

# MOUNTAIN-PLAINS CONSORTIUM

MPC 20-422 | S. Bartlett, E. Lawton, and Z. Gibbs

Evaluation of Secondary Consolidation Settlement Associated with Embankment Construction for Fast-paced Transportation Projects



A University Transportation Center sponsored by the U.S. Department of Transportation serving the Mountain-Plains Region. Consortium members:

Colorado State University  
North Dakota State University  
South Dakota State University

University of Colorado Denver  
University of Denver  
University of Utah

Utah State University  
University of Wyoming

# **Evaluation of Secondary Consolidation Settlement Associated with Embankment Construction for Fast-paced Transportation Projects**

Steven F. Bartlett, Ph.D., P.E.  
Evert C. Lawton, Ph.D., P.E.  
Zach M. Gibbs

Department of Civil and Environmental Engineering  
University of Utah

October 2020

## **Acknowledgments**

The authors acknowledge the Utah Department of Transportation (UDOT) for funding this research. The following individuals from UDOT and other organizations on the Technical Advisory Committee helped advise and guide the study.

David Stevens (UDOT)  
Grant Gummow (UDOT)  
Jon Bischoff (UDOT)  
James Higbee (UDOT)  
Richard J. Porter (U of U – MPC)  
Travis Gerber (BYU)  
Scott M. Olson (U. of Illinois)  
Steven Saye (Kiewit)  
Shun Li (U of U)  
Ramesh Neupane (U of U)

## **Disclaimer**

The contents of this report reflect the views of the authors, who are responsible for the facts and the accuracy of the information presented. This document is disseminated under the sponsorship of the Department of Transportation, University Transportation Centers Program, in the interest of information exchange. The U.S. Government assumes no liability for the contents or use thereof.

NDSU does not discriminate in its programs and activities on the basis of age, color, gender expression/identity, genetic information, marital status, national origin, participation in lawful off-campus activity, physical or mental disability, pregnancy, public assistance status, race, religion, sex, sexual orientation, spousal relationship to current employee, or veteran status, as applicable. Direct inquiries to: Vice Provost, Title IX/ADA Coordinator, Old Main 201, 701-231-7708, [ndsueoaa@ndsu.edu](mailto:ndsueoaa@ndsu.edu).

## ABSTRACT

This report discusses the design and implementation of surcharging technology and the required laboratory, field, and engineering evaluations. It is hoped that such information will provide a more consistent and technically defensible rationale for deploying this technology on highway projects constructed atop soft soils. Surcharging or preloading of the earthen embankments and underlying compressible soils is the most commonly deployed strategy to reduce the magnitude of secondary compression. Surcharging or overconsolidating of the foundation soils can be used to reduce the post-construction secondary settlement. In this research, 22 consolidation tests and 88 time-rate of consolidation tests were performed on Pleistocene and recent fine-grained, cohesive, lacustrine deposits composed of Lake Bonneville and more recent clays, most likely of Utah Lake origin located along the Wasatch Front in Utah. Plots of the adjusted amount of surcharge (AAOS) were plotted versus the normalized rate of secondary settlement ( $C\alpha'/C\alpha$ ) and compared with prior laboratory data. The data from our research plots agree better with the long-term settlement performance monitoring data obtained from the I-15 Reconstruction Project in Salt Lake County, Utah. Also, this report presents a recommended method for designing surcharge fills, considering post-construction (i.e., secondary compression) settlement effects.

# TABLE OF CONTENTS

<b>1. INTRODUCTION .....</b>	<b>1</b>
1.1 Overview .....	1
1.2 Scope and Purpose of Research .....	2
<b>2. BACKGROUND .....</b>	<b>3</b>
2.1 General Discussion .....	3
2.2 Mesri et al. Concept of Secondary Compression .....	4
2.3 Surcharging to Reduce Secondary Compression .....	5
2.4 Surcharge Design Using Methodology Developed by Mesri .....	5
2.5 Surcharge Design Using Methodology Developed by Ladd .....	6
2.6 Application of Ladd's Method to the I-15 Reconstruction Project.....	8
<b>3. RESEARCH OBJECTIVES AND TASKS .....</b>	<b>13</b>
3.1 Research Objectives .....	13
3.2 Research Plan.....	13
3.3 Tasks .....	13
<b>4. FIELD INVESTIGATIONS .....</b>	<b>14</b>
4.1 Introduction.....	14
4.2 Field Investigations.....	14
<b>5. LABORATORY TESTING .....</b>	<b>38</b>
5.1 Test Procedures .....	38
5.1.1 Introduction .....	38
5.1.2 Testing Equipment .....	38
5.1.3 Sample Setup.....	39
5.2 Laboratory Test Program .....	44
5.2.1 Introduction .....	44
5.2.2 Determination of the Preconsolidation Stress .....	45
5.2.3 Determination of the Rate of Secondary Compression $C_\alpha$ .....	45
5.2.4 Determining $C_\alpha'$ .....	46
<b>6. RESULTS AND INTERPRETATIONS .....</b>	<b>47</b>
6.1 Laboratory Tests and Data Screening .....	47
6.2 Relationships for $C_\alpha$ , $C_\alpha'$ and $C_\alpha'/C_\alpha$ .....	52
6.3 $C_\alpha/CR$ Ratio .....	58
6.4 Moisture Content Correlations.....	62
<b>7. CONCLUSIONS .....</b>	<b>67</b>
7.1 Summary of Research Objectives.....	67
7.2 Mesri's Concept of Secondary Compression.....	67
7.2.1 $C_\alpha/CR$ .....	67
7.2.2 Creep Behavior as a Function of AAOS .....	67
7.2.3 The Time Before Creep Resumes After the Removal of a Surcharge.....	68
7.2.4 Recommendations for Laboratory Testing Program .....	68
7.3 Additional Design Guidance.....	68
7.4 Recommendations for Additional Testing .....	68
7.5 Recommended Method for Design .....	69
<b>8. REFERENCES.....</b>	<b>70</b>

<b>APPENDIX A. PLOTS FOR PRECONSOLIDATION STRESS .....</b>	<b>72</b>
<b>APPENDIX B. PLOTS OF RATE OF SECONDARY SETTLEMENT .....</b>	<b>336</b>
<b>APPENDIX C. LABORATORY TESTING PROCEDURE .....</b>	<b>425</b>
<b>APPENDIX D. CPT PLOTS OF SOIL BEHAVIOR TYPES .....</b>	<b>435</b>
<b>APPENDIX E. COMPARISON OF INCREMENTAL LOADING AND INSTANTANEOUS LOADING .....</b>	<b>440</b>
<b>APPENDIX F. METHOD FOR DESIGNING SURCHARGE FILLS CONSIDERING POST-CONSTRUCTION SECONDARY COMPRESSION SETTLEMENT .....</b>	<b>444</b>
Introduction .....	445
Required Information and Design Inputs .....	445
Primary Consolidation Settlement .....	445
Estimation of Amount of Primary Consolidation Settlement for Design .....	446
Estimation of Time Rate of Primary Consolidation Settlement for Design .....	446
Secondary Consolidation Settlement .....	451
Estimation of Secondary Compression for Normally Consolidated Soils .....	451
Estimation of Secondary Compression for Surcharged Soils .....	451
Recommended Surcharge Layout and Extents .....	457
Instrumentation for Monitoring Progression of Primary Consolidation .....	461
Settlement Plates .....	461
Settlement Manometer .....	462
Magnet Extensometer .....	464
Sondex System .....	466
Piezometers .....	466
Interpretation of Field Data for Surcharge Release .....	467
Consequences of Premature Surcharge Removal .....	469
References (Appendix F only) .....	471

## LIST OF TABLES

Table 4.1	Boring locations, depths, and drilling dates.....	15
Table 4.2	CPT locations.....	15
Table 6.1	Listing of sites, depths, moisture content, preconsolidation stress, compression and recompression ratio, rate of secondary settlement and OCR values.....	49
Table 6.2	Values of strain at $\sigma'_{vo}$ and the corresponding rating of SQD.....	50
Table 6.3	Site, depth, effective vertical stress, and SQD.....	51

## LIST OF FIGURES

Figure 2.1	Definition of $C_\alpha$ from 1D time rate of consolidation test (after Raymond and Wahls, 1976; Ng 1998).....	4
Figure 2.2	Mesri's basic concepts of the effects of surcharge on secondary compression from Terzaghi et. al. 1996 .....	6
Figure 2.3	The effects of surcharging (i.e., preloading) on the rate of secondary compression (after Ladd, unpublished notes). .....	8
Figure 2.4	Typical cone penetrometer (CPT) log and soil descriptions for downtown segment of I-15 Reconstruction Project, Salt Lake City, Utah (Farnsworth et al., 2008). .....	9
Figure 2.5	Typical Fill Height versus Settlement Record for the 1960s, I-15 Construction, Salt Lake Valley, x-axis is elapsed time since beginning of fill placement since April 1964, y-axis (green) is fill height (ft) and y-axis (red) is settlement measured at original ground surface (ft) .....	10
Figure 2.6	Relationship between rate of secondary compression and compression ratio for Lake Bonneville clays (Ng, 1998). Ng (1998) data are labeled MIT and Woodward-Clyde Consultants are labeled WCC (Saye and Ladd, 2000).....	11
Figure 2.7	(Top) $C_\alpha' / C_\alpha$ as a function of AAOS (Bottom) Log( $t_s/t_r$ ) ratios as a function of AAOS (Saye and Ladd, 2000).....	12
Figure 4.1	400 South site (400 South 800 West). (Top) Vicinity map for drilling site (Bottom) Close up of drilling site .....	166
Figure 4.2	drilling South Layton site (Layton Parkway and Main Street). (Top) Vicinity map for site (Bottom) Close up of drilling site .....	177
Figure 4.3	Springville site (400 South and 1700 West). (Top) Vicinity map for drilling site (Bottom) Close up of drilling site.....	188
Figure 4.4	Provo site (Southbound I-15 on ramp for University Avenue). (Top) Vicinity map for drilling site (Bottom) Close up of drilling site and CPT location.....	19
Figure 4.5	CPT for 400 South and I-15, Salt Lake City, 06-SC-159.....	20
Figure 4.6a	CPT for South Layton CPT-01 .....	21
Figure 4.7a	CPT for Springville, CPT-01 .....	24
Figure 4.8a	CPT for Springville CPT-07.....	30
Figure 4.9a	CPT for Provo CPT-07 .....	33
Figure 4.10	Test Hole Log for 400 South and I-15, Salt Lake City.....	33
Figure 4.11	Test Hole Log for South Layton Test Hole I.....	34
Figure 4.12	Test Hole Log for South Layton Test Hole II.....	35
Figure 4.13	Test Hole Log for Springville.....	36
Figure 4.14	Test Hole Log for Provo.....	37
Figure 5.1	Tabletop oedometer .....	39
Figure 5.2	Consolidation ring and cell.....	39
Figure 5.3	Horizontal ban saw used to cut samples for testing.....	40
Figure 5.4	Extruding sample from Shelby tube .....	41
Figure 5.5	Sample in turntable. ....	42
Figure 5.6	Sample in consolidation ring .....	43
Figure 5.7	Sample fully assembled in cell. ....	43
Figure 5.8	Fully assembled cell in table top oedometer.....	44
Figure 6.1	Plot of preconsolidation stress vs. depth for 400 South, South Layton, Springville, and Provo.....	52



Figure 6.2	Plot of $C_\alpha$ and $C_\alpha'$ vs. OCR for 400 South, South Layton, Springville, and Provo Sites	53
Figure 6.3	Plot of $C_\alpha'/C_\alpha$ vs. OCR for 400 South, South Layton, Springville, and Provo Sites	54
Figure 6.4	Plot of AAOS vs. $C_\alpha'/C_\alpha$ using an average exponential trend line .....	56
Figure 6.5	Comparison plot of AAOS vs. $C_\alpha'/C_\alpha$ on a semi log plot with data acquired by MIT	57
Figure 6.6	Rate of Foundation Creep Extrapolated to 10 Years of Post-Construction (from Farnsworth et al., 2008).....	58
Figure 6.7	Plot of CR vs. $C_\alpha$ for all sites .....	59
Figure 6.8	Comparison plot of CR vs. $C_\alpha$ with data collected from MIT and WCC.....	60
Figure 6.9	Comparison plot of AAOS vs. LOG(ts/tr) with data collected from MIT and WCC	61
Figure 6.10	Plot of moisture content vs. virgin compression ratio .....	63
Figure 6.11	Plot of moisture content vs. virgin compression ratio (Bartlett and Lee, (2004).....	64
Figure 6.12	Plot of moisture content vs. rate of secondary settlement .....	64
Figure 6.13	Plot of moisture content vs. $C_\alpha/CR$ ratio.....	655
Figure 6.14	Plot of moisture content vs. normalized rate of secondary settlement .....	666

# UNIT CONVERSION FACTORS

SI* (MODERN METRIC) CONVERSION FACTORS				
APPROXIMATE CONVERSIONS TO SI UNITS				
Symbol	When You Know	Multiply By	To Find	Symbol
<b>LENGTH</b>				
in	inches	25.4	millimeters	mm
ft	feet	0.305	meters	m
yd	yards	0.914	meters	m
mi	miles	1.61	kilometers	km
<b>AREA</b>				
in <sup>2</sup>	square inches	645.2	square millimeters	mm <sup>2</sup>
ft <sup>2</sup>	square feet	0.093	square meters	m <sup>2</sup>
yd <sup>2</sup>	square yard	0.836	square meters	m <sup>2</sup>
ac	acres	0.405	hectares	ha
mi <sup>2</sup>	square miles	2.59	square kilometers	km <sup>2</sup>
<b>VOLUME</b>				
fl oz	fluid ounces	29.57	milliliters	mL
gal	gallons	3.785	liters	L
ft <sup>3</sup>	cubic feet	0.028	cubic meters	m <sup>3</sup>
yd <sup>3</sup>	cubic yards	0.765	cubic meters	m <sup>3</sup>
NOTE: volumes greater than 1000 L shall be shown in m <sup>3</sup>				
<b>MASS</b>				
oz	ounces	28.35	grams	g
lb	pounds	0.454	kilograms	kg
T	short tons (2000 lb)	0.907	megagrams (or "metric ton")	Mg (or "t")
<b>TEMPERATURE (exact degrees)</b>				
°F	Fahrenheit	5 (F-32)/9 or (F-32)/1.8	Celsius	°C
<b>ILLUMINATION</b>				
fc	foot-candles	10.76	lux	lx
fl	foot-Lamberts	3.426	candela/m <sup>2</sup>	cd/m <sup>2</sup>
<b>FORCE and PRESSURE or STRESS</b>				
lbf	poundforce	4.45	newtons	N
lbf/in <sup>2</sup>	poundforce per square inch	6.89	kilopascals	kPa
APPROXIMATE CONVERSIONS FROM SI UNITS				
Symbol	When You Know	Multiply By	To Find	Symbol
<b>LENGTH</b>				
mm	millimeters	0.039	inches	in
m	meters	3.28	feet	ft
m	meters	1.09	yards	yd
km	kilometers	0.621	miles	mi
<b>AREA</b>				
mm <sup>2</sup>	square millimeters	0.0016	square inches	in <sup>2</sup>
m <sup>2</sup>	square meters	10.764	square feet	ft <sup>2</sup>
m <sup>2</sup>	square meters	1.195	square yards	yd <sup>2</sup>
ha	hectares	2.47	acres	ac
km <sup>2</sup>	square kilometers	0.386	square miles	mi <sup>2</sup>
<b>VOLUME</b>				
mL	milliliters	0.034	fluid ounces	fl oz
L	liters	0.264	gallons	gal
m <sup>3</sup>	cubic meters	35.314	cubic feet	ft <sup>3</sup>
m <sup>3</sup>	cubic meters	1.307	cubic yards	yd <sup>3</sup>
<b>MASS</b>				
g	grams	0.035	ounces	oz
kg	kilograms	2.202	pounds	lb
Mg (or "t")	megagrams (or "metric ton")	1.103	short tons (2000 lb)	T
<b>TEMPERATURE (exact degrees)</b>				
°C	Celsius	1.8C+32	Fahrenheit	°F
<b>ILLUMINATION</b>				
lx	lux	0.0929	foot-candles	fc
cd/m <sup>2</sup>	candela/m <sup>2</sup>	0.2919	foot-Lamberts	fl
<b>FORCE and PRESSURE or STRESS</b>				
N	newtons	0.225	poundforce	lbf
kPa	kilopascals	0.145	poundforce per square inch	lbf/in <sup>2</sup>

\*SI is the symbol for the International System of Units. (Adapted from FHWA report template, Revised March 2003)

## LIST OF ACRONYMS

AAOS	Adjusted Amount of Surcharge
AOS	Amount of Surcharge
CL	Low Plastic Clay
CH	High Plastic Clay
CR	Compression Ratio
EOP	End of Primary Consolidation
FHWA	Federal Highway Administration
MH	High Plasticity Silt
ML	Low Plasticity Silt
MIT	Massachusetts Institute of Technology
OCR	Overconsolidation Ratio
RR	Recompression Ratio
SC	Clayey Sand
SHANSEP	Stress History and Normalized Soil Engineering Properties
SM	Silty Sand
UDOT	Utah Department of Transportation
WCC	Woodward Clyde Consultants

## EXECUTIVE SUMMARY

Secondary compression of foundation soils can cause long-term settlement damage to bridges, their foundations and approach embankments, overlying pavements, and other nearby constructed works. Because this type of settlement is long-term and manifests itself many months to years following embankment construction, it often goes unnoticed until it damages overlying or nearby infrastructure.

This report discusses the design and implementation of surcharging technology and the required laboratory, field, and engineering evaluations. Surcharging or preloading of the earthen embankments and underlying compressible soils is the most commonly deployed strategy to reduce the magnitude of secondary compression. Surcharging or overconsolidating of the foundation soils can be used to reduce the post-construction secondary settlement. In the course of this research, 22 consolidation tests and 89 time-rate tests were performed on Pleistocene and recent fine-grained, cohesive, lacustrine deposits composed of Lake Bonneville and more recent clays, most likely of Utah Lake origin located along the Wasatch Front in Utah. Before analyzing the data, the test results were screened using the sample quality designation (SQD).

Plots of the adjusted amount of surcharge (AAOS) were plotted versus the normalized rate of secondary compression settlement ( $C_{\alpha}'/C_{\alpha}$ ) with the research performed by Ng (1998), where  $C_{\alpha}'$  is the reduced rate of secondary compression due to surcharging. The value of  $C_{\alpha}$  is the rate associated with normally consolidated sediments (i.e., un-surcharged). The data obtained from this study plot higher than those reported by Ng (1998), suggesting more elevated amounts of secondary settlement will occur. As additional support, this observed trend is in better agreement with the long-term settlement performance monitoring data obtained from the I-15 Reconstruction Project from 2000 to 2012 in the northern part of the Salt Lake Valley in Utah. Data from the time rate tests associated with this study were used to determine the  $C_{\alpha}/CR$  ratio, giving a mean value of  $C_{\alpha}/CR = 0.0442$ , where CR is defined as the compression ratio. This value was also compared with the research performed by Ng (1998), which had a value of  $C_{\alpha}/CR = 0.0433$ , which correlates well with the results obtained from this study. A plot of moisture content vs. CR was developed and compared with research done by Bartlett and Lee (2004). The data from this thesis trend line are slightly lower than those reported by Bartlett and Lee (2004), but still correlate well. The correlation of moisture content vs. the  $C_{\alpha}/CR$  ratio was explored and also shows promise, but more observations are needed to improve the statistical support for this relation.

Also provided in this report is a recommended method for designing surcharge fills considering the amount of post-construction, secondary compression settlement.

# 1. INTRODUCTION

## 1.1 Overview

Secondary compression or secondary settlement or creep settlement is a continuation of the volume change of a compressible soil under a constant (i.e., non-changing) loading without the associated changes in the effective stress of the soil fabric. This behavior begins to be manifested near the end of primary consolidation and continues indefinitely, but at a non-linear diminishing rate. In contrast to primary consolidation, which is associated with compression due to pore water pressure dissipation, secondary compression begins when the specimen achieves a constant effective stress after essentially all excess pore water pressure has dissipated that was initially induced by the initial loading event (Holtz et al., 2011). Secondary compression of foundation soils at deep, compressible, soil sites can cause long-term settlement damage to bridges, their foundations and approach embankments, overlying pavements and other nearby constructed works. Because this type of settlement is long-term and manifests itself many months to years following embankment construction, it often goes unnoticed until it damages overlying or nearby infrastructure. For example, the collective secondary compression is often significantly large enough to produce a severe “bump” at pile-supported bridges where the approach embankment has settled differentially relative to the bridge and bridge abutments.

The magnitude and potential deleterious effects of secondary compression on the future performance of the interstate system were important geotechnical design and performance considerations during the reconstruction of I-15 in the northern part of Salt Lake Valley, Utah, from 1998 to 2001. Surcharging or preloading of the earthen embankments and underlying compressible soils was the most commonly deployed strategy to reduce the magnitude of secondary compression; however, soil improvement and lightweight embankment materials were also used as settlement mitigative measures. An important part of embankment design for the I-15 project was a systematic evaluation of the required amount (i.e., height) of surcharge to reduce the secondary compression to acceptable, post-construction, performance goals. Associated with this issue is also the required time that such surcharge is to remain in place to achieve the desired long-term settlement performance goal. For the I-15 project, the performance goal was to surcharge the foundation soils sufficiently enough that the embankment in the bridge approach area did not settle more than three inches in a 10-year, post-construction period. Whatever the desired outcome, the settlement performance goals should be clearly defined by the project team in consultation with the owner. For fast-paced construction, the corresponding settlement calculations and design, construction settlement monitoring, and project communication are vital if these goals are to be realized. In addition to the amount of surcharging employed, the time or duration that the surcharge is to remain in-place (i.e., surcharge duration) strongly impacts the post-construction settlement performance and the construction schedule. Because the surcharge duration can be long for deep soil sites, this can significantly impact the construction schedule; hence, there is an inherent tendency by the contractor and the project team to try to shorten the surcharge duration to expedite the construction. Therefore, construction settlement monitoring to assess the progression of primary consolidation settlement and a decision framework for selecting when to remove the surcharge are essential in achieving the settlement performance goals and delivering a timely project.

## **1.2 Scope and Purpose of Research**

The primary purpose of this research is: (1) to quantify the effects that surcharging (i.e., preloading) has on secondary compression settlement for fine-grained soils located along the Wasatch Front, Utah, area using one-dimensional (1D) consolidation tests performed on conventional tabletop oedometers; (2) to develop the information, relations, equations, charts, etc. required to develop and implement a surcharge design for these sediments using the framework developed by Ladd (1989) and Ng (1998); (3) to confirm or recommend changes, if any, to the relations required for surcharge design as presented by Ladd (1989) and Ng (1998); and (4) to make other recommendations about the implementation of the results of this research in regard to surcharge calculations and design.

These purposes and objectives were explored via: (1) reviewing the geotechnical literature that supports the approaches of Mesri et al., (Mesri and Castro, 1987; Mesri et al., 1994) and of Ladd (Ladd, 1989; and Ng, 1998); (2) undisturbed sampling of cohesive soils from four soft soil sites located along the urban Wasatch Front, Utah; (3) laboratory testing of these specimens in conventional oedometers to determine the rate of secondary compression as a function of preloading (i.e., overconsolidation ratio); (4) evaluating and presenting the results of the laboratory test program in the analysis framework developed by (Ladd, 1989, and Ng, 1998); and (5) making recommendations, if any, about modifications to the relationships or methods developed by Ladd (1989) and Ng (1998).

## 2. BACKGROUND

### 2.1 General Discussion

Consolidation settlement of soil occurs from three general mechanisms: (1) quasi elastic compression of the soil fabric upon reloading that occurs below the preconsolidation stress, (2) primary consolidation settlement resulting from significant compression of the soil fabric from an applied stress that exceeds the preconsolidation stress, and (3) secondary consolidation or secondary compression of the soil fabric, which is a complex combination of processes that initiates near the end of primary consolidation and continues as a long-term process under a constant load or unchanging effective stress (Holtz et al., 2011). Secondary compression is generally thought of as void ratio change in the soil fabric occurring at a relatively slow rate after primary consolidation is essentially completed. However, some researchers have noted that secondary compression occurs in conjunction with primary consolidation settlement, but at a slower rate; hence its effects are in a large part masked by the significantly greater magnitude and faster rate of primary consolidation settlement realized during the initial part of the consolidation process. Therefore, it is difficult to distinguish secondary compression from experimental data when the sample is undergoing large void ratio changes associated with primary consolidation (Takeda et al., 2013). Although such distinctions are important for the advancement of consolidation theory, this research will adopt the classical construction shown in Figure 2-1 to define the time corresponding to the end of primary consolidation,  $t_p$ , which also marks the beginning of secondary compression (Raymond and Wahls, 1976). In this definition,  $t_p$  is calculated as the intersection of the straight lines that define primary consolidation and secondary compression on a void ratio,  $e$ , versus log of time plot.

As the rate of primary consolidation diminishes, secondary compression becomes the dominant process. At this point, almost all of the excess pore water pressure (i.e., pore water pressure above hydrostatic) has dissipated from the soil fabric that was caused by the initial loading event. Hence, secondary compression is also defined as void ratio change or settlement occurring when the effective stress in the soil fabric is no longer significantly changing (Holtz et al., 2011). The continued settlement at a diminishing rate is a result of creep, viscous behavior of the soil fabric, compression of organic matter, and other processes.

Holtz et al. (2011) suggest that the following assumptions must be adopted to provide a working hypothesis about the behavior of fine-grained sediments undergoing secondary compression based on work by Ladd (1971) and Raymond and Wahls (1976). They discuss the relative merits and practical consequences associated with these assumptions, which have been briefly summarized below:

1. The rate of secondary compression is independent of time, at least during the time span of engineering interest. (This assumption is discussed later in this report.)
2. The rate of secondary compression is independent of the soil layer.
3. The rate of secondary compression is independent of the load increment ratio (LIR), as long as some primary consolidation occurs.
4. The ratio of the rate of secondary compression to the compression index is approximately constant for many geo-materials over the range of engineering stresses (also discussed later in this report).

The amount of volume change during secondary compression is calculated from the secondary compression index,  $C_{\alpha}$ , which represents the rate of secondary compression defined by:

$$C_{\alpha} = \Delta e / \Delta \log t \quad (2-1)$$

where:  $\Delta e$  is the change in void ratio,  $\Delta \log t$  is  $\log t - \log t_p$ . The value of  $C_{\alpha}$  represents the change in void ratio,  $e$ , divided by the change in log of time for the portion of the time rate of consolidation curve extending beyond the end-of-primary (EOP) consolidation (Figure 2-1) (Holtz et al., 2011). When plotted

on a semi-log plot,  $C_\alpha$  represents the slope of this semi-log linear portion of secondary compression that occurs beyond EOP consolidation (Figure 2-1).

The magnitude of secondary compression or settlement for a specimen or layer is typically calculated by the following formula for 1D consolidation:

$$S = [C_\alpha / (1 + e_o)] H_o \log t / t_p \quad (2-2)$$

where:  $H_o$  is the height of the specimen or layer,  $e_o$  is the initial void ratio,  $C_\alpha$  is the rate of secondary compression,  $t$  is the elapsed time after the end of primary consolidation, and  $t_p$  is the time required to reach the end of primary consolidation (Figure 2.1) (Holtz et al., 2011; Terzaghi et al., 1996).

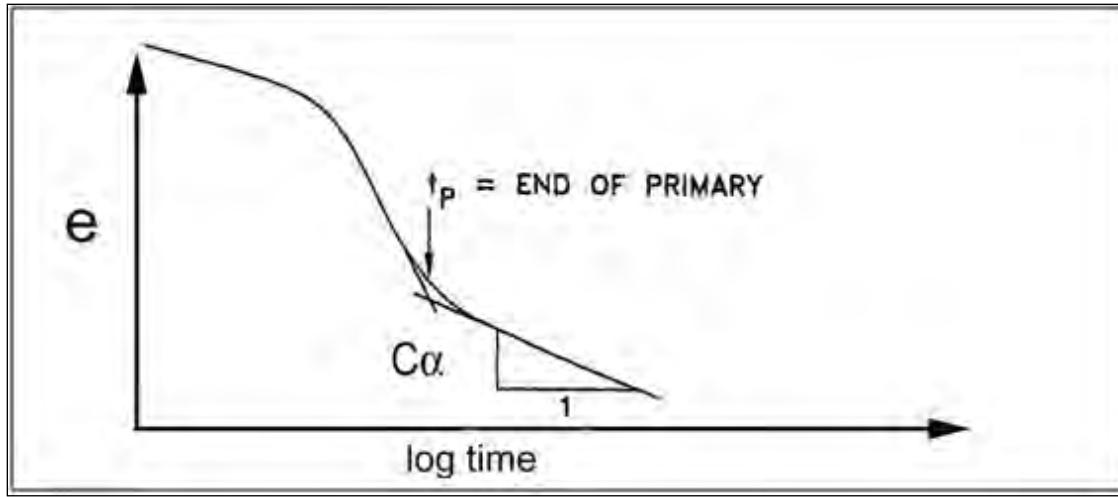


**Figure 2.1** Definition of  $C_\alpha$  from 1D time rate of consolidation test (after Raymond and Wahls, 1976; Ng 1998)

## 2.2 Mesri et al. Concept of Secondary Compression

Mesri et al. have shown that the secondary compression index for a normally consolidated soil,  $C_{\alpha NC}$ , is correlated with and can be estimated from the virgin compression index,  $C_c$ , or the compression ratio CR of that soil (Mesri and Castro, 1987; Mesri and Feng, 1991; Mesri et al., 1994; Terzaghi et al. 1996; Ladd, 1989; Ng, 1998; Saye and Ladd, 2000) where the compression ratio is defined as:

$$CR = C_c / (1 + e_o) \quad (2-3)$$

Because of this correlation, the method proposed by Mesri et al. (Mesri and Castro, 1987; Mesri et al., 1994) is often used to estimate the rate of secondary compression for a given geologic unit. In the approach proposed by Mesri et al., the ratio of  $C_\alpha/C_c$  or  $C_\alpha/CR$  has been found to be considered relatively constant for sediments of the same geologic origin. Therefore, this ratio can be used to estimate  $C_\alpha NC$  if  $C_c$  or CR has been determined for the soil of interest. It should be noted that the  $C_\alpha/CR$  ratio used in this research is the same as  $C_\alpha/C_c$  ratio of Mesri and Castro (1987) and Mesri et al. (1994) because for  $C_\alpha/CR$ , the unit of strain in  $C_\alpha = d\varepsilon_v / d\log t$  and that found in  $CR = d\varepsilon_v / d\log \sigma'_{vc}$  cancel each other; and for  $C_\alpha/C_c$ , the unit of change in void ratio  $C_\alpha = de / d\log t$  and that found in  $C_c = de / d\log \sigma'_{vc}$  cancel each other (Ng, 1998), thus  $C_\alpha/CR$  or  $C_\alpha/C_c$  can be used interchangeably.

To implement the Mesri et al. method (Mesri and Castro, 1987; Mesri et al., 1994), values of  $C_\alpha/C_c$  or  $C_\alpha/CR$  are typically determined from a laboratory consolidation testing program from each geologic unit



of interest. Once this ratio is established, additional estimates of  $C_\alpha$  can be made for a given deposit using laboratory or field estimates of  $C_c$  or CR and the corresponding values of  $C_\alpha/C_c$  or  $C_\alpha/CR$  ratio for that deposit.

## 2.3 Surcharging to Reduce Secondary Compression

Terzaghi et al. (1996) recognized that if the final in situ state of stress resulting from a loading event imparted to a foundation soil is higher than the original preconsolidation stress of the soil, and if the time for primary consolidation,  $t_p$ , is small perhaps due to the installation of prefabricated vertical drains (PVD), then the amount of secondary compression settlement can be relatively large. However, this can be reduced to acceptable levels by using surcharging of the foundation soil during the last stage of embankment construction. Surcharging has the effect of preloading the soil (i.e., overconsolidating) and reducing the rate of secondary compression when compared with the rate of secondary compression for a normally consolidated soil (i.e., a soil that has not been surcharged).

Surcharge methodologies developed by Ladd (1989) and by Mesri (1986) have been used in engineering practice to develop a surcharge approach to reduce the effects of secondary compression associated with embankment construction atop relatively soft, compressible, foundation soils. The next two sections of this report describe Mesri's and Ladd's methodologies. Section 5 of this report discusses how Ladd (1989) methodology was applied to the I-15 Reconstruction Project in the Salt Lake Valley, Utah, to reduce the effects of secondary compression. The data developed from this roadway project in conjunction with additional field and laboratory testing and evaluations performed as part of this research become, in part, the basis for the surcharge design guidance developed herein.

## 2.4 Surcharge Design Using Methodology Developed by Mesri

Mesri (Terzaghi et al., 1996) has shown the behavior of a soil subjected to surcharging (Figure 2-2). The removal of the surcharge leads to rebound of the specimen, including primary rebound up to the time  $t_{pr}$  and secondary rebound that levels off at time  $t_l$  and is followed by secondary compression occurring at a nonlinear rate on a log of time plot. In this figure,  $t_{pr}$ ,  $t_l$  and  $t$  are measured from the time when the surcharge load was removed (i.e.,  $t'_s$ ). The post-surge secondary compression behavior,  $C'_\alpha$ , shown in Figure 2.2 is initially small and subsequently gradually increases with time. Mesri has shown that at large values of  $t$ , the behavior of the secondary compression depends on the initial shape of the EOP  $e$  vs.  $\log \sigma'_v$  curve at the state of stress with the surcharged load applied. Hence, because  $C'_\alpha$  is not constant with time, a secant value  $C''_\alpha$  is used in evaluations where the slope of  $C''_\alpha$  is defined by the line connecting  $t_l$  with  $t$ .

In Mesri's approach, the surcharging effort is expressed as the total surcharge ratio:

$$R_s = (\sigma_{vs} / \sigma'_{vf}) - 1 \quad (2-4)$$

where:  $\sigma_{vs}$  is equal to  $\sigma'_{vf} + \Delta\sigma_{vs}$  and  $\sigma'_{vf}$  is the final effective vertical stress after removal of surcharge and  $\Delta\sigma_{vs}$  is the total stress applied by the surcharge load. The surcharging time ratio,  $t'_s / t'_{ps}$ , affects the behavior of the curve where  $t'_s$  is the duration of the surcharge, and  $t'_{ps}$  is the time to EOP compression under the surcharge load. For cases where the surcharge load is removed before EOP compression, the above equation is rewritten as:

$$R'_s = (\sigma'_{vs} / \sigma'_{vf}) - 1 \quad (2-5)$$

where:  $\sigma'_{vs}$  is the maximum effective vertical stress reached before the removal or surcharge. Hence, when  $t'_s / t'_{ps} = 1$ , then  $R_s = R'_s$ .

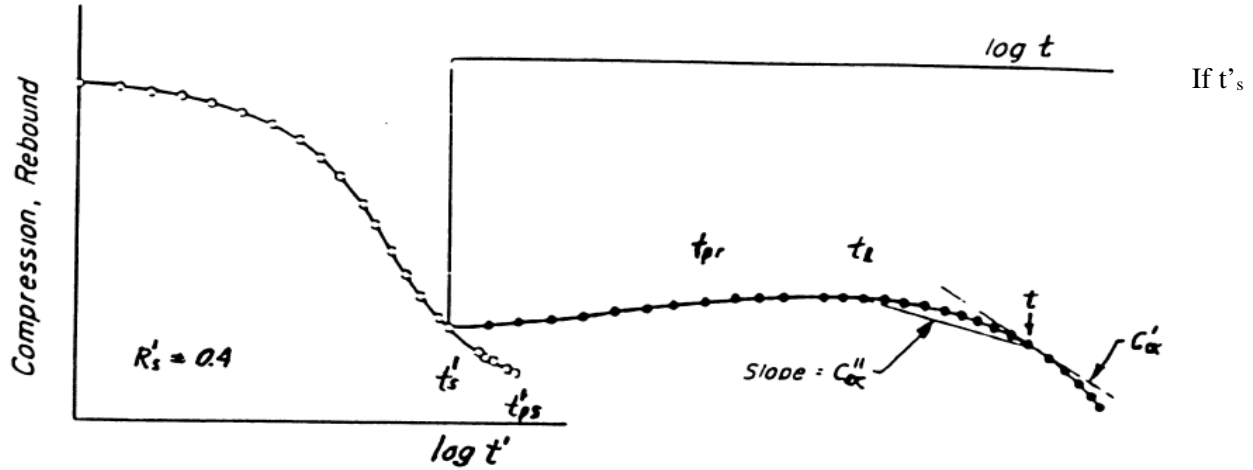


**Figure 2.2** Mesri's basic concepts of the effects of surcharge on secondary compression from Terzaghi et al. 1996

exceeds the time to the EOP compression, then the value of  $R'_s$  is adjusted to reflect the aging and the effective surcharge ratio,  $R'_s$ , is equal to:

$$R'_s = (\sigma'_p - \sigma'_{vf}) / \sigma'_{vf} \quad (2-6)$$

where:  $\sigma'_p$  is the apparent preconsolidation stress due to aging of the soil under the surcharge load.

## 2.5 Surcharge Design Using Methodology Developed by Ladd

The methodology of Ladd (1989) has many aspects that are similar to that of Mesri, but the part of the curve that defines secondary compression has been simplified (Figure 2-3). The most important difference is that Ladd's method assumes the rate of secondary compression is linear when plotted on a semi-log plot. The linear portion begins after the start of secondary compression,  $t_s$ , and continues thereafter (Figure 2-3). Hence  $C'_\alpha$  is calculated from the slope of a line fitted through the linear most part of the vertical strain measurements that follow  $t_s$ . This construction makes Ladd's method easier to apply than that of Mesri.

In Ladd's method, if the soil is surcharged (i.e., overconsolidated) and subsequently aged under this surcharge load, it undergoes secondary compression at a reduced rate,  $C'_\alpha$ , when compared with the, un-surcharged, unaged rate of secondary compression  $C_\alpha$  (Figure 2-3). The aging time of the soil under the surcharge stress (i.e., elapsed time between  $t_p$  and  $t_r$ ) reduces the rate of secondary compression from  $C_\alpha$ , the normally consolidated value, to a lesser, overconsolidated value,  $C'_\alpha$ , which has a reduced slope (Figure 2.3). Hence, if a soil can be surcharged and aged, the amount of post-construction creep settlement is reduced when compared with the un-surcharged, normally consolidated value. Therefore, in applying this concept to developing the surcharge design for an embankment and its foundation soil, an evaluation is made to provide sufficient surcharging of the foundation soil so as to reduce  $C'_\alpha$  to a value that will reduce the amount of secondary compression. The value of  $C'_\alpha$  required is a function of the thickness of the foundation soil layer undergoing secondary compression and the post-construction

settlement goal selected by the project team. The amount of secondary compression settlement for normally consolidated sediments (i.e., un-surcharged soils) is calculated from:

$$S_s = H_1 C_\alpha \log (t / t_p) \quad (2-7)$$

where:  $S_s$  is the amount of secondary compression settlement,  $H_1$  is the thickness of the layer undergoing secondary compression,  $C_\alpha$  is the normally consolidated rate of secondary compression,  $t_p$  is time to end of primary consolidation, and  $t$  is the time beyond  $t_p$ . If the soil has been surcharged (i.e., overconsolidated) and then unloaded, then a reduced rate of secondary compression,  $C_\alpha'$ , is used in lieu of  $C_\alpha$ :

$$S_s = H_1 C_\alpha' \log (t / t_p) \quad (2-8)$$

When using Ladd's methodology for a surcharge design, the soil is loaded from  $(\sigma'_v)$  to the surcharge stress  $(\sigma'_{vs})$  and then is unloaded to the final stress  $(\sigma'_{vf})$ . The difference between these values is defined as the amount of surcharge (AOS), which is determined from the following:

$$AOS = (\sigma'_{vs} - \sigma'_{vf}) / \sigma'_{vf} \quad (2-9)$$

For staged embankment construction,  $\sigma'_{vs}$  should be calculated using the full embankment height plus the height of surcharge, and  $\sigma'_{vf}$  should be calculated using the final embankment height after surcharge removal, but including the weight of the overlying pavement system, if present.

If the surcharge stress  $\sigma'_{vs}$  exceeds the preconsolidation stress of the soil (i.e., primary consolidation is initiated) and primary consolidation is allowed to go to completion, but significant secondary compression is not allowed under the surcharge load (i.e., soil is not allowed to age by removing the surcharge,  $t_r$ , at the same time as  $t_p$  is achieved), then Equation 2-9 is appropriate and Equation 2-8 should be used to calculate the secondary compression of the soil using  $C_\alpha'$  appropriate for the AOS achieved by the surcharge load. The amount of surcharge, AOS, and the overconsolidation ratio, OCR, are related by:

$$AOS = OCR - 1 \quad (2-10)$$

If the soil is aged by allowing the surcharge to remain in place for some time after the end of primary consolidation (i.e.,  $t_r > t_p$ ), then the AOS is adjusted to account for the apparent increase of  $\sigma'_p$  above  $\sigma'_{vs}$ , due to the aging. The adjusted amount of surcharge (AAOS) is determined using the following:

$$AAOS = (\sigma'_p - \sigma'_{vf}) / \sigma'_{vf} \quad (2-11)$$

$$\text{where: } \sigma'_p = \sigma'_{vs} (t_r / t_p)^{C_\alpha / CR}.$$

Figure 2.3 also shows a time delay between the removal of the surcharge,  $t_r$ , and the initiation of the reduced rate of secondary compression,  $t_s$ . Initially, there is a brief heave event, followed by the initiation of secondary compression at a reduced rate represented by  $C_\alpha'$ . The length of this time delay is a function of AAOS (Ladd, 1989, and Ng, 1998). The time delay is longer for higher AOS values, as discussed in the next section using data from the I-15 Reconstruction Project (Ng, 1998). This delay is also beneficial in reducing the amount of secondary compression occurring in the post-construction period. For evaluation purposes, the value of  $t_s$  represents the point in time when the soil has reached its maximum heave value (Figure 2.3).

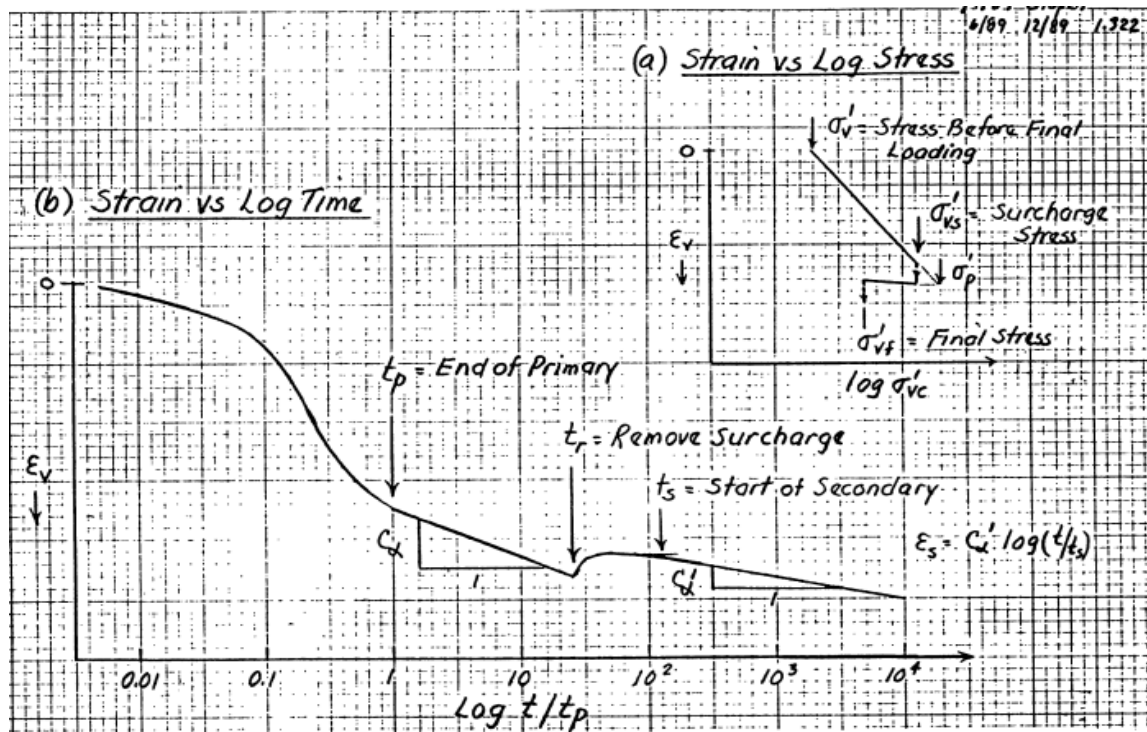


**Figure 2.3** The effects of surcharging (i.e., preloading) on the rate of secondary compression (after Ladd, unpublished notes).

## 2.6 Application of Ladd's Method to the I-15 Reconstruction Project

The I-15 project was a fast-paced Reconstruction Project that began during the spring of 1998 and ended in the fall of 2001, just prior to the 2002 Winter Olympic Games in Salt Lake City, Utah. At that time, it was the largest public highway construction project to be accomplished using a design-build project delivery system. During this 3.5-year period, the design-build consortium demolished and rebuilt 26 km (16.2 miles) of urban interstate, widening the roadway from six to up to 12 lanes at a total cost of about \$1.4 billion. A large part of this cost was spent erecting 144 overpass bridge structures, constructing 160 mechanically stabilized earth (MSE) retaining walls and placing 3.8 million m<sup>3</sup> (134 million ft<sup>3</sup>) of new embankment. The design-build contract featured a 50-year design life and an optional 10-year corrective maintenance agreement (Farnsworth et al., 2008).

The strict project completion date presented unique challenges to the design-build team. Perhaps the most demanding was developing strategies to address the impacts of consolidation settlement in the northern segment of the project near the downtown area. Here, compressible, fine-grained lacustrine sediments deposited by Pleistocene-age Lake Bonneville underlie about 5 m (16.4 ft) of Holocene alluvium (Figure 2.4). The lacustrine sediments are approximately 15-m (49.2 ft) thick, consisting of inter-bedded silty clay and clayey silt (CL, ML), plastic clays and silts (CH, MH), and fine clayey and silty sands (SC, SM), and are lightly overconsolidated ( $OCR \approx 1.5$ ). Interbedded, subaqueous silts, fine sands and low plasticity clays are found in the middle of the Lake Bonneville sediments and separate the upper and lower Lake Bonneville clays. These upper and lower clay units are compressible (CR values ranging from 0.1 to 0.35), have relatively low undrained shear strength (25 to 50 kPa) and require substantial time to complete primary consolidation. In this regard, settlement records from the mid-1960s construction of I-15 show that a typical 8- to 10-m high embankment underwent 1 to 1.5 m of primary consolidation settlement over a period of two to three years. For example, Figure 2.5 shows a settlement record from the

mid-1960s construction, for an embankment constructed over the typical soil conditions represented in Figure 2.4. The record shown in Figure 2-5 is typical of those recorded during the mid-1960s construction for this type of soil condition. This figure shows that fill placement was performed in multiple stages to reach the peak loading condition and then the primary settlement was allowed to take place prior to removal of the surcharge. These large magnitudes of settlement (1.4 m or 4.5 ft) and long consolidation settlement durations (approximately two years) can be attributed directly to the soft, thick, compressible Lake Bonneville clay layers. In the mid-1960s, the bridge foundations, bridge, approaches, and pavement were not placed until such settlement was essentially finished (Farnsworth et al., 2008). The I-15 Reconstruction Project team established a long-term performance goal to limit the amount of post-construction settlement (i.e., secondary compression settlement) of the foundation soils to 3 inches, or less, in a 10-year post construction period. The design surcharge height and surcharge duration were calculated to meet this performance goal (Saye and Ladd, 2000).

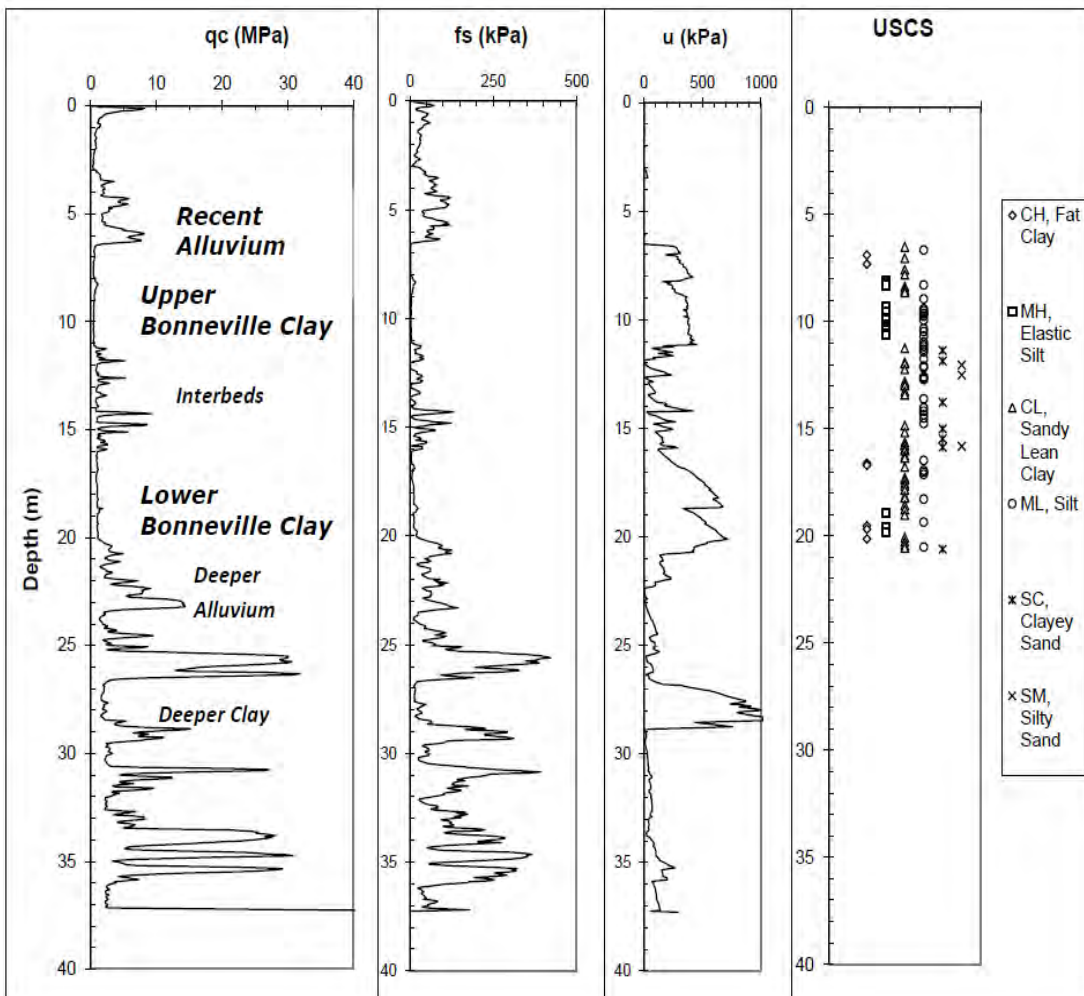


**Figure 2.4** Typical cone penetrometer (CPT) log and soil descriptions for downtown segment of I-15 Reconstruction Project, Salt Lake City, Utah (Farnsworth et al., 2008).

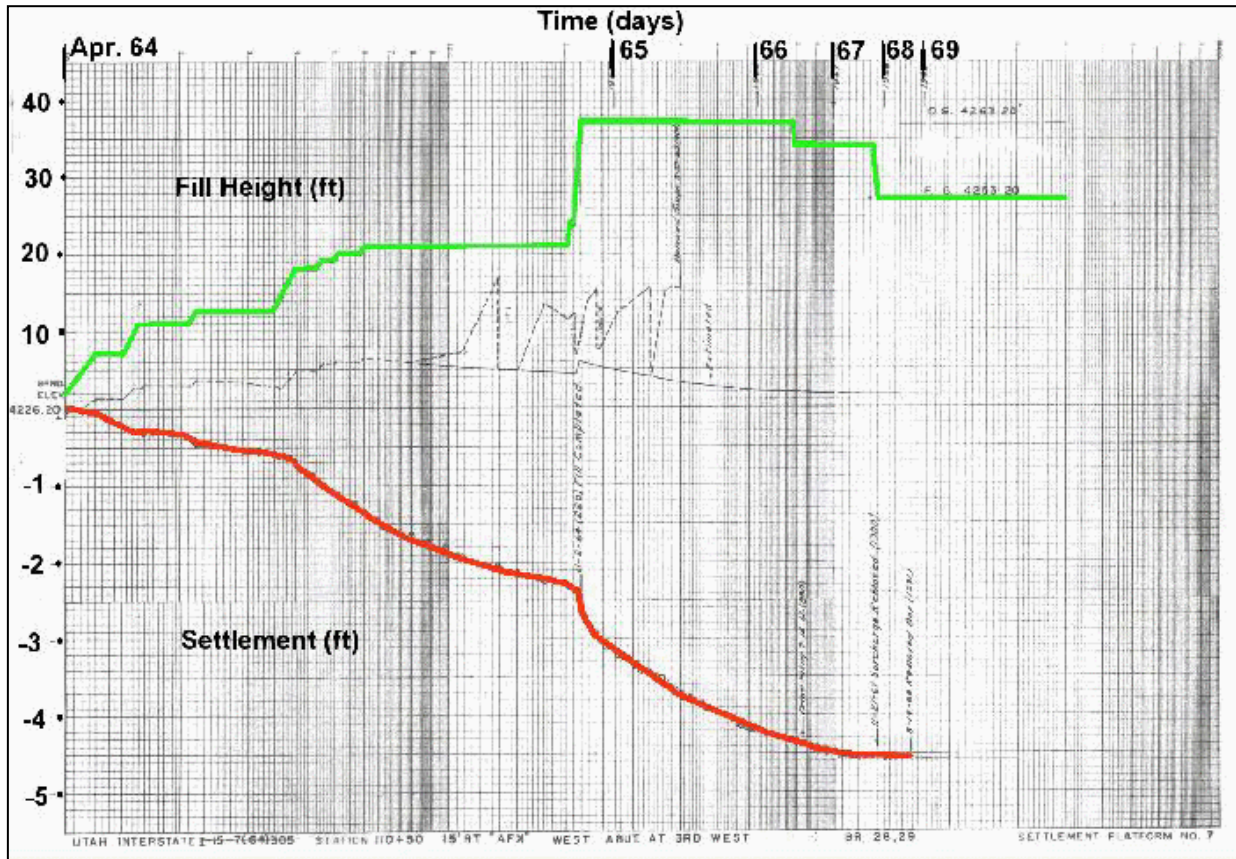


**Figure 2.5** Typical fill height versus settlement record for the 1960s, I-15 construction, Salt Lake Valley, x-axis is elapsed time since beginning of fill placement since April 1964, y-axis (green) is fill height (ft) and y-axis (red) is settlement measured at original ground surface (ft)

The I-15 Reconstruction Project utilized three geotechnologies to address the large and potentially damaging effects of primary and secondary consolidation originating from compression of the soft foundation soils prevalent beneath much of the northern part of the project. The first and most widely utilized approach was to apply surcharging in conjunction with the construction of two-stage mechanically stabilized earth (MSE) walls and/or sloped, reinforced earthen embankments. For these types of construction, prefabricated vertical drains (PVDs) were installed in the foundation soils prior to wall or embankment construction. Once the surcharged embankments had reached their design height, primary consolidation settlement of the foundation soil was allowed to take place, followed by surcharge removal. The second approach was to essentially eliminate most of the potential foundation settlement by using lightweight fill (e.g., scoria and EPS geofoam), thus greatly minimizing the loading condition imposed on the foundation soils.

The third approach involved strengthening the foundation soils by installing lime cement columns prior to placing an MSE wall, thus reducing the magnitude of settlement within the stiffened foundation soils (Farnsworth et al., 2008). Ladd's (1989) method was used to develop the surcharge design for the MSE walls and earthen embankment construction. For this, it was important to determine the thickness of the compressible layer(s) and to estimate the reduced rate of secondary compression for the underlying sediments as a function of the amount of surcharge and the surcharge duration. The former was determined from field investigations (i.e., soil boring and CPT soundings) at various locations along the project, and the latter soil properties were evaluated from a laboratory test program using "undisturbed"



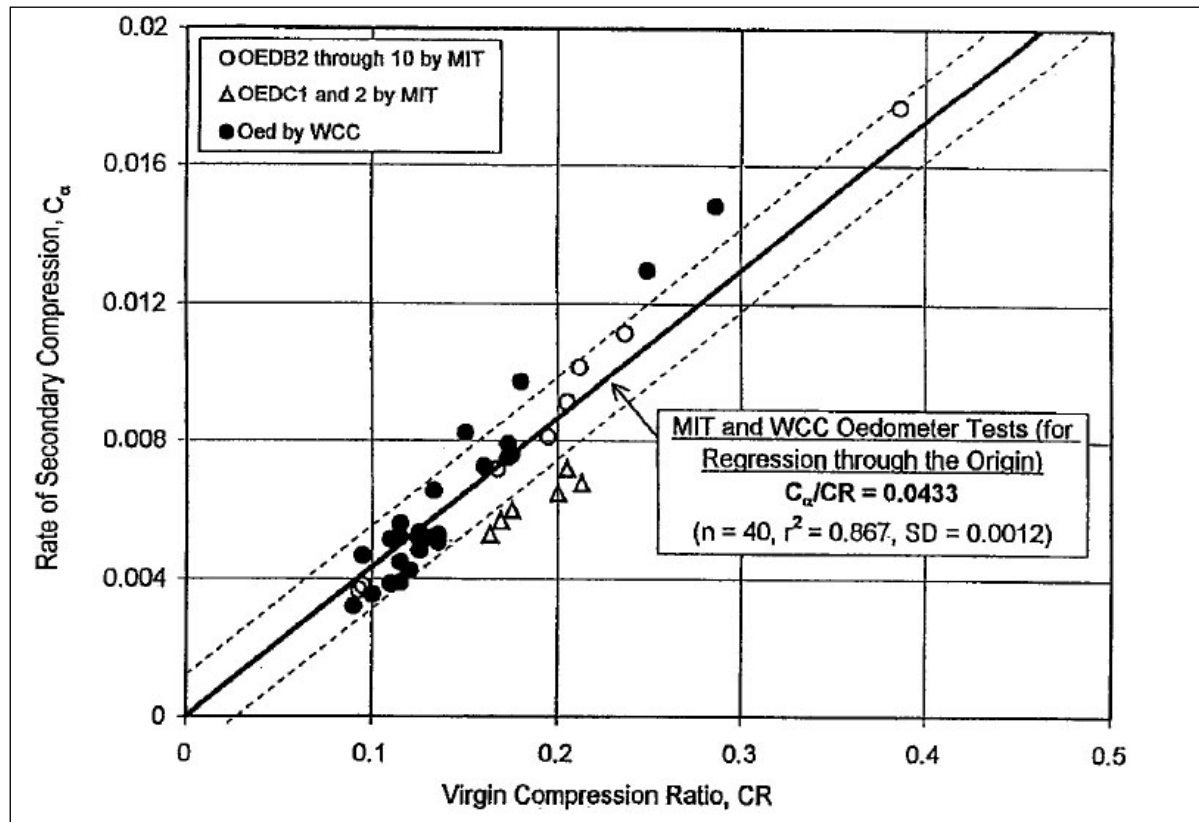


**Figure 2.6** Relationship between rate of secondary compression and compression ratio for Lake Bonneville clays (Ng, 1998). Ng (1998) data are labeled MIT and Woodward-Clyde Consultants are labeled WCC (Saye and Ladd, 2000)

samples obtained from the field investigation program (Ng, 1998). The laboratory testing was done in a relatively rigorous manner for the project because C. C. Ladd was retained by Woodward-Clyde Consultants as a senior consultant and reviewer for the project. The consolidation and shear strength testing to support the design were done at Massachusetts Institute of Technology (MIT) soil mechanics laboratory under the supervision of C. C. Ladd and the results were reported in Ng (1998). While Ng's (1998) evaluations were being performed and finalized, the project team used interim values of  $C_\alpha/CR$  equal to 0.0425 from preliminary laboratory testing for the Lake Bonneville deposits performed by Woodward-Clyde Consultants (Saye and Ladd, 2000). Estimates of CR values were back-calculated using soil models developed in MS Excel spreadsheets for the Lake Bonneville deposits. To calibrate the CR values used in these models, foundation settlement versus time data were used as obtained by the Utah Department of Transportation (UDOT) from the original I-15 embankment construction records from the northern part of Salt Lake Valley. To constrain the layer thickness used in these models, soil layering was developed from borehole logs at the corresponding locales as obtained from baseline geotechnical investigations performed just prior to the I-15 Reconstruction Project by various geotechnical consulting firms. As the MIT report (Ng, 1998) became available, the average  $C_\alpha/CR$  of 0.0433 was adopted based on laboratory testing by Woodward-Clyde Consultants (WCC) and MIT for the Lake Bonneville deposits as shown in Figure 2.6.

In addition to this design chart, the effects of AAOS on  $C_\alpha'$  and the time of initiation of secondary compression,  $t_s$ , were needed to complete the design. For the AAOS versus  $C_\alpha'/C_\alpha$  relation (Figure 2.7 top), the maximum reduction line (i.e., bottom solid line surrounded by black dots) was used. This was

selected because it was based on site-specific samples obtained from the I-15 project as tested by Ng (1998). Figure 2.7 (bottom) quantifies this as the time delay between surcharge removal,  $t_r$ , and start of secondary compression,  $t_s$ , as a function of AAOS based on testing done by Ladd (1989) and Ng (1998). This figure shows that the start of secondary compression has greater delay for higher amounts of surcharge. Such delay is beneficial in reducing the amount of secondary compression over a given post-construction period. In regards to  $t_s/t_r$  versus AAOS, the average line was selected for design purposes for the I-15 Reconstruction Project (Saye and Ladd, 2000).

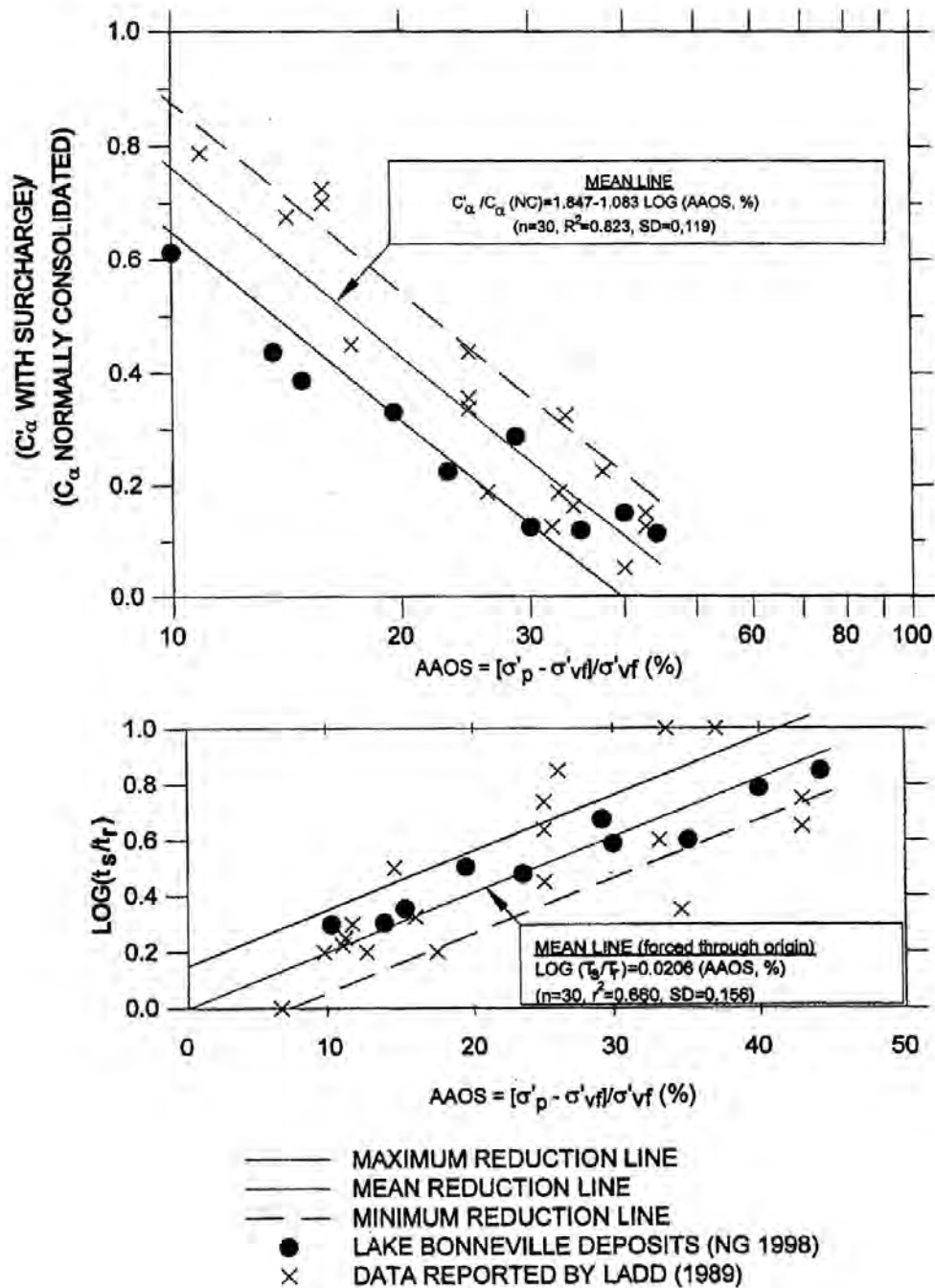


**Figure 2.7** (Top)  $C'_\alpha / C_\alpha$  as a function of AAOS (Bottom)  $\text{Log}(t_s/t_r)$  ratios as a function of AAOS (Saye and Ladd, 2000)



### **3. RESEARCH OBJECTIVES AND TASKS**

#### **3.1 Research Objectives**

The primary objectives addressed in this research are as follows: 1) corroborate Mesri's concept of secondary compression (i.e.,  $C_\alpha/CR$  is relatively constant) for the Lake Bonneville deposits along the Wasatch Front in Utah; 2) supplement and/or revise, as necessary, the design relationships developed by Ng (1998) for the I-15 surcharge design using a larger set of field and laboratory test data; (3) recommend an appropriate laboratory testing and evaluation program to support project-specific surcharge design for future highway embankment projects sponsored by the Utah Department of Transportation (UDOT) in the Wasatch Front Area; and (4) develop additional design guidance and/or recommendations for developing and evaluating the surcharge design.

#### **3.2 Research Plan**

To accomplish these research objectives, a field investigation and collection of undisturbed samples of soils in the Wasatch Front area was performed. The specimens acquired during the field investigation were tested to develop design charts consistent with the design parameters required to implement Ladd's (1989) method. In addition, the data acquired from this research were evaluated and compared with existing data and relations developed by Ng (1998).

#### **3.3 Tasks**

The major tasks needed to achieve the above research objective are:

- 1) Review of the existing literature regarding secondary compression and how a surcharging program can be implemented to reduce secondary settlement. This will include a description of Ladd's and Mesri's methodologies. This has been completed and is summarized in Chapter 2.
- 2) Obtain undisturbed samples from four locations located along the Wasatch Front, Utah, including: (1) 400 South Street in Salt Lake City, (2) Provo South Interchange, (3) Springville 400 South Overpass Structure, and (4) Layton Interchange. The undisturbed samples were obtained using mud rotary drilling and piston sampling at sites where long-term monitoring of settlement has been ongoing as part of instrument arrays sponsored by UDOT. Soil samples from the area near these arrays were used in the laboratory test program.
- 3) Develop and implement a laboratory test program to acquire secondary compression consolidation data and the design parameters associated with Ladd's (1989) method. The undisturbed samples and the associated laboratory tests were performed on fine-grained, cohesive soils to determine design parameters such as  $\sigma_p$ ,  $CR$ ,  $RR$ ,  $C_\alpha$ , and  $C_\alpha'$ .
- 4) Evaluate the design parameters obtained from the laboratory testing program and compare them with those published by Ng (1998). Specifically, the parameters compared will be the  $C_\alpha/CR$  ratio of Ng (1998) and the normalized  $C_\alpha'/C_\alpha$  and  $\log(t_s/t_r)$  versus AAOS.
- 5) Make recommendations regarding the implementation of a laboratory testing program and the steps and procedures required to implement a site-specific surcharge design for future UDOT embankment projects founded on soft soil sites.

## **4. FIELD INVESTIGATIONS**

### **4.1 Introduction**

A field investigation was performed for the purpose of collecting samples of fine-grained soils along the Wasatch Front at sites where long-term settlement data were available. These sites were selected because long-term instrumentation and settlement monitoring had been performed at these sites over the past 10 years. These undisturbed soil samples were tested in the U of U Civil and Environmental Engineering Soil Mechanics laboratory to determine soil properties and design parameters required for engineering evaluations such as  $\sigma_p$ , CR, RR,  $C_\alpha$ , and  $C_\alpha'$ .

### **4.2 Field Investigations**

The four drilling sites were: (1) 400 South at 400 South and 800 West just east of I-15 in Salt Lake City, Utah (Figure 4.1), (2) South Layton at Layton Parkway and Main Street in South Layton, Utah, in an empty lot northeast of the Layton Parkway and Main Street intersection west of I-15 (Figure 4.2), (3) Springville at 400 South and about 1700 West in Springville, Utah, at a site located west of the railroad tracks and on the south side of the railroad tracks overpass (Figure 4.3), and (4) Provo at the University Avenue I-15 southbound on-ramp in Provo, Utah, at a point where the southbound on-ramp for University Avenue and the on- and off-ramp for southbound traffic for 1860 South meet (Figure 4.4). The location, drilling depths, and dates are found in Table 4.1.

**Table 4.1** Boring locations, depths, and drilling dates

Site	Latitude	Longitude	BH Depth (ft.)	Drilling Date
400 South	40°45'40.02"N	111°54'45.61"W	92	12/5/2012
S. Layton	41° 3'23.25"N	111°57'47.63"W	142	2/5/2013
Springville	40° 9'39.78"N	111°38'18.43"W	129	4/1/2013
Provo	40°12'26.41"N	111°39'39.43"W	127	4/5/2013

The drilling was performed with the use of a truck-mounted CME 75 drill rig using mud rotary drilling in a 4-inch casing. The primary purpose of the drilling was to obtain piston samples from the cohesive, fine-grained soils of Lake Bonneville and recent lacustrine deposits. The piston sampling used standard galvanized-steel Shelby tubes with a 2.8-inch inner diameter and a 3.0-inch outer diameter, with an overall length of 30 inches.

The depths selected for soil sampling were determined using CPT logs that were performed by others at or near the locations of the boreholes. The locations of the CPT soundings are shown in Table 4.2. For the CPT logs, see Figures 4.5 to 4.9.

**Table 4.2** CPT Locations

Site	CPT	Latitude	Longitude
400 South, Salt Lake	06-SC-159	40° 45' 39.06"N	111° 54' 49.02"W
S. Layton	CPT-01	41° 3' 16.42"N	111° 57' 47.63"W
Springville	CPT-01	40° 9' 39.89"N	111° 38' 20.03"W
Springville	CPT-07	40° 9' 39.90"N	111° 38' 17.75"W
Provo	CPT-07	40°12' 25.08"N	111° 39' 39.30"W

The samples were immediately logged and labeled by location and depth. The logs for the boreholes are given in Figures 4.10 to 4.14. Samples were sealed with plastic Shelby caps and wrapped with duct tape to maintain their in situ moisture content. They were carefully transported and stored in a humidified room in the University of Utah Concrete Laboratory until the consolidation testing could be performed.





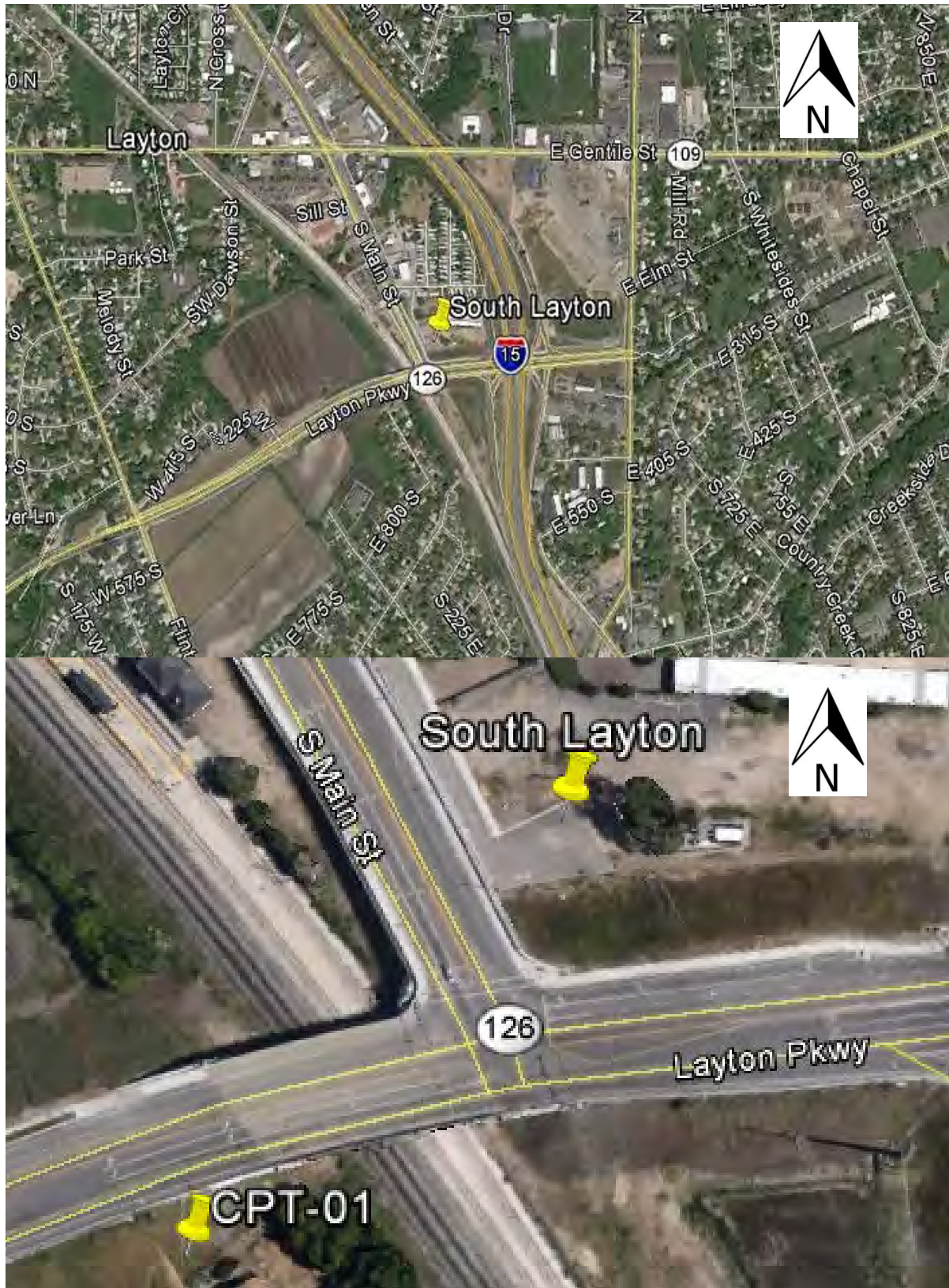


**Figure 4.2** South Layton site (Layton Parkway and Main Street). (Top) Vicinity map for drilling site (Bottom) Close-up of drilling site





**Figure 4.3** Springville site (400 South and 1700 West). (Top) Vicinity map for drilling site (Bottom) Close-up of drilling site





**Figure 4.4** Provo site (Southbound I-15 on ramp for University Avenue). (Top) Vicinity map for drilling site (Bottom) Close-up of drilling site and CPT location

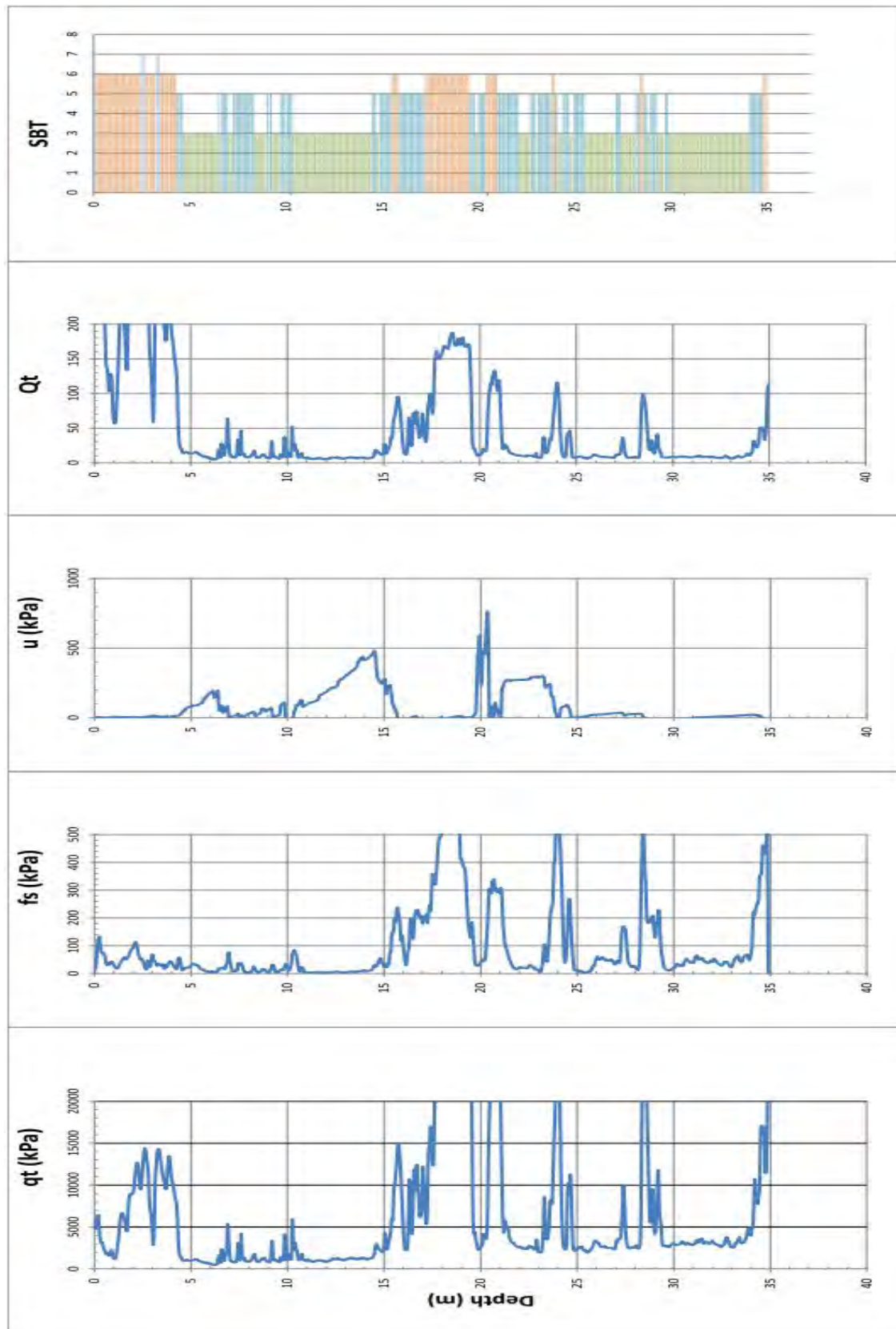


**Figure 4.5** CPT for 400 South and I-15, Salt Lake City, 06-SC-159



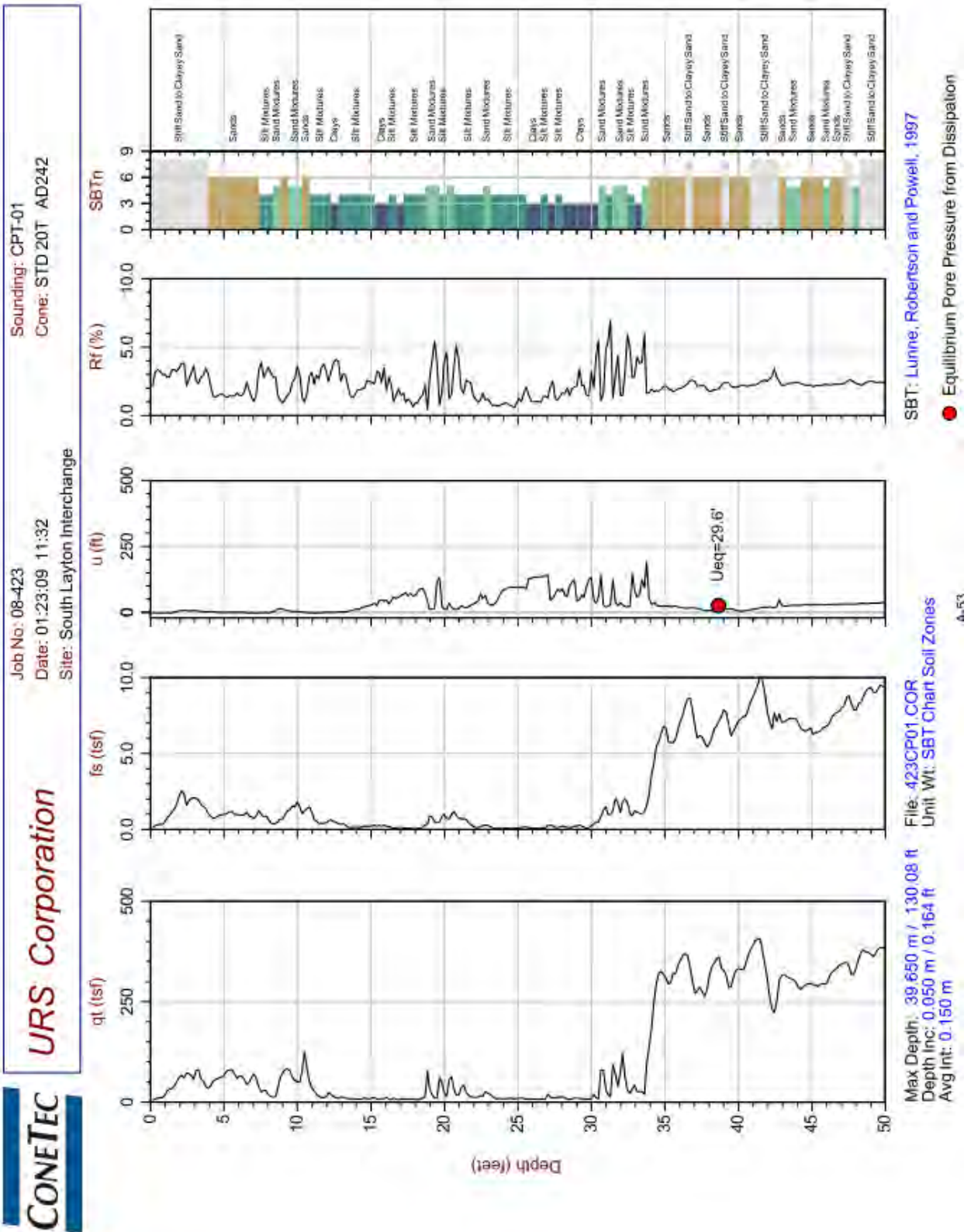
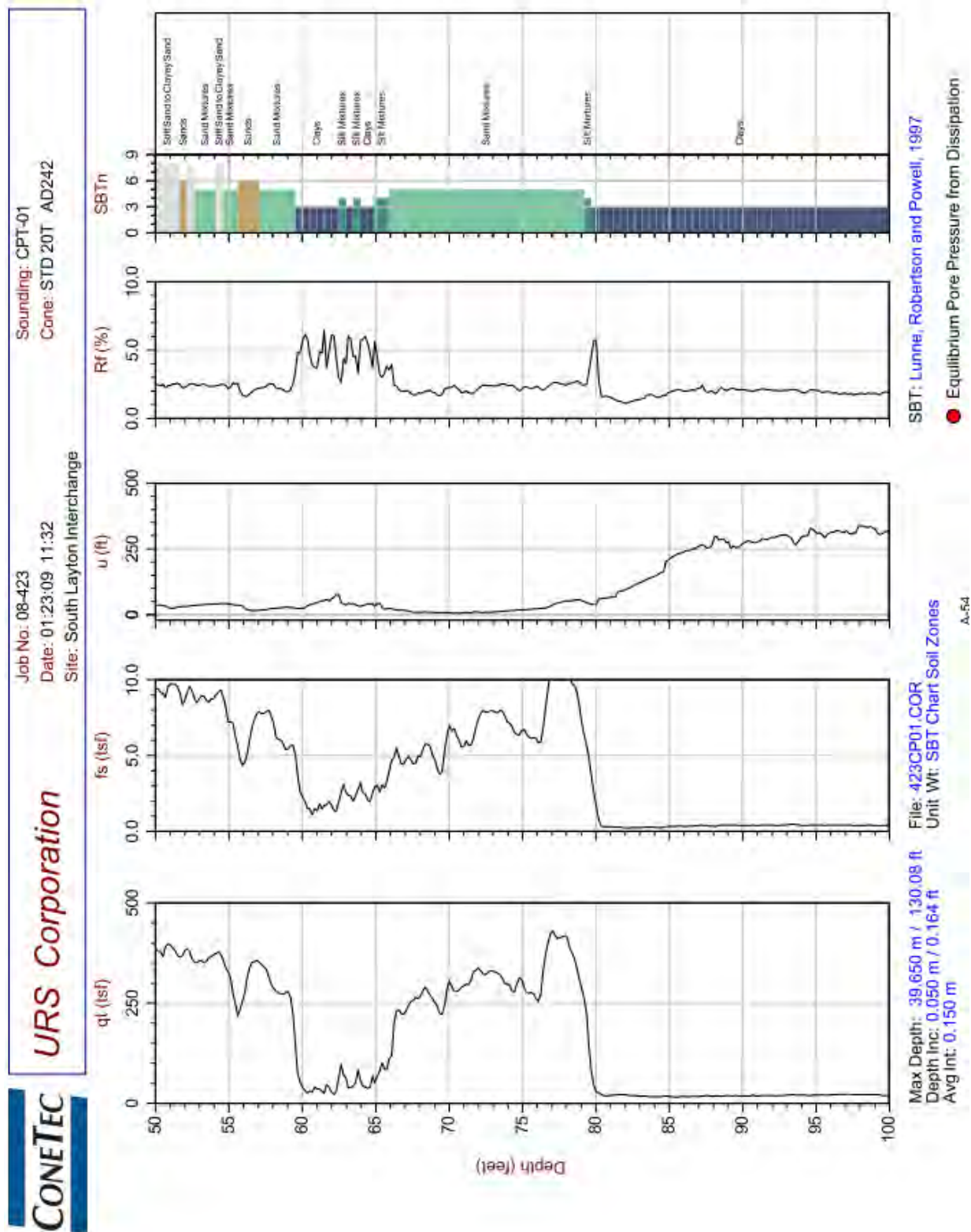


Figure 4.6a CPT for South Layton CPT-01



**Figure 4.6b** CPT for South Layton CPT-01

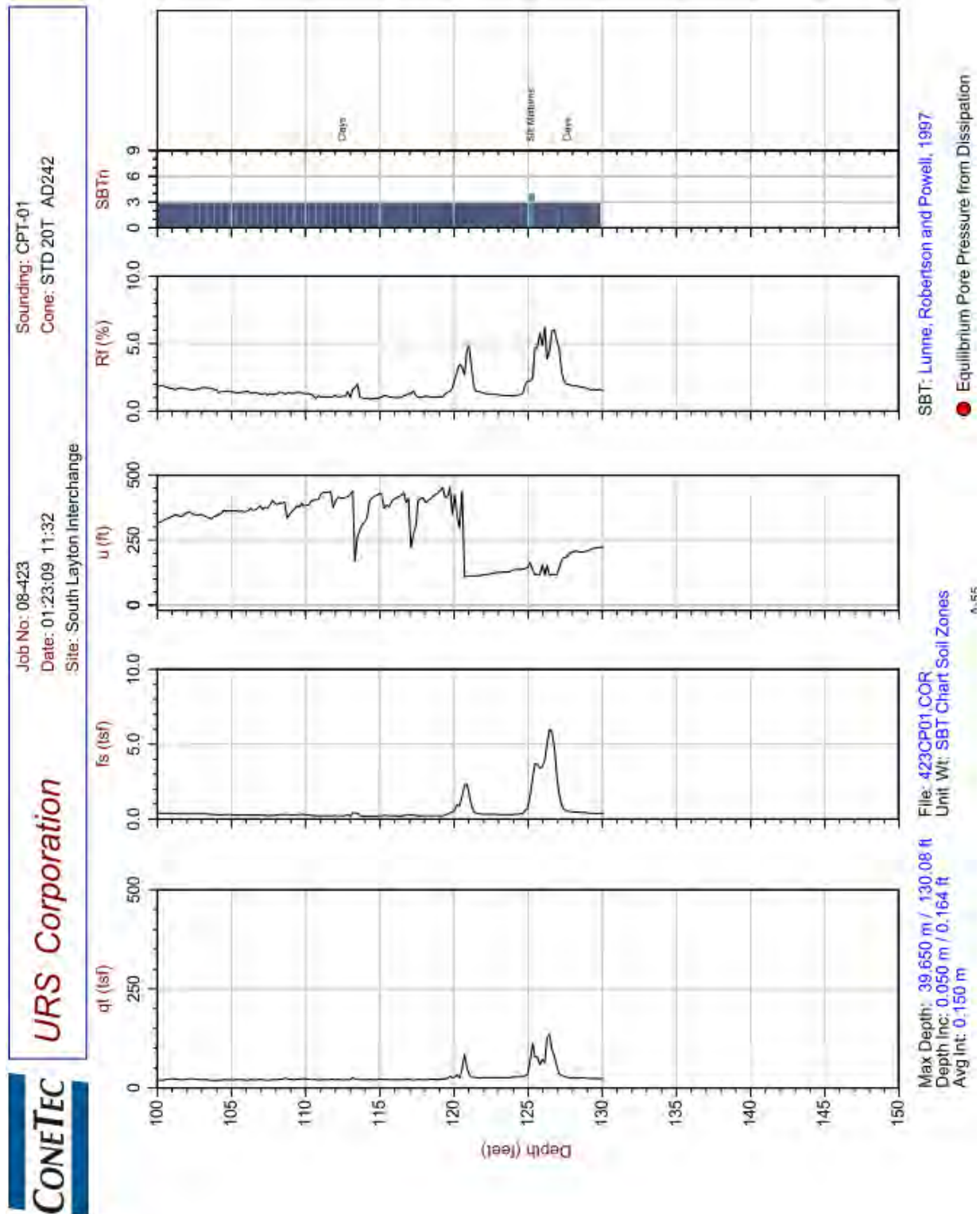


Figure 4.6c CPT for South Layton CPT-01



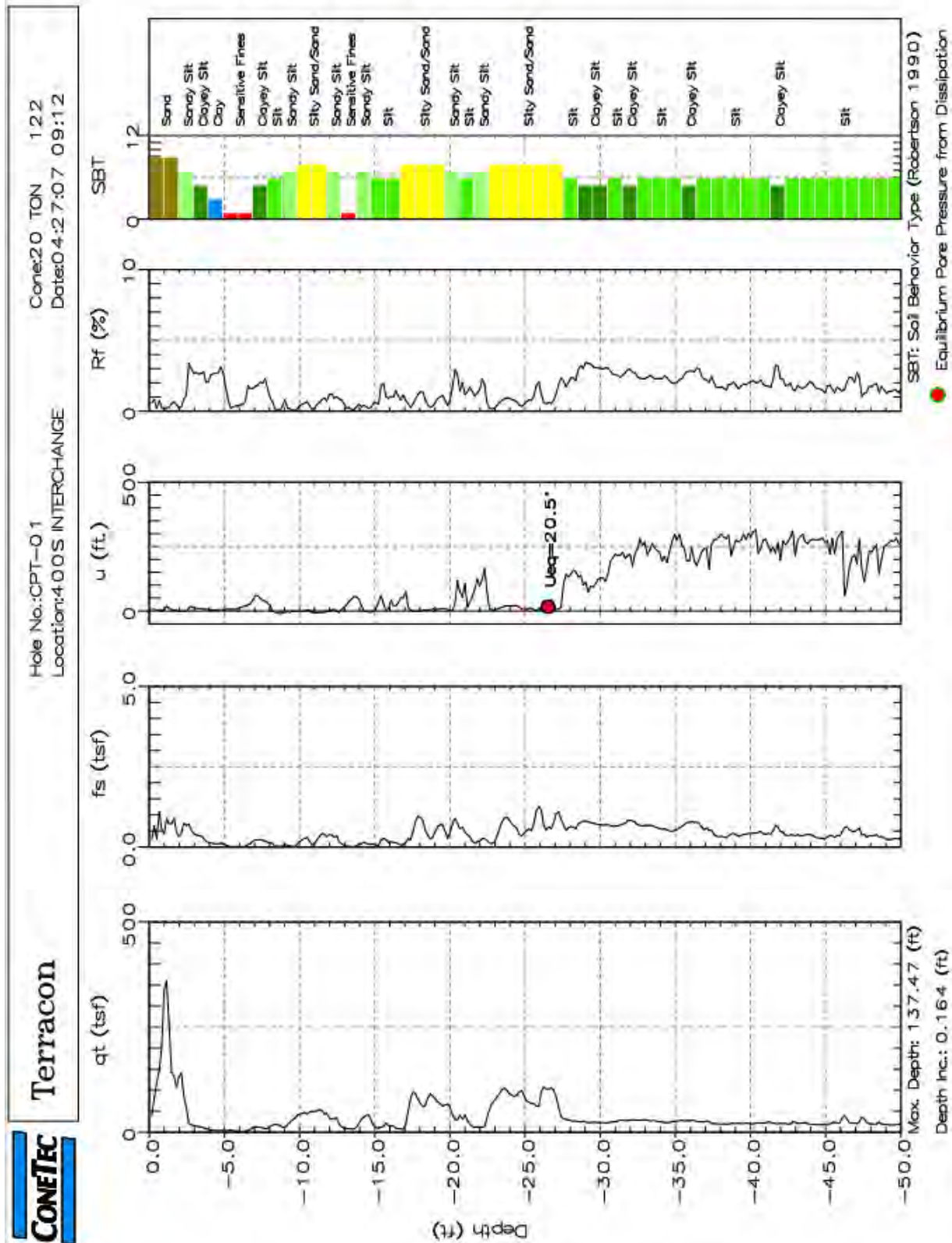


Figure 4.7a CPT for Springville, CPT-01

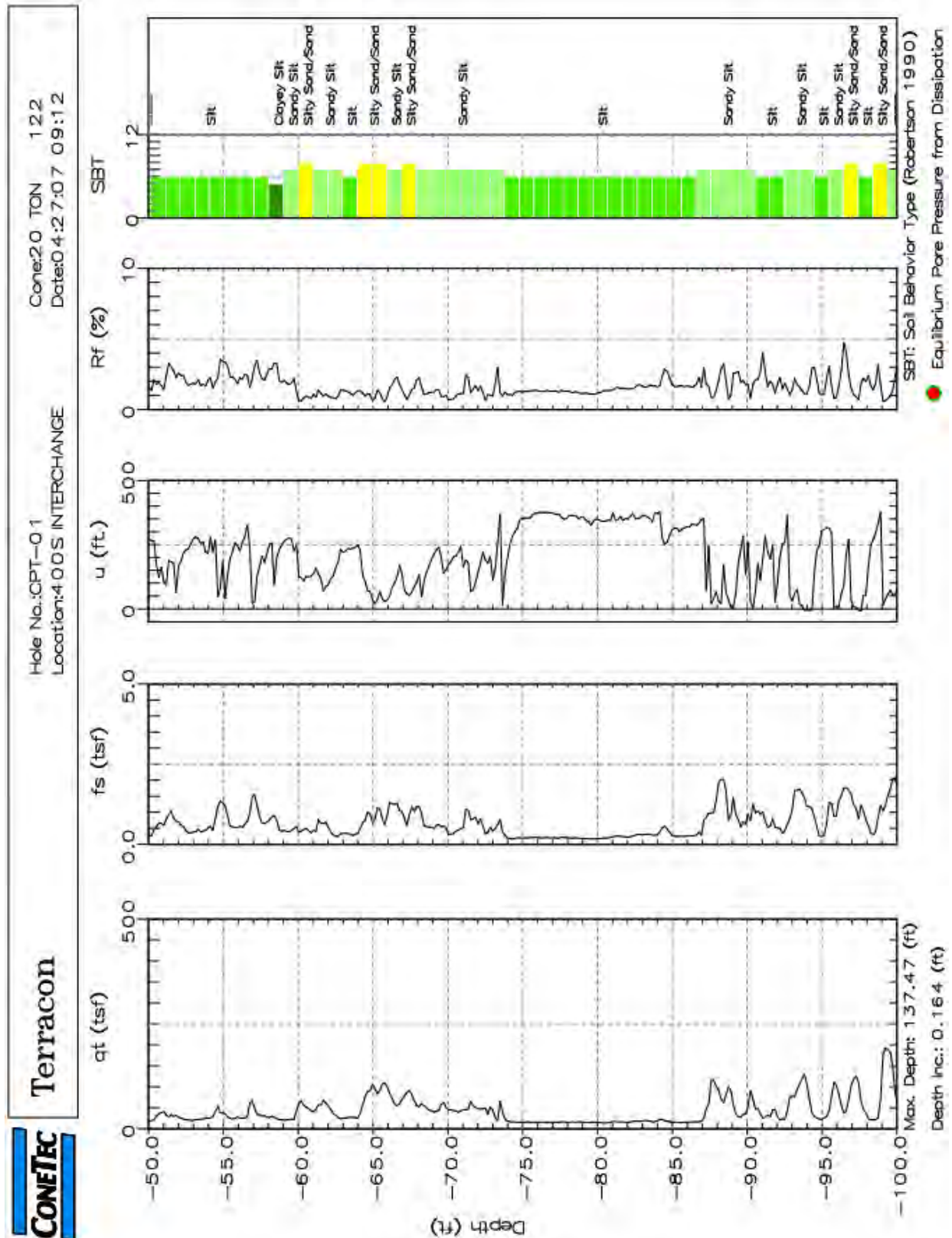


Figure 4.7b CPT for Springville, CPT-01

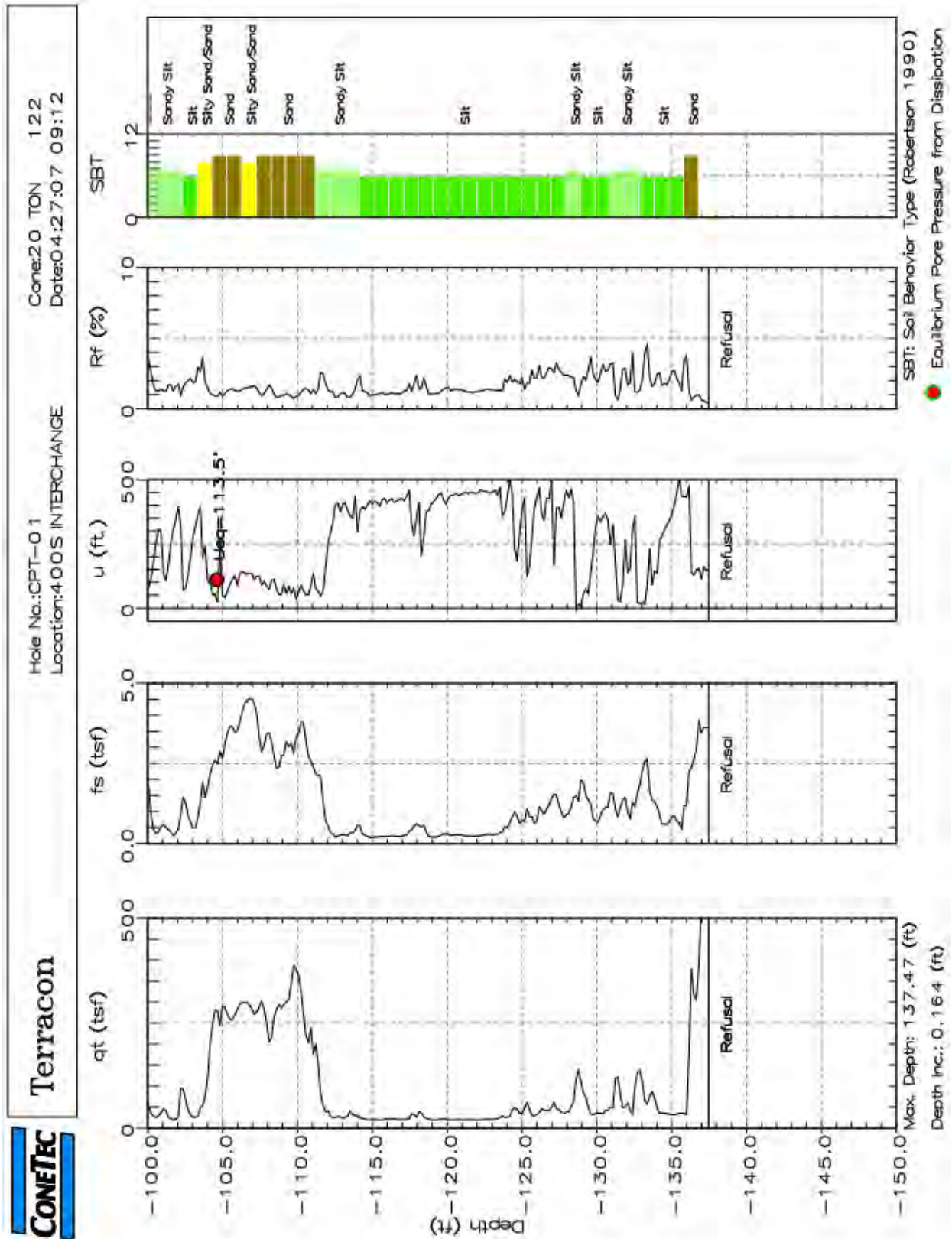
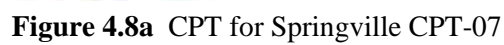


Figure 4.7c CPT for Springville, CPT-01





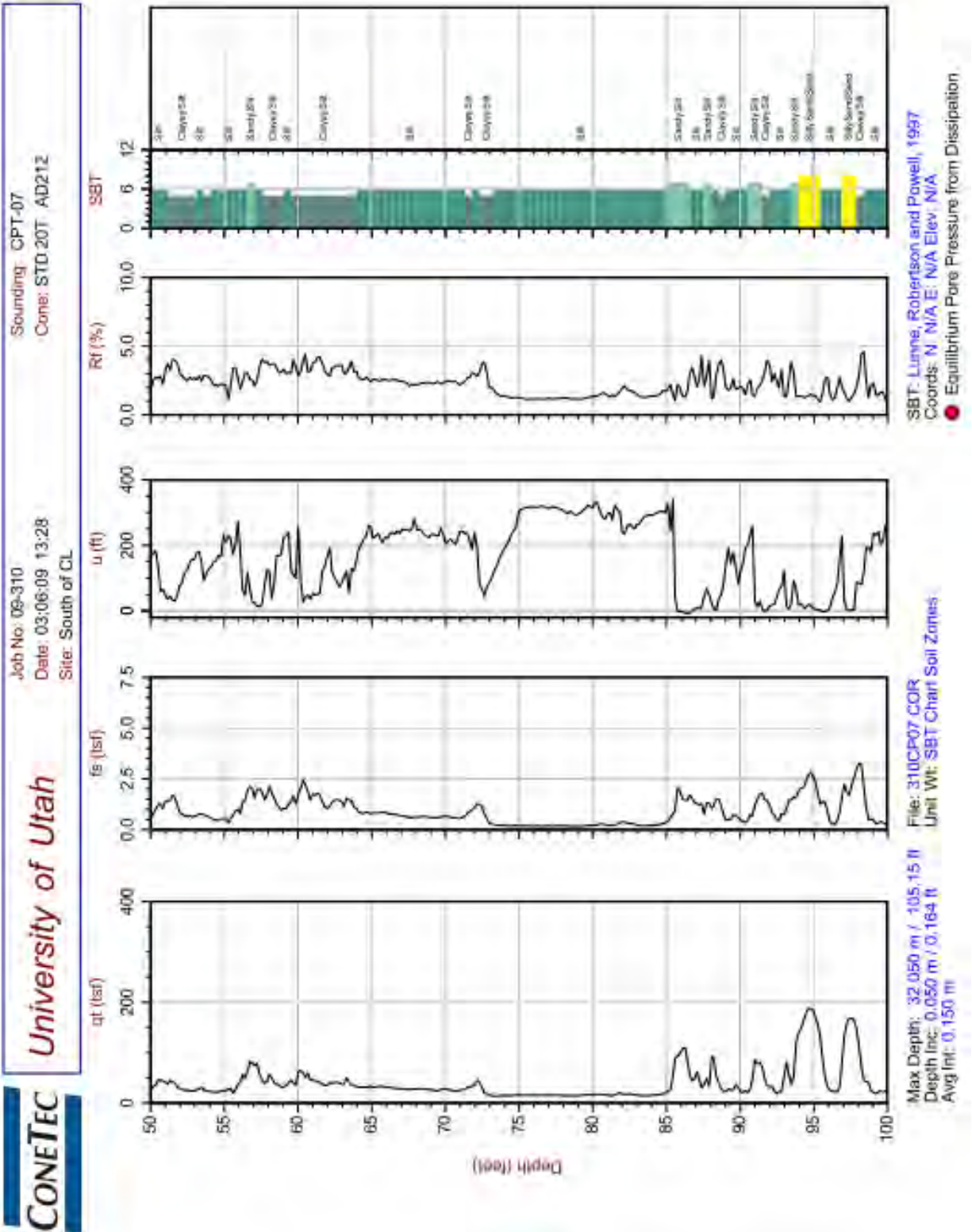
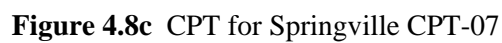


Figure 4.8b CPT for Springville CPT-07





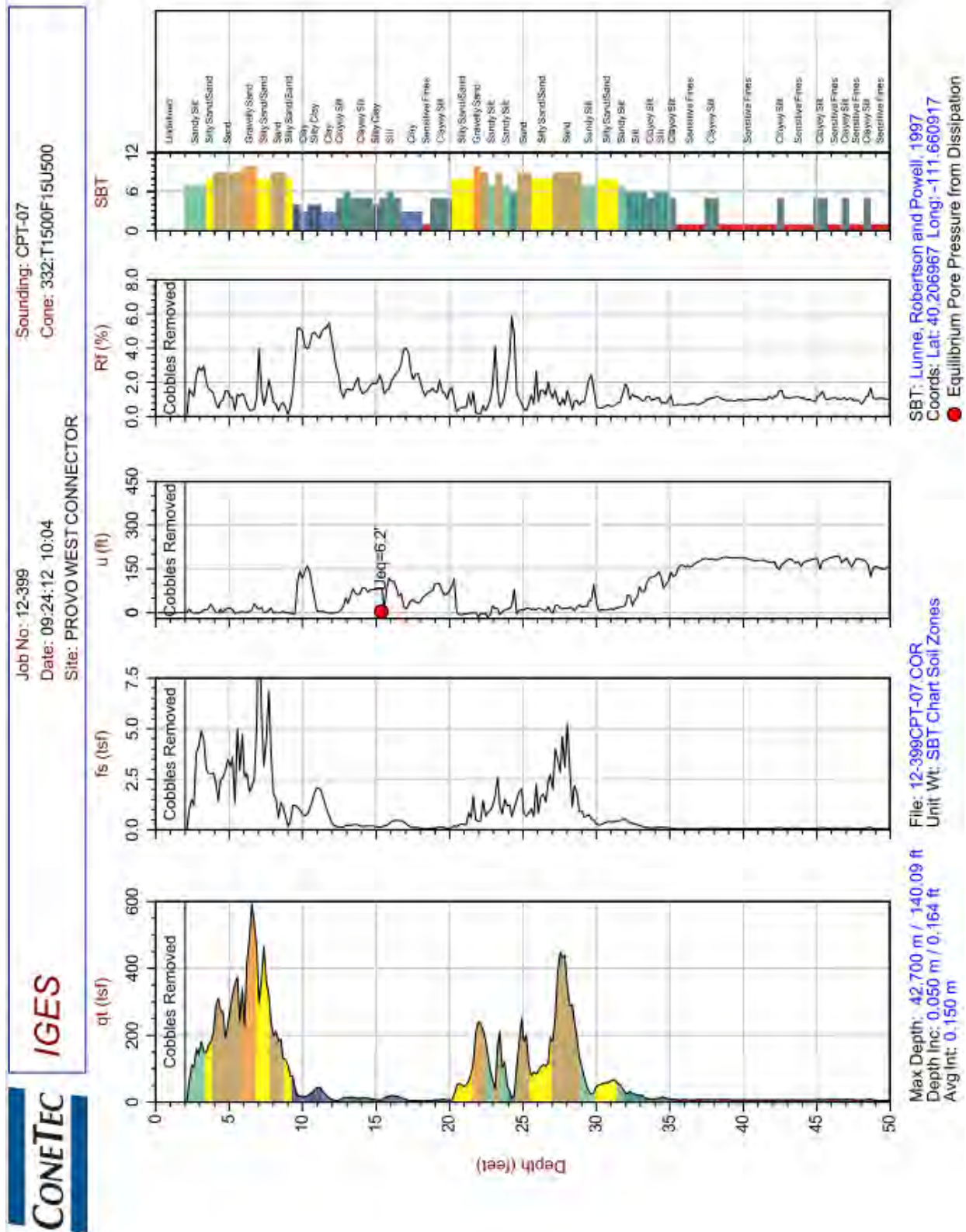
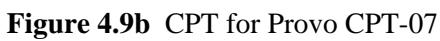
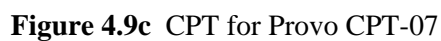





Figure 4.9a CPT for Provo CPT-07










400 South						
By Zach Gibbs		Test Hole I				
Elevation (ft)	Sample Depth (ft)	Visual Soil Description	Sample Recovery (in)	Soil Symbols	Penetration N (blows/ft)	Remarks and raw SPT data
4196						- No samples taken
4185	10-12	SAND, medium grained, gray to green gray (SP)	24		20	- 5 9 9 11
	12.5-14.5	CLAY, silty, gray (CL)	24		0	- 0 weight of hammer
	15-17	SILT, soft, gray (MH)	24		ST	
	17.5-19.5	SILT, soft, gray (MH)	24		ST	
4175	20-22	SILT, soft, gray (MH)	24		ST	- sluff sand had to clean out the hole
	22.5-24.5	CLAY, silty, gray (CL)	24		ST	
	25-27	CLAY, silty, gray (CL)	24		ST	- Inter beds
	27.5-29.5	CLAY, silty, gray (CL)	24		ST	
4165	30-32	CLAY, silty, gray (CL)	24		ST	
	32.5-34.5	SILT, soft, gray (ML)	24		ST	
	35-37	No recovery	0		ST	- probably sands
	37.5-39.5	CLAY, silty, gray (CH)	24		ST	
4155	40-42	CLAY, silty, gray (CH)	24		ST	
	42.5-44.5	CLAY, silty, gray (CL)	24		ST	
	45-47	CLAY, silty, gray (CL)	24		ST	
	47.5-49.5	CLAY, silty, gray (CL)	24		ST	
4145	50-52	CLAY, silty, with sand, gray (CL)	24		ST	
	52.5-54.5	CLAY, silty, with sand, gray (CL)	24		ST	
	55-57	No recovery	0		14	- put a spt after no recovery 5 4 5 9
4135	60-62	CLAY, silty, with sand, gray (CL)	24		ST	
	65-67	CLAY, silty, gray (CL)	24		ST	
4125	70-72	SAND, silty (SM)	24		ST	
4115	80-82	SAND, clayey, fine grained (SC)	24		ST	
4105	90-92	CLAY, gray (CL)	24		ST	
Soil Symbols		Other Symbols		Driller : Bedke		
Sand: 				Boring Number : 400 South		
Silt: 				Date Drilled : 12/5/2012		
Clay: 				Job Number : 1		
				Site Location : Salt Lake City, Ut.		
				400 South		
Notes :				Test Method : ASTM D 1586		
				Hammer Type : Automatic Trip Hammer		
				140 lb		
				Sampler : Shelby tube		
				24 in. Sampler		
				Drilling Method : Mud Rodery		
				4" casing		
				Make of Drilling Rig : CME 75		
				(Truck Mounted)		

**Figure 4.10** Test Hole Log for 400 South and I-15, Salt Lake City



South Layton						
By Zach Gibbs		Test Hole II				
Elevation (ft)	Sample Depth (ft)	Visual Soil Description	Sample Recovery (in)	Soil Symbols	Penetration N (blows/ft)	Remarks and raw SPT data
4341						
4337.5	2.5-4.5	SAND, silty (SM)	24		ST	
4335	5-7	SAND, silty (SM)	24		ST	
4332.5	7.5-9.5	SAND, silty (SM)	24		ST	
4330	10-12	SAND, silty (SM)	24		ST	
4327.5	12.5-14.5	CLAY (CL)	24		ST	
4325	15-17	CLAY (CL)	24		ST	
4322.5	17.5-19.5	CLAY (CL)	24		ST	
4320	20-22	CLAY, sandy (CL)	24		ST	
4290	50-52	SAND, clayey (SC)	24		ST	
4285	55-57	SAND, clayey (SC)	24		ST	
4260	80-82	CLAY (CL)	24		ST	
4255	85-87	CLAY (CL)	24		ST	
4250	90-92	CLAY (CL)	24		ST	
4245	95-97	CLAY (CL)	24		ST	
4240	100-102	CLAY (CL)	24		ST	
4235	105-107	CLAY (CL)	24		ST	
4230	110-112	CLAY (CL)	24		ST	
4225	115-117	CLAY (CL)	24		ST	
4220	120-122	CLAY (CL)	24		ST	
4215	125-127	CLAY (CL)	24		ST	
4210	130-132	CLAY (CL)	24		ST	
4205	135-137	CLAY (CL)	24		ST	
4200	140-142	CLAY (CL)	24		ST	
<b>Soil Symbols</b>		<b>Other Symbols</b>		<b>Driller :</b> Bedke		
Sand: 				<b>Boring Number :</b> South Layton		
Silt: 				<b>Date Drilled :</b> 2/5/2013 - 2/6/2013		
Clay: 				<b>Job Number :</b> 2		
				<b>Site Location :</b> South Layton Ut.		
				Layton Parkway and Main street		
<b>Notes :</b> BH II is located 5 ft. north of BH I				<b>Test Method :</b> ASTM D 1586		
				<b>Hammer Type :</b> Automatic Trip Hammer		
				140 lb		
				<b>Sampler :</b> Shelby tube		
				24 in. Sampler		
				<b>Drilling Method :</b> Mud Rodery		
				4" casing		
				<b>Make of Drilling Rig :</b> CME 75		
				(Truck Mounted)		

**Figure 4.12** Test Hole Log for South Layton Test Hole II







## **5. LABORATORY TESTING**

### **5.1 Test Procedures**

#### **5.1.1 Introduction**

One of the outcomes of this research is to produce a recommended laboratory testing program that can be routinely executed by geotechnical consulting firms to develop surcharge evaluations and design for support of highway transportation projects. Recent research by the University of Utah (Ozer et al., 2012; Bartlett and Ozer, 2005) and that of Ng (1998) has shown that the controlled rate of strain consolidation (CRS) test (D4186M-12e1) is generally preferable to standard incremental loading oedometer tests (ASTM D2435M-11) for producing high quality laboratory data for consolidation evaluations. CRS testing better defines the shape of the consolidation curve due to the higher density of data points produced by this test, especially as the specimen transitions from recompression to virgin compression behavior.

Notwithstanding, conventional incremental load oedometer tests were selected instead of CRS consolidation tests for this research. This was done in discussions with the UDOT technical advisory committee, and the reasons for this selection were: (1) incremental load tests are the standard of practice, (2) multiple secondary compression tests needed to be performed simultaneously for this research and there was not sufficient CRS devices at the university for such testing, (3) it is unclear if the CRS test offers any advantage over incremental load oedometer tests when secondary compression is the primary topic of the research.

Therefore, it is hoped that careful sample preparation and incremental load testing in conventional tabletop oedometers would produce data that are of sufficient quality to be incorporated in the research plan. In addition, it is hoped that if consulting engineers and technicians review and follow, as applicable, the procedures and recommendations developed herein, sufficient data quality and quantity can be obtained to support future surcharge design and evaluation strategies for UDOT projects.

The following sections describe the test procedures that were used to perform the laboratory testing that supports this research.

#### **5.1.2 Testing Equipment**

The equipment used for the laboratory test program were tabletop oedometers (Figure 5.1) located in the University of Utah Soil Mechanics Laboratory. These devices consisted of 1.0-inch high and 2.5-inch diameter stainless steel consolidation rings, a standard consolidation cell with base plate having an O-ring, two 2.5-inch diameter porous stones, a top reservoir, a top cap to provide evenly dispersed pressure on the sample, and three bolts to hold the cell together (Figure 5.2). Filter paper was used between the porous stones and the soil sample to prevent plugging of the stones. Suspended weights, which produced a reaction on the sample equivalent to 0.25, 0.5, 1.0, and 2.0 tsf, were used to load the specimens. These weights were used in various combinations to produce the loading increments discussed in Section 5.2. The dial gages used for the vertical settlement readings had a precision of 0.0001 inch.



**Figure 5.1** Tabletop oedometer

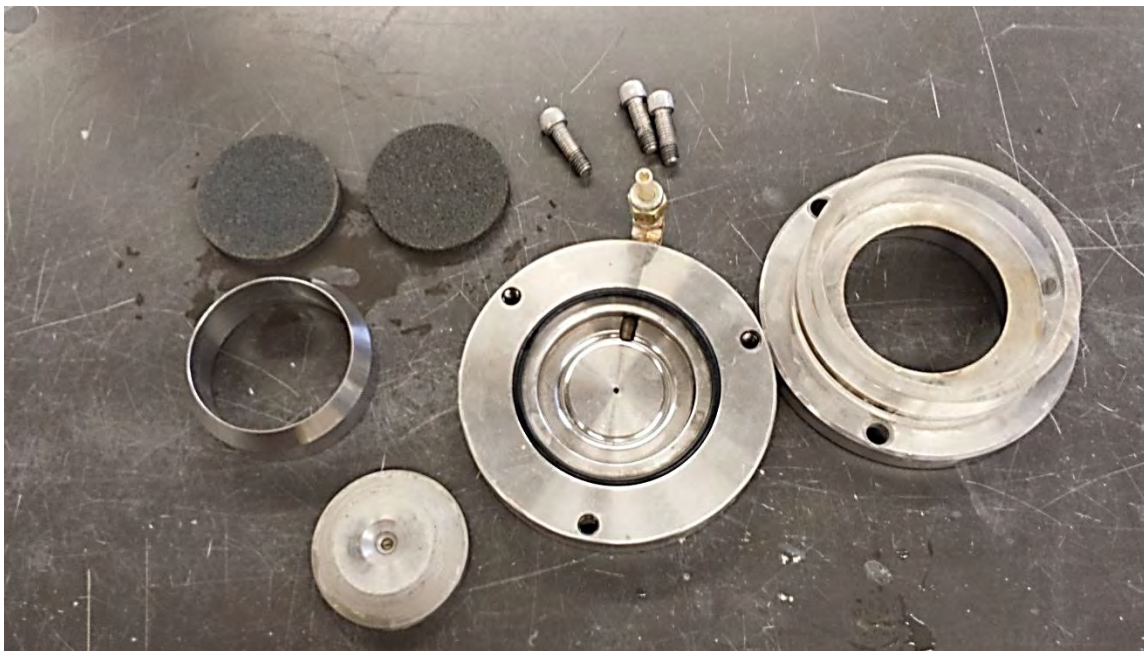


**Figure 5.2** Consolidation ring and cell

### 5.1.3 Sample Setup

All Shelby tubes collected from the sites remained sealed and were stored in a humidified room in the University of Utah Concrete Laboratory to preserve their initial water content. The Shelby tubes were cut with a commercial band saw (Figure 5.3). The sample was cut approximately 1 inch above and below the test specimen to provide sufficient soil for trimming and moisture content testing without producing a lot of waste.



**Figure 5.3** Horizontal band saw used to cut samples for testing

Ng (1998), Ladd (1999) and Bartlett and Ozer (2005) have found that radiography can serve as an aid to detecting variations in the soil fabric (e.g., heterogeneity, layer, anomalies, disturbance) if desired, but radiography was not performed on specimens used for this research. In addition, prior to extrusion of soft samples, it is recommended that a piano wire be inserted between the outer edge of the specimen and the cut Shelby tube and carefully be used to cut or break the perimeter adhesion bond between the tube and the specimen to reduce sample disturbance (Ladd et al., 1998).

The samples were carefully extruded from the tubes using the sample extruder shown in Figure 5.4. Immediately following extruding, they were trimmed to fit the consolidation ring using a turntable (Figure 5.5), a fine-gauge wire saw, and reference straight edge. Soil trimmings were immediately weighed to prevent change in mass due to drying and were subsequently placed in the drying oven for moisture content determinations. It is important to obtain accurate moisture content measurements of the specimens for determination of the initial void ratio, which is required in the consolidation calculation, and also as an index of compressibility.





**Figure 5.4** Extruding sample from Shelby tube

Regarding this latter point, Bartlett and Lee (2004) have shown that the compression index of the soil,  $C_c$ , can be reasonably estimated from the in situ moisture content of the soil, because moisture content is highly correlated with void ratio, which is in turn correlated with soil compressibility. Because of this, it is recommended that moisture content and other index properties be obtained for the specimens for further correlation with laboratory-determined consolidation properties.

The height, weight, and diameter of the consolidation ring were recorded using precision scales and a micrometer. The consolidation rings used had heights of 1 inch and diameters of 2.5 inches. To reduce the friction between the soil and the consolidometer rings, the inner circumference of the rings were lubricated with a low-friction, silicone-based lubricant.

The samples were then carefully placed into the consolidation ring and trimmed flush with the top and bottom of the ring (Figure 5.6). If there were any small voids present on the top or bottom of the specimens from the trimming process, these imperfections were carefully filled with trimmed soil.



**Figure 5.5** Sample in turntable

After the trimming and preparation were completed, the weights of the rings with the soil present were then recorded. Porous stones were boiled in deionized water and soaked in de-aired water prior to assembly. Standard 0.15-mm thick filter paper was used between the sample and the porous stones on both top and bottom of the specimens to prevent clogging of the stones and the loss of the solids during the tests.

The samples in the consolidation ring were then assembled in the cell with porous stones and filter paper, and the top caps were placed on the top reservoir and secured with bolts to prevent leakage (Figure 5.7). The cells were then placed in tabletop oedometers and deionized, and de-aired water was used to fill the reservoir to saturate the specimen (Figure 5.8). Testing was then performed using the interpretive methodologies described in the following section.



**Figure 5.6** Sample in consolidation ring



**Figure 5.7** Sample fully assembled in cell



**Figure 5.8** Fully assembled cell in table top oedometer

## 5.2 Laboratory Test Program

### 5.2.1 Introduction

The specimens selected for testing were determined by evaluating nearby CPT soundings and selecting the sampling depth having the most clay-like behavior. This was usually manifest on the adjacent CPT sounding as low tip resistance and relatively high excess pore water pressure relative to hydrostatic conditions. The CPT sounding used in the evaluations is found in Chapter 4. At the 400 South site, a CPT sounding from the I-15 Reconstruction Project was available (Figure 4.5). For the borehole completed at this location, the sampling depths started at 15 feet (i.e., below the alluvium) and sampling was done every 5 feet until a depth of 50 feet was reached. All of these samples from 400 South appeared to be very similar to each other and were cohesive sediments.

For each sampling interval, the specimens were used to determine the following consolidation properties: (1) preconsolidation stress ( $\sigma_p$ ), (2) rate of secondary compression for normally consolidated specimen,  $C_{\alpha}$ , (3) rates of secondary compression for overconsolidated specimens,  $C'_{\alpha}$ , for OCR values of 1.25, 1.5,



and 2.0. The preconsolidation stress was determined using 1-D incremental loading tests with time rate of consolidation measurements taken for each loading increment. The following describes the procedures used to determine these properties.

## 5.2.2 Determination of the Preconsolidation Stress

The preconsolidation stress of the specimens was evaluated using a 1-D incremental loading consolidation test with the sample preparation described in Section 5.1. The following loading schedule was implemented: 0.25, 0.5, 1.0, 2.0, 4.0, 8.0, and 16.0 tsf (500, 1,000, 2,000, 4,000, 8,000, 16,000, and 32,000 psf, respectively), and the unloading schedule was 16.0, 4.0, 1.0, and 0.25 tsf (32,000, 8,000, 2,000, and 500 psf, respectively). This is equivalent to applying a load increment ratio,  $\Delta P/P$ , of unity (1.0), which is most commonly used in practice. However, Jamiolkowski et al. (1985) recommend that the  $\Delta P/P$  ratio be reduced to about 0.5 to obtain better defined consolidation curves in the vicinity of the preconsolidation stress as used by Canadian practice for sensitive clays in eastern Canada.

In standard geotechnical practice, each load increment is usually maintained for one day (24 hours) to define the consolidation curve and estimate the preconsolidation stress. However, because the end of primary consolidation usually occurs less than one hour after the newly applied load, the virgin portion of consolidation curves based on 24-hour waiting periods is displaced downward by one or more cycles of secondary compression (Jamiolkowski et al., 1985). This is not desirable for two obvious reasons: (1) it makes interpretation of the preconsolidation stress more variable, especially for soft soils, (2) data needed for interpretation of the rate of secondary compression at the applied stress are not obtained.

Thus, contrary to standard practice and in order to produce as little secondary compression as possible between each incremental loading, time rate of consolidation tests were done for every loading increment. These data were used to decide when end of primary consolidation was essentially completed so that the next load increment could be applied. To this end, Taylor's square root of time method (as found in Holtz and Kovacs, 2011) was performed on the time rate of consolidation data to determine when 90% of primary consolidation had occurred. Ninety-percent of primary consolidation was selected mainly to accelerate the consolidation process; when consolidating soft clays it can take substantially more time to reach 95% or 100% of consolidation. When this value was reached, the next load increment was then applied. This accomplished three things: (1) it allowed for the incremental loading test to be completed in a more expeditious manner similar to that of CRS testing, (2) it allowed for a more consistent interpretation of the preconsolidation stress, and (3) it produced more repeatable results for the rate of secondary compression.

The incremental loading results were then plotted and the preconsolidation stress ( $\sigma'_p$ ) was determined using the work/strain method (Becker et al., 1987) and Casagrande's method (Casagrande, 1936). The compression ratio (CR) and recompression ratio (RR) were also determined from plots of log of applied stress versus vertical strain.

## 5.2.3 Determination of the Rate of Secondary Compression $C_\alpha$

The rate of secondary compression varies with the preconsolidation stress and amount of aging (Jamiolkowski et al., 1985; Ng, 1998). For this research it is important to determine rate of secondary compression for the normally consolidated condition, i.e.,  $C_\alpha$ . This was done by first determining the preconsolidation stress from the incremental load tests described in the previous section. After this, specimens from the same depth interval and borehole were loaded to a new stress state that was 1.5 to 2.0 times the in situ  $\sigma'_p$  value. This ensured that specimens had reached a new normally consolidated state and any effects of aging or past preconsolidation had been removed.

Ladd's (1989) method was used to interpret the time rate of consolidation data for secondary compression (Figure 2.3). When using Ladd's methodology, the value of secondary settlement  $C_\alpha$  is the slope of the line through the linear-most portion of the data, after primary consolidation has occurred, on the strain vs. log of time plot.

The reading schedule used for this part of the test was: 4 min, 8 min, 15 min, 30 min, 1 hour, 2 hours, and 4 hours. Then readings were taken about once a day for the remainder of the test, usually about once every 24 hours. The first few readings were removed because they have very little effect on the value of  $C_\alpha$ . It was decided to take the first reading at 4 minutes to increase the number of tests that could be run at one time. This test ran for one to two weeks to be sure that a good value of  $C_\alpha$  was achieved.

#### **5.2.4 Determining $C_\alpha'$**

The process for determining  $C_\alpha'$  was done using the same procedure to determine  $C_\alpha$  but with a few variations. The specimen was loaded to a state of stress that is 1.5 to 2.0 times the in situ  $\sigma'_p$  value as was done in the section stated above.

After the one- or two-hour reading was taken, the load was then reduced to a known OCR of 1.25, 1.5, or 2.0. These values were selected because this range is likely to bracket the values used for surcharge design. The reading schedule for this part of the test was the same as stated above and ran for one to two weeks.

Ladd's (1989) method was also used to interpret the time rate of consolidation data for secondary compression. Additional detail was provided in Chapter 2.

## 6. RESULTS AND INTERPRETATIONS

### 6.1 Laboratory Tests and Data Screening

In the course of this research, a total of five 1-D consolidation tests were performed at each sampling depth from the individual boreholes completed during the field investigations. For each depth, one test was performed to determine the preconsolidation stress, and the remaining four tests consisted of time rate of consolidation tests to determine the rate of secondary compression at OCR values of 1.0, 1.25, 1.5, and 2.0. These OCR values were selected to represent a reasonable range of overconsolidation states that could be effectively achieved in the foundation soils during embankment construction.

At the 400 South Street site in Salt Lake City, Utah, specimens from eight sample depths were tested. At the South Layton, Utah, site located just off of Layton Parkway and Main Street, a total of four sample depths were tested. At the Springville, Utah, 400 South Street site, specimens from seven sample depths were tested. Similarly at the Provo, Utah, interchange, specimens from seven sample depths were tested. Thus, in total, 26 consolidation tests and 104 time rate tests were performed on Pleistocene and recent fine-grained, cohesive, lacustrine deposits composed of Lake Bonneville and more recent clays, most likely of Utah Lake origin. A list of the locations, sample depths, and results of these tests are presented in Table 6.1.

Prior to developing the consolidation parameters from the specimens, the consolidation test results were screened using the sample quality designation (SQD) developed by Andresen and Kolstad (1979) of the Norwegian Geotechnical Institute (NGI). This method uses the recompression vertical strain during the initial reloading loading of the specimen back to the in situ effective vertical stress. For example, in this method, an SQD value of 4 indicates that the specimen underwent 4% vertical strain during the reloading. Andresen and Kolstad (1979) developed an SQD nomenclature that corresponds with the vertical strain values given in Table 6.2. For example, an SQD value between 2 and 4 receives a “fair” designation. Saye and Ladd (2000) used SQD values of 4 or greater to screen out (i.e., omit) consolidation data from their evaluations. The 1D consolidation data used by these authors were obtained by the various geotechnical firms during the baseline investigations for the I-15 Reconstruction Project and had varying levels of quality. Therefore, in general, based on Andersen and Kolstad (1979) and Saye and Ladd (2000), it is recommended that an SQD criterion of 4 or higher be used as a screening criterion for future project evaluations.

However, some of the specimens obtained for this research exceeded this recommended screening threshold (Table 6.3). In order to improve the sample size for the statistical analysis herein, it was decided to slightly relax this criterion. Thus, consolidation tests results having SQD greater than 6 were excluded from the subsequent analysis herein. The footnotes in Table 6.1 give information on which specimens were screened from the statistical analyses due to poor SQD, or other testing or data reduction issues.

Some of the specimens sampled from the 400 South Street site in Salt Lake City, Utah, and from the Provo, Utah, South Interchange site had relatively high SQD values, indicating higher amounts of sample disturbance. The reasons for this are unclear, but may be partly attributable to the softer soil deposits found at these locations. Such soils may be more susceptible to disturbance effects associated with sampling, handling, and preparation processes.

The consequences of sample disturbance appear to have had a larger impact on specimens tested at or slightly above the normally consolidated state of stress (i.e.,  $OCR \approx 1$ ). For example, when the screened tests results for  $C_\alpha$  and  $C_\alpha'$  from this research are plotted versus OCR values (Figure 6.2), the variance (i.e., scatter) of the data is higher for results obtained at lower OCR values when compared with that obtained at higher OCR values. This holds true for both the total variance (scatter of data from all sites) and for the sample variance (scatter of data obtained from a particular site). Some of this variation is due to natural variability of the layered sediments at a given site, because not all specimens at each site were obtained from the same layer. However, it is also likely that some of the variation can be attributed to the effects of sample disturbance. Therefore, it is reasonable to conclude that the apparent decrease in variance with increasing OCR values is, in part, due to the ameliorating effect of overconsolidation of the soil specimens prior to performing the time rate of consolidation tests to determine  $C_\alpha'$ . A similar beneficial effect of overconsolidating soils prior to performing undrained shear strength tests have been discussed by Ladd and Foott (1974) in developing the SHANSEP (Stress History and Normalized Soil Engineering Properties) method.

**Table 6.1** Listing of sites, depths, moisture content, preconsolidation stress, compression and recompression ratio, rate of secondary settlement, and OCR values

Site	Avg. depth (ft)	$\omega$ (%)	Casagrande $\sigma'_p$ (psf)	Work $\sigma'_p$ (psf)	CR	RR	$C_\alpha$	$C'_\alpha$ OCR 1.25	$C'_\alpha$ OCR 1.5	$C'_\alpha$ OCR 2.0
400 South	16 <sup>b</sup>	53.0	2671	2780	0.21	0.021	0.0164	0.0230	0.0017	0.0009
	21	52.0	6338	6420	0.20	0.026	0.0127	0.0089	0.0044	0.0020
	26	49.2	2989	3040	0.18	0.021	0.0095	0.0072	0.0028	0.0007
	31	47.2	5473	5280	0.15	0.018	0.0066	0.0022	0.0012	0.0003
	39	40.3	5423	5520	0.15	0.024	0.0105	0.0058	0.0015	0.0010
	41 <sup>a</sup>	46.7	1610	1660	0.13	0.016	0.0103	0.0103	0.0029	0.0010
	46 <sup>a</sup>	40.3	4262	4240	0.12	0.018	0.0036	0.0047	0.0026	0.0010
	51 <sup>a</sup>	48.5	2350	2120	0.17	0.016	0.0049	0.0047	0.0041	0.0018
S. Layton	16	32.8	5067	5120	0.13	0.012	0.0030	0.0017	0.0007	0.0004
	91	34.7	6510	6580	0.07	0.013	0.0026	0.0015	0.0006	0.0005
	106	28.4	6408	7140	0.04	0.008	0.0023	0.0018	0.0011	0.0005
	131	25.5	5974	6320	0.11	0.017	0.0048	0.0033	0.0012	0.0006
Springville	31	26.7	7101	7060	0.09	0.023	0.0018	0.0012	0.0006	0.0003
	41	26.8	6682	6780	0.09	0.014	0.0021	0.0011	0.0003	0.0002
	66	23.6	5810	6040	0.05	0.008	0.0024	0.0022	0.0014	0.0010
	71	27.7	12125	12420	0.12	0.018	0.0040	0.0026	0.0012	0.0012
	76	32.8	6274	6280	0.15	0.022	0.0051	0.0050	0.0019	0.0007
	81 <sup>a</sup>	41.9	6643	6880	0.19	0.023	0.0074	0.0060	0.0016	0.0007
	85 <sup>a</sup>	40.6	5503	5503	0.17	0.023	0.0047	0.0025	0.0006	0.0001
Provo	13	45.5	7358	7820	0.11	0.017	0.0046	0.0023	0.0007	0.0004
	18	35.2	2969	3120	0.14	0.013	0.0036	0.0021	0.0008	0.0016
	51 <sup>a</sup>	51.1	3803	4000	0.12	0.020	0.0037	0.0014	0.0010	0.0004
	61 <sup>a</sup>	32.6	4740	4800	0.10	0.017	0.0032	0.0026	0.0015	0.0009
	81	47.8	6331	6340	0.18	0.023	0.0075	0.0027	0.0018	0.0018
	91	34.1	7014	7300	0.13	0.015	0.0045	0.0040	0.0007	0.0005
	111 <sup>a</sup>	41.3	5512	5520	0.14	0.021	0.0037	0.0030	0.0008	0.0005

**a** Data that have been removed from analysis due to a high SQD value.

**b** Data were removed from analysis due to poor result for  $C_\alpha$  by not running long enough.

**Table 6.2** Values of strain at  $\sigma'_{vo}$  and the corresponding rating of SQD

Strain on Reloading to $\sigma'_{vo}$ (%)	Sample Quality Designation (SQD)
<1	A, Very good to excellent
1-2	B, Good
2-4	C, Fair
4-8	D, Poor
>8	E, Very poor

A plot of preconsolidation stress versus depth for the higher quality samples shows that the soils at the various test sites are overconsolidated at all depths (Figure 6.1). This is a typical finding, which has been documented by many geotechnical investigations for the surficial alluvium and underlying lacustrine sediments in the Wasatch Front Area. The apparent overconsolidation originates from aging, void ratio change due to repeated drying and wetting cycles resulting from groundwater fluctuations, and, in some cases, minor cementation from calcium carbonate.

The effective vertical stress profile is also shown on Figure 6.1 using an estimation of the water table level determined from piezometer readings for CPT soundings performed nearby. The CPT soundings were used to infer the equilibrium water table condition instead of the boreholes because the drilling operations required that the boreholes be “abandoned” (filled with grout) soon after the drilling had ceased. The in situ OCR values ranged from 1.3 to 5.8, where the higher values of OCR tend to be at shallow depths and then decreases with depth.



**Table 6.3** Site, Depth, Effective Vertical Stress, and SQD

Site	Avg. Depth (ft)	$\sigma'_v$ (psf)	SQD
400 S	16	1198	2.7
	21	1436	2.7
	26	1674	5.5
	31	1912	4.7
	38.5	2269	5.6
	41	2388	11.2
	46	2626	8.2
	51	2864	11.8
S. Layton	16	1483	3.0
	91	5803	5.0
	106	6667	3.3
	131	8107	7.0
Springville	31	2067	2.8
	41	2593	4.3
	66	3908	3.0
	71	4171	2.4
	76	4434	5.2
	81	4697	8.9
	85	4908	6.5
Provo	13	1245	1.4
	18	1508	3.2
	51	3244	17.5
	61	3770	8.1
	81	4822	7
	91	5348	6.4
	111	6400	13.5

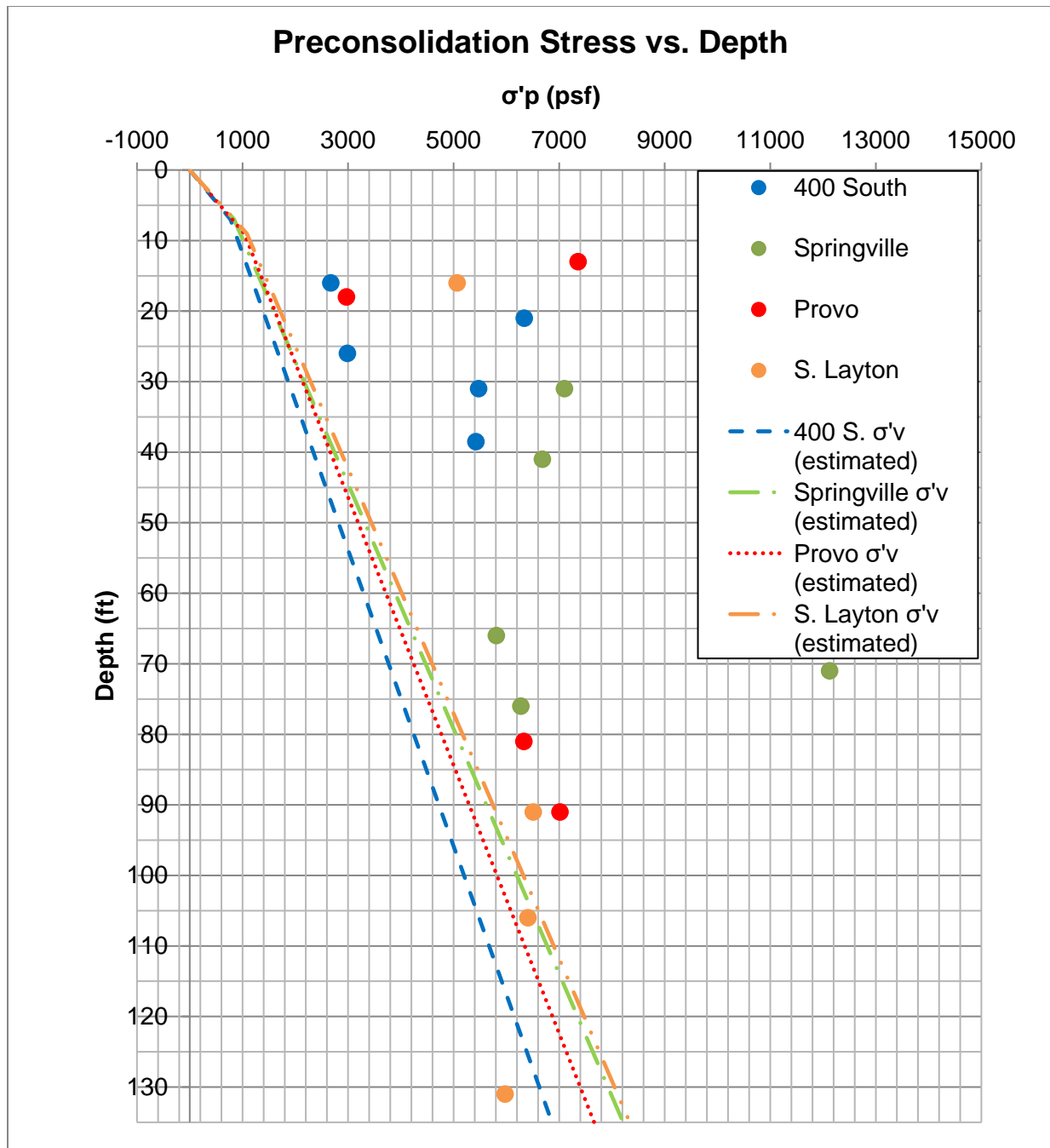


**Figure 6.1** Plot of preconsolidation stress vs. depth for 400 South, South Layton, Springville, and Provo

## 6.2 Relationships for $C_\alpha$ , $C'_\alpha$ and $C'_\alpha/C_\alpha$

The plot of  $C_\alpha$  and  $C'_\alpha$  versus OCR shows there is a non-linear trend that exists between the dependent and independent variables. This trend is best fit using the exponential trend line feature in MS Excel. This plot and its corresponding non-linear relationships indicate a relatively small change in  $C'_\alpha$  for OCR values greater than about 1.5. At higher OCR values, the  $C'_\alpha$  values appear to converge to a value slightly less than 0.001 (Figure 6.2). From an application standpoint, this behavior suggests there is a point of

diminishing return when surcharging soils beyond an OCR value of about 1.5 for the sediments tested in this study.

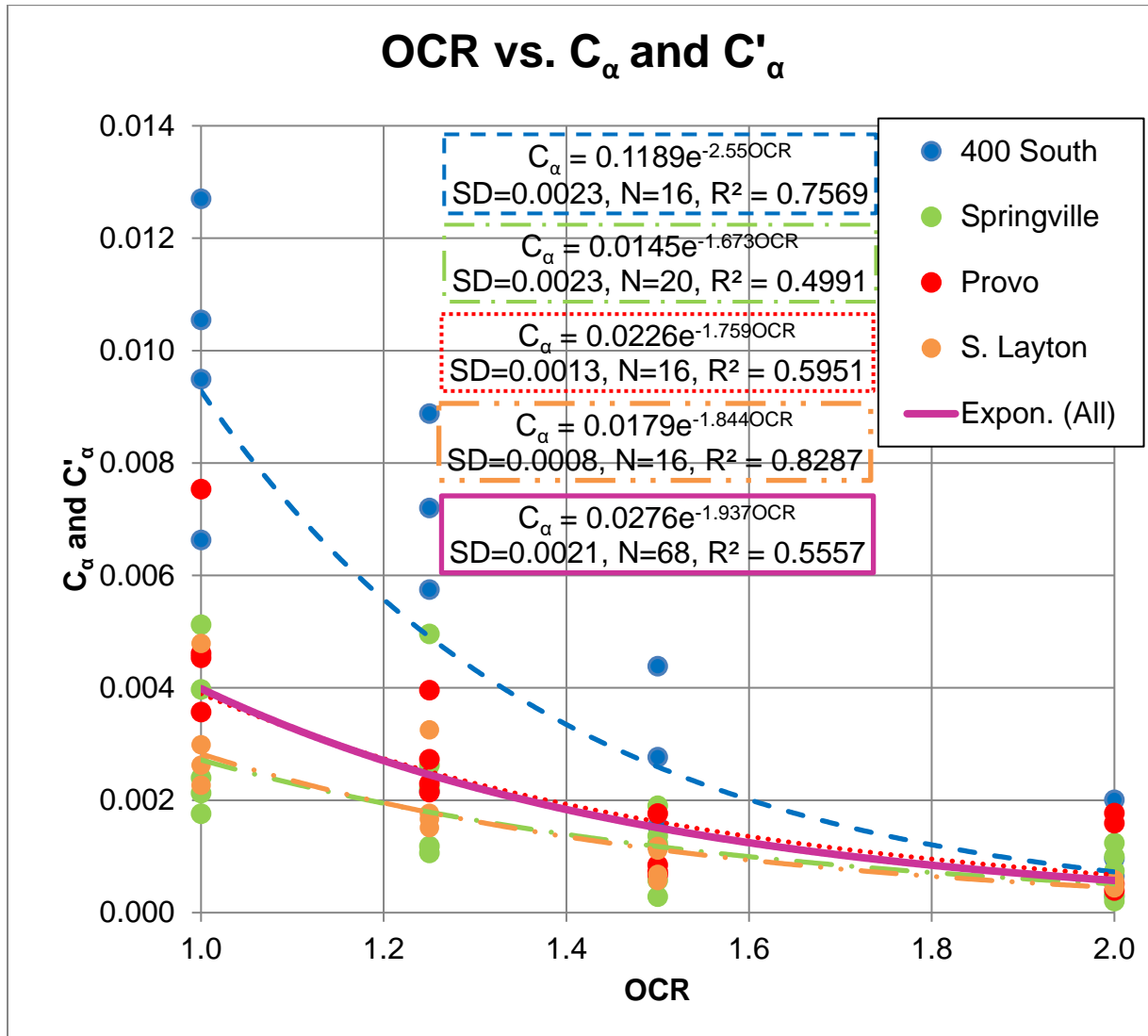


**Figure 6.2** Plot of  $C_\alpha$  and  $C_\alpha'$  vs. OCR for 400 South, South Layton, Springville, and Provo Sites

While the  $C_\alpha'$  values for the various sites tend to converge at an OCR value of 2.0, it is also apparent that the fitted relationship for the 400 South Site in Salt Lake City is higher than the average fitted trend line; whereas, the fitted trend lines for Springville and South Layton tend to be lower than the average trend line. A possible reason for this difference in behavior may be attributed to the nature of the lacustrine sediments. In the Salt Lake Valley, the lacustrine sediments sampled are solely from Lake Bonneville deposits. Whereas at the Provo and Springville sites, in Utah Valley, the sampled sediments consisted of recent Utah Lake and earlier Lake Bonneville sediments. In general, it appears that the Utah Lake sediments are siltier than those obtained from Lake Bonneville, and this may be causing the difference in the  $C_\alpha'$  values.

Because of these relatively large differences in the trend lines for the various sites, a better interpretation and graphical representation of the data are required. This can be done by normalizing  $C_\alpha'$  using  $C_\alpha$  (i.e., forming  $C_\alpha'/C_\alpha$  ratios) and plotting the normalized values versus OCR (Figure 6.3). This method

produces a normalized average trend line for  $C'_\alpha/C_\alpha$  that fits all data reasonably well and which can be used as a good representation of the average of all data.

Ladd (1989) introduced the concepts of amount of surcharge (AOS) and adjusted amount of surcharge (AAOS) instead of OCR to represent the data trends. These factors are more useful for applied surcharge purposes (see Chapter 2). A plot of  $C'_\alpha/C_\alpha$  versus AAOS is shown in Figure 6.4.

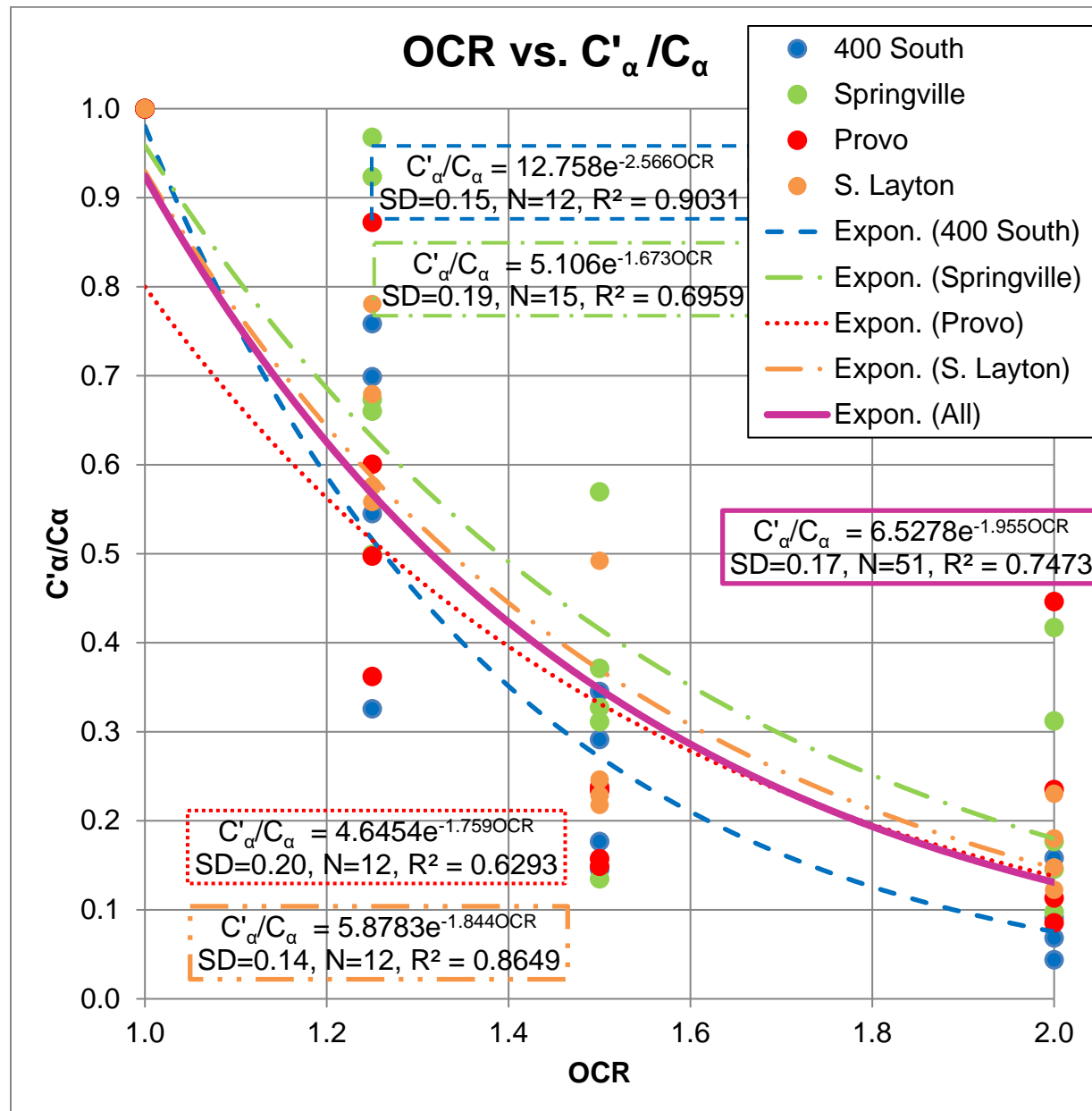


**Figure 6.3** Plot of  $C'_\alpha/C_\alpha$  vs. OCR for 400 South, South Layton, Springville, and Provo Sites

Ng (1998) plotted  $C'_\alpha/C_\alpha$  versus AAOS values from testing developed for the I-15 Reconstruction Project on a semi log plot. The data from this study have been superimposed on the Ng (1998) relationship for comparative purposes in Figure 6.5. The average trend line for this research plots significantly higher

than that developed by Ng (1998). There are several possible explanations for this, as discussed in the next few paragraphs.

First, the soil specimens from this research may be significantly different from those tested by Ng (1998). The Provo and Springville sites are located about 40 to 50 miles to the south of Salt Lake City, respectively, in an adjacent valley and appear to be siltier in nature due to the presence of near shore sediments deposited in Utah Lake. Only one test site (400 S. Street in Salt Lake City) was geographically near the drill hole locations where Ng (1998) and Woodward-Clyde Consultants obtained soil samples for the I-15 project. When the results for the 400 South Street site (blue line in Figure 6-5) are compared with those of Ng (1998), significant differences still remain. But the lower bound data points from the 400 South Site plot within the upper range of the Ng (1998) data.

Second, the trend of the Ng (1998) relationship appears to overstate the reduction in  $C_a'/C_a$  as a function of AAOS. For example, if extrapolated to an AAOS value of 50% (i.e., OCR = 1.5), the average trend line of Ng (1998) would predict a  $C_a'/C_a$  ratio of near zero, which appears to be unlikely, especially when considering that this research shows a minimum value of  $C_a'/C_a$  of about 0.1 at an OCR value of 2.0. This latter result appears to be more realistic and intuitive based on the data presented in this report.

Third, long-term settlement performance monitoring data obtained from the I-15 Reconstruction Project for the surcharged earthen embankments and MSE walls show that the measured creep settlement is somewhat larger than the desired performance goal (Figure 6.6) (Farnsworth et al., 2008). The settlement performance goal adopted by the project was to limit the creep settlement to 75 mm, or less, in a 10-year post-construction period. Large earthen embankments located at 400 S. and 2400 S. Streets were constructed with surcharged embankments designed to meet this performance goal. However, the 10-year post-construction settlement at these sites is projected to exceed this settlement goal by a factor of about 1.5 to 2 (Figure 6.6). This suggests that the rate of secondary compression in the subsurface soils at these locales is greater than that anticipated in the surcharge design. One possible reason for the underestimation of the actual settlement could rest in the value of  $C_a'$  selected for the design calculations. Because the amount of secondary compression settlement is directly proportional to  $C_a'$  based on Eq 2-8, the additional settlement incurred at these sites may have resulted from an underestimation of the actual  $C_a'$  for the foundation settlement for these locales. For example, if the design  $C_a'$  values were approximately 1.5 to 2.0 times higher than those reported by Ng (1998), then such a change would produce a more reasonable result that is in better agreement with the average  $C_a'/C_a$  trend line developed for the 400 South Street site in Salt Lake City from this research.

Nonetheless, despite the various interpretations of the existing laboratory and field data that could be offered, it is clear that site-specific field and laboratory evaluations are needed for future sites to avoid pitfalls associated with applying data and relationships developed from other sites that may have significantly differing soil conditions than the site of interest.



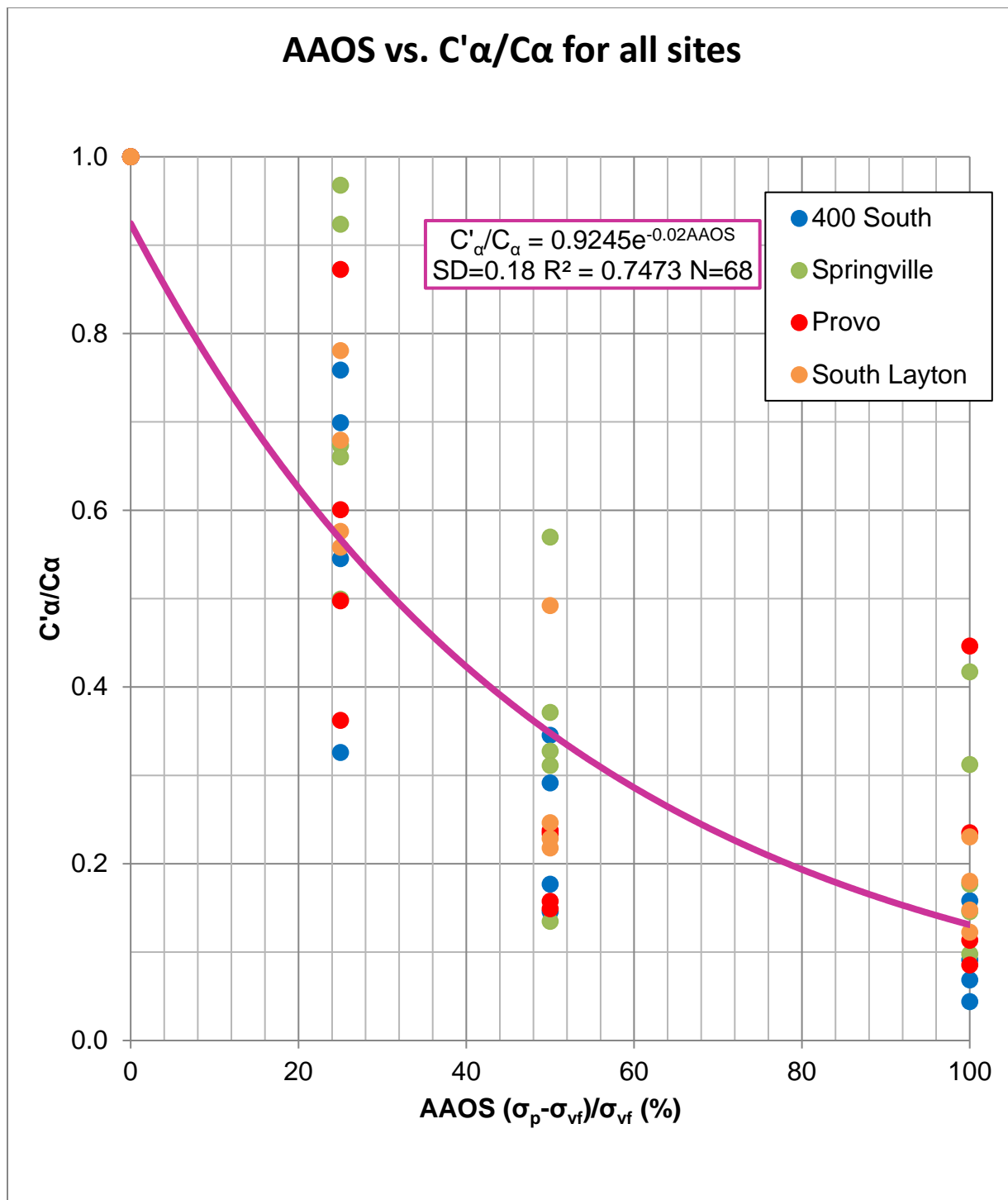


**Figure 6.4** Plot of AAOS vs.  $C\alpha'/C\alpha$  using an average exponential trend line

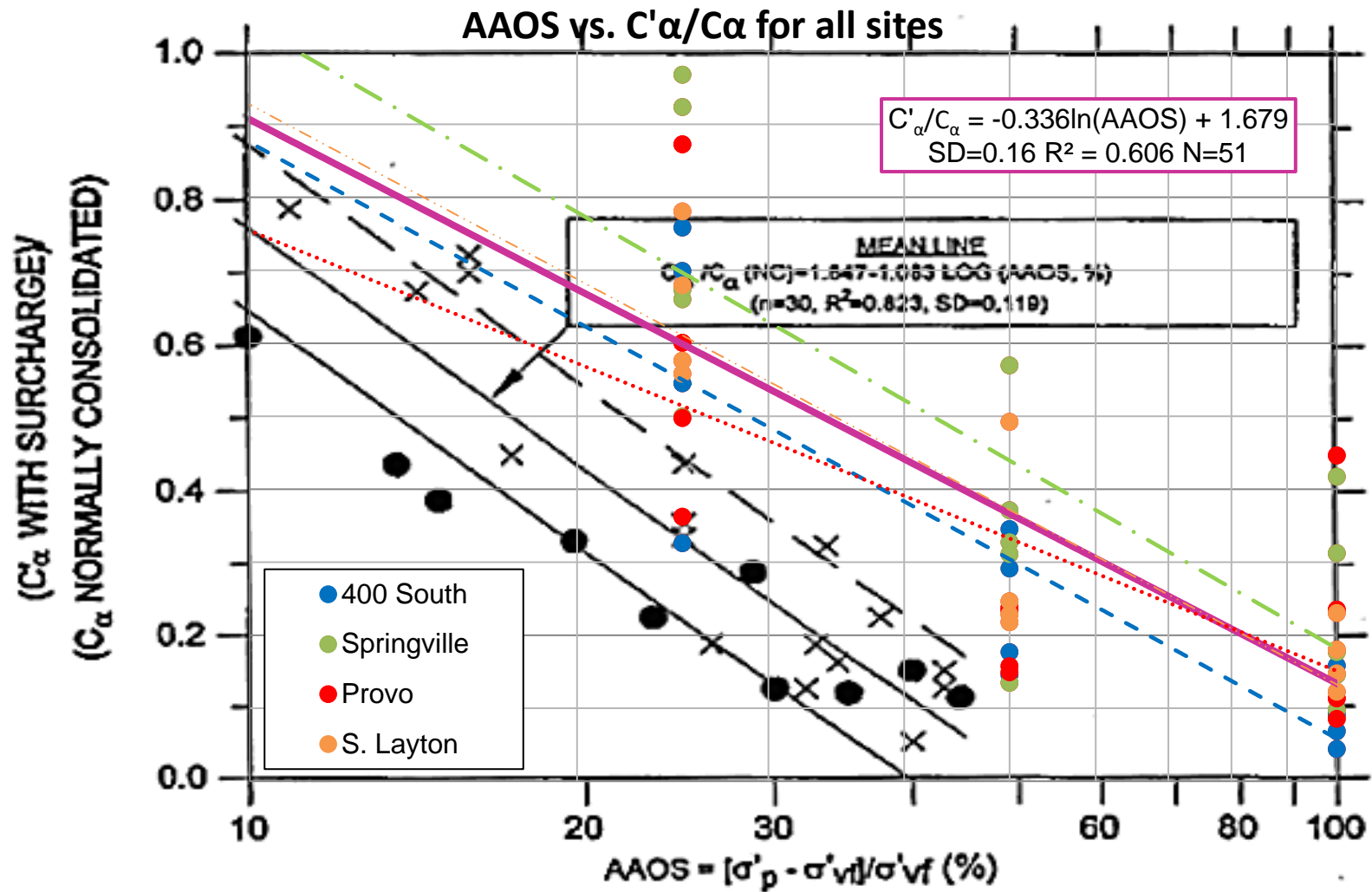


**Figure 6.5** Comparison plot of AAOS vs.  $C'_\alpha/C_\alpha$  on a semi log plot with data acquired by MIT

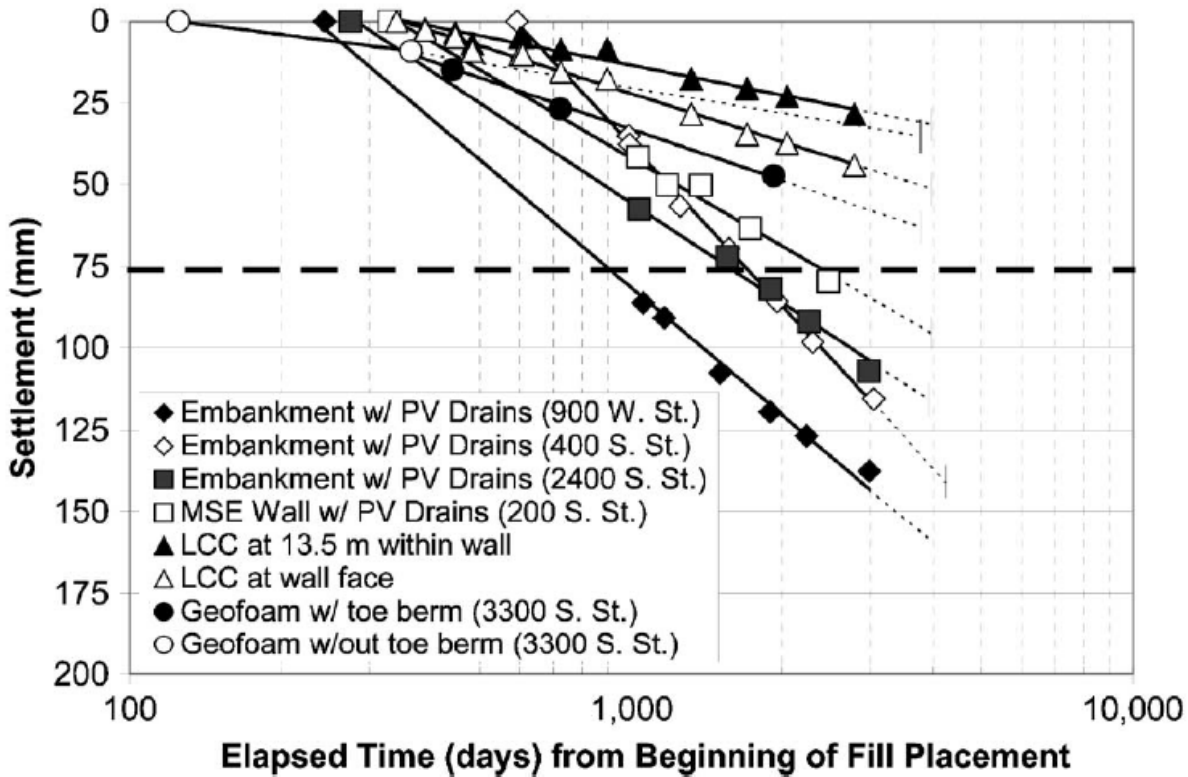


**Figure 6.6** Rate of Foundation Creep Extrapolated to 10 Years of Post-Construction (from Farnsworth et al., 2008)

### 6.3 $C_a/CR$ Ratio

Mesri has shown that the  $C_a/CR$  ratio is relatively constant for a given soil type. Knowledge of this ratio has proven to be very helpful in performing secondary settlement calculations because  $C_a$  can be estimated if values of CR and the  $C_a/CR$  ratio are known for a particular soil or can be reasonably estimated. Values of CR are easily attainable from standard consolidation testing, and  $C_a/CR$  ratios can be estimated from this research and that of Ng (1998) as shown in Figures 6.7 and 6.8, respectively.

The ratios developed by this research (Figure 6.7) were calculated using a linear trendline function and by forcing the trend line through the origin; hence, the slopes of these lines also represent the  $C_a/CR$  ratio. These results show that each individual research site has a slightly different  $C_a/CR$  relationship when compared with the average trend line. In short, the 400 South Street site in Salt Lake City has a somewhat steeper slope (higher ratio) than the South Layton, Springville, and Provo sites. However, when the average slope of all the data from the four research sites is calculated, the corresponding value is  $C_a/CR = 0.0442$ . This average ratio correlates reasonably well with that of Ng (1998) of  $C_a/CR = 0.0433$ . The Ng (1998) average relation included consolidation tests performed at MIT and by Woodward-Clyde Consultants for the Lake Bonneville deposits (Figure 6.8). Although this research supports a similar average  $C_a/CR$  ratio when compared with Ng (1998), the results for the 400 S. Street site in Salt Lake City plot somewhat above the average trend line of Ng (1998).

In addition to this, the time delay for when secondary compression resumes is shown in Figure 6.9 as a plot of AAOS vs.  $\text{LOG}(t_s/t_r)$ . When comparing the data from this research and the data from MIT and WWC (Ng, 1998) the trend line is slightly lower but compares well with previous work.

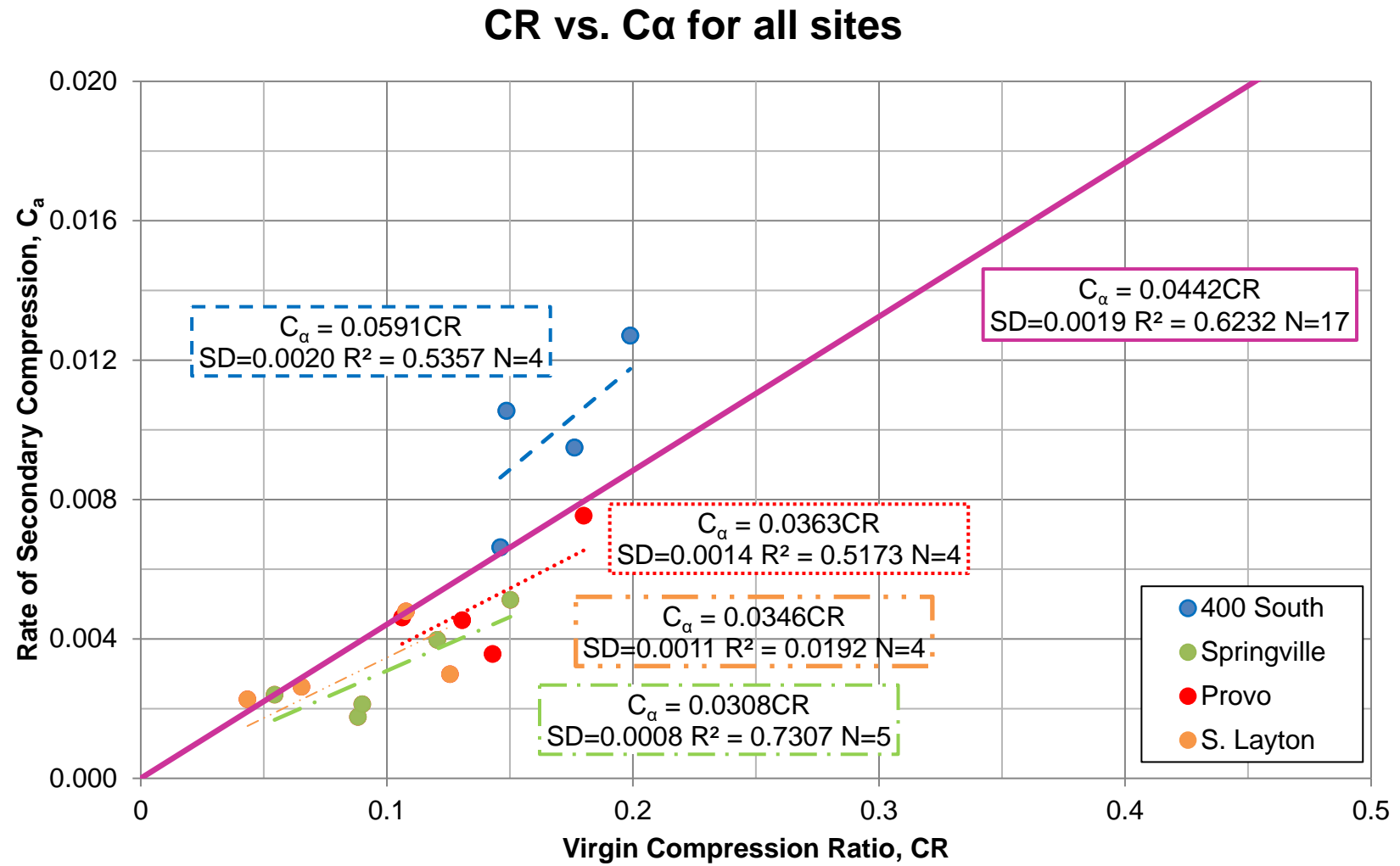


**Figure 6.7** Plot of CR vs.  $C_\alpha$  for all sites

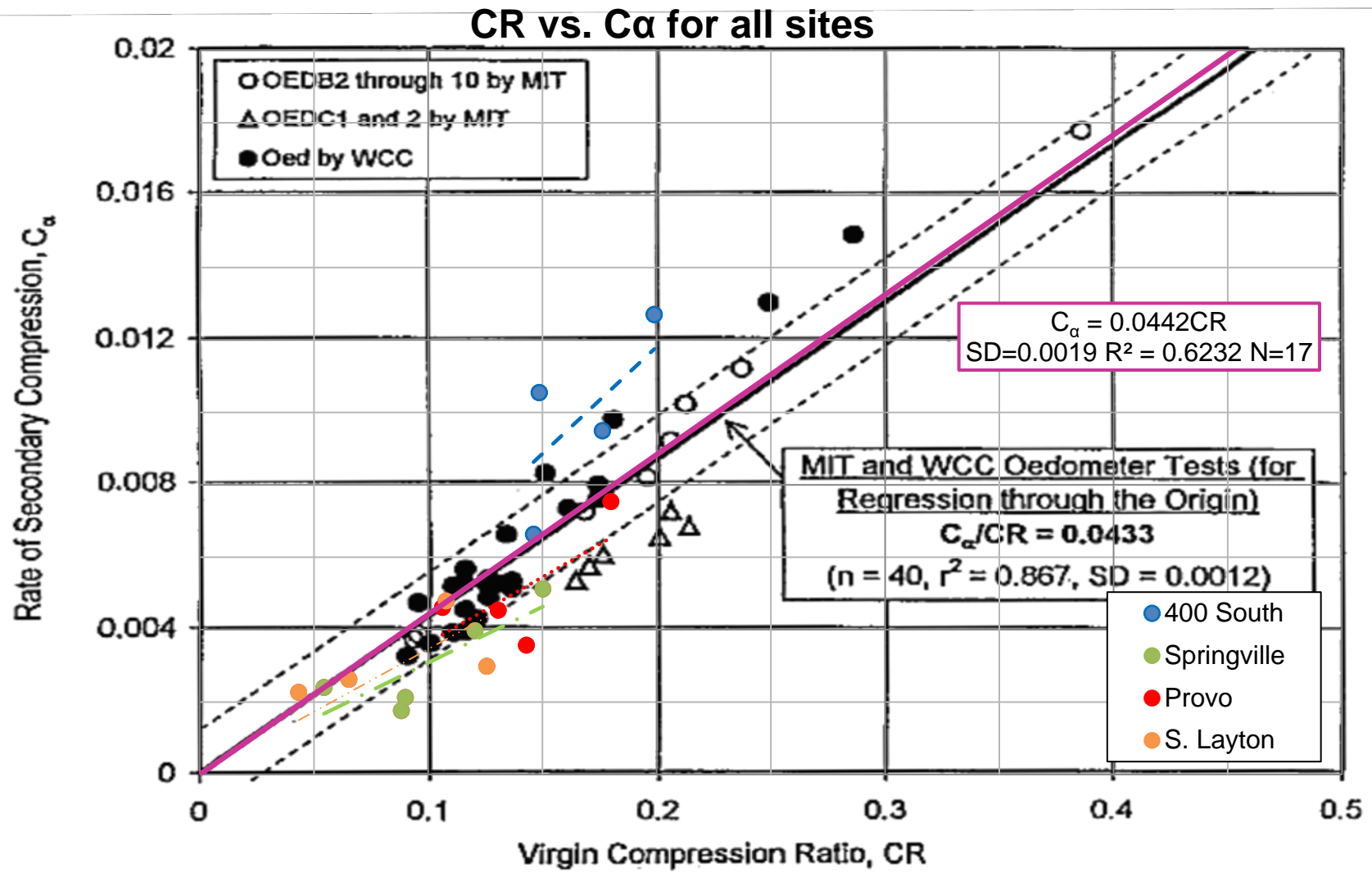


**Figure 6.8** Comparison plot of CR vs.  $C_\alpha$  with data collected from MIT and WCC

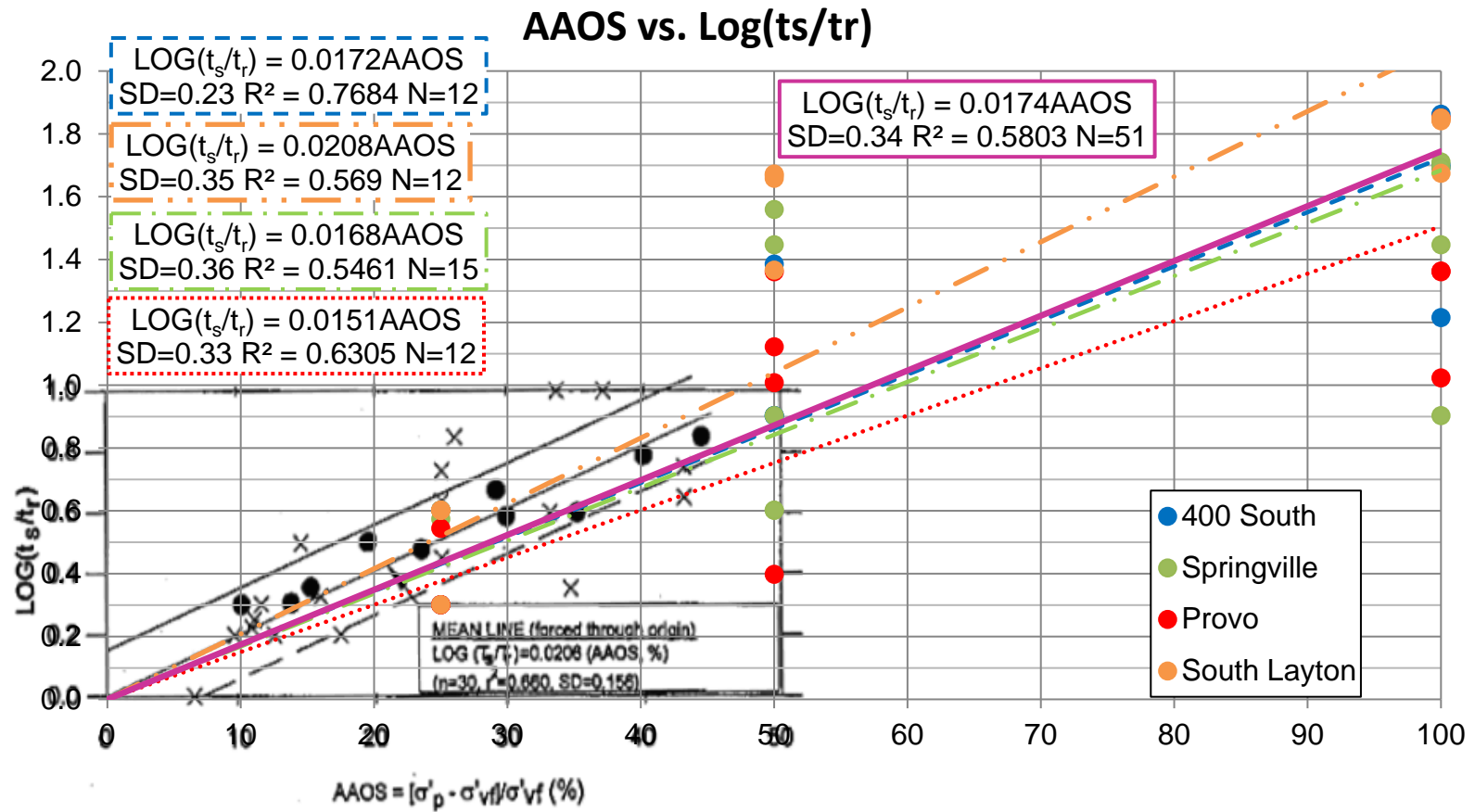


**Figure 6.9** Comparison plot of AAOS vs. LOG(ts/tr) with data collected from MIT and WCC



## 6.4 Moisture Content Correlations

Many researchers have shown that the moisture content,  $\omega$ , of soil is highly correlated with soil compressibility (i.e.,  $C_c$  and CR) for saturated soils. This is because when the soil fabric is saturated, the in situ moisture content is directly correlated with the in situ void ratio for soils with a given specific gravity. For many cohesive soils, there is a relatively minor variation in the specific gravity of the soil solids; hence, moisture content is an excellent predictor of void ratio. In addition, void ratio in turn is highly correlated with  $C_c$  and CR because soils with high voids have more opportunity for compression (i.e., void ratio reduction) upon loading.

Figure 6.10 shows a  $\omega$  versus CR relation using the test results from this research. The data indicate a relatively good correlation between these properties. In addition to this, Bartlett and Lee (2004) developed moisture content and compressibility correlations for the Lake Bonneville deposits. These correlations were made from laboratory data obtained from various geotechnical reports associated with the I-15 Reconstruction Project. Test results with a SQD value greater than 4 were screened (excluded) from their evaluations (Figure 6.11). The data from this research have been superimposed on the Bartlett and Lee (2004) plot for comparative purposes. The trend line developed from this research plots somewhat lower than that of Bartlett and Lee (2004). However, this does not imply that the two equations are inconsistent for the following reasons: (1) the soils from this research appear to be somewhat siltier, on average, than those used by Bartlett and Lee (2004); (2) the Bartlett and Lee (2004) relation has more statistical support because of the larger sample size; and (3) the data from this research do not plot outside the data range of the Bartlett and Lee (2004) relation, suggesting the two data sets are not entirely inconsistent. For application purposes, it is recommended the Bartlett and Lee relation be used because of its greater statistical support.

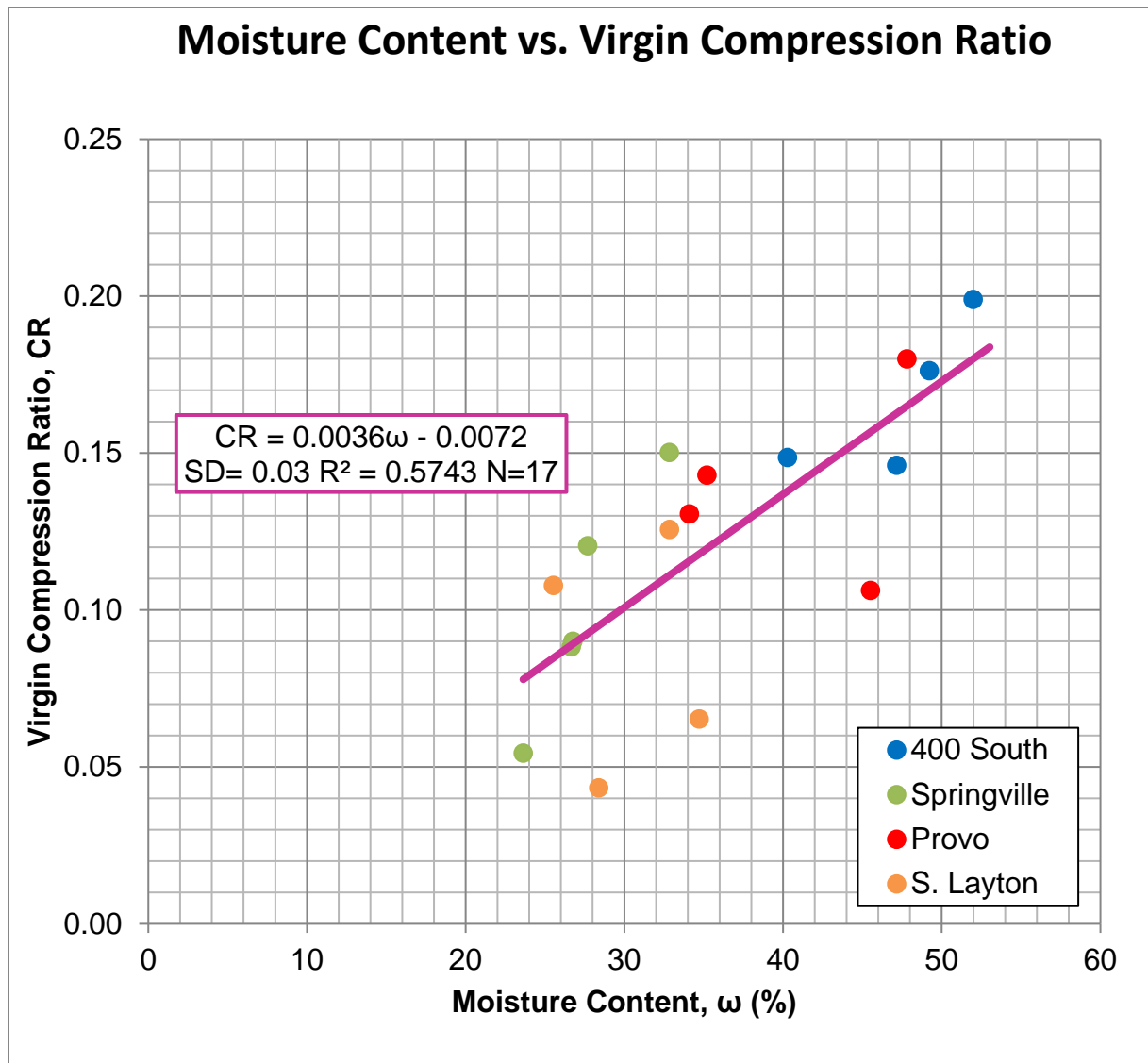


**Figure 6.10** Plot of moisture content vs. virgin compression ratio

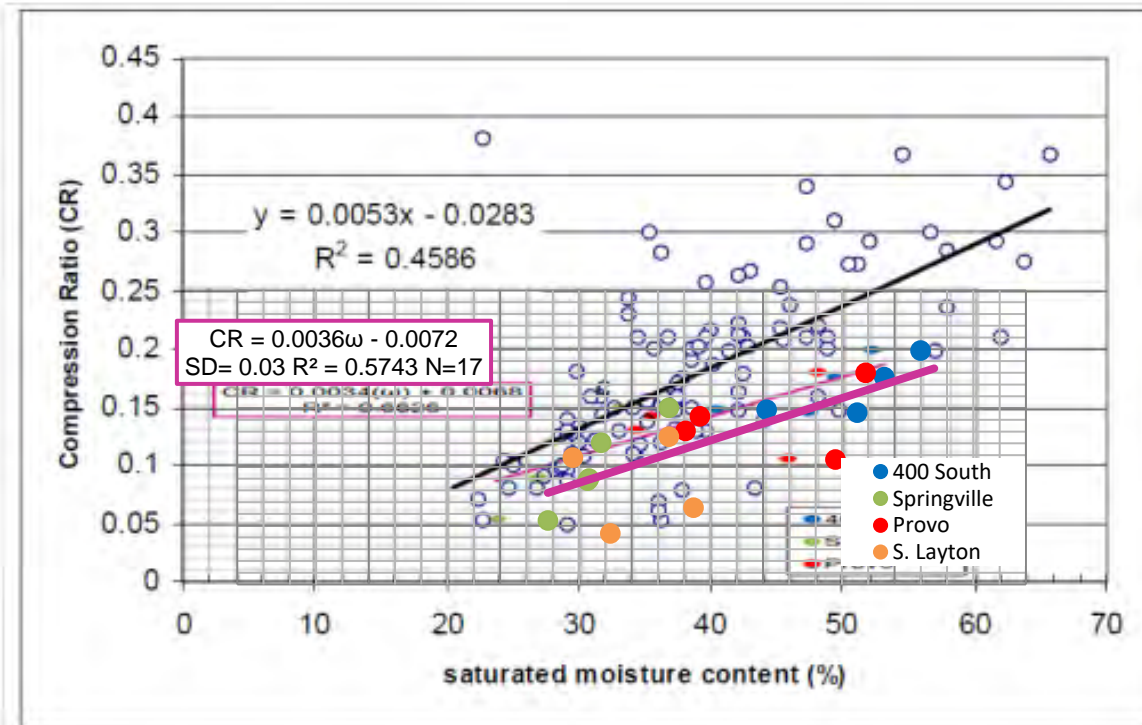


**Figure 6.11** Plot of moisture content vs. virgin compression ratio (Bartlett and Lee, (2004))

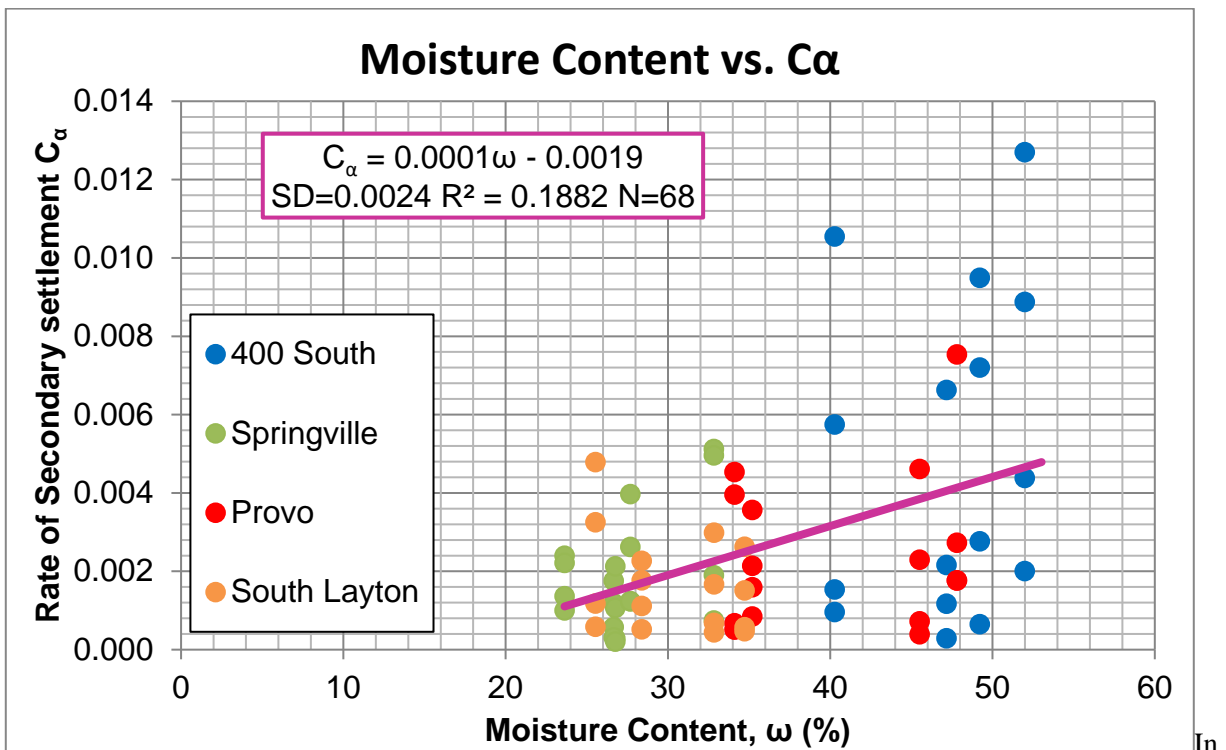


**Figure 6.12** Plot of moisture content vs. rate of secondary settlement

In addition to the correlations just discussed, correlations that included rate of secondary compression properties and moisture content were explored. The correlations as attempted included:  $C_\alpha$ ,  $C_\alpha/CR$ ,  $C_\alpha'/C_\alpha$  as shown in Figures 6.12 to 6.14, respectively. Based on these plots, there is poor to very poor

correlation between  $C_\alpha$  and  $C_\alpha'/C_\alpha$  and  $\omega$  (Figures 6.12 and 6.14, respectively). However, the correlation between  $C_\alpha/CR$  and  $\omega$  has some promise for future development and application (Figure 6.13). However, more observations are needed to improve the statistical support for this relation.

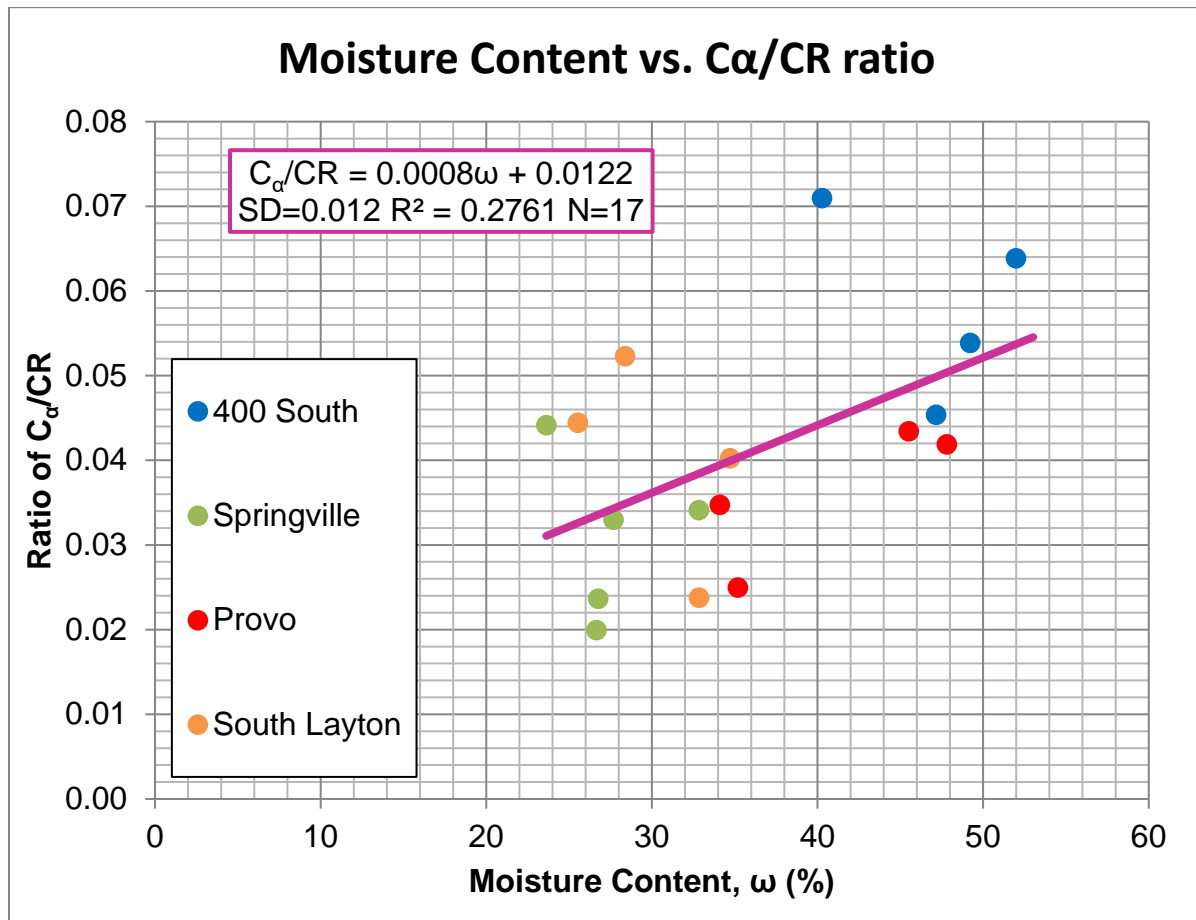


**Figure 6.13** Plot of moisture content vs.  $C_\alpha/CR$  ratio

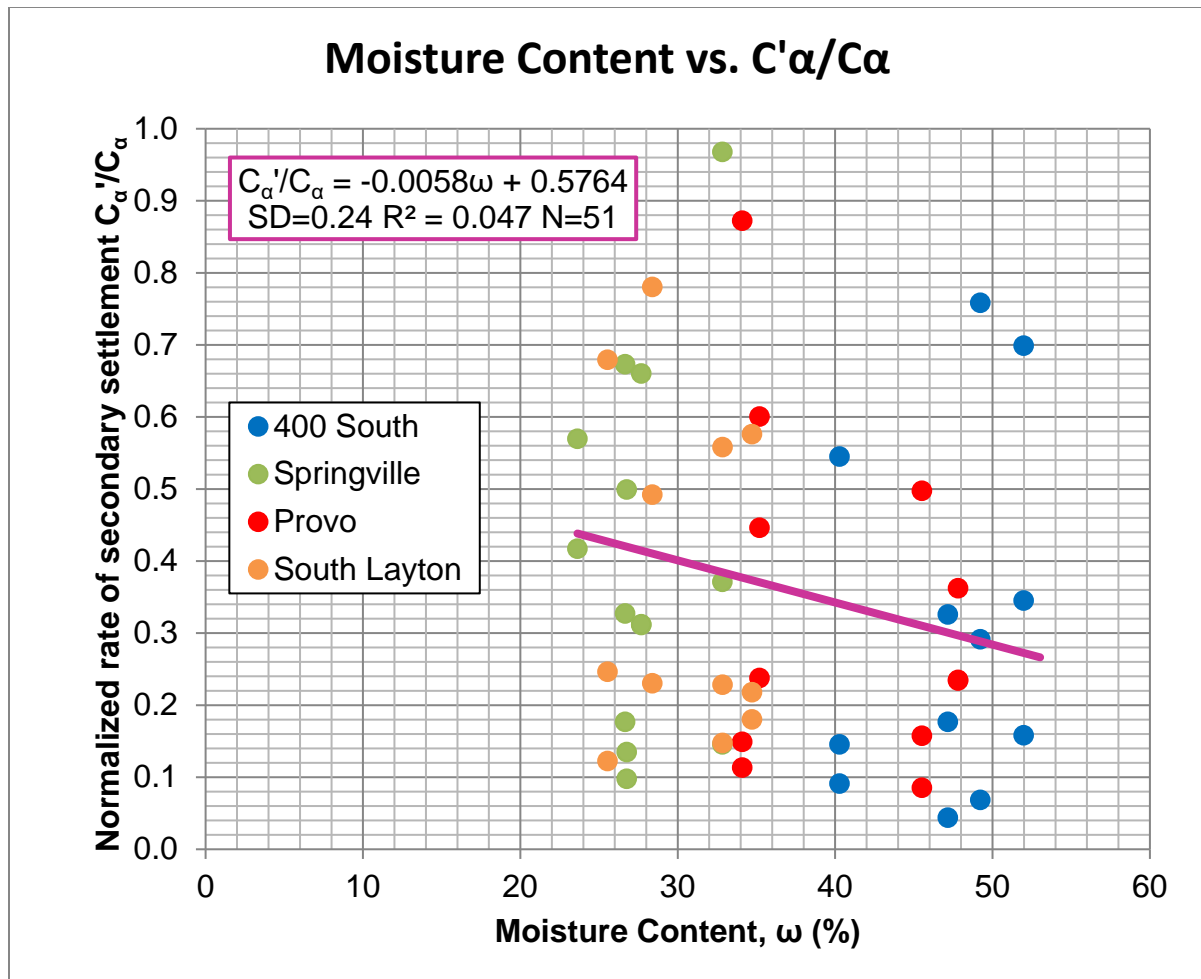


**Figure 6.14** Plot of moisture content vs. normalized rate of secondary settlement

## 7. CONCLUSIONS

### 7.1 Summary of Research Objectives

The main objectives in this research were: 1) corroborate Mesri's concept of secondary compression (i.e.,  $C_\alpha/CR$  is relatively constant) for the Lake Bonneville deposits along the Wasatch Front in Utah; 2) supplement and/or revise, as necessary, the design relationships developed by Ng (1998) for the I-15 surcharge design using a larger set of field and laboratory test data; (3) recommend an appropriate laboratory testing and evaluation program to support project-specific surcharge design for future highway embankment projects sponsored by the Utah Department of Transportation (UDOT) in the Wasatch Front Area; and (4) develop additional design guidance and/or recommendations for developing and evaluating the surcharge design.

### 7.2 Mesri's Concept of Secondary Compression

Based on the results of the oedometer tests run at MIT and WCC, they have recommended values of the following creep properties: 1)  $C_\alpha/CR$ , 2) creep behavior as a function of AAOS, and 3) the delay to the amount of time before creep resumes after the removal of a surcharge as a function of AAOS. The data acquired during testing from this research were compared with that produced by MIT and WCC.

#### 7.2.1 $C_\alpha/CR$

Based on analysis from this research, the  $C_\alpha/CR$  ratio with the regression line passing through the origin (Figure 6.8) gives an average value of  $C_\alpha/CR = 0.0442$ . The various site ratio values include: 400 South  $C_\alpha/CR = 0.0591$ , South Layton  $C_\alpha/CR = 0.0346$ , Springville  $C_\alpha/CR = 0.0308$ , and Provo  $C_\alpha/CR = 0.0363$  (Figure 6.7). The trend at the 400 S. Street site in Salt Lake City has a somewhat steeper slope (higher ratio) than the South Layton, Springville, and Provo sites.

The average ratio obtained through this research of  $C_\alpha/CR = 0.0442$  correlates reasonably well with that obtained by the results from Ng's (1998) of  $C_\alpha/CR = 0.0433$ . This confirms that Mesri's concept of secondary compression as expressed as a  $C_\alpha/CR$  ratio is constant along the Wasatch Front for the lacustrine deposits tested in this sampling program.

#### 7.2.2 Creep Behavior as a Function of AAOS

Using the methodology developed by Ladd (1989), when plotting AAOS vs.  $C'_\alpha/C_\alpha$  on a semi-log plot and comparing this with research done by Ng (1998), these data show that the trend seems to be higher than that estimated by Ng (1998) (Figure 6.5). In fact, the trend seems to be closer to the upper bound of the data from Ng (1998). During the I-15 Reconstruction Project, the lower bound was used for the calculations of long-term settlement. The 10-year post construction settlement at some of the sites is projected to be almost 1.5 to 2 times that of what was calculated (Figure 6.6). This suggests that the rate of secondary compression in the subsurface soils at these locales is greater than that anticipated in the surcharge design.

In Figure 6.5, it can be seen that with AAOS above 50% ( $OCR = 1.5$ ) the average trend line of Ng (1998) would predict a  $C'_\alpha/C_\alpha$  ratio of near zero. The data from this research show a minimum value of  $C'_\alpha/C_\alpha$  of about 0.1 at an AAOS of 100% ( $OCR = 2.0$ ) (Figure 6.5). However, the data seem to fit better with the use of an exponential trend line (Figure 6.4).



Therefore, it is recommended that when estimating the value of  $C'_a/C_a$  from AAOS to use the exponential equation  $C'_a/C_a = 0.9245e^{-0.02(\text{AAOS})}$ , or if using the plot produced by MIT and an AAOS below 50% to use the upper bound trend line.

### 7.2.3 The Time Before Creep Resumes After the Removal of a Surcharge.

When comparing the data from this research with that done by MIT and WWC (Ng 1998) for the plot of AAOS vs.  $\text{Log}(t_s/t_r)$  (Figure 6.9), it can be seen that the average trend line through the origin is lower than that produced by MIT, where Ng (1998) has the equation of  $\text{Log}(t_s/t_r) = 0.0206 (\text{AAOS})$ , and the equation for the average trend from this research is  $\text{Log}(t_s/t_r) = 0.0174 (\text{AAOS})$ . This trend line is slightly lower but compares well with previous work.

### 7.2.4 Recommendations for Laboratory Testing Program

When performing laboratory testing to determine the Mesri's  $C_a/\text{CR}$  ratio, the procedure is as follows:

(1) Perform a 1-D consolidation test on the sample; this is done to determine the consolidation properties such as  $\sigma_p$ , CR, and RR. (2) Determine the rate of secondary compression for normally consolidated specimen,  $C_a$ , by loading the soil sample to 1.5 to 2.0 times that of  $\sigma_p$  (to remove any disturbance from the soil sample and to be sure that the soil is normally consolidated). (3) Determine the rates of secondary compression for overconsolidated specimens,  $C'_a$ . Refer to Appendix C for the detailed procedure used in this research.

It is recommended that when determining the preconsolidation stress that each loading step should be moved to the next step with as little secondary settlement as possible occurring. If a large amount of secondary settlement occurs, the soil then becomes aged and it can have an impact on the results of the consolidation data. It is also advantageous to move to the next loading step with as little secondary compression occurring because the tests can be run in a shorter amount of time as opposed to the traditional 24-hour loading steps.

## 7.3 Additional Design Guidance

The moisture content can be used for the estimating of  $C_c$  and CR of a saturated soil (Figures 6.10 and 6.11). For application purposes, it is recommended the Bartlett and Lee (2004) equation  $\text{CR} = 0.0053(\omega) - 0.0283$  be used because of its greater statistical support.

Correlations for  $C_a$ ,  $C_a/\text{CR}$ , and  $C'_a/C_a$  with  $\omega$  were explored in this research (Figures 6.12 to 6.14). Based on these plots, there is poor to very poor correlation between  $C_a$  and  $C'_a/C_a$  with  $\omega$  (Figures 6.12 and 6.14, respectively). The correlation between  $C_a/\text{CR}$  and  $\omega$  has some promise for future development and application (Figure 6.13). However, more observations are needed to improve the statistical support for this relation.

## 7.4 Recommendations for Additional Testing

It is recommended that when future testing is being performed, that Atterberg limits and fines wash be performed on every test specimen for a better classification of the soil being tested. This will also lead to a better understanding of how each type of soil behaves during long-term settlement.

It is also recommended that in the future a more advanced testing with pore water pressure measurements be performed, so as to know when primary settlement is complete and to have very little secondary settlement occur.

## **7.5 Recommended Method for Design**

In Appendix F, a recommended method is provided for designing surcharge fills considering post-construction, secondary compression settlement. The recommended method is based partly on the research presented in this report. Note that current UDOT Geotechnical Manual of Instruction requirements take precedence over the narrative in the design method.

## 8. REFERENCES

- Andresen, A.A. and Kolstad, P. (1979). "The NGI 54-mm samplers for undisturbed sampling of clays and representative sampling of coarser material." Proceedings of the International Symposium on Soil Sampling, Singapore. 13-21.
- ASTM D2435 / D2435M-11, "Standard Test Methods for One-Dimensional Consolidation Properties for Soils Using Incremental Loading."
- ASTM D4186 / D4186M-12e1, "Standard Test Method for One-Dimensional Consolidation Properties of Saturated Cohesive Soils Using Controlled-Strain Loading."
- Bartlett, S. F., and Lee, H., 2004, "Estimation of Compression Properties of Clayey Soils, Salt Lake Valley, Utah," Utah Department of Transportation Research Report No. UT-04.28, 44 p.
- Bartlett, S.F., and Ozer, T., 2005, "Estimation of Consolidation Properties from In-Situ and Laboratory Testing," Utah Department of Transportation Research, Research Division, Report, 206 p. (unpublished).
- Becker, D.E., Crooks, J.H.A., Been, K., and Jeffries, M.G. (1987). "Work as a criterion for determining in situ and yield stresses in clays." *Can. Geotech. J.*, 24(4):549–564.
- Casagrande, A. (1936). "The determination of pre-consolidation load and its practical significance." In Casagrande, A., Rutledge, P.C., and Watson, J.D. (Eds.), Proc. 1st Int. Conf. Soil Mech. Found. Eng., Am. Soc. Civ. Eng., 3:60–64.
- Farnsworth, C. F., Bartlett S. F., Negussey, D. and Stuedlein, A. (2008). "Construction and Post-Construction Settlement Performance of Innovative Embankment Systems, I-15 Reconstruction Project, Salt Lake City, Utah," *Journal of Geotechnical and Geoenvironmental Engineering*, ASCE (Vol. 134 pp. 289-301, March 2008).
- Germaine, John T., and Germaine, Amy V., (2009). Geotechnical Laboratory Measurements for Engineers.
- Holtz, R. D., Kovacs, W. D., and Sheahan, T. C. (2011). An Introduction to Geotechnical Engineering, Second Edition, Prentice Hall.
- Jamiolkowski, M., Ladd, C. C., Germanie, J. T., and Lancellotta, R., (1985). "New developments in field and laboratory testing of soils," Proceedings of the Eleventh International Conference on Soil Mechanics and Foundation Engineering, Vol. 1, San Francisco, 57-153
- Ladd, C. C. (1971). "Settlement Analyses for Cohesive Soils," Research Report R71-2, Soils Publication 272, Department of Civil Engineering, Massachusetts Institute of Technology, 107 p.
- Ladd, C. C., and Foott, R. (1974). "A new design procedure for stability of soft clays." *Journal of Geotechnical Engineering Division, ASCE*, 100(7), 763-786.
- Ladd, C. C. (1989). Unpublished class notes for course 1.322, Soil Behavior, Department of Civil and Environmental Engineering, MIT, Cambridge, MA.
- Ladd, C. C., 1998, "Engineering Properties of Boston Blue Clay from Special Testing Program," Proceedings of Special Geotechnical Testing Central Artery/Tunnel Project in Boston Massachusetts, ASCE Geotechnical Special Publication (GSP) No. 91, October 18-21, Boston Massachusetts.
- Ladd, C. C., 1999, "Parameter Development For Estimating Settlements Due to Primary Consolidation and Secondary Compression," Proceedings of the 34th Symposium on Engineering Geology and Geotechnical Engineering, Utah State University, Logan Utah, April 28-30, 1999.

- Mesri, G., and Castro, A. (1987). "C<sub>a</sub>/C<sub>c</sub> concept and K<sub>o</sub> during secondary compression," *Journal of Geotechnical Engineering Division, ASCE*, 113 (30), 230-249.
- Mesri, G., and Feng, T. W. (1991). "Surcharging to Reduce Secondary Settlements," *Geo-Coast '91*, September 1991, Yokohama, Japan.
- Mesri, G., Lo, D.O., and Feng, T. W. (1994). "Settlement of embankments on soft clay," *Proceedings Vertical Deformations of Foundations and Embankments*, ASCE Geotechnical Special Publication No. 40, Vol. 1, pp. 8-56.
- Ng, N. S. Y. (1998). "Characterization of consolidation and creep properties of Salt Lake City clays," Msc. Thesis, Department of Civil and Environmental Engineering, Massachusetts Institute of Technology, Cambridge, Massachusetts.
- Ozer, A. T., Lawton, E. C., and Bartlett, S. F., 2012, "New Method to Determine Proper Strain Rate for Constant Rate of Strain Consolidation Tests." *Canadian Geotechnical Journal*, Vol. 49, No. 1, January, pp. 18-26.
- Raymond, G. P., and Wahls, H. E. (1976). "Estimating One-Dimensional Consolidation, Including Secondary Compression of Clay Loaded from Overconsolidated to Normally Consolidated State," Special Report 163, Transportation Research Board, pp. 17-23.
- Saye, S. R., and Ladd, C. C. (2000). "Design and Performance of the Foundation Stabilization Treatments for the Reconstruction of Interstate 15 in Salt Lake City, Utah," Unpublished report presented to URS Consultants, June 24, 2000, 92 p.
- Takeda, T., Sugiyama, M., Akaishi, M., and Chang, H. (2013). "Initial Rate of Secondary Compression in One-Dimensional Consolidation Analysis," *Journal of GeoEngineering*, Vol. 8, No. 2, pp. 55-60, August 2013.
- Terzaghi, K., Peck, R. B., and Mesri, G. (1996). *Soil Mechanics in Engineering Practice*, John Wiley and Sons, Inc., New York, New York.

## **APPENDIX A PLOTS FOR PRECONSOLIDATION STRESS**

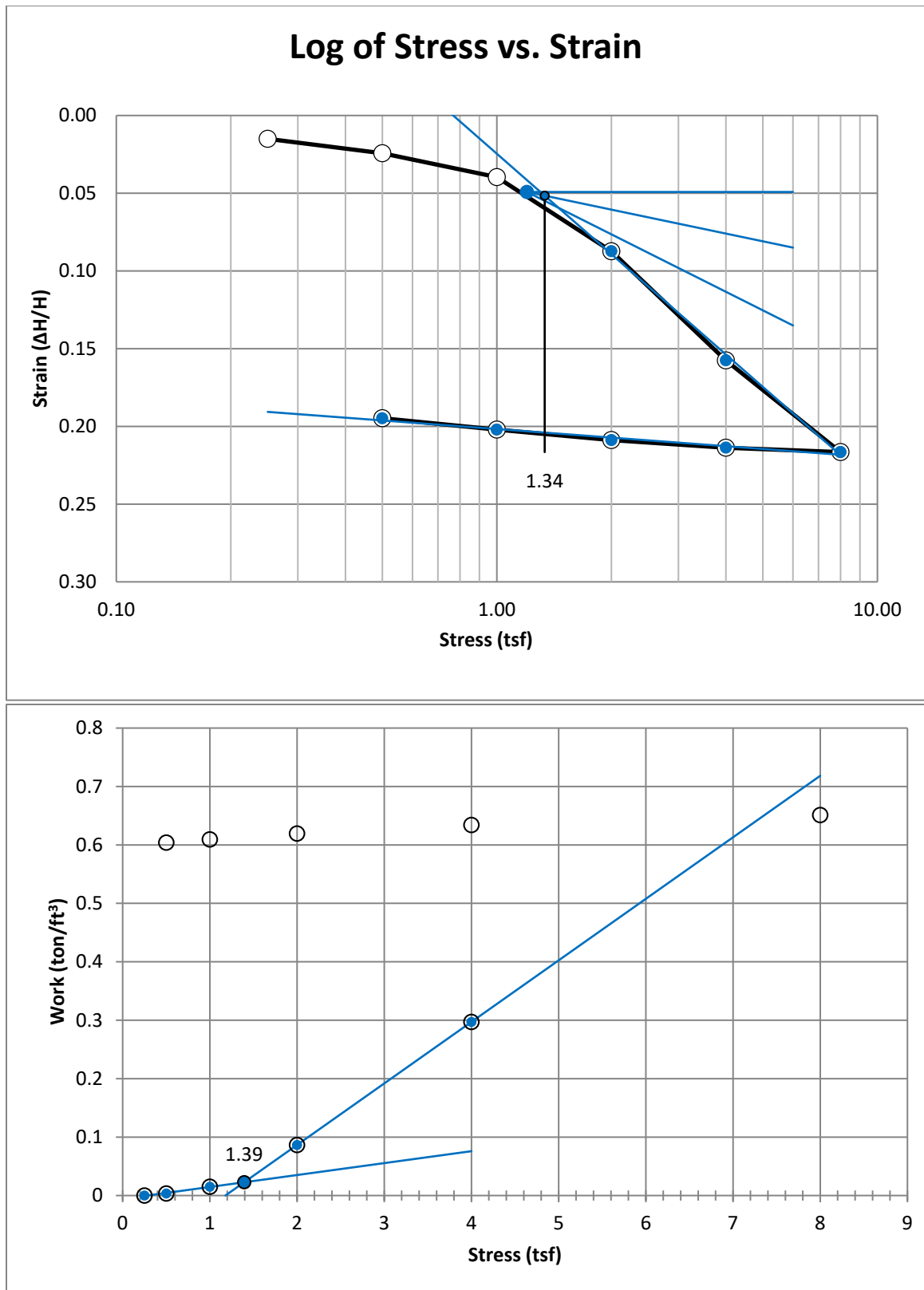


Figure A1 400 South at 15-17 feet



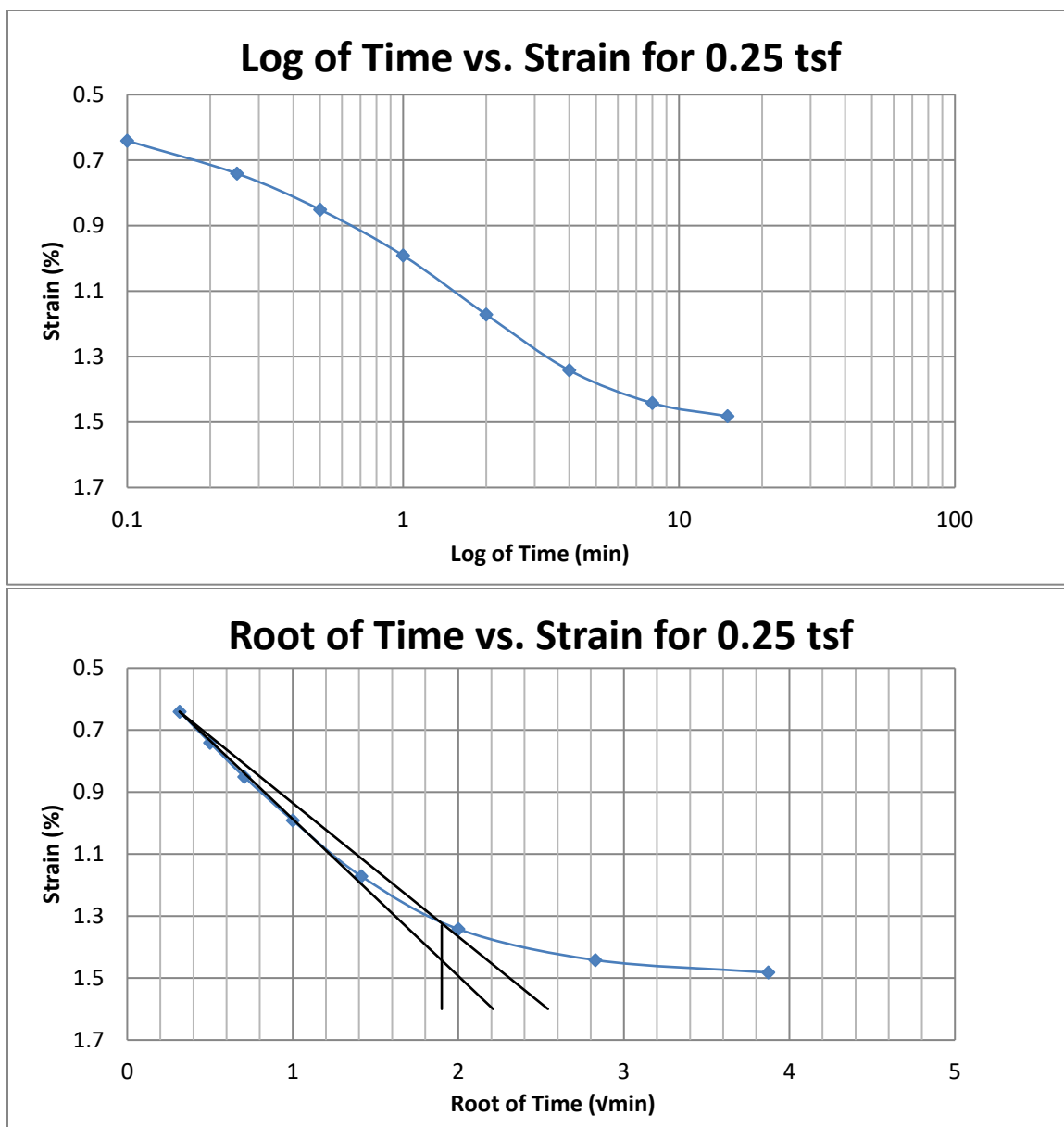


Figure A2 400 South at 15-17 feet

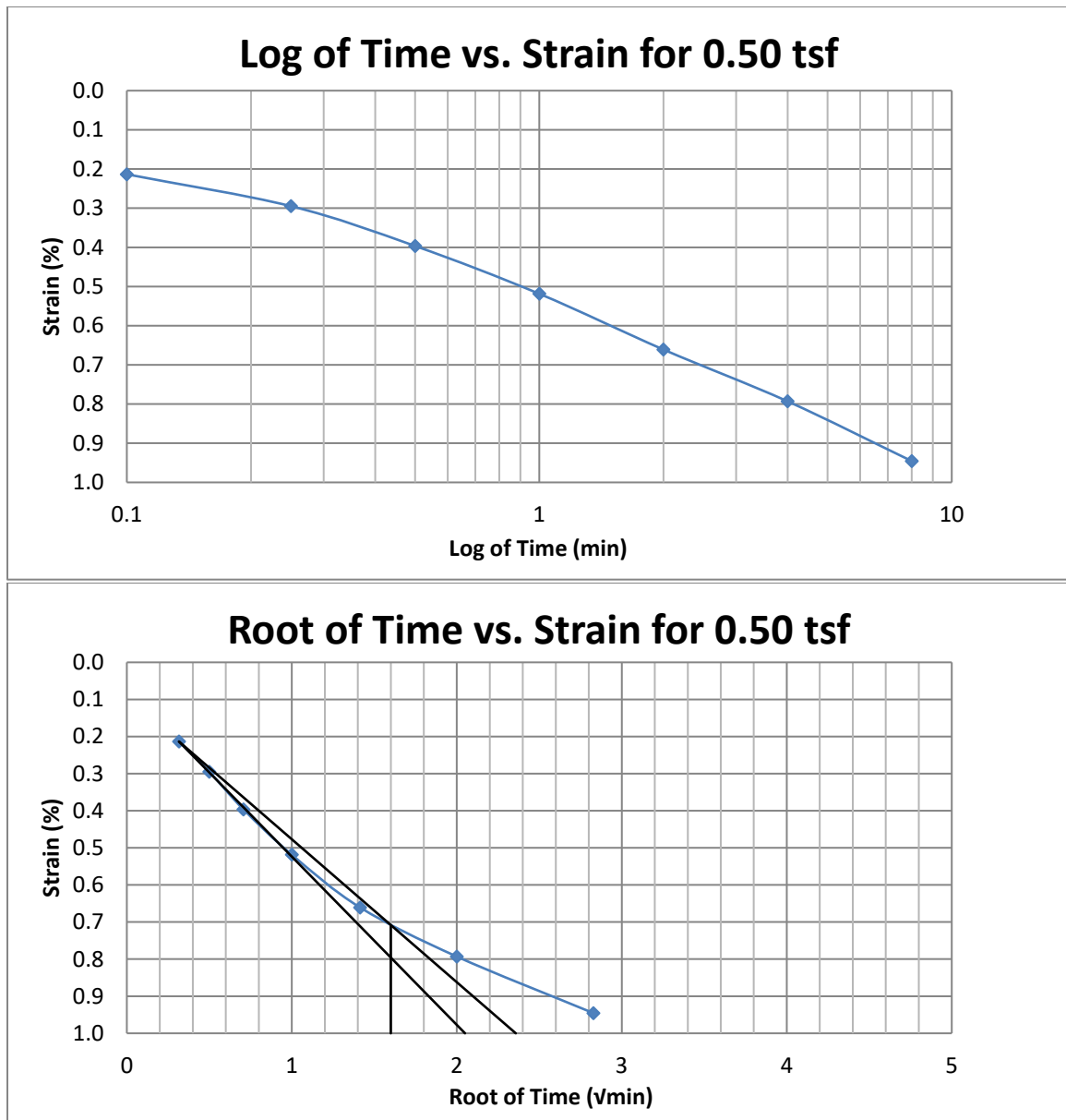


Figure A3 400 South at 15-17 feet

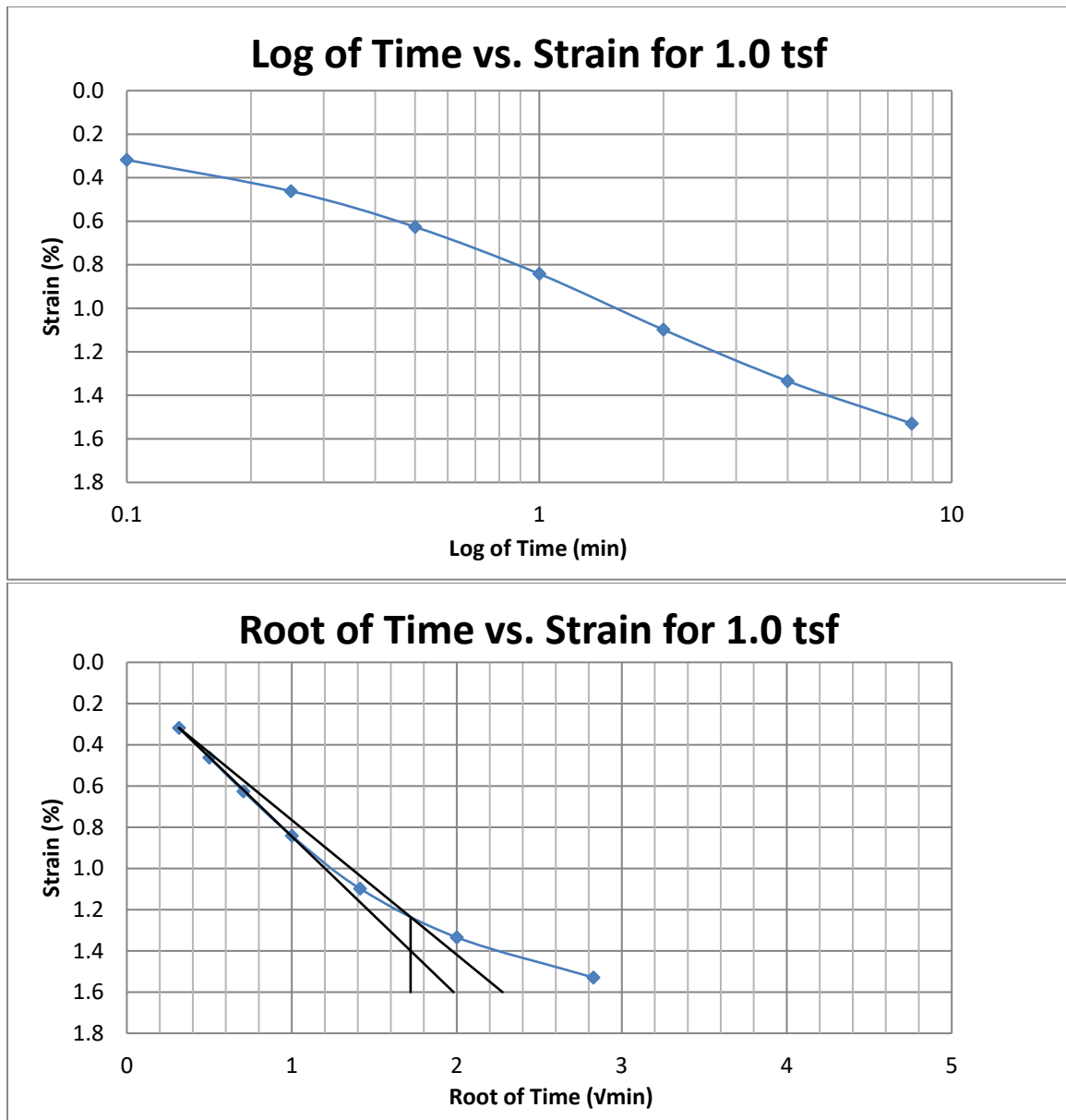


Figure A4 400 South at 15-17 feet

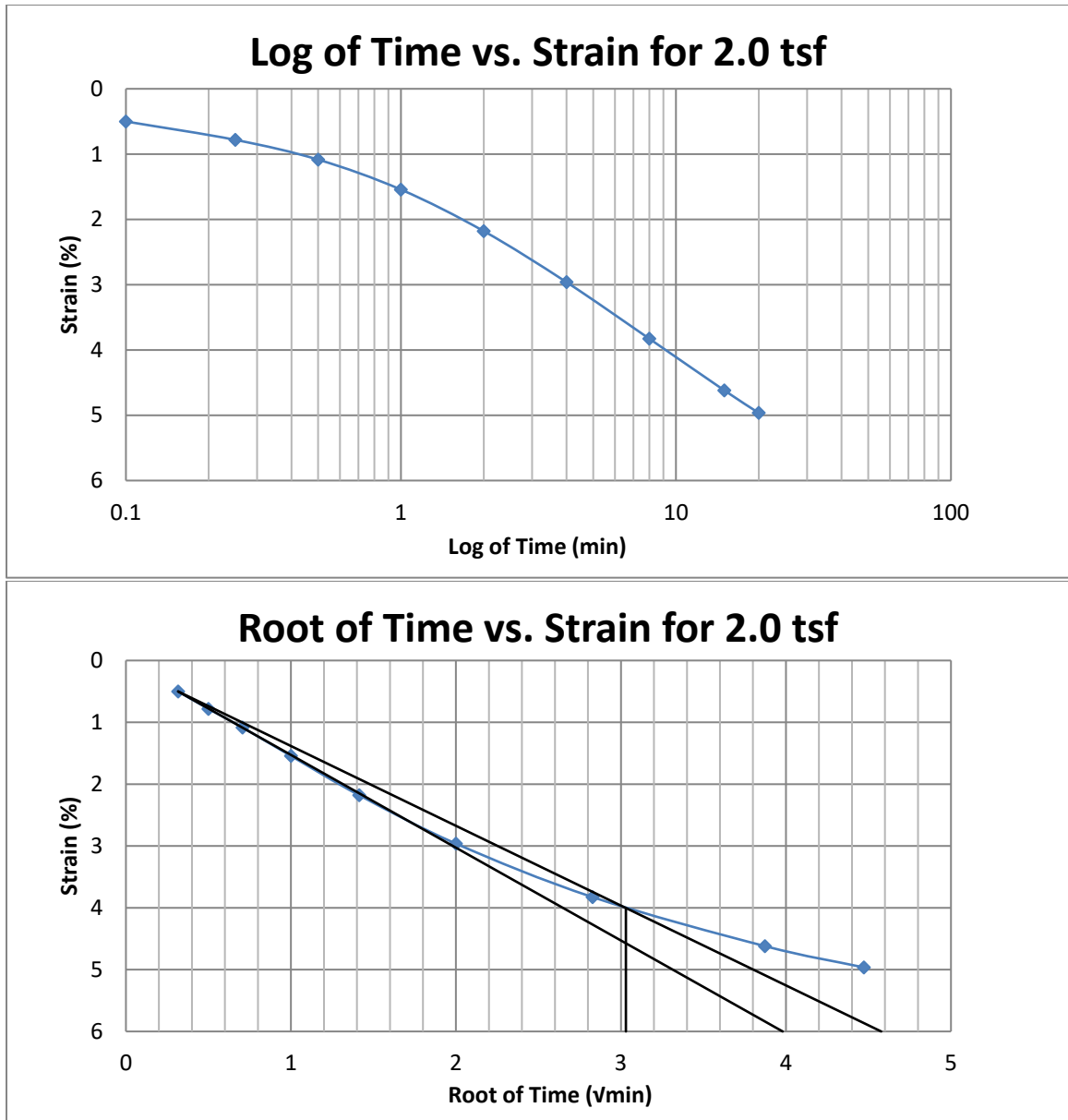


Figure A5 400 South at 15-17 feet

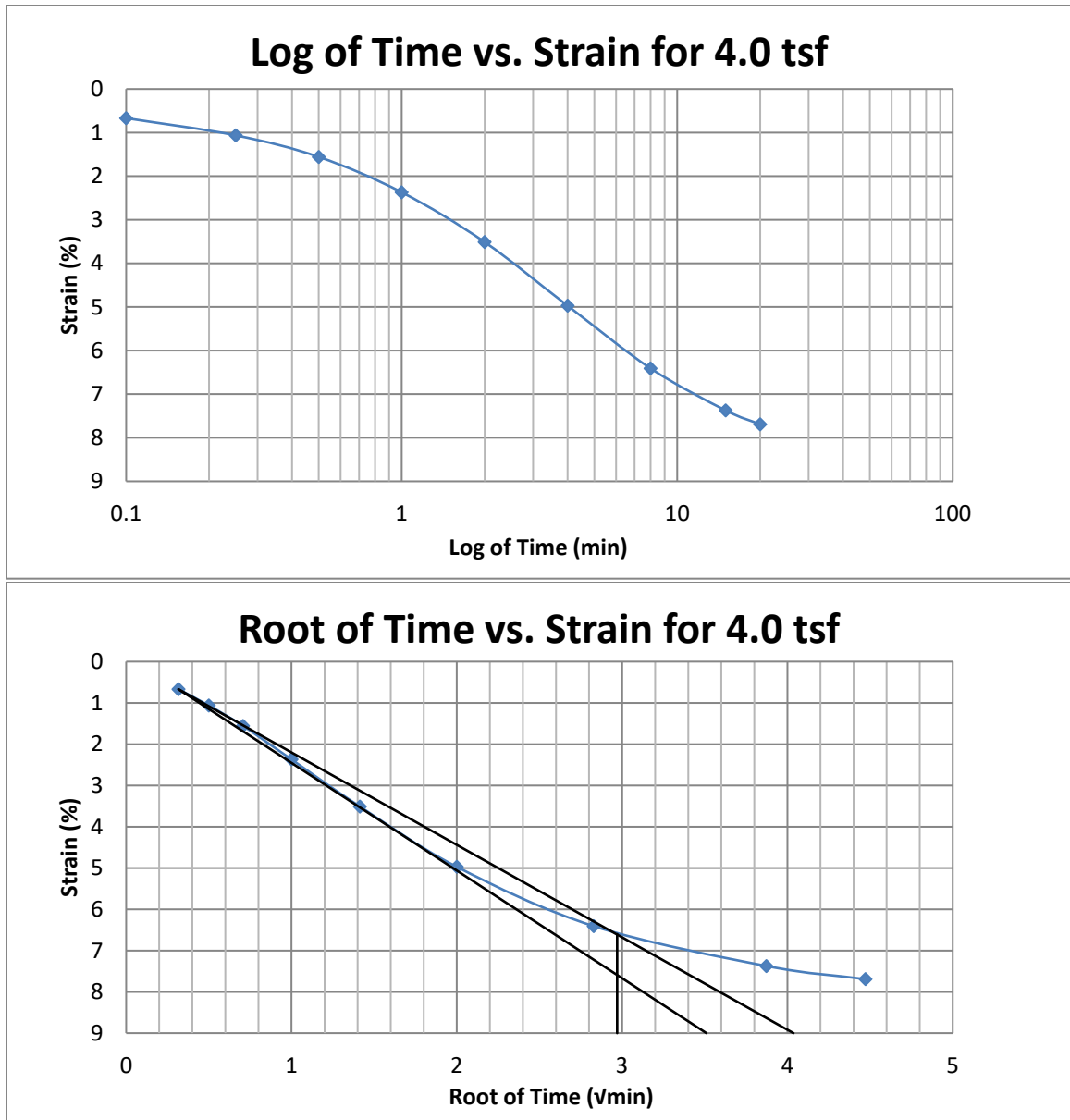


Figure A6 400 South at 15-17 feet

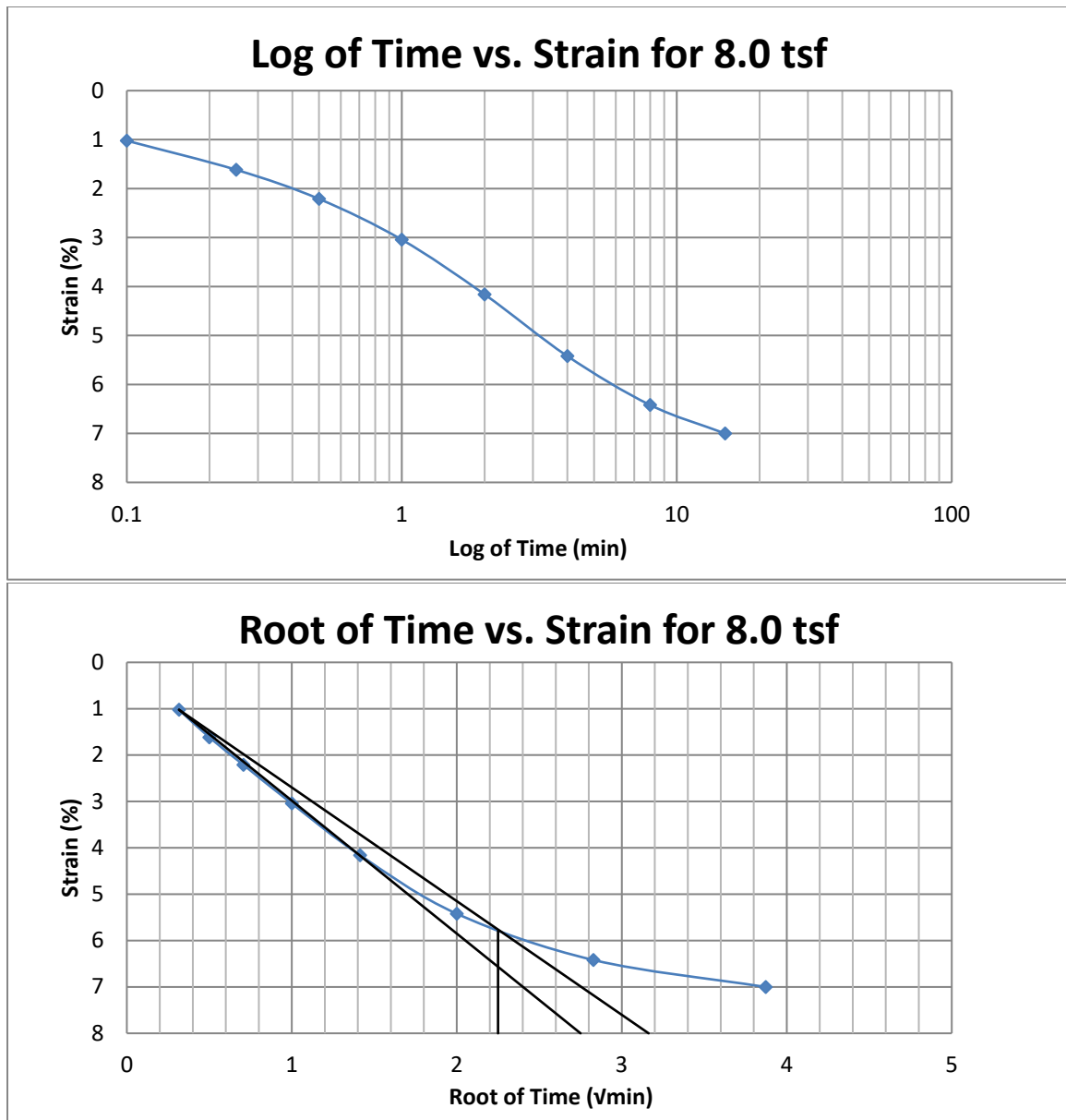


Figure A7 400 South at 15-17 feet



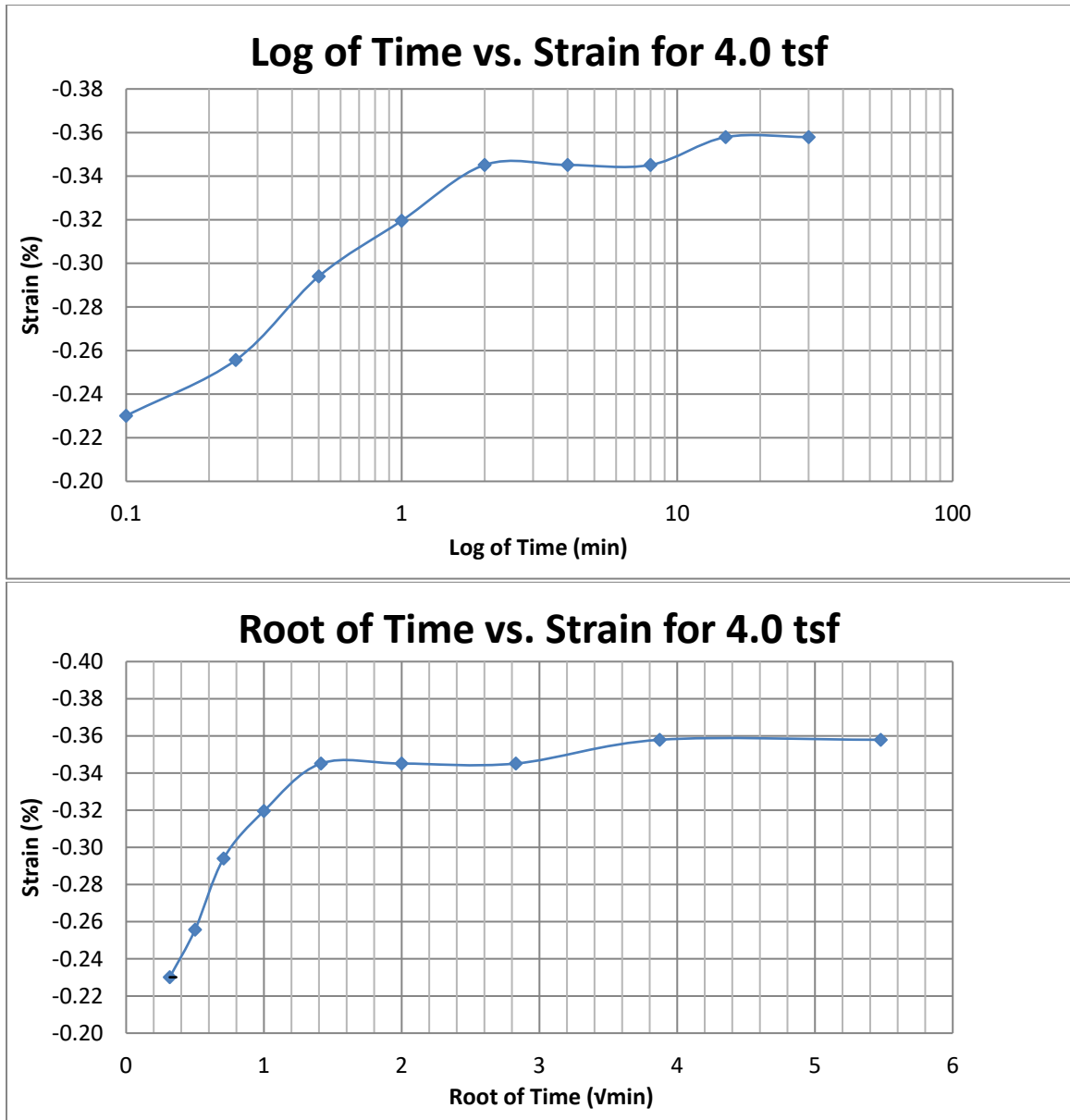


Figure A8 400 South at 15-17 feet

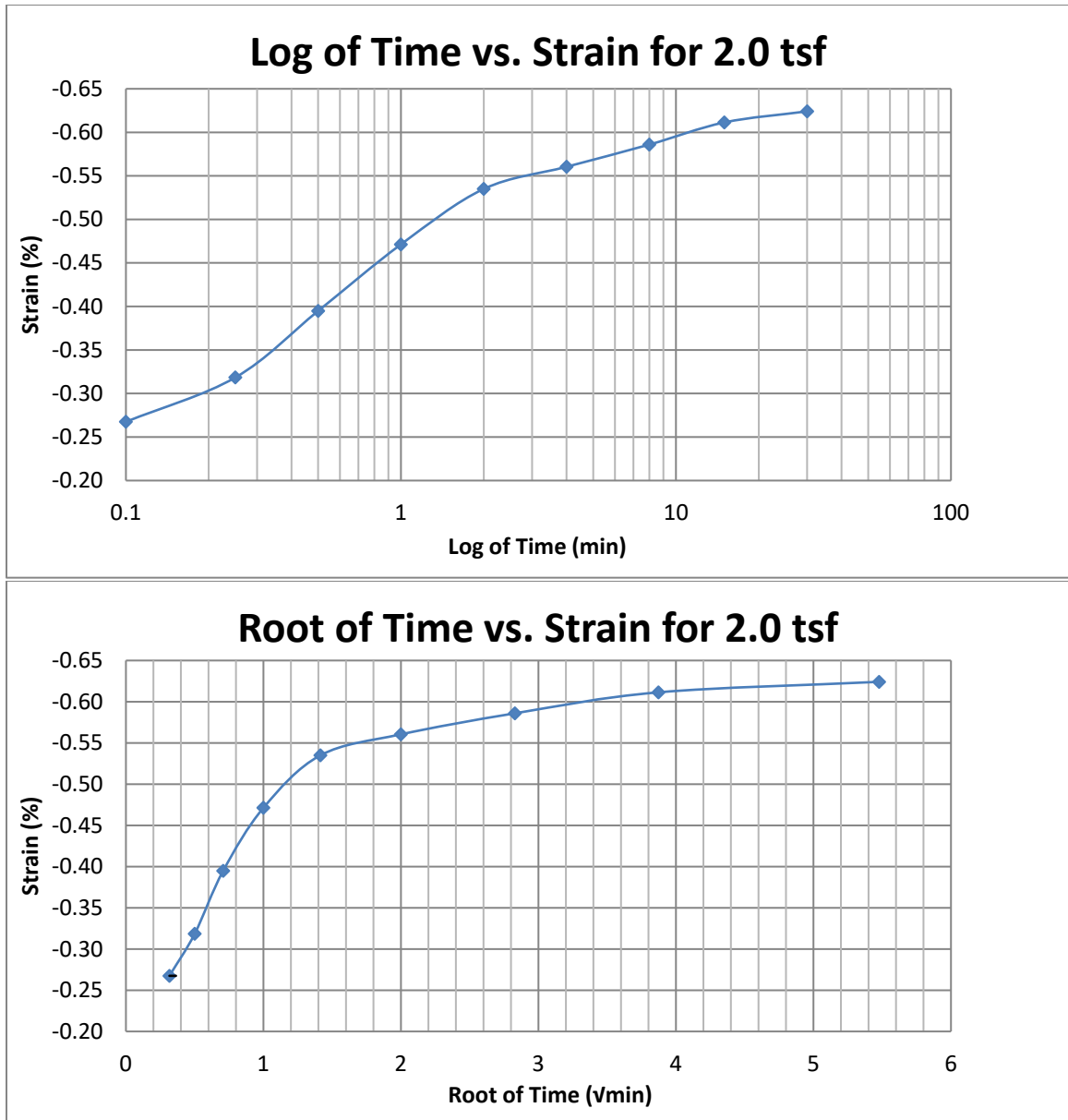


Figure A9 400 South at 15-17 feet

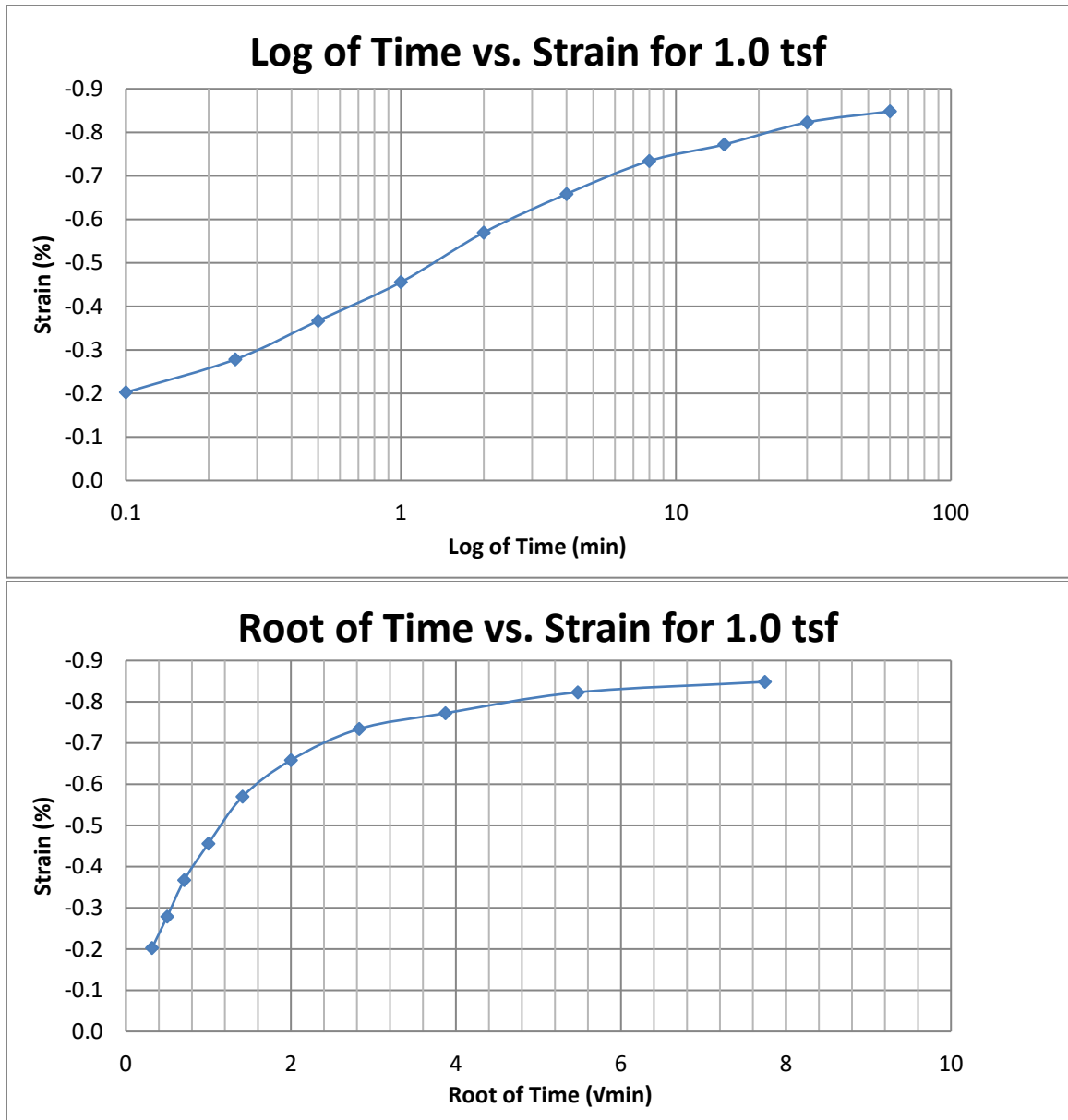
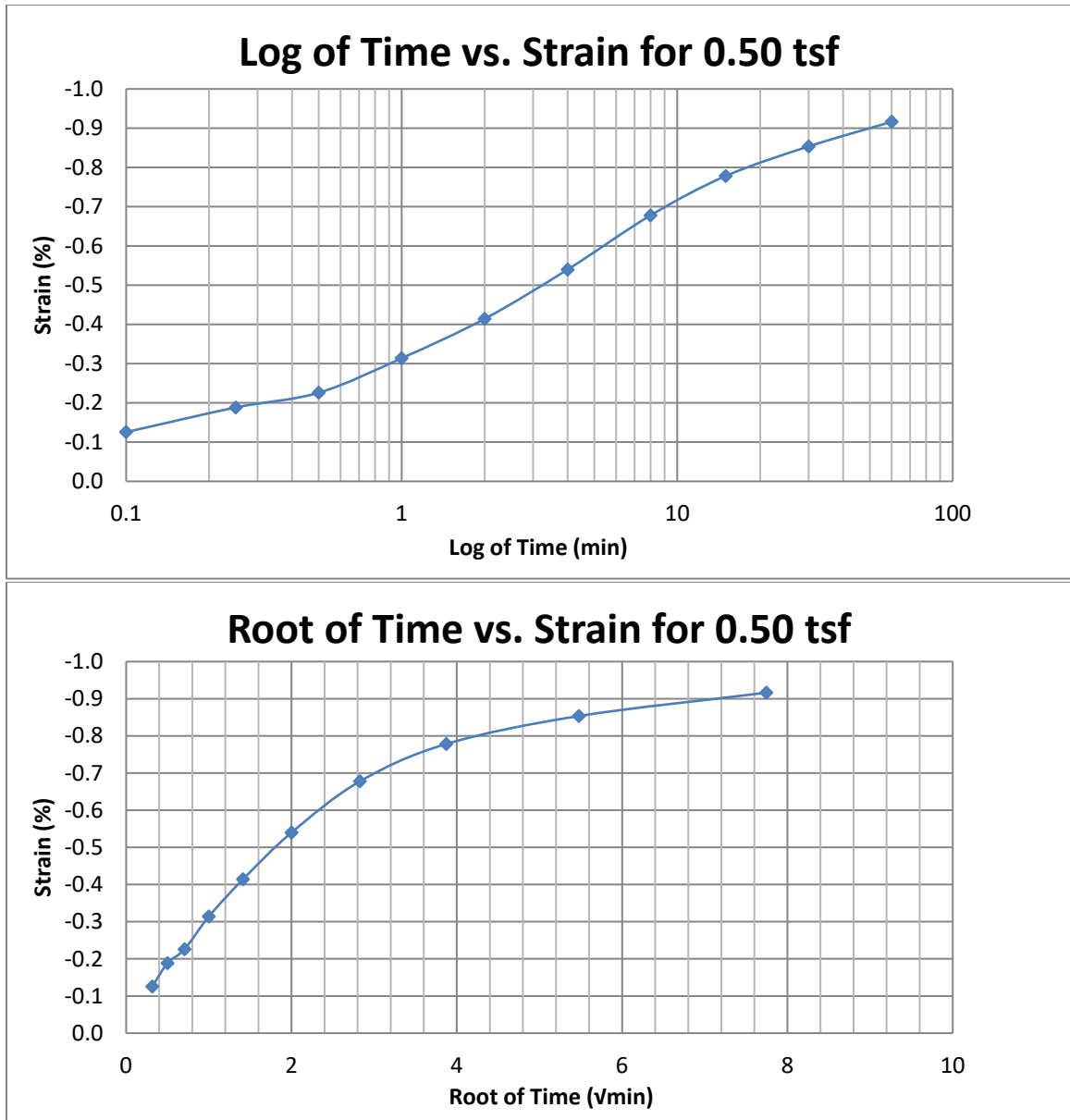


Figure A10 400 South at 15-17 feet



**Figure A11 400 South at 15-17 feet**

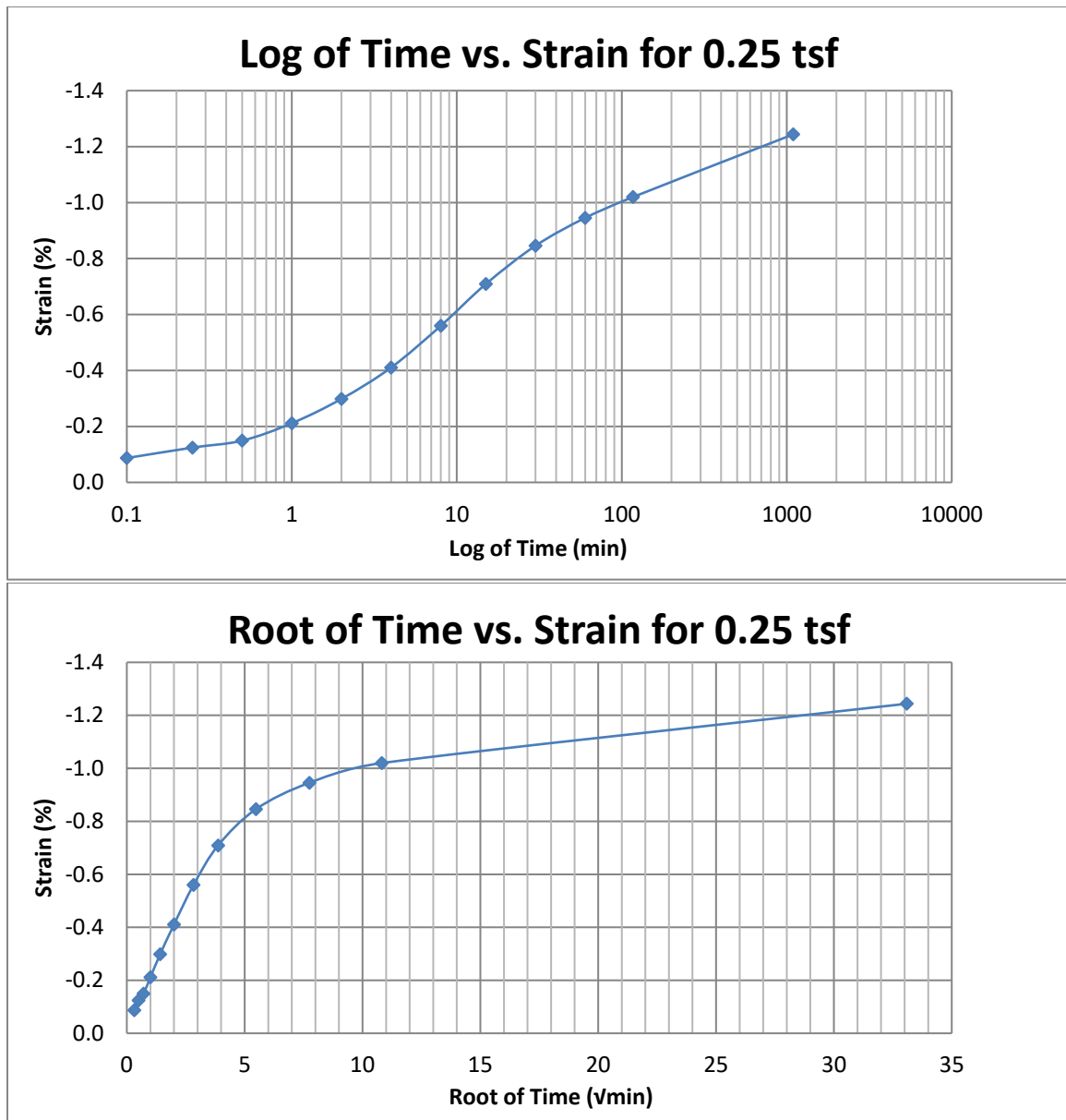
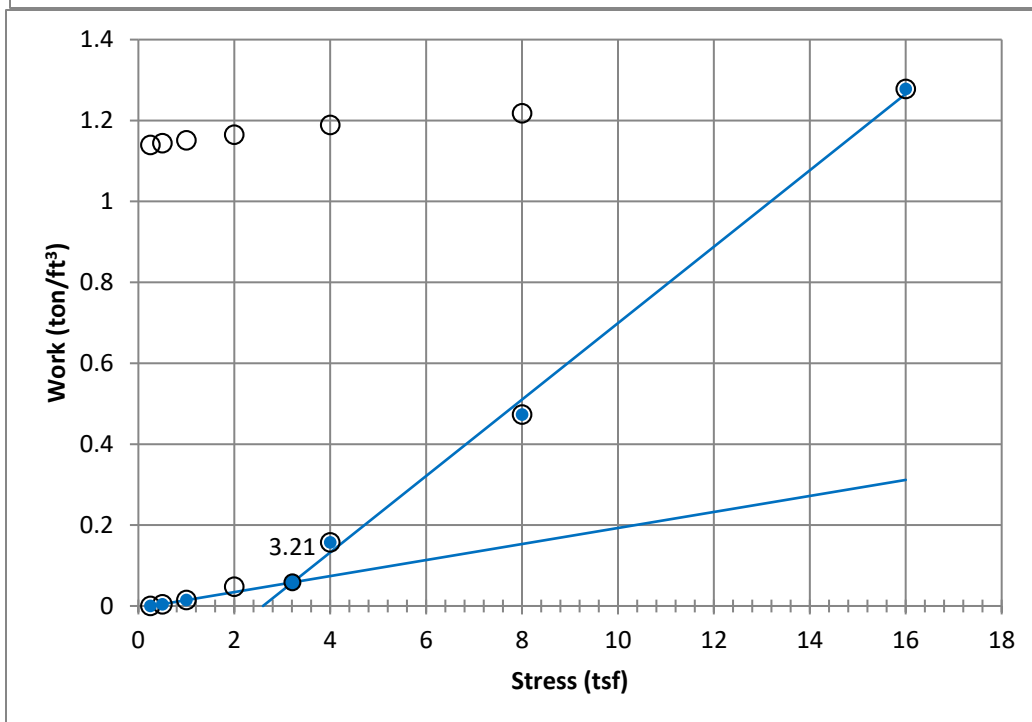
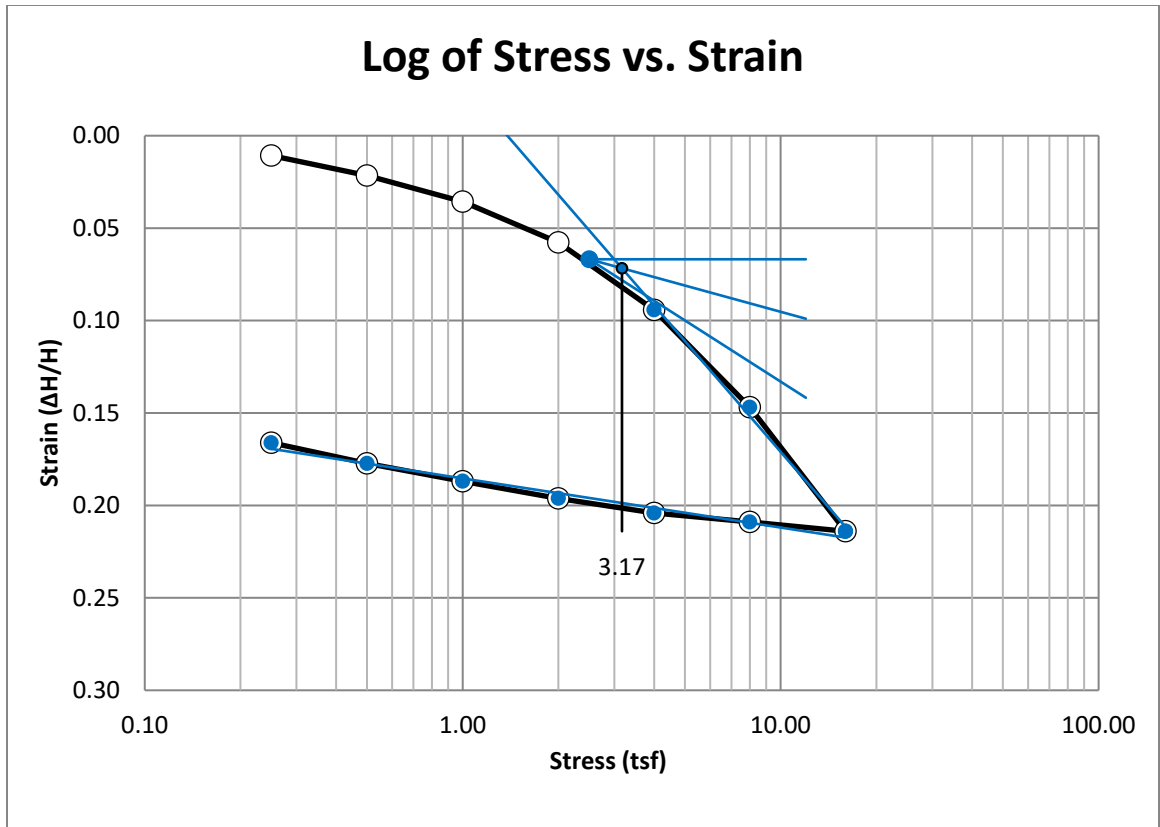


Figure A12 400 South at 15-17 feet



**Figure A13 400 South at 20-22 feet**



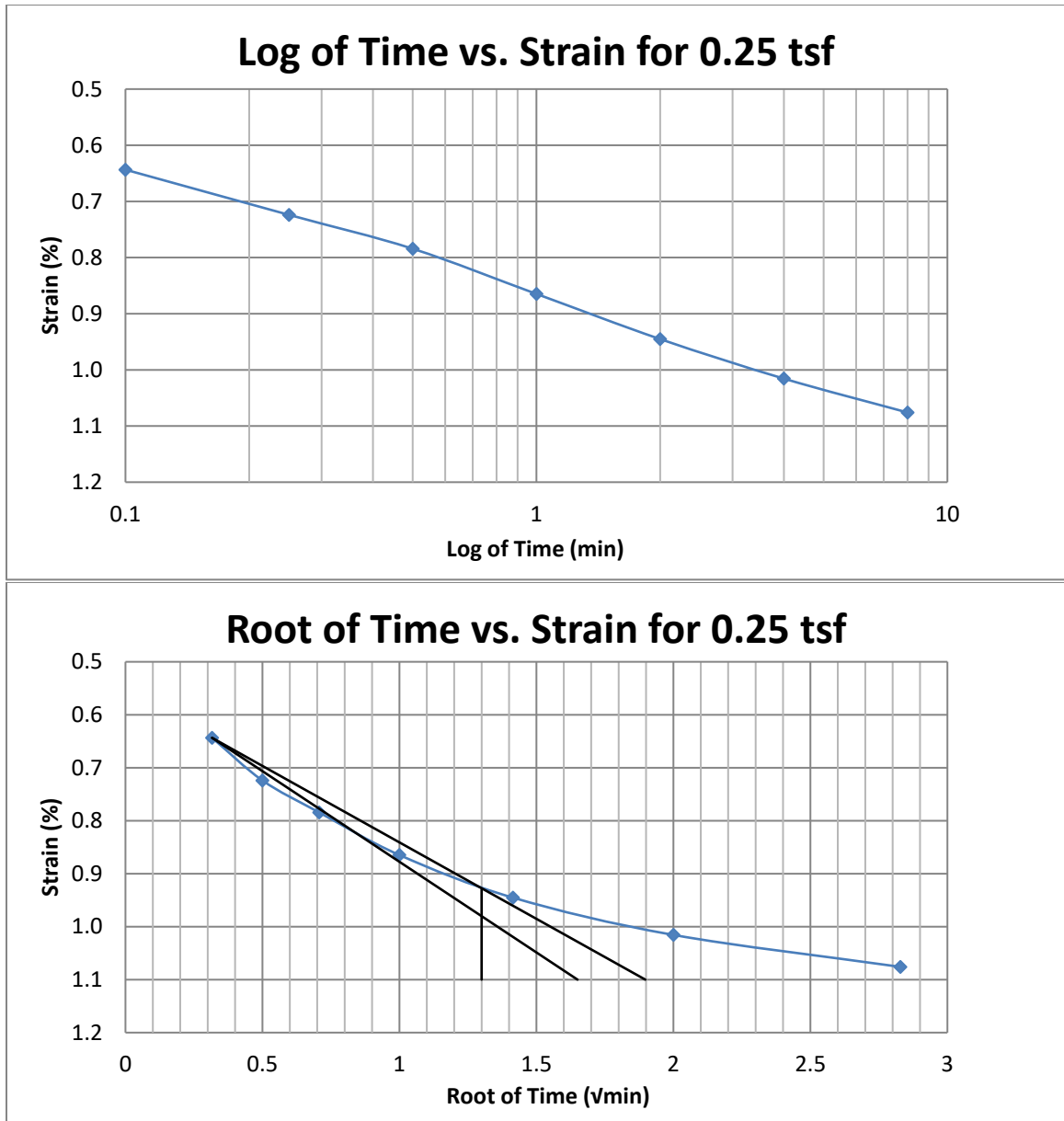


Figure A14 400 South at 20-22 feet

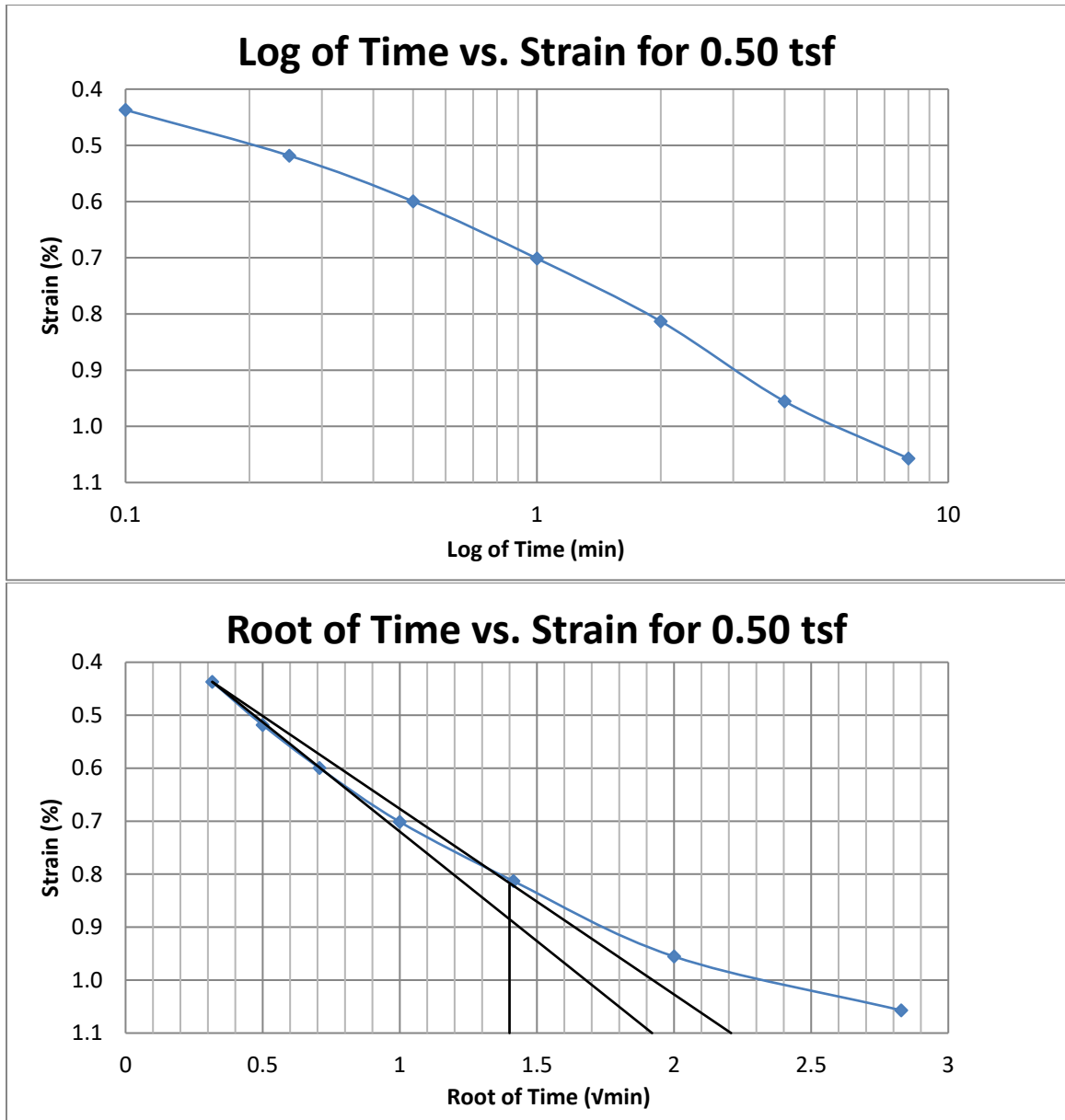


Figure A15 400 South at 20-25 feet

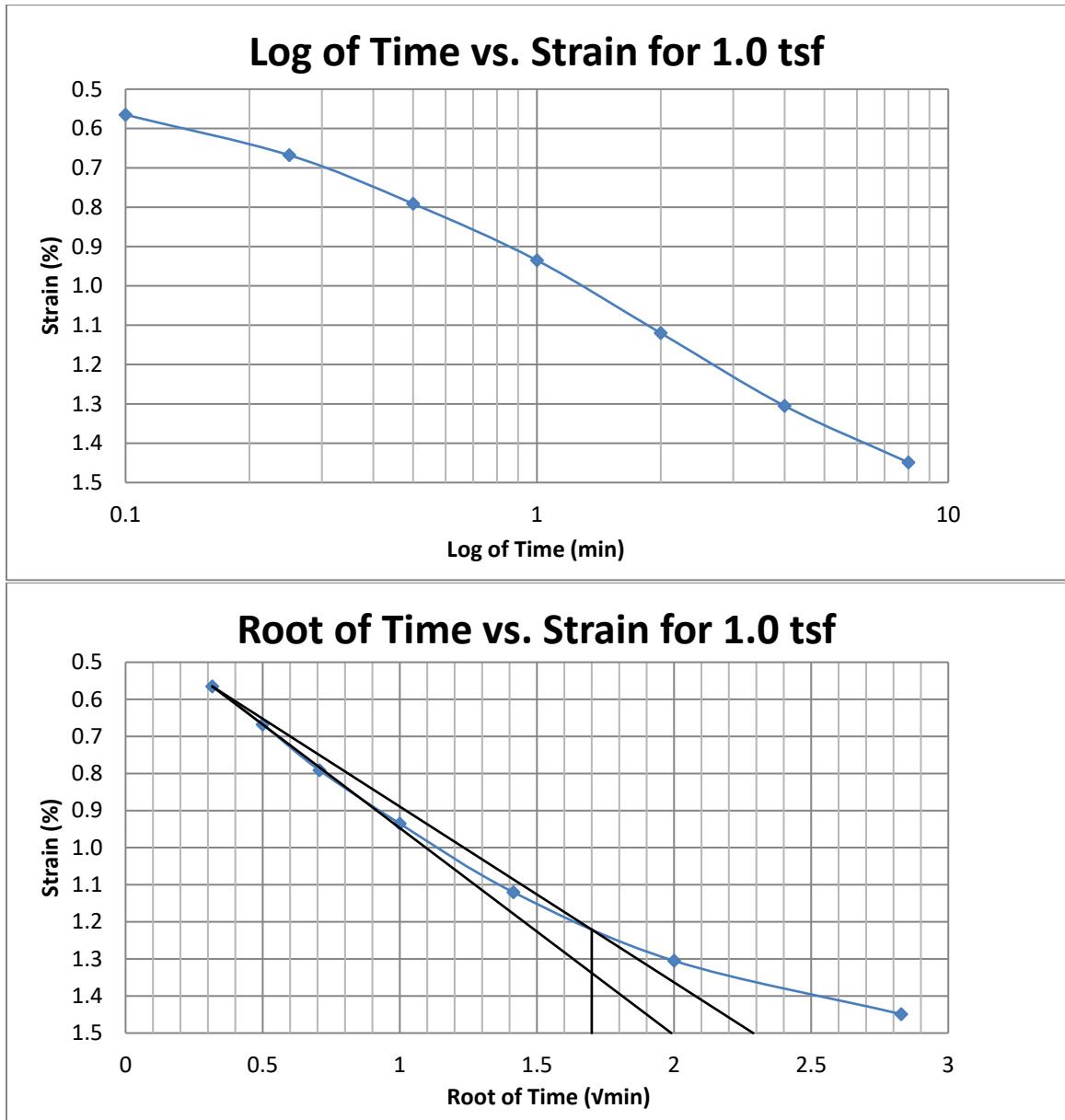


Figure A16 400 South at 20-25 feet

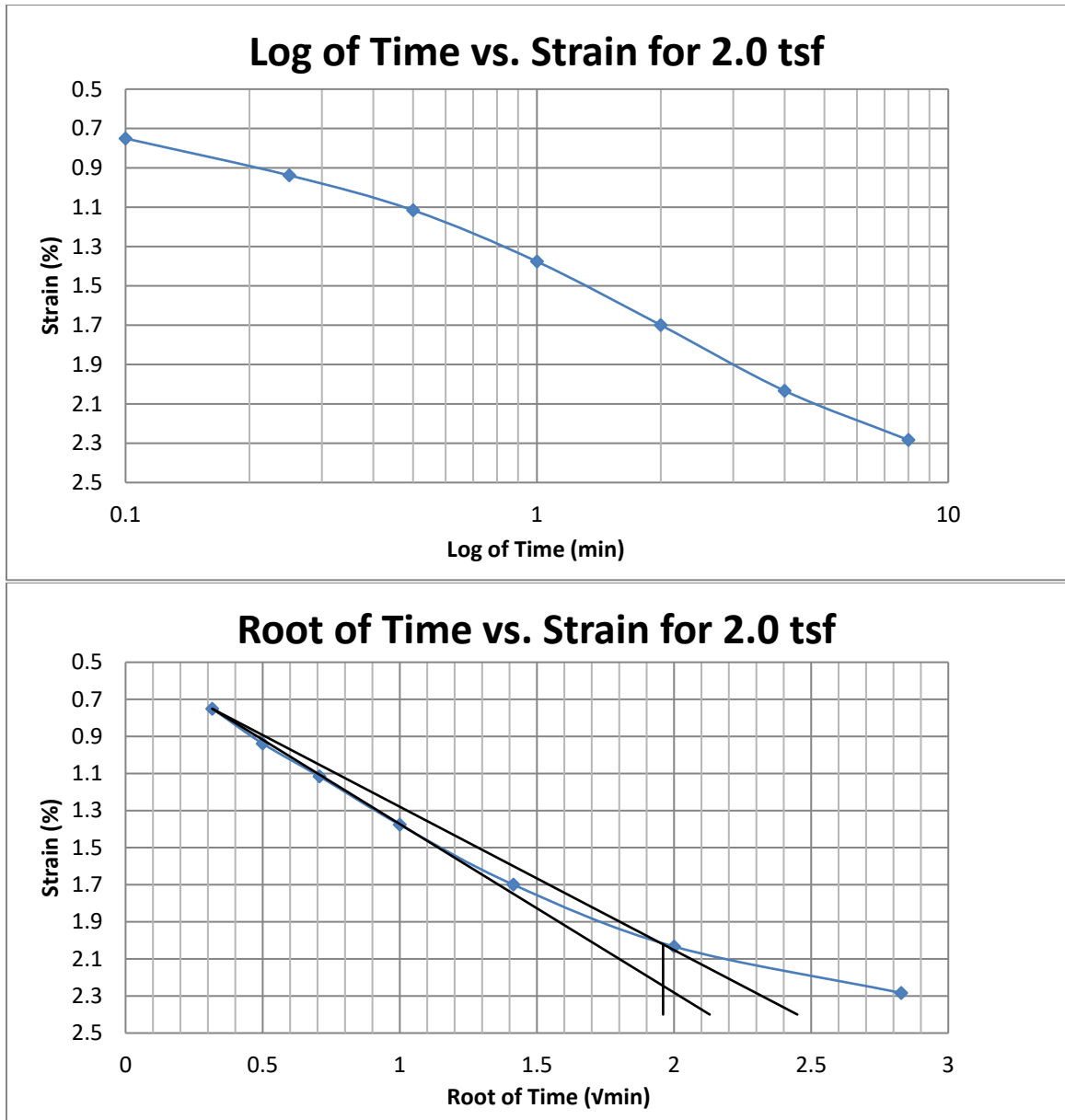


Figure A17 400 South at 20-22 feet

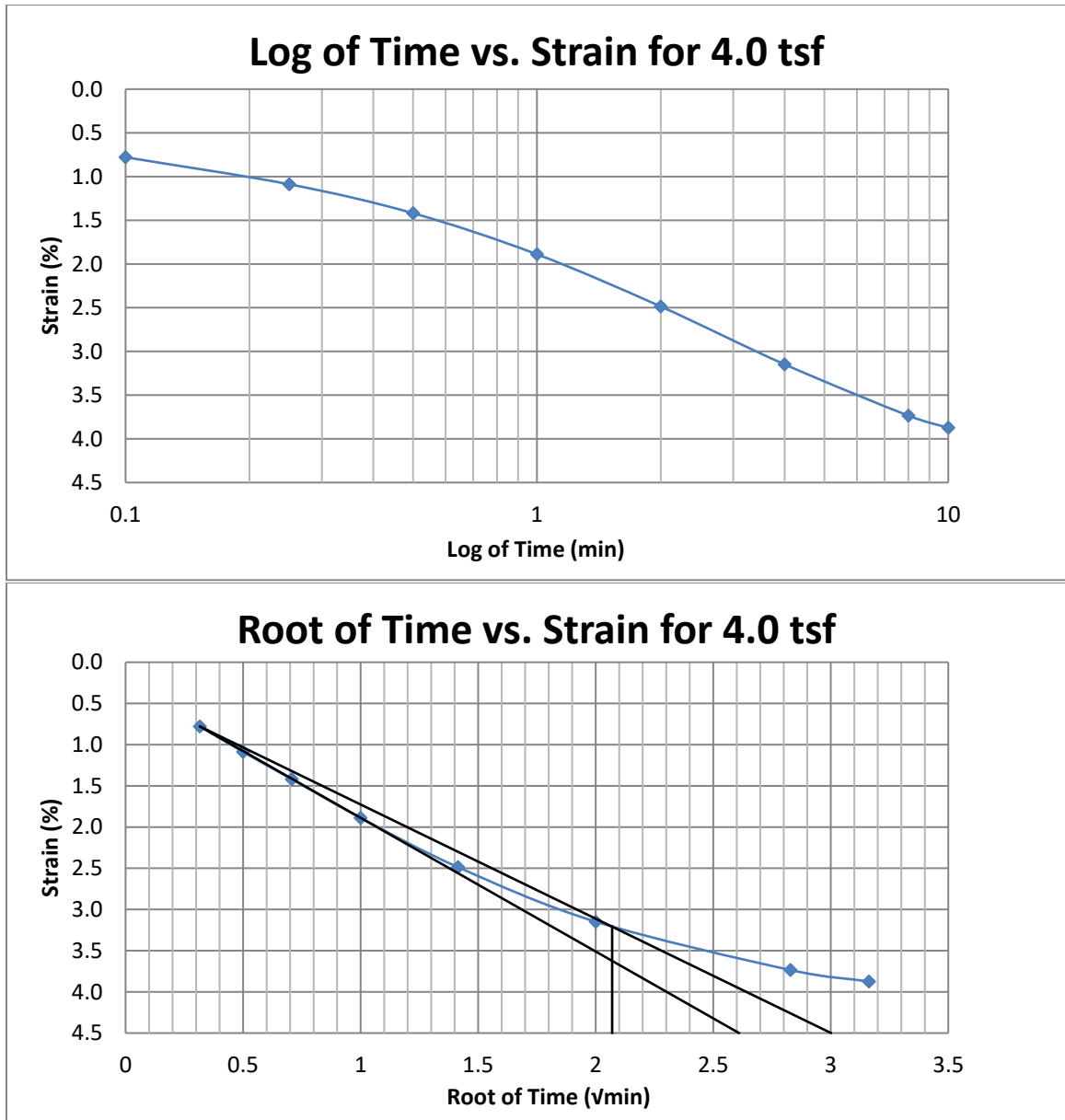


Figure A18 400 South at 20-22 feet

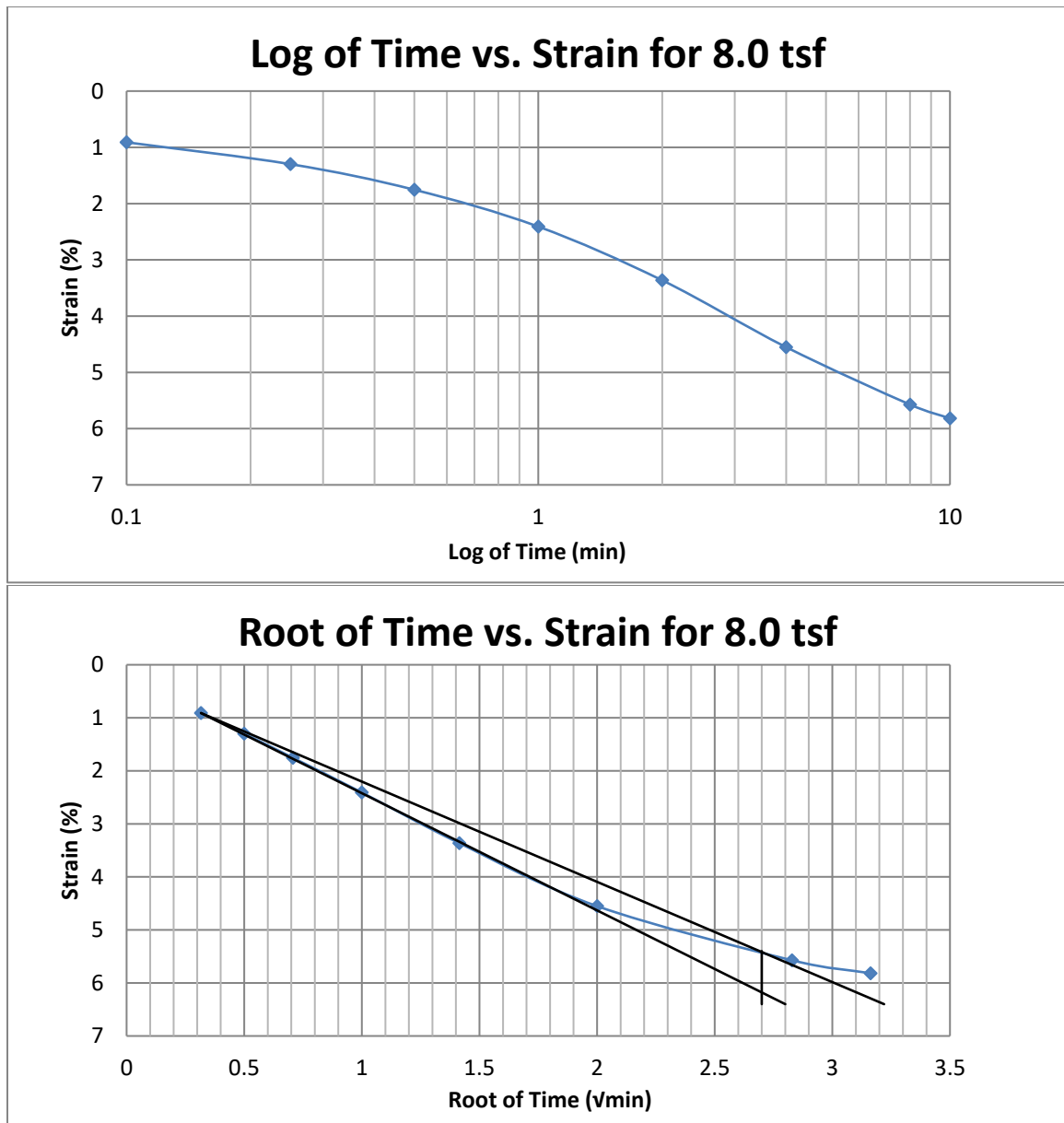


Figure A19 400 South at 20-22 feet



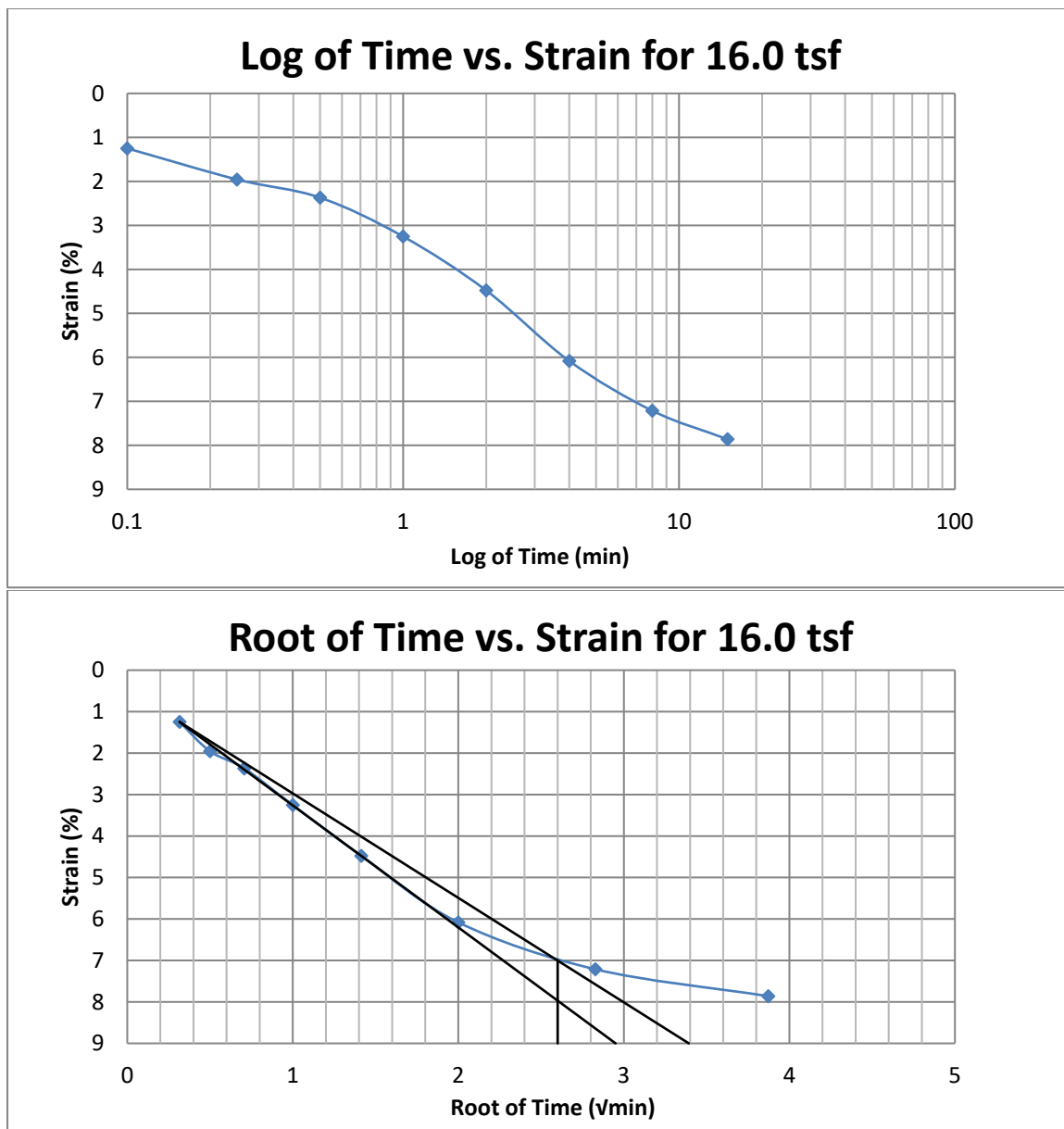


Figure A20 400 South at 20-22 feet

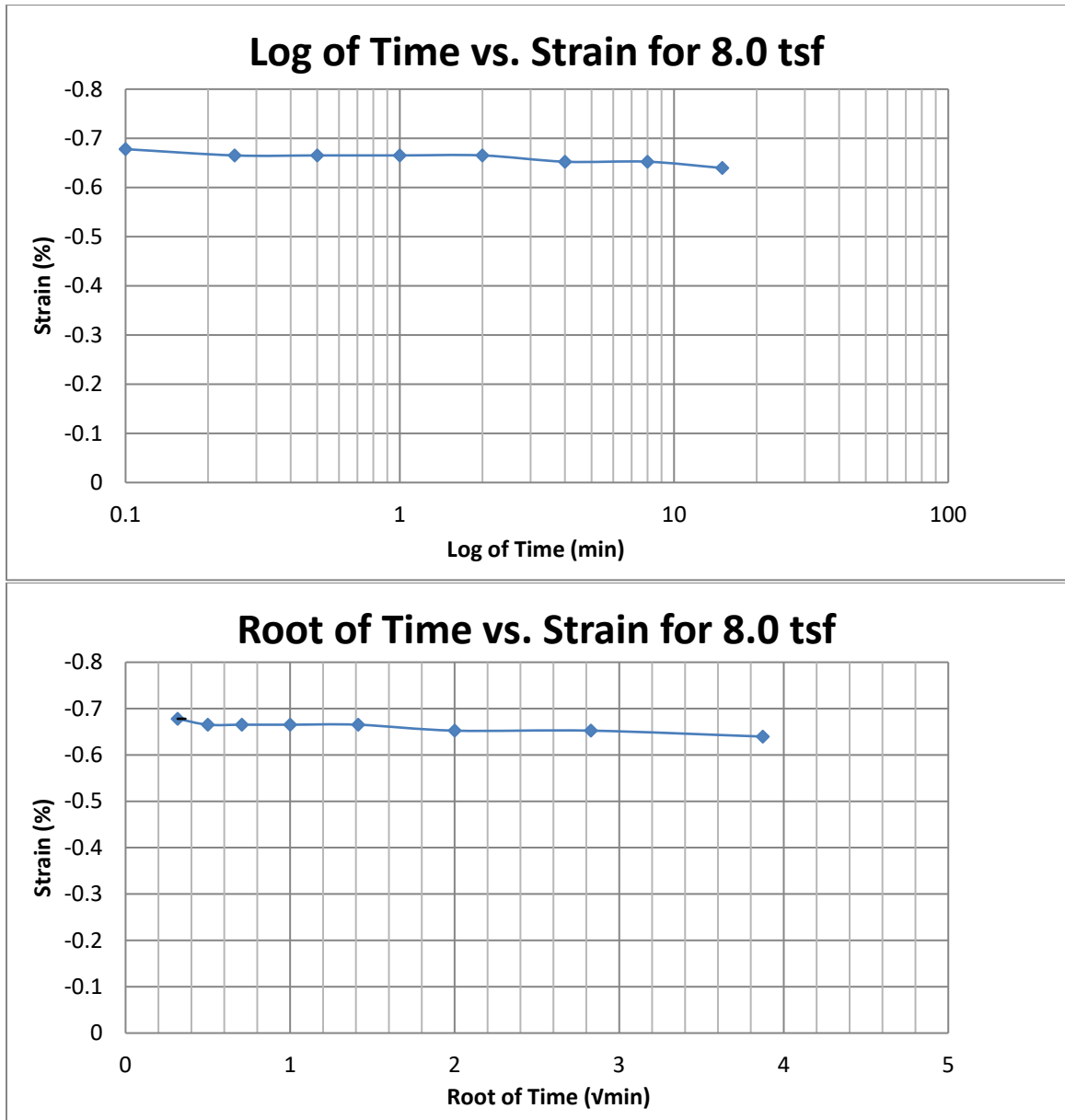


Figure A21 400 South at 20-22 feet

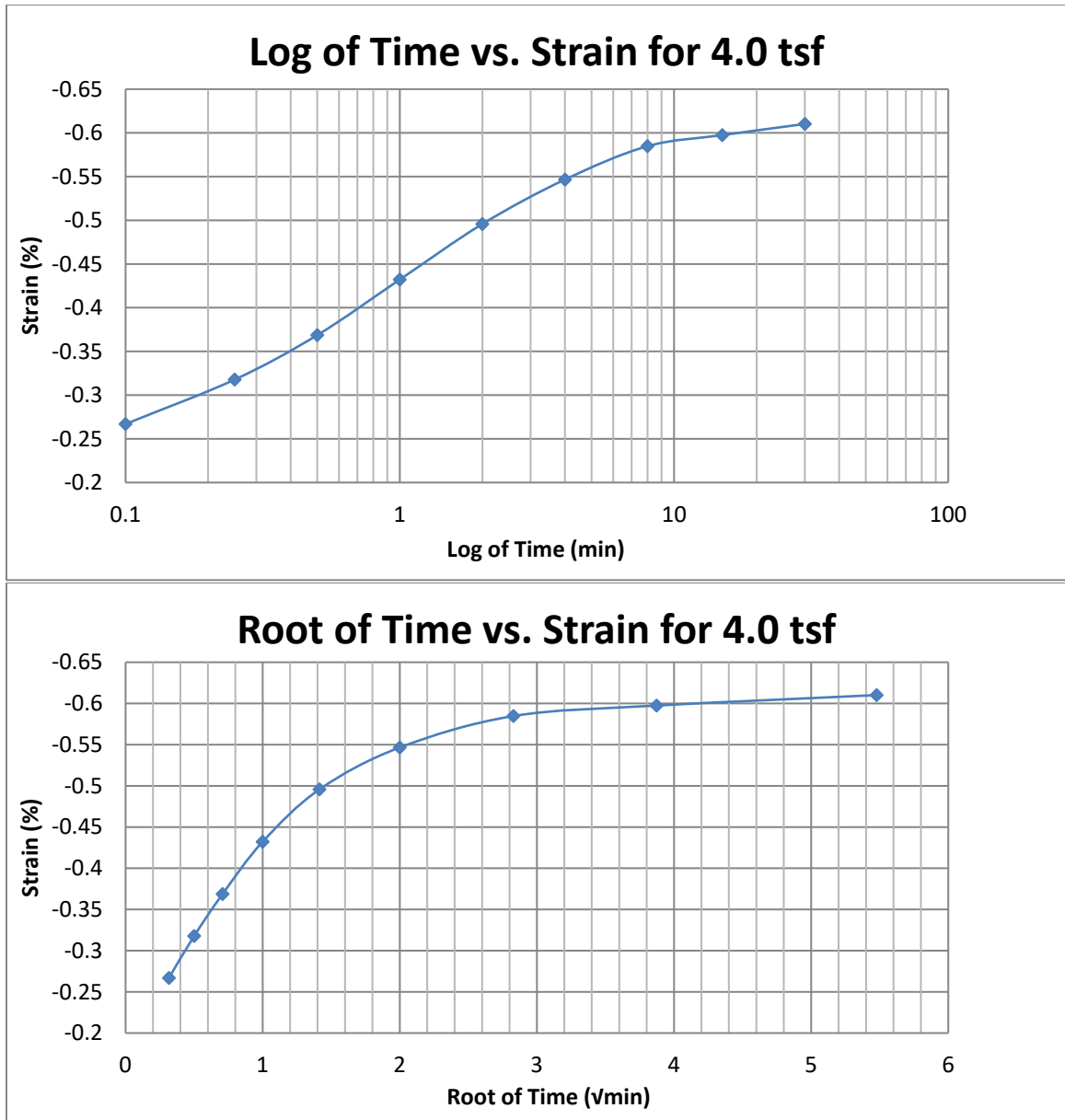


Figure A22 400 South at 20-22 feet

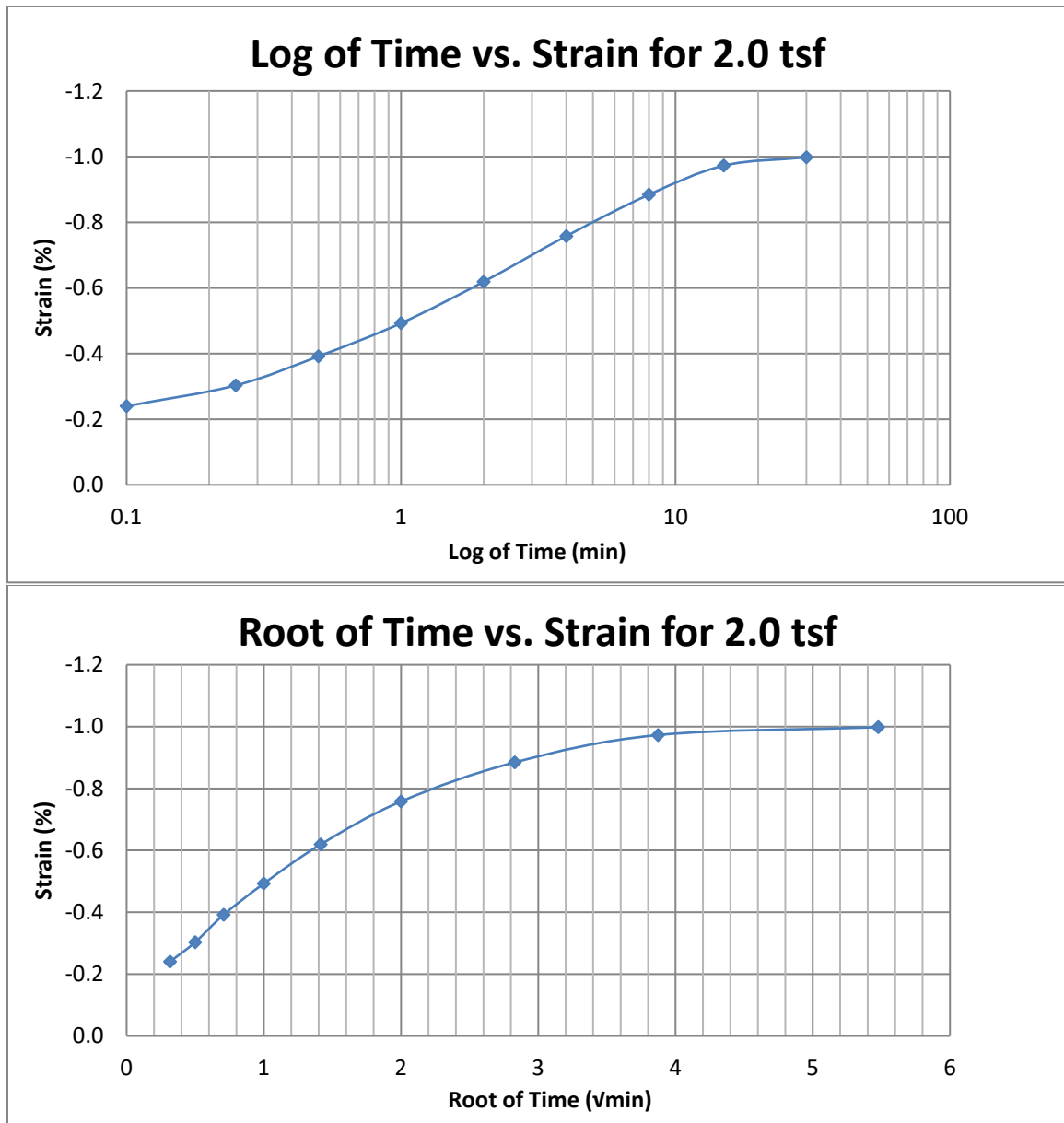


Figure A23 400 South at 20-22 feet

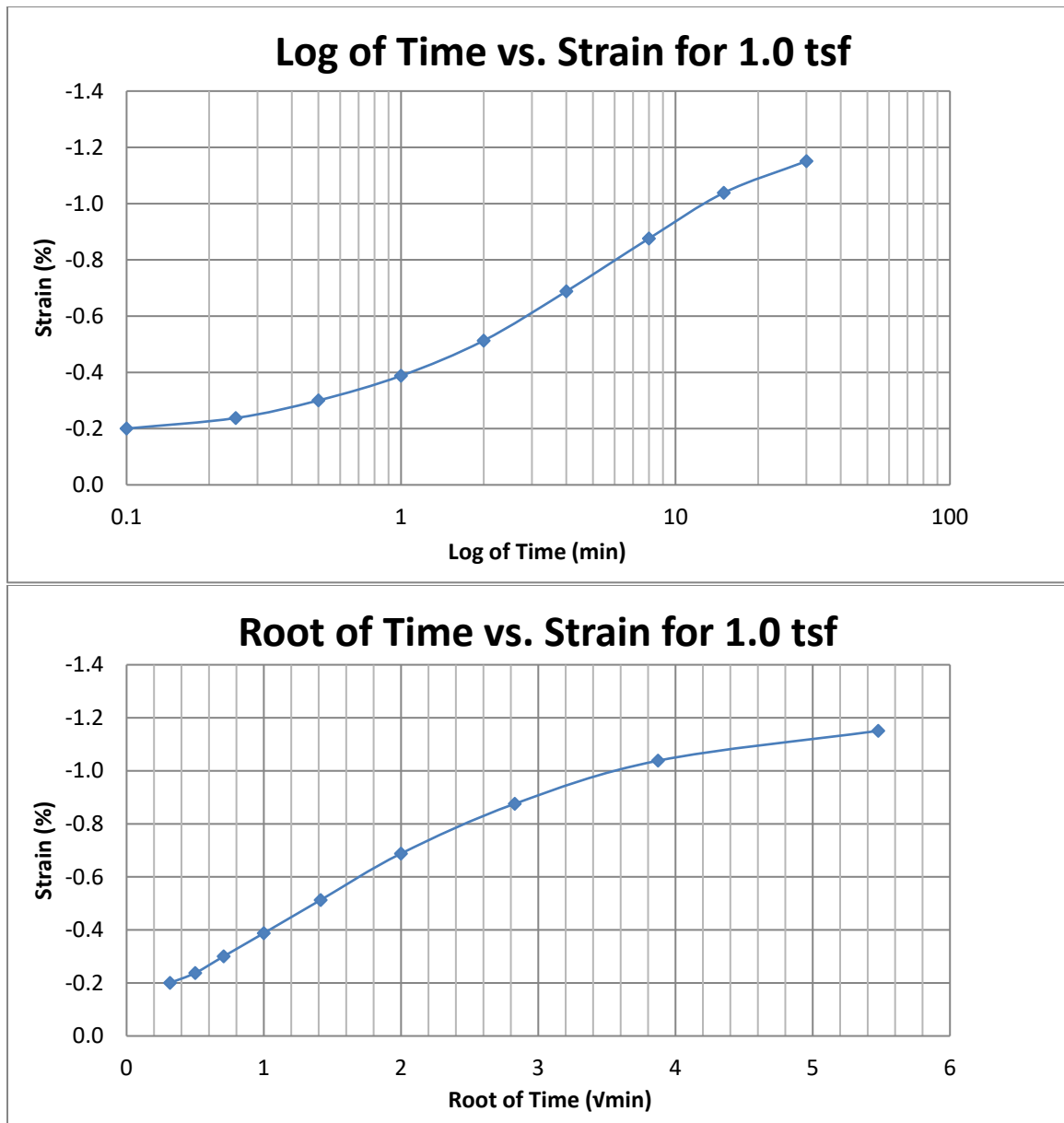


Figure A24 400 South at 20-22 feet

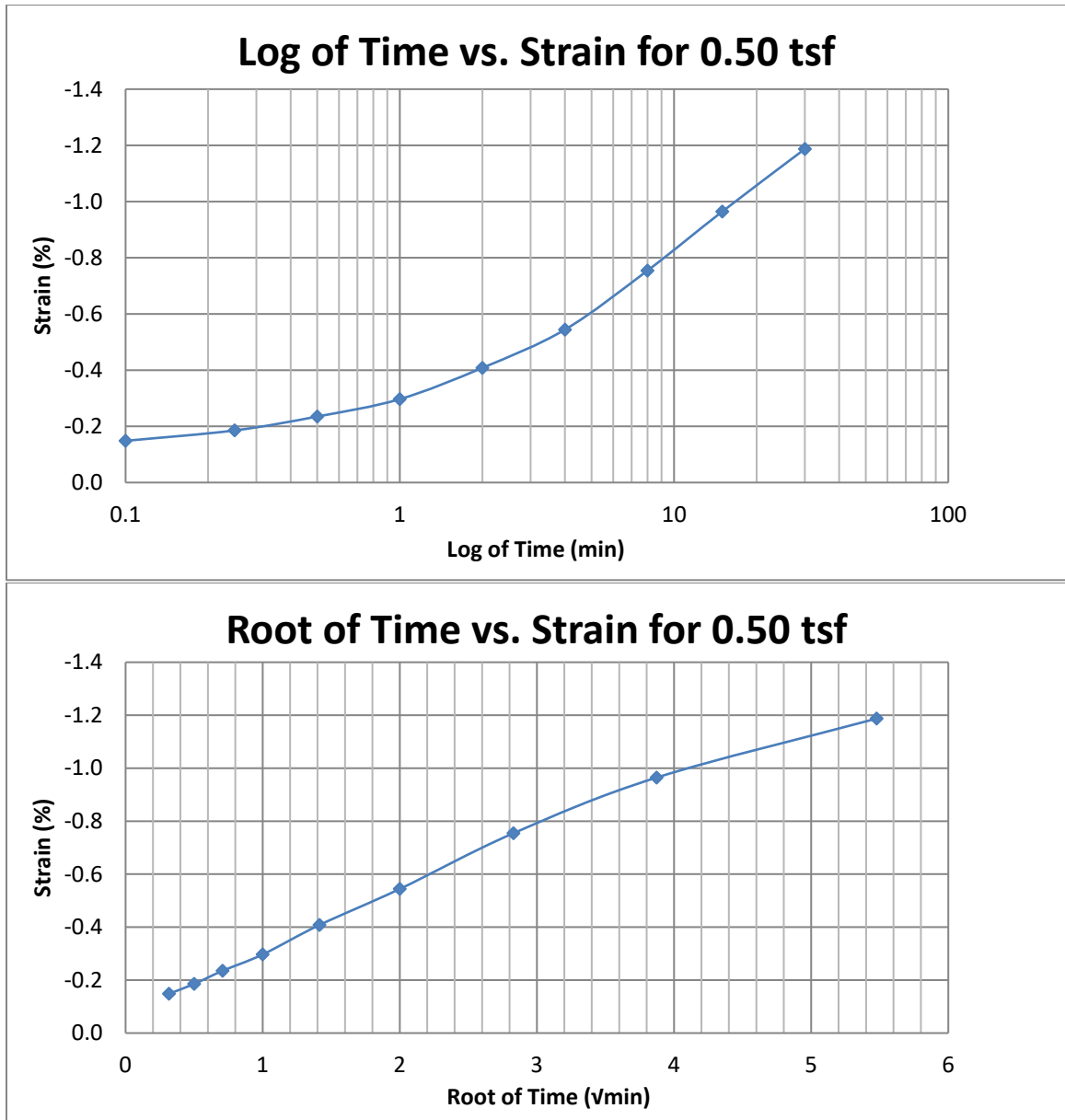


Figure A25 400 South at 20-22 feet

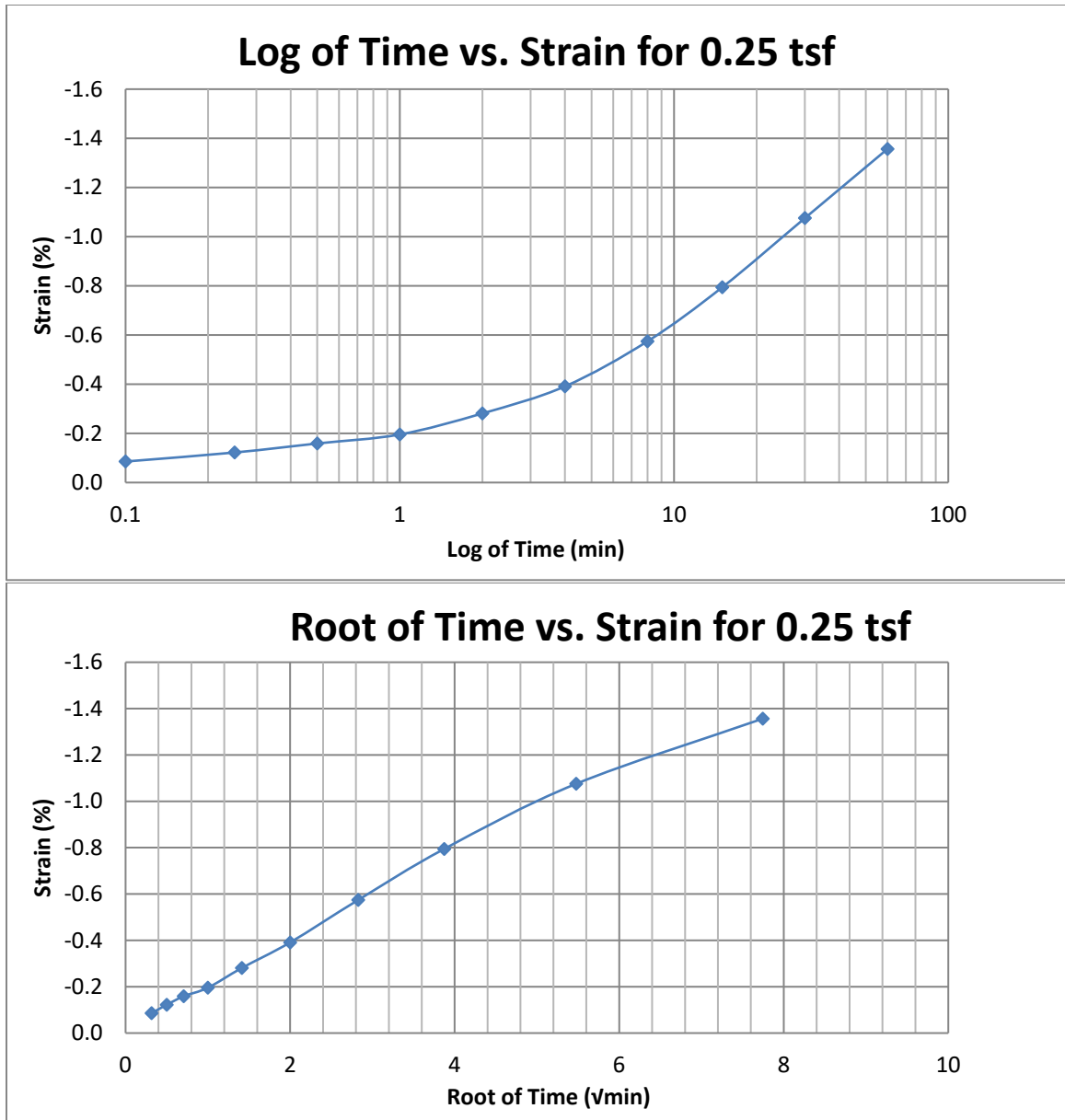


Figure A 26 400 South at 20-22 feet



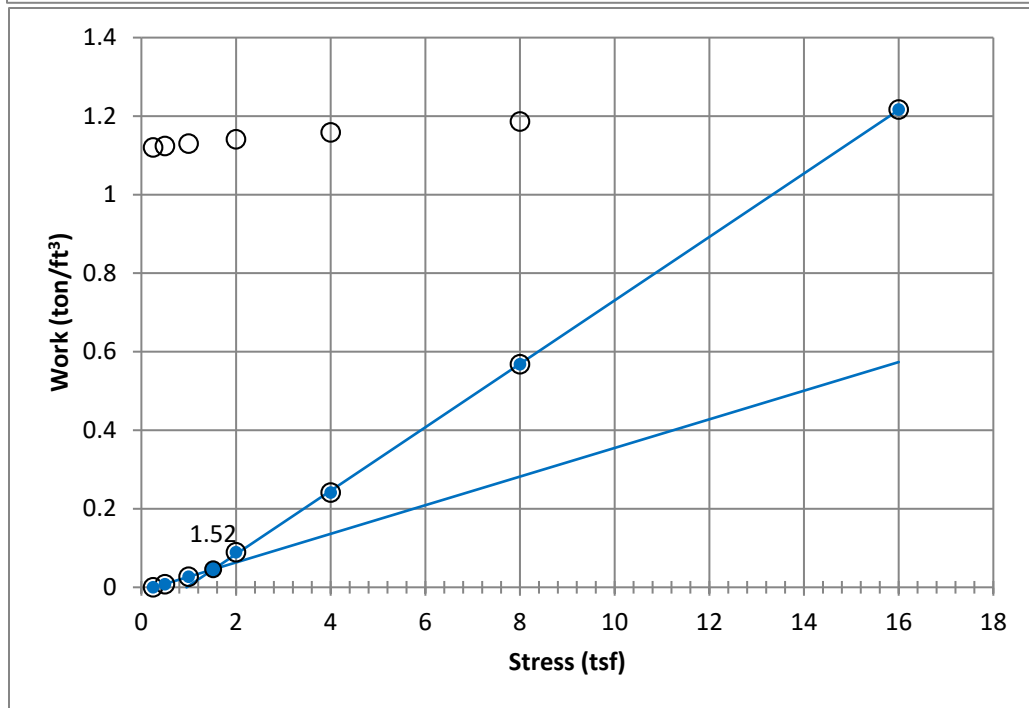
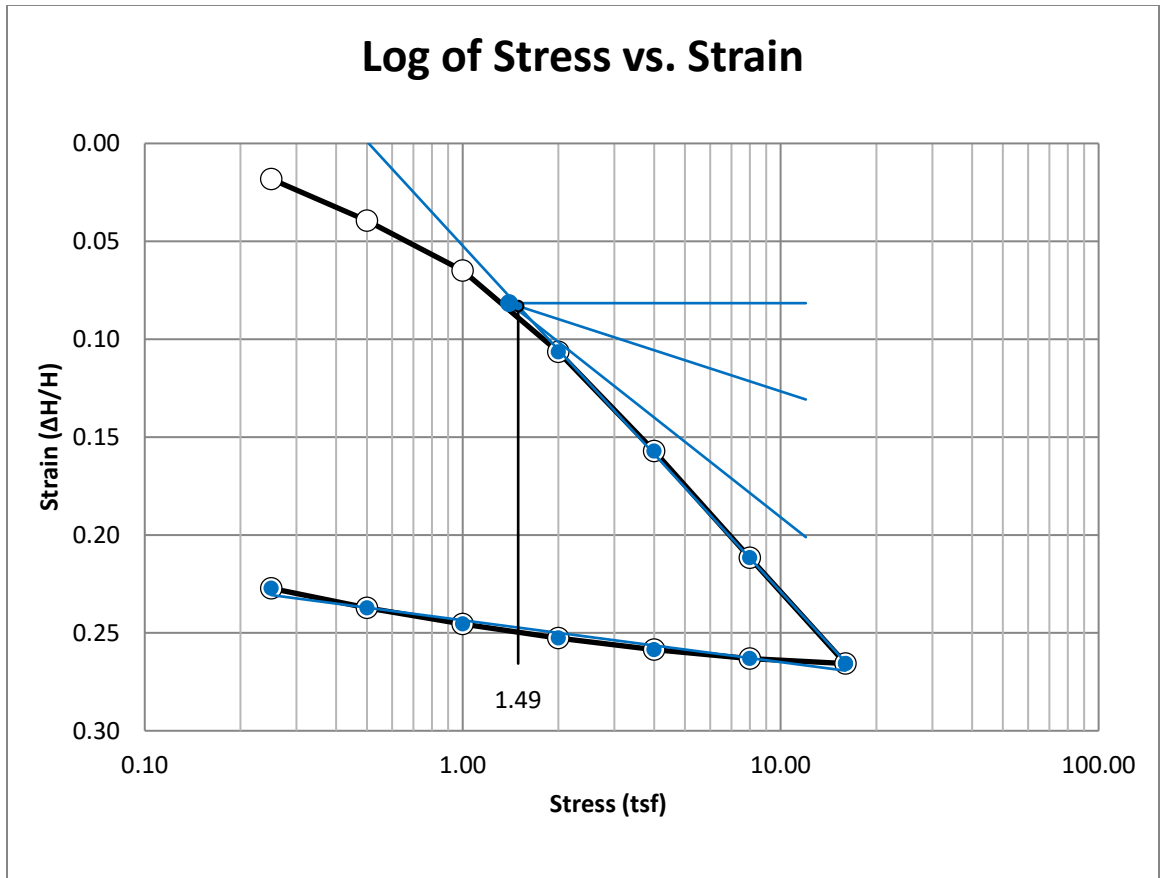


Figure A27 400 South at 25-27 feet

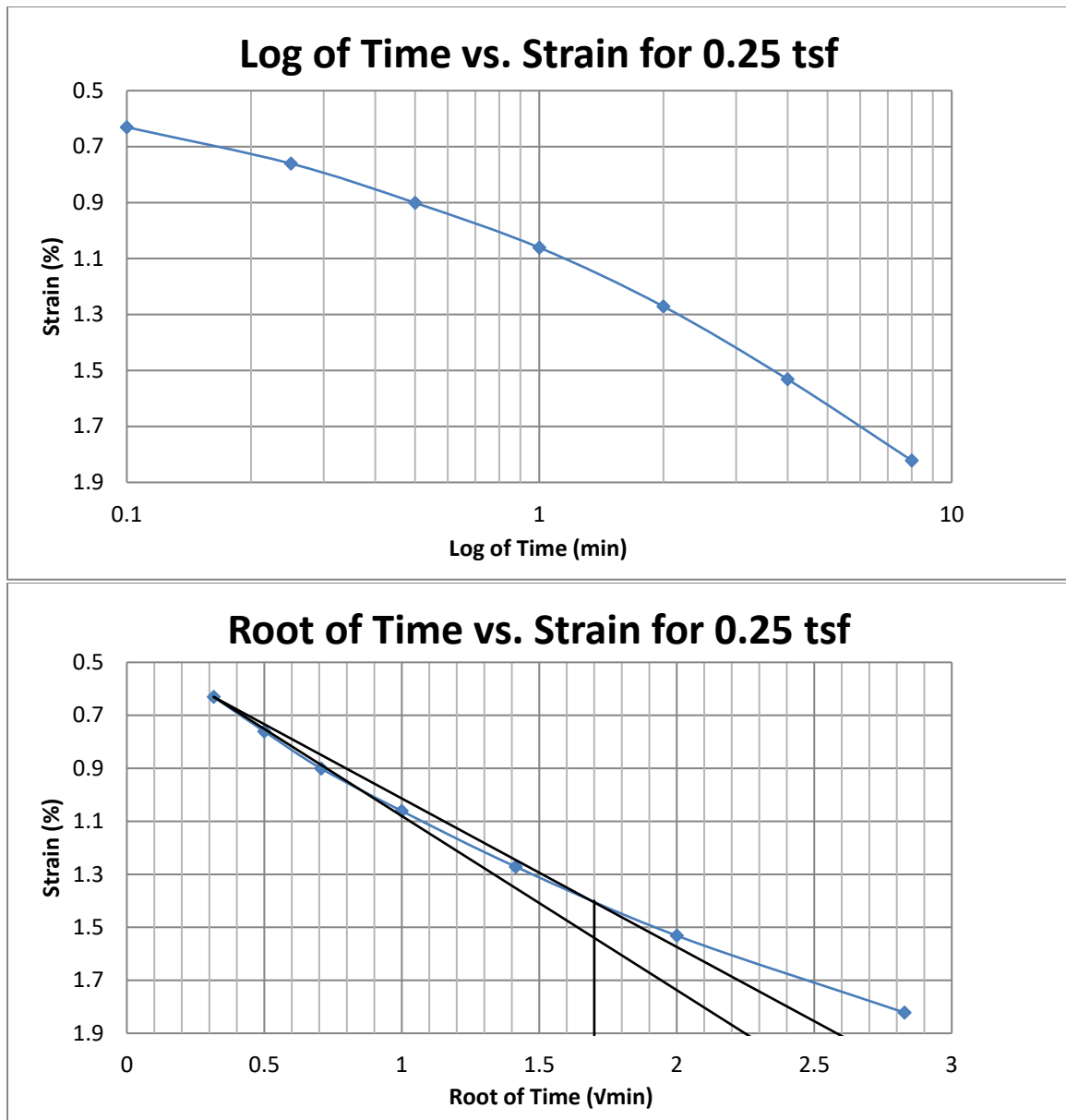


Figure A28 400 South at 25-27 feet

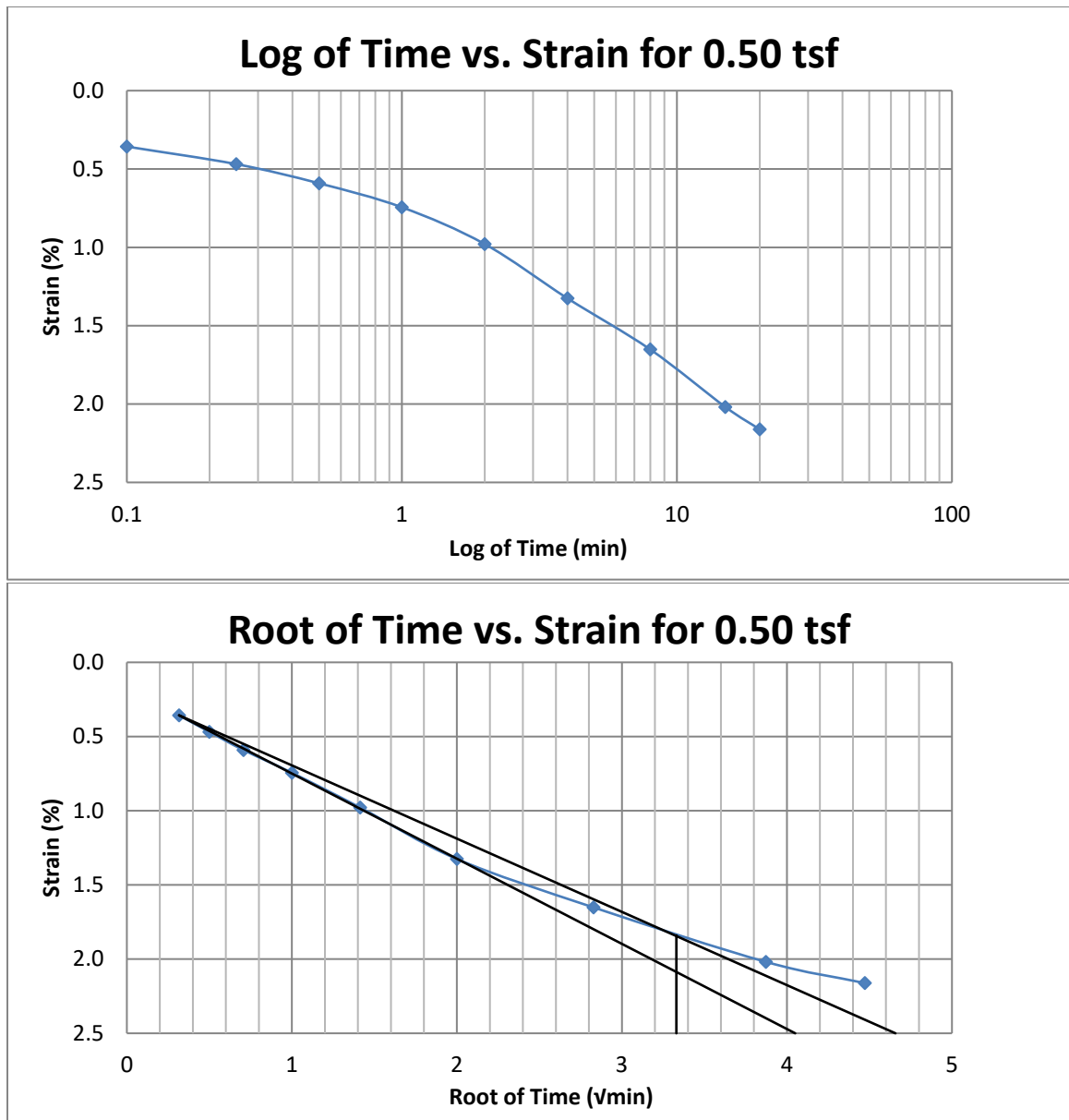


Figure A29 400 South at 25-27 feet

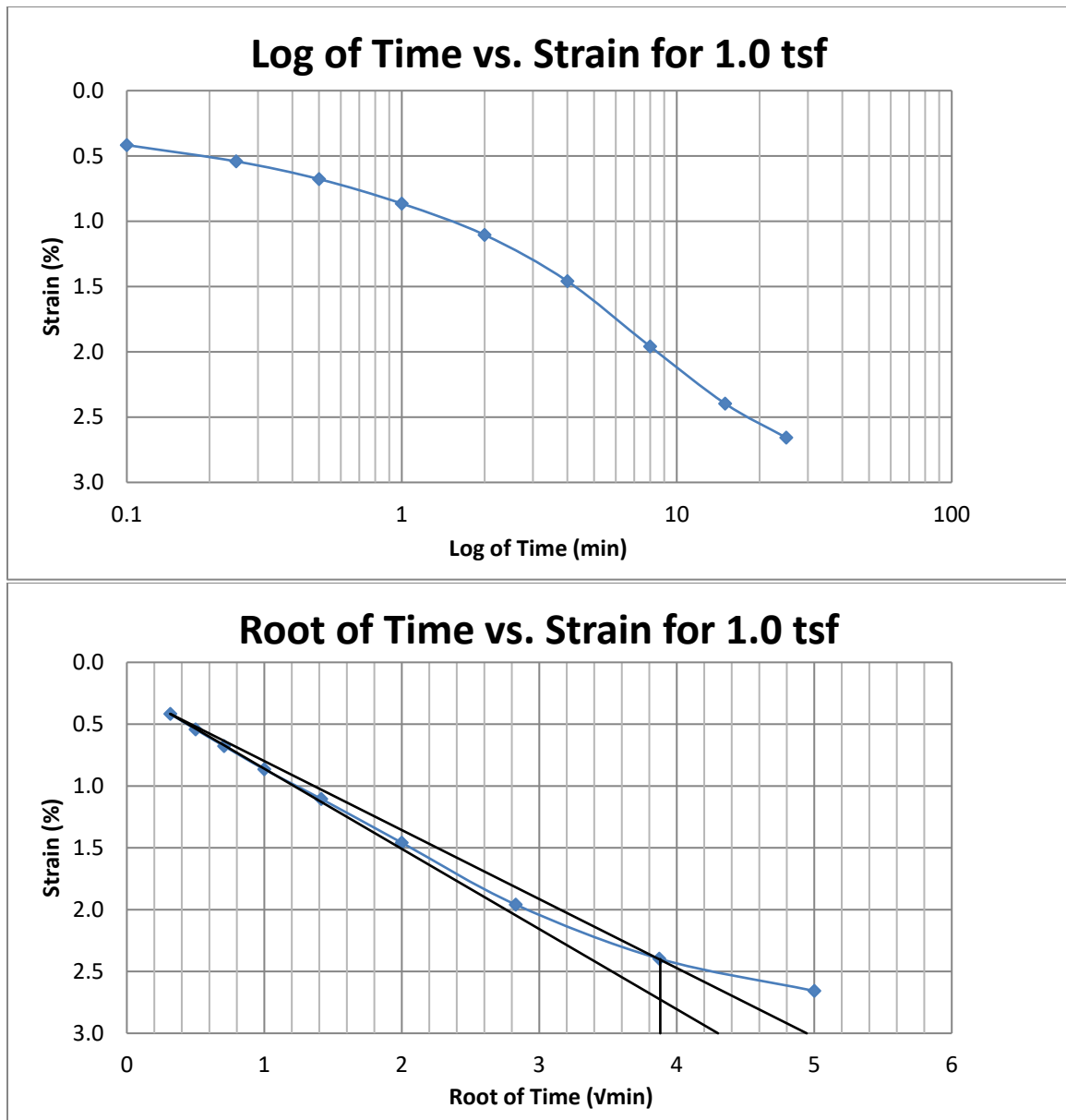


Figure A30 400 South at 25-27 feet

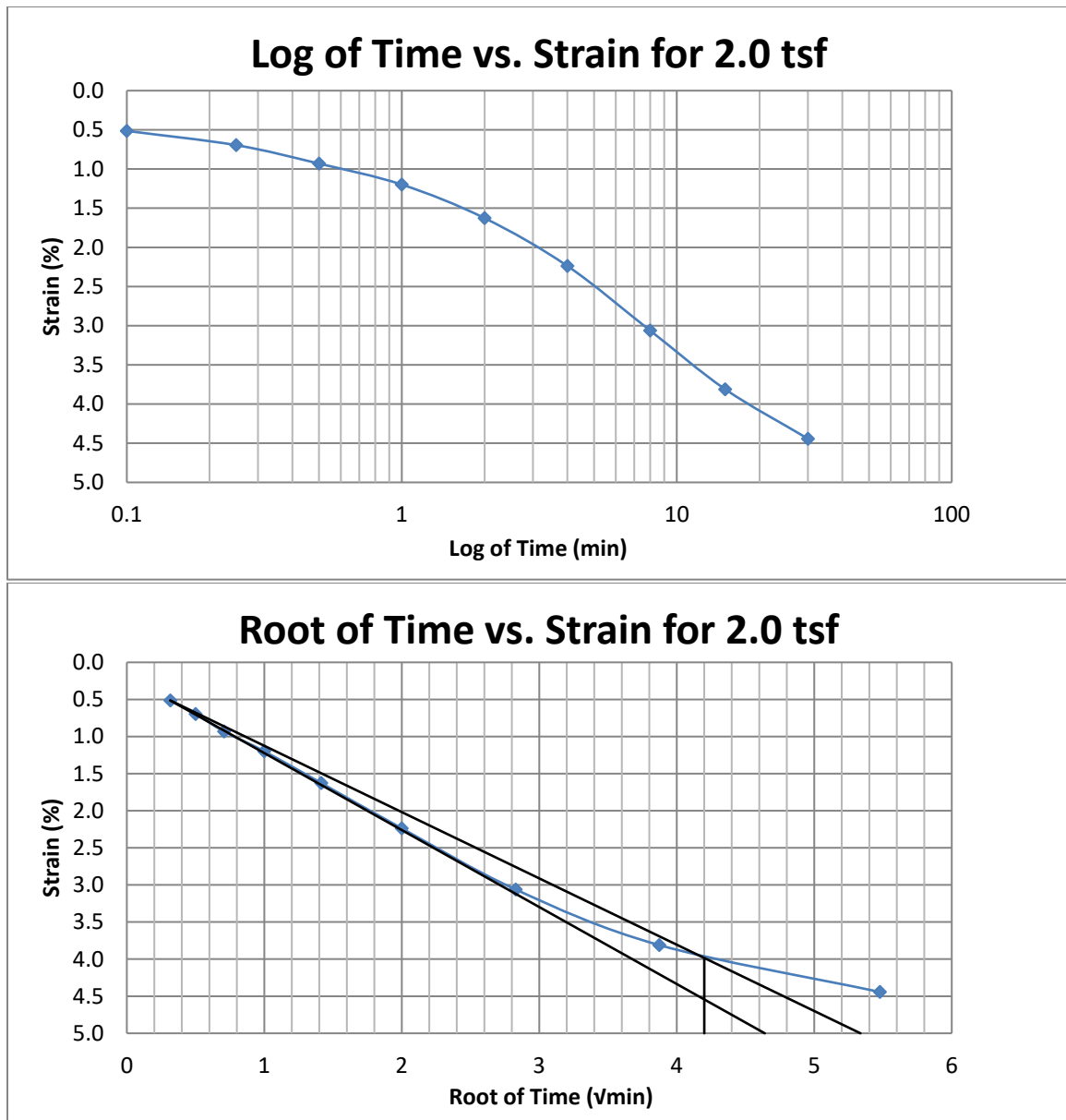


Figure A31 400 South at 25-27 feet

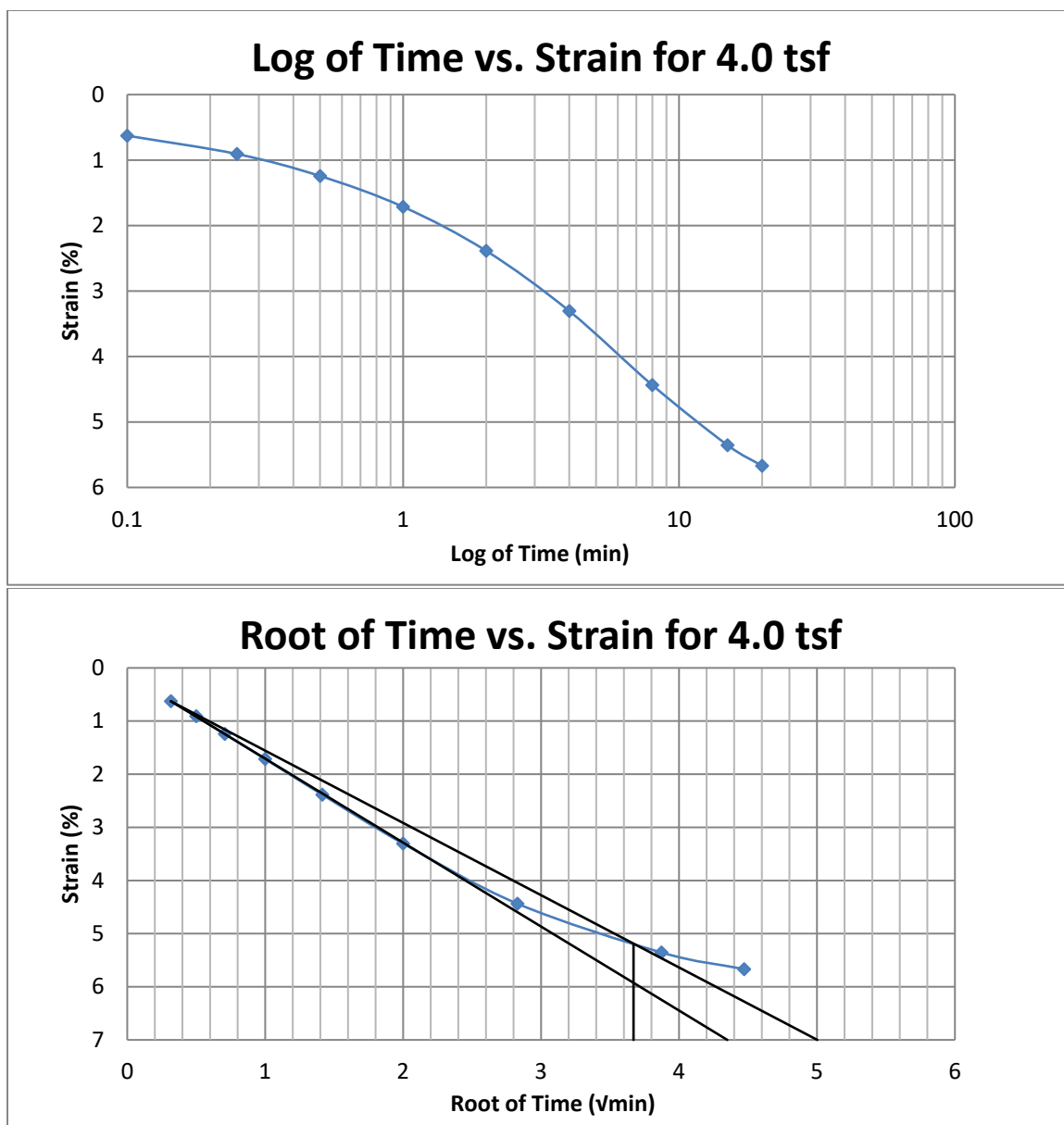


Figure A32 400 South at 25-27 feet

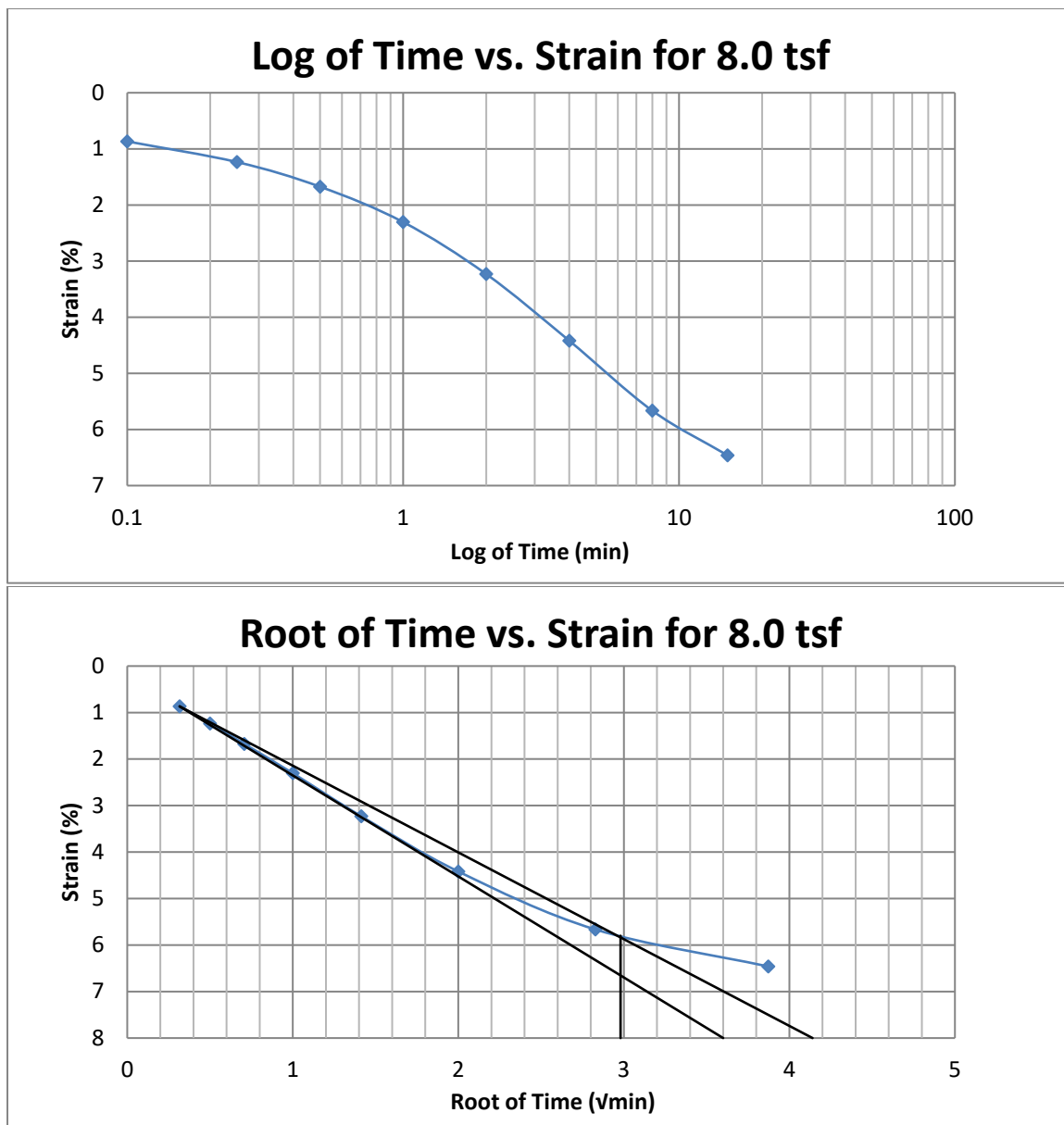


Figure A33 400 South at 25-27 feet

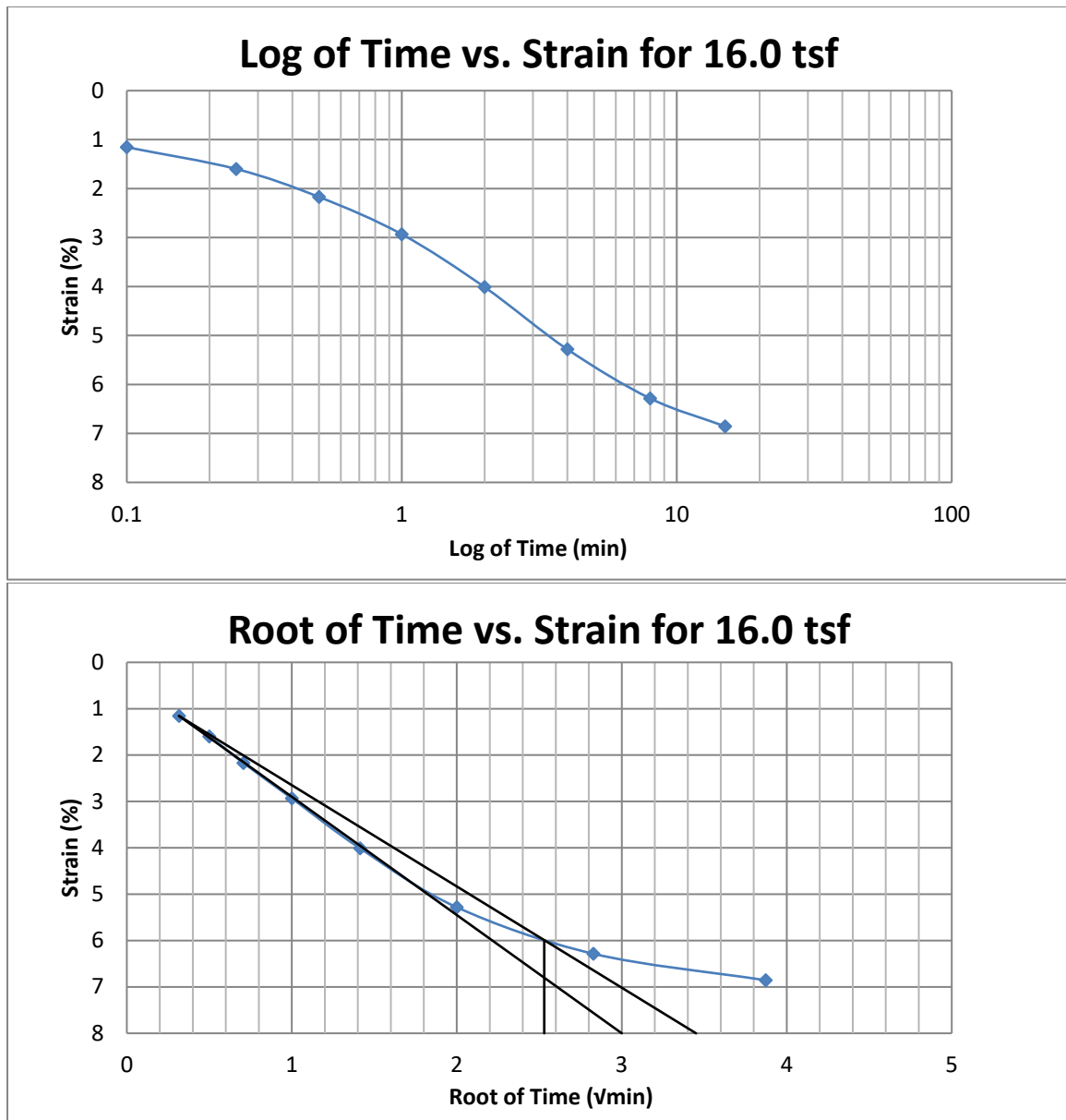


Figure A34 400 South at 25-27 feet



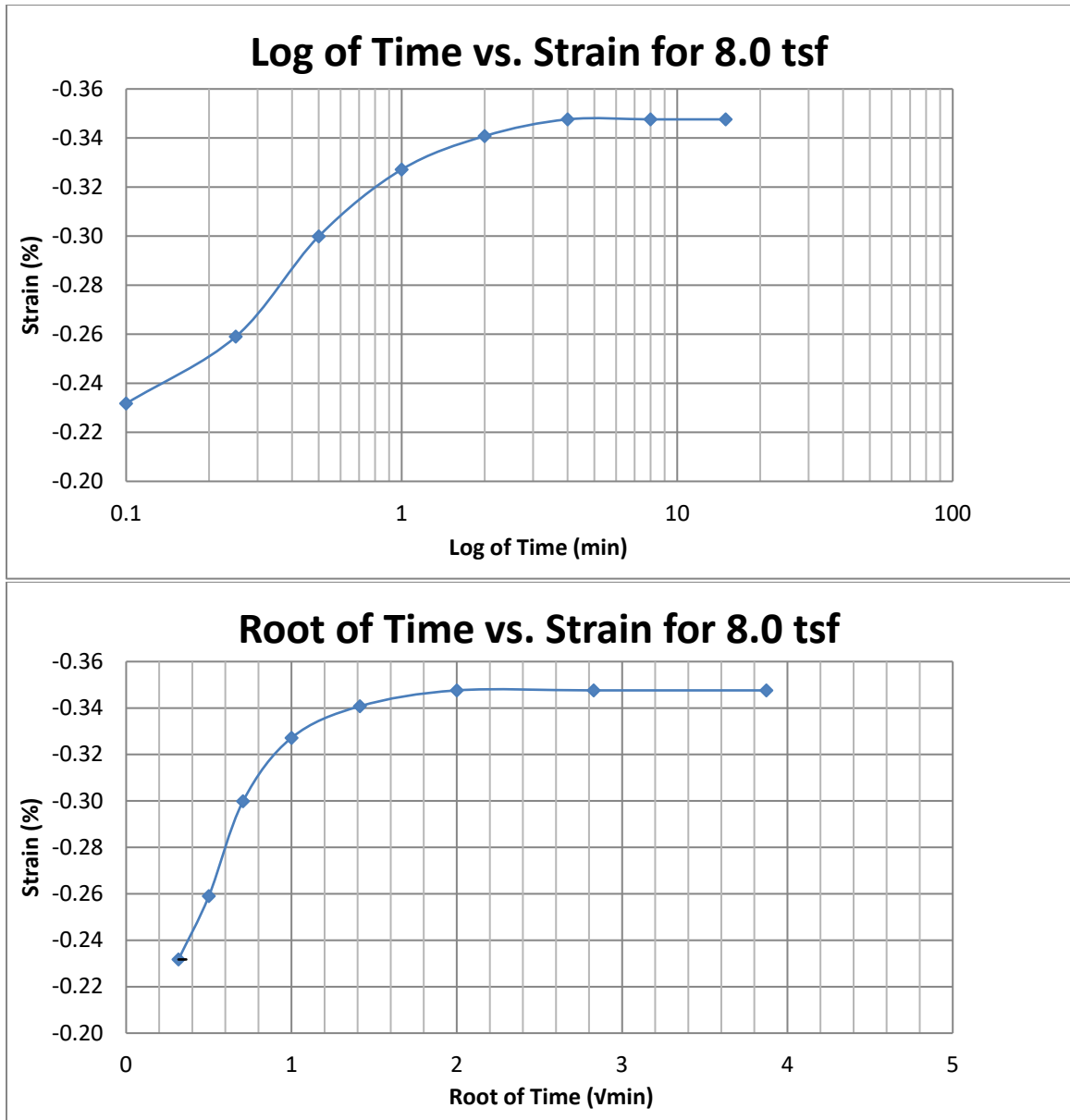


Figure A35 400 South at 25-27 feet

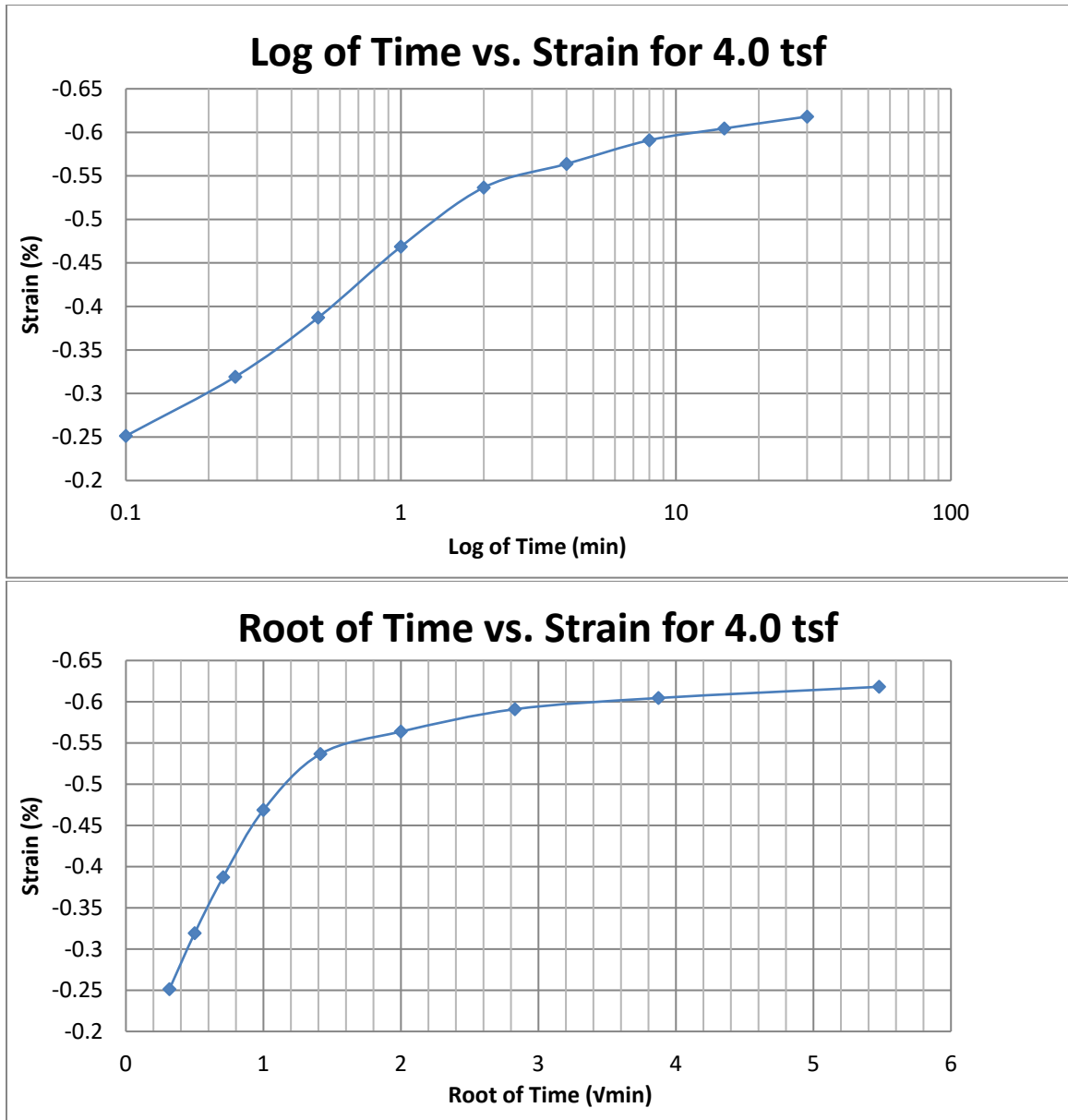


Figure A36 400 South at 25-27 feet

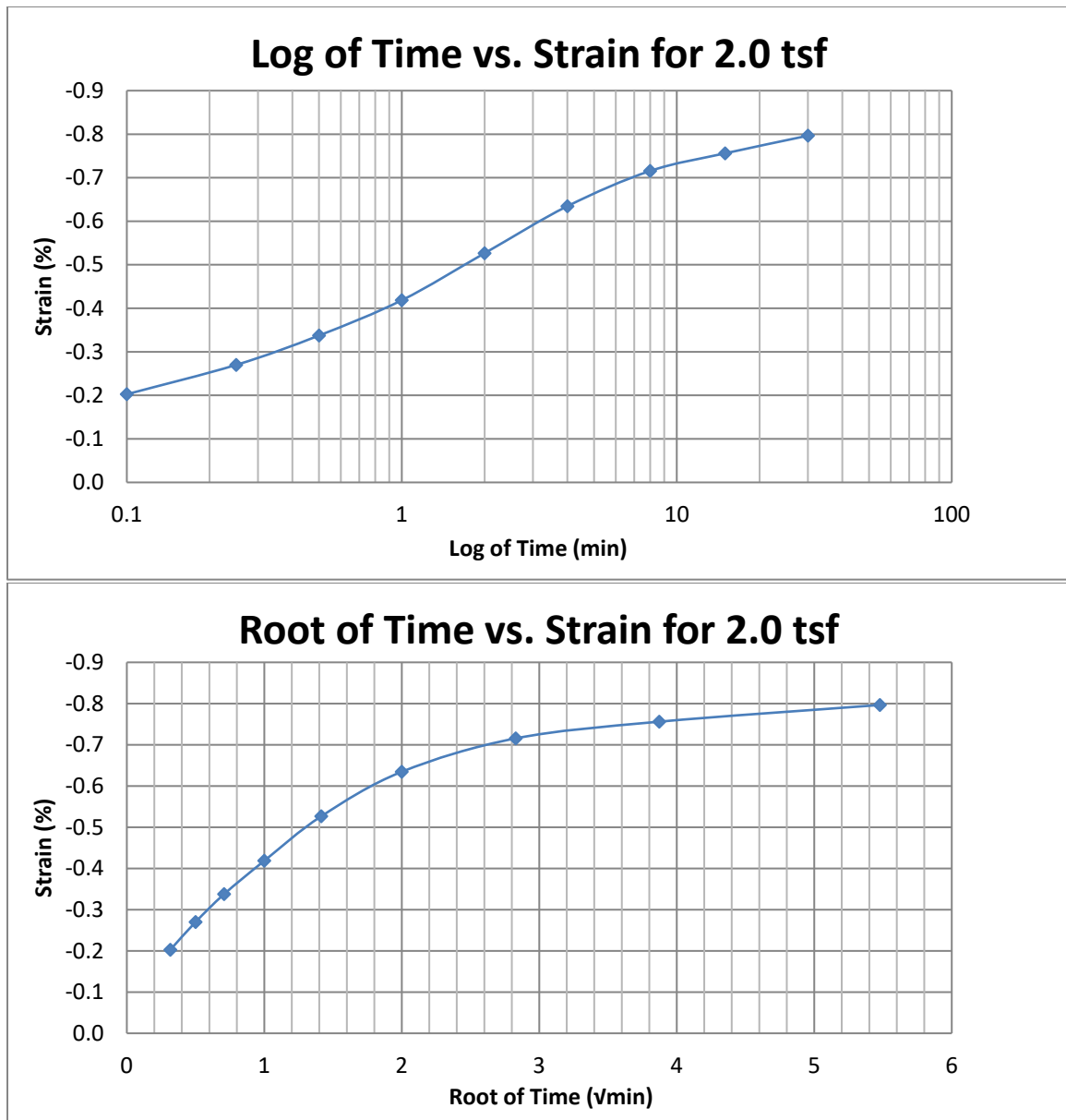


Figure A37 400 South at 25-27 feet

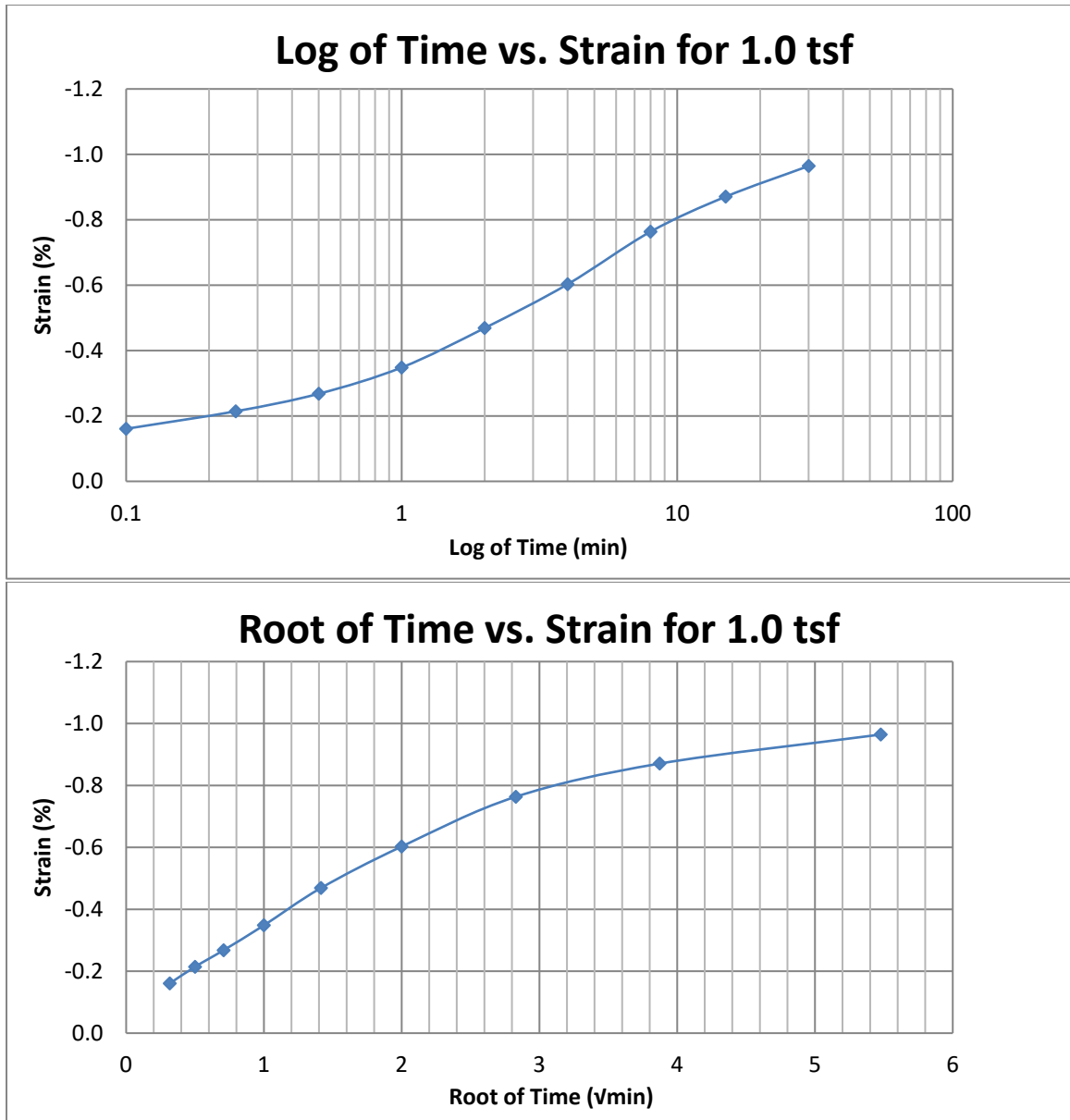
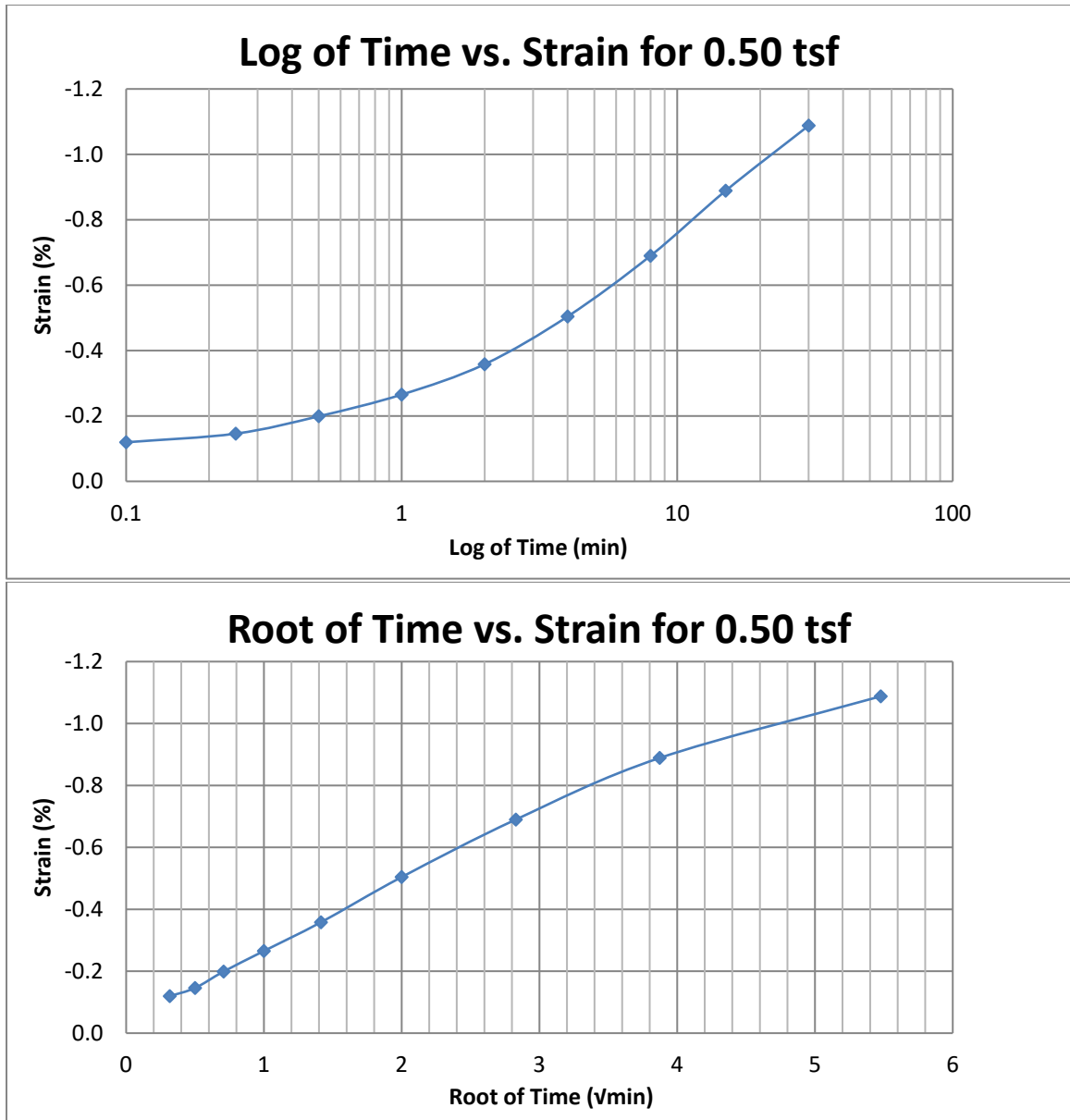


Figure A38 400 South at 25-27 feet



**Figure A39 400 South at 25-27 feet**

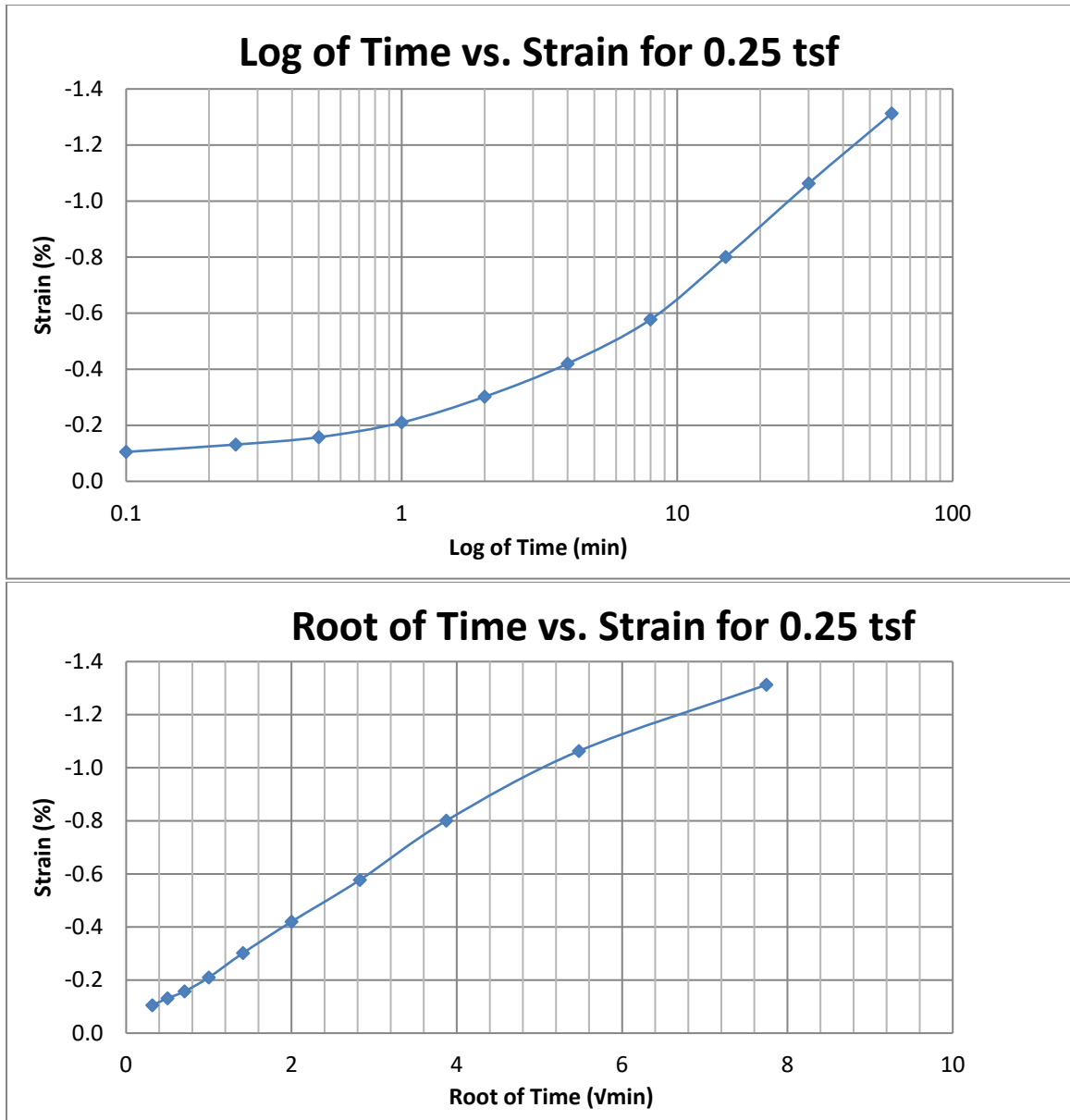


Figure A40 400 South at 25-27 feet

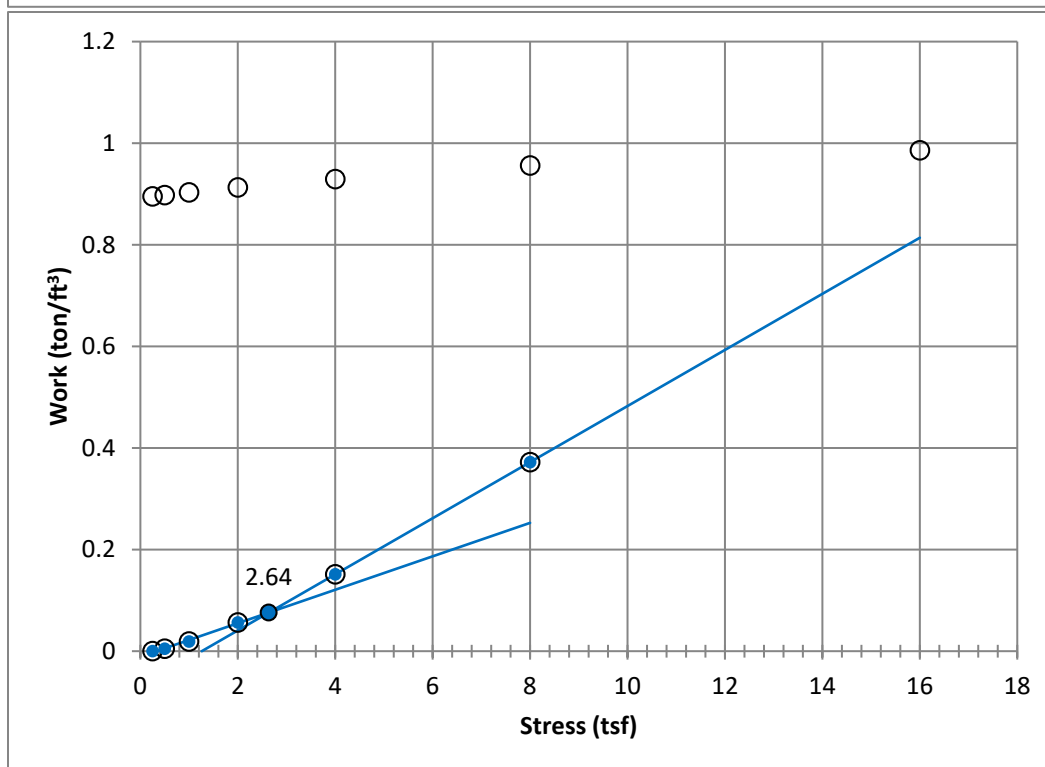
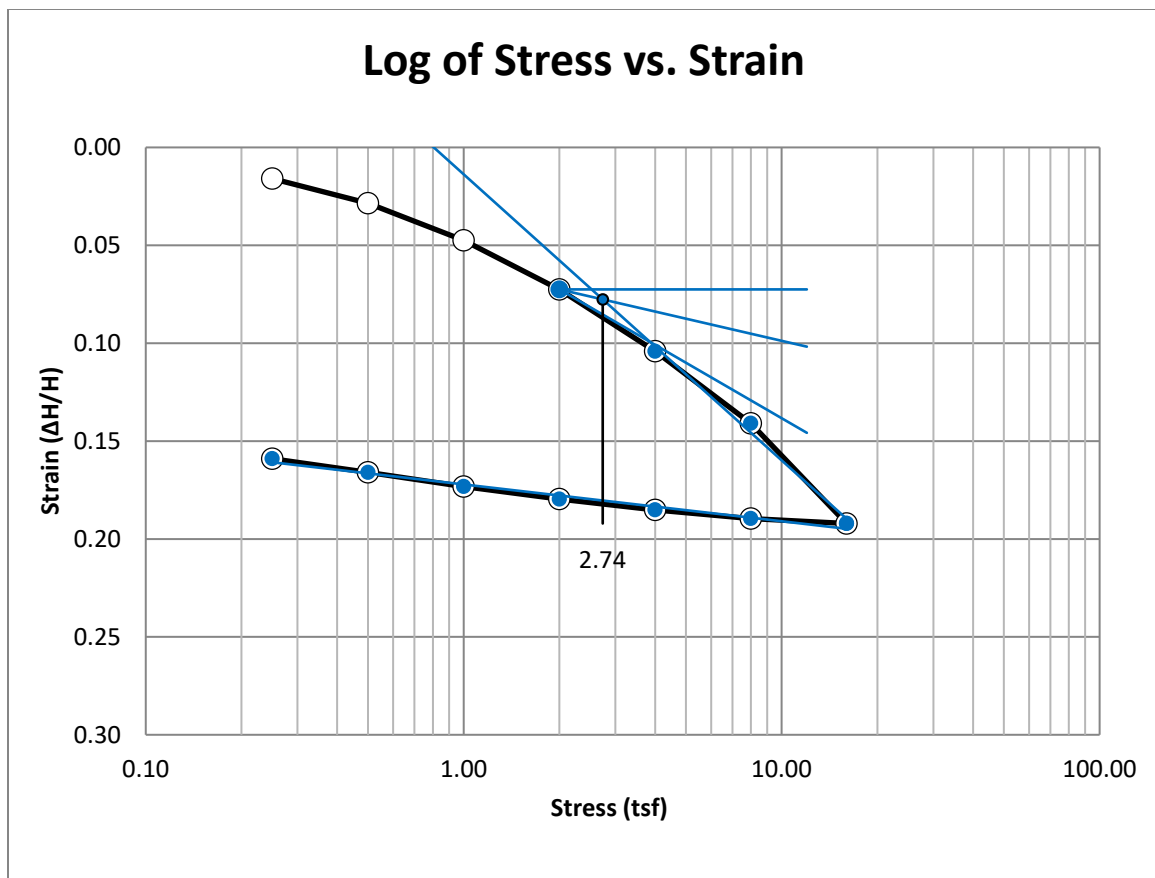


Figure A41 400 South at 30-32 feet

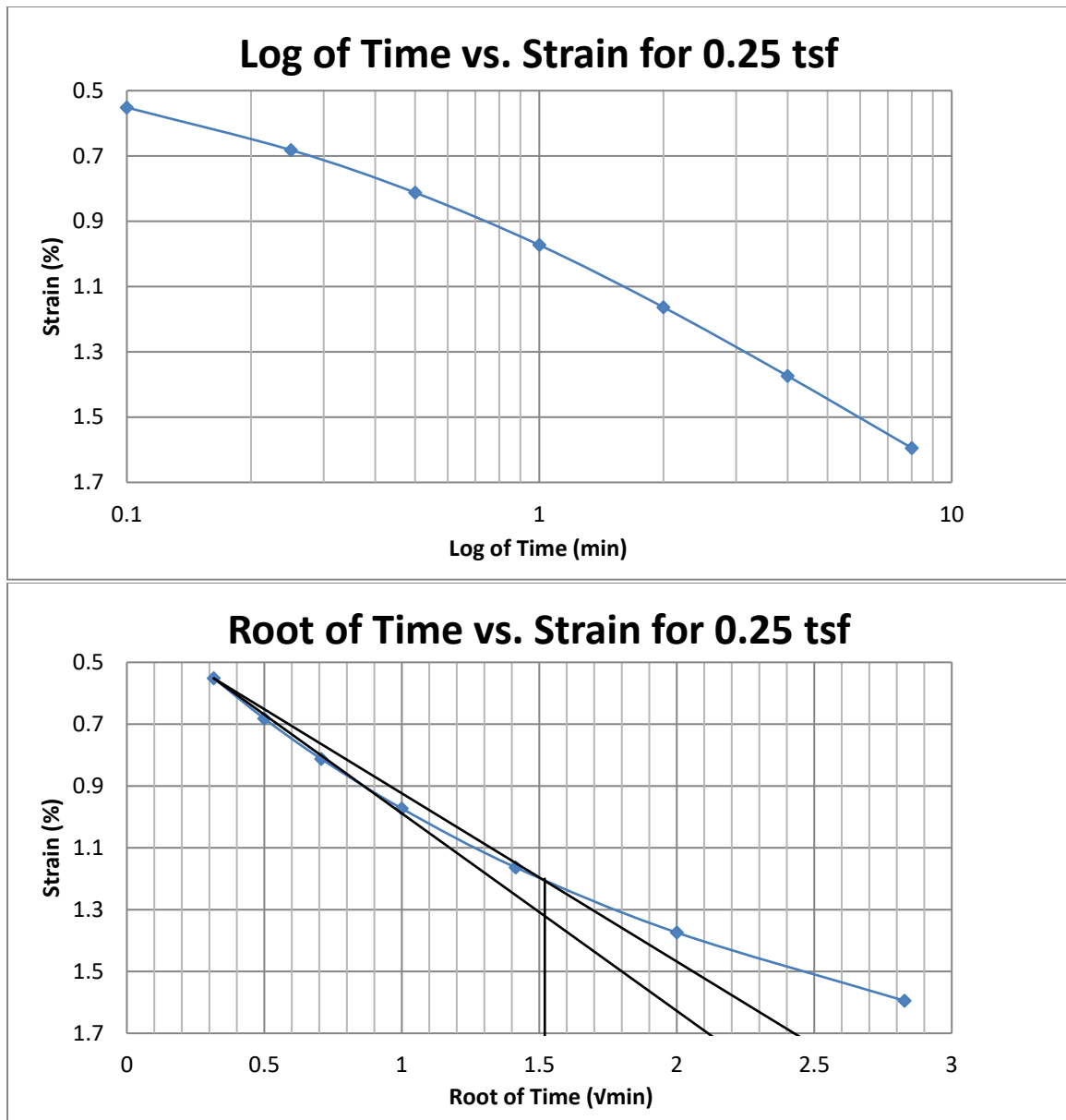


Figure A42 400 South at 30-32 feet



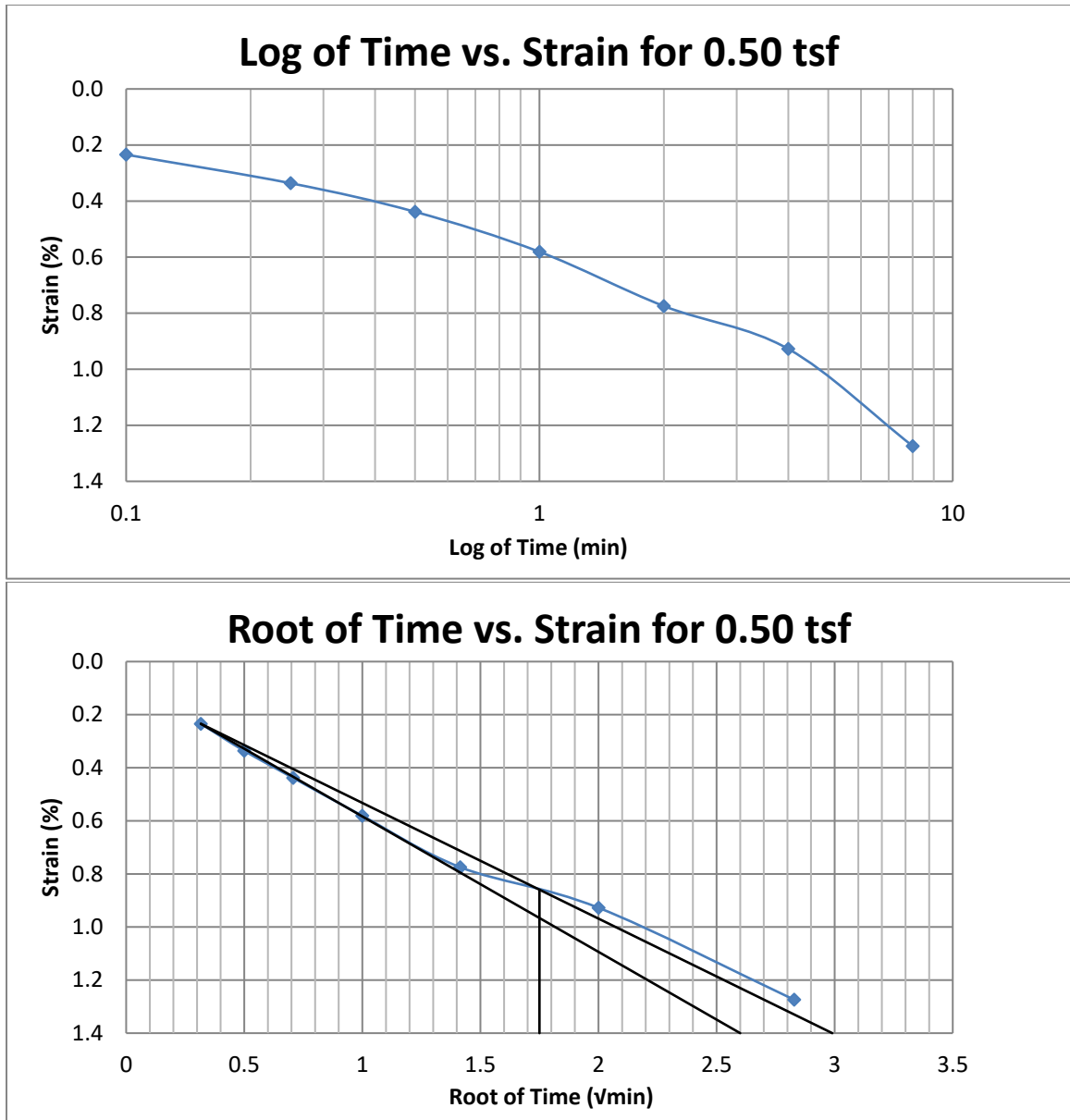


Figure A43 400 South at 30-32 feet

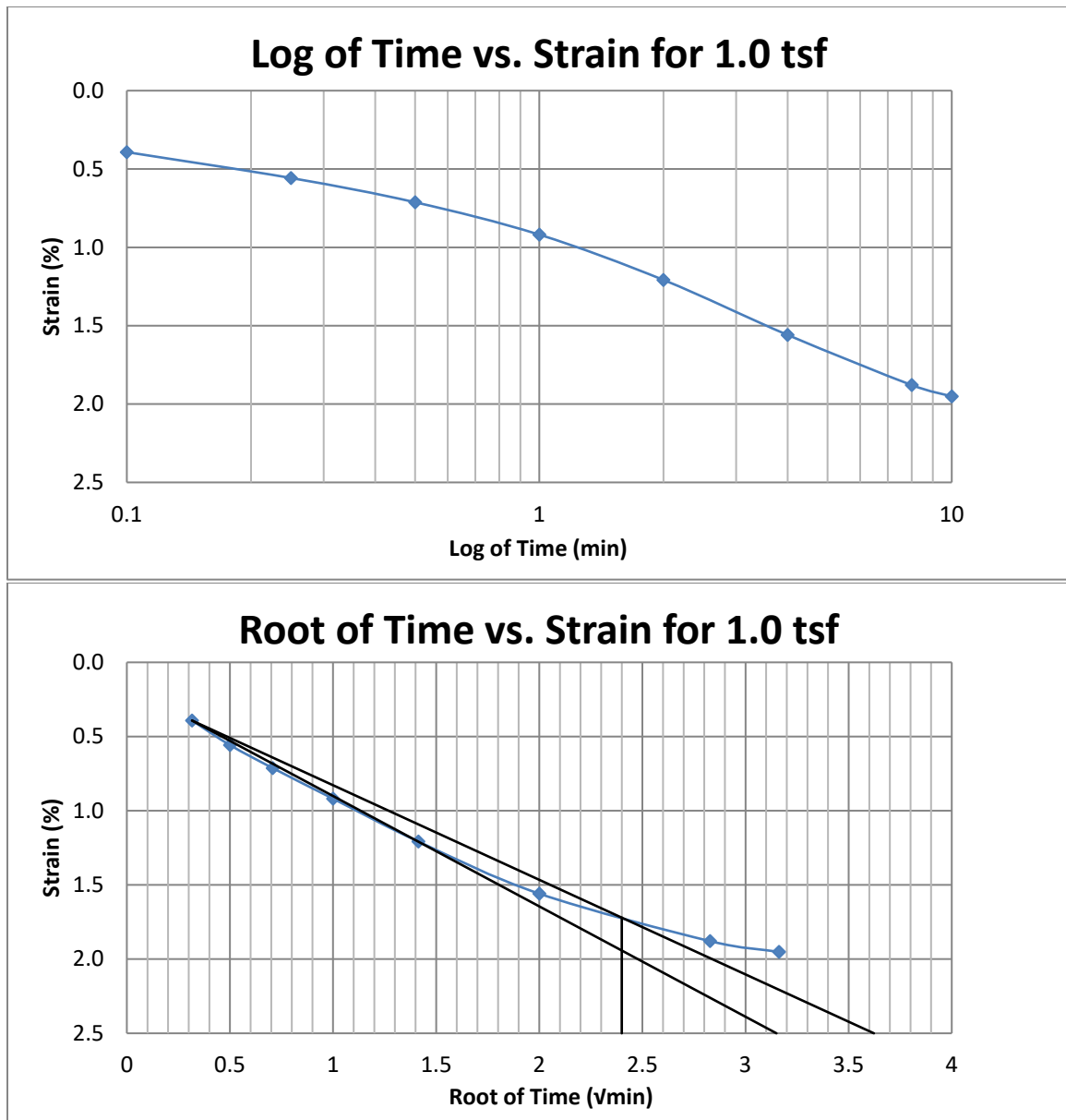


Figure A44 400 South at 30-32 feet

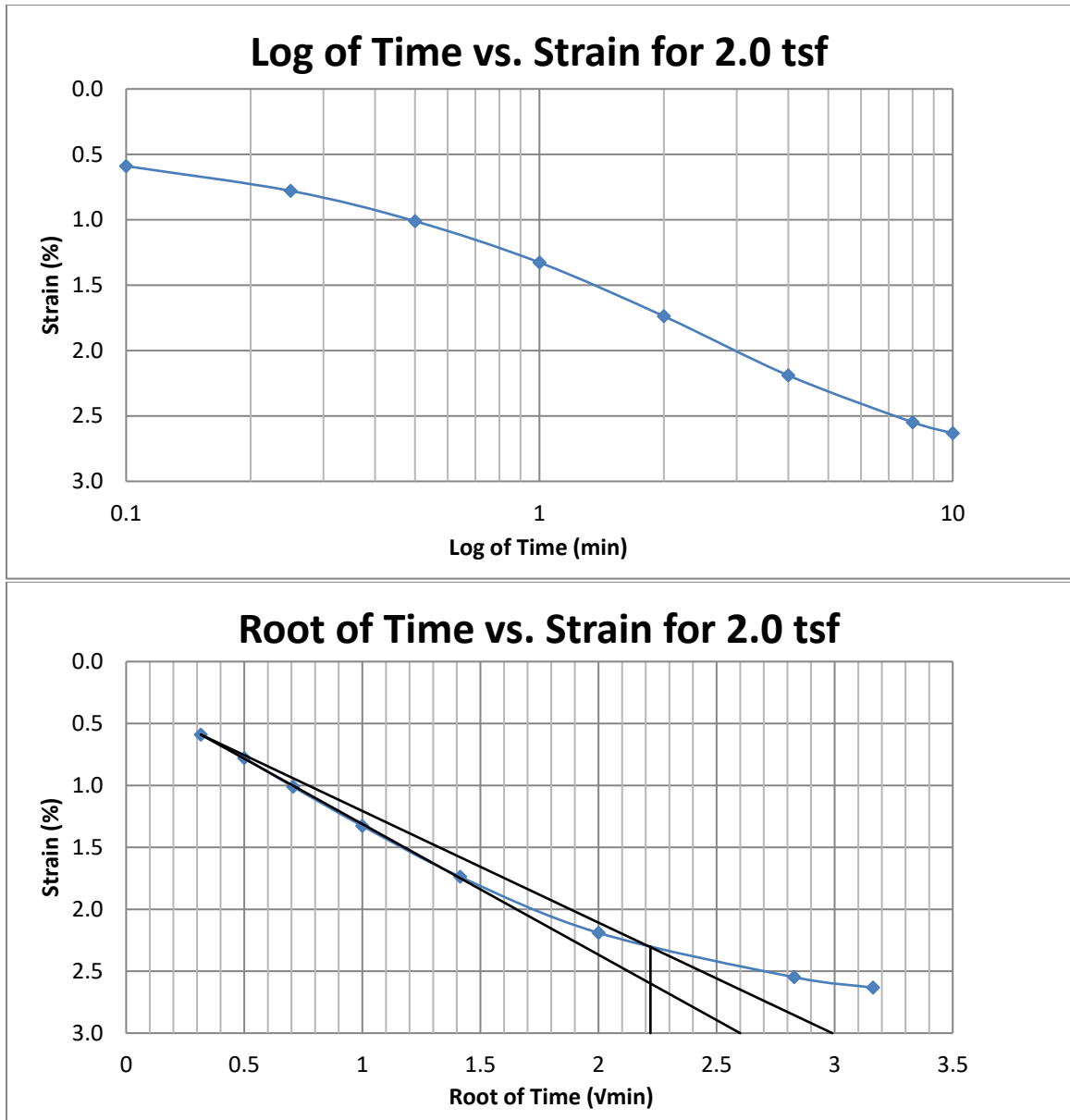


Figure A45 400 South at 30-32 feet

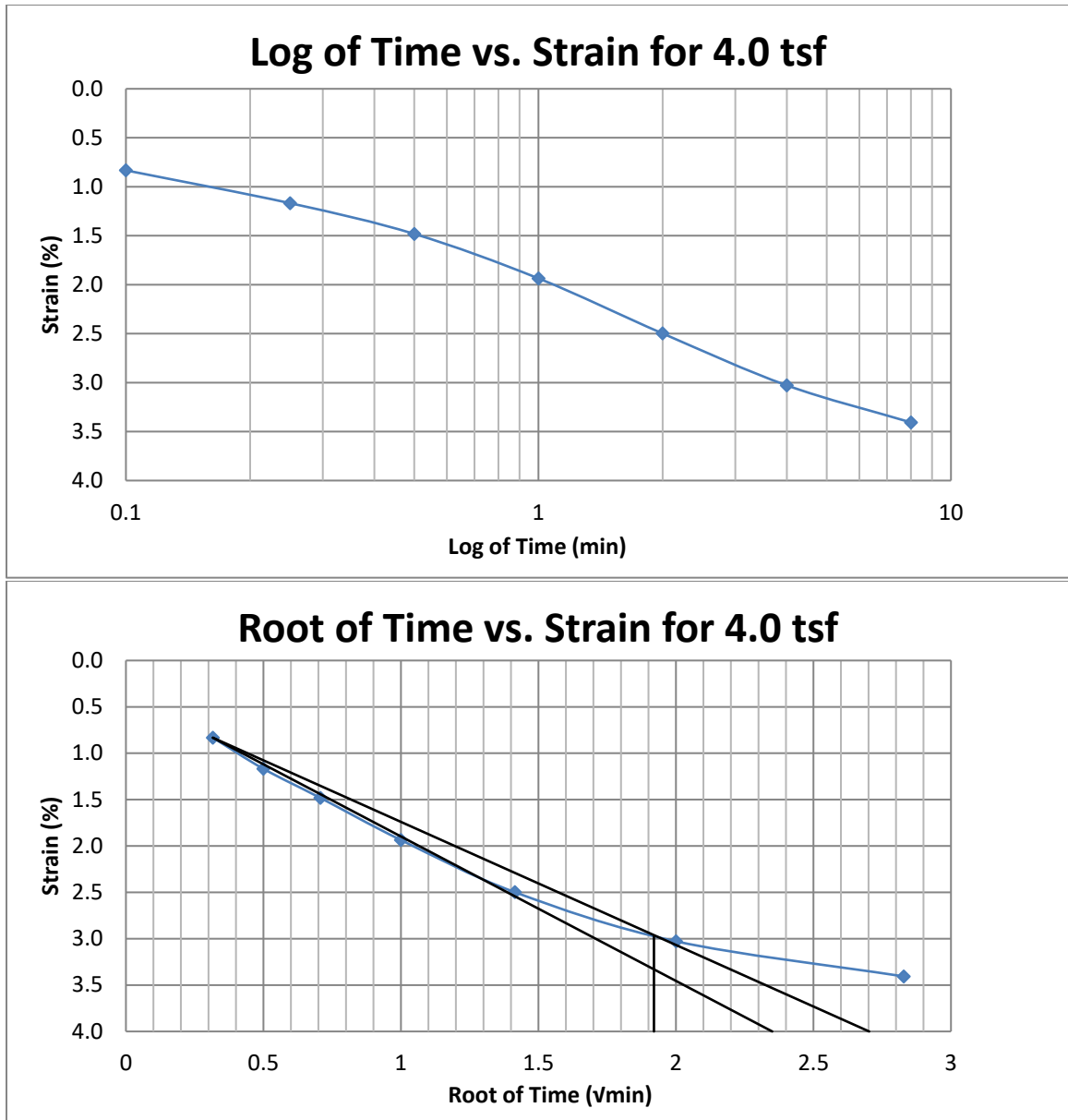


Figure A46 400 South at 30-32 feet

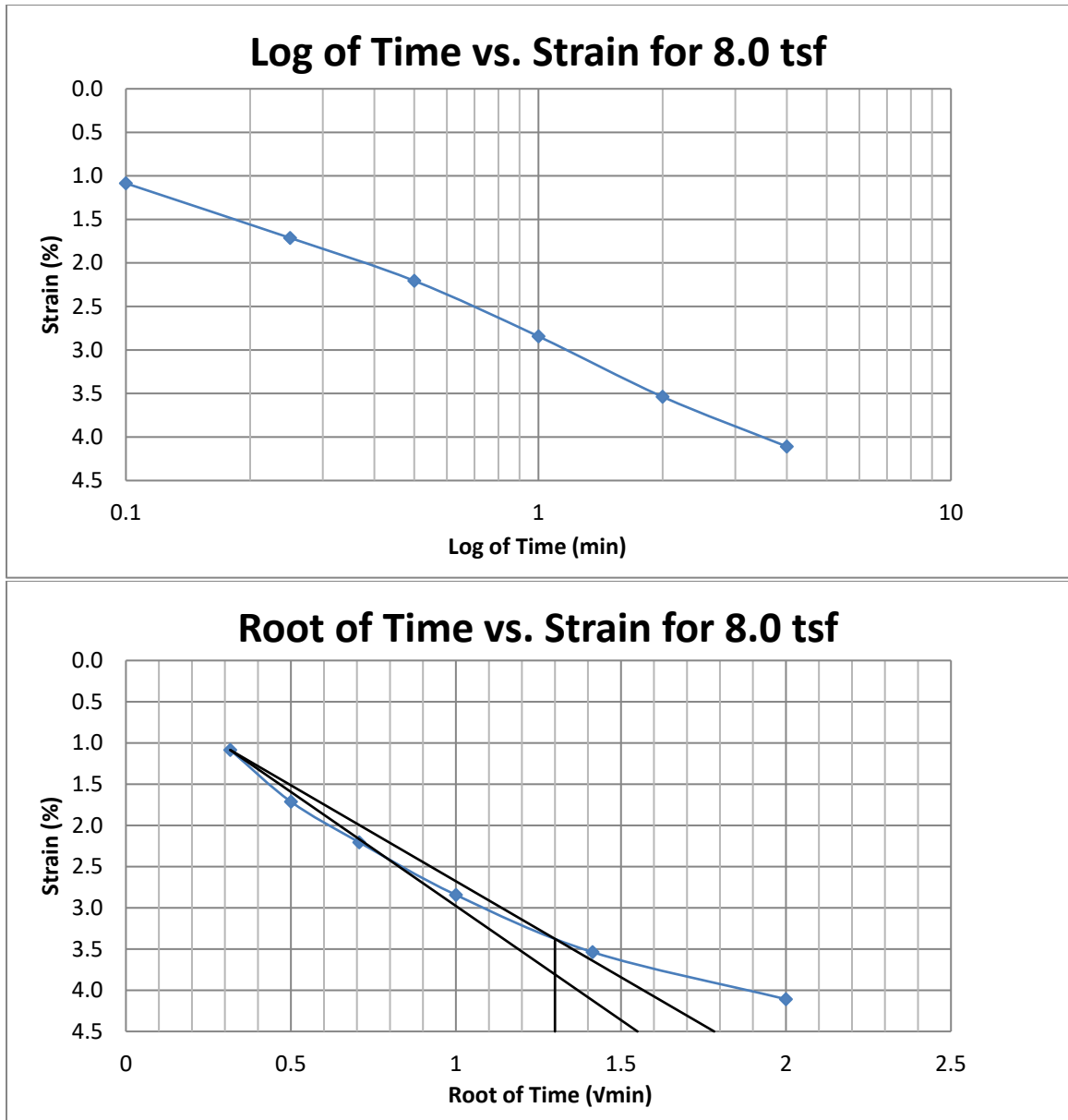


Figure A47 400 South at 30-32 feet

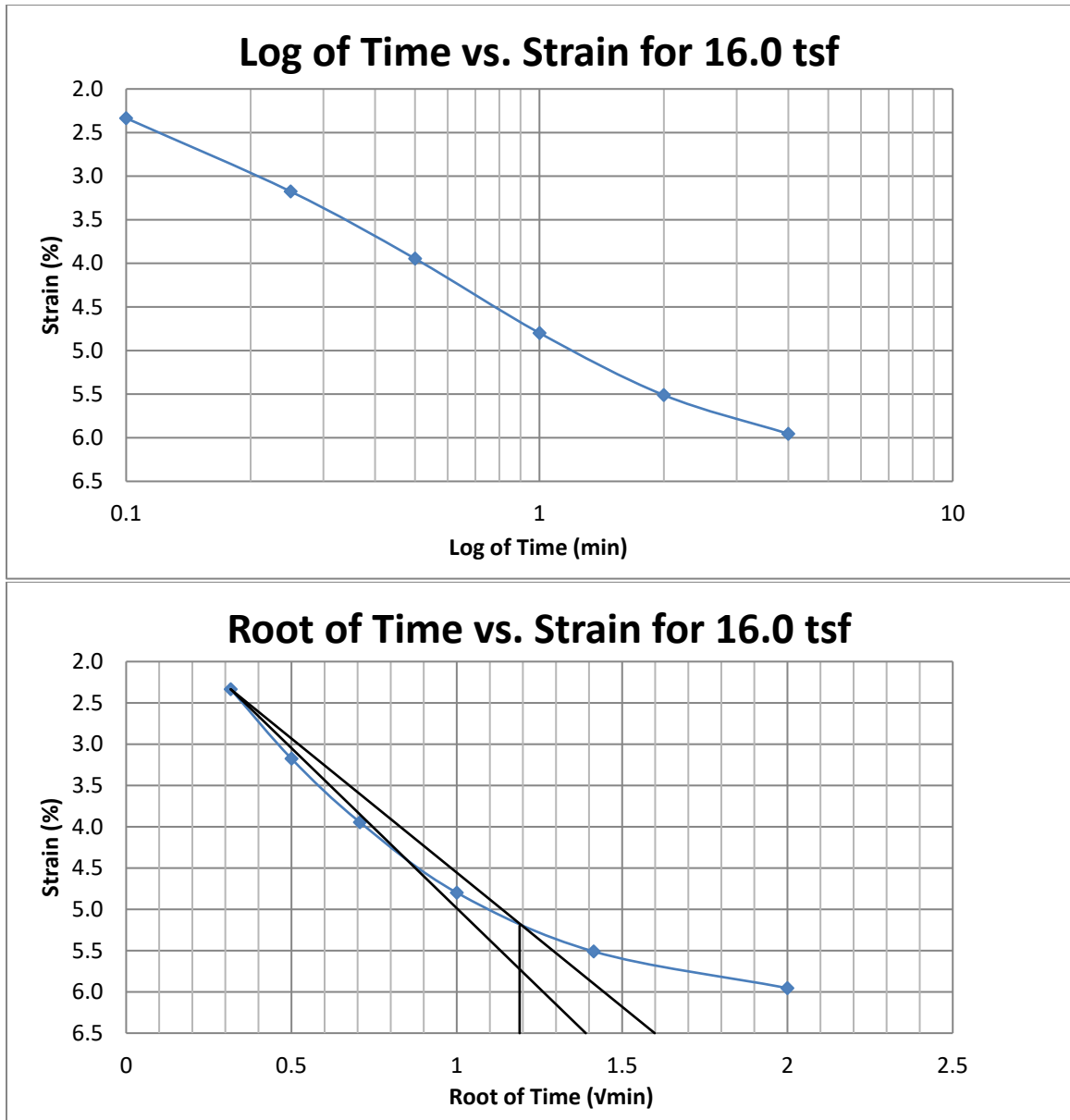


Figure A48 400 South at 30-32 feet

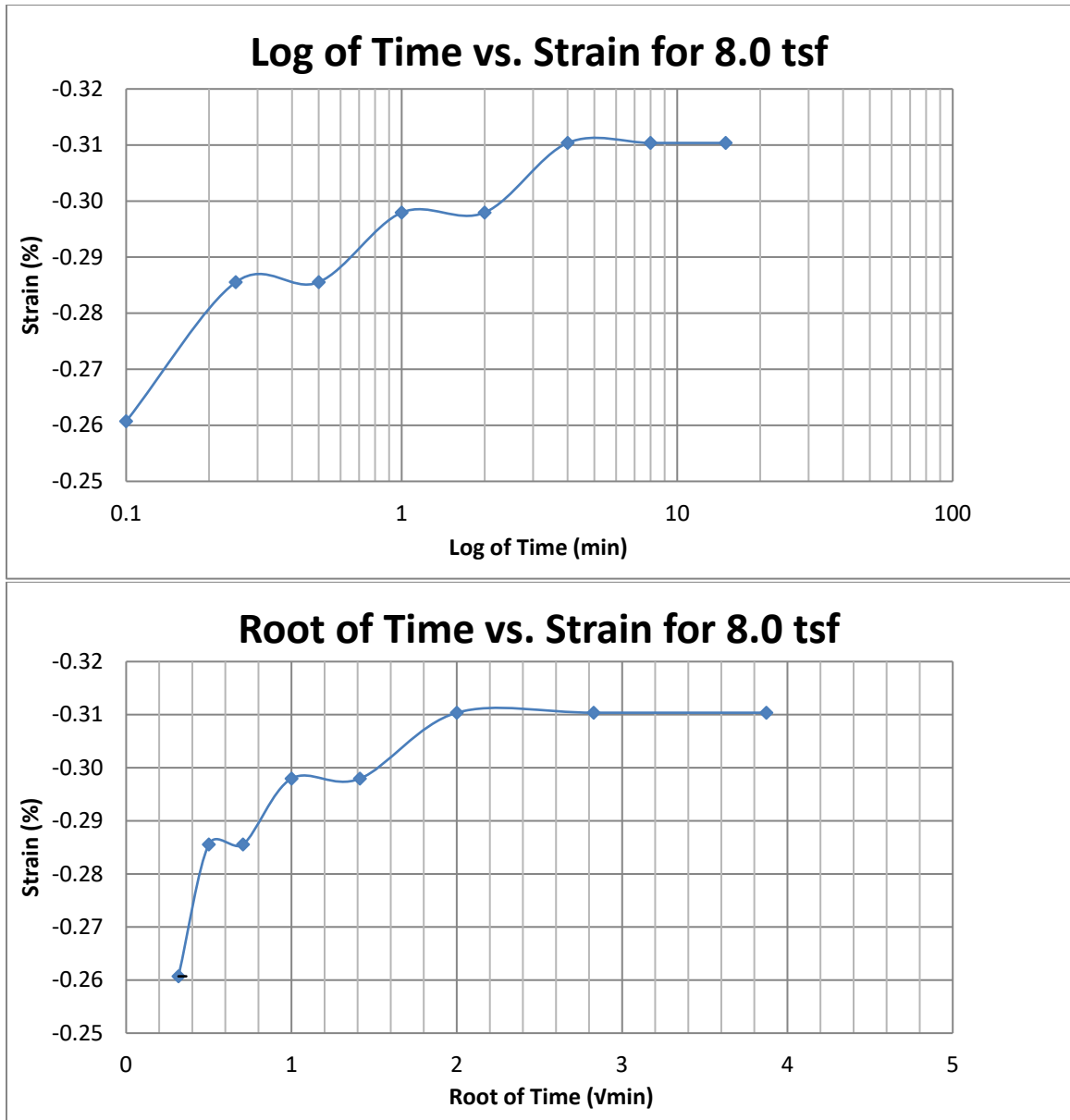


Figure A49 400 South at 30-32 feet

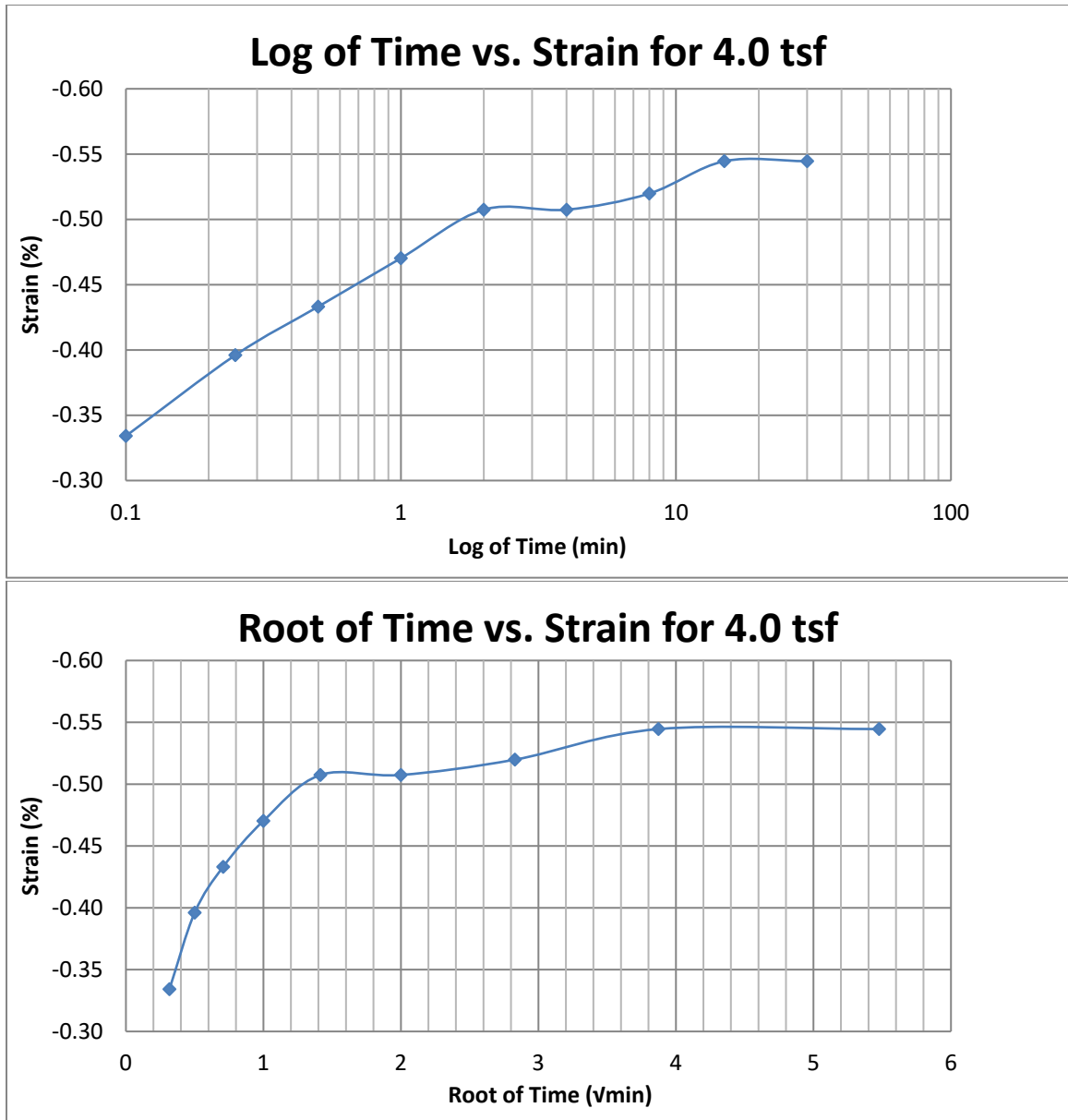


Figure A50 400 South at 30-32 feet



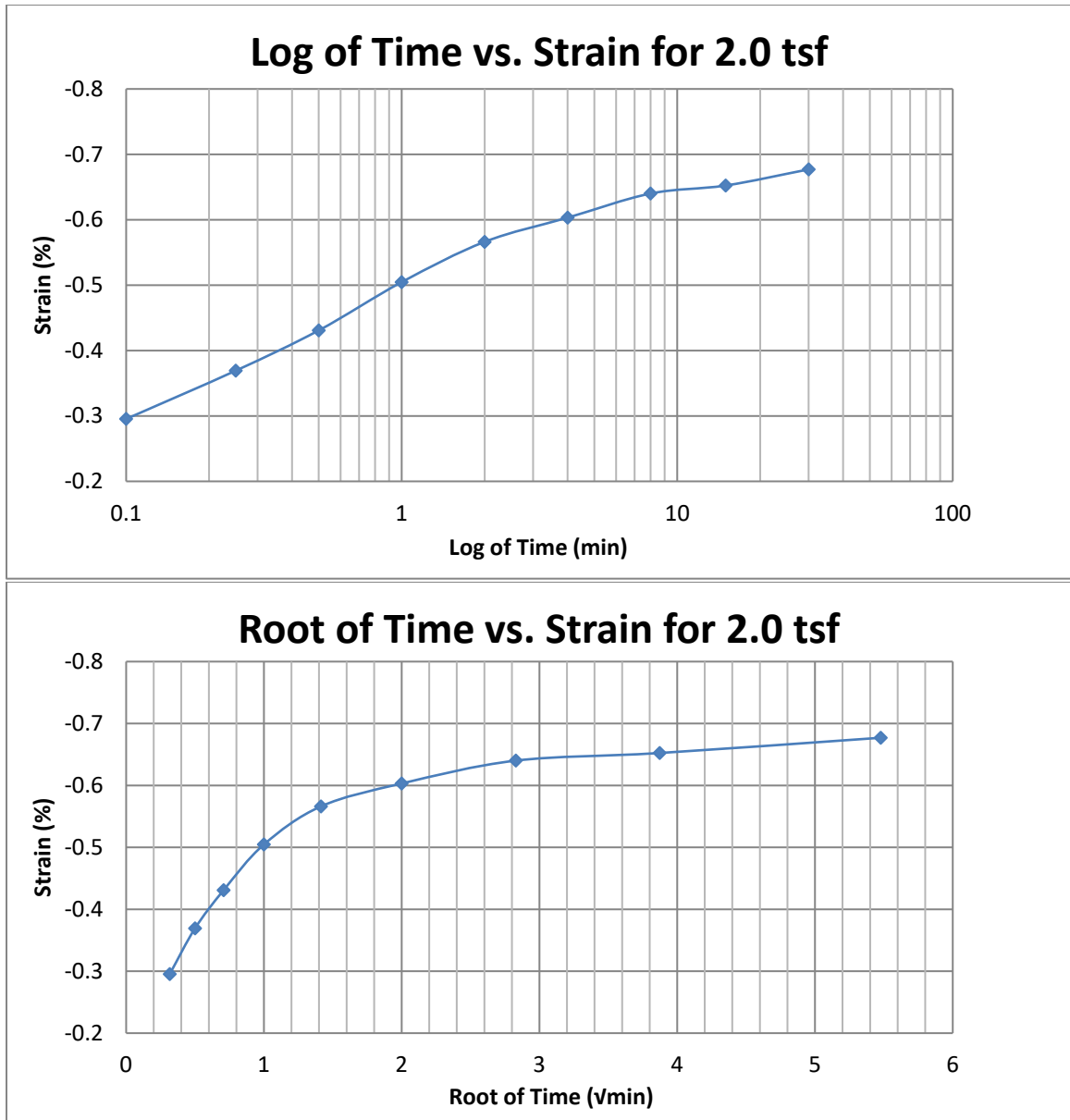


Figure A51 400 South at 30-32 feet

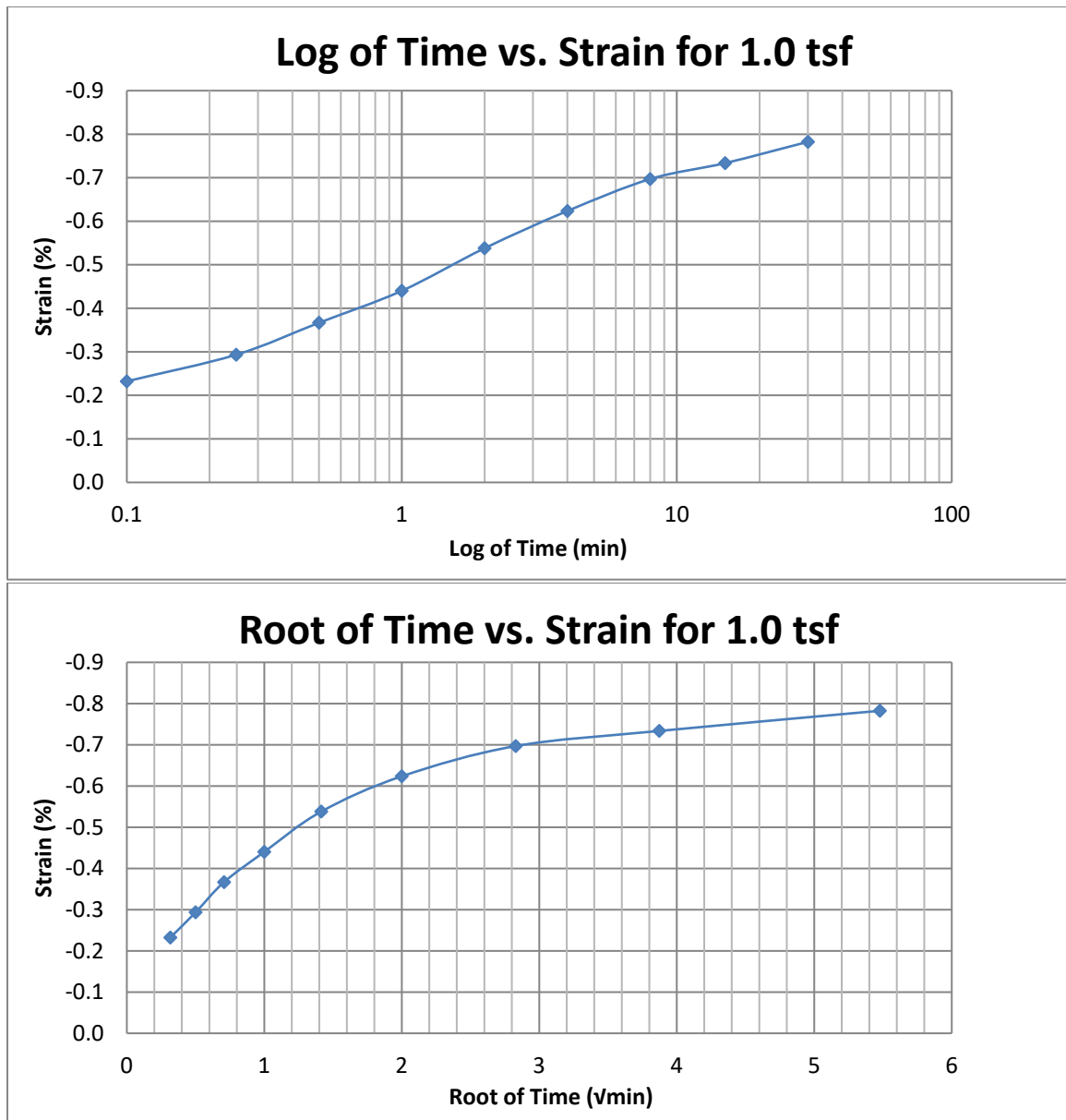


Figure A52 400 South at 30-32 feet

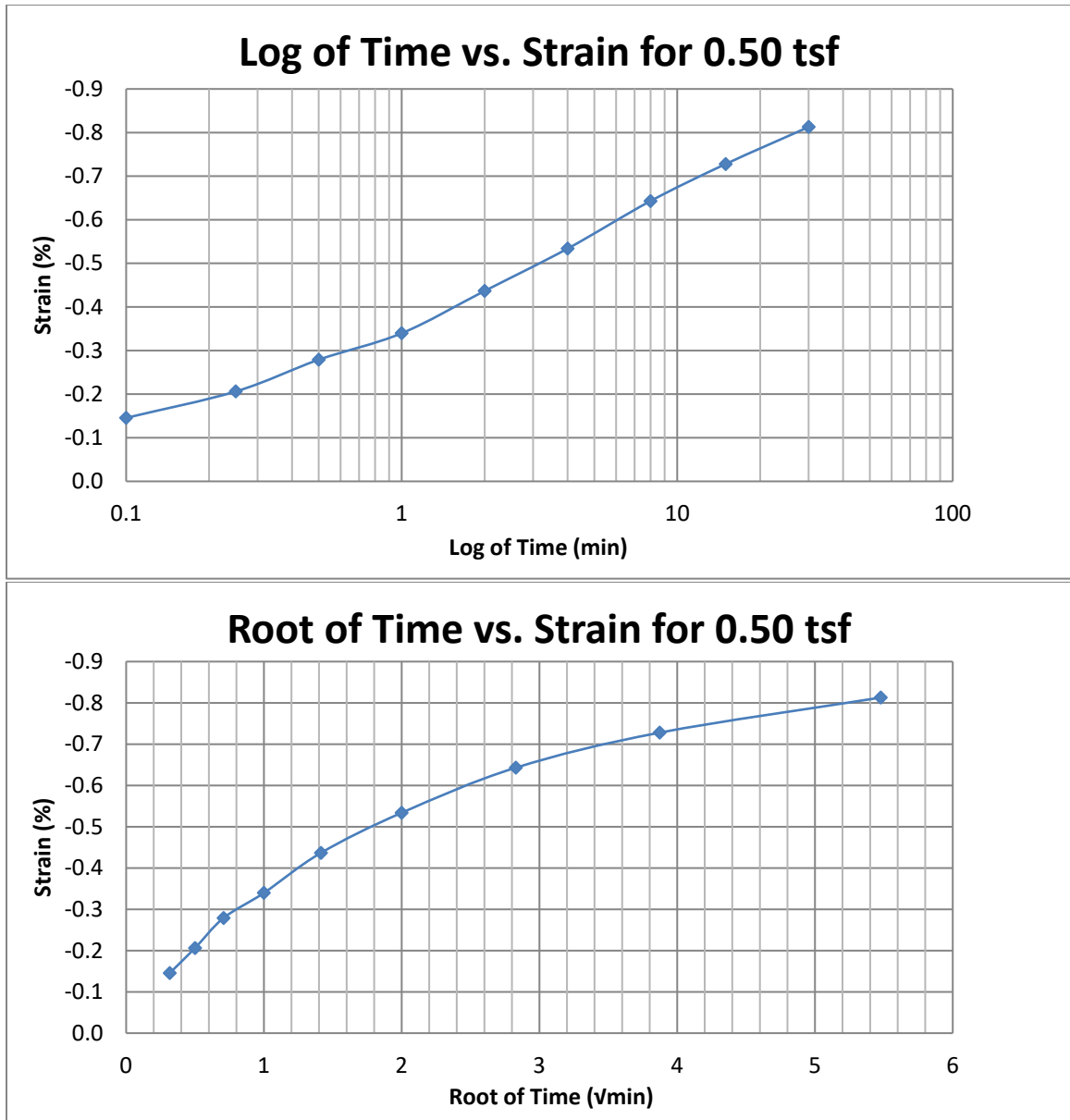


Figure A53 400 South at 30-32 feet

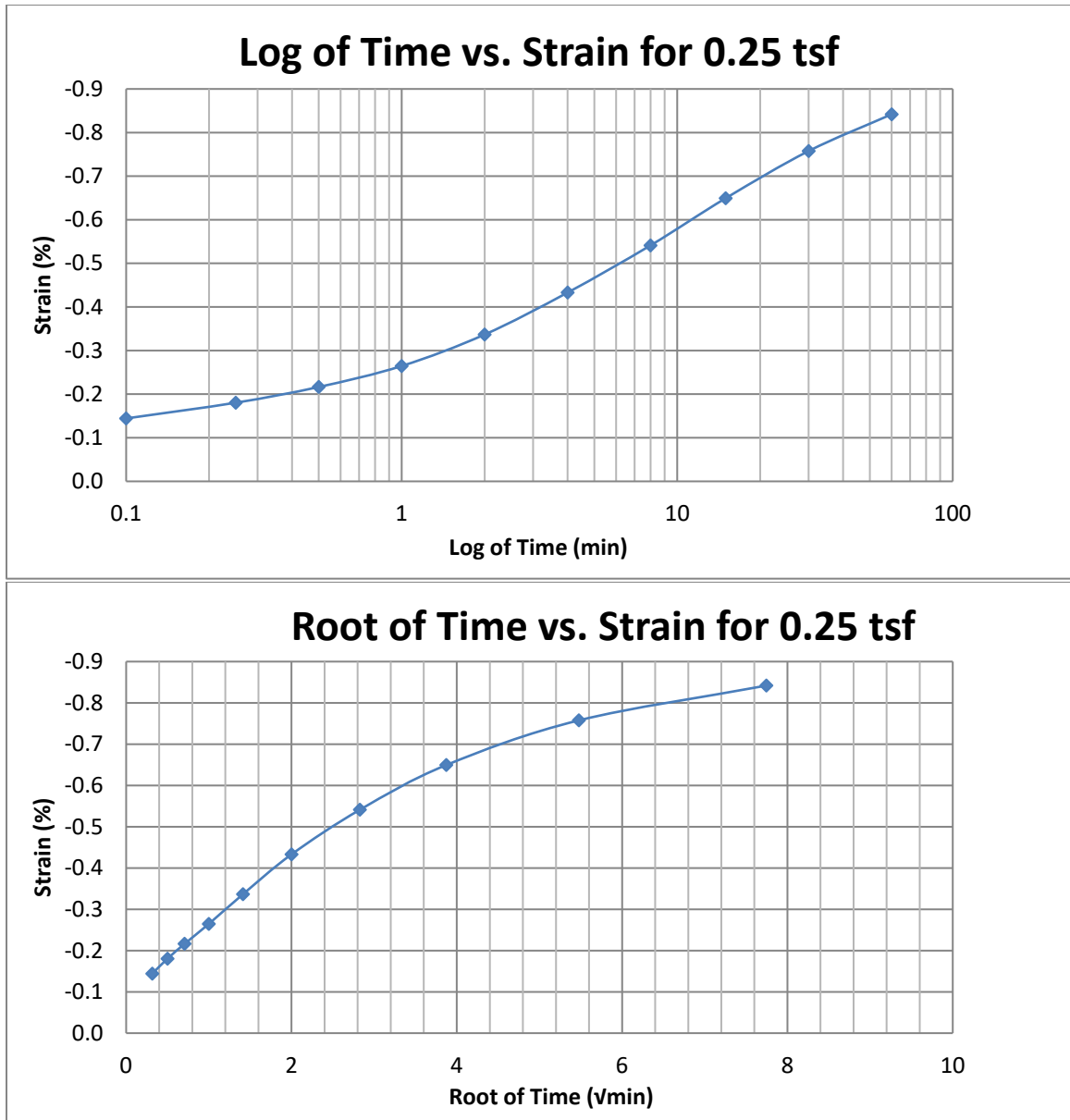


Figure A54 400 South at 30-32 feet

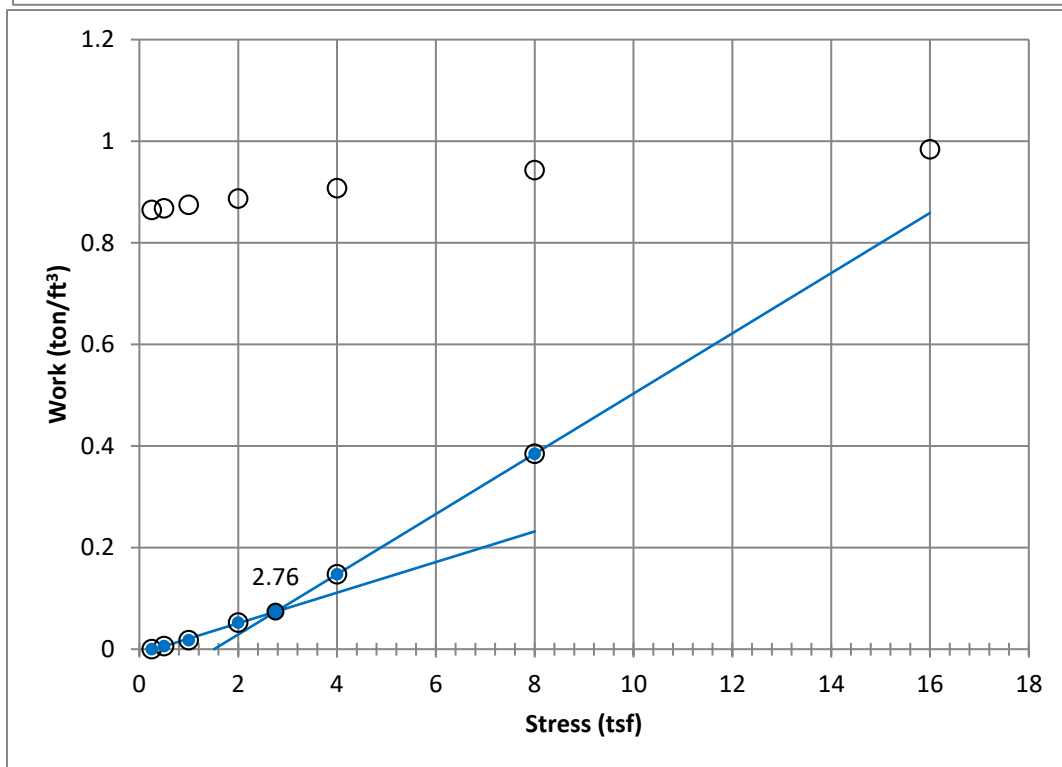
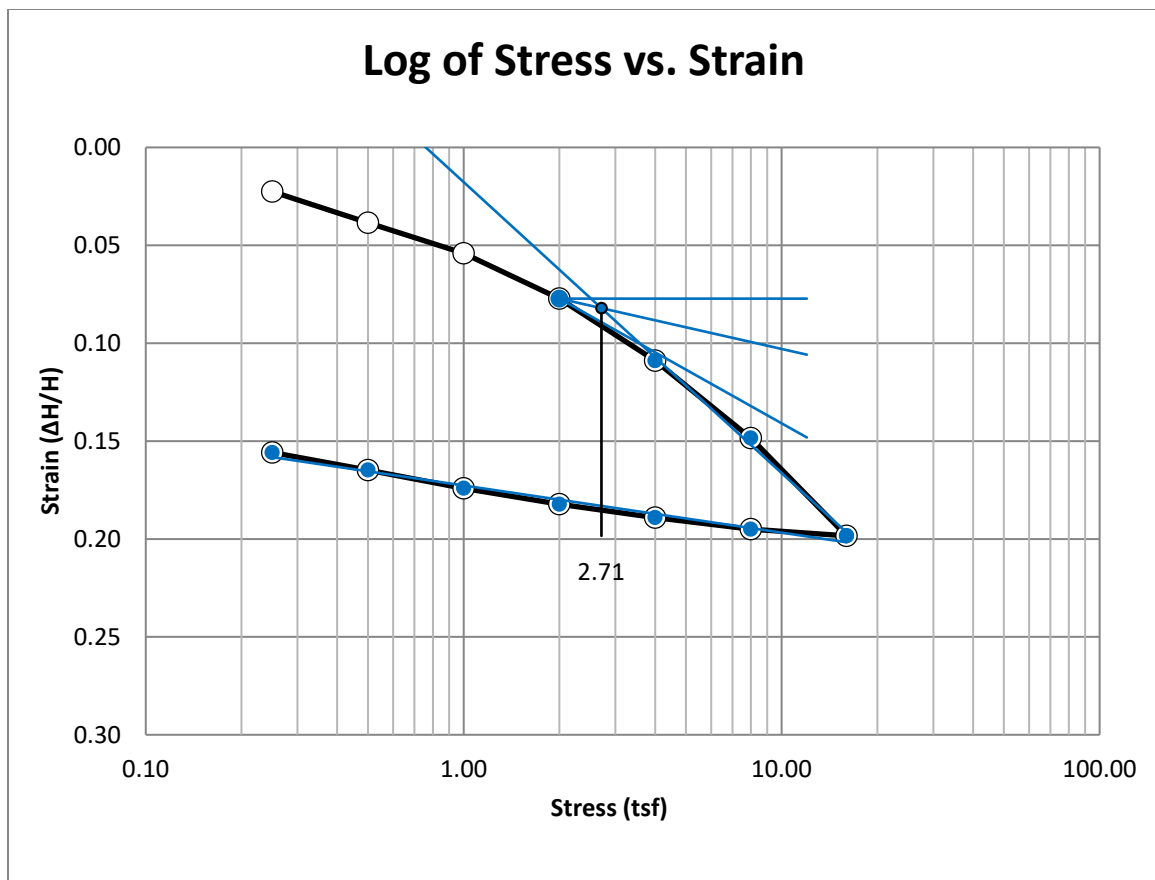


Figure A55 400 South at 37.5-39.5 feet

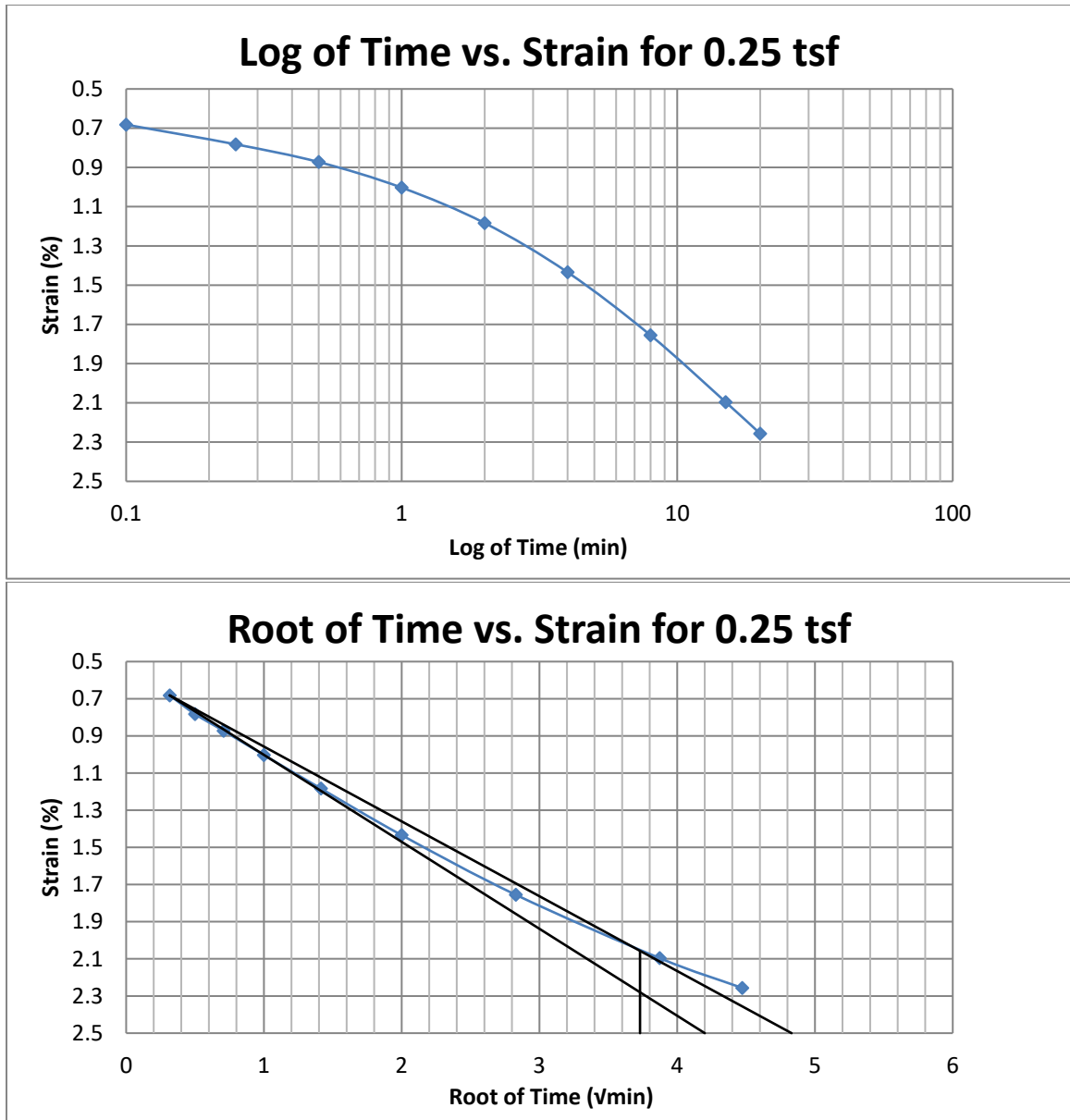


Figure A56 400 South at 37.5-39.5 feet

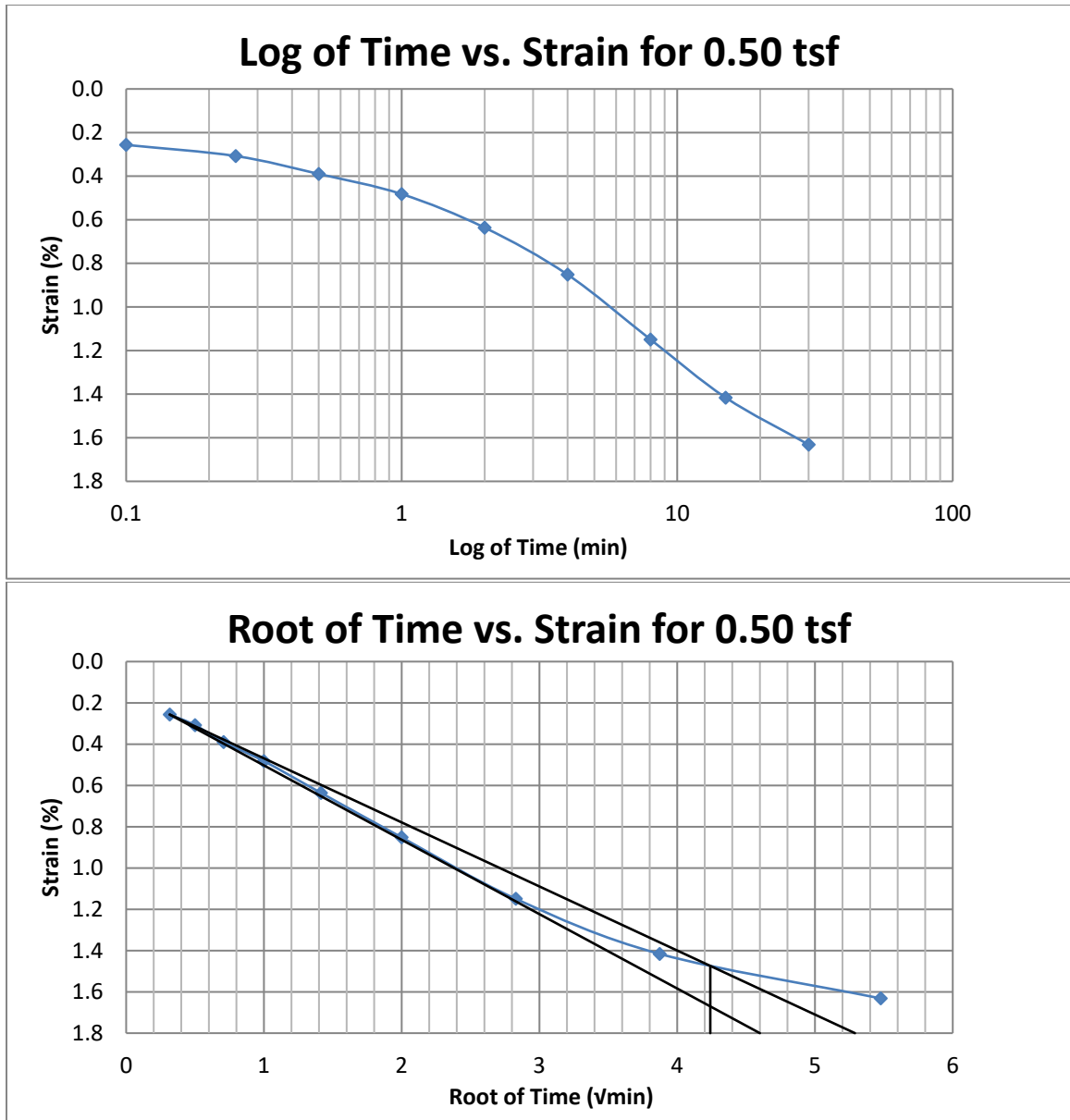


Figure A57 400 South at 37.5-39.5 feet

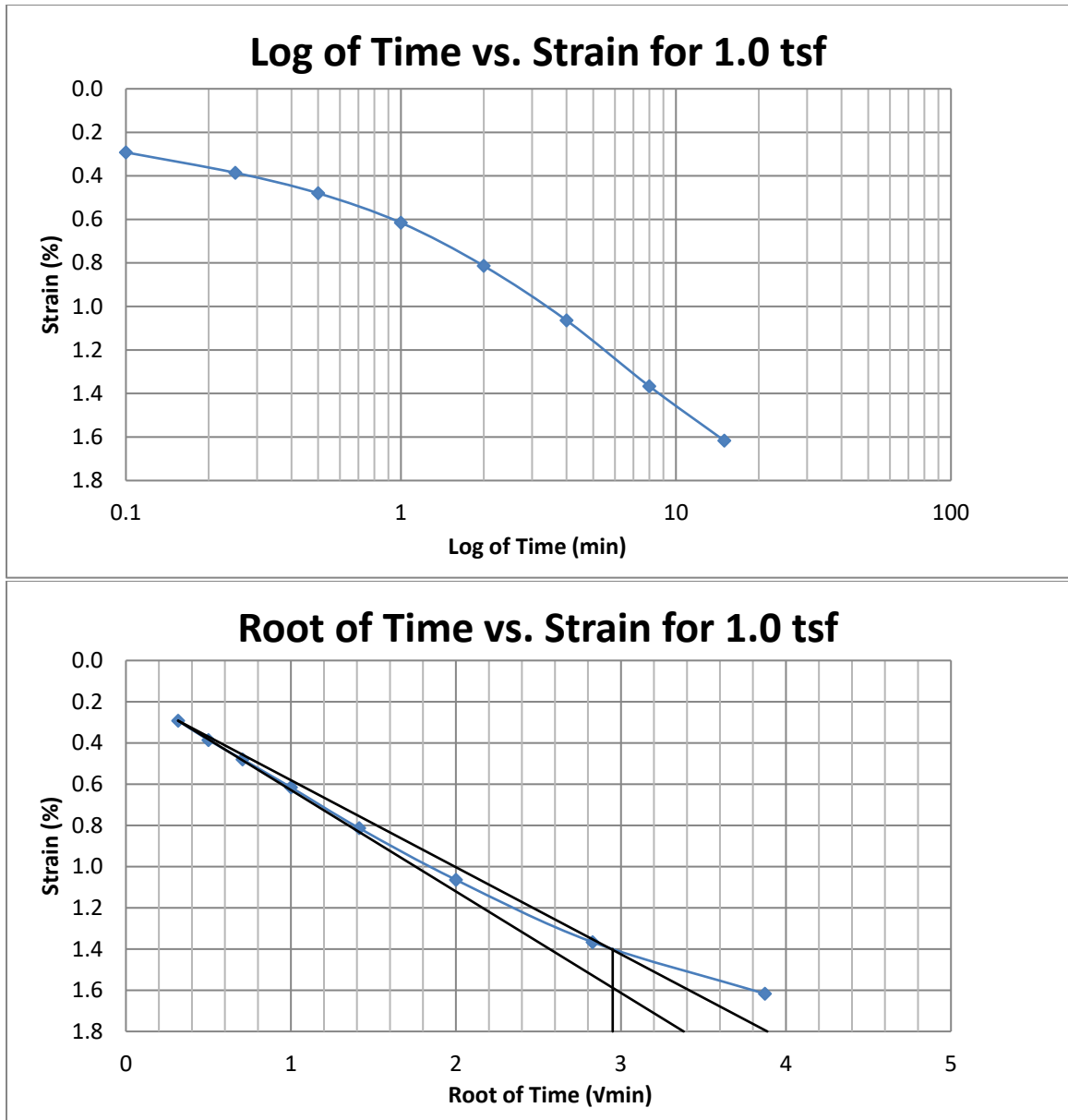


Figure A58 400 South at 37.5-39.5 feet



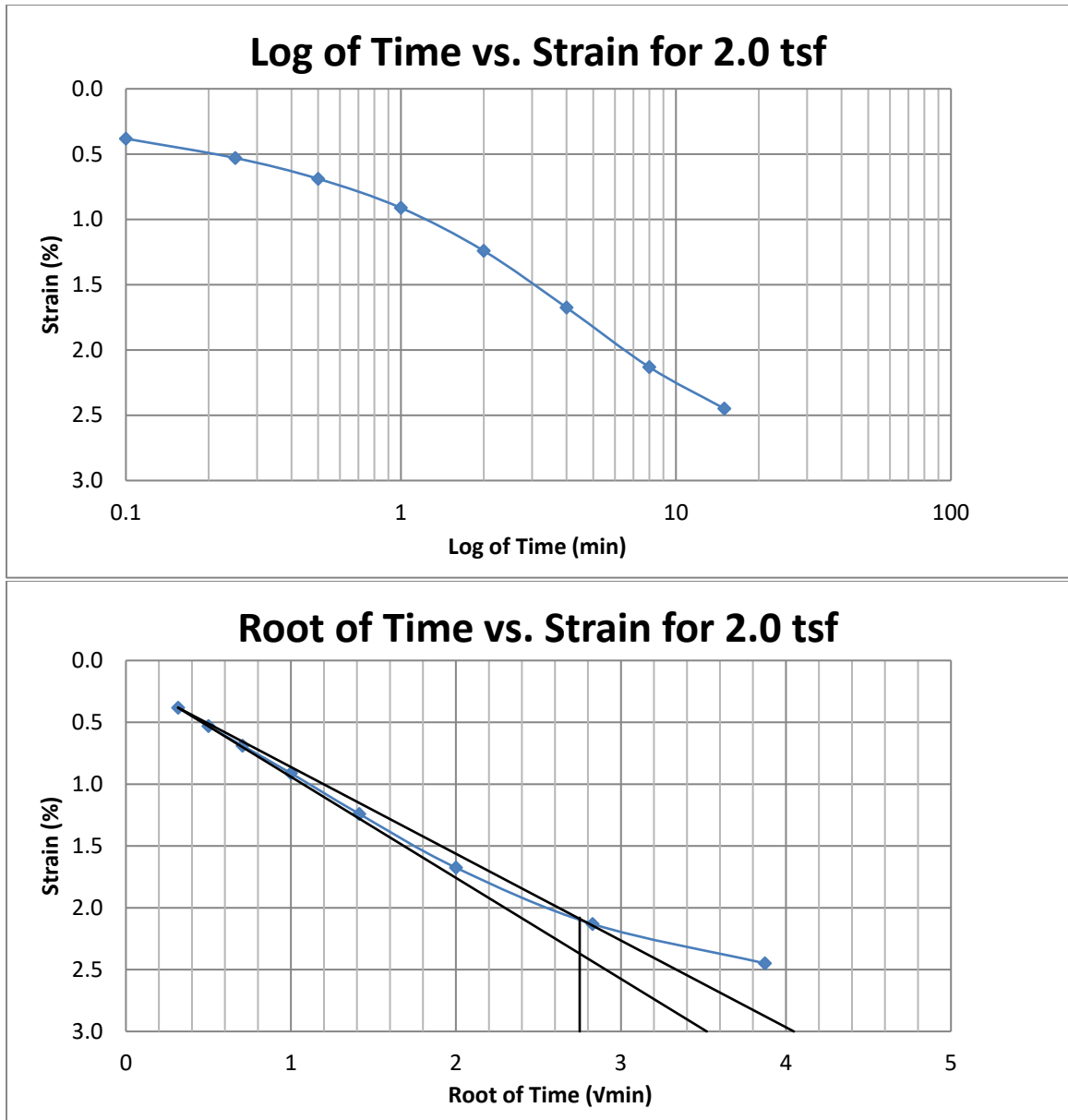


Figure A59 400 South at 37.5-39.5 feet

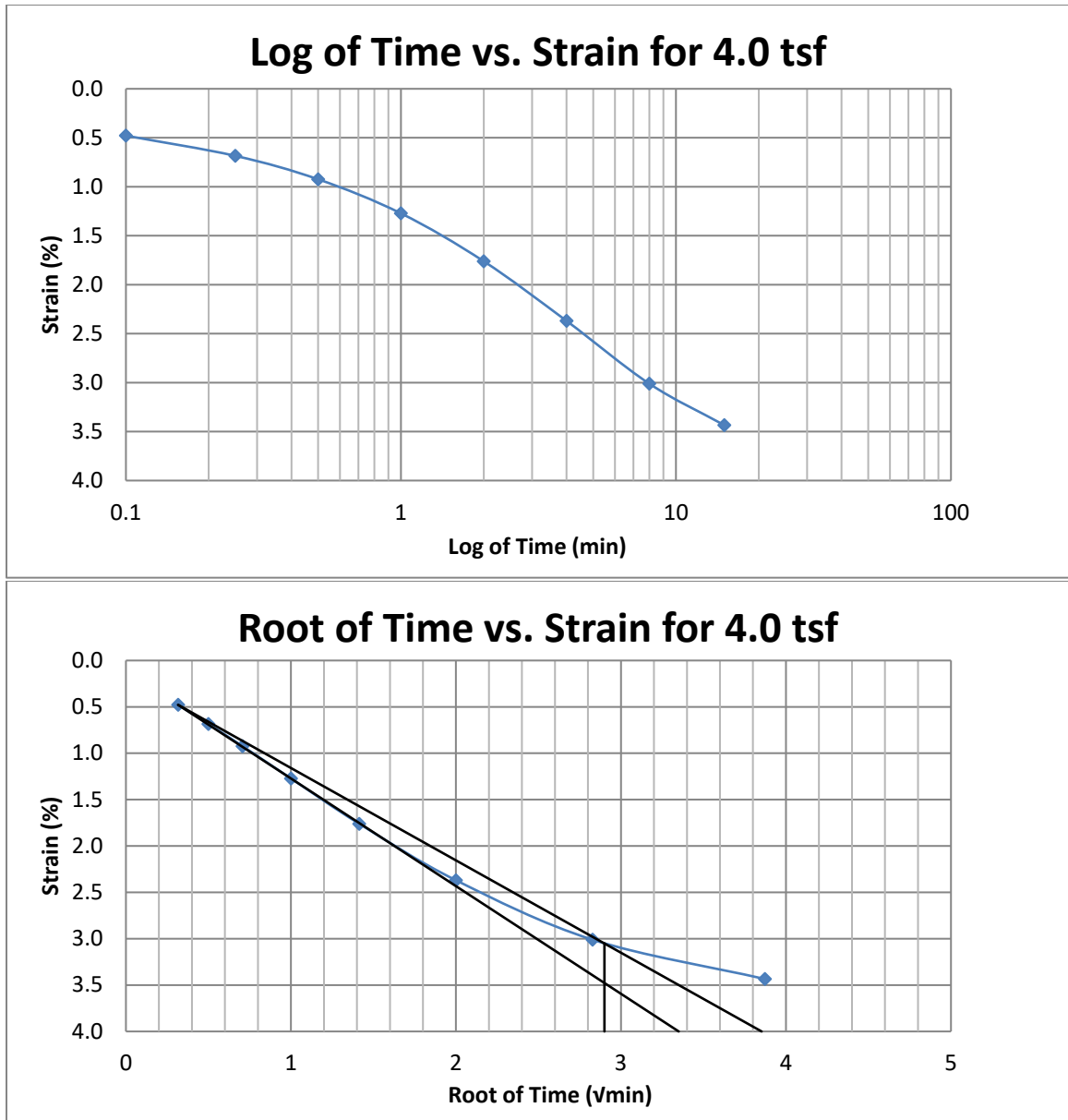


Figure A60 400 South at 37.5-39.5 feet

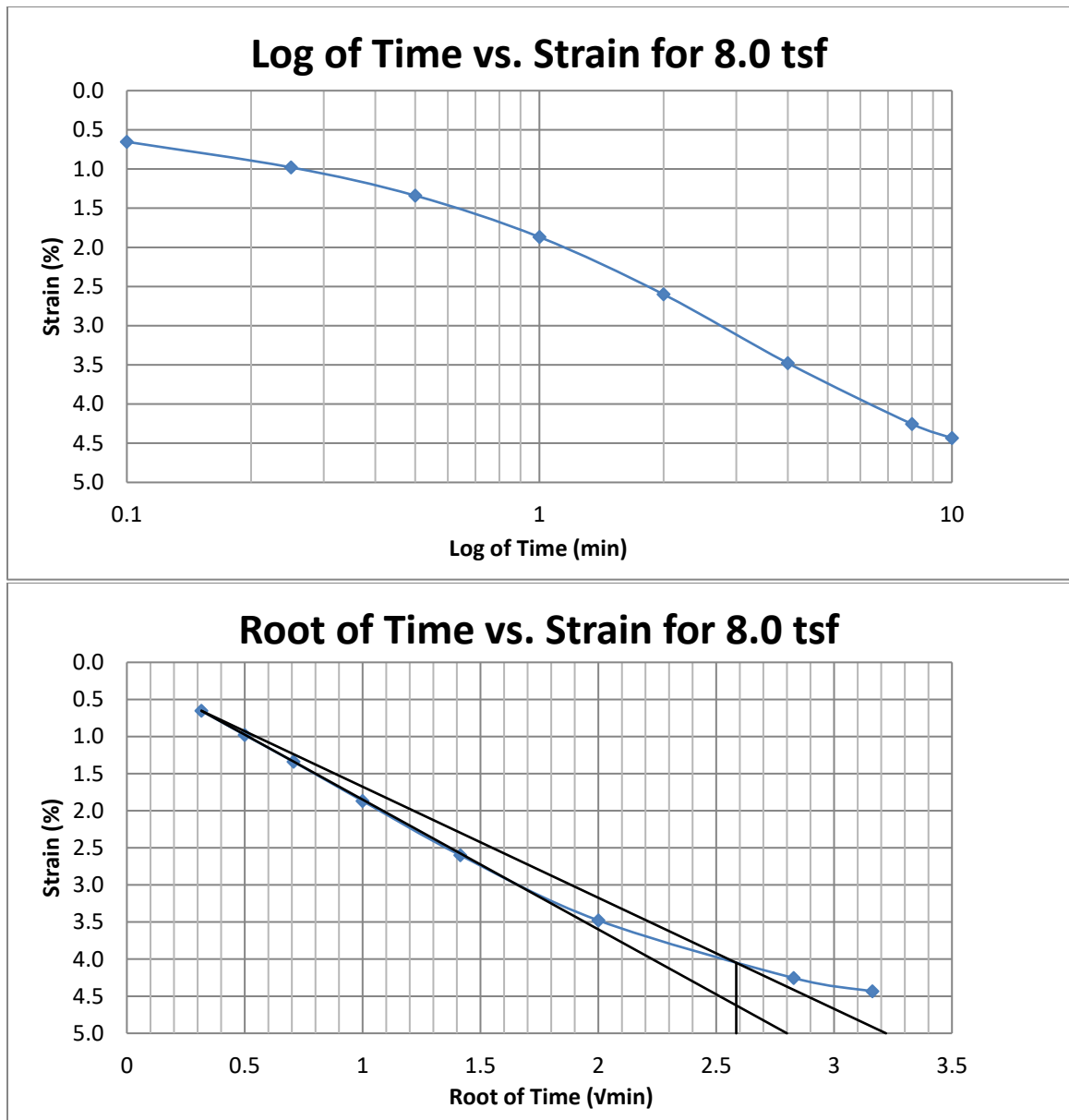


Figure A61 400 South at 37.5-39.5 feet

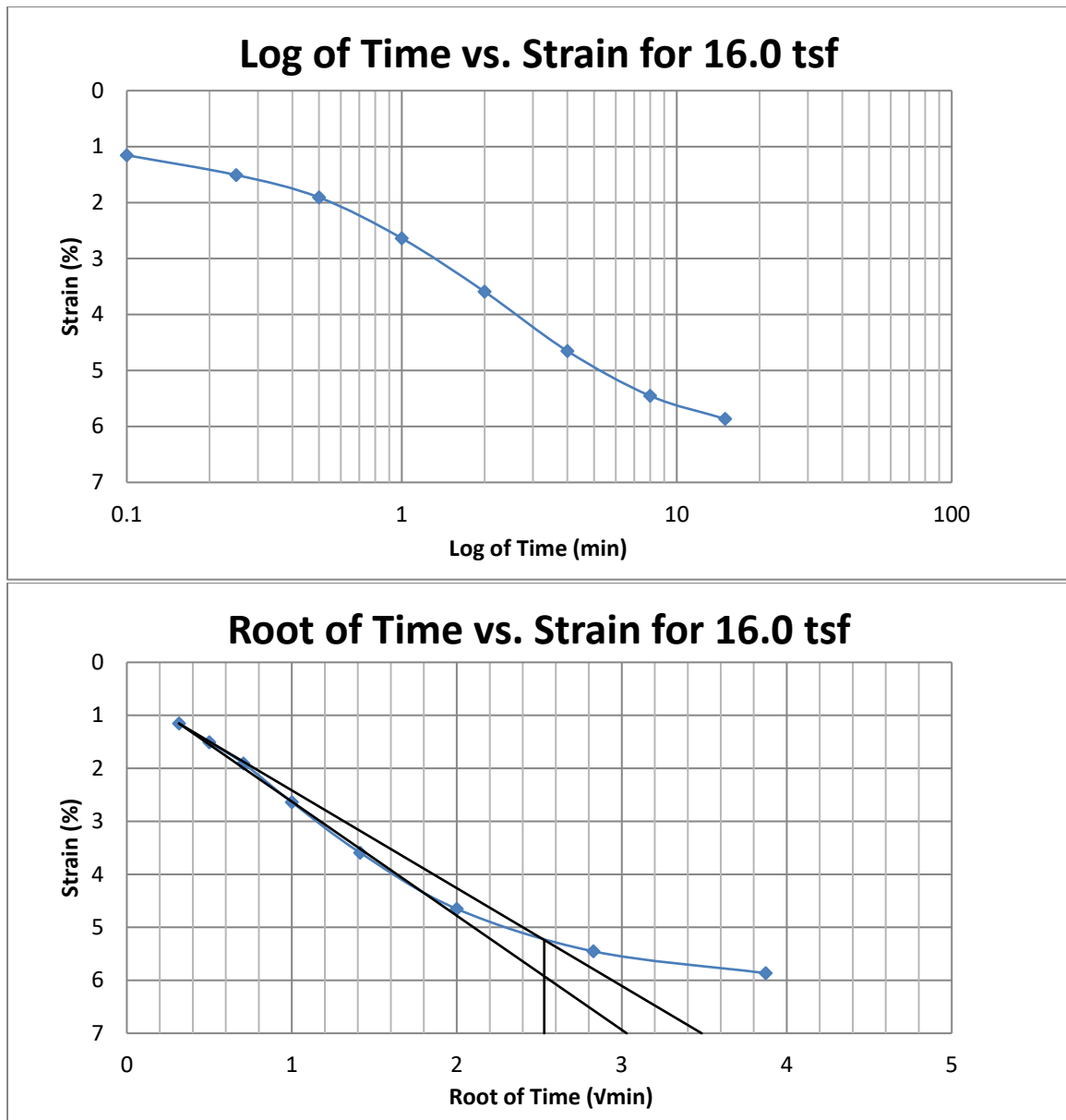


Figure A62 400 South at 37.5-39.5 feet

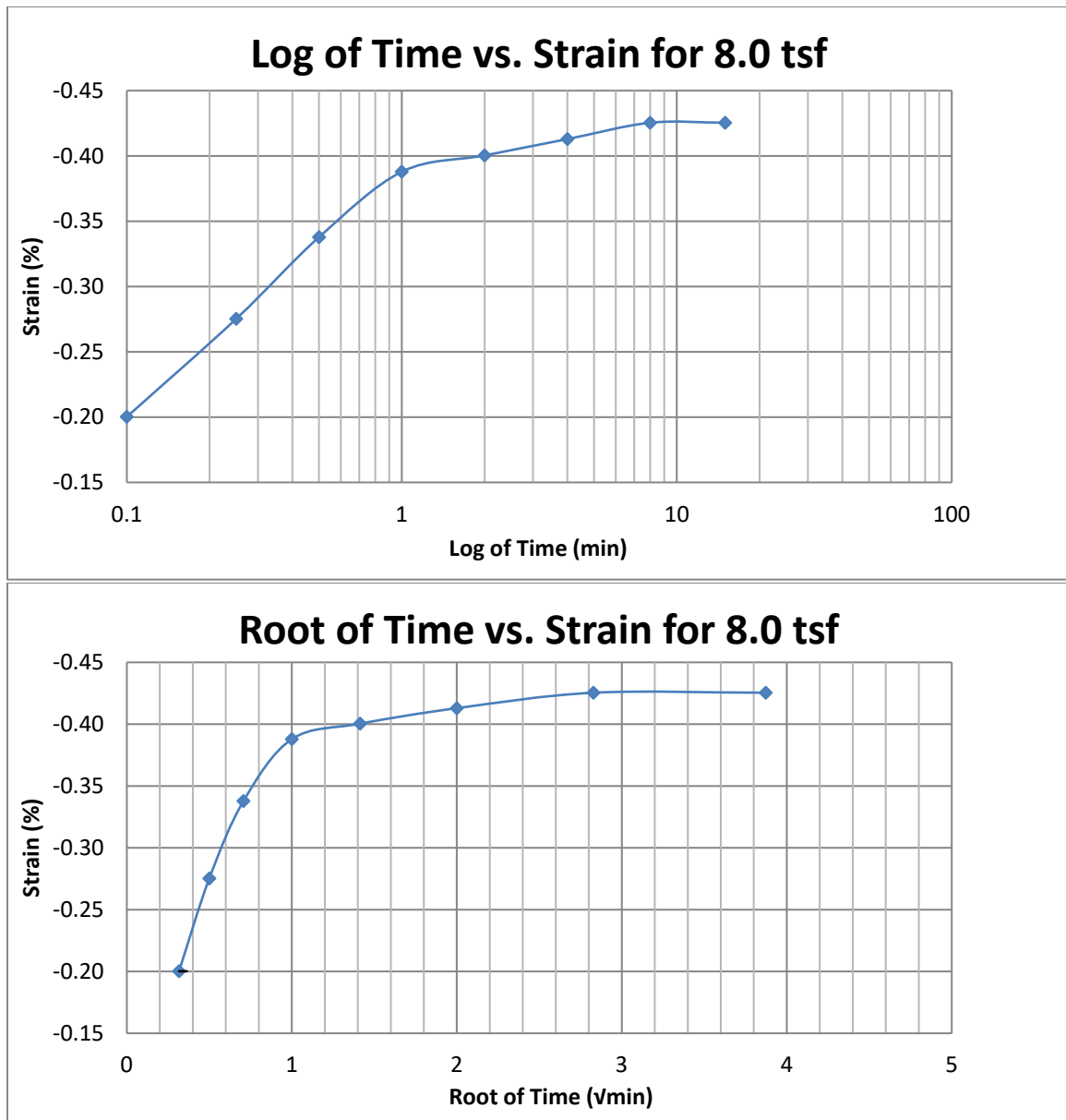


Figure A63 400 South at 37.5-39.5 feet

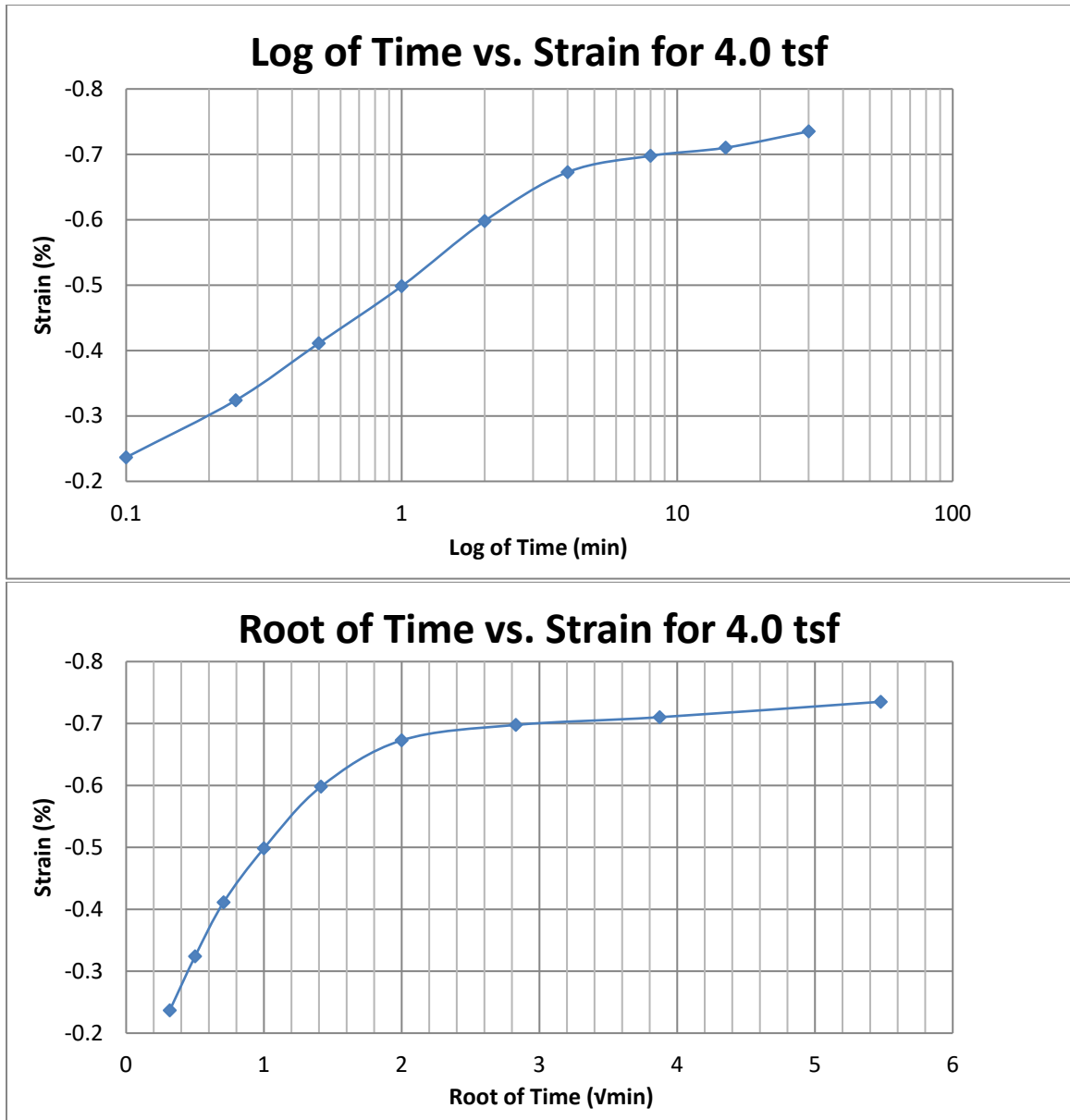


Figure A64 400 South at 37.5-39.5 feet

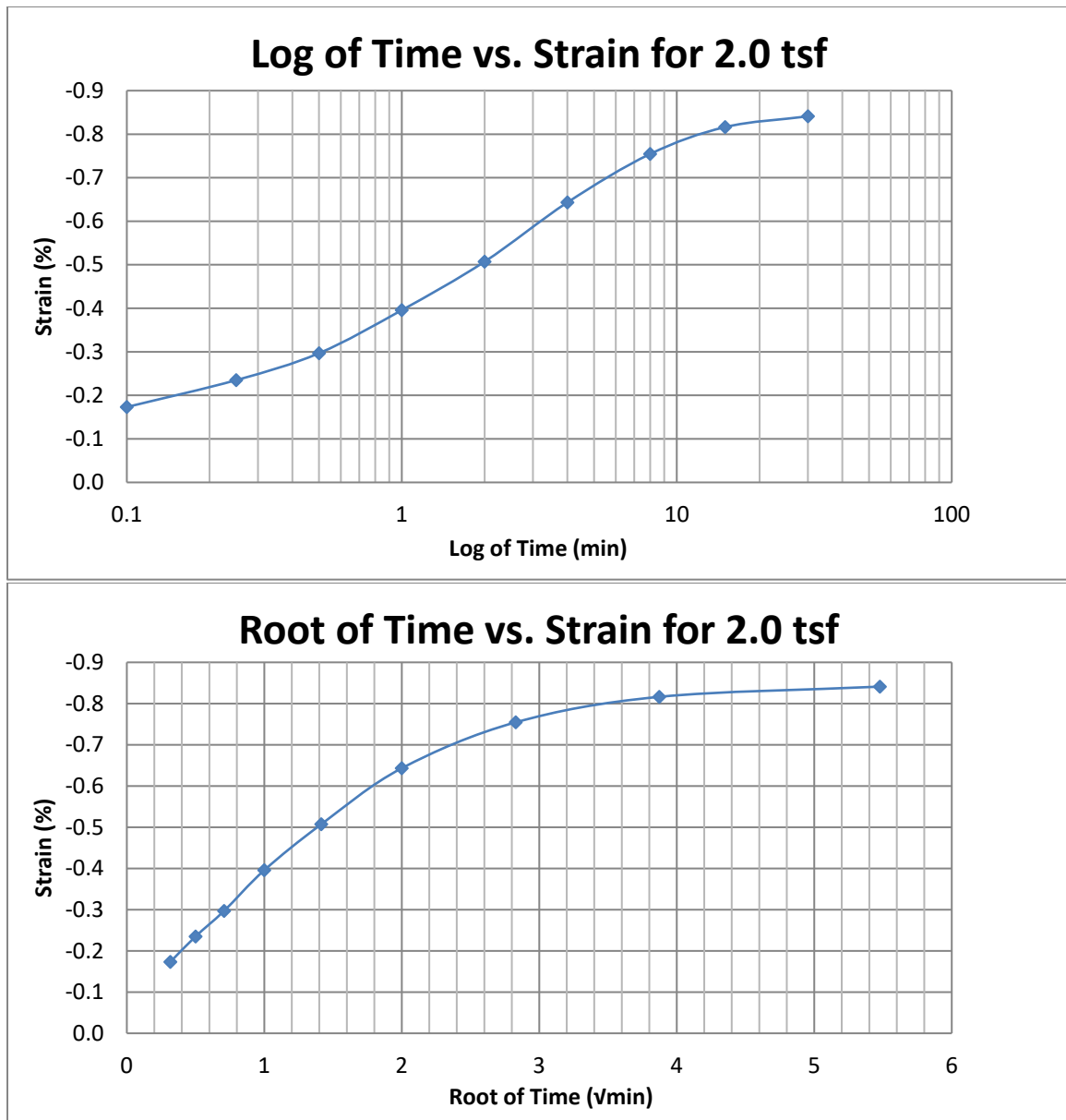


Figure A65 400 South at 37.5-39.5 feet

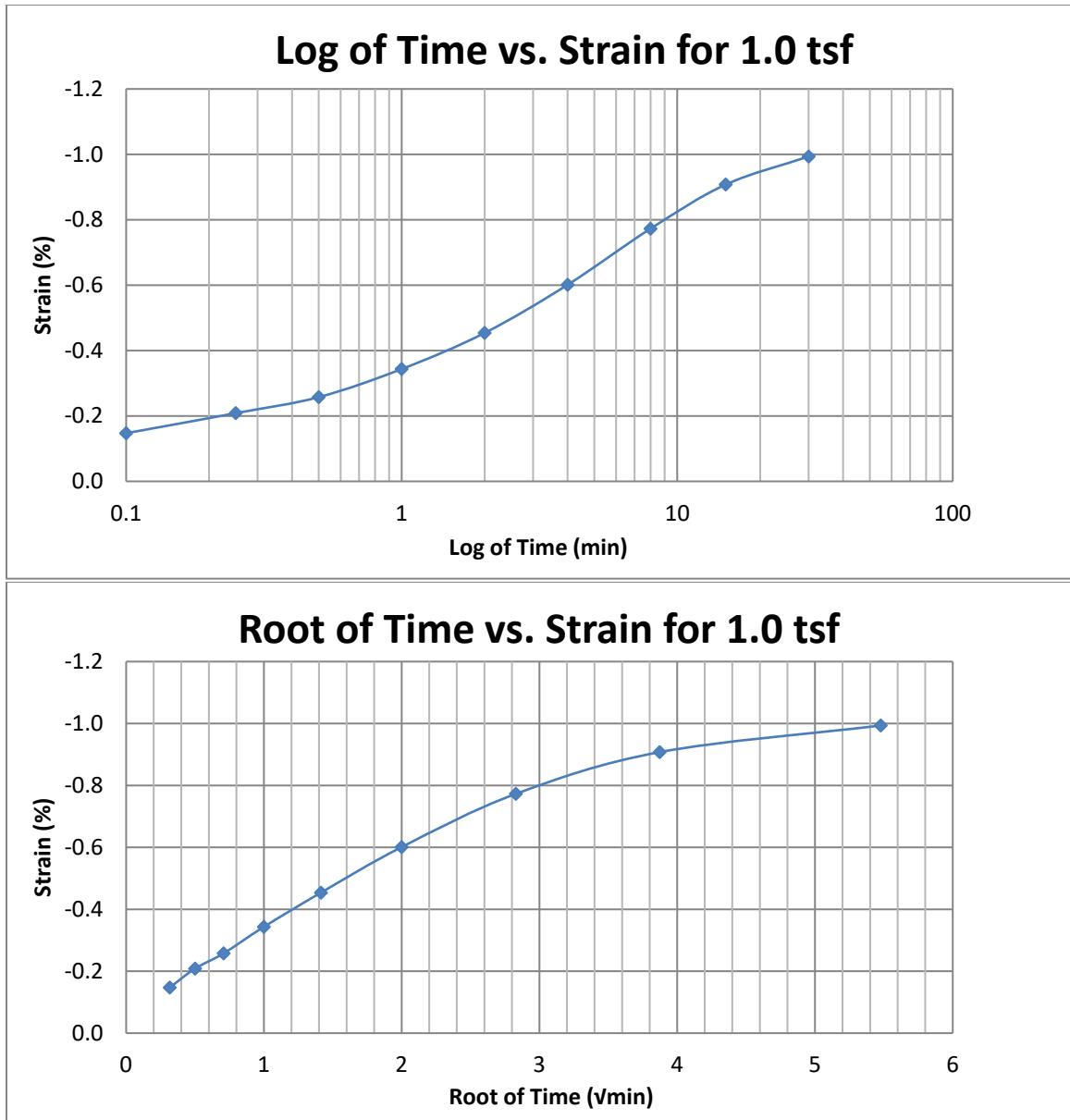


Figure A66 400 South at 37.5-39.5 feet



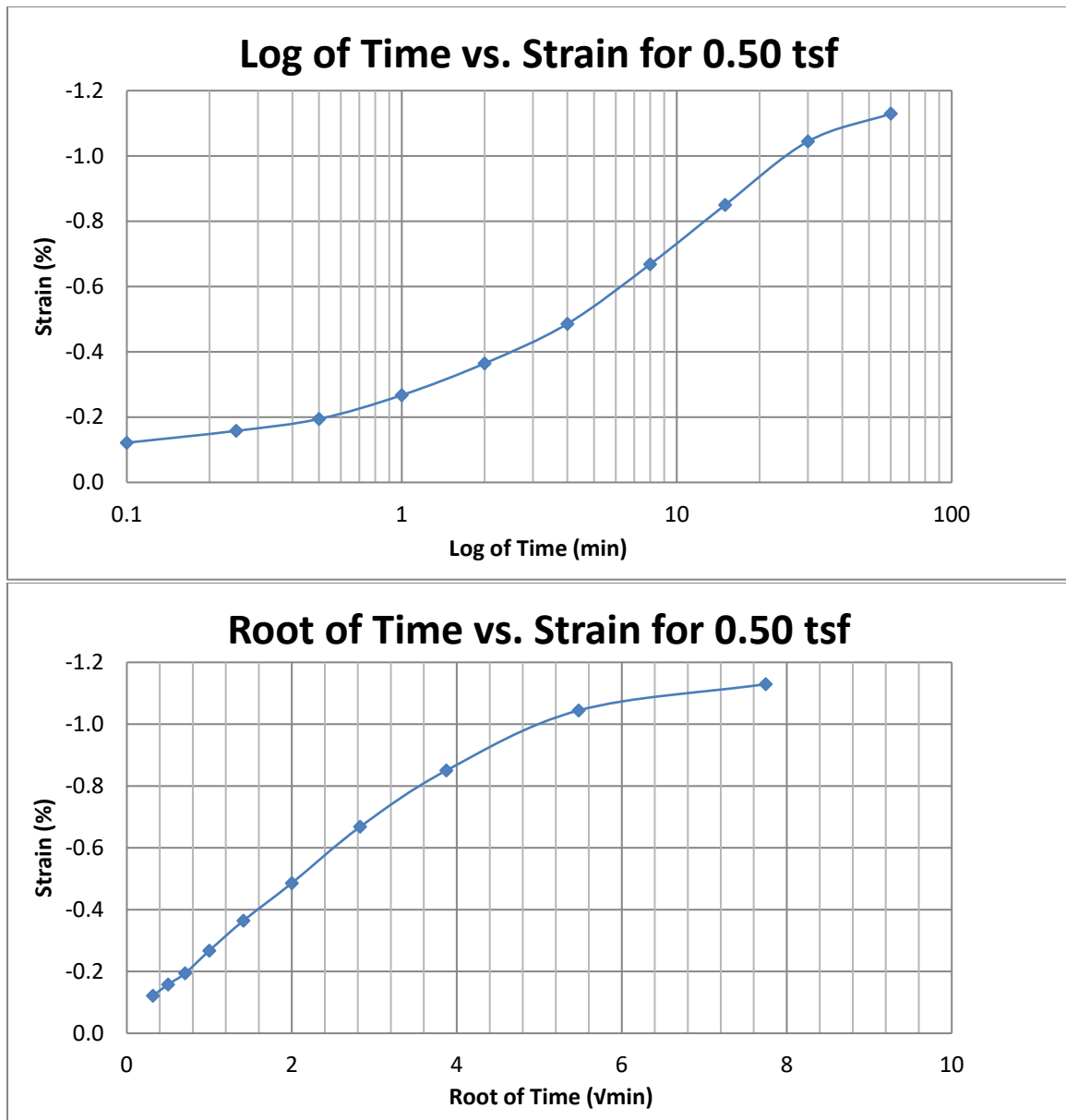
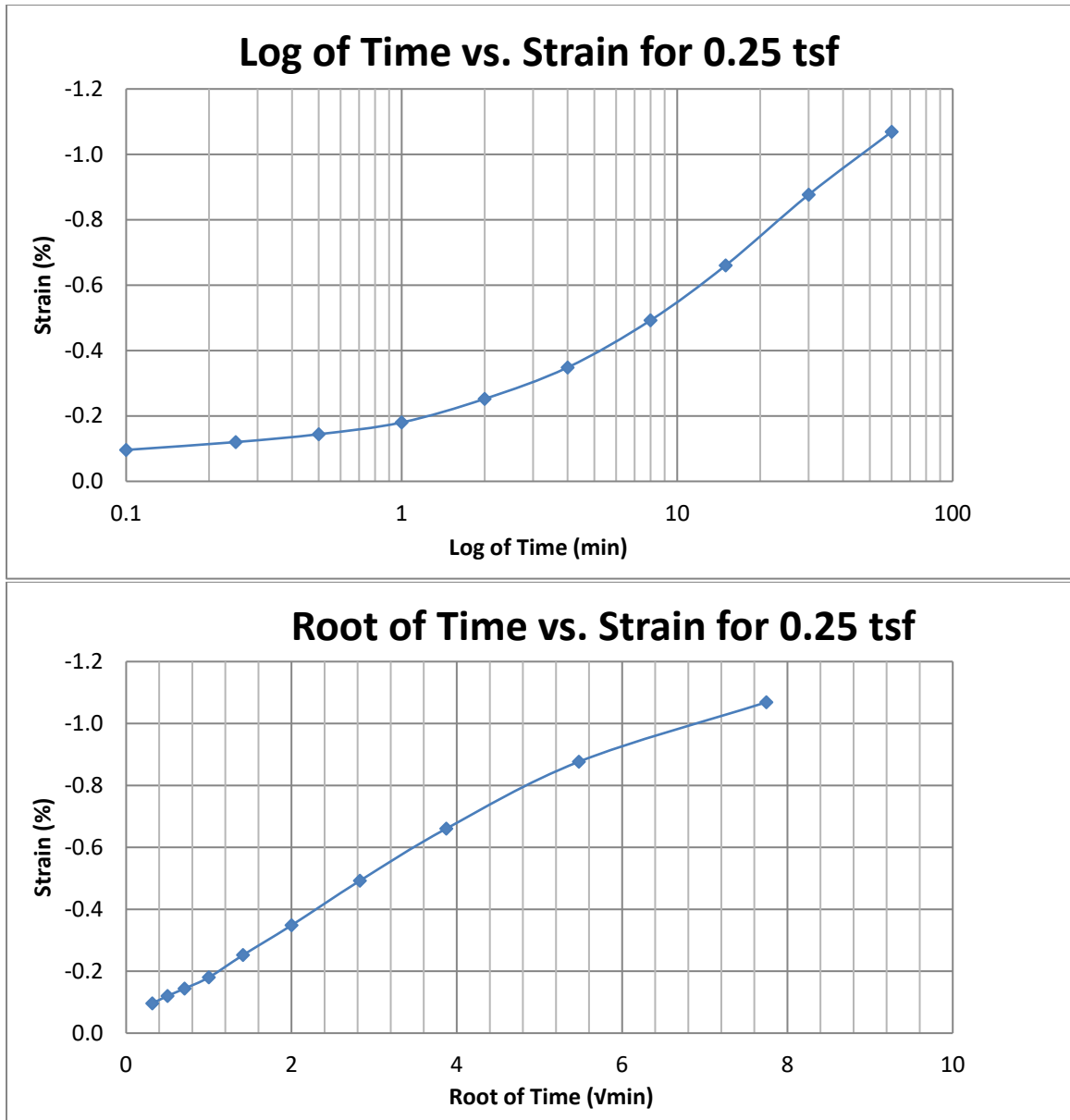


Figure A67 400 South at 37.5-39.5 feet



**Figure A68 400 South at 37.5-39.5 feet**

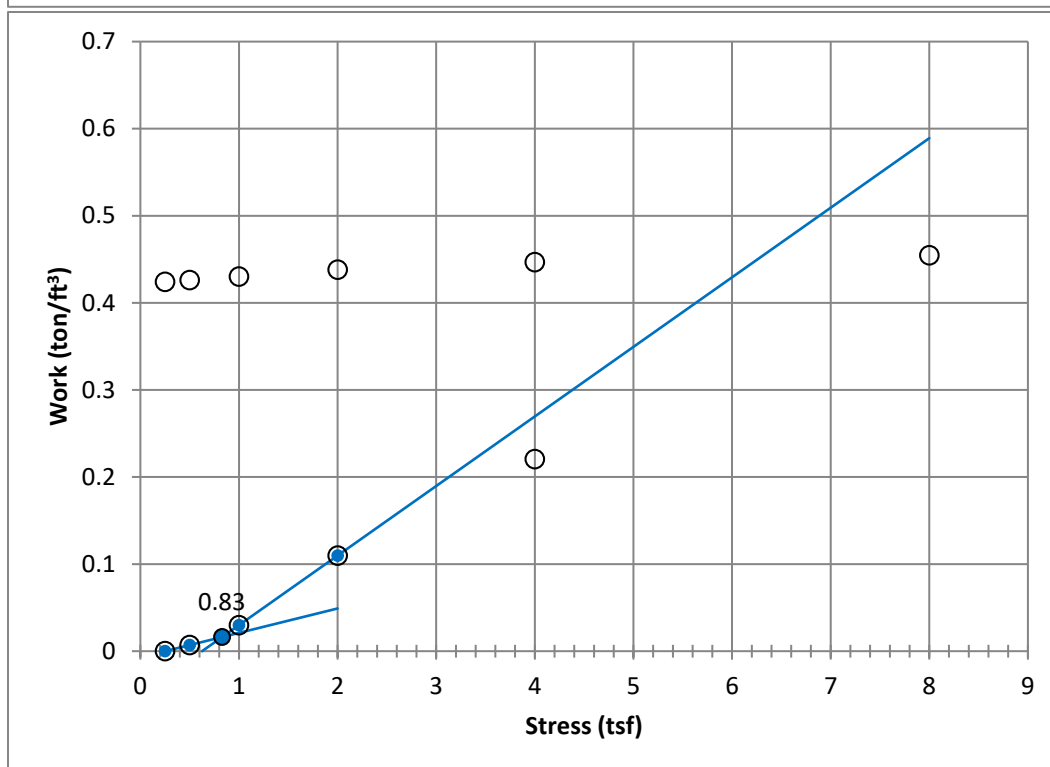
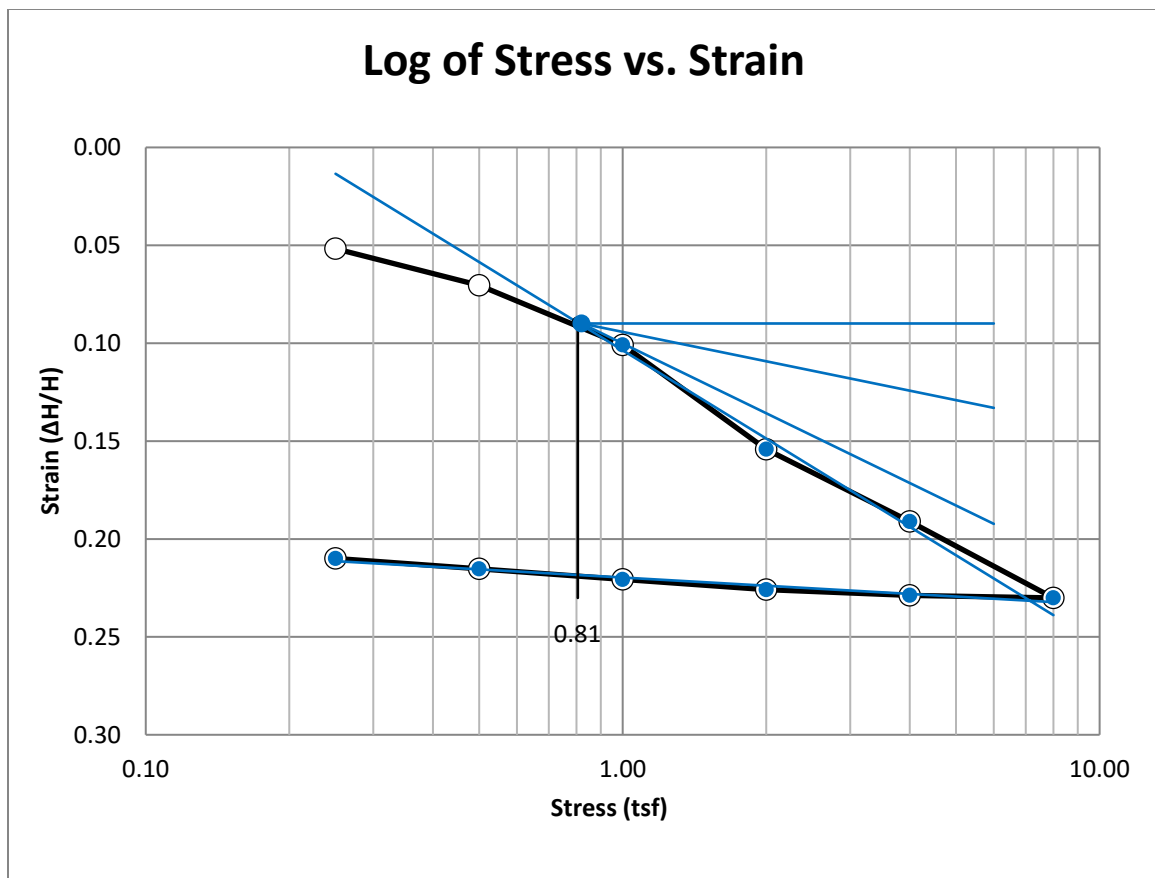


Figure A69 400 South at 40-42 feet

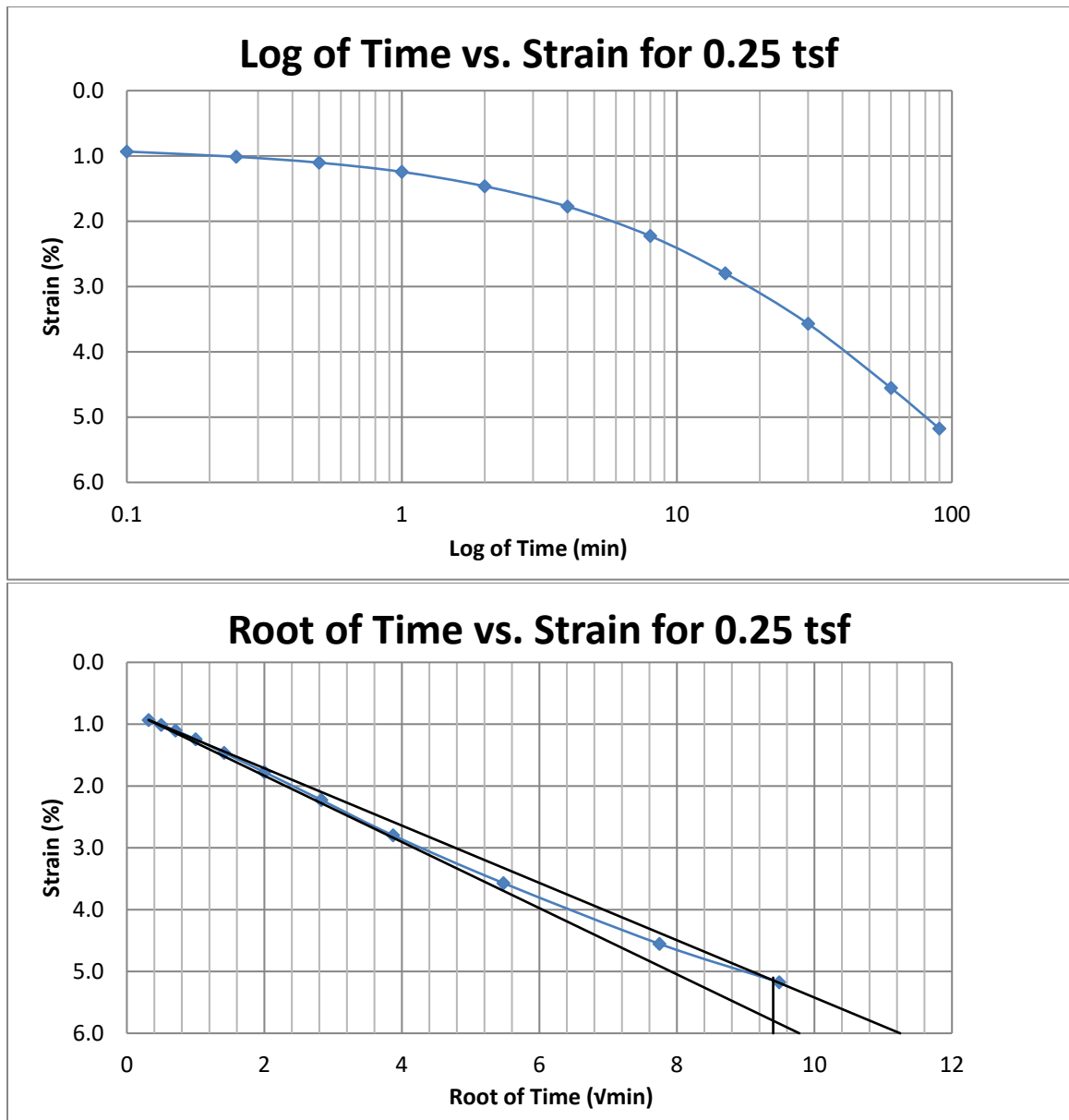


Figure A70 400 South at 40-42 feet

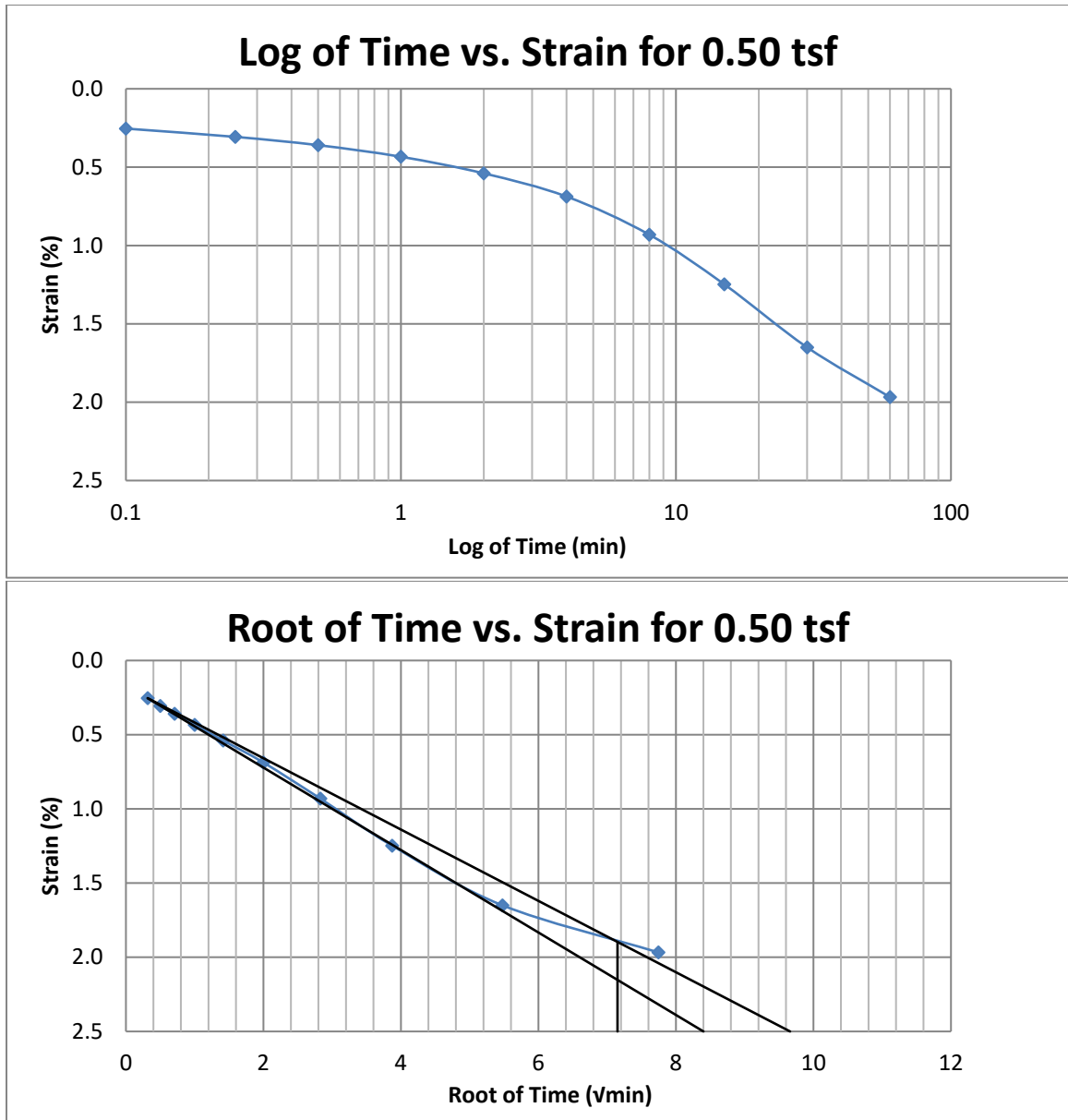


Figure A71 400 South at 40-42 feet

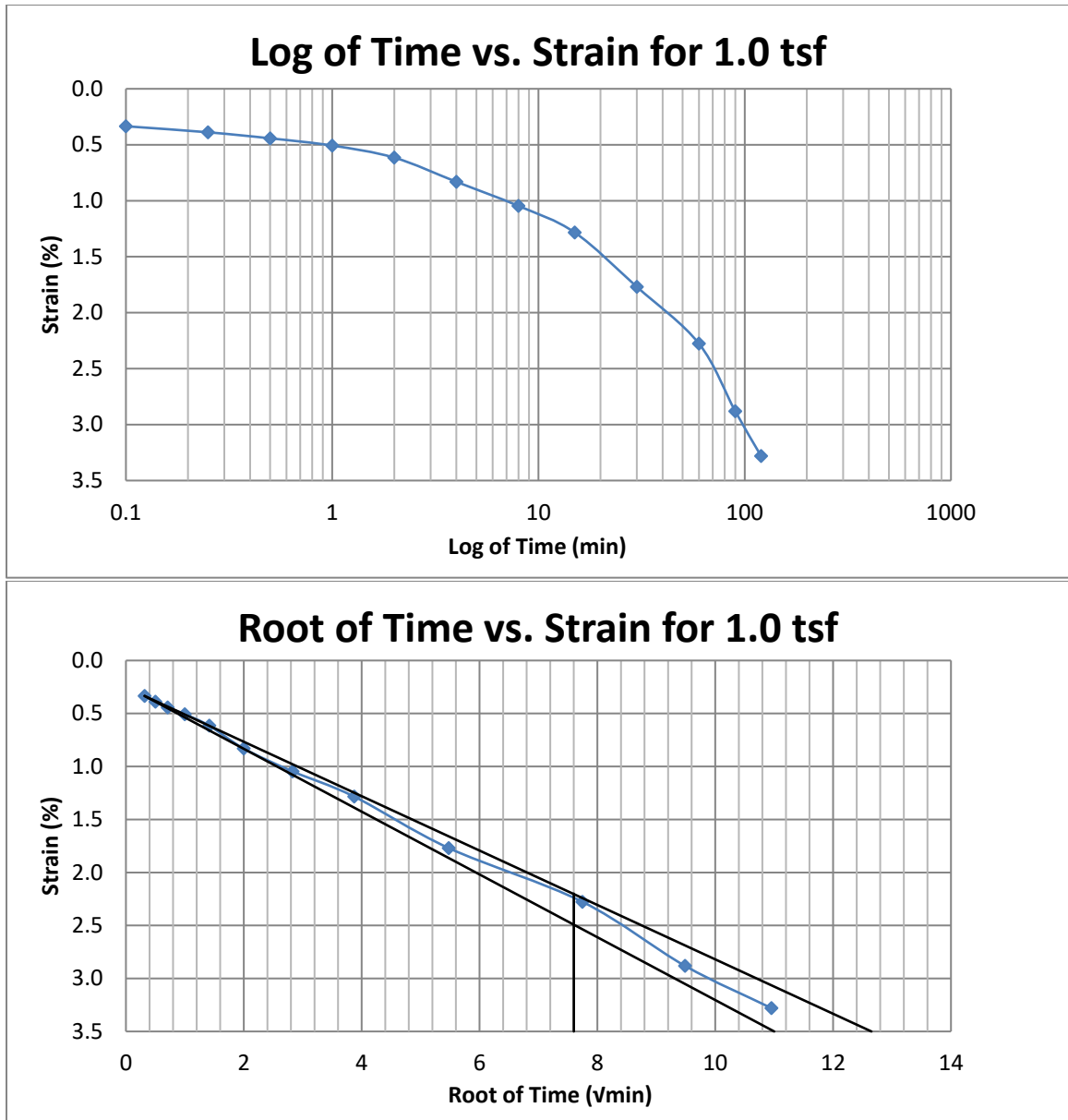


Figure A72 400 South at 40-42 feet

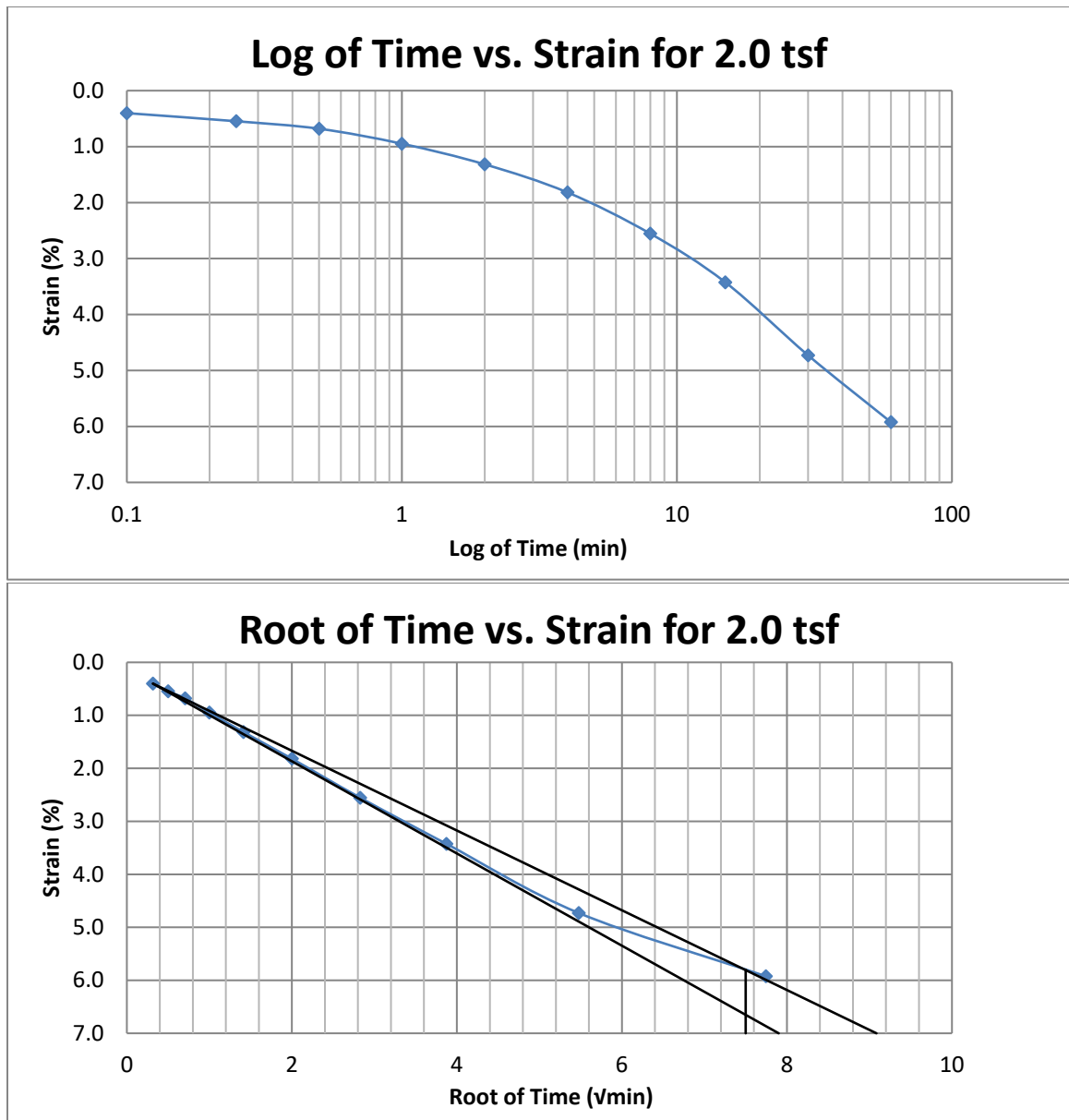


Figure A73 400 South at 40-42 feet

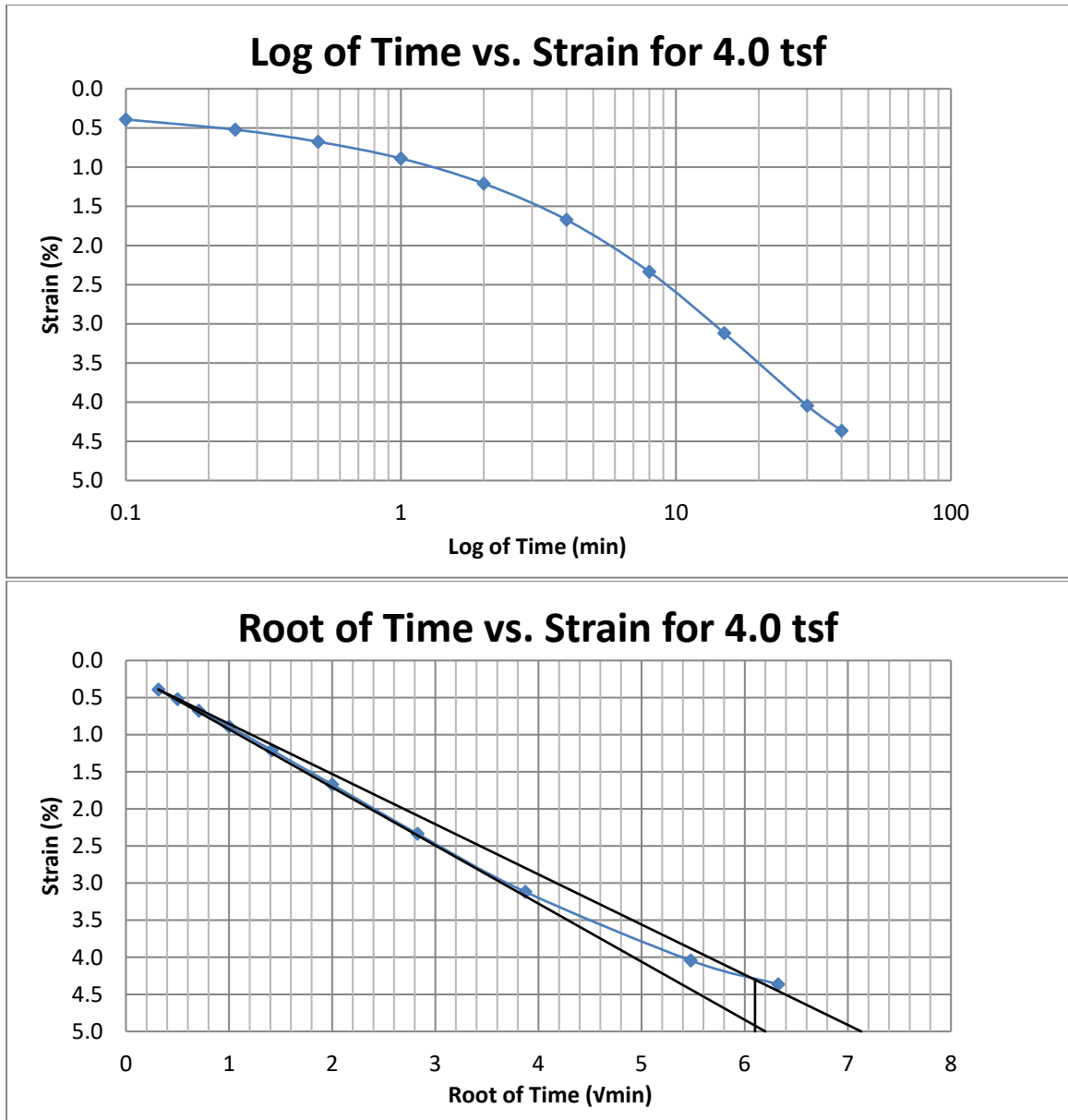


Figure A74 400 South at 40-42 feet



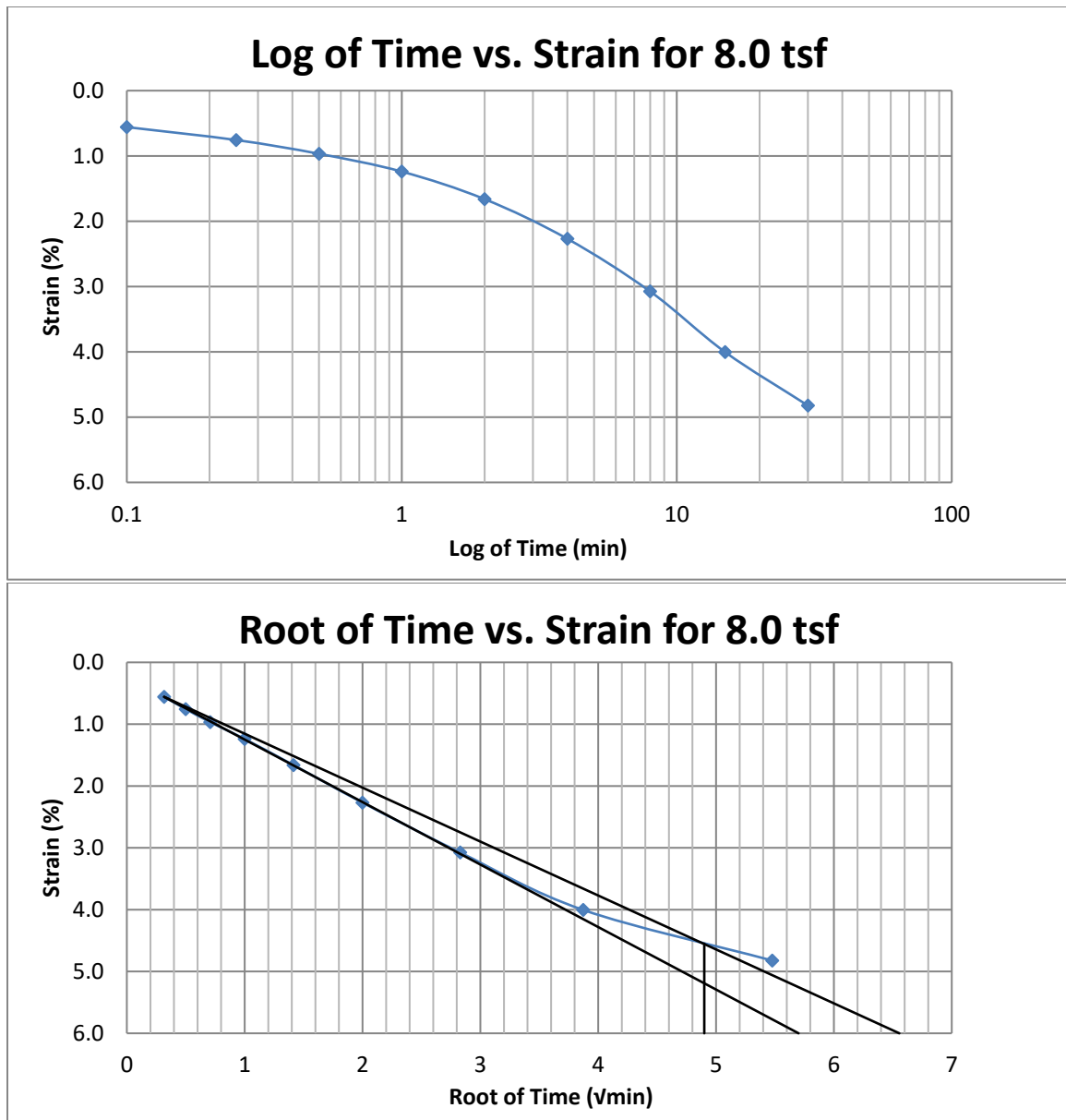


Figure A75 400 South at 40-42 feet

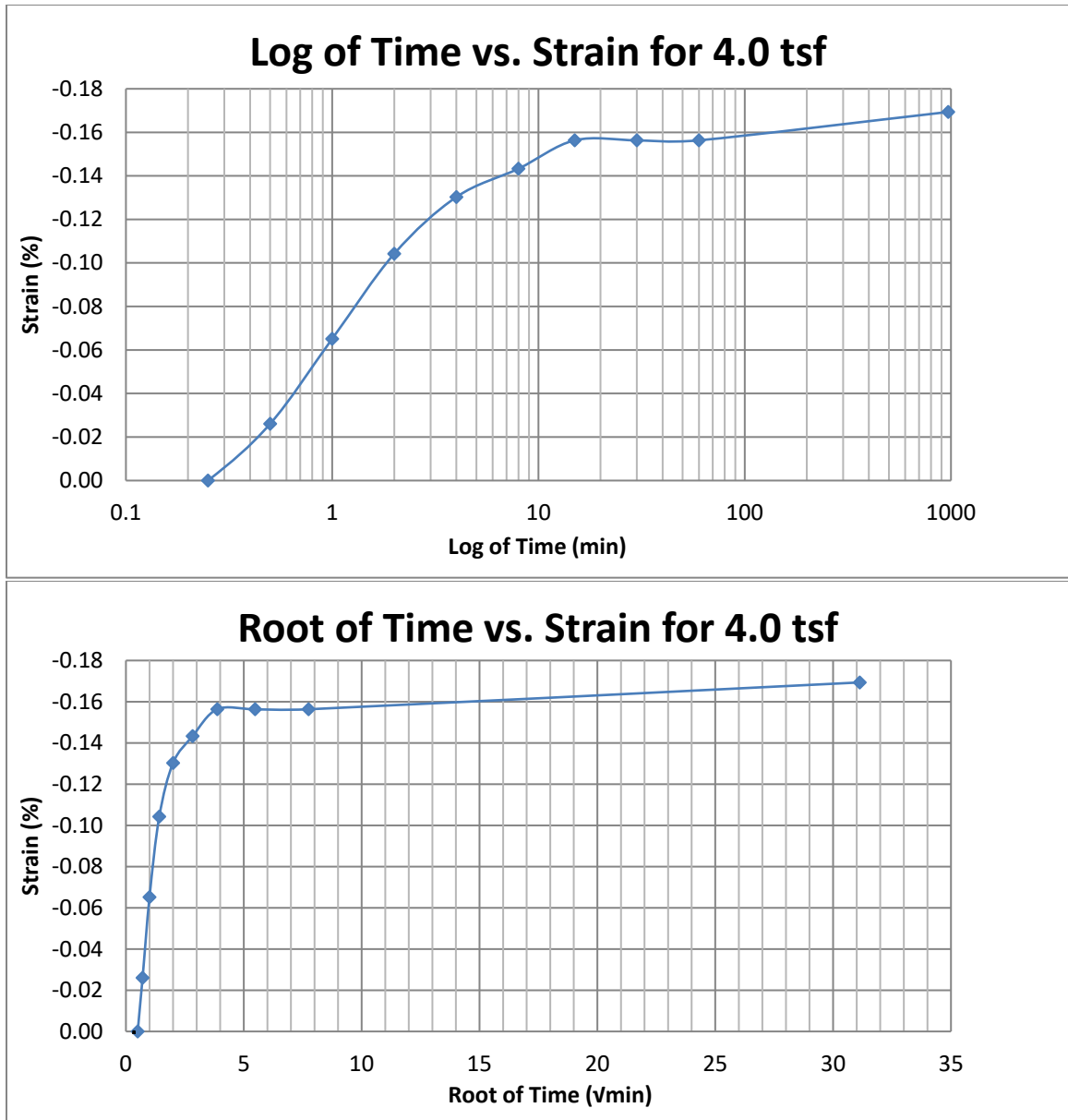


Figure A76 400 South at 40-42 feet

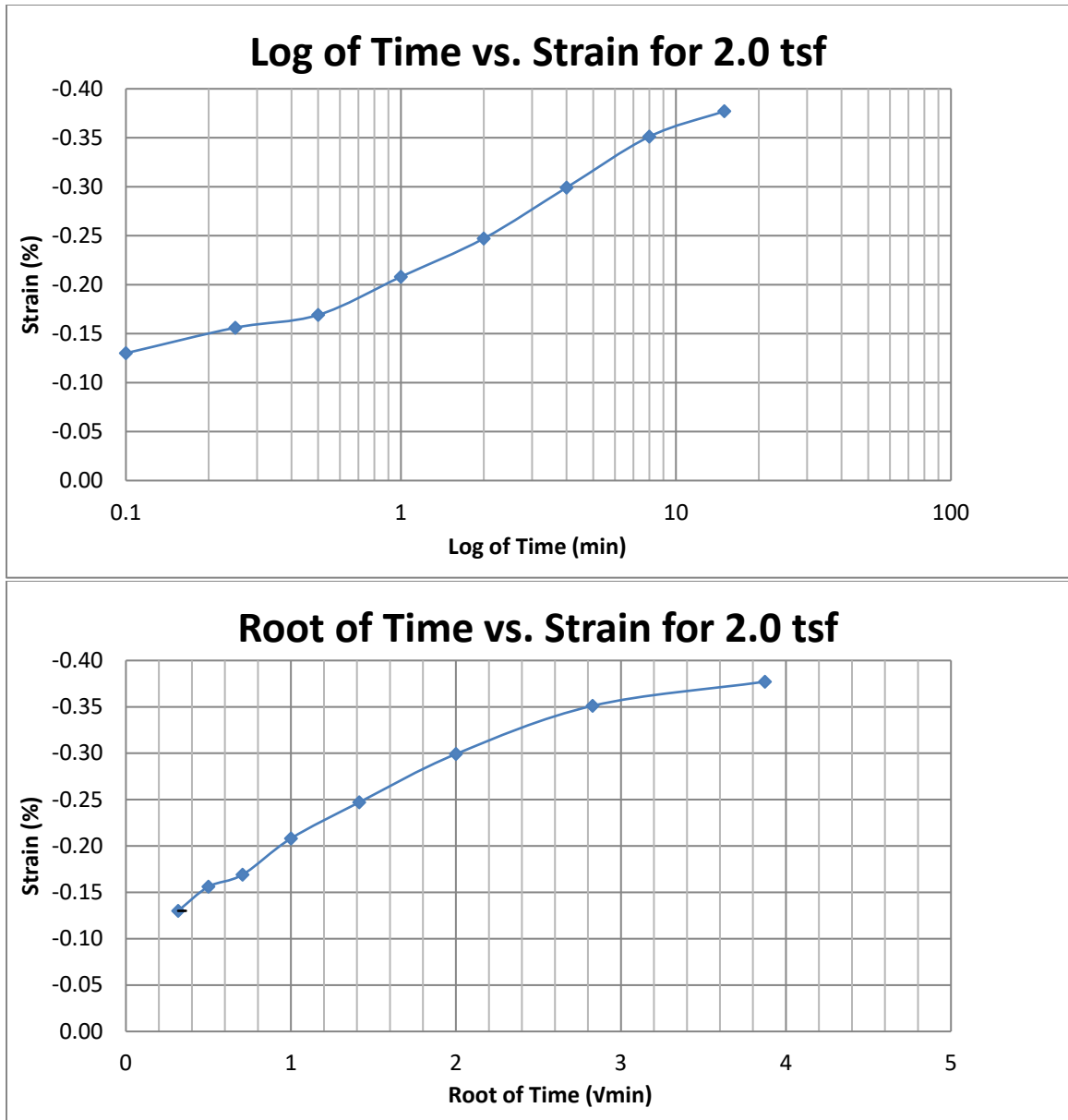


Figure A77 400 South at 40-42 feet

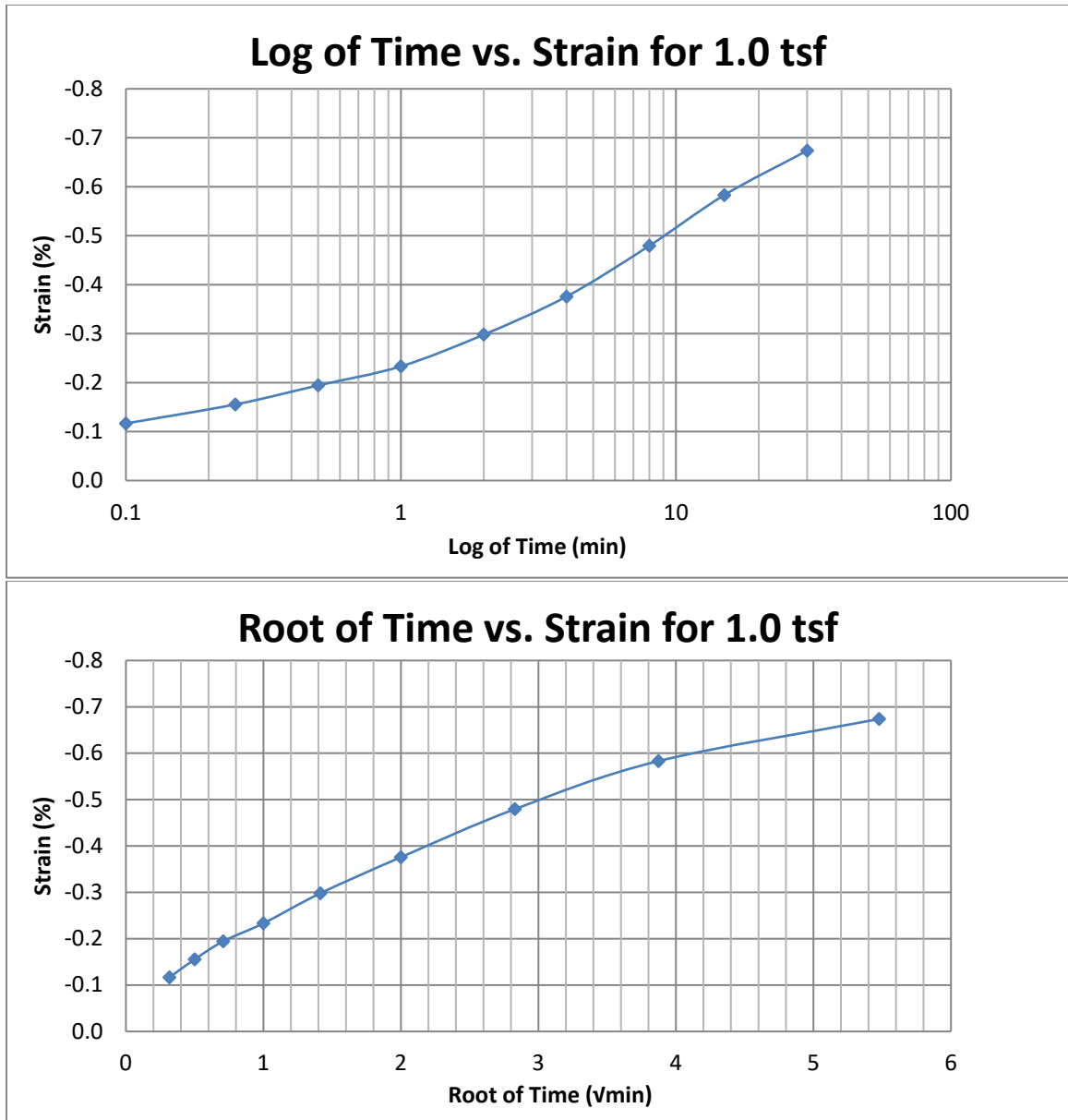


Figure A78 400 South at 40-42 feet

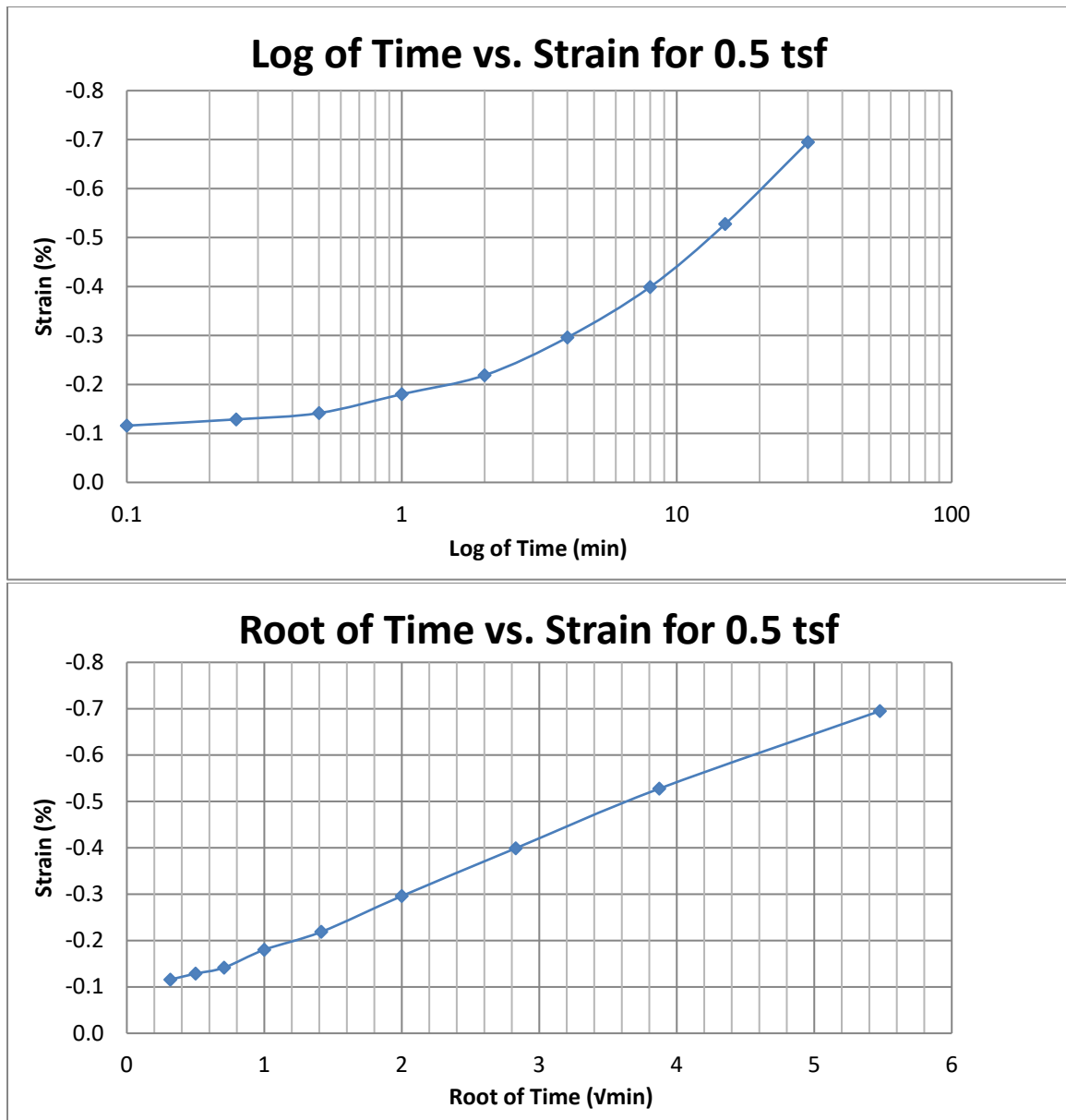


Figure A79 400 South at 40-42 feet

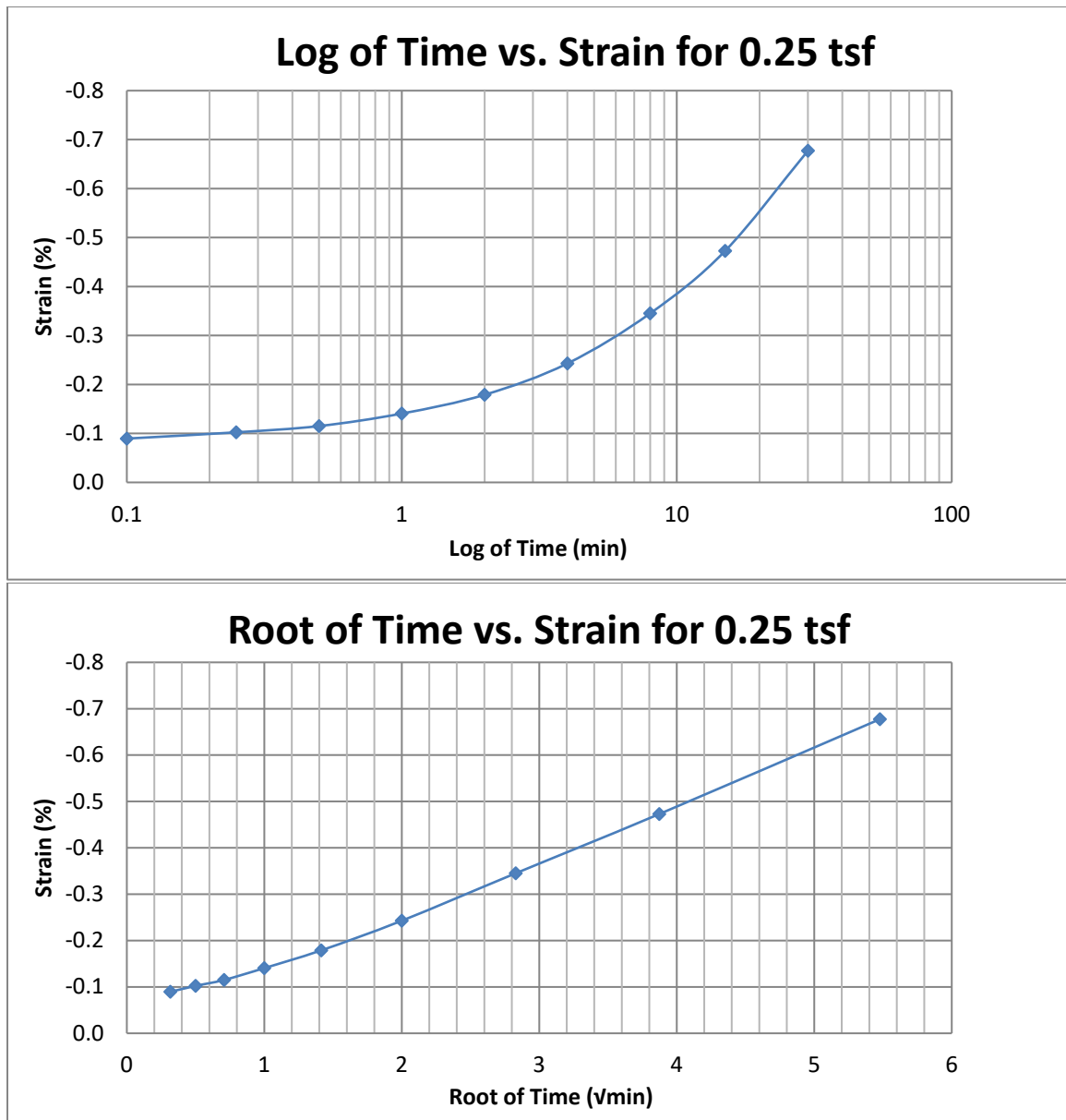


Figure A80 400 South at 40-42 feet

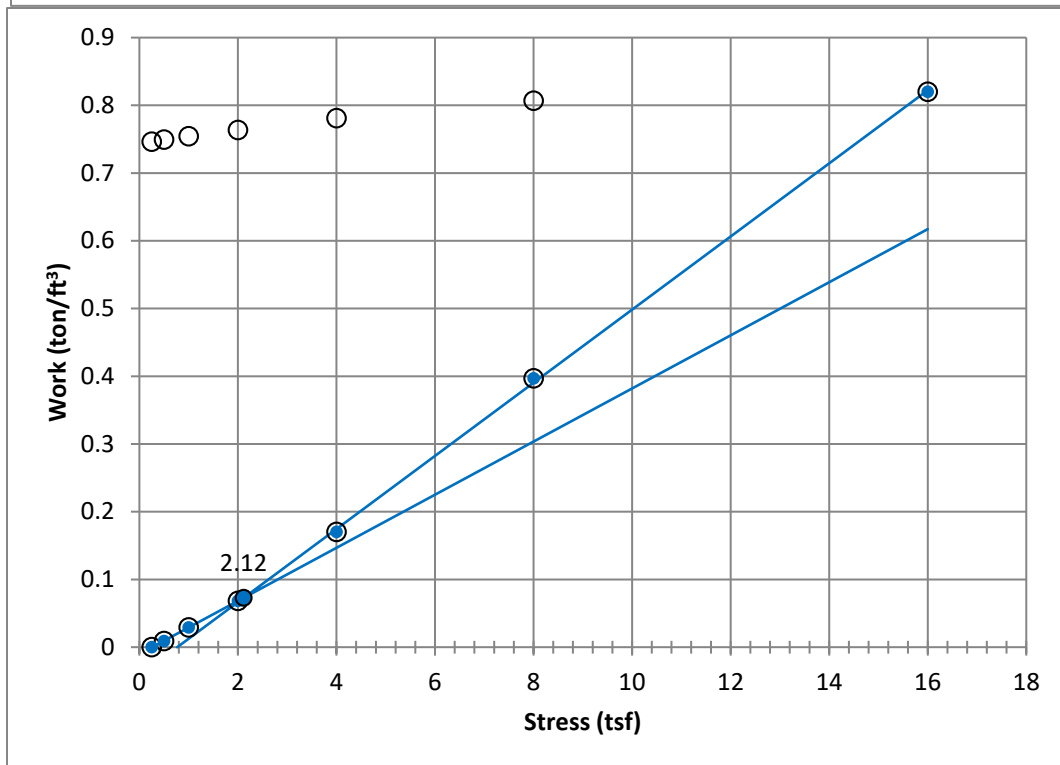
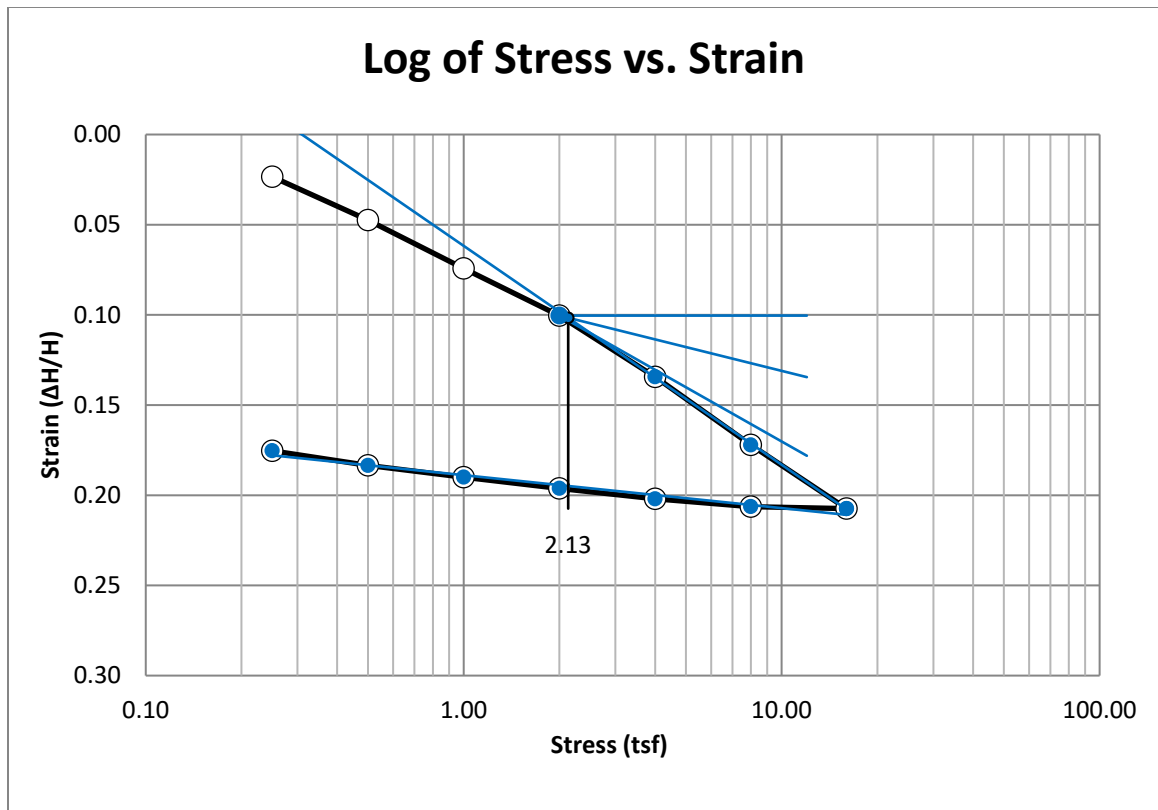


Figure A81 400 South at 45-47 feet

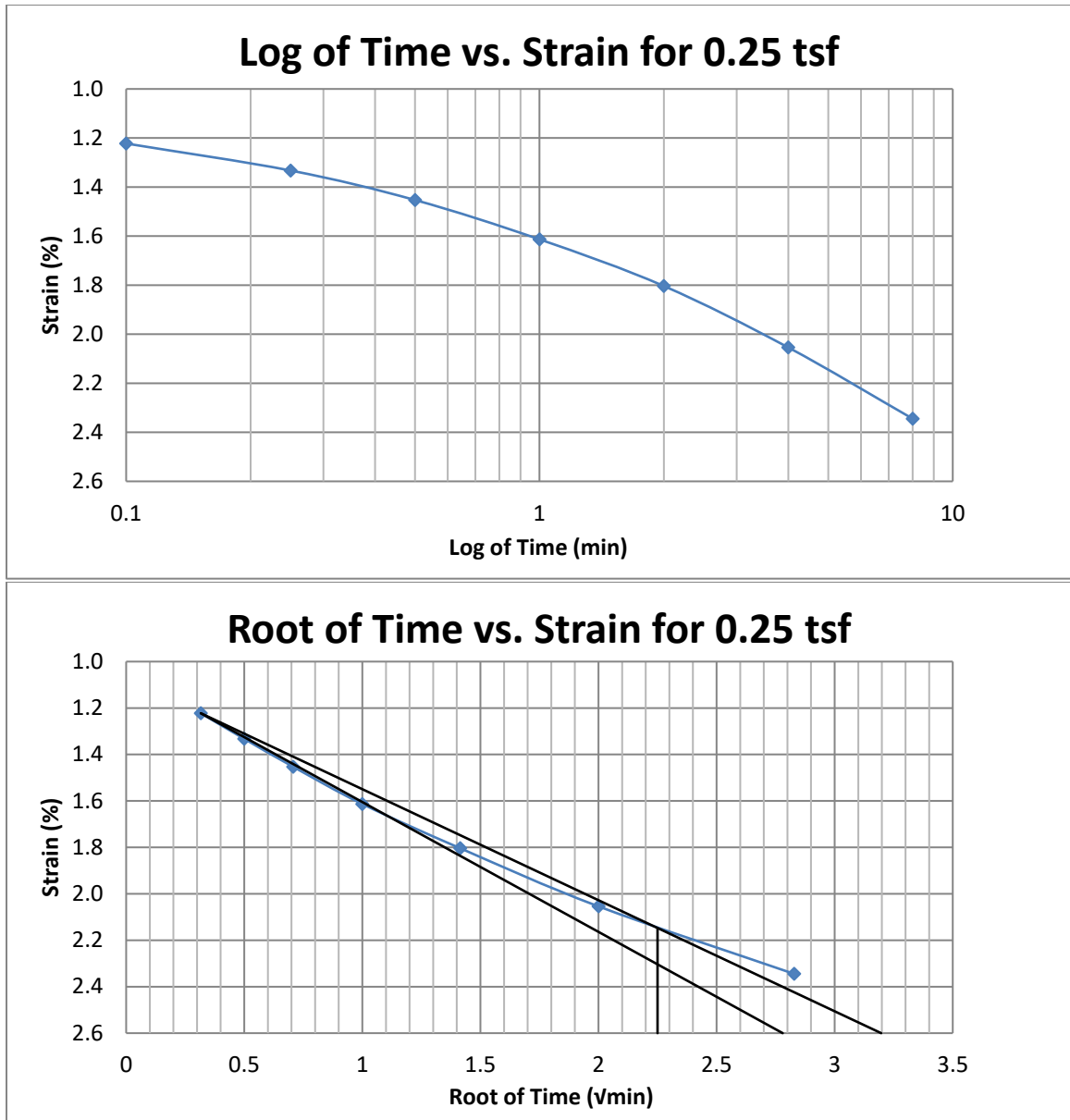


Figure A82 400 South at 45-47 feet



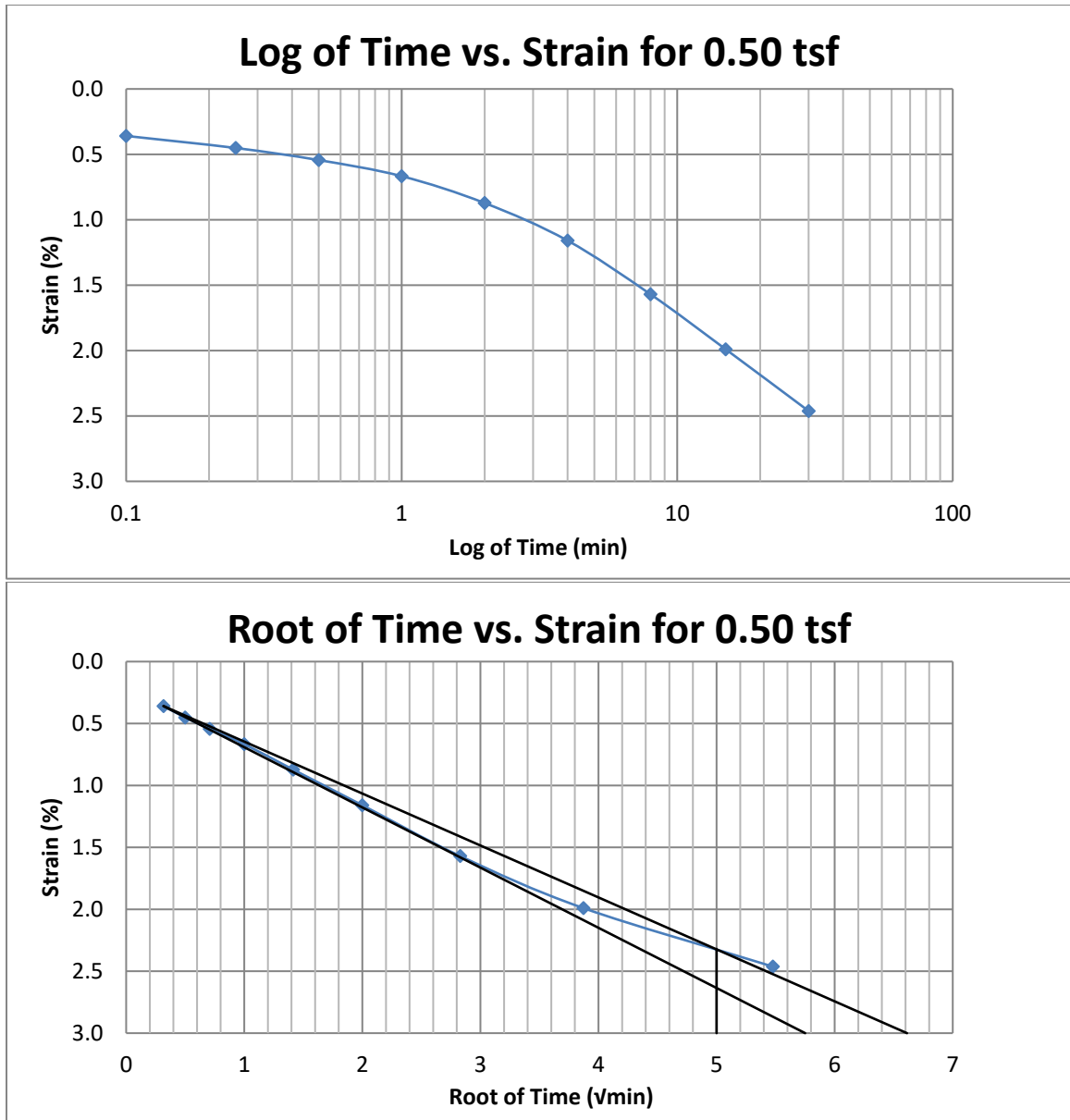


Figure A83 400 South at 45-47 feet

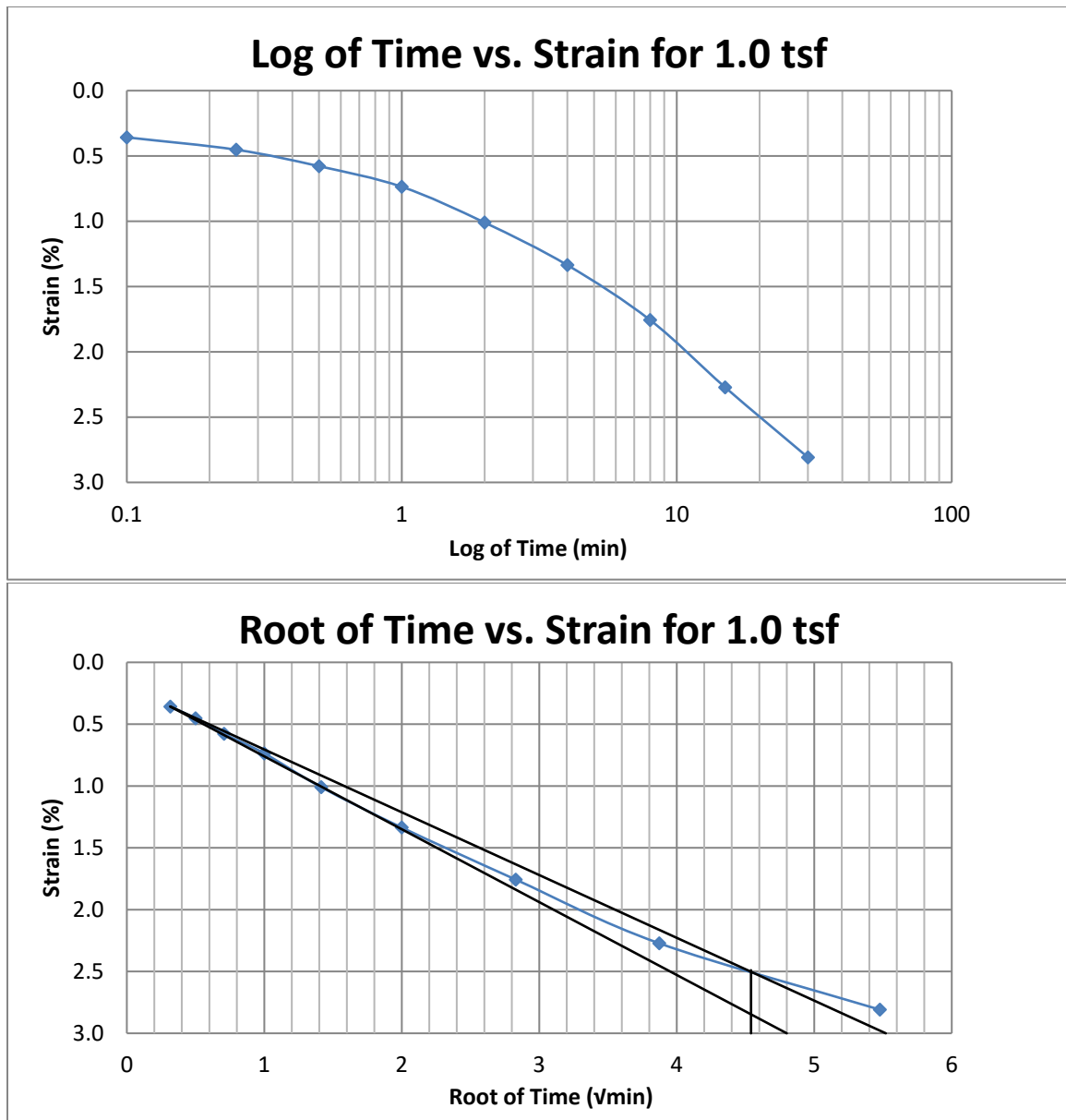


Figure A84 400 South at 45-47 feet

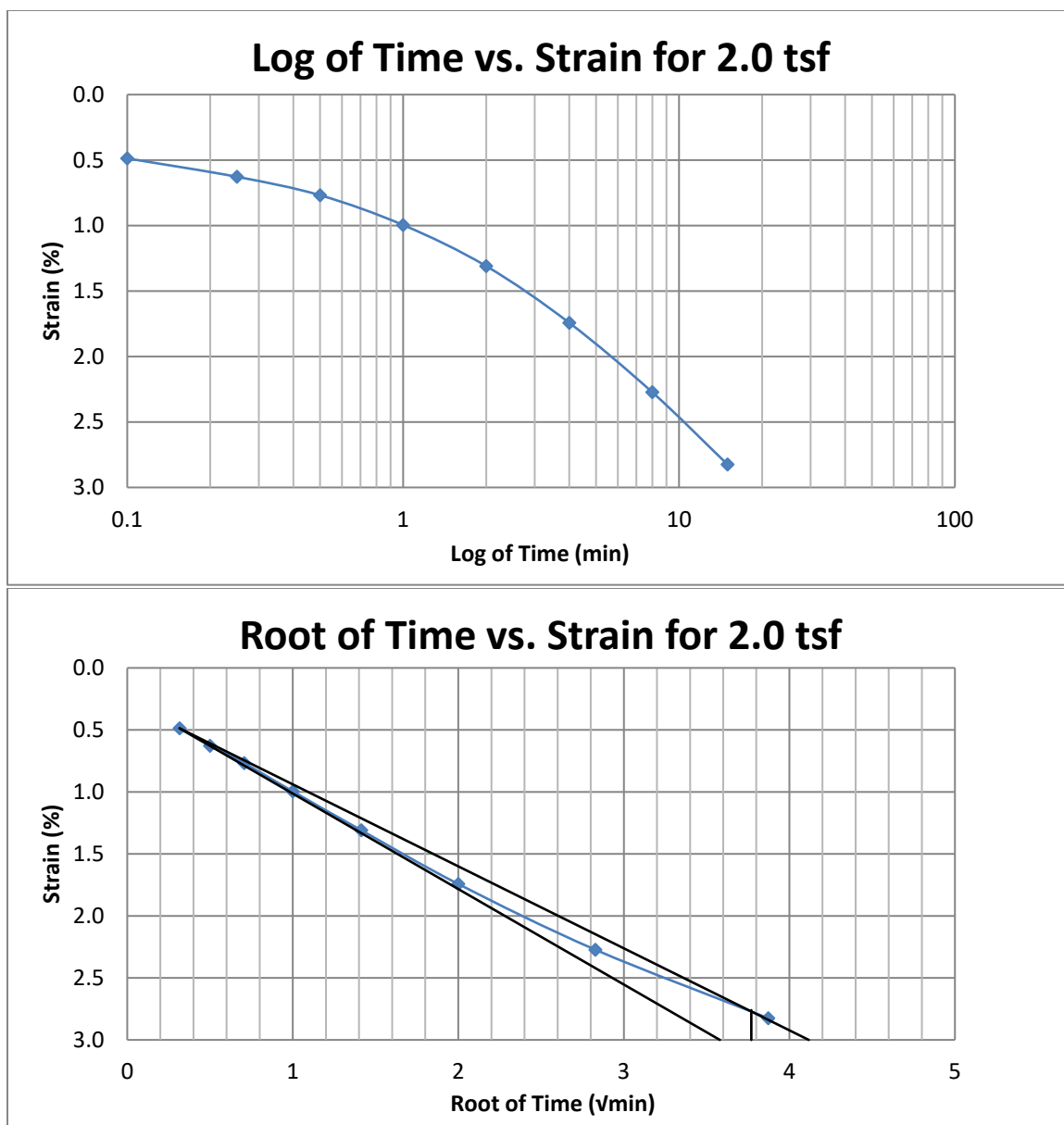


Figure A85 400 South at 45-47 feet

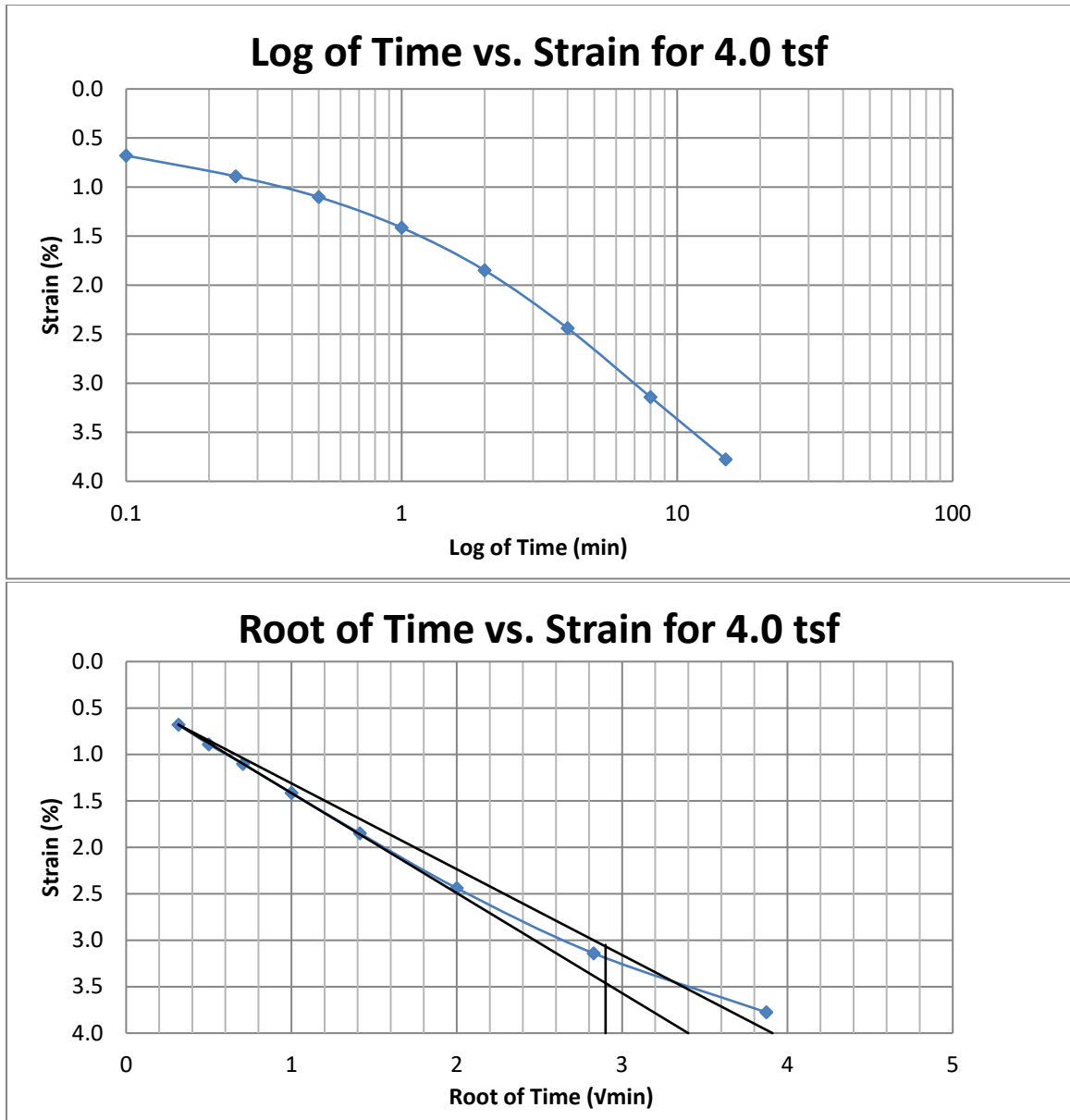


Figure A86 400 South at 45-47 feet

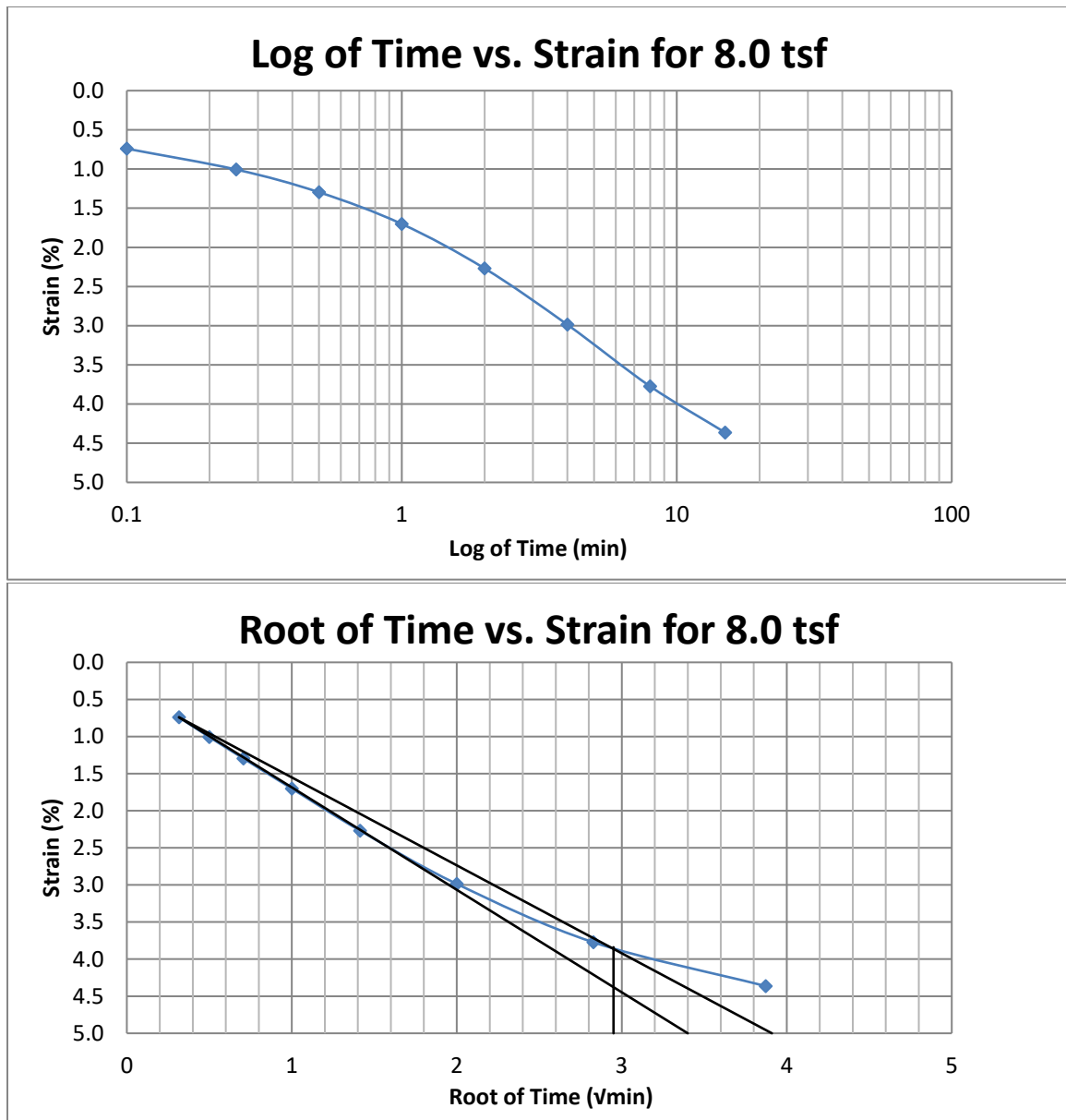


Figure A87 400 South at 45-47 feet

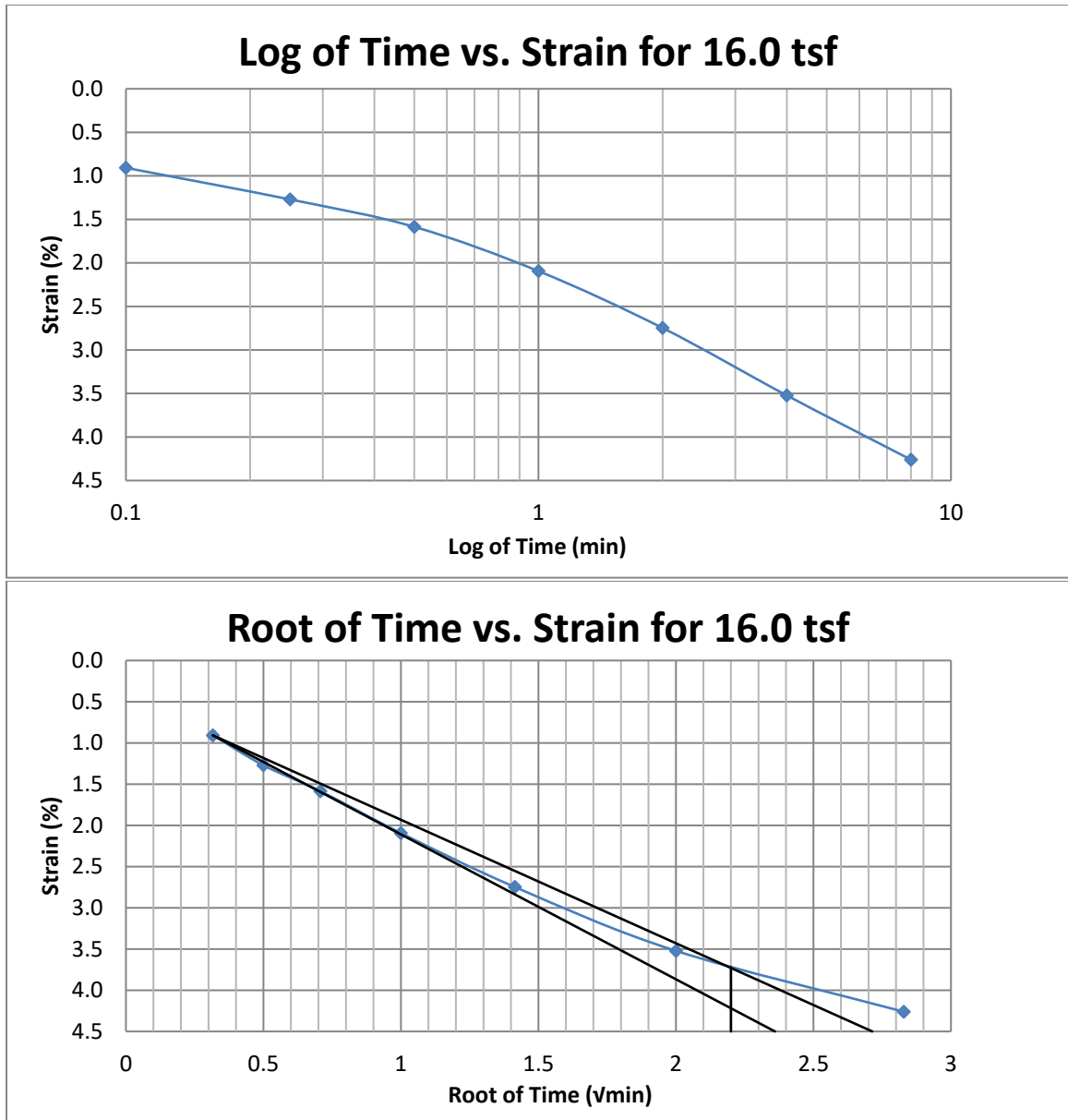


Figure A88 400 South at 45-47 feet

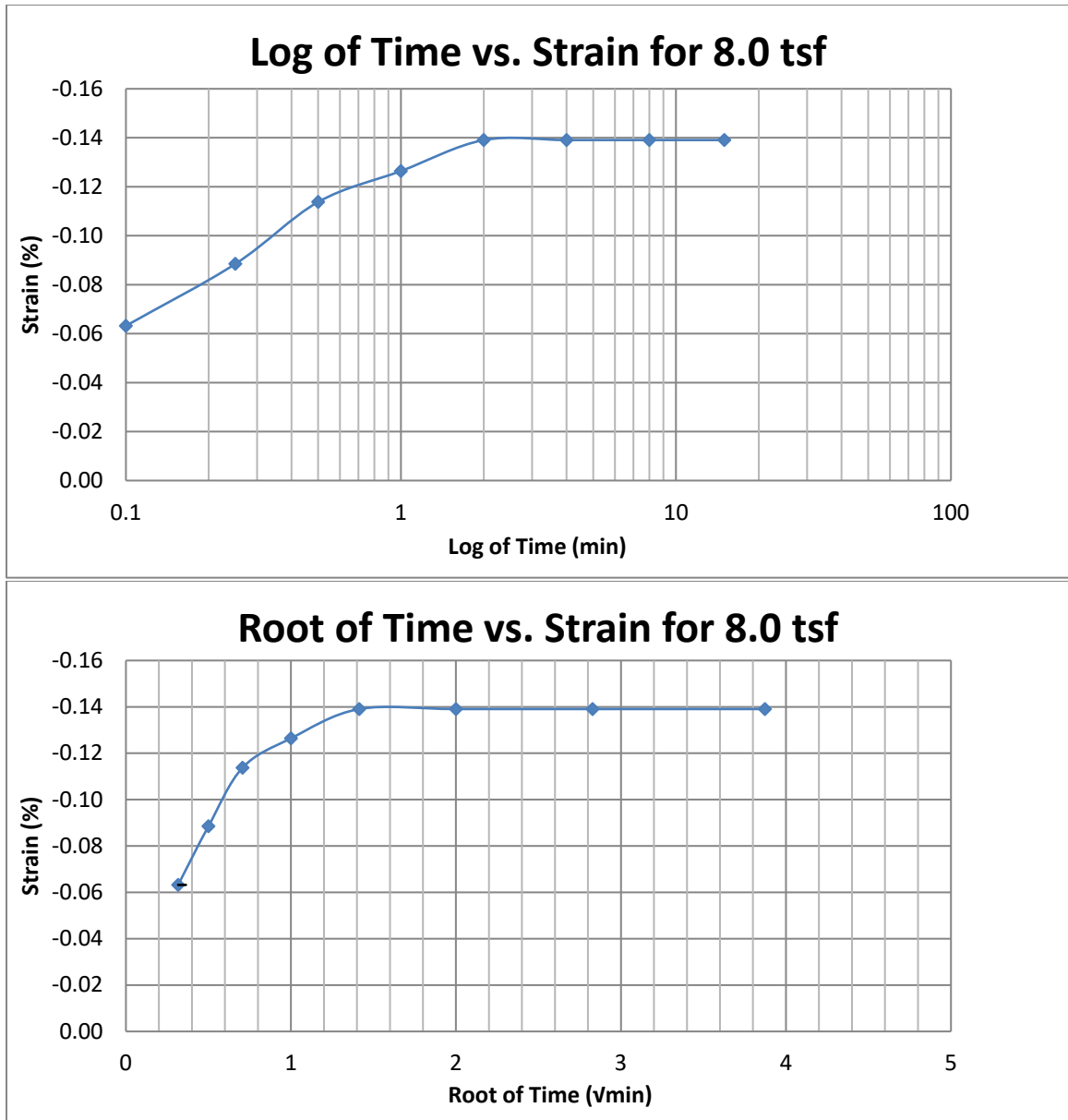


Figure A89 400 South at 45-47 feet

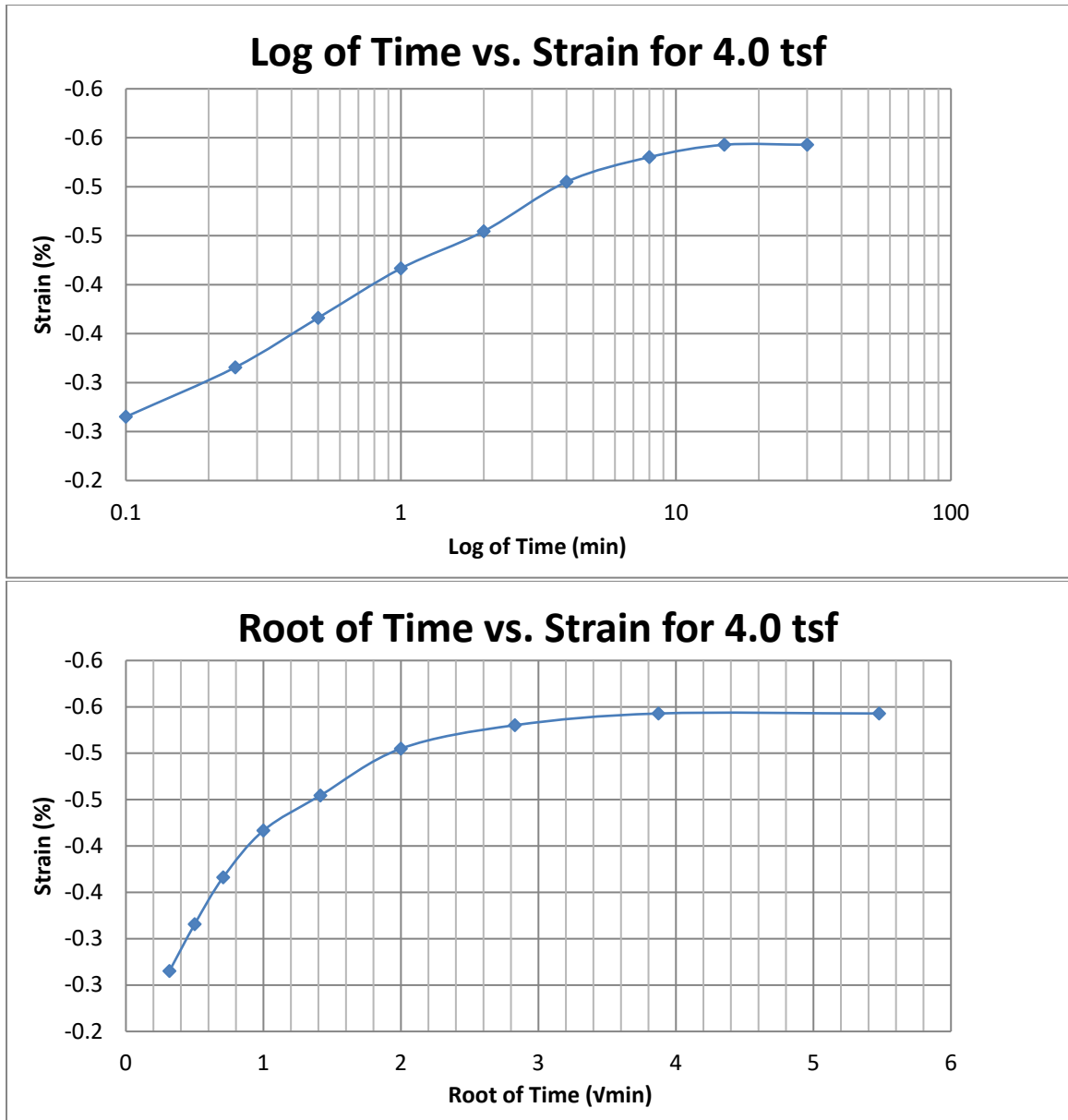


Figure A90 400 South at 45-47 feet



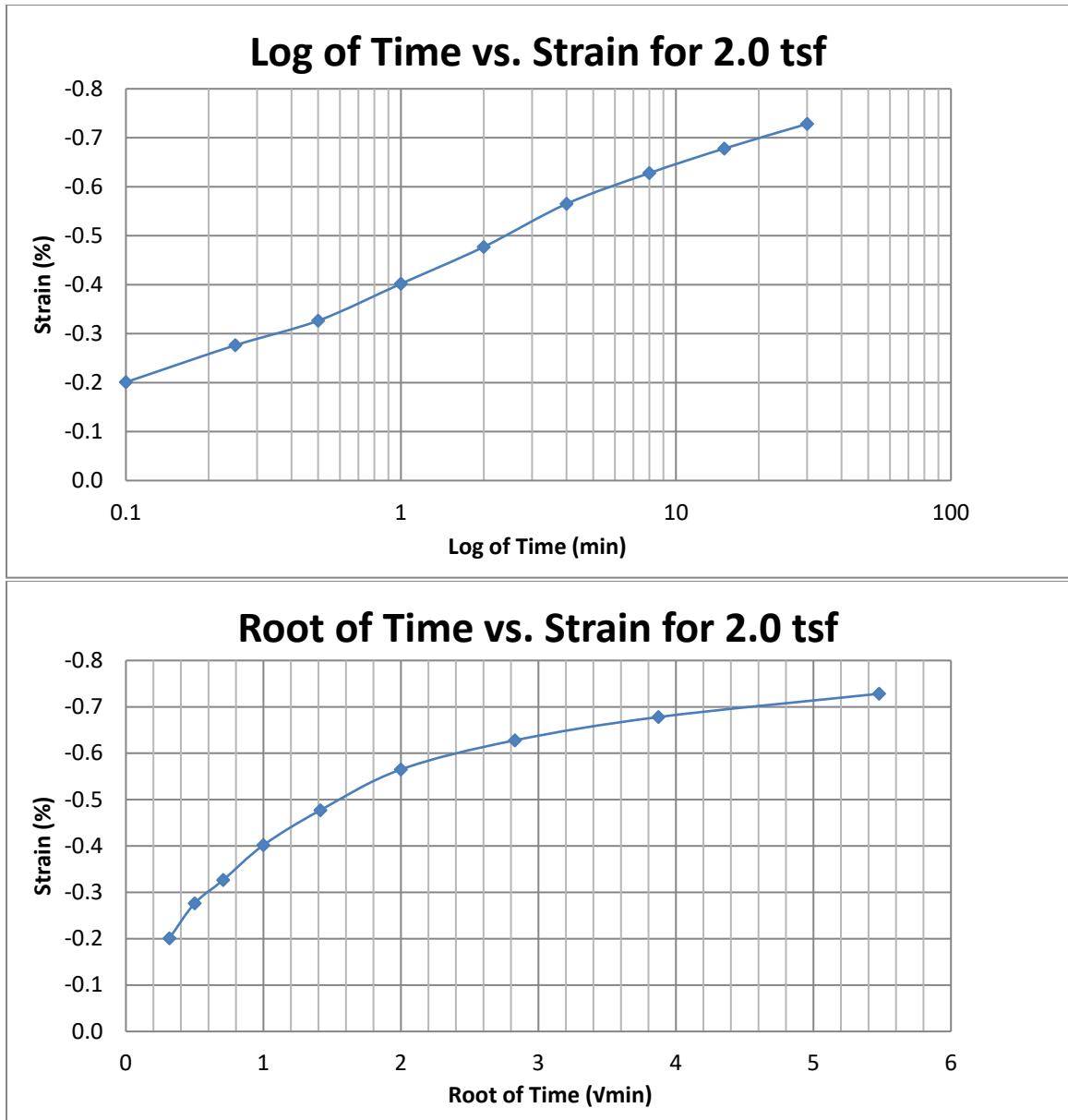


Figure A91 400 South at 45-47 feet

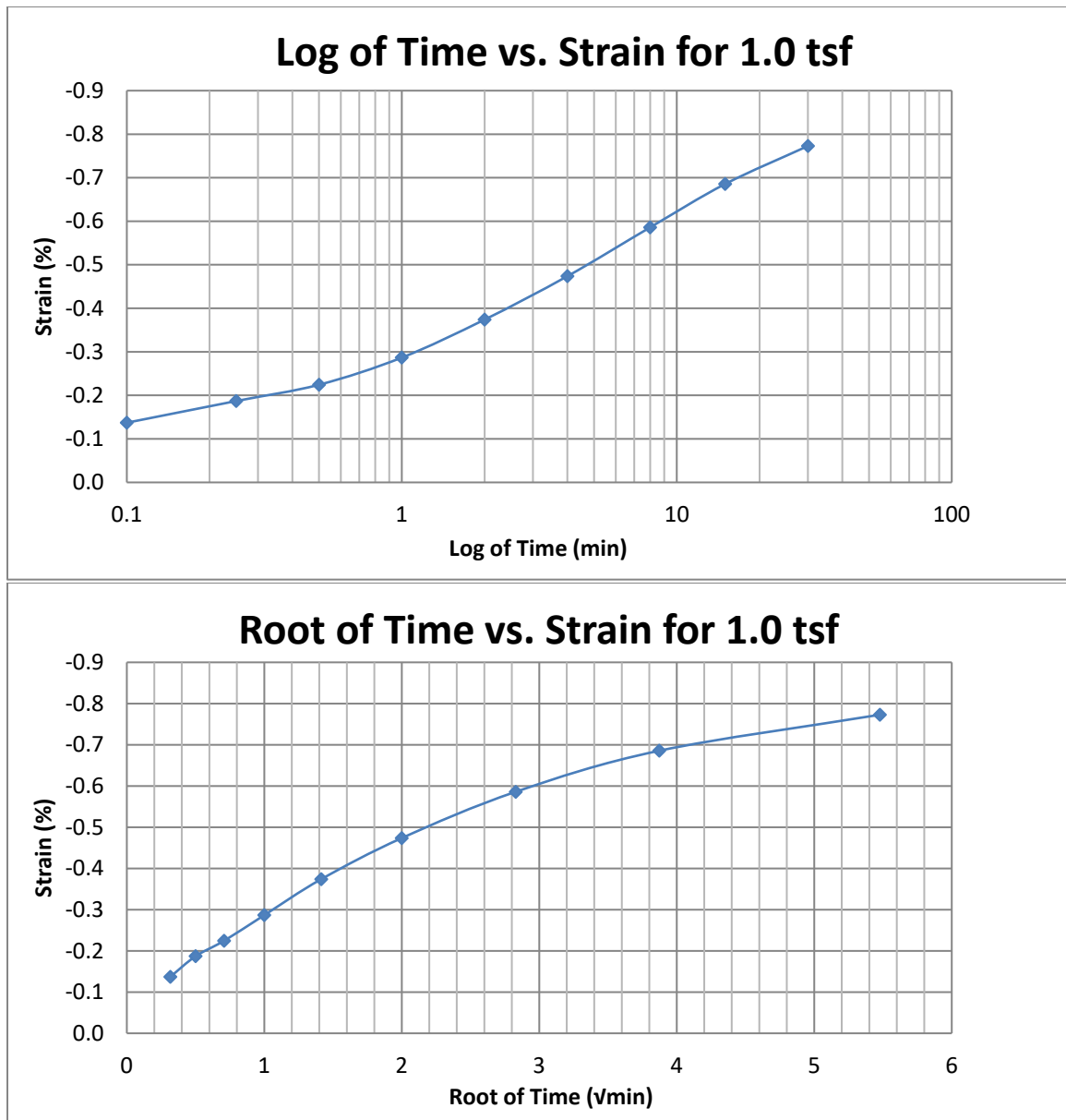


Figure A92 400 South at 45-47 feet

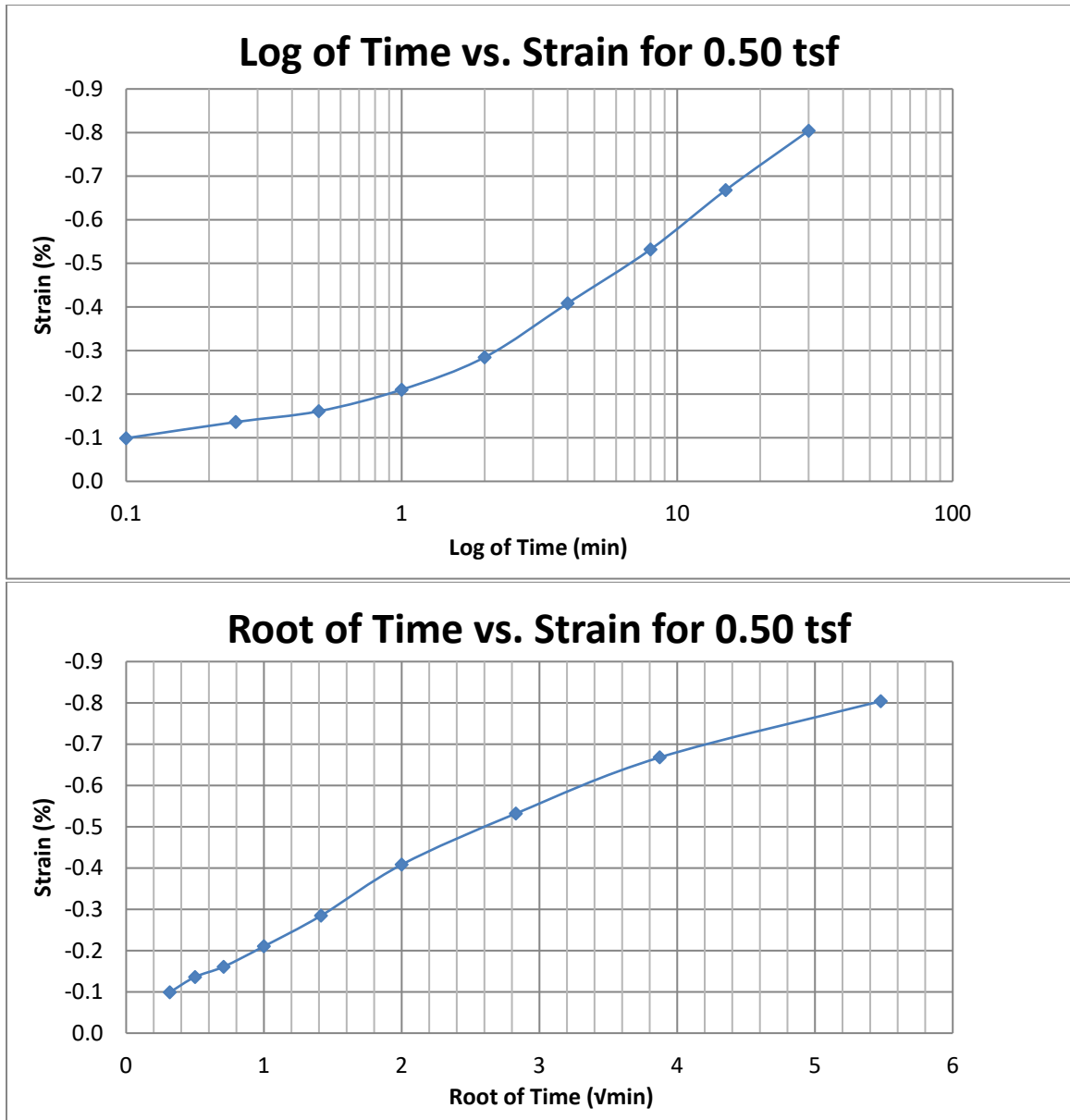


Figure A93 400 South at 45-47 feet

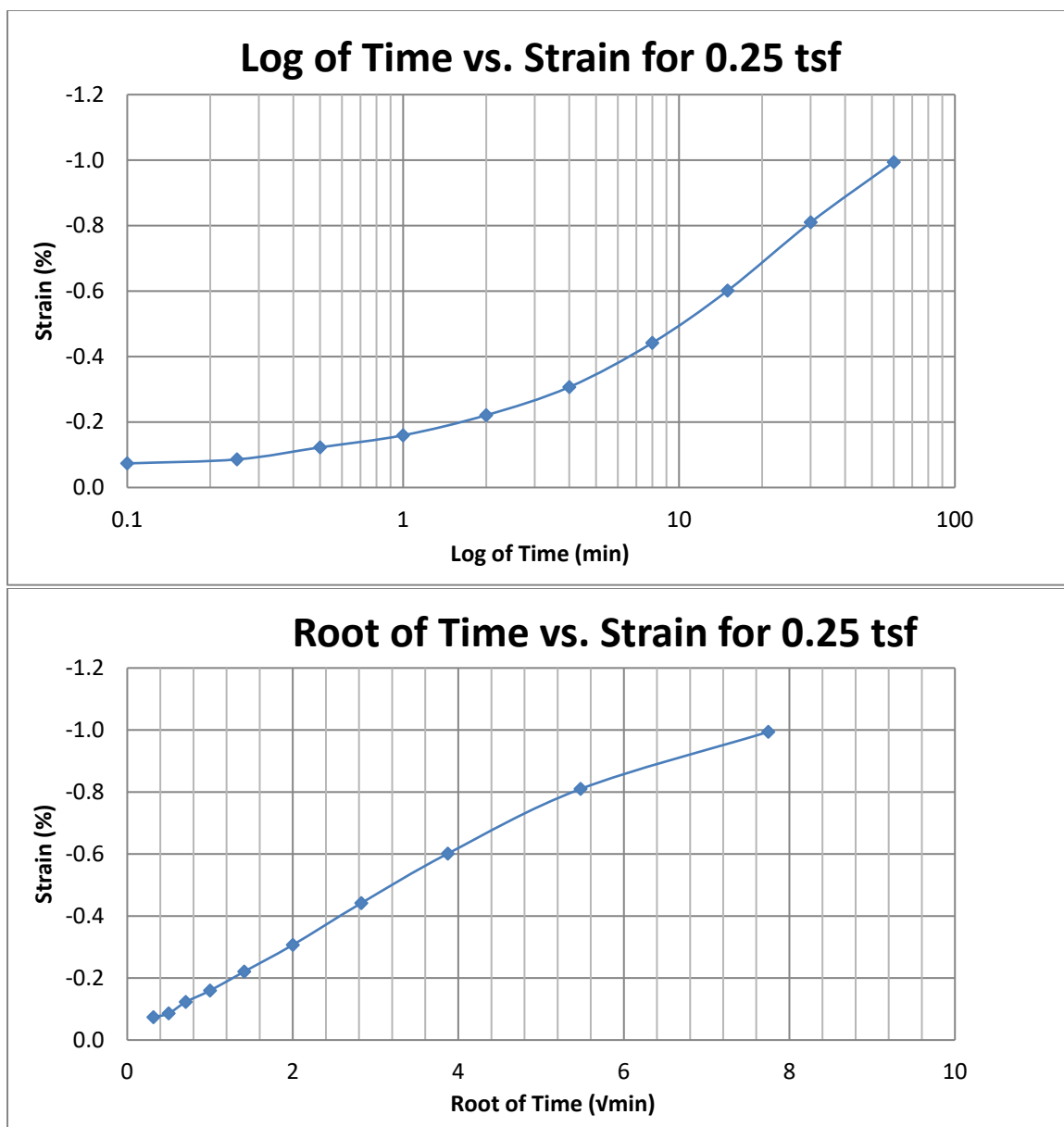


Figure A94 400 South at 45-47 feet

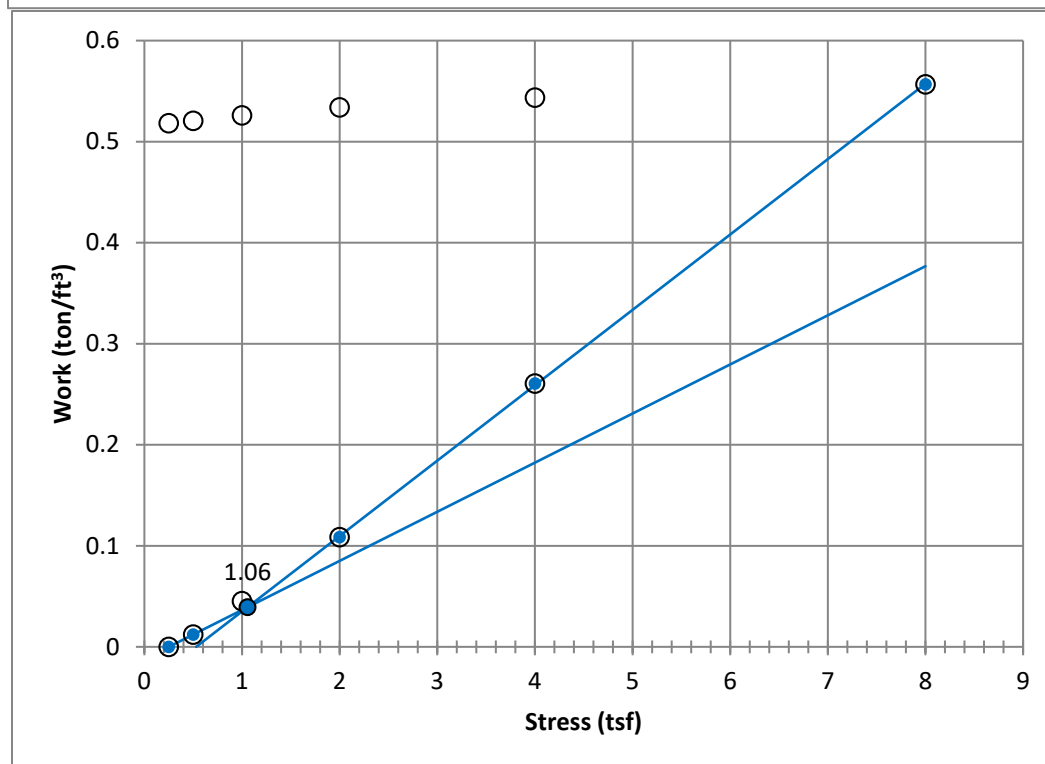
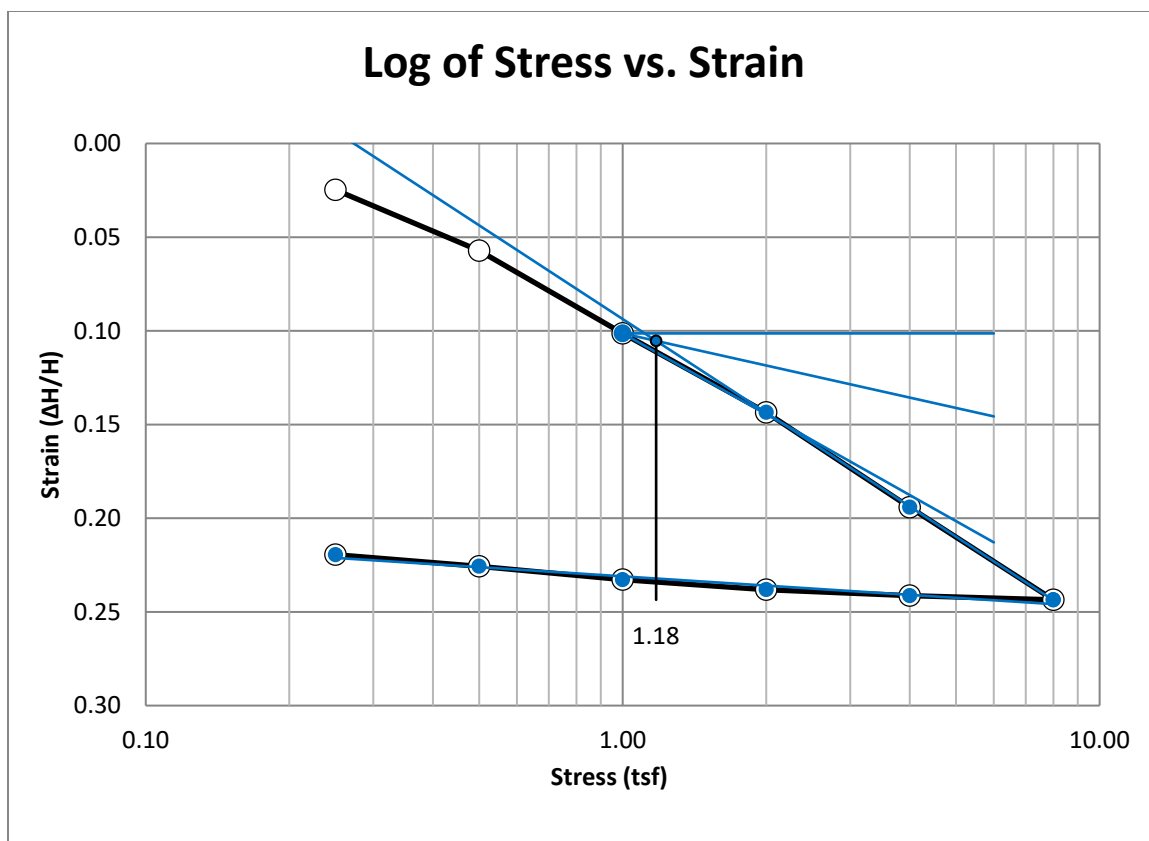


Figure A95 400 South at 50-52 feet

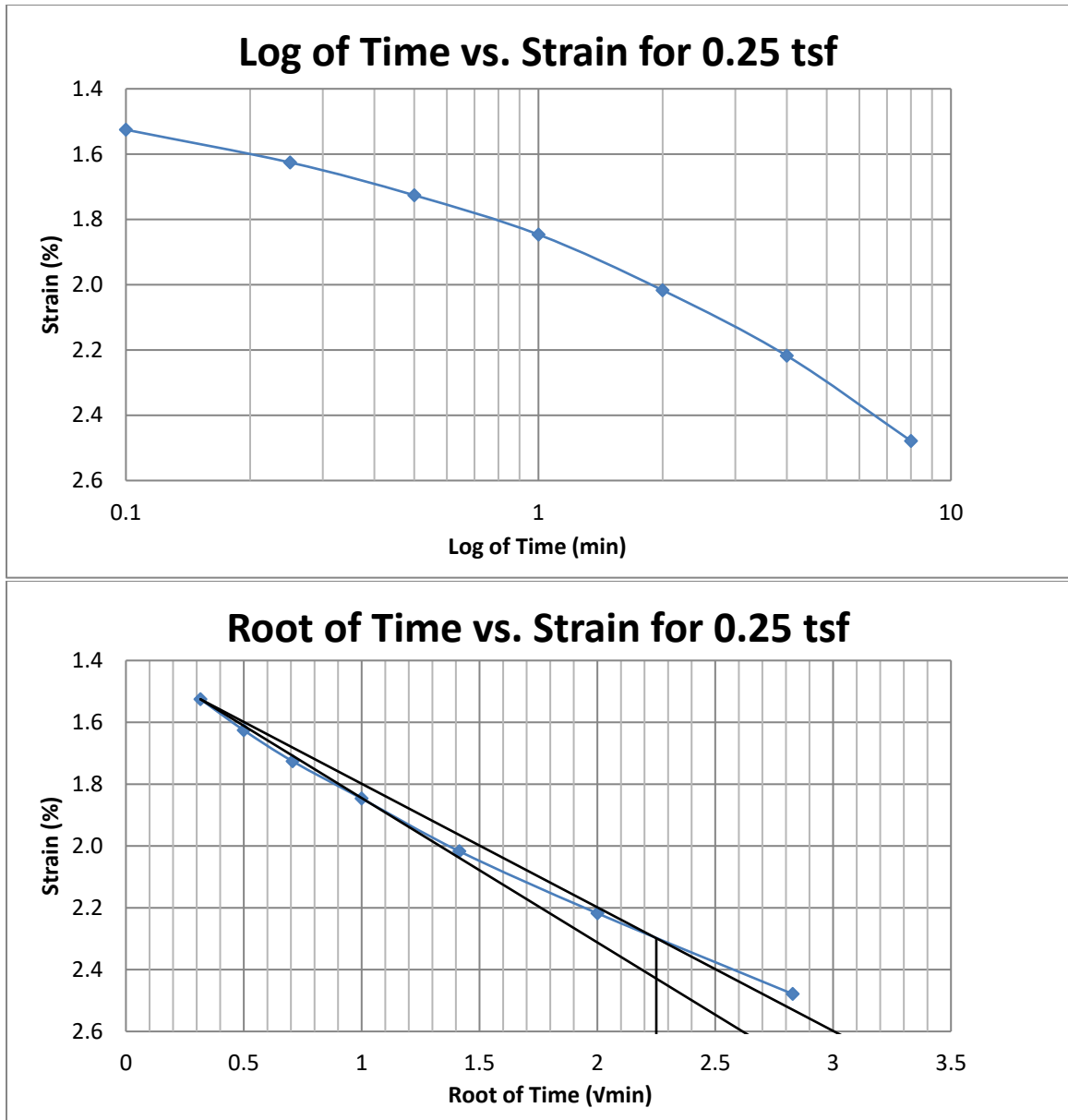


Figure A96 400 South at 50-52 feet

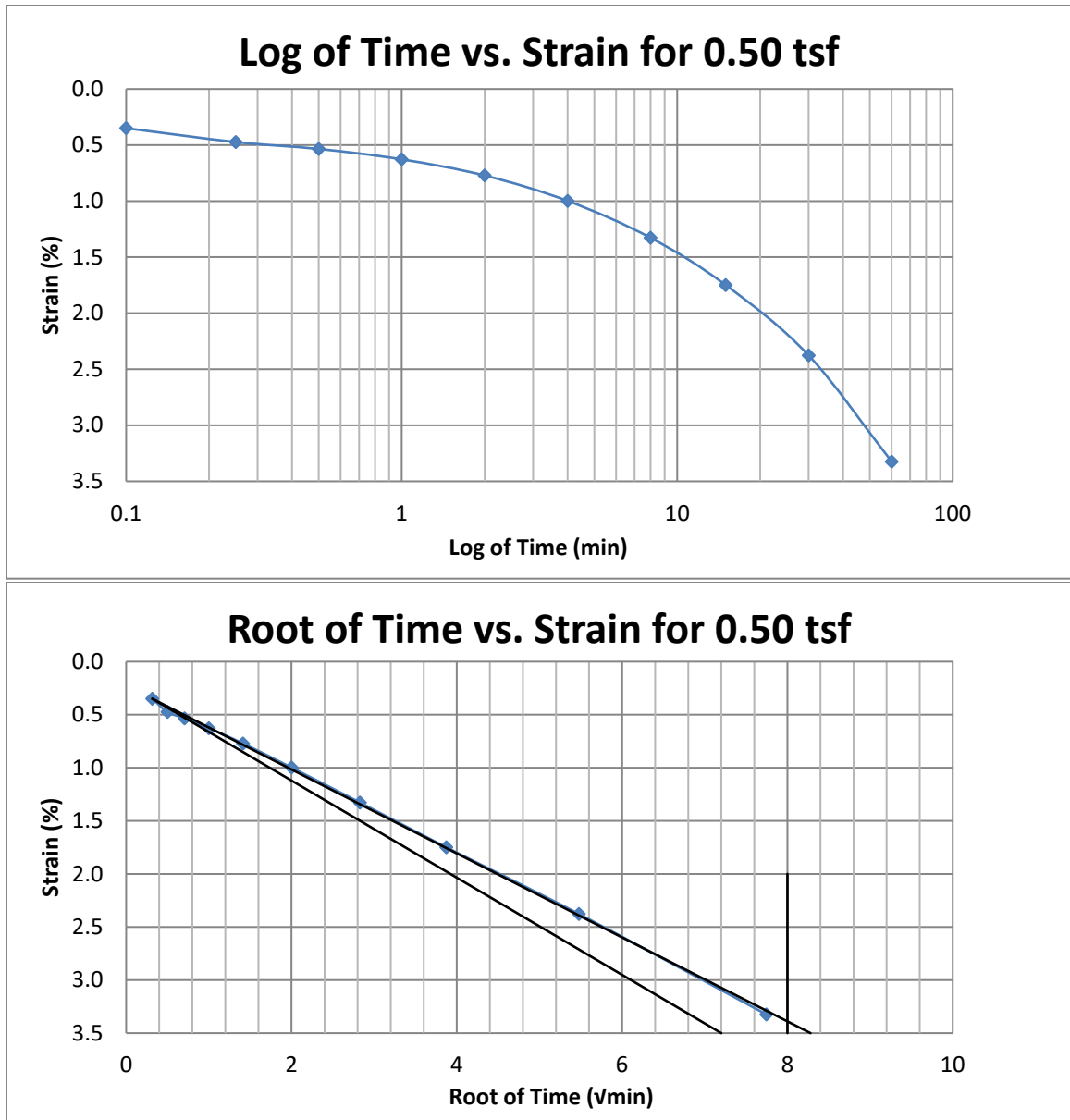


Figure A97 400 South at 50-52 feet

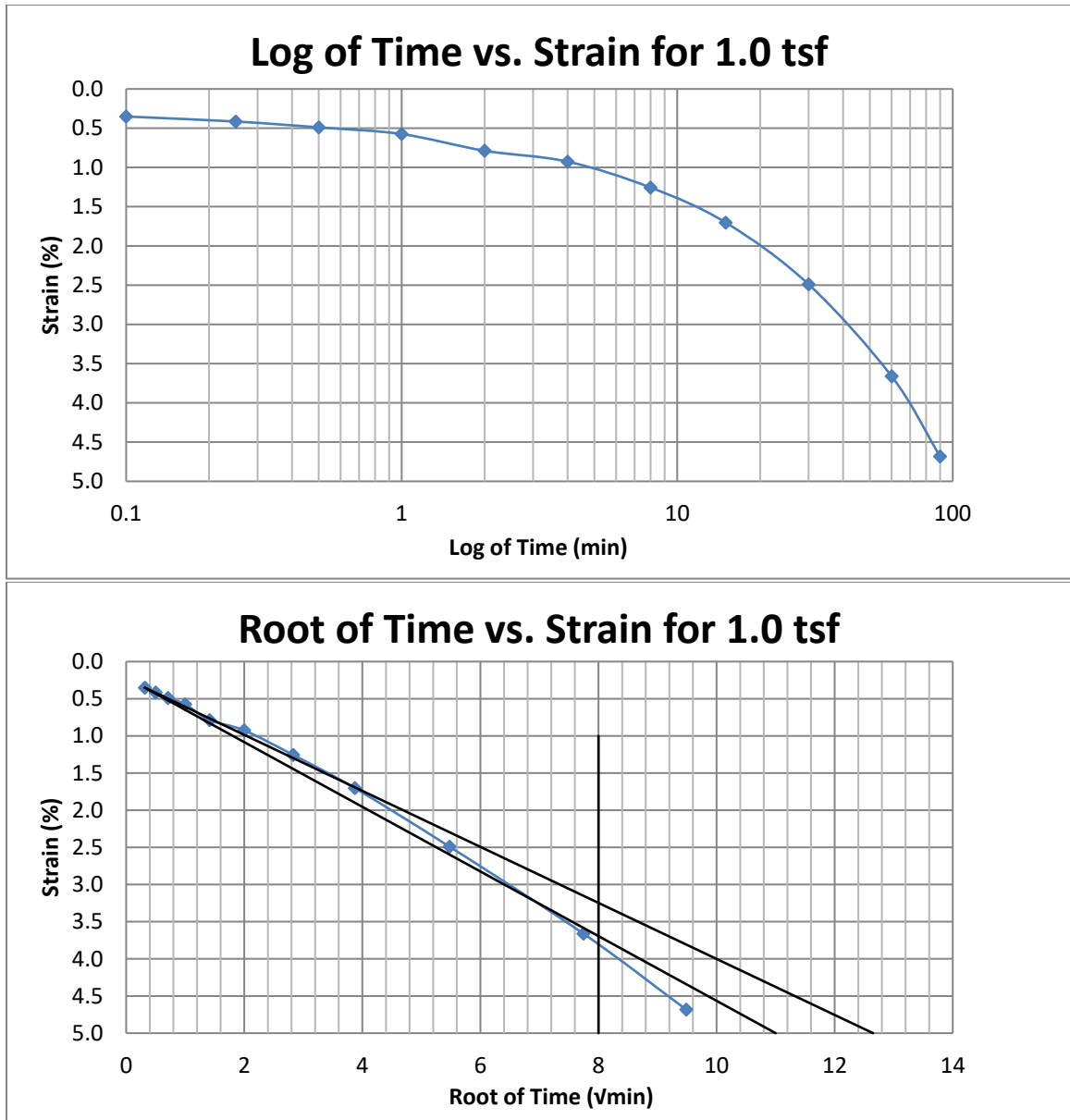


Figure A98 400 South at 50-52 feet



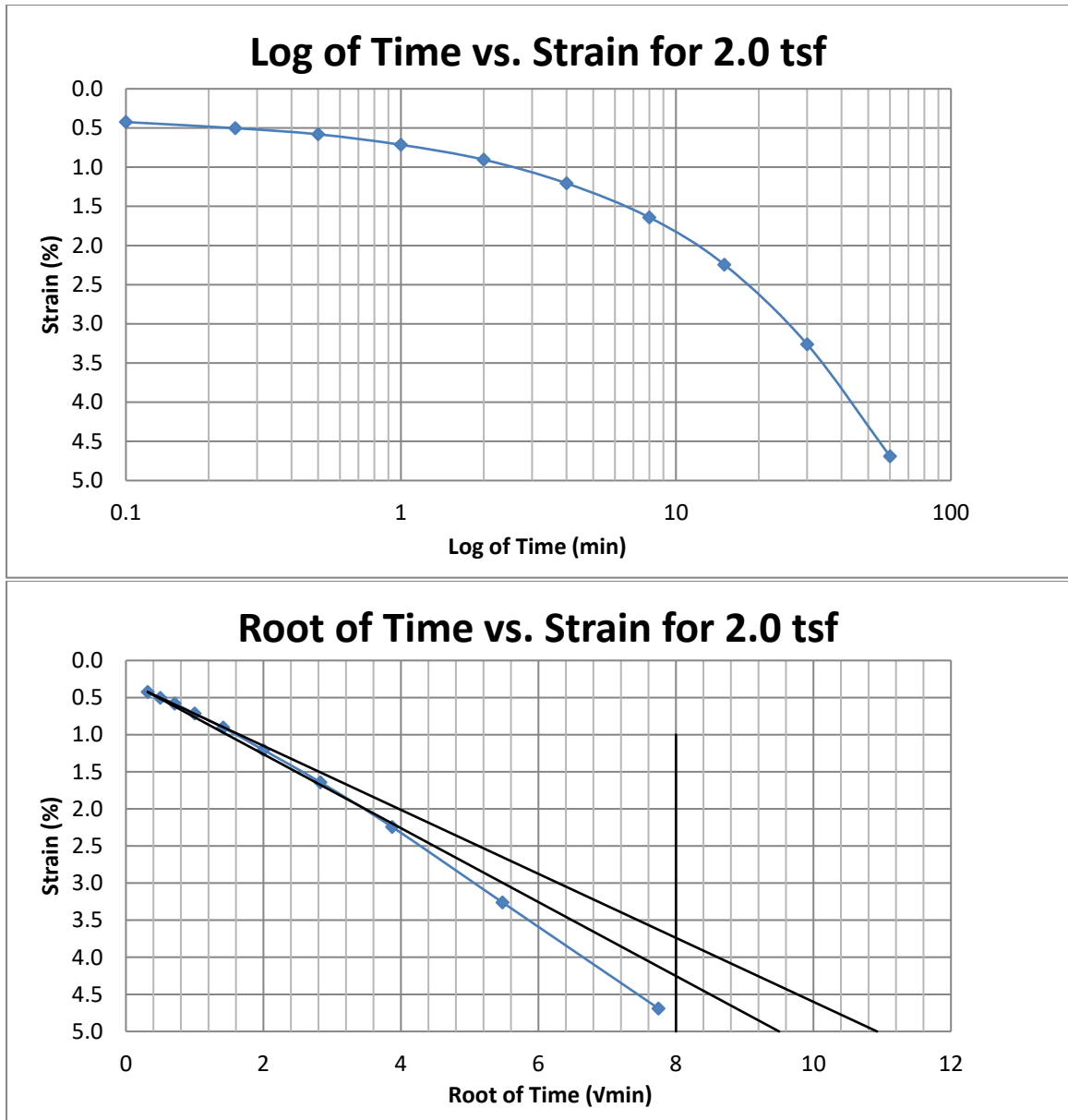


Figure A99 400 South at 50-52 feet

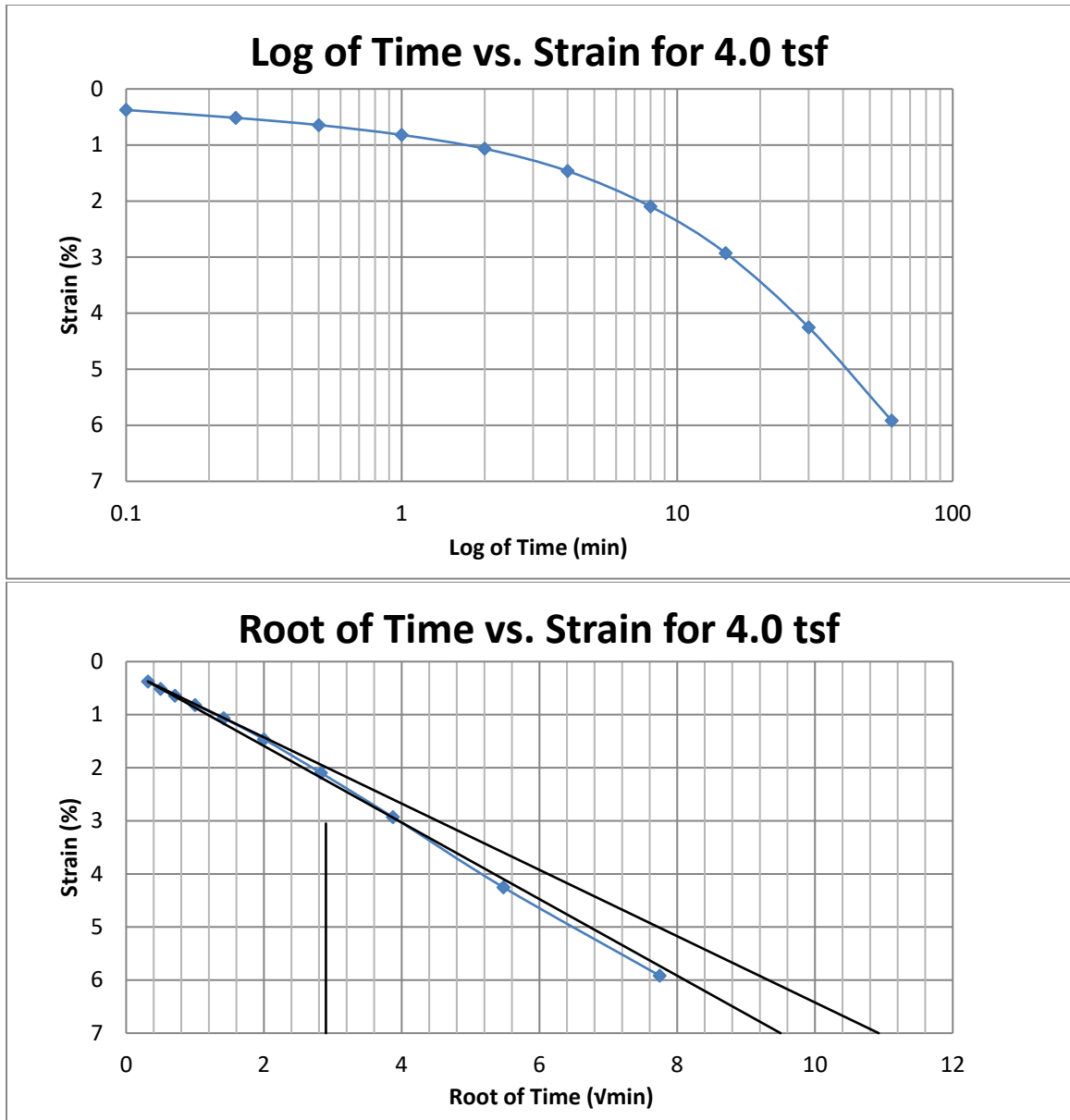


Figure A100 400 South at 50-52 feet

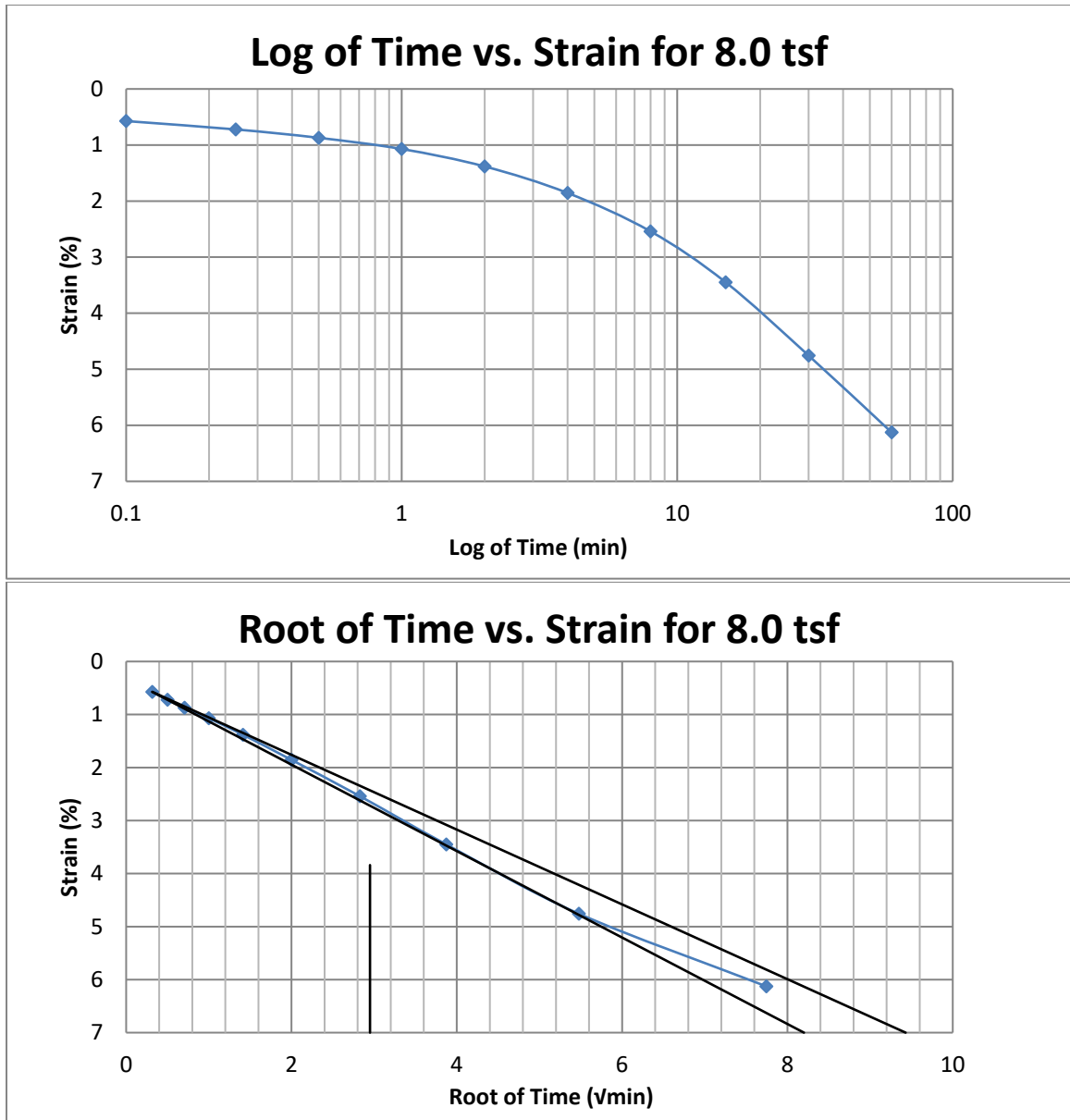


Figure A101 400 South at 50-52 feet

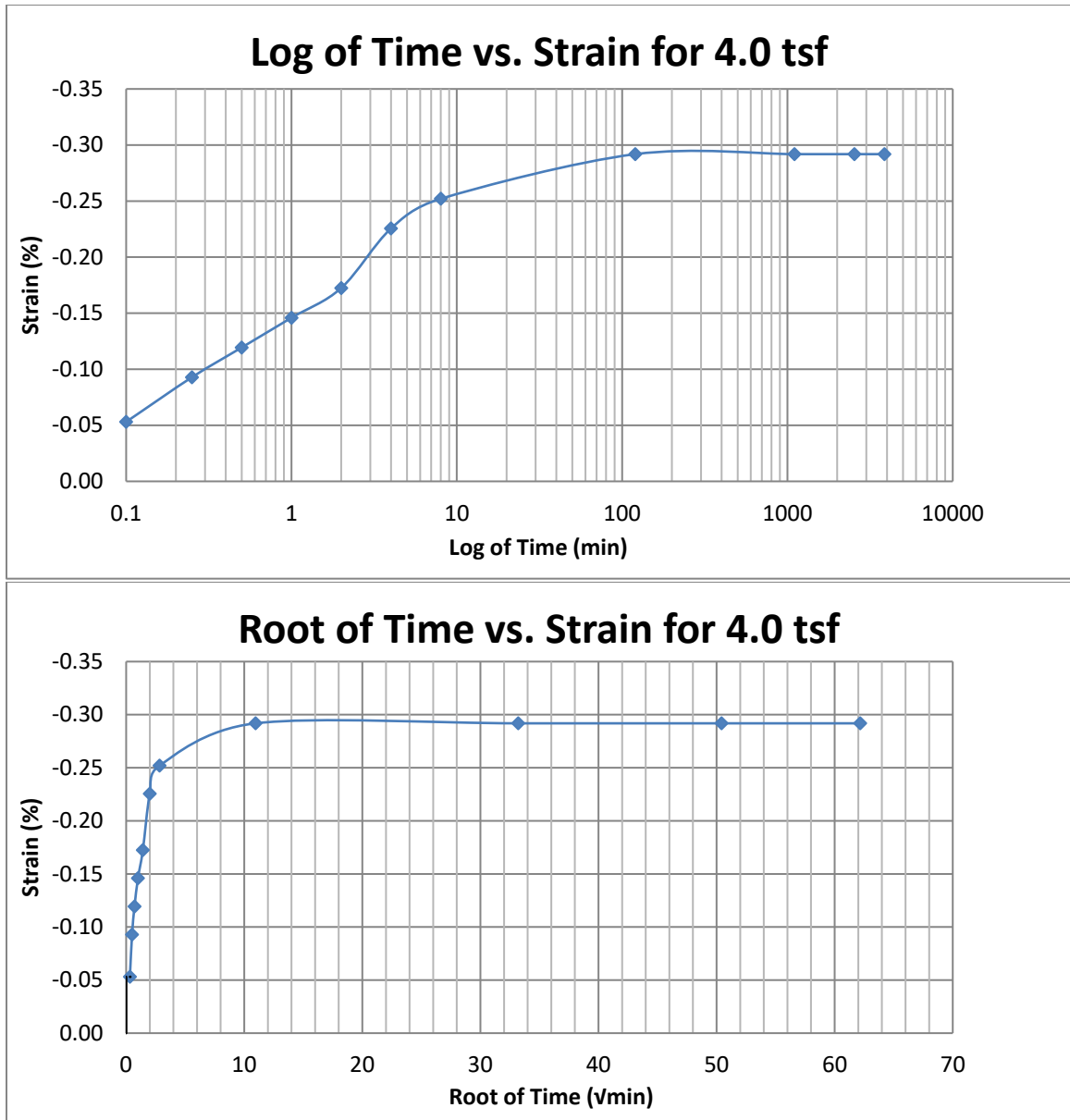


Figure A102 400 South at 50-52 feet

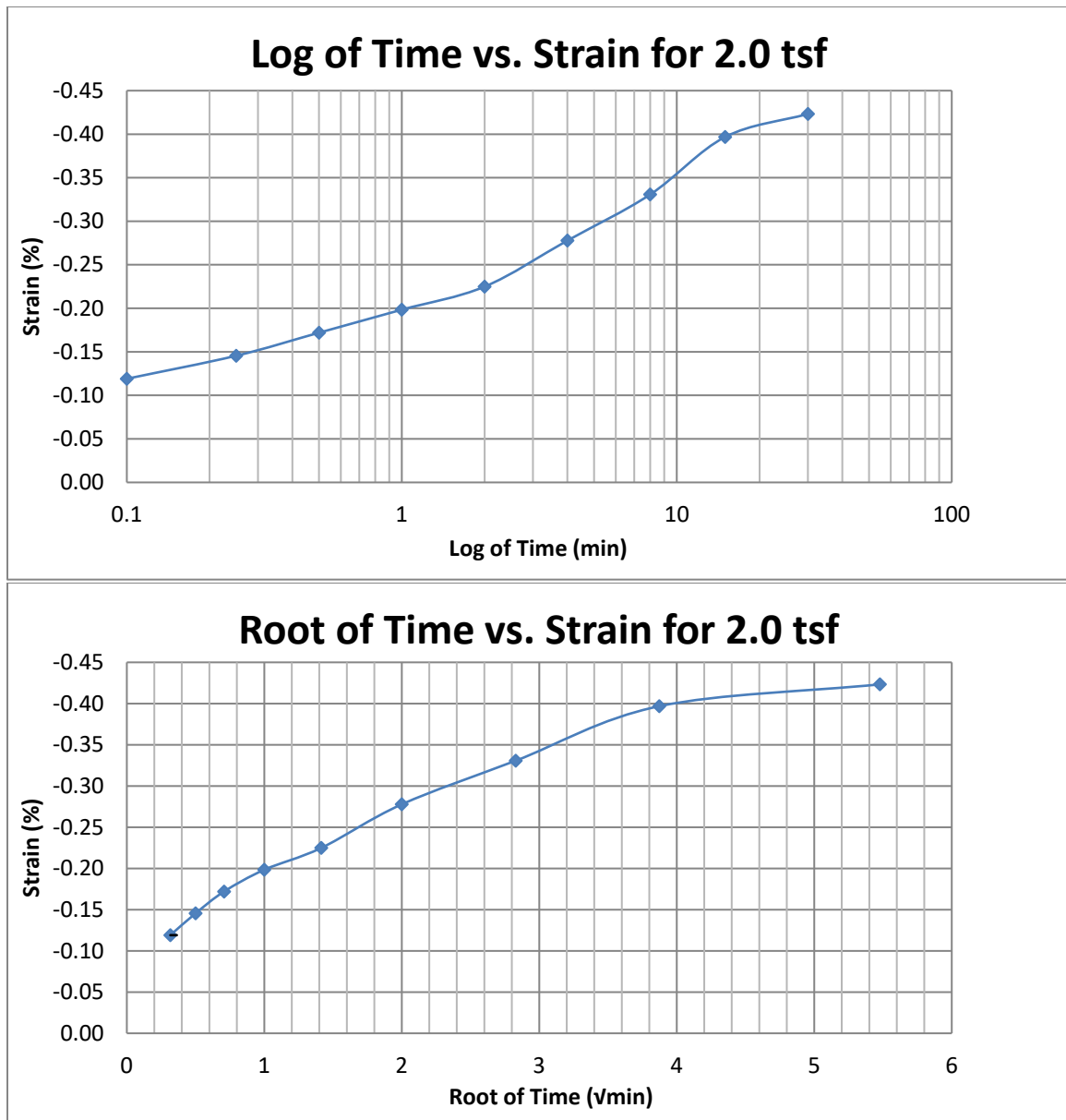


Figure A103 400 South at 50-52 feet

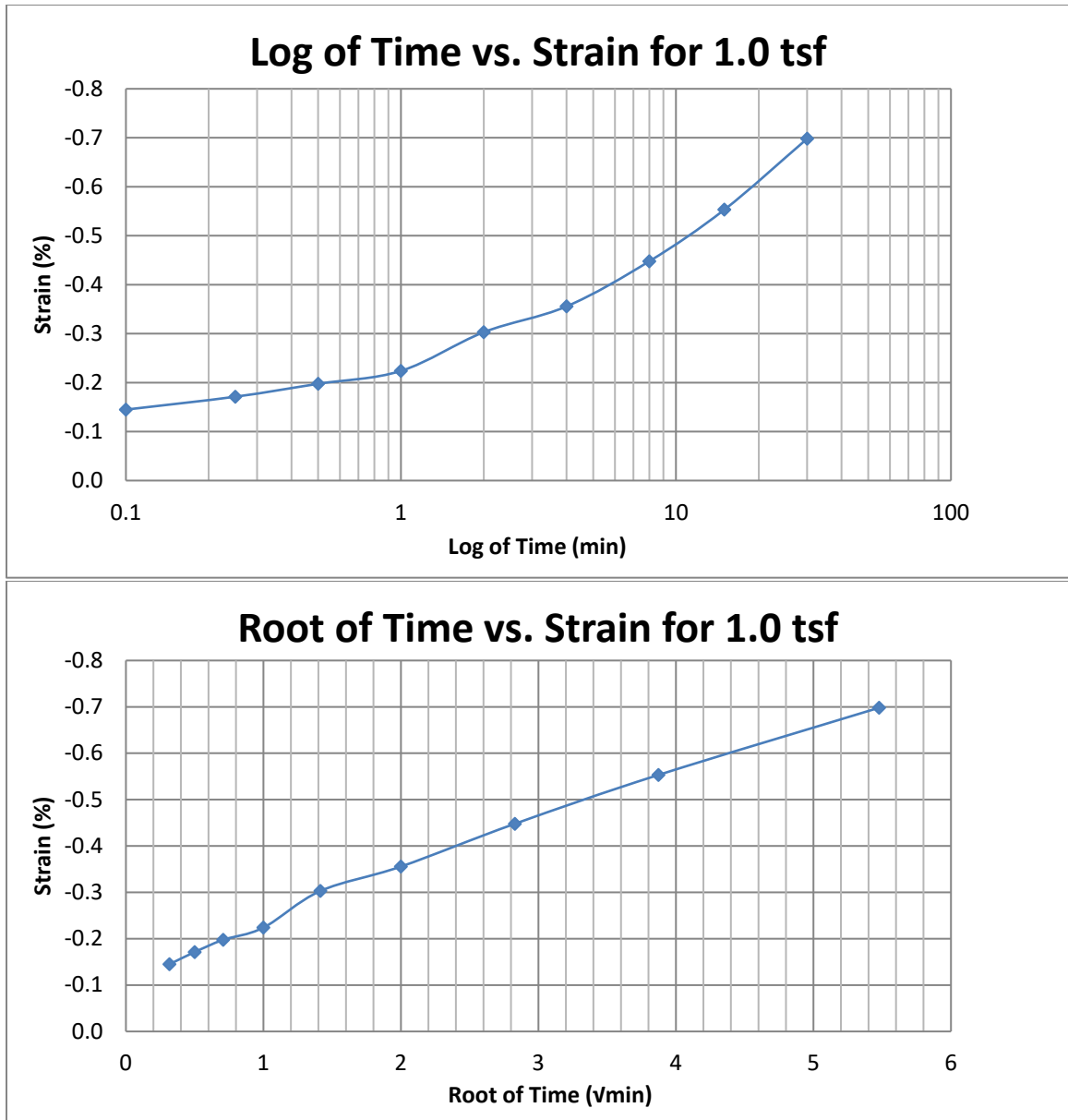


Figure A104 400 South at 50-52 feet

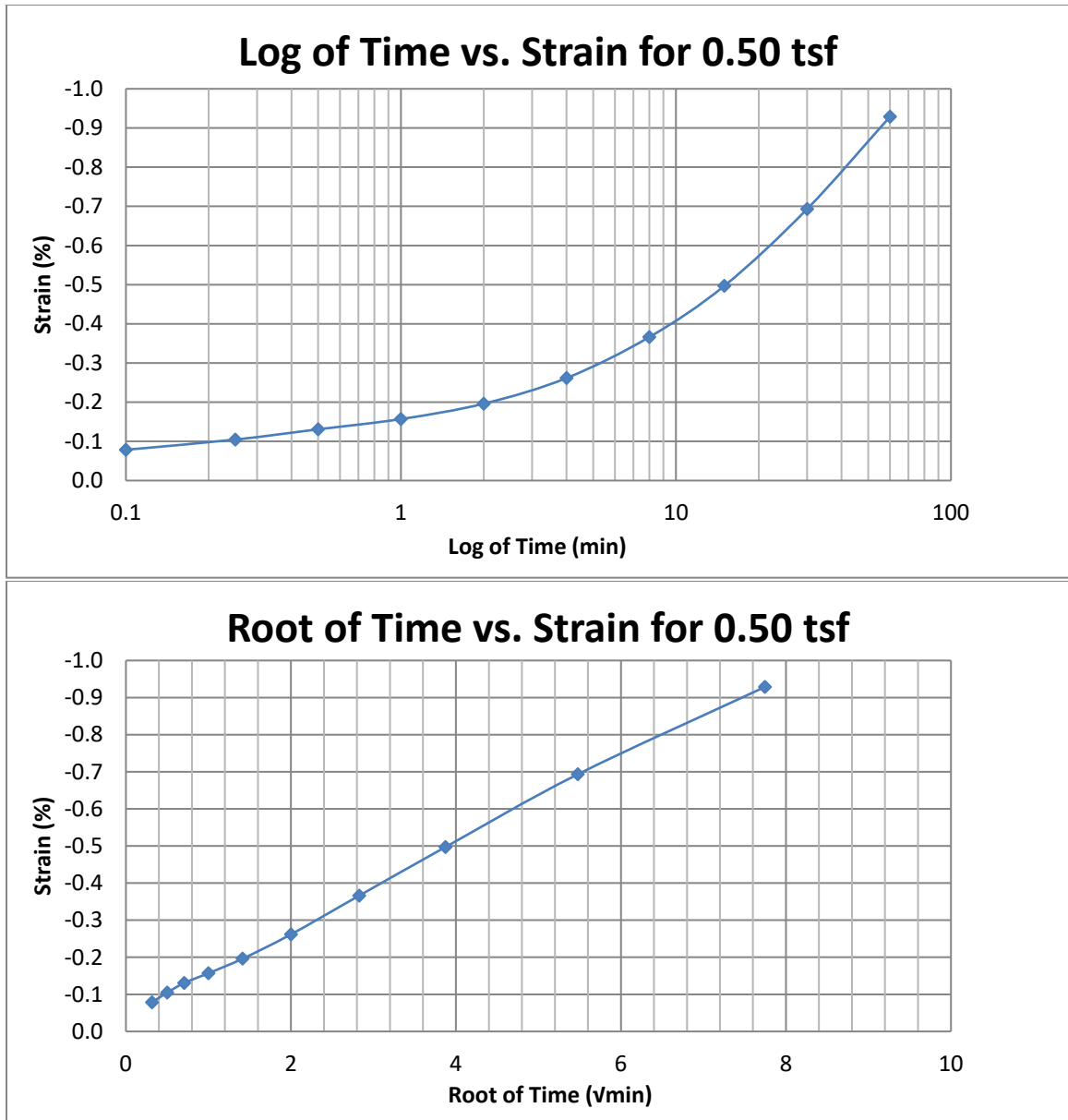
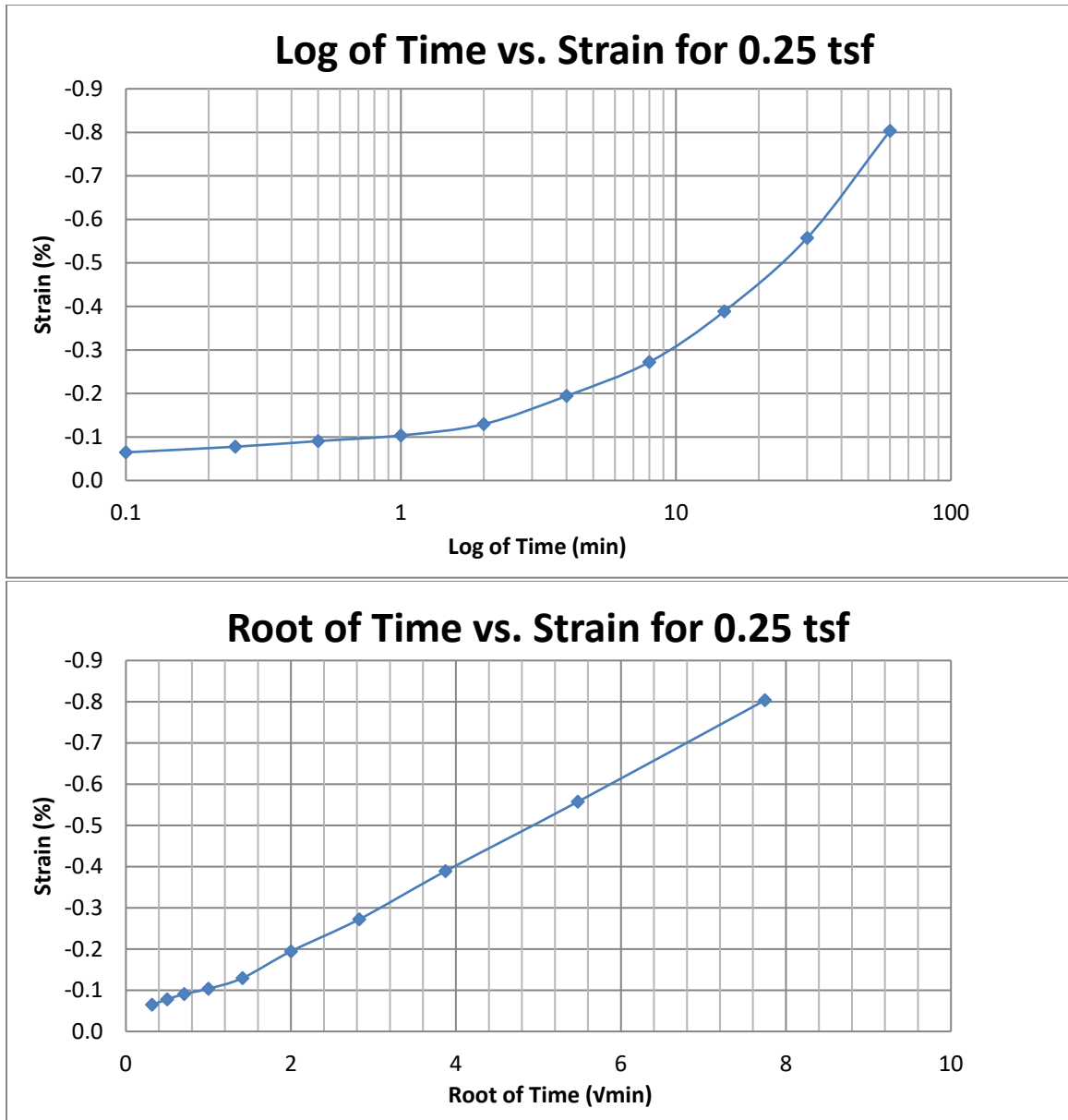
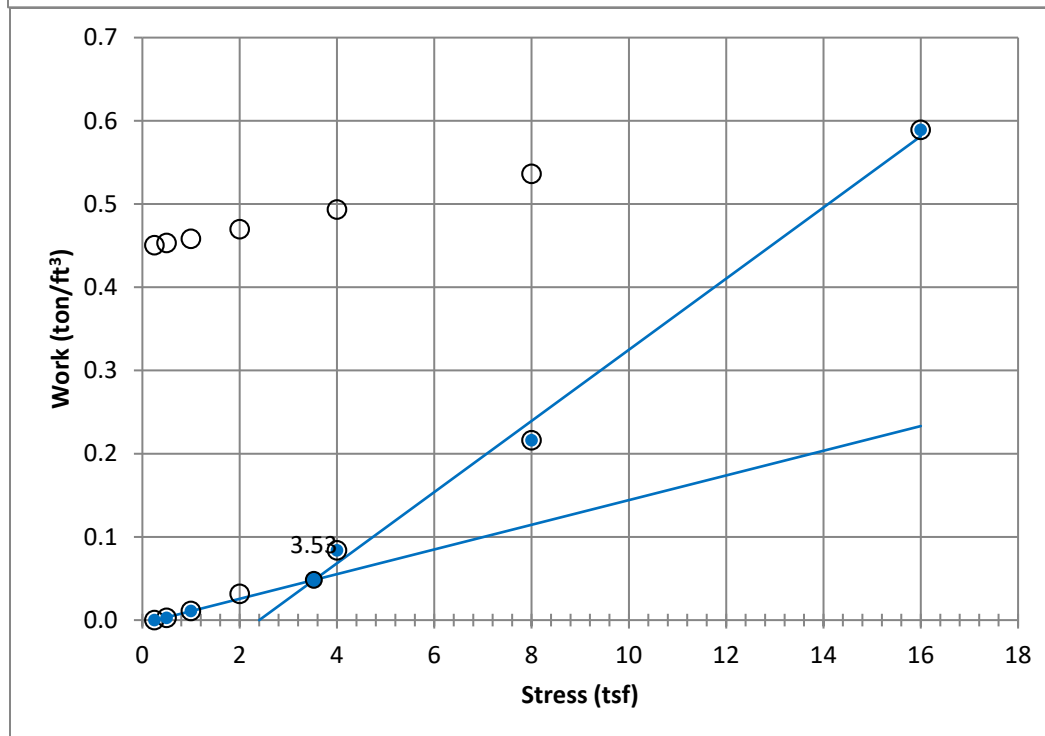
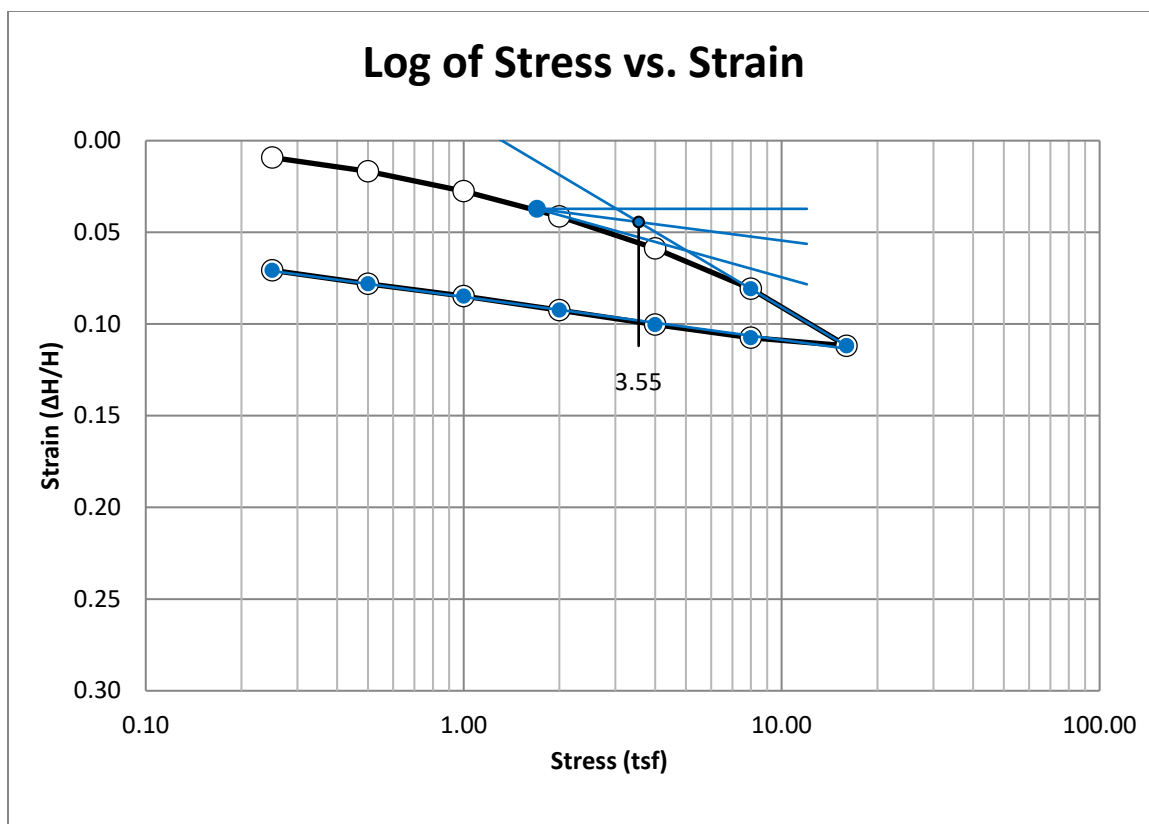


Figure A105 400 South at 50-52 feet



**Figure A106 400 South at 50-52 feet**





**Figure A107 Springville at 30-32 feet**

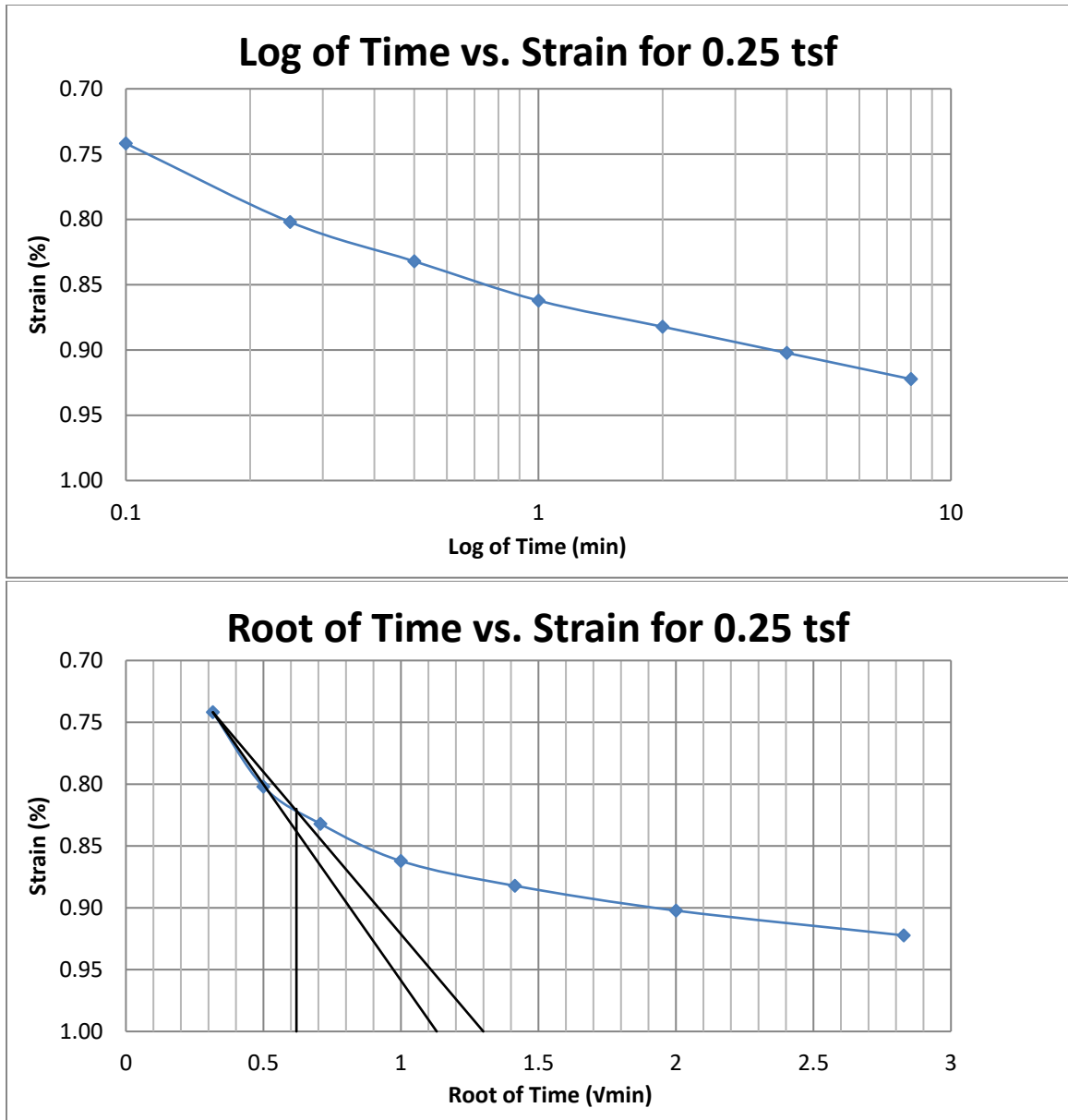


Figure A108 Springville at 30-32 feet

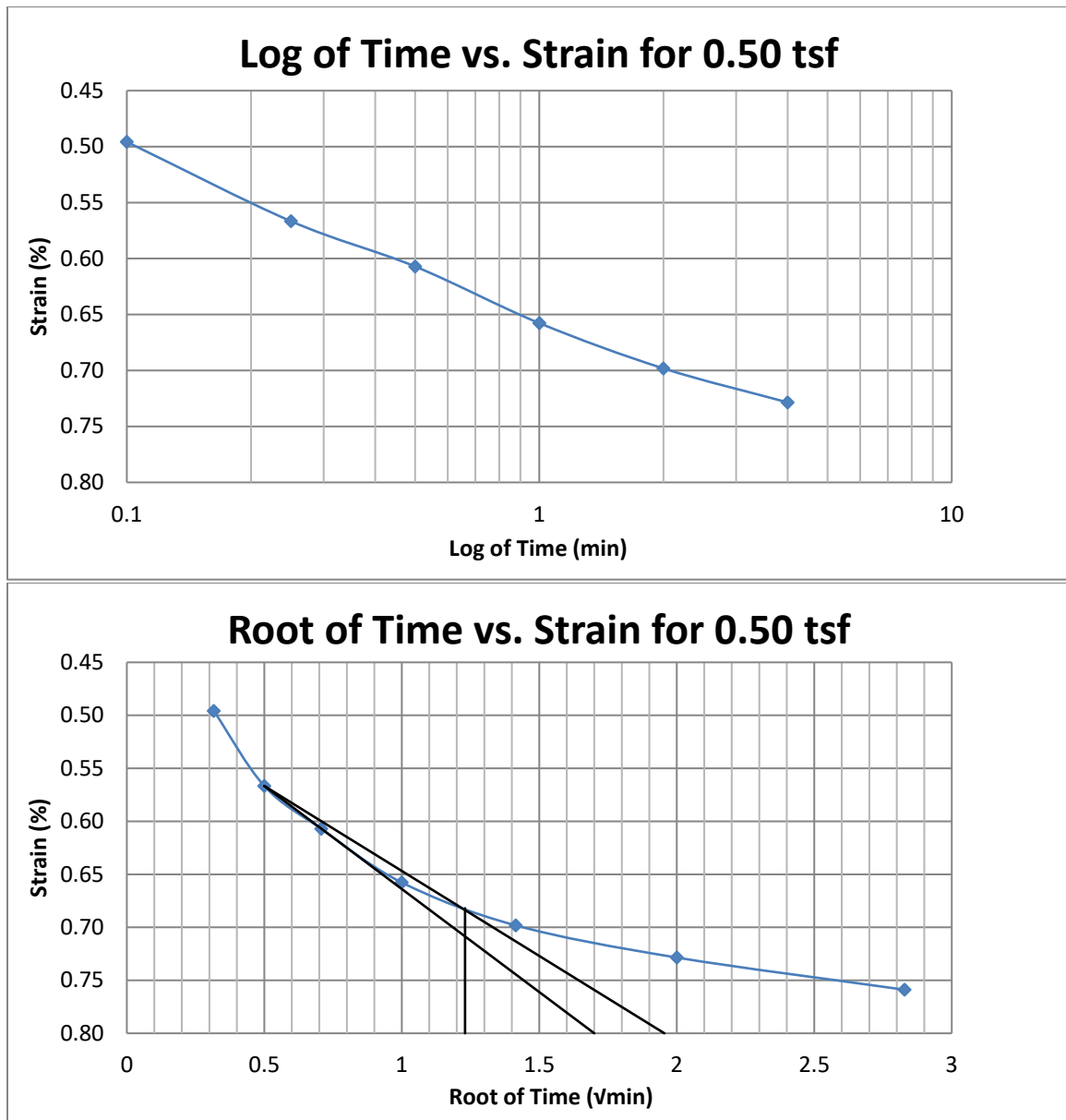


Figure A109 Springville at 30-32 feet

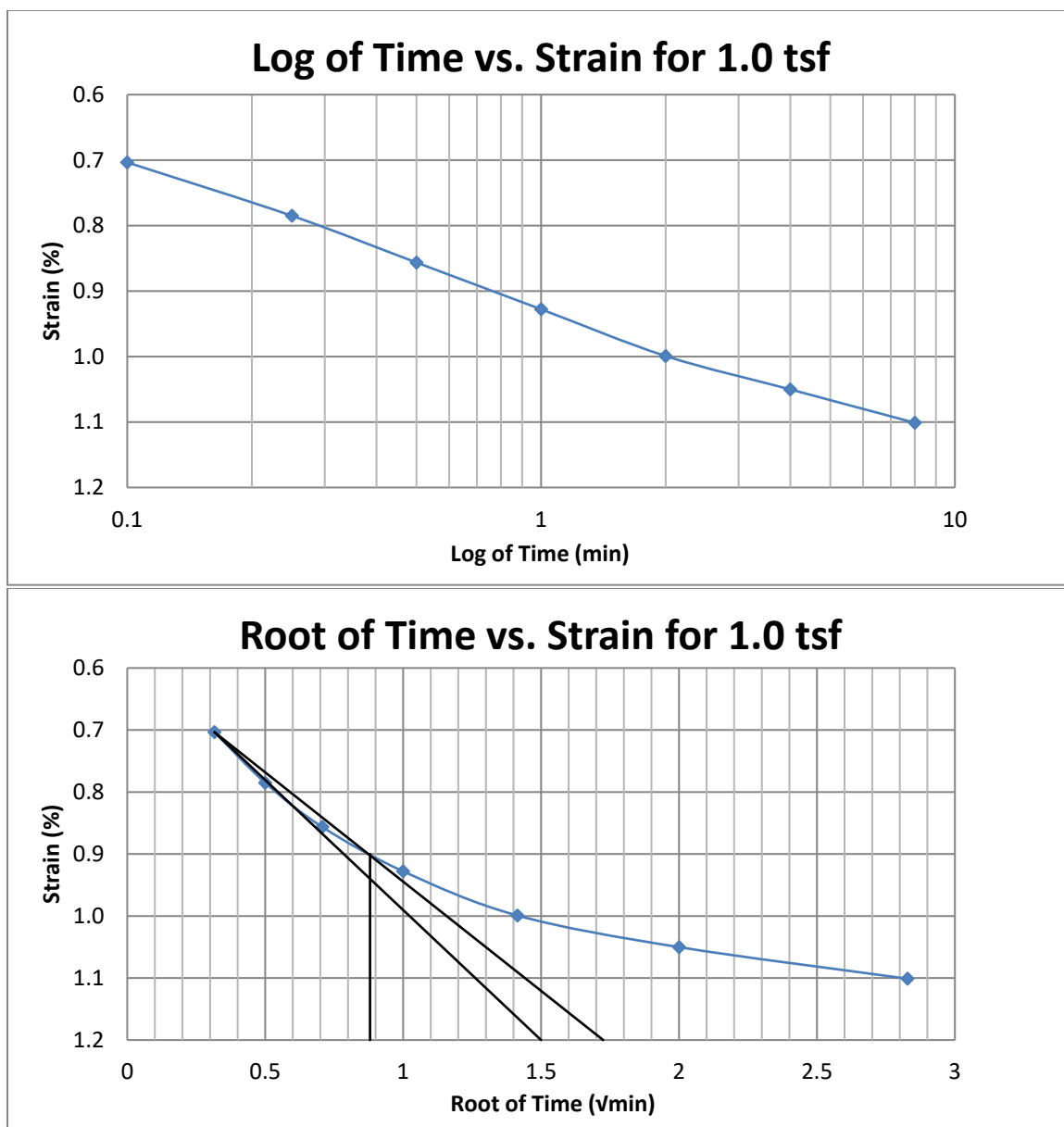


Figure A110 Springville at 30-32 feet

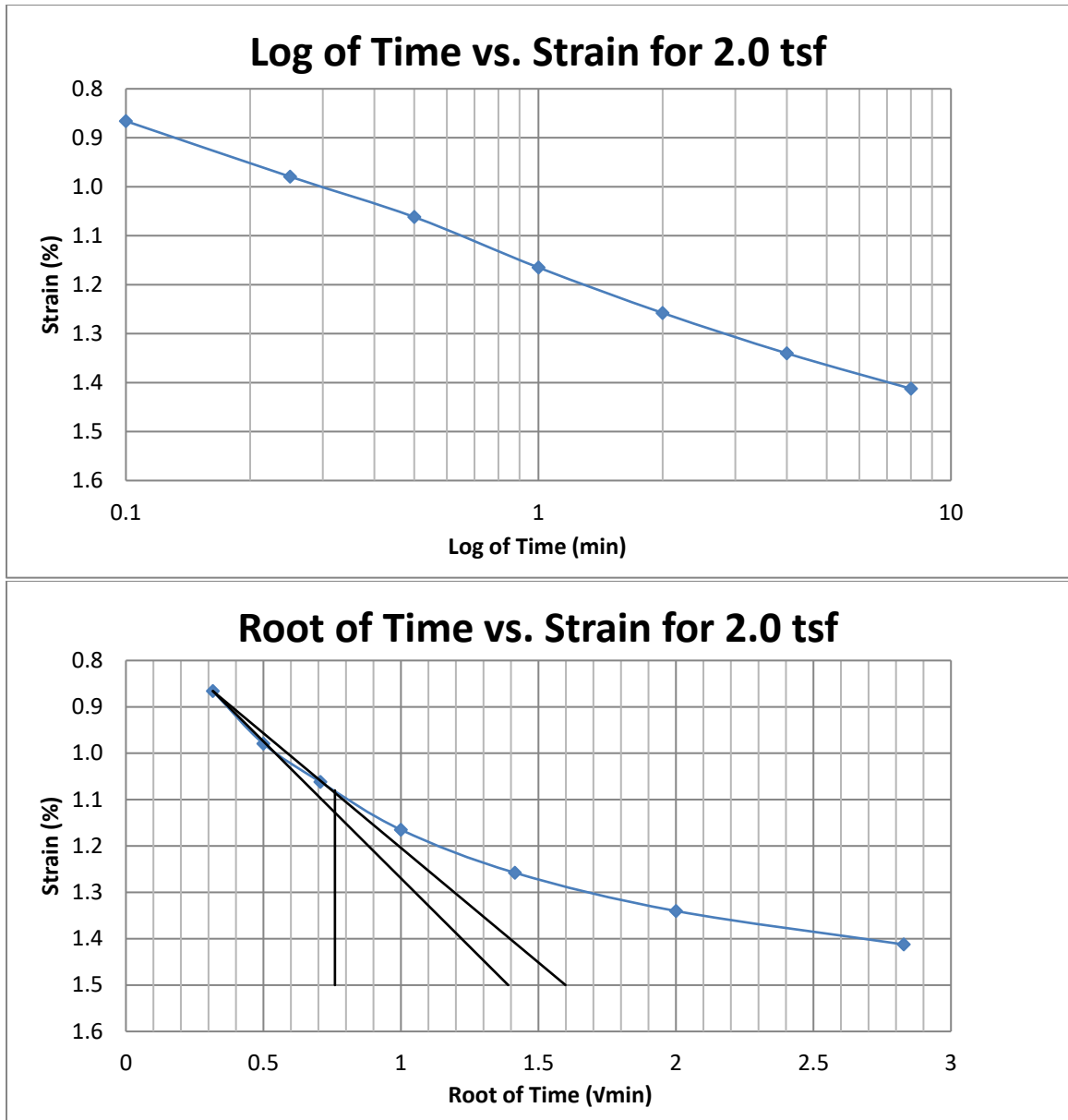


Figure A111 Springville at 30-32 feet

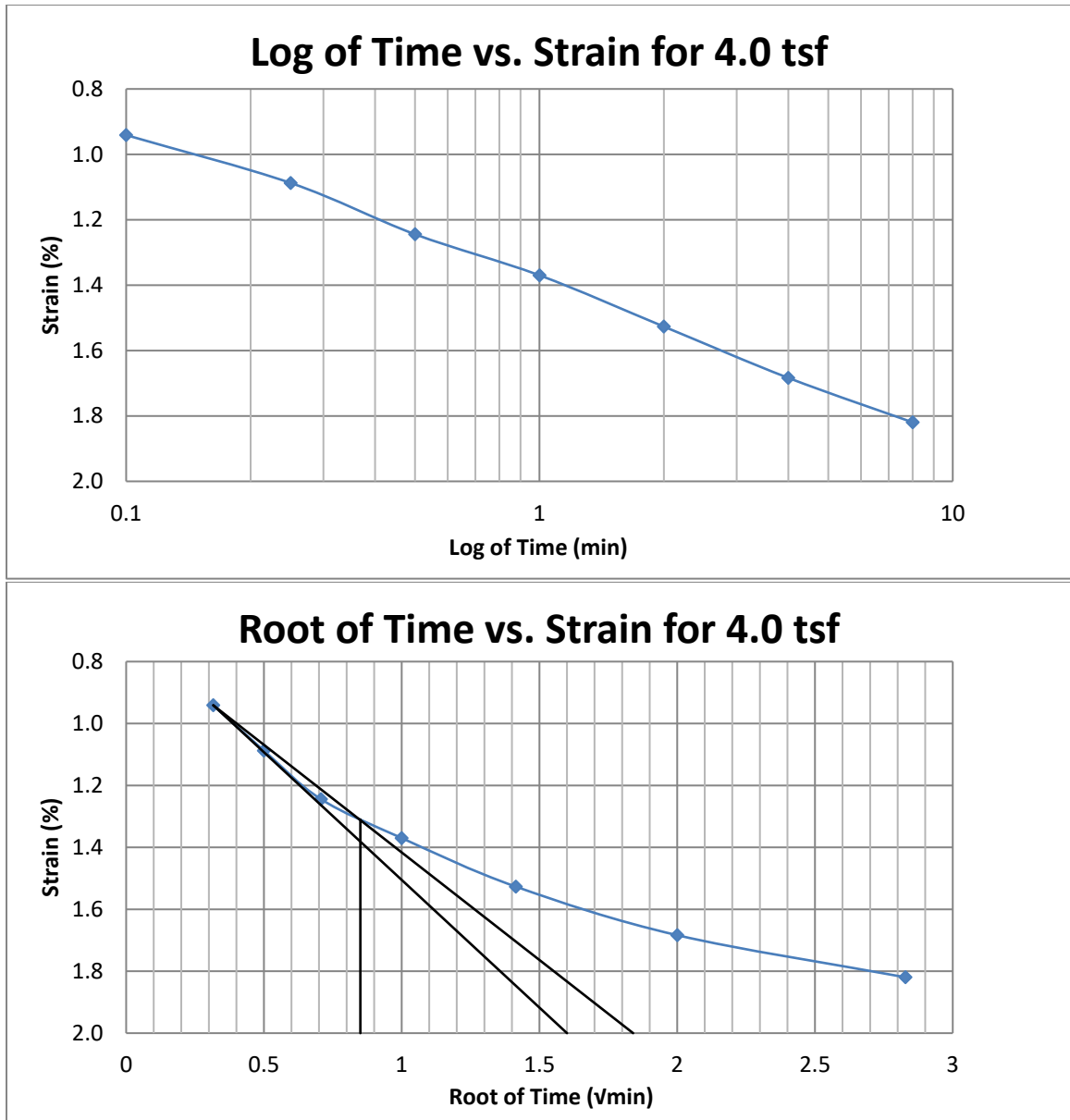


Figure A112 Springville at 30-32 feet

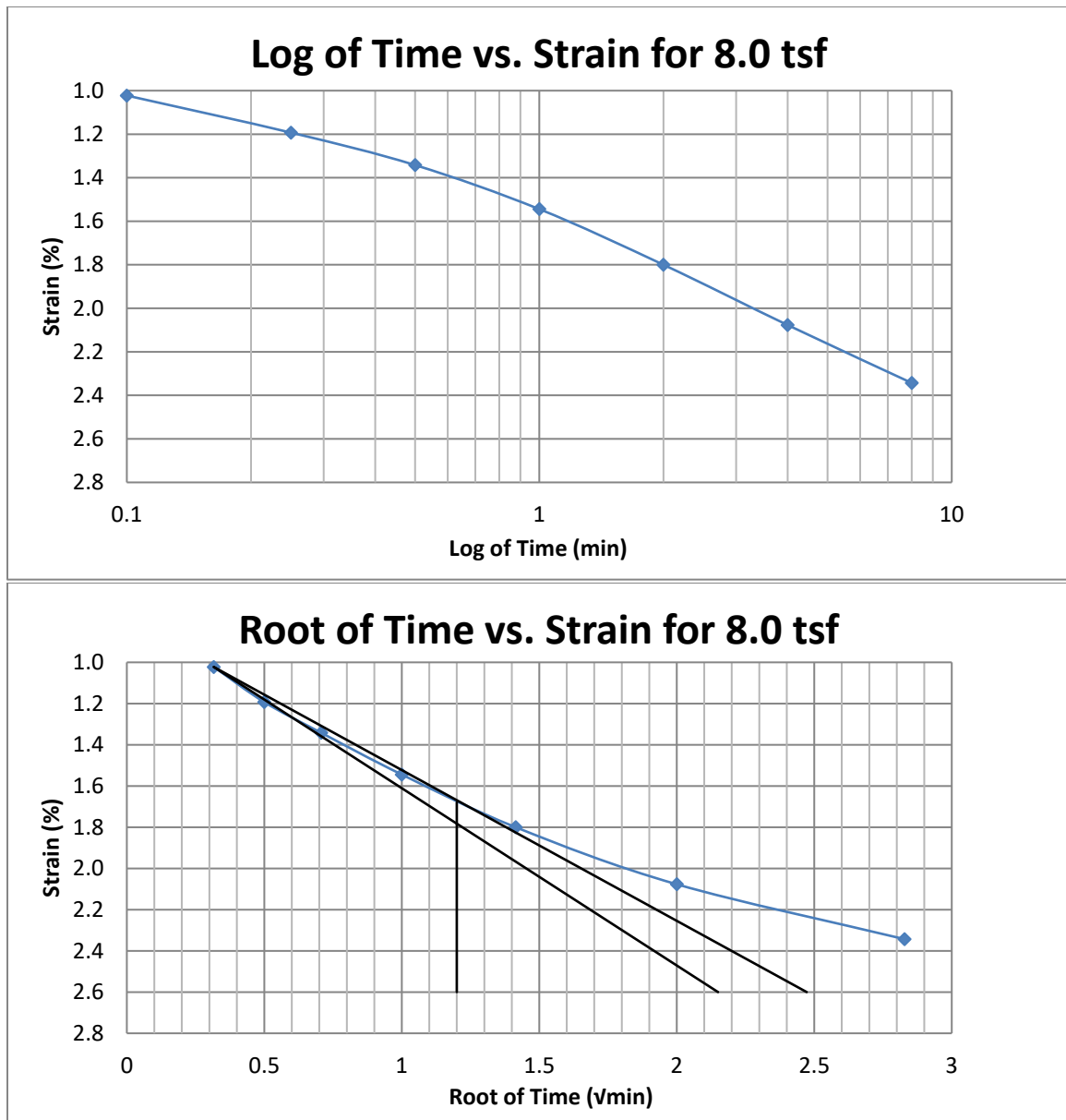


Figure A113 Springville at 30-32 feet

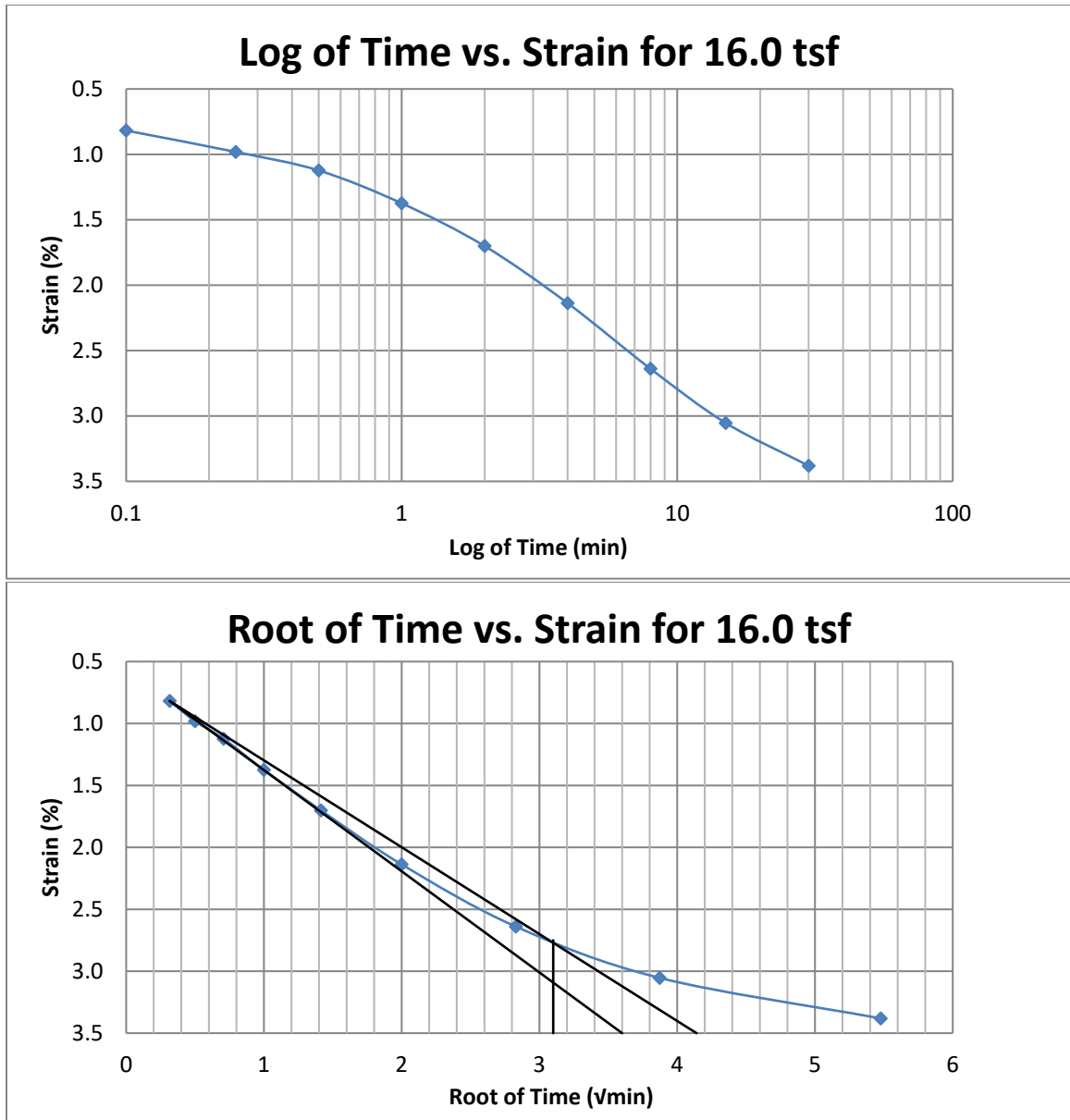


Figure A114 Springville at 30-32 feet



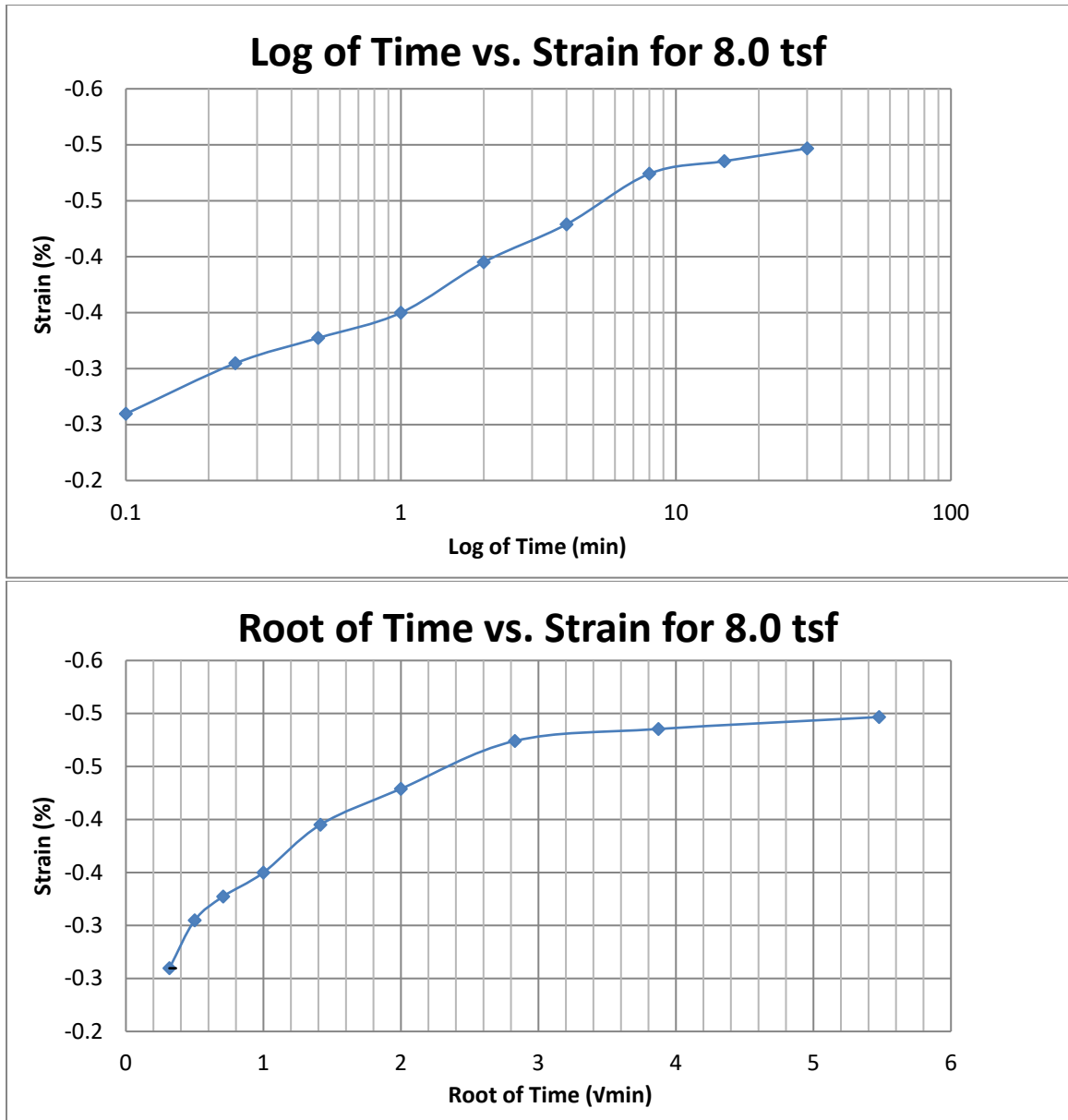


Figure A115 Springville at 30-32 feet

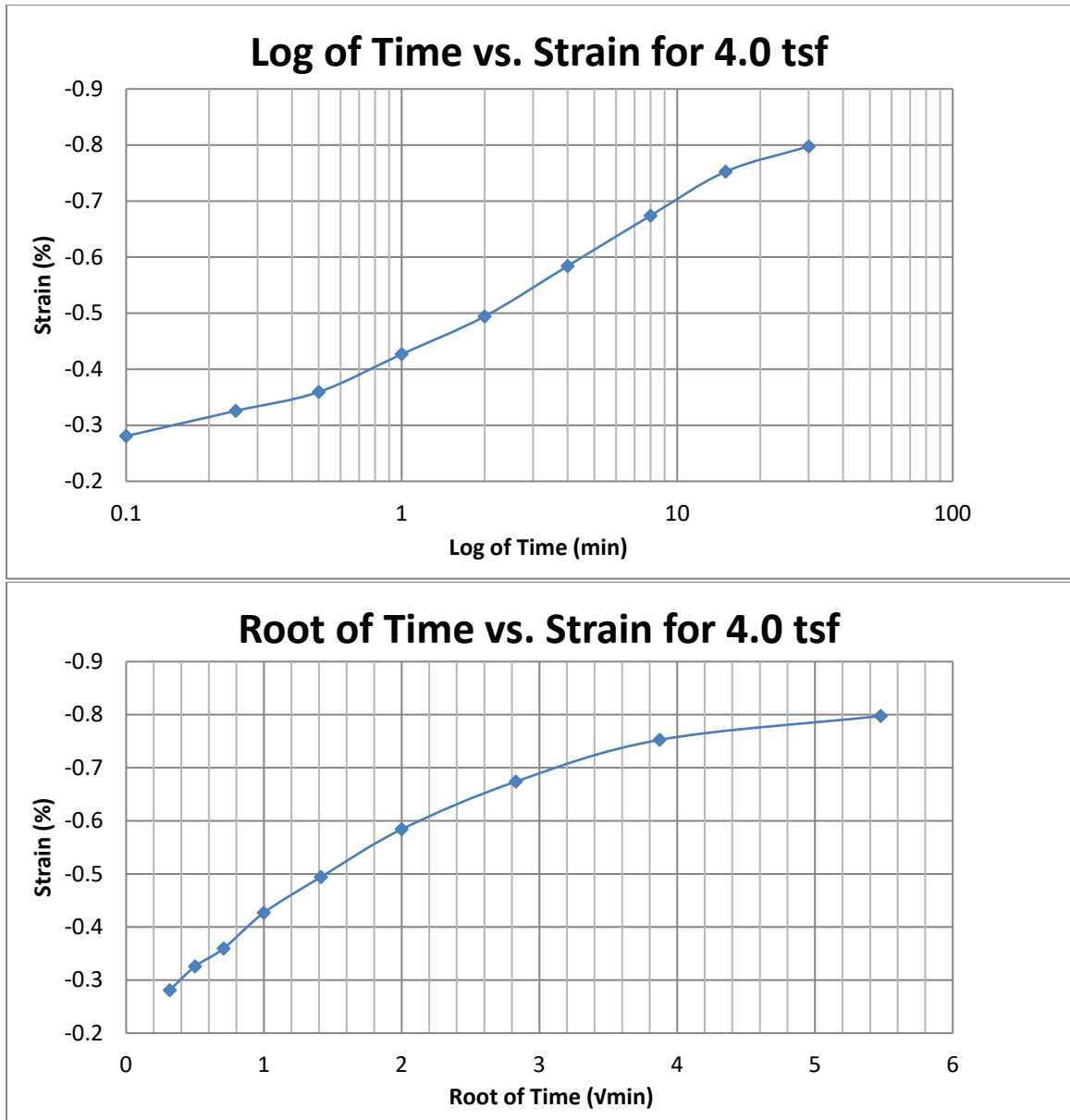


Figure A116 Springville at 30-32 feet

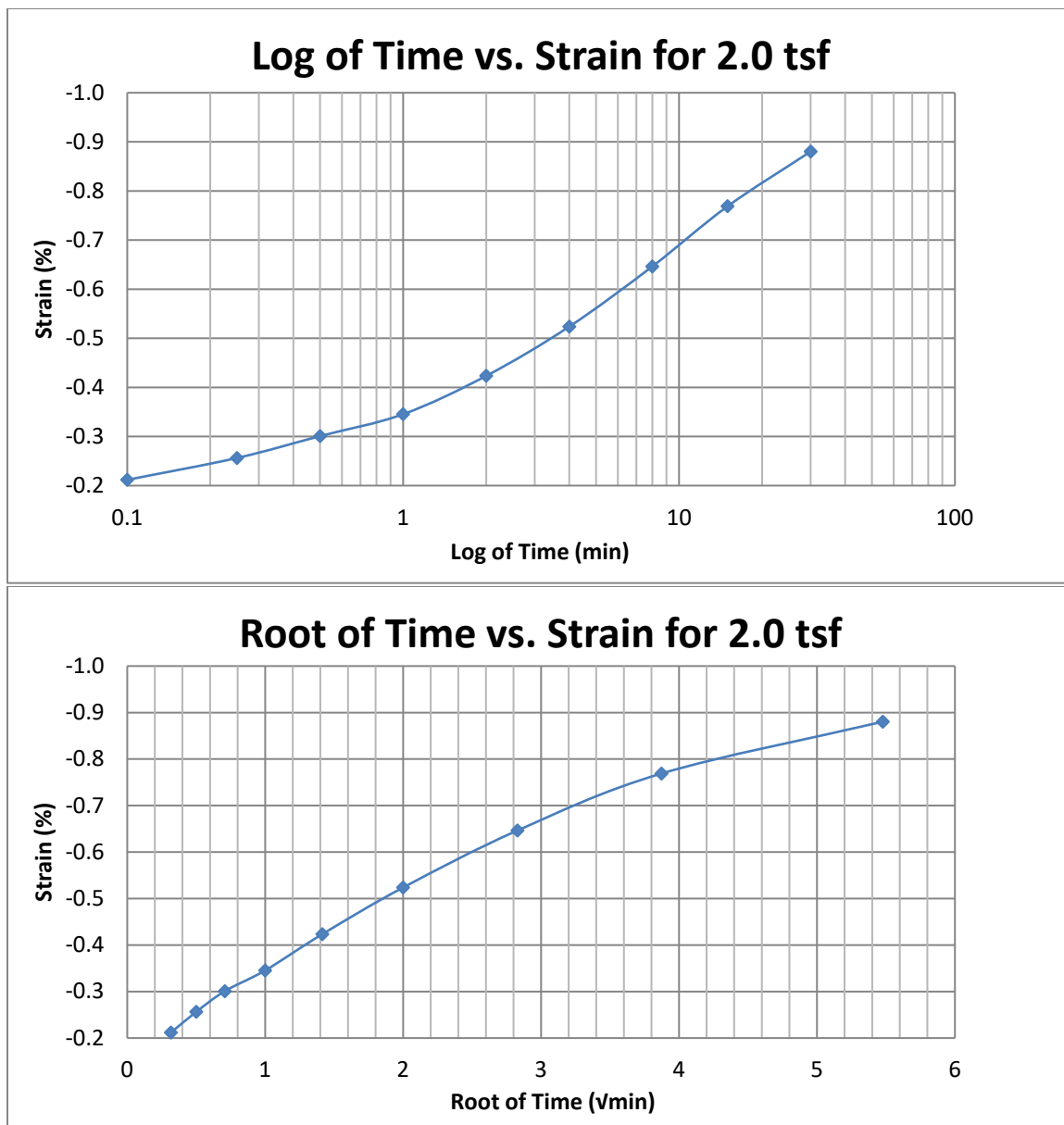


Figure A117 Springville at 30-32 feet

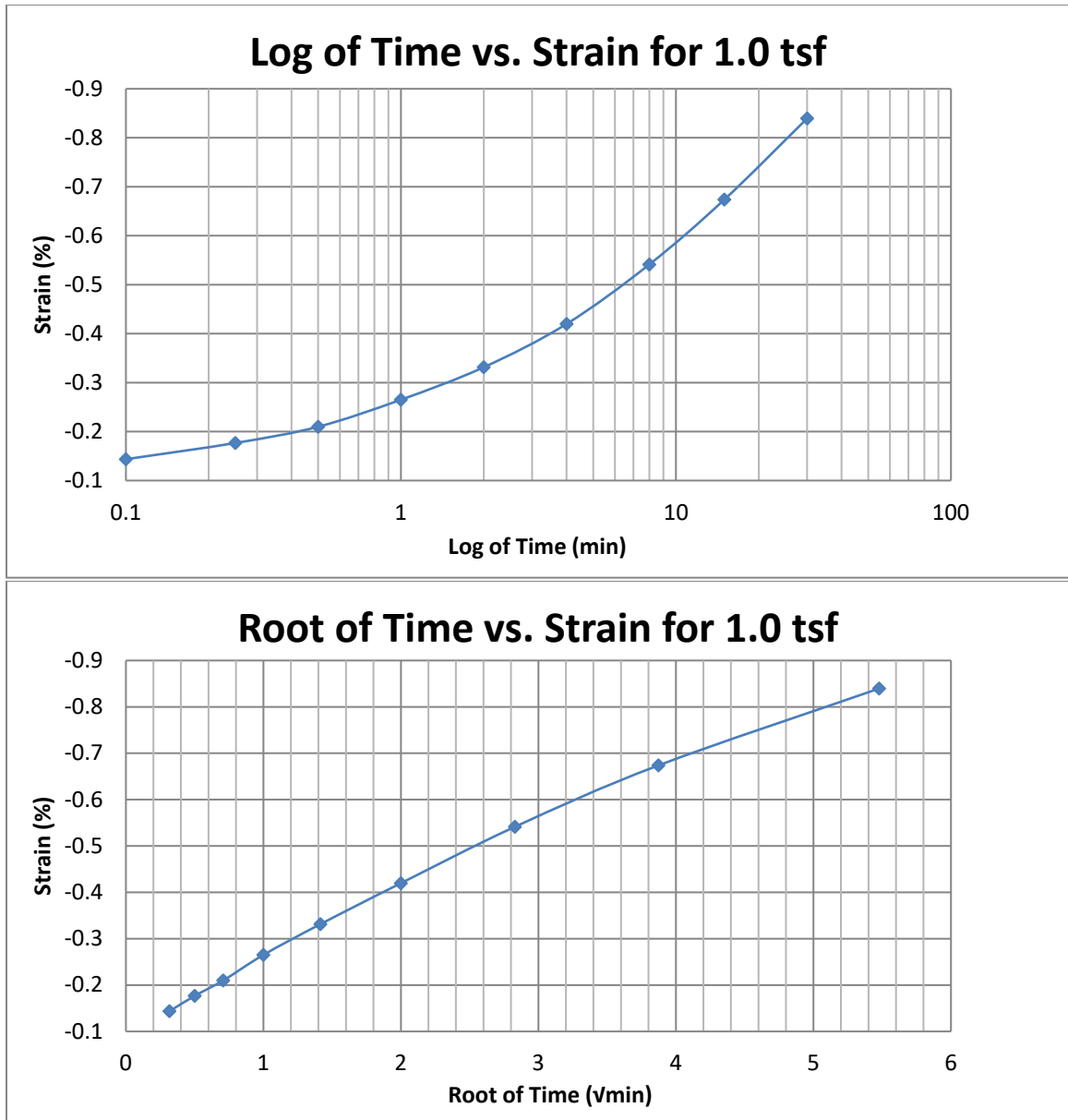


Figure A118 Springville at 30-32 feet

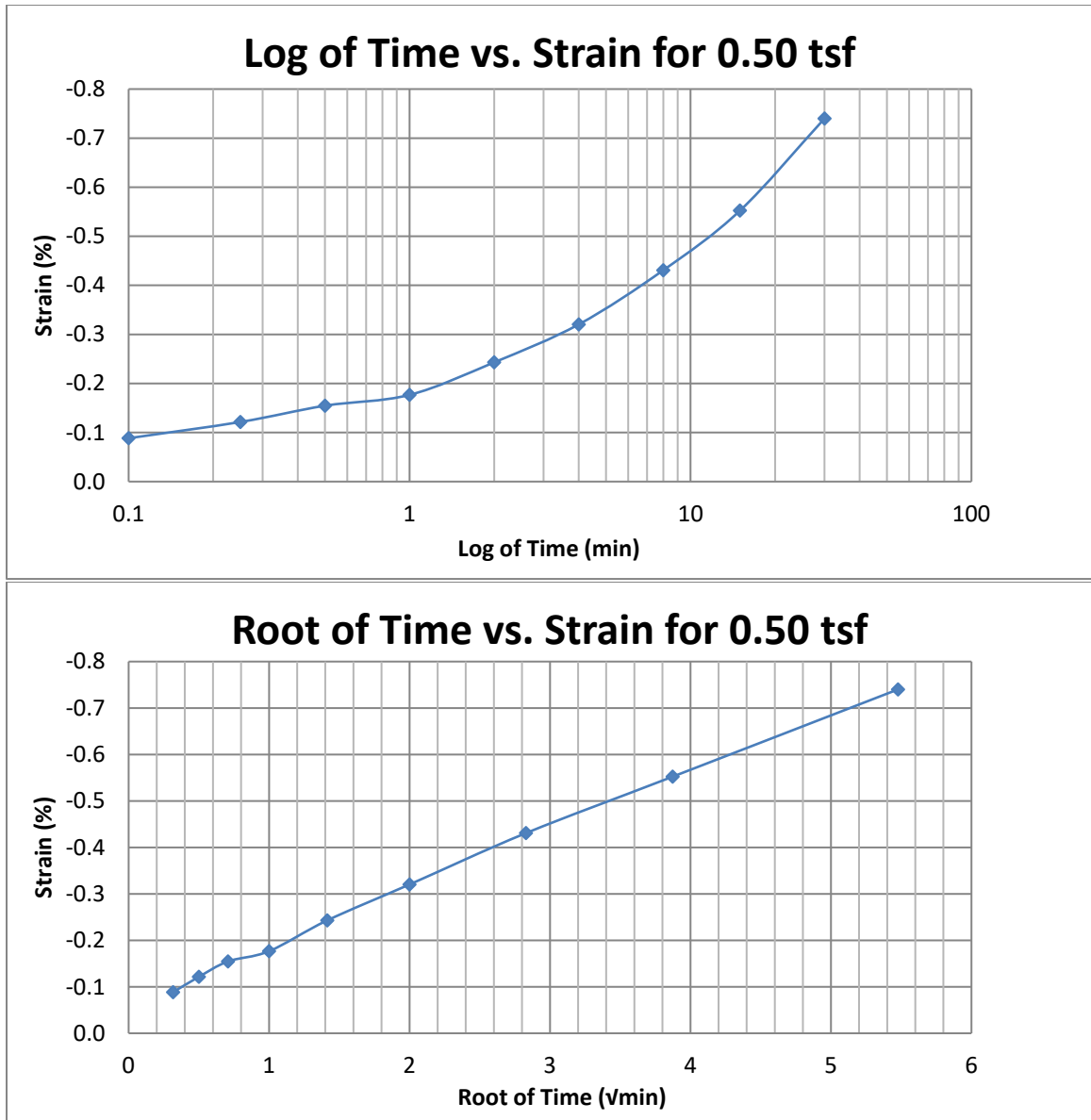


Figure A119 Springville at 30-32 feet

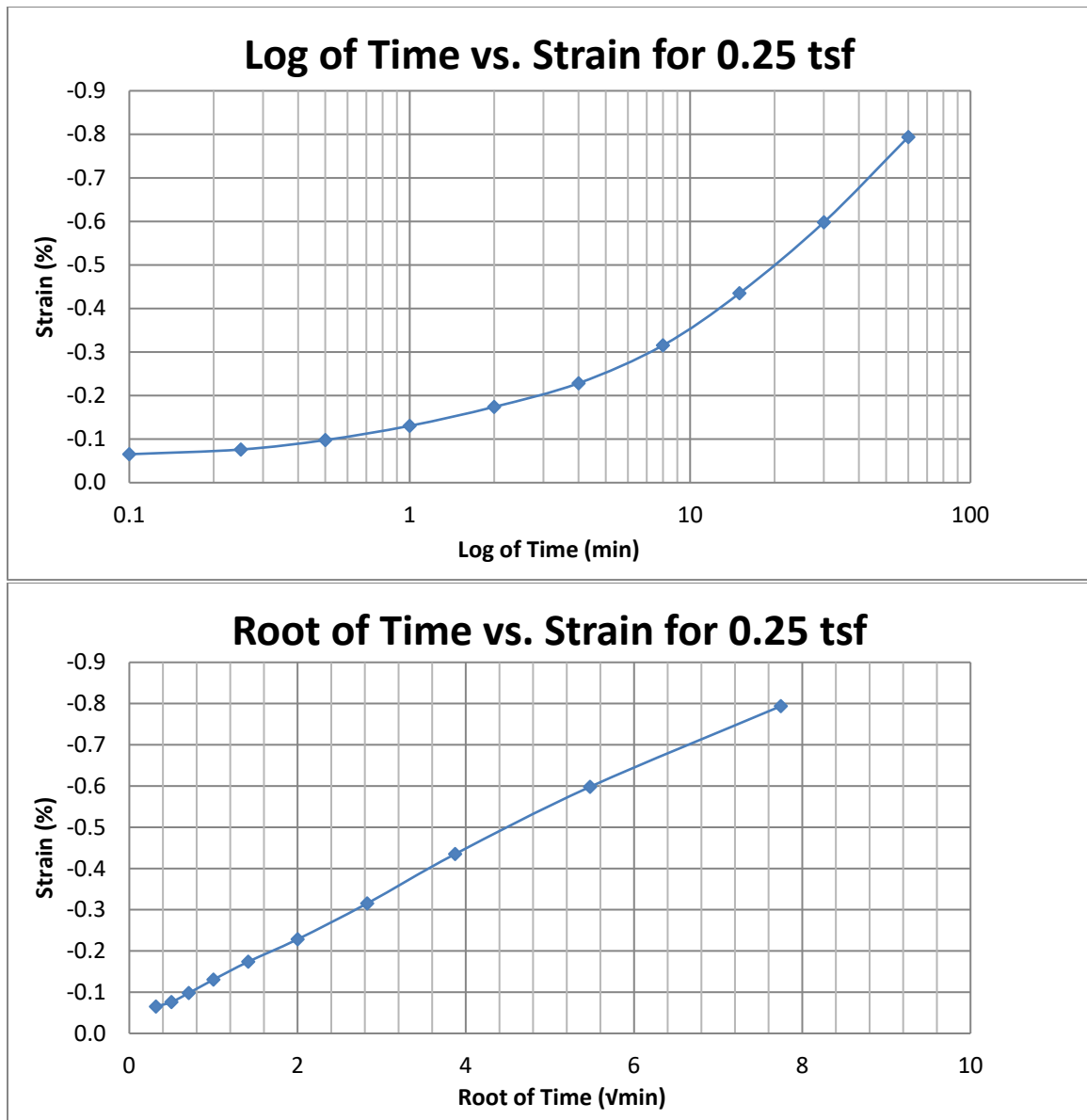
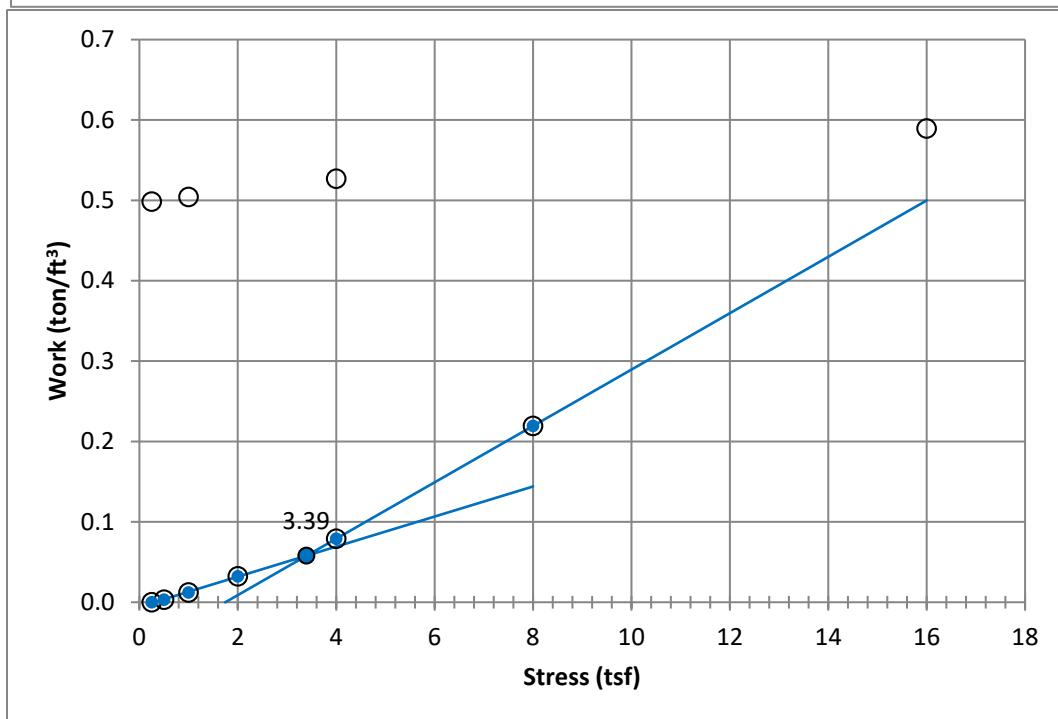
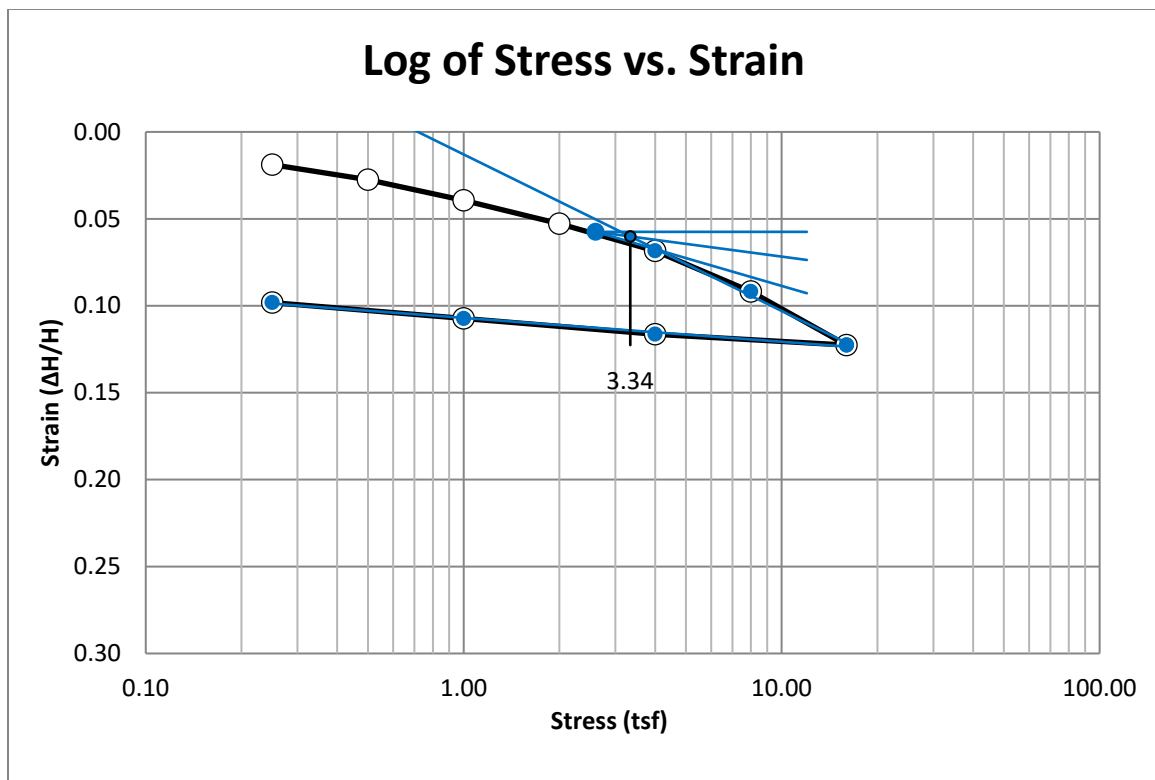


Figure A120 Springville at 30-32 feet



**Figure A121 Springville at 40-42 feet**

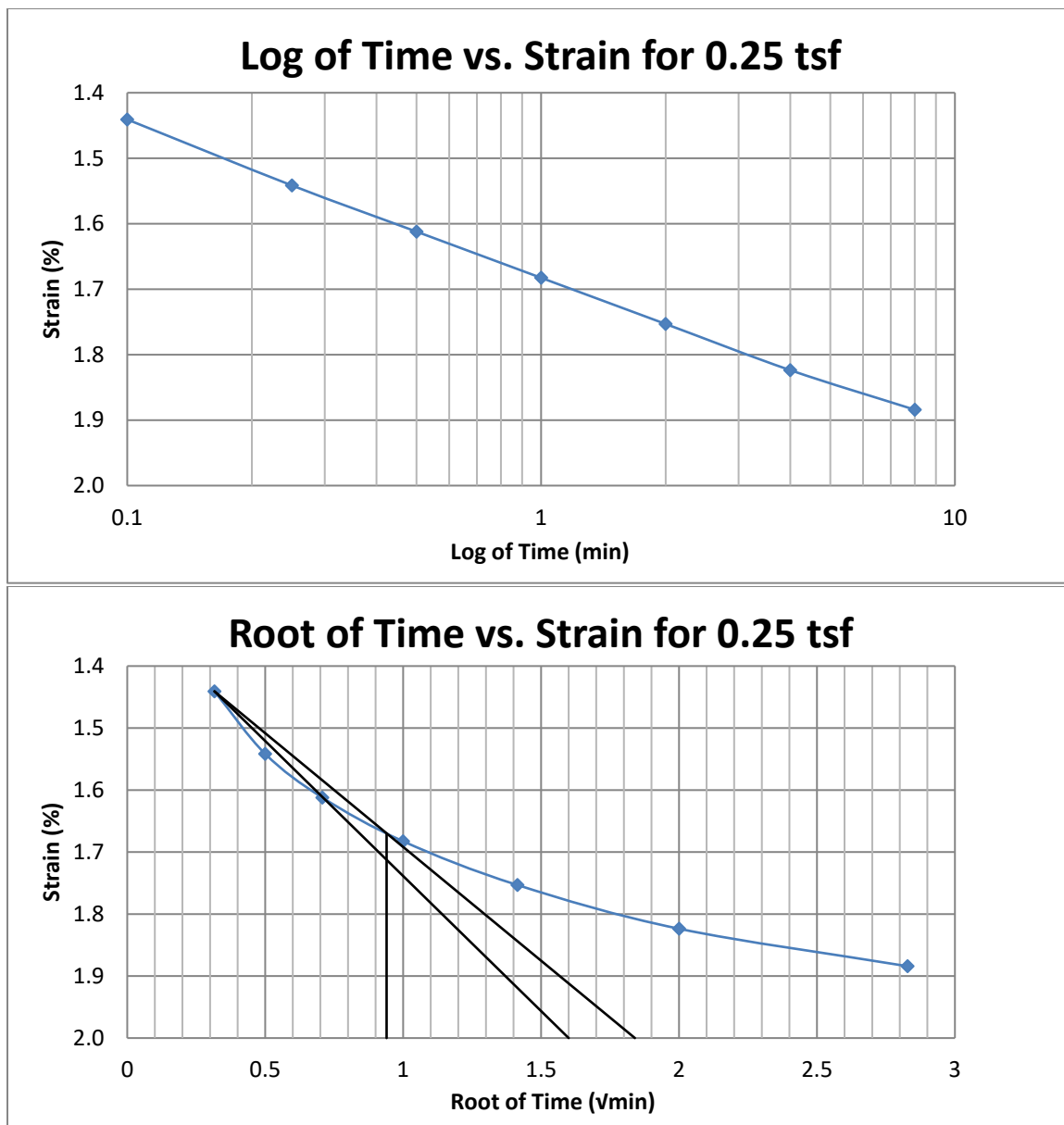


Figure A122 Springville at 40-42 feet



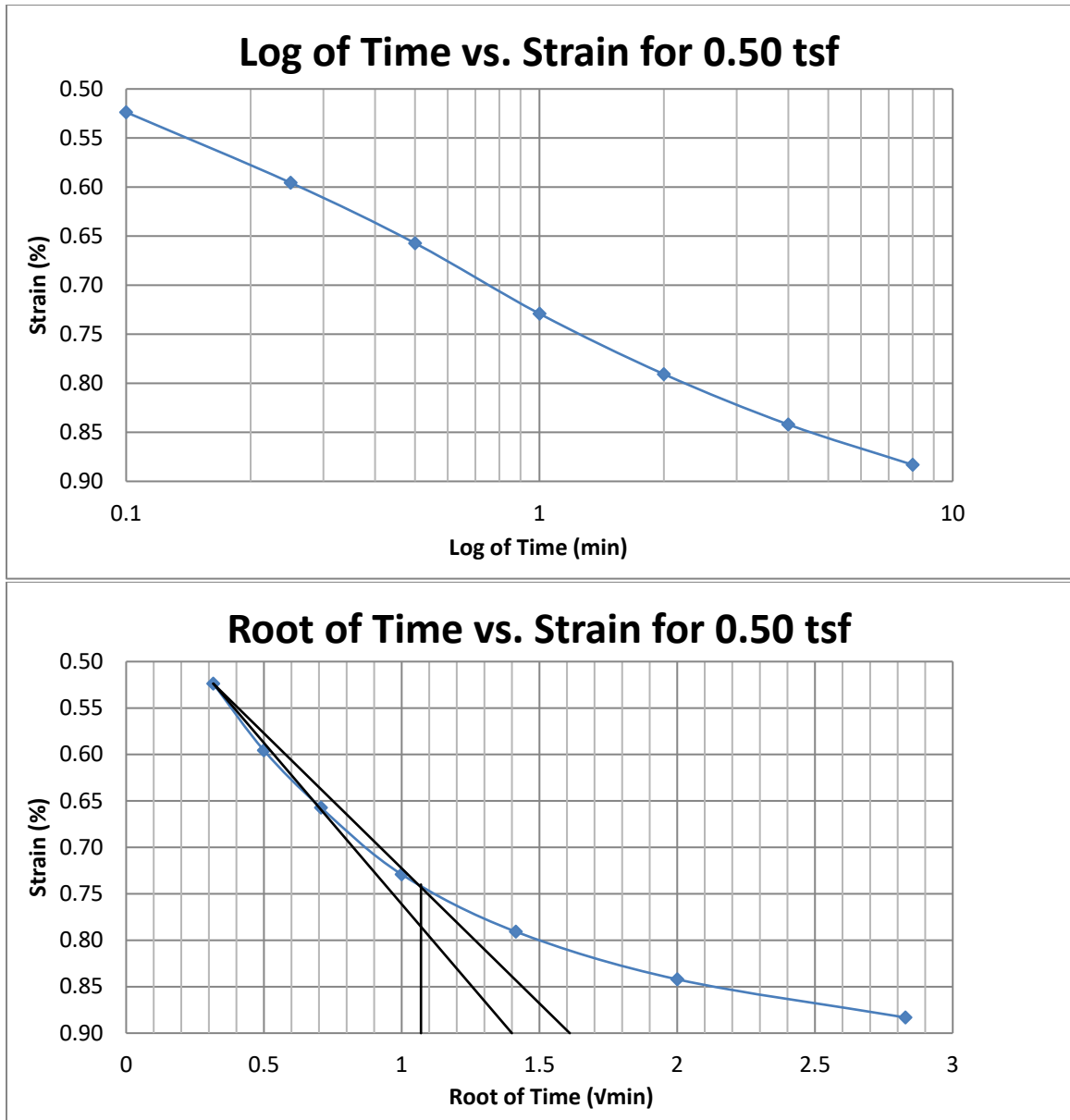


Figure A123 Springville at 40-42 feet

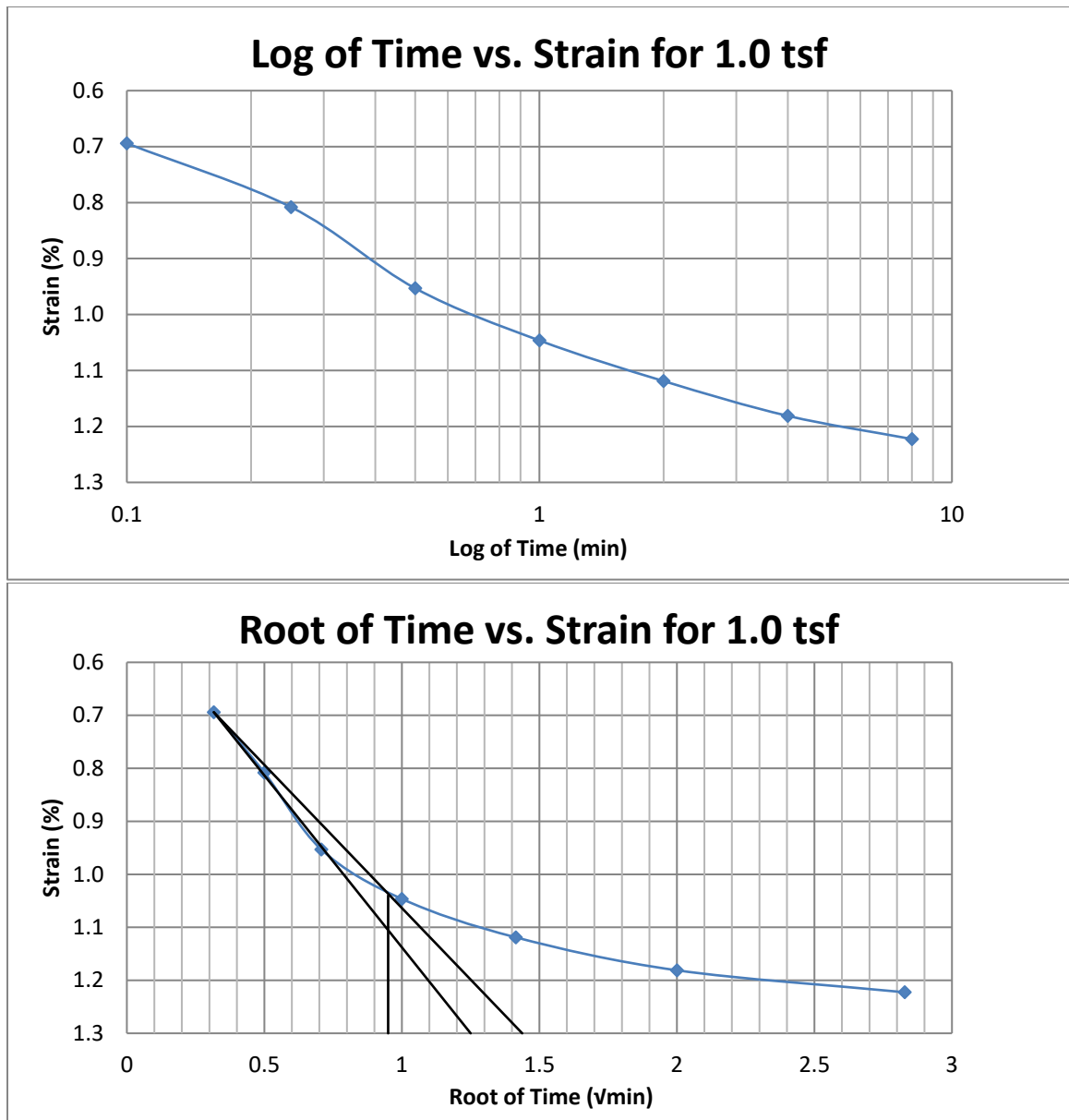


Figure A124 Springville at 40-42 feet

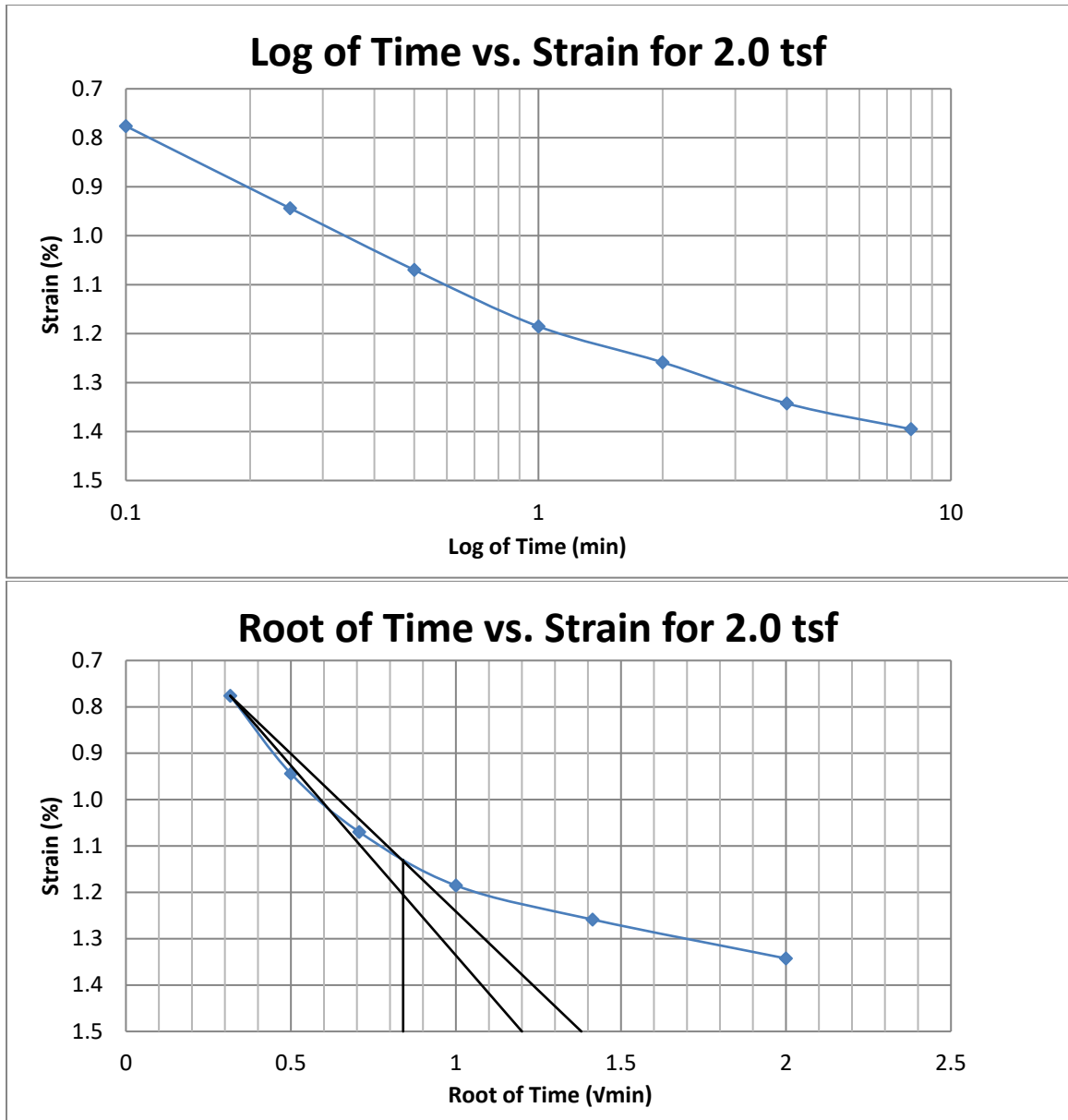


Figure A125 Springville at 40-42 feet

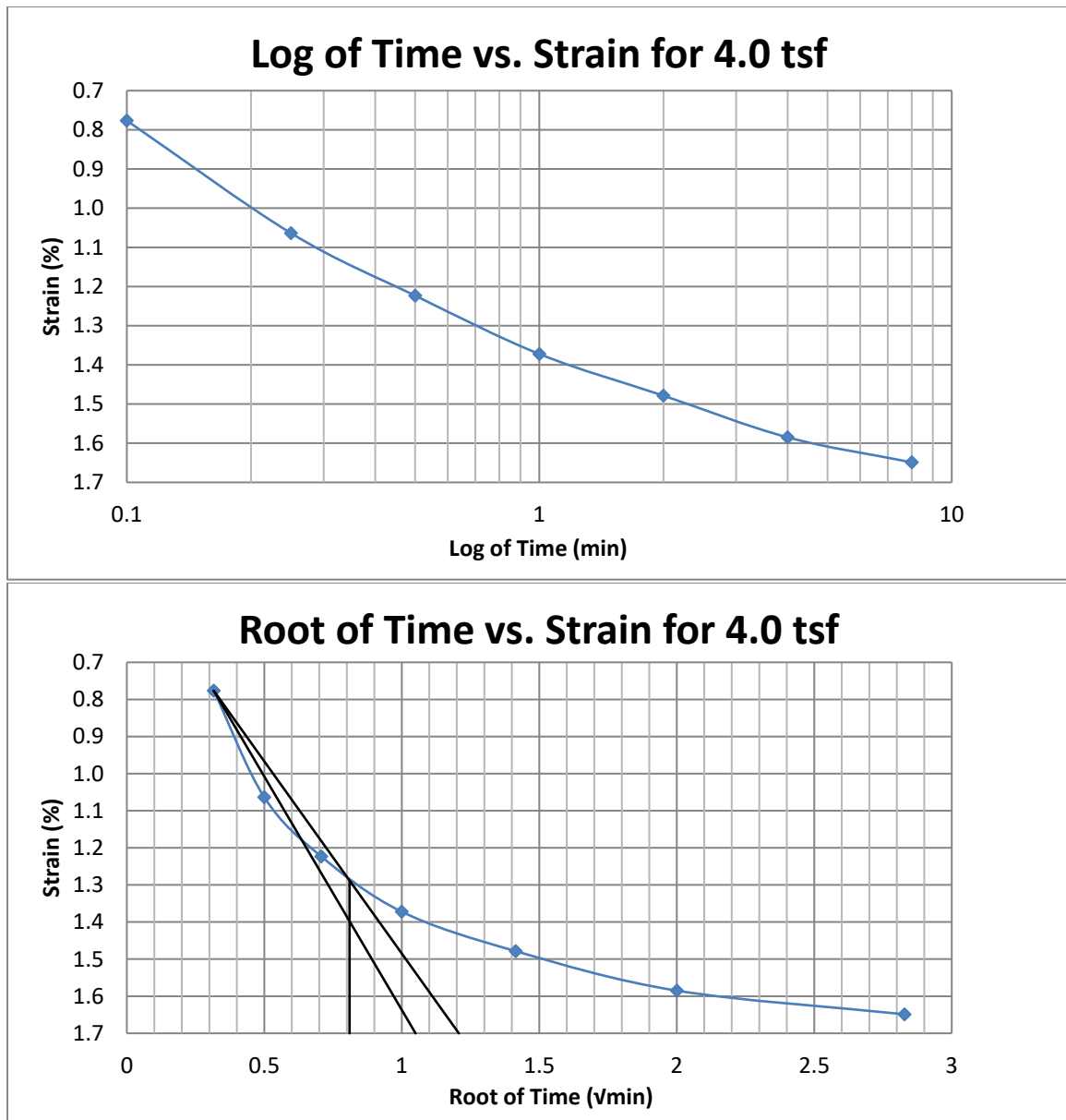


Figure A126 Springville at 40-42 feet

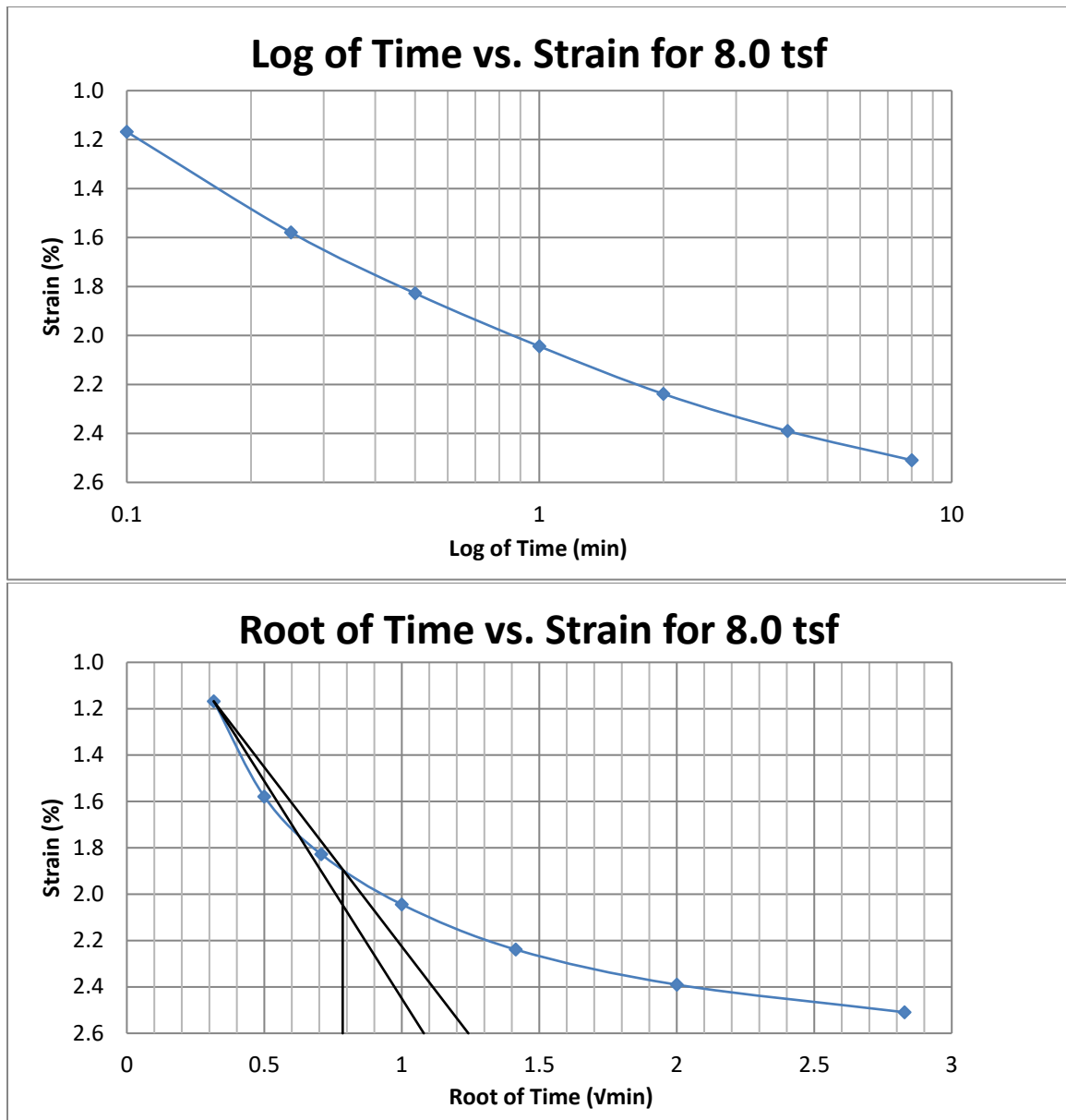
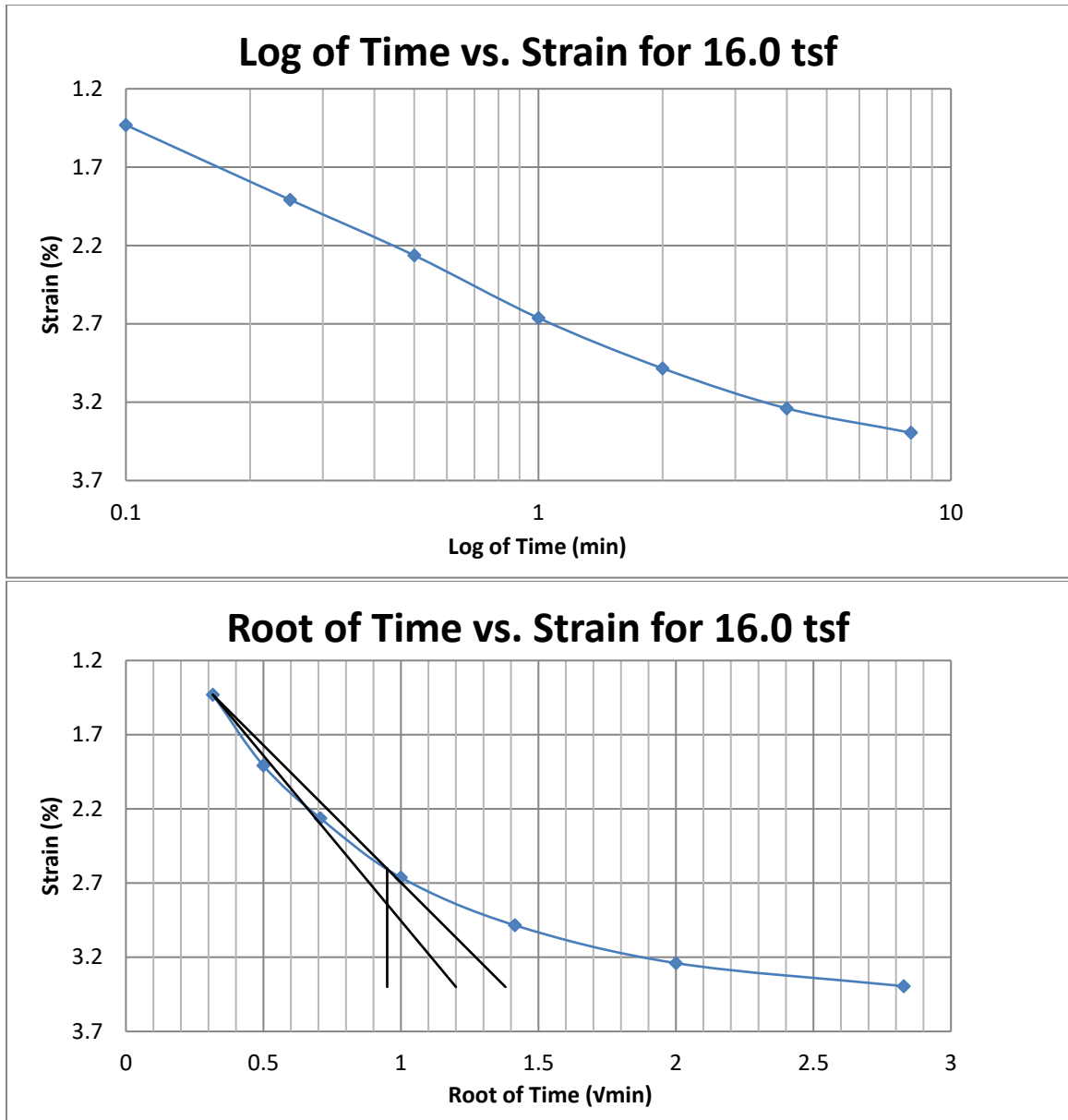


Figure A127 Springville at 40-42 feet



**Figure A128 Springville at 40-42 feet**

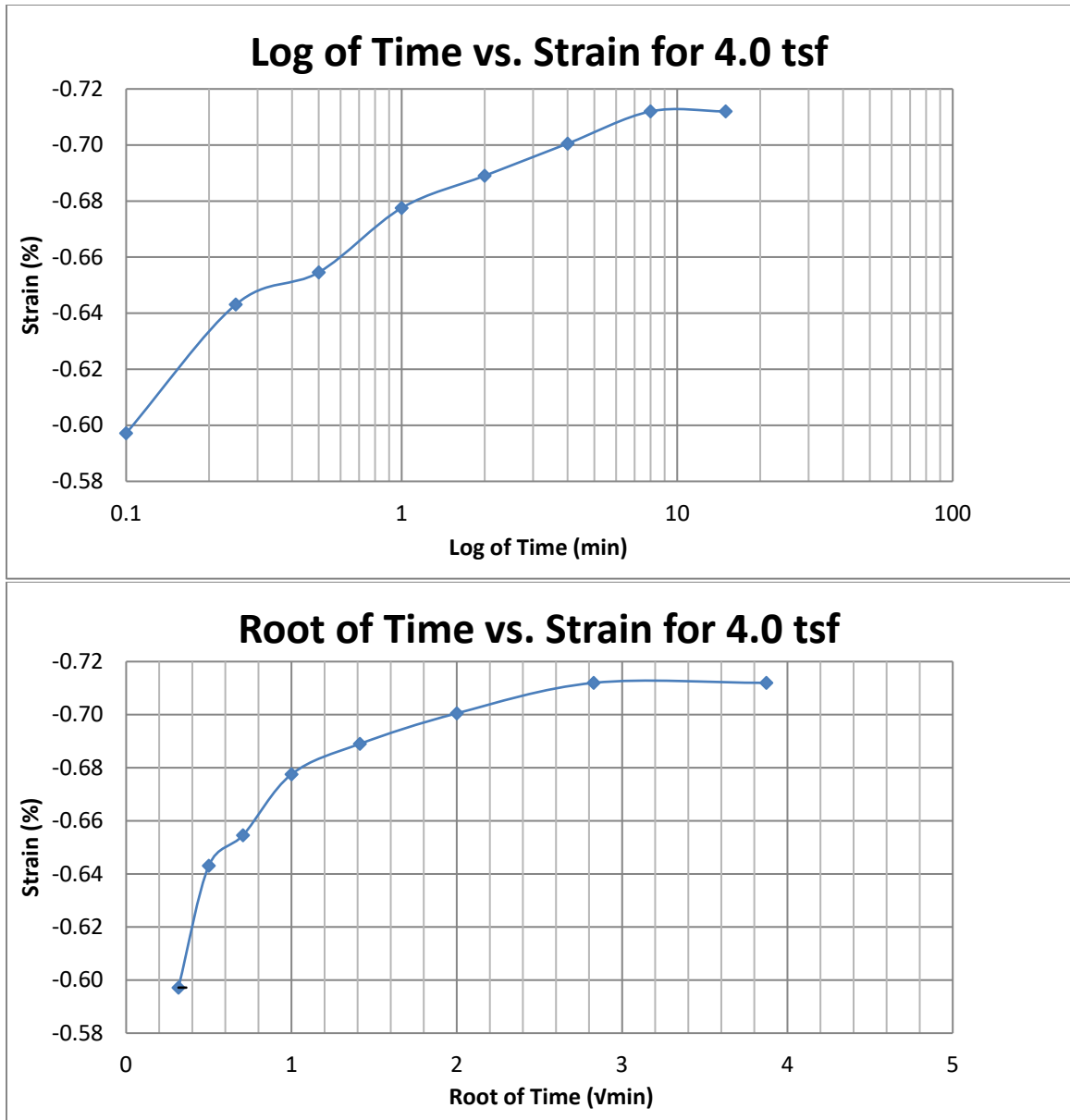


Figure A129 Springville at 40-42 feet

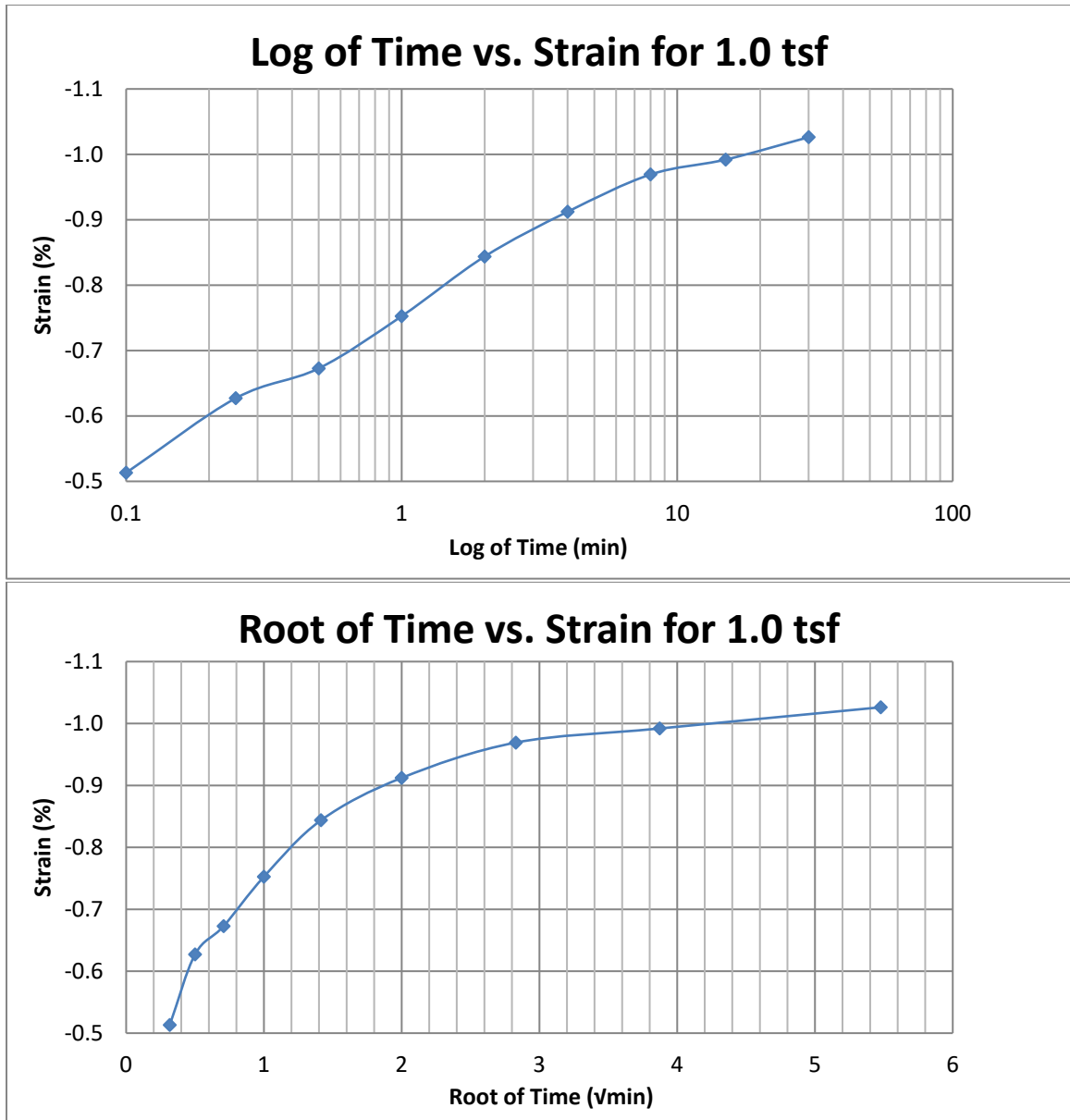


Figure A130 Springville at 40-42 feet



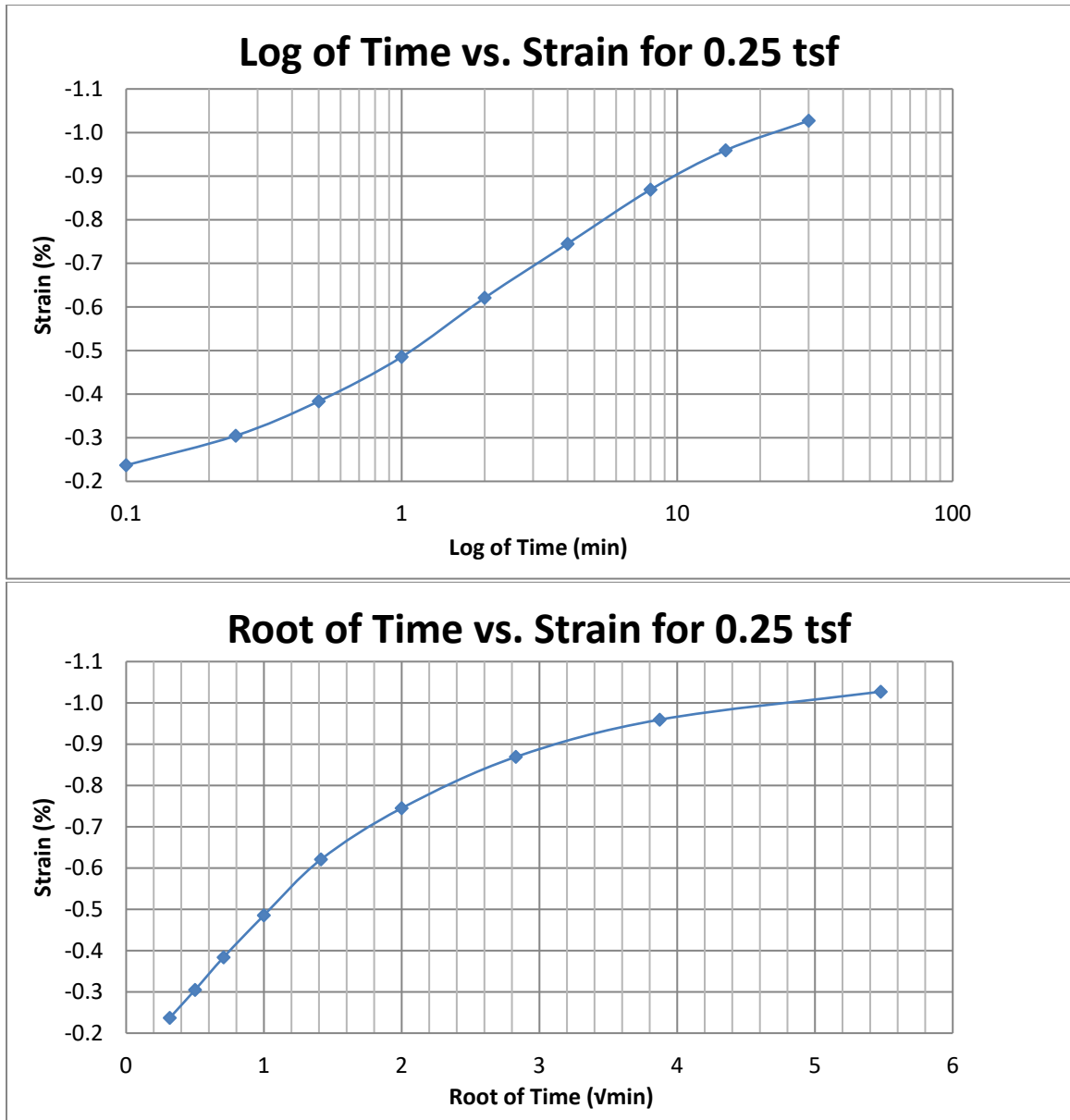
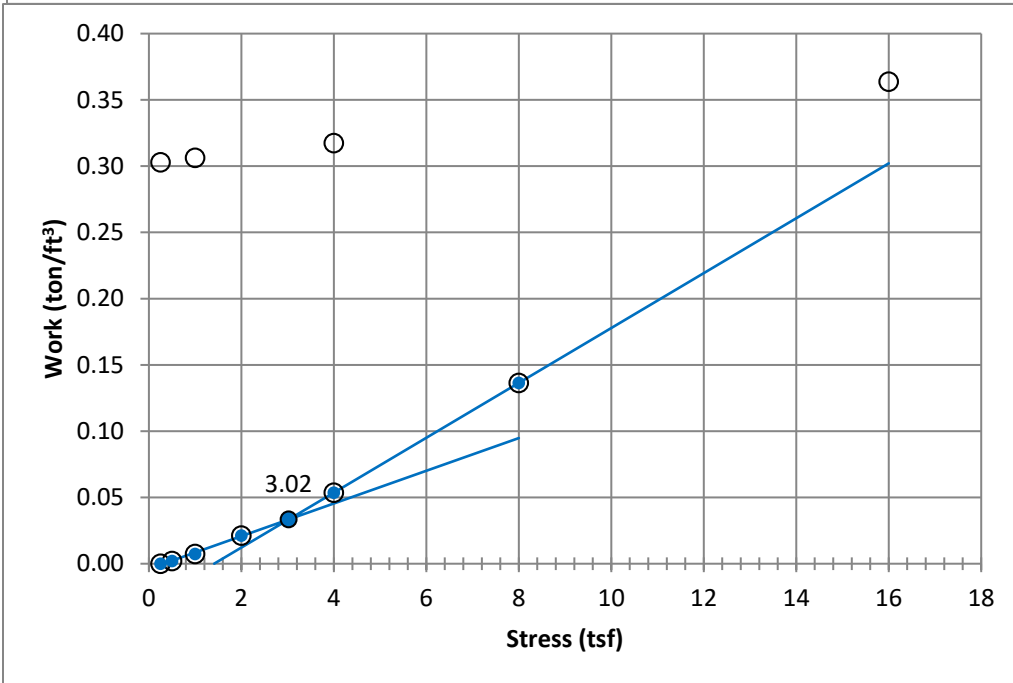
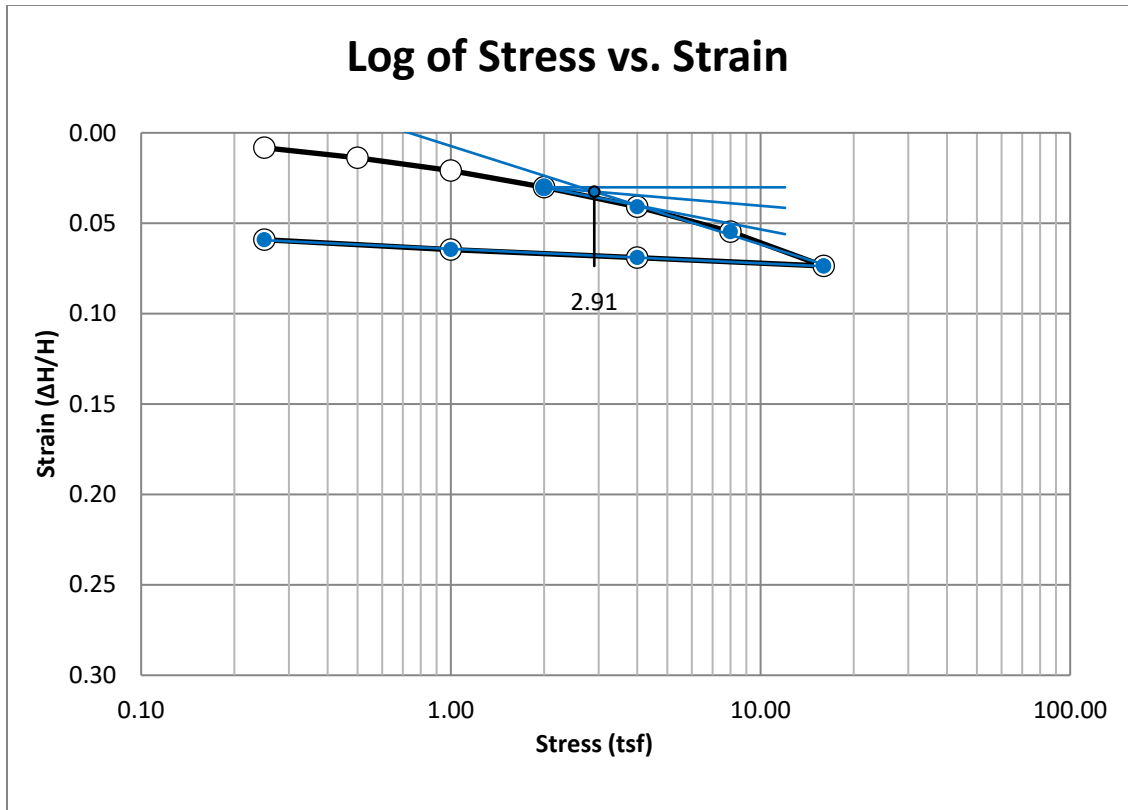


Figure A131 Springville at 40-42 feet



**Figure A132 Springville at 65-67 feet**

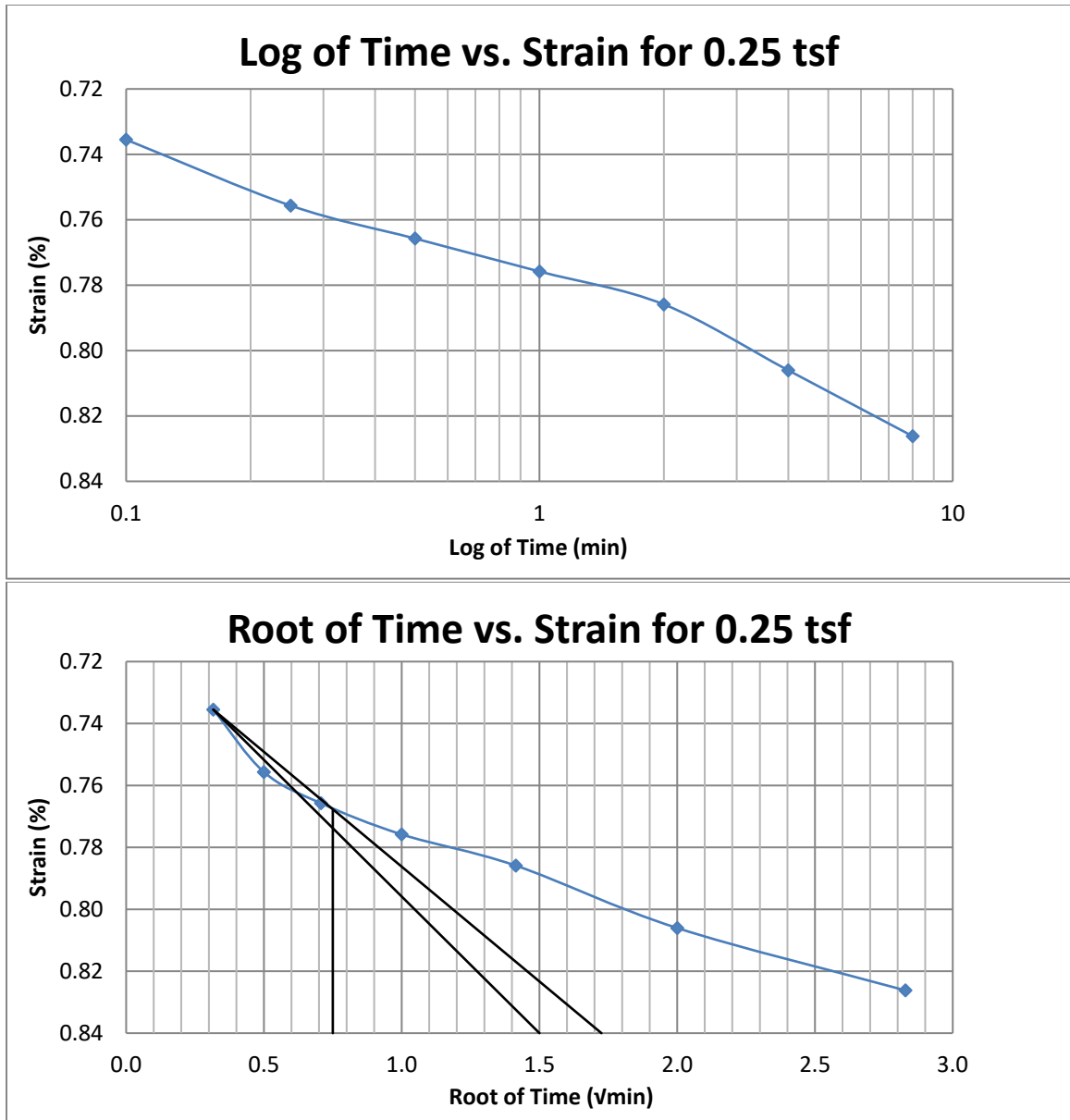


Figure A133 Springville at 65-67 feet

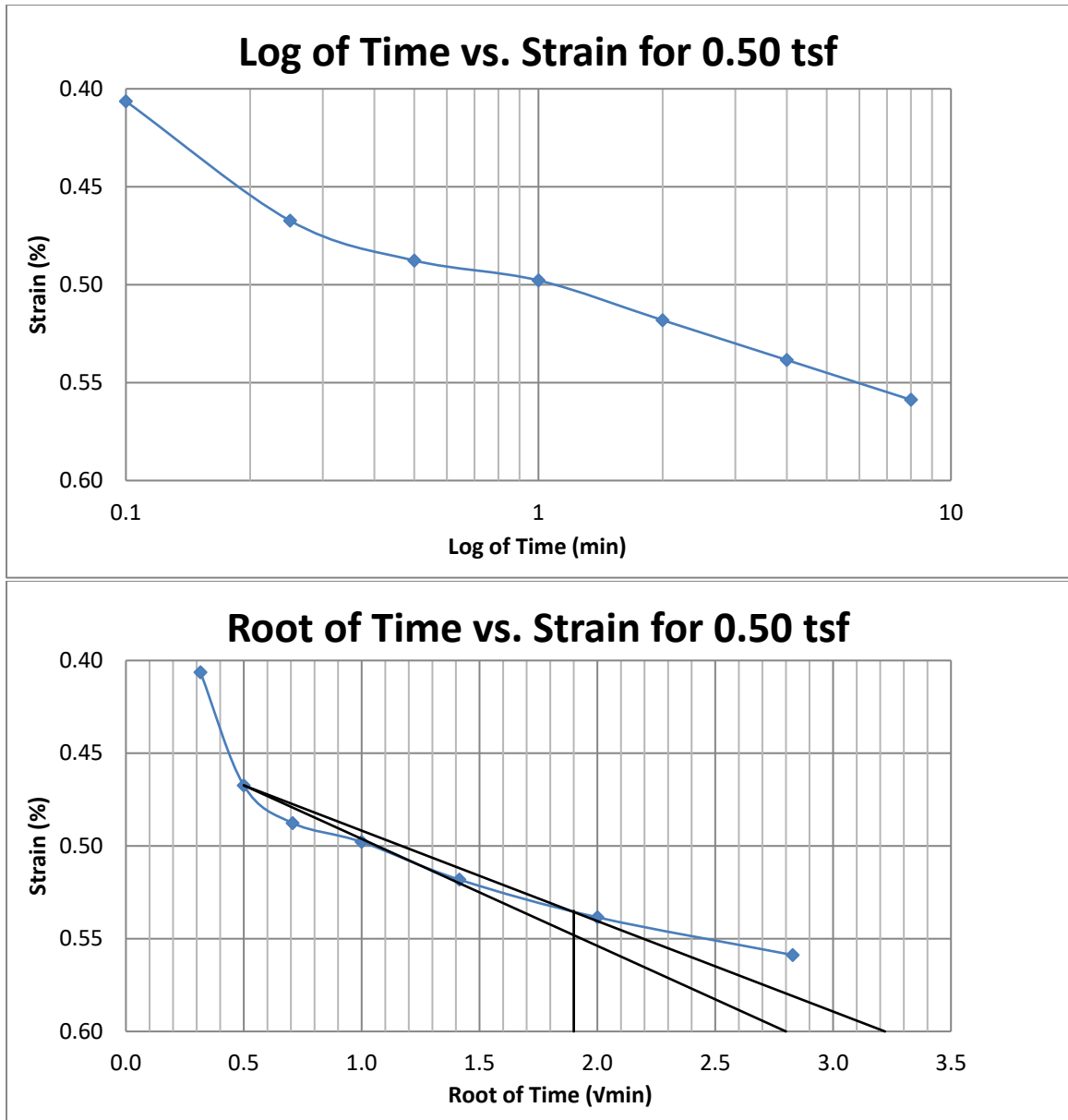


Figure A134 Springville at 65-67 feet

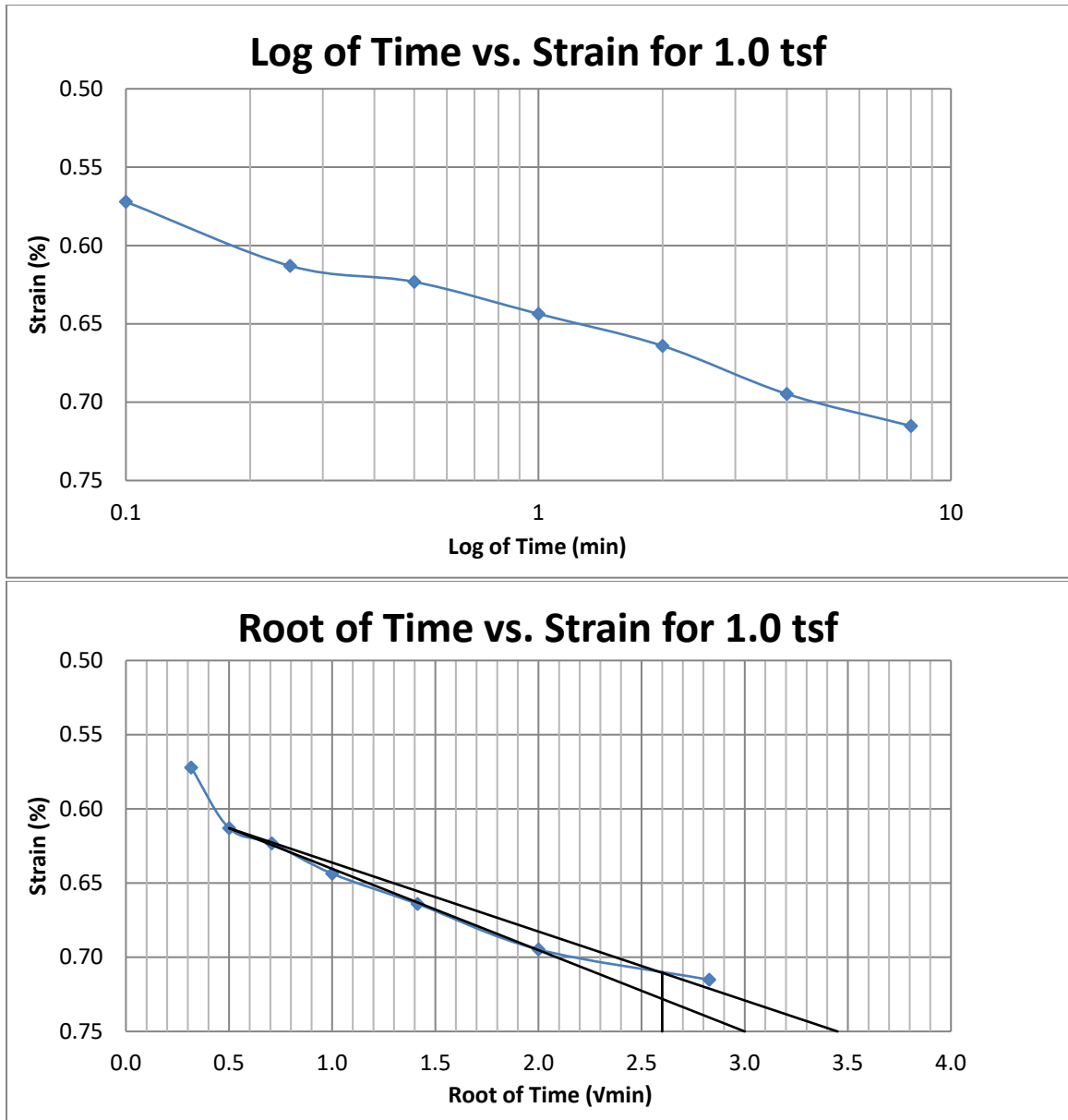


Figure A135 Springville at 65-67 feet

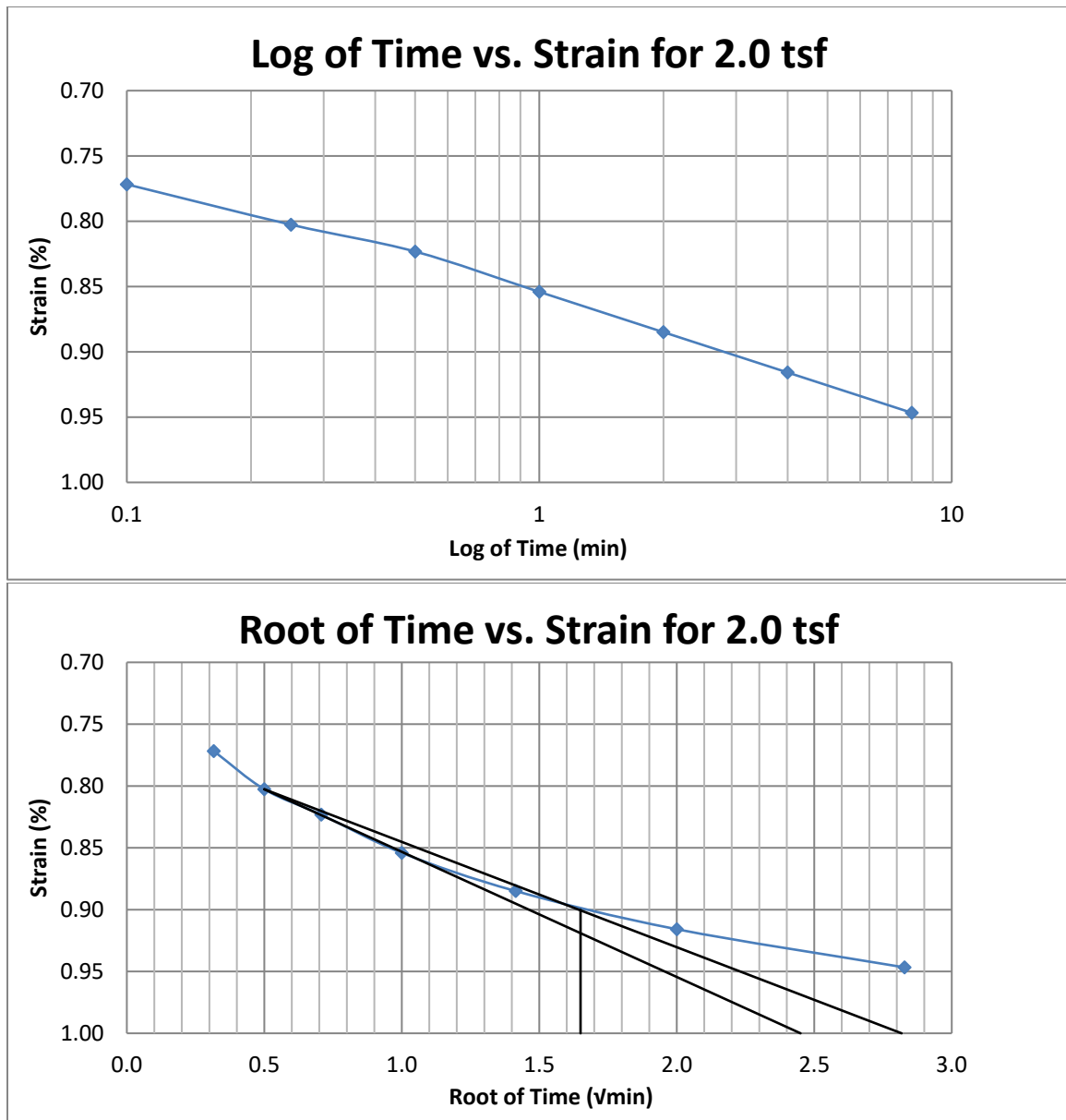


Figure A136 Springville at 65-67 feet

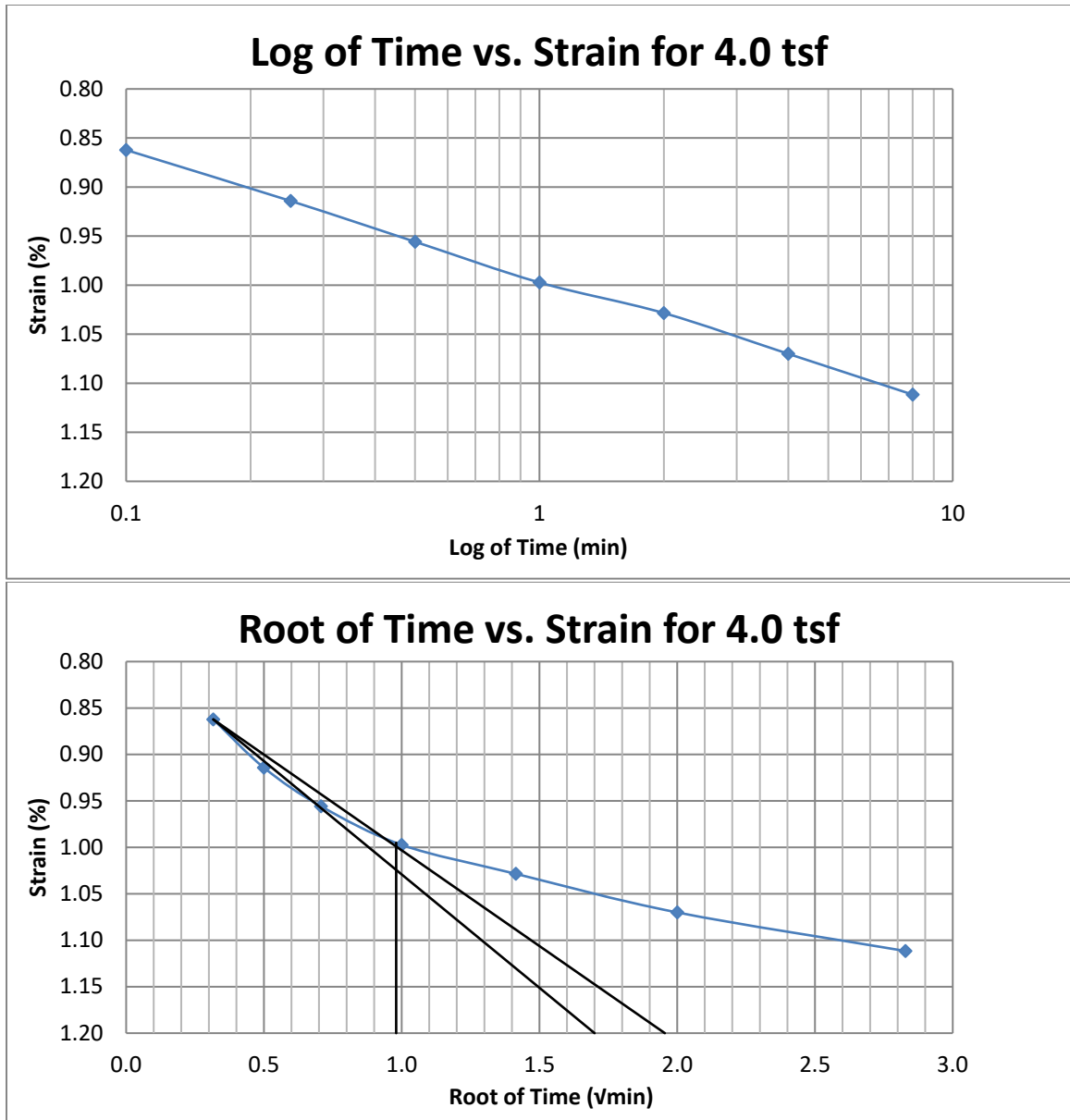


Figure A137 Springville at 65-67 feet

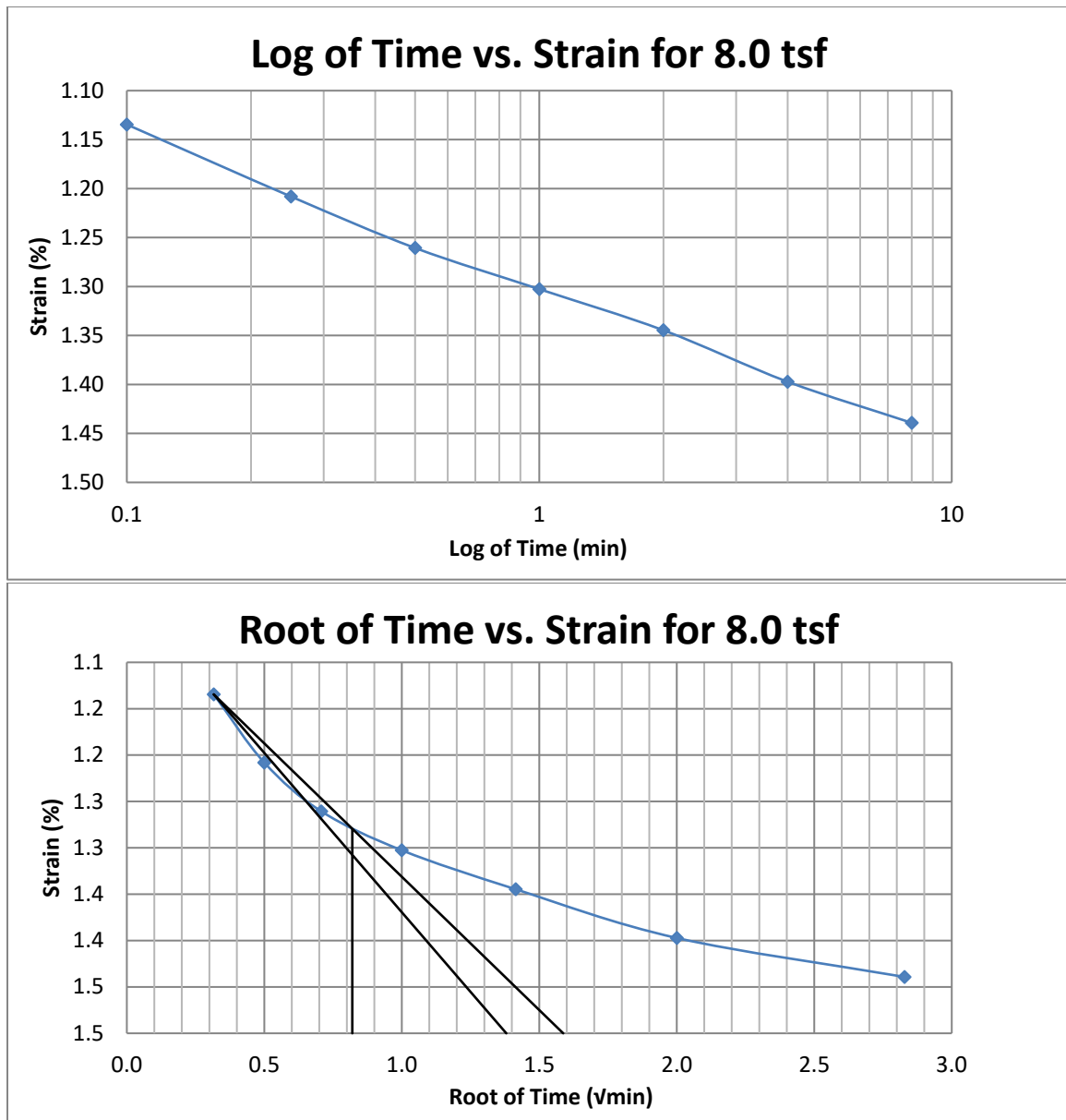


Figure A138 Springville at 65-67 feet



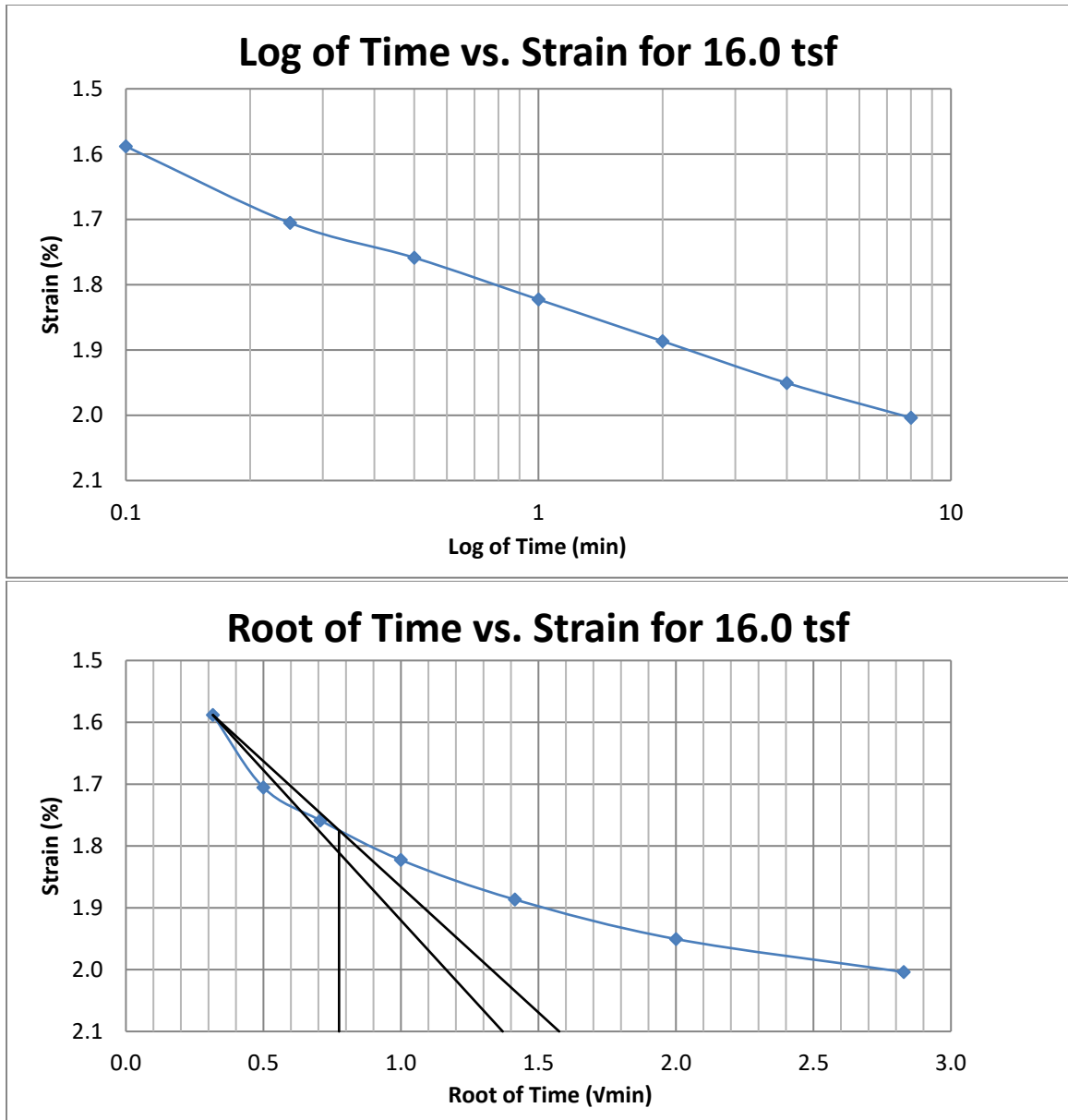


Figure A139 Springville at 65-67 feet

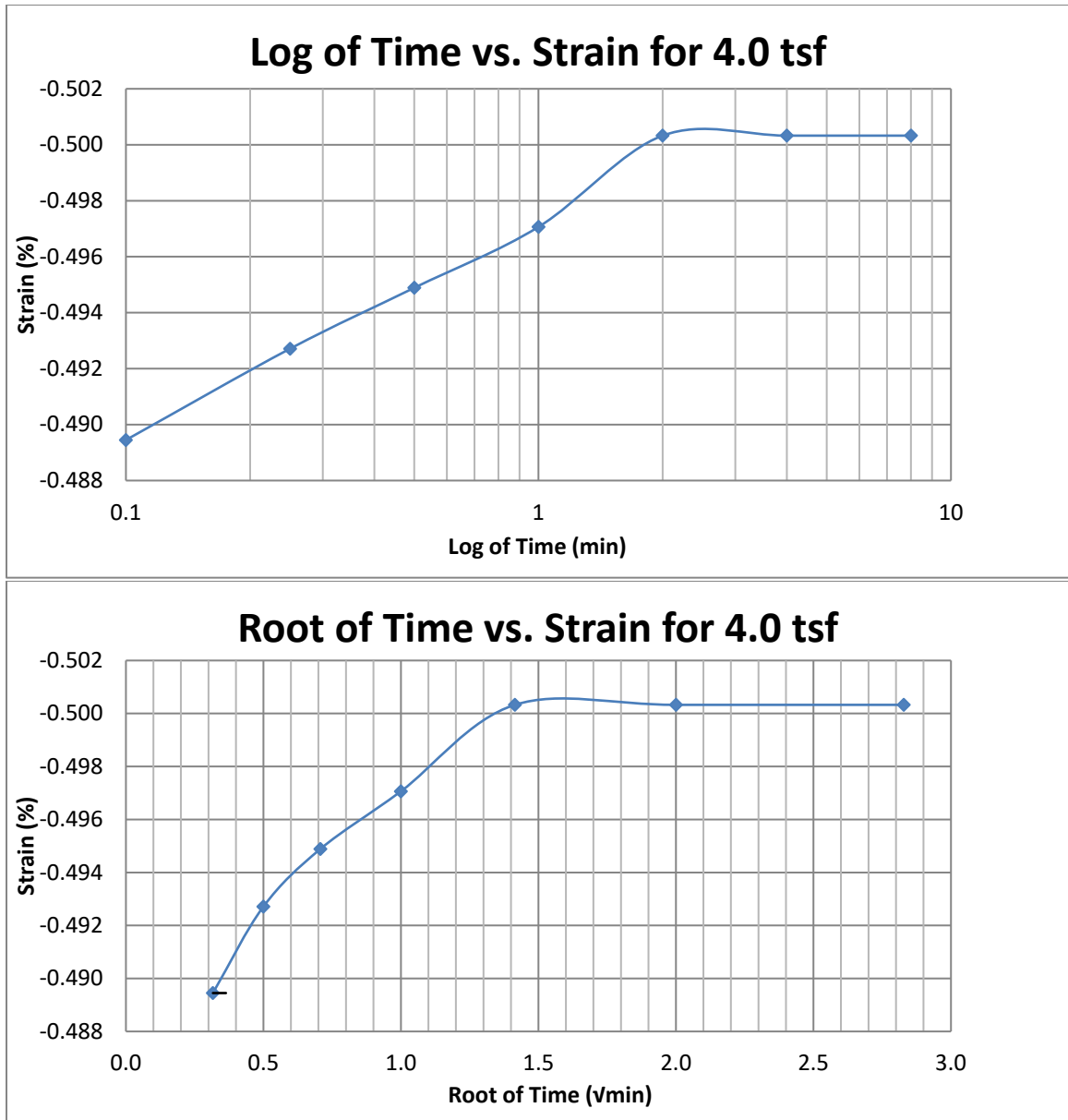


Figure A140 Springville at 65-67 feet

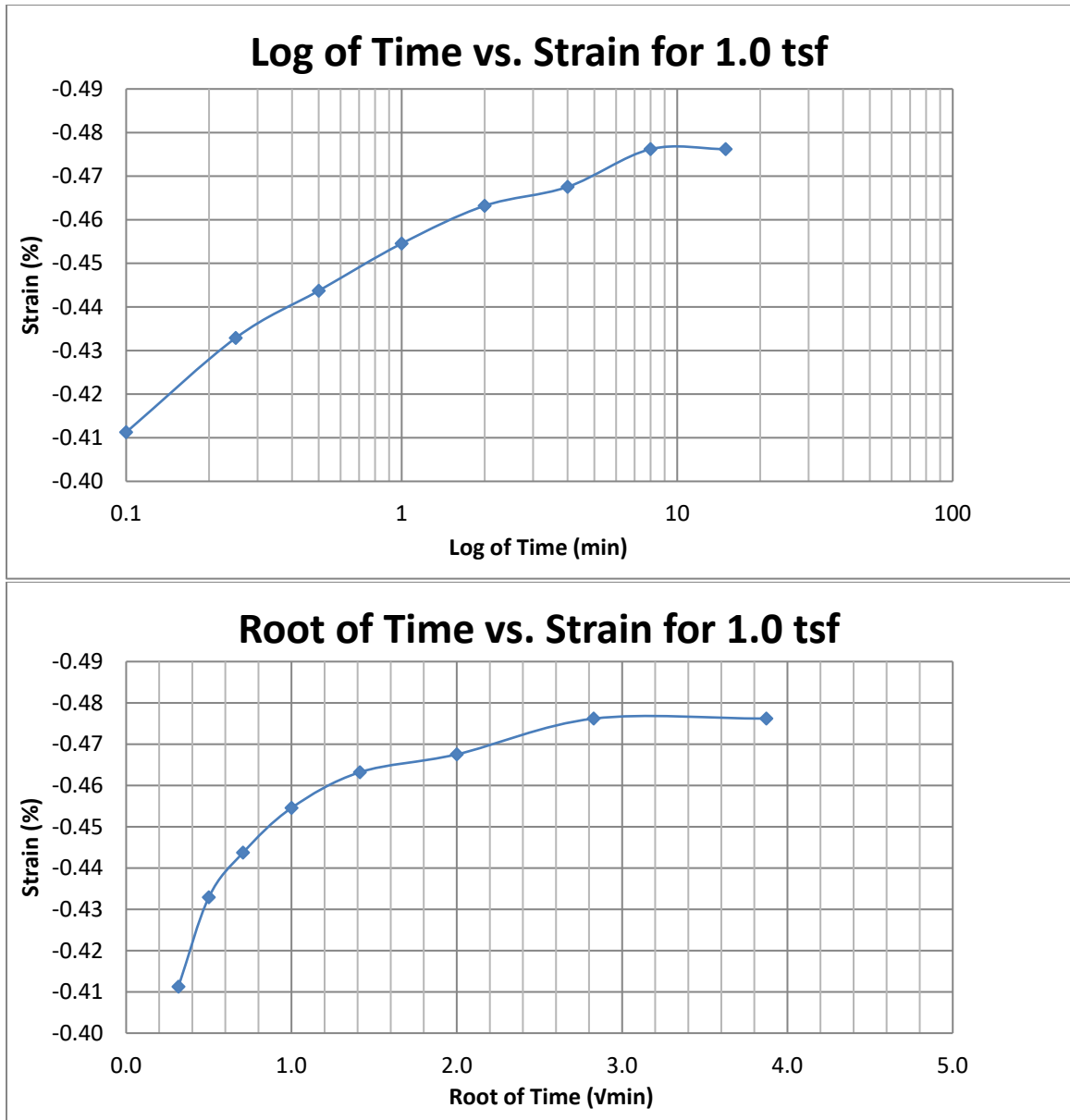


Figure A141 Springville at 65-67 feet

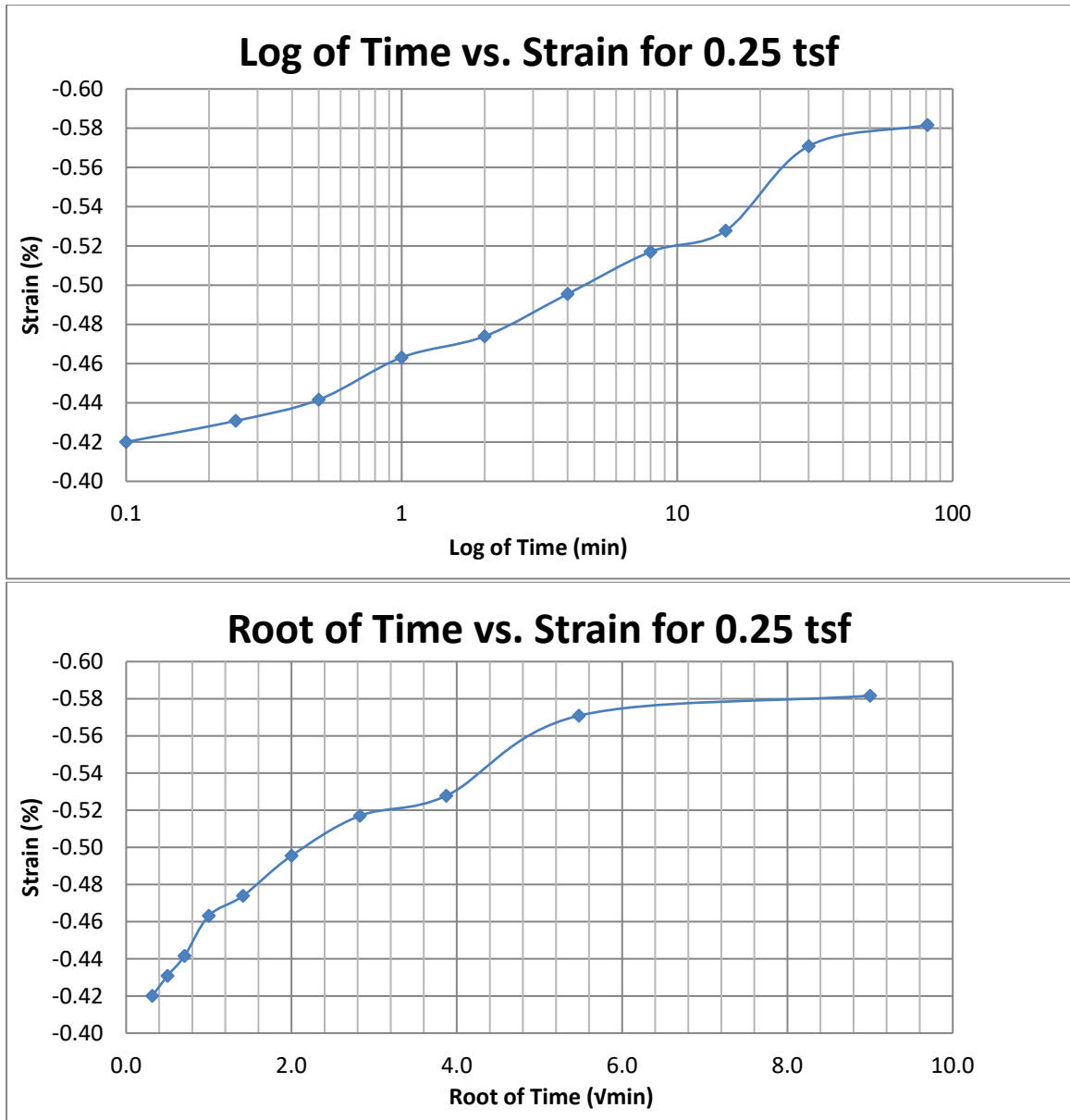


Figure A142 Springville at 65-67 feet

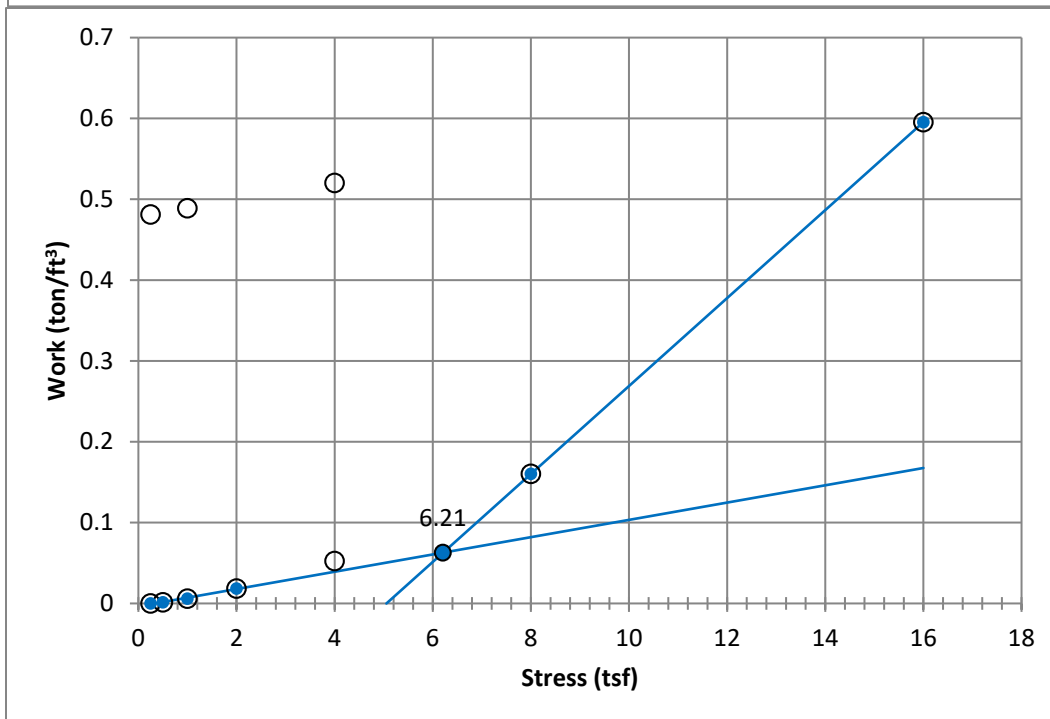
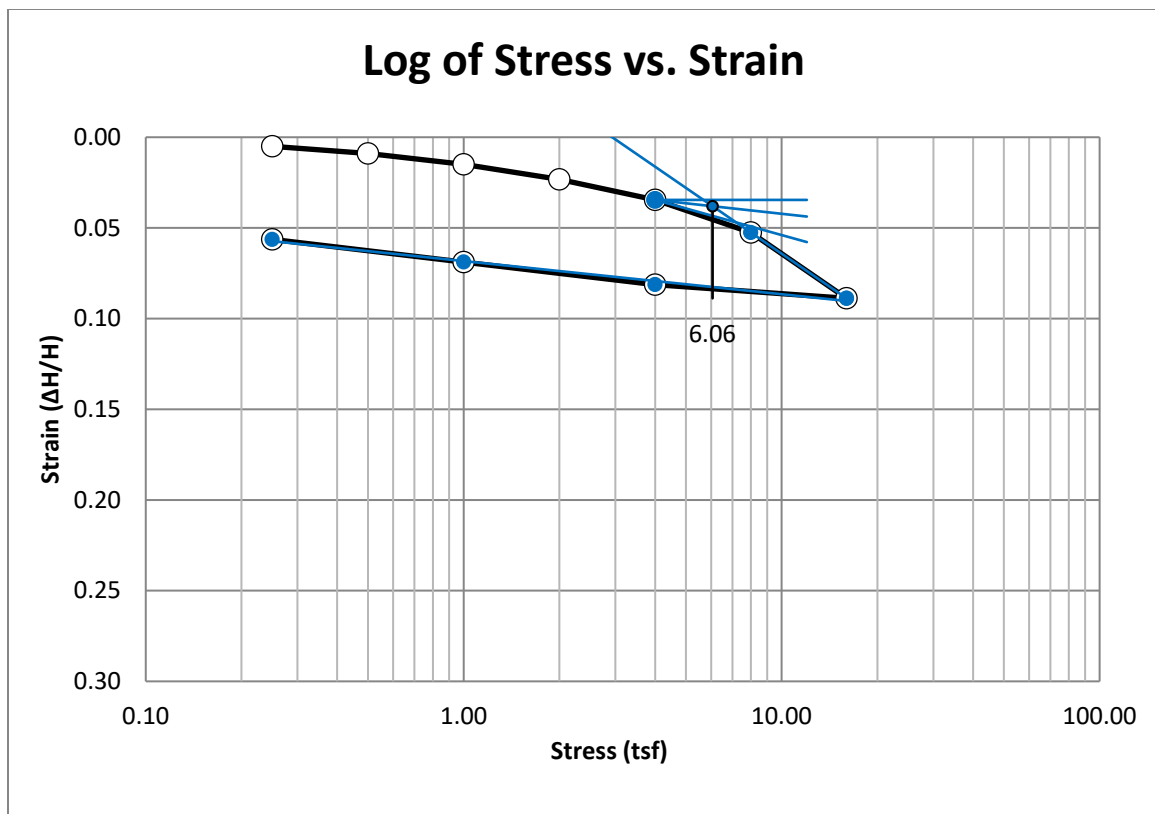


Figure A143 Springville at 70-72 feet

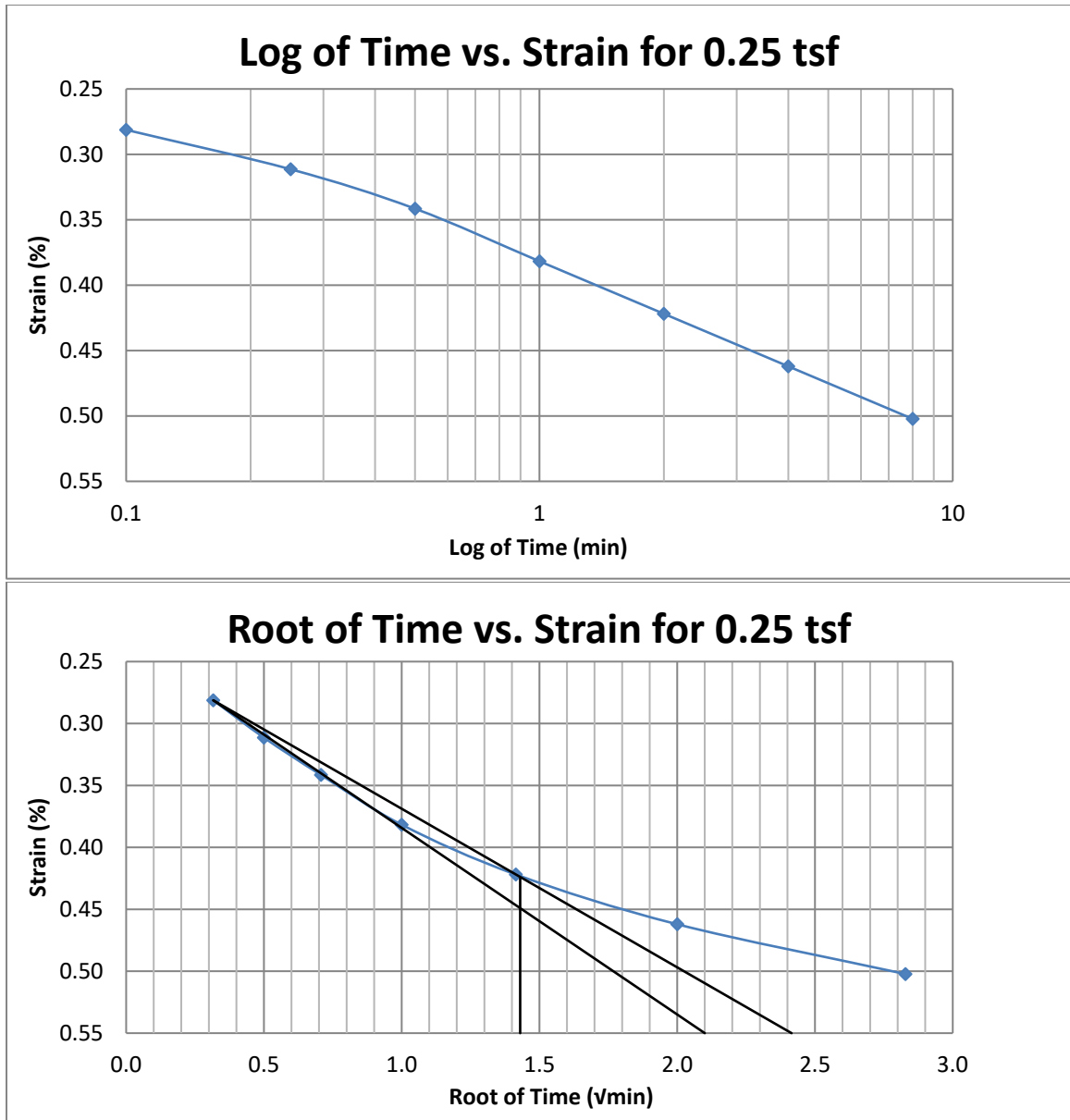


Figure A144 Springville at 70-72 feet

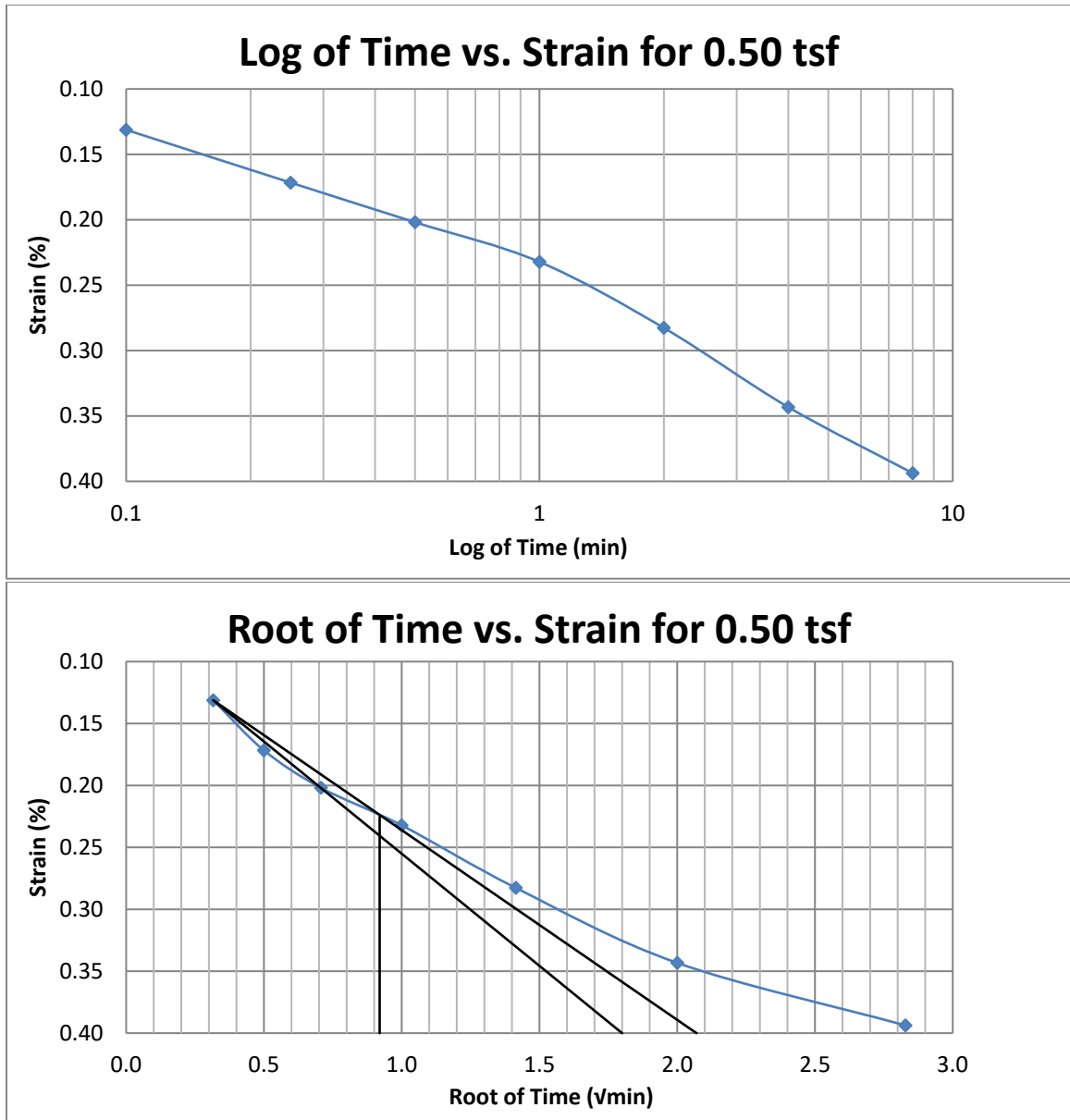


Figure A145 Springville at 70-72 feet

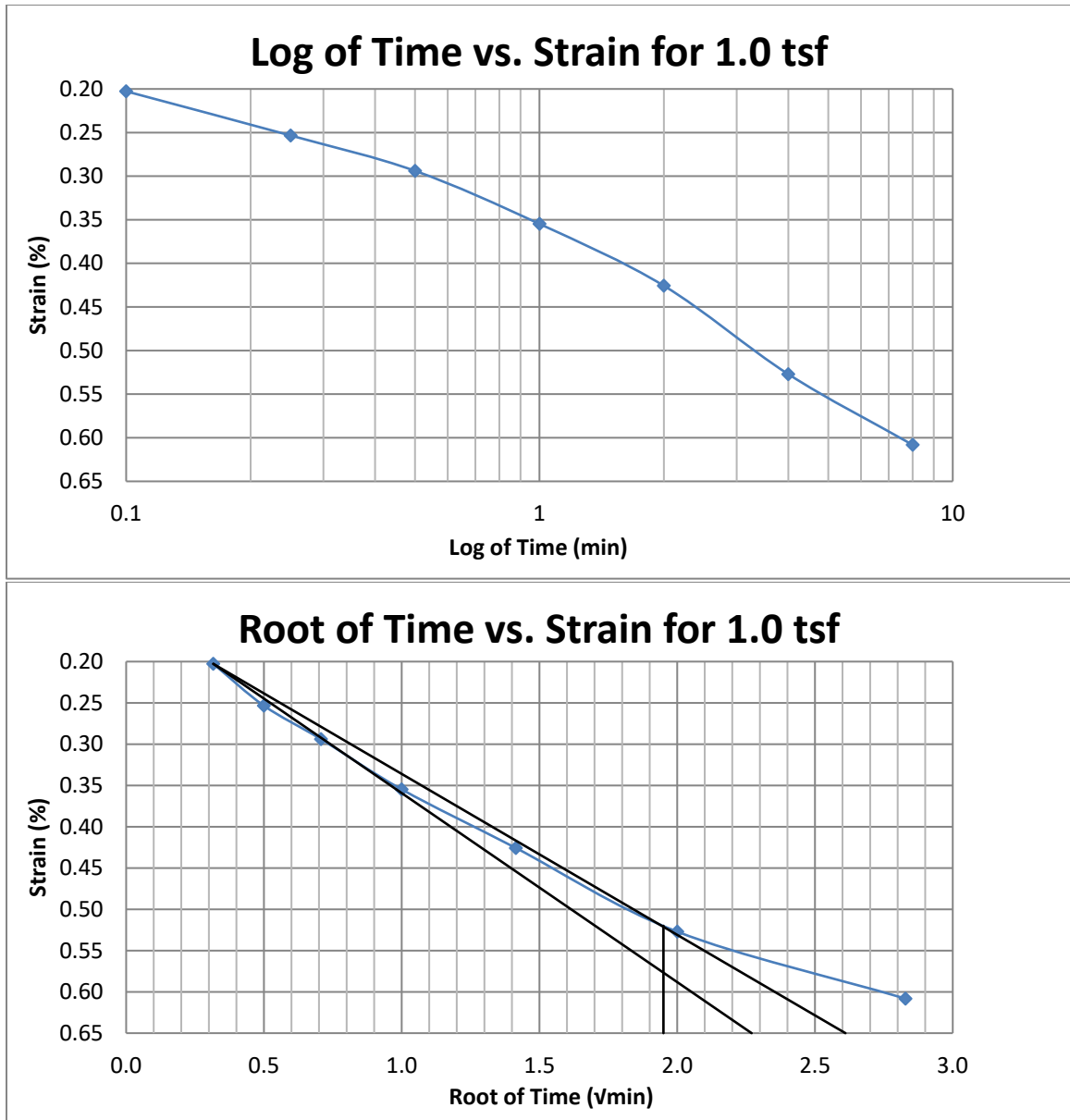


Figure A146 Springville at 70-72 feet



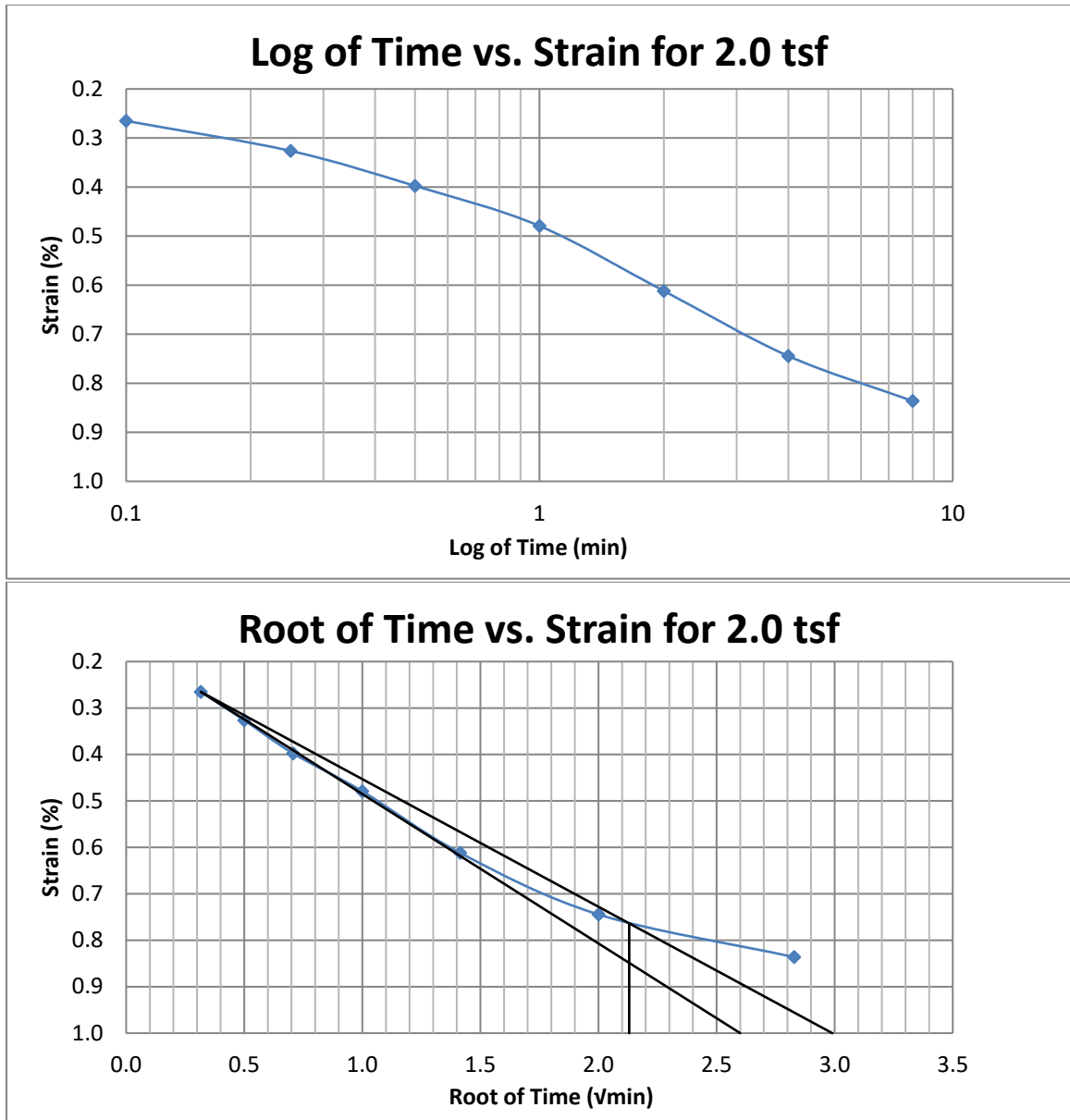


Figure A147 Springville at 70-72 feet

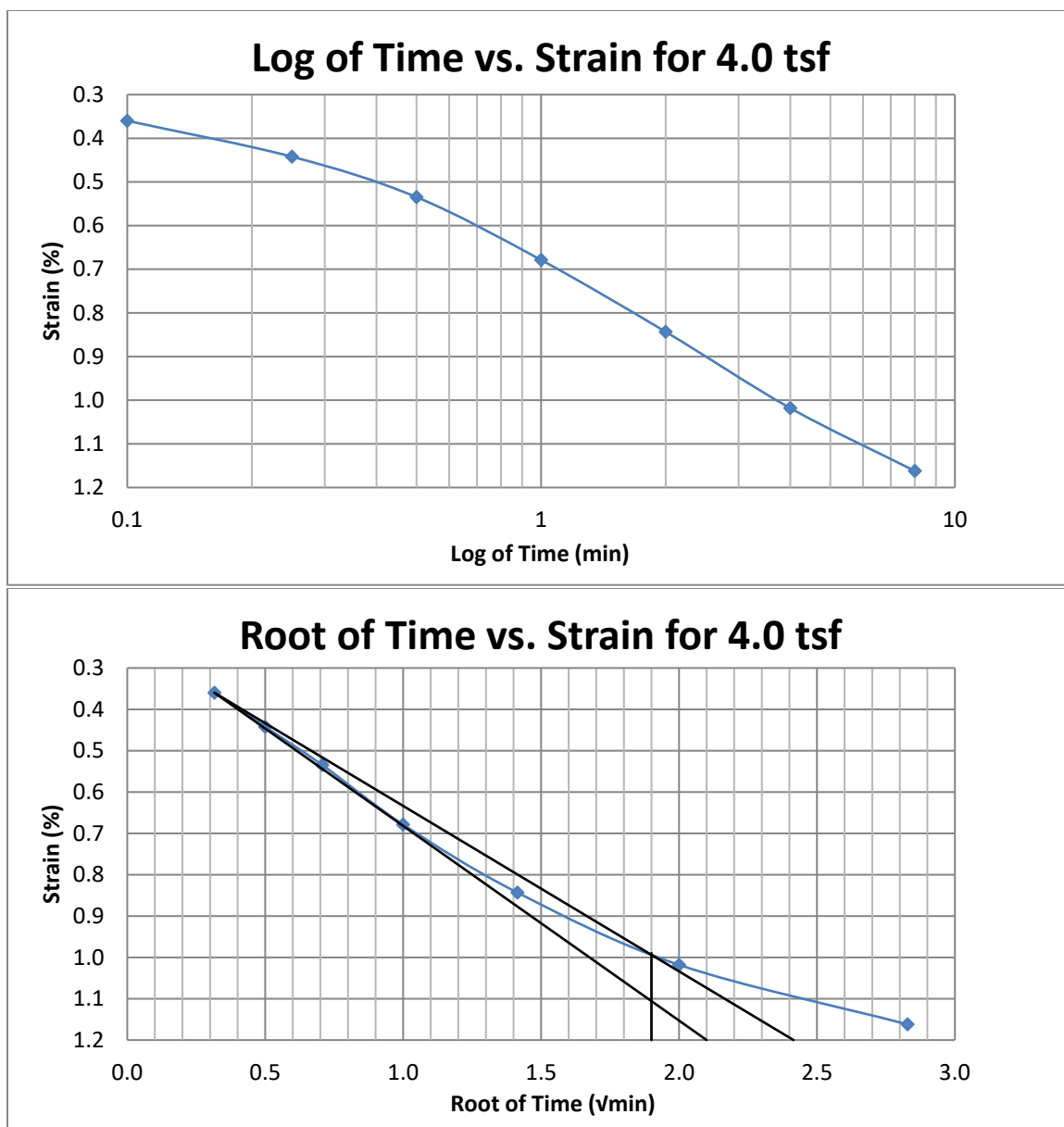


Figure A148 Springville at 70-72 feet

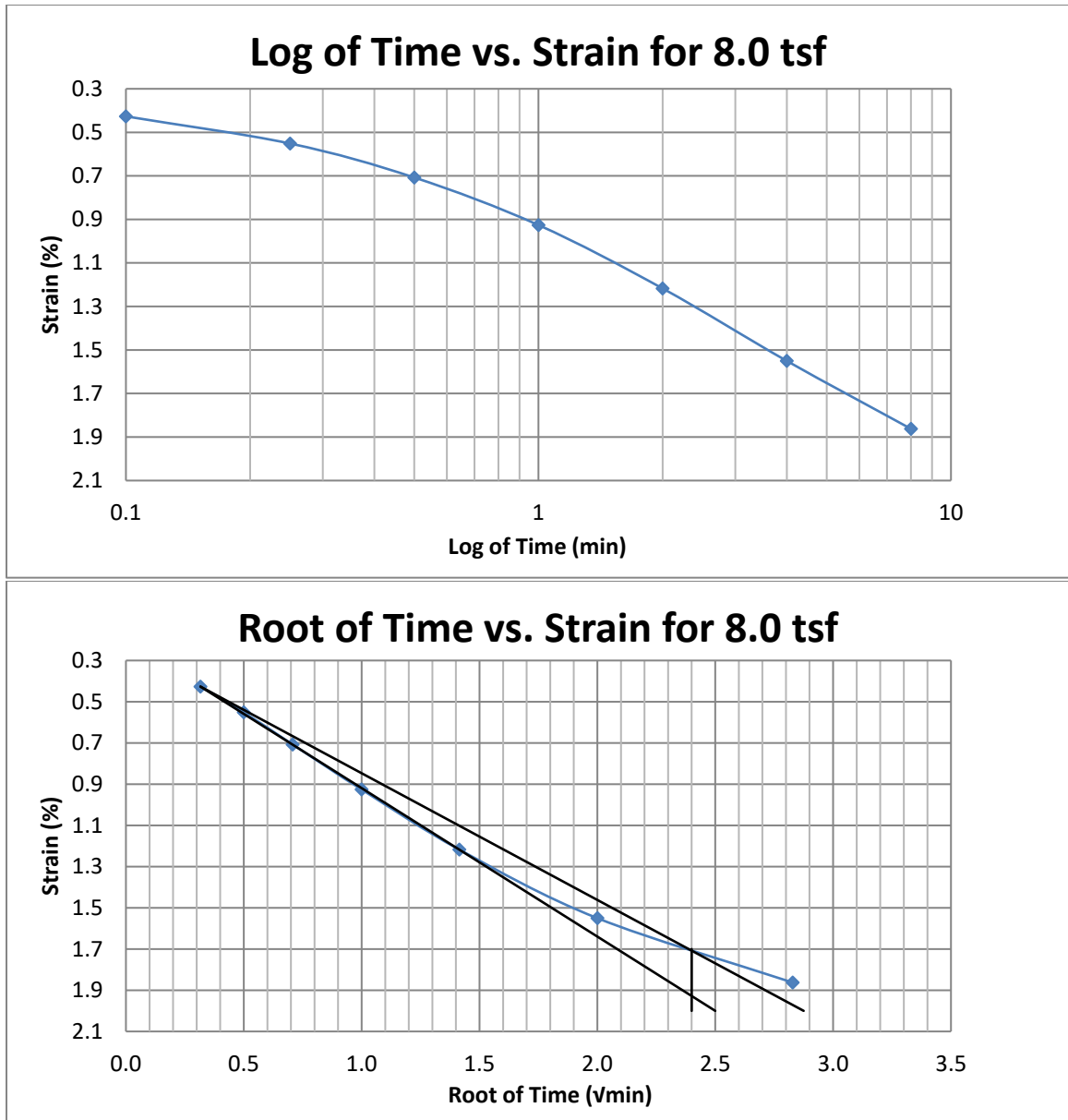


Figure A149 Springville at 70-72 feet

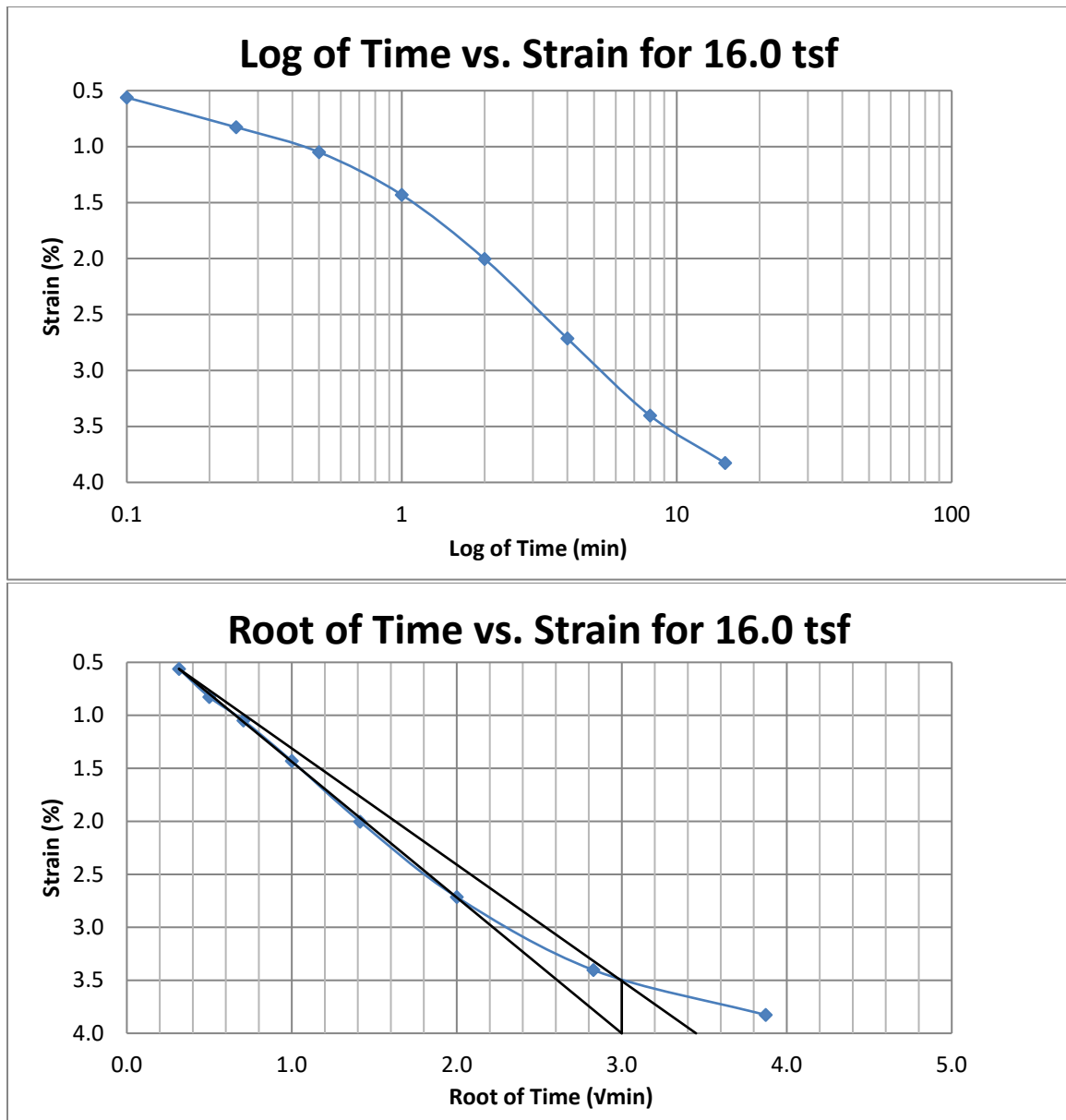


Figure A150 Springville at 70-72 feet

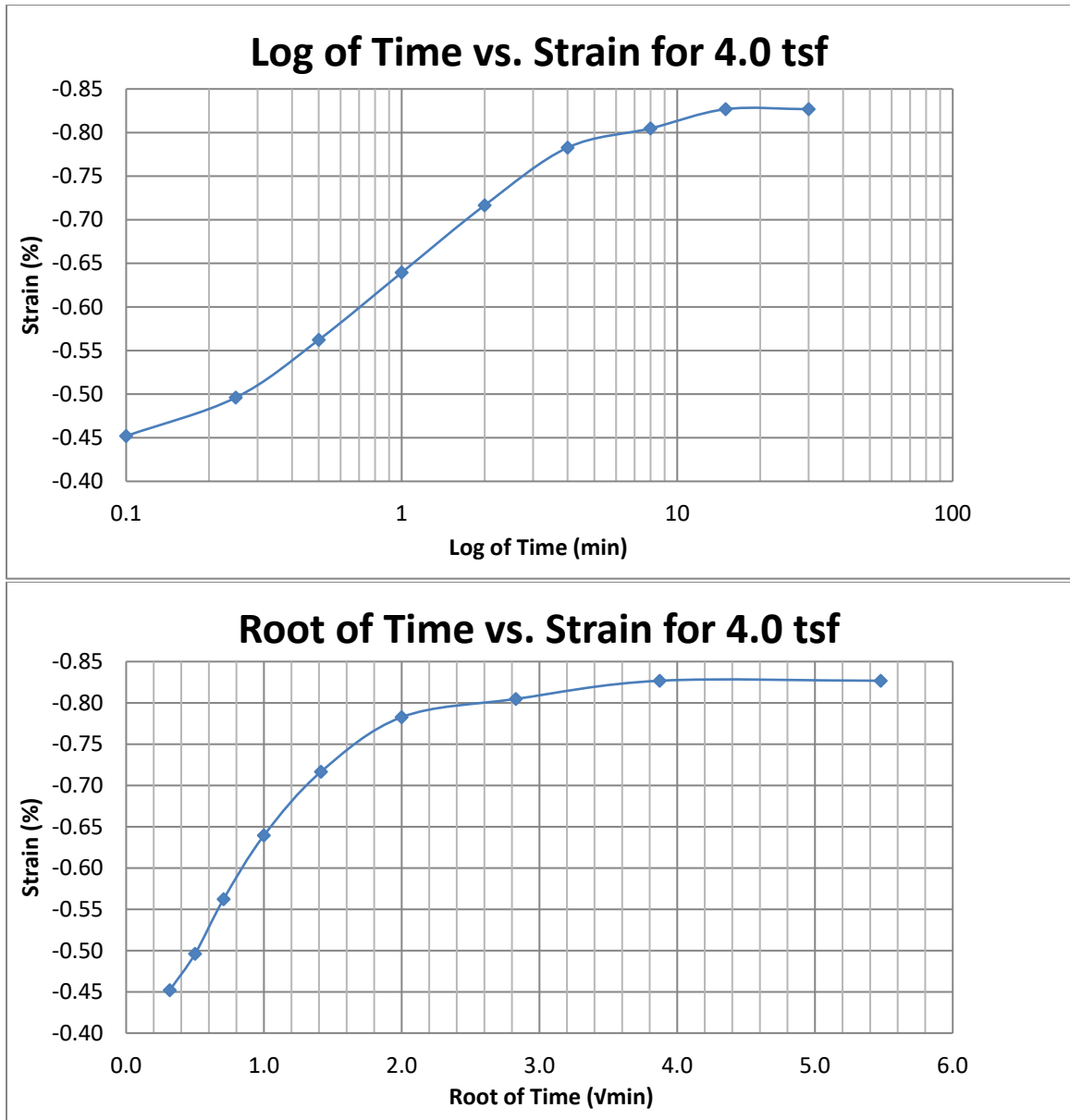


Figure A151 Springville at 70-72 feet

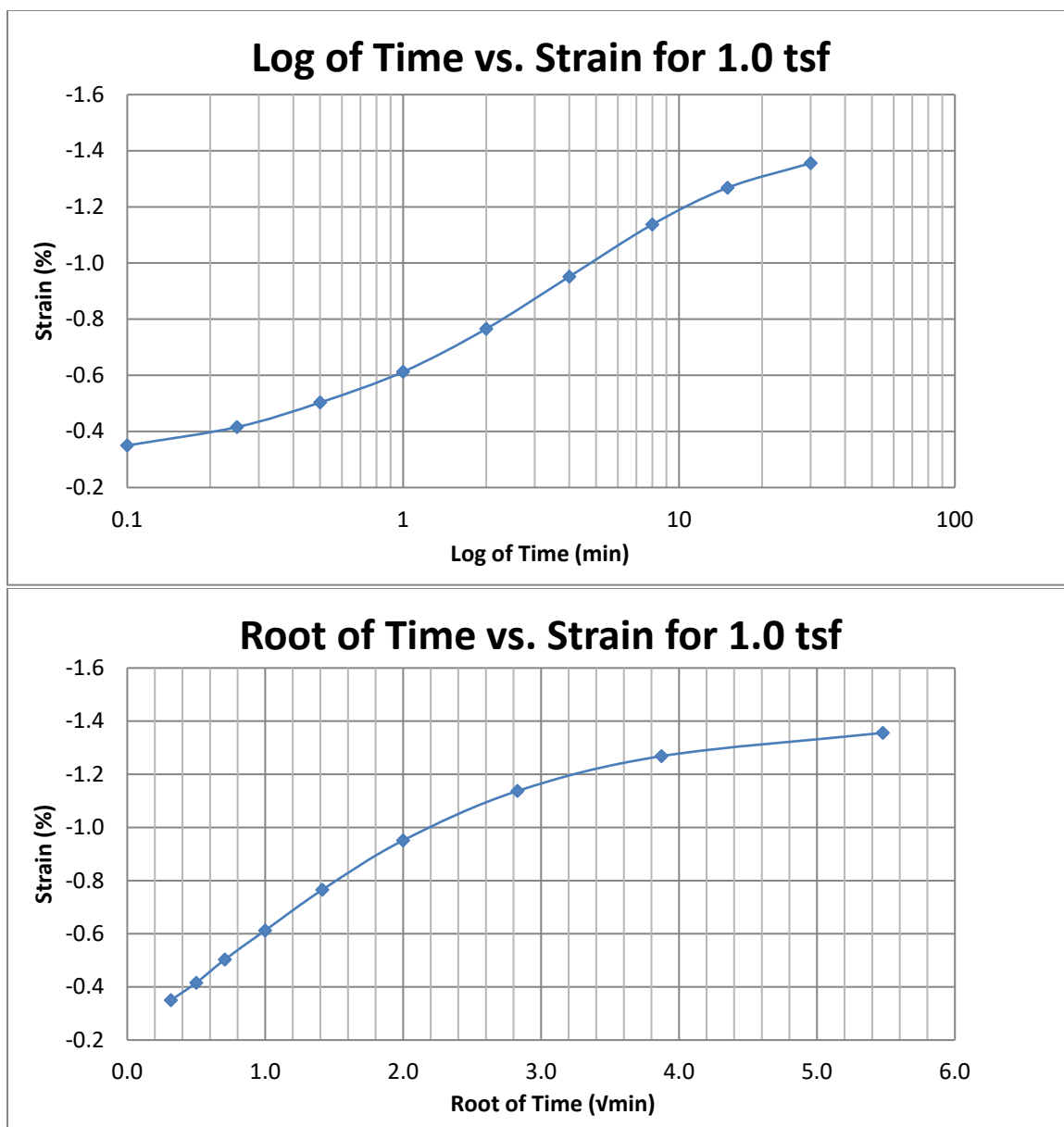


Figure A152 Springville at 70-72 feet

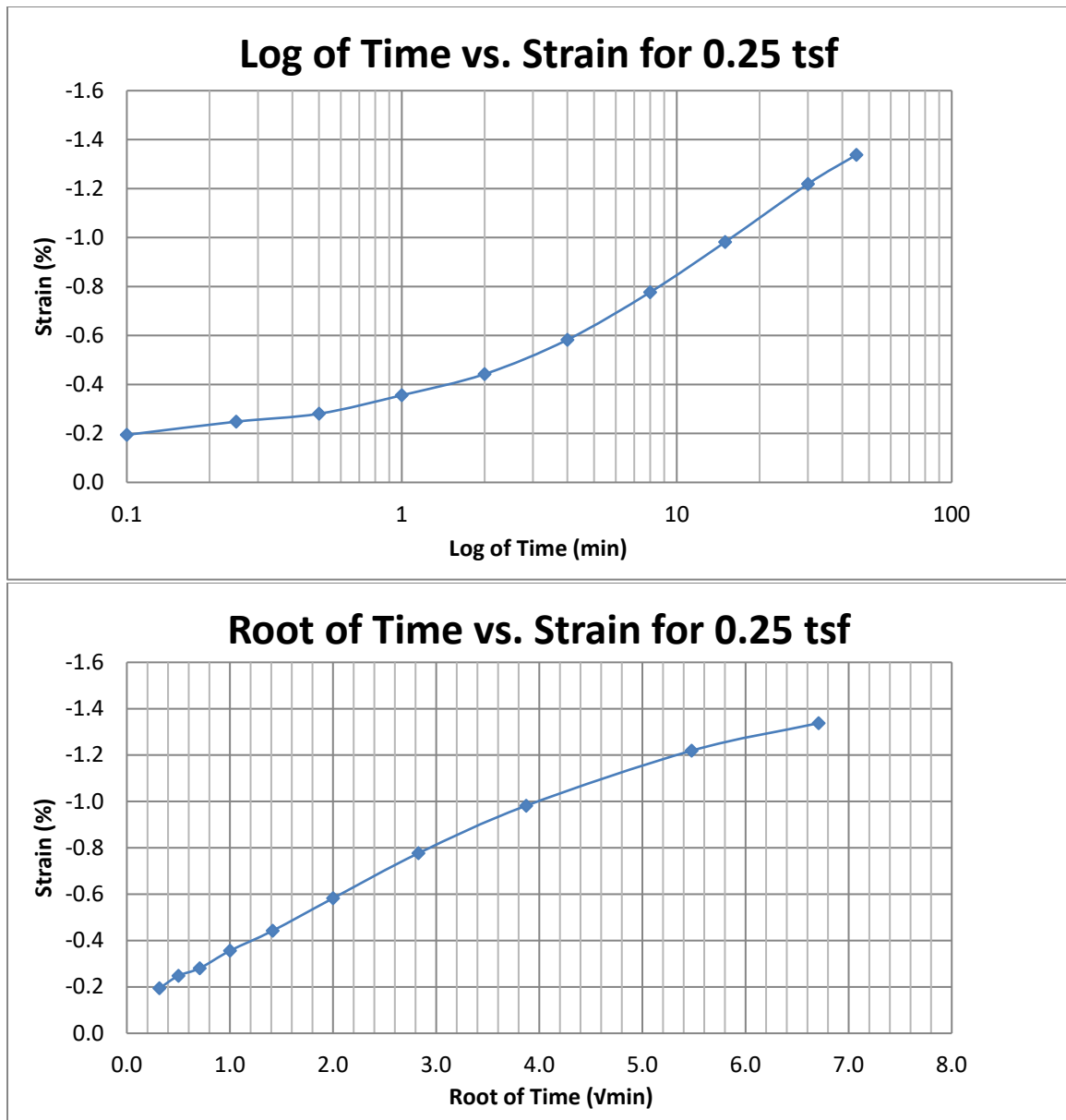


Figure A153 Springville at 70-72 feet

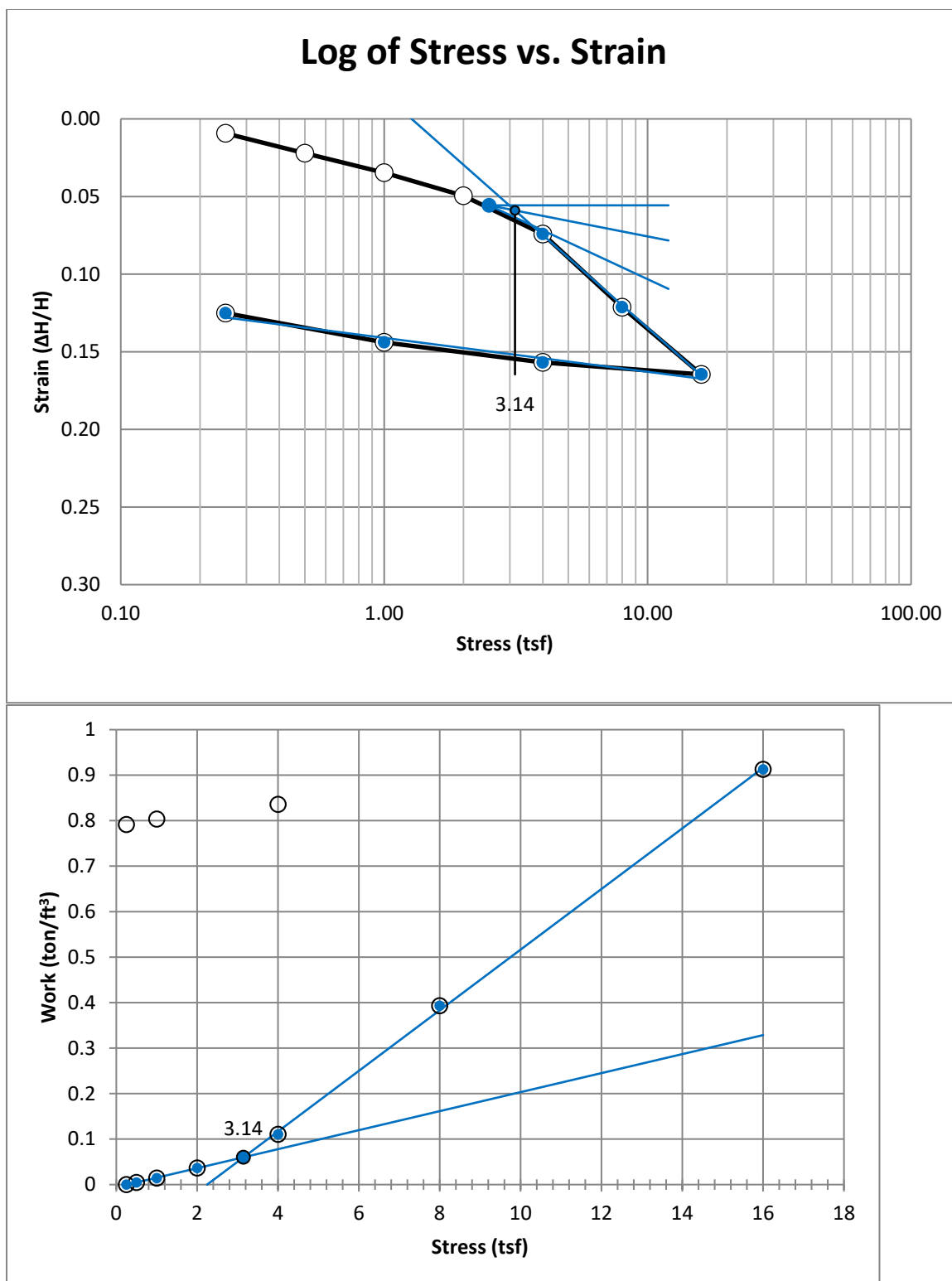


Figure A154 Springville at 75-77 feet



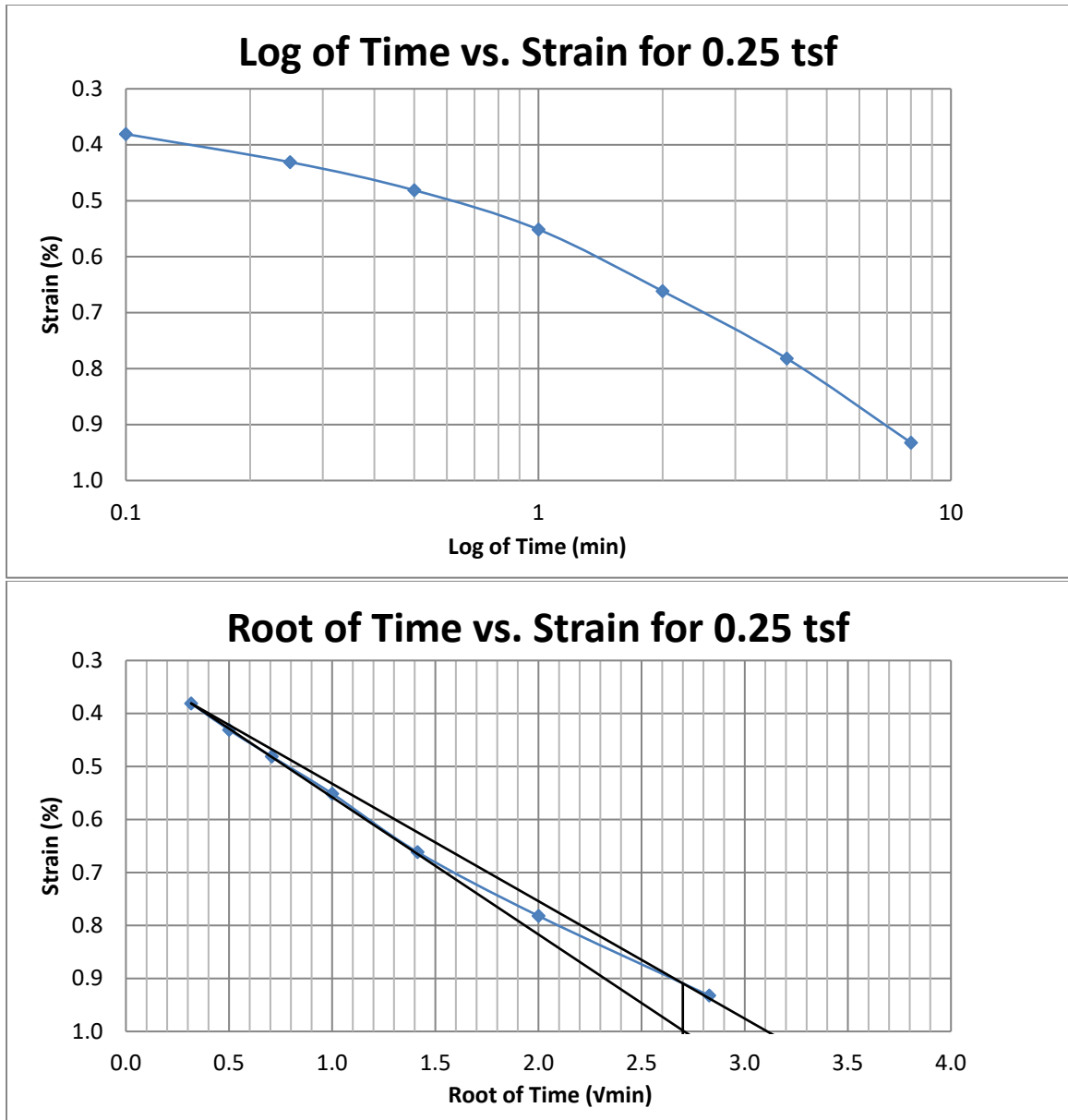


Figure A155 Springville at 75-77 feet

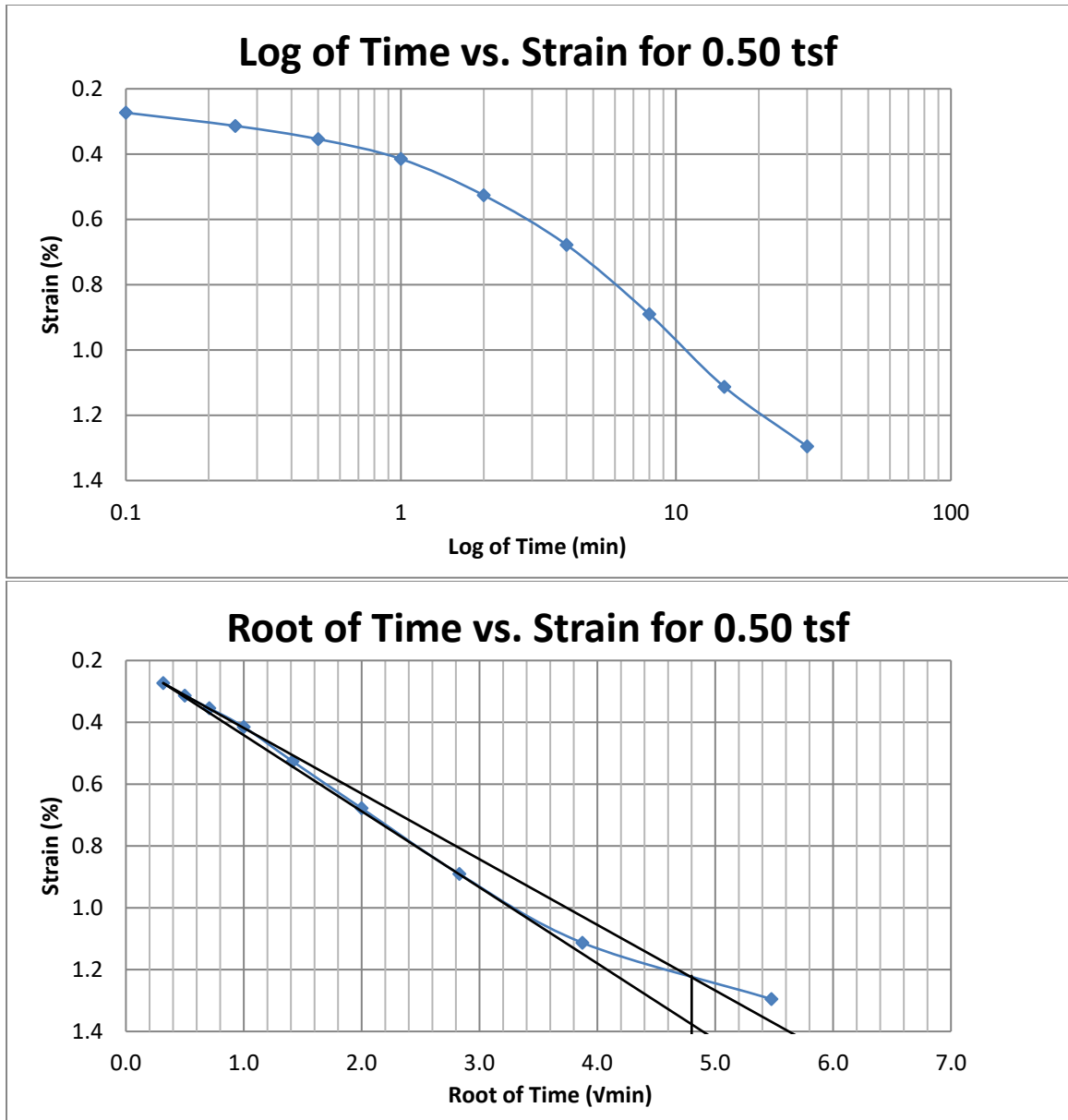


Figure A156 Springville at 75-77 feet

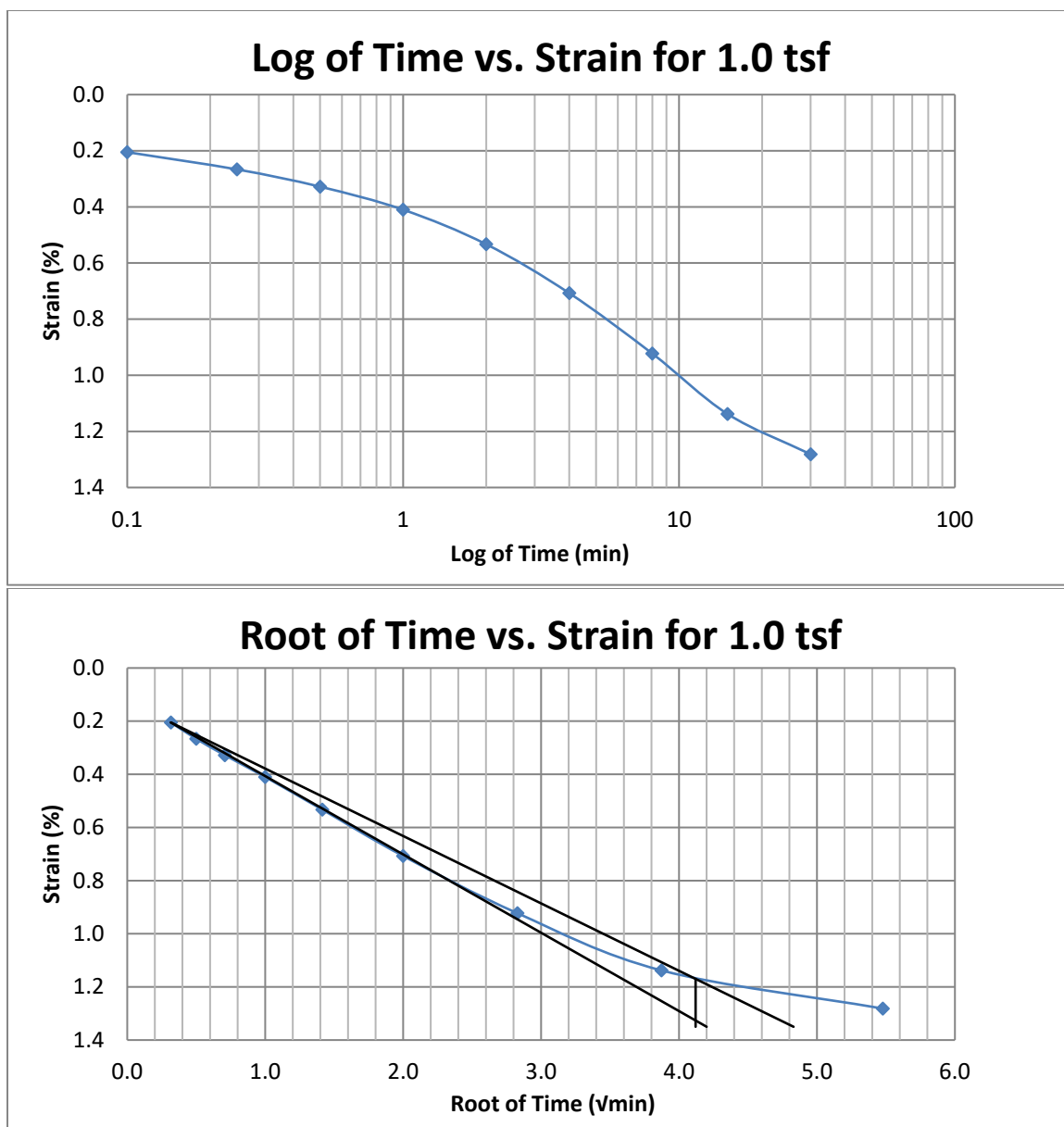


Figure A157 Springville at 75-77 feet

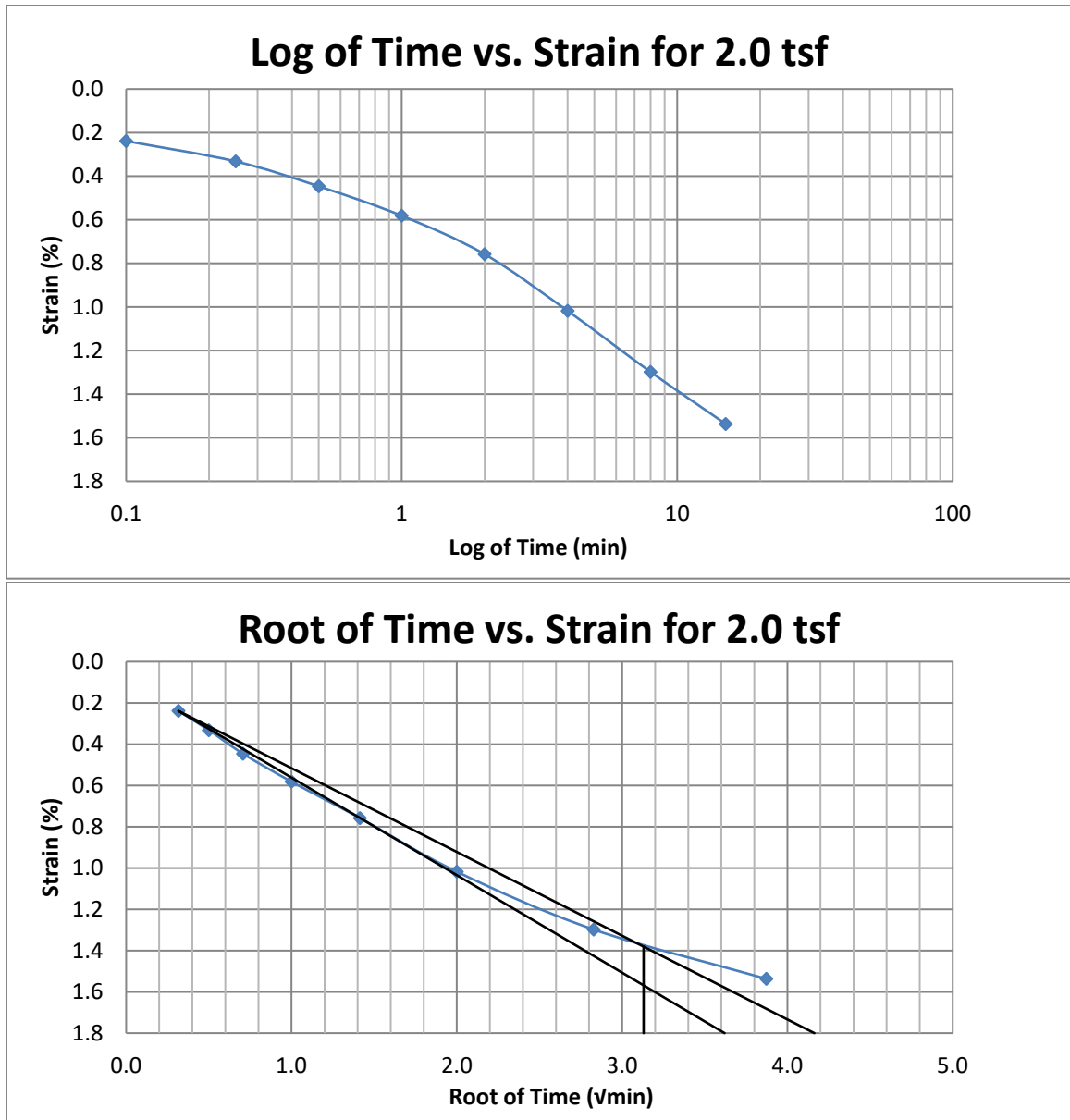


Figure A158 Springville at 75-77 feet

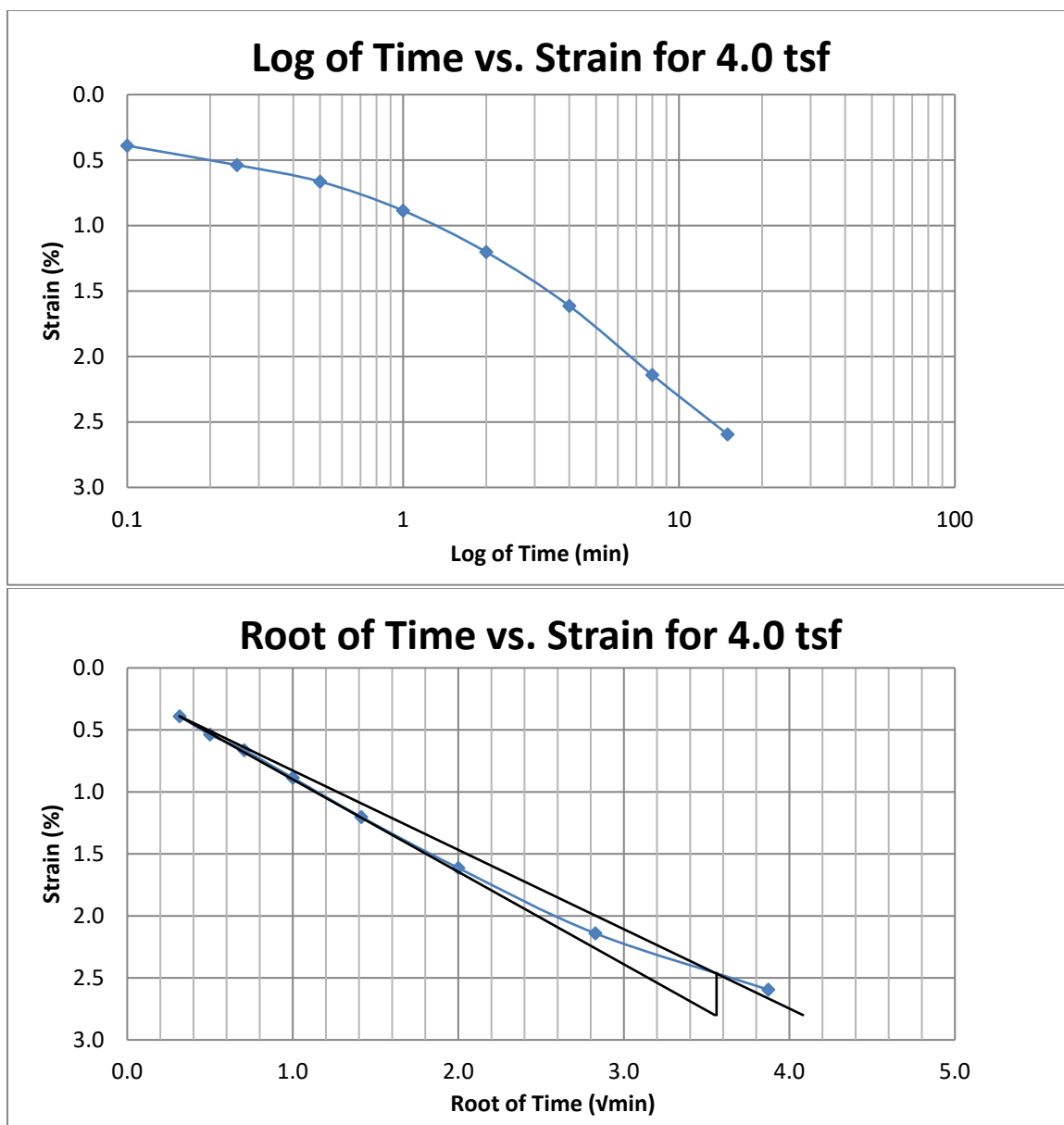


Figure A159 Springville at 75-77 feet

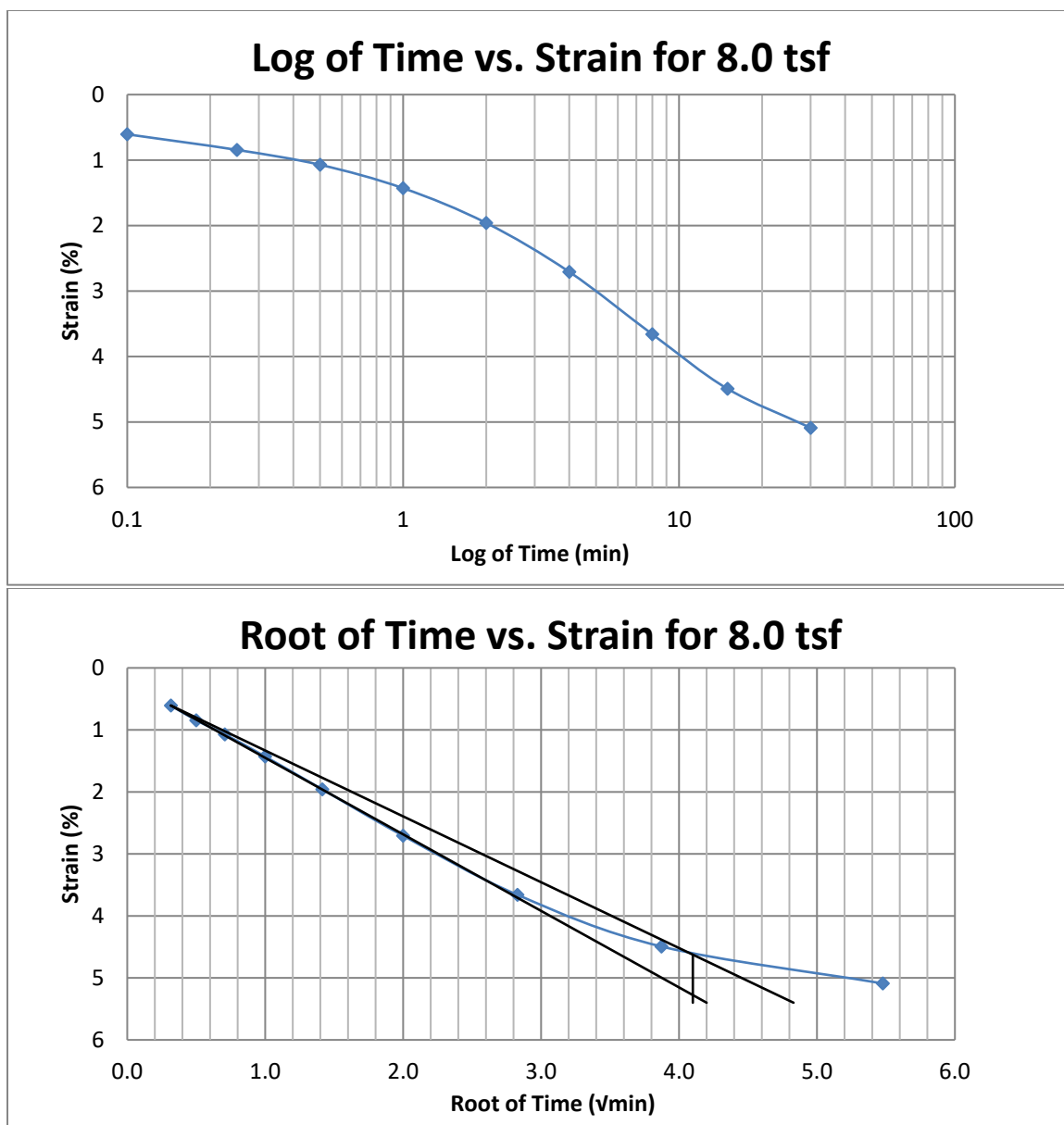


Figure A160 Springville at 75-77 feet

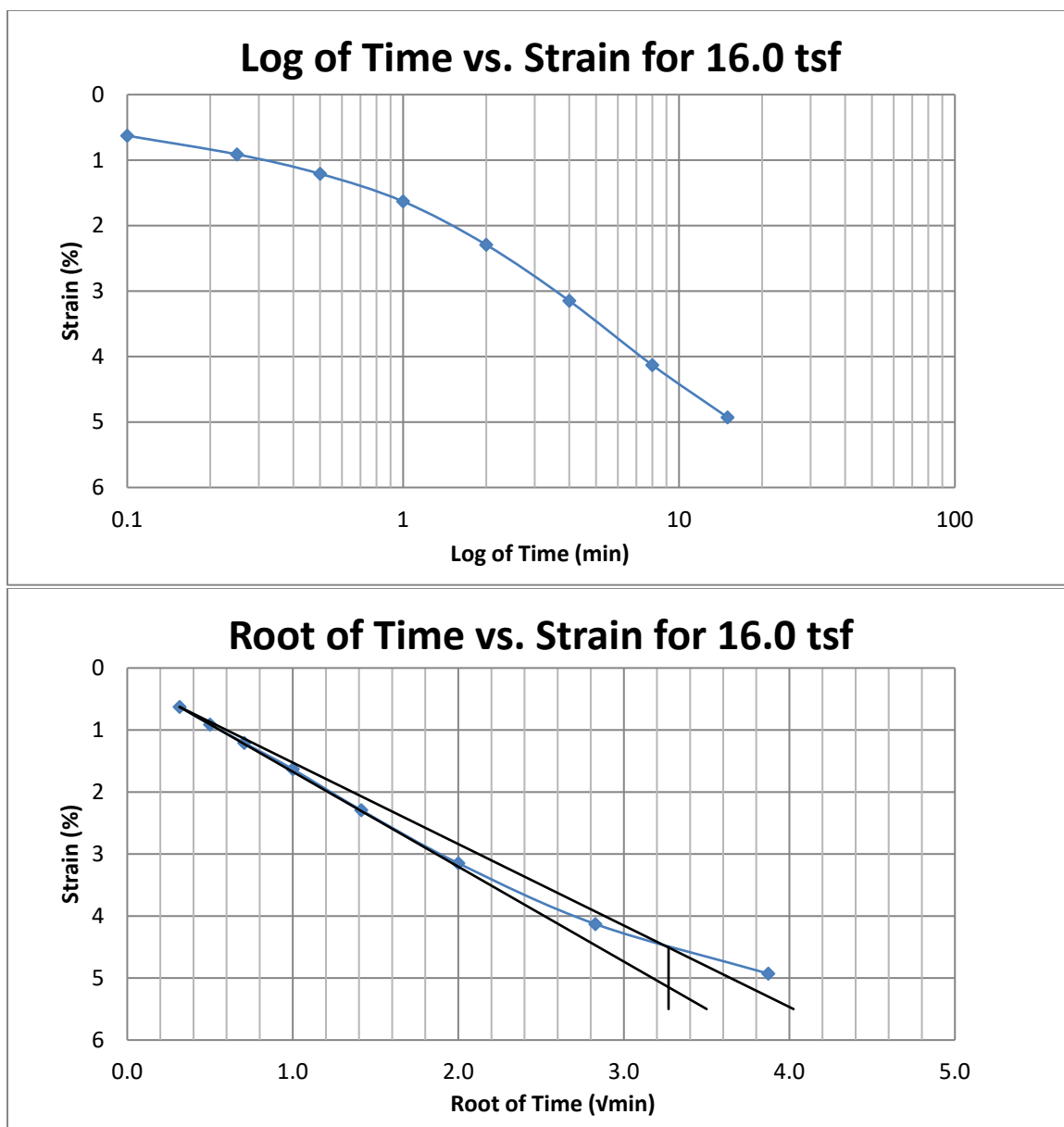


Figure A161 Springville at 75-77 feet

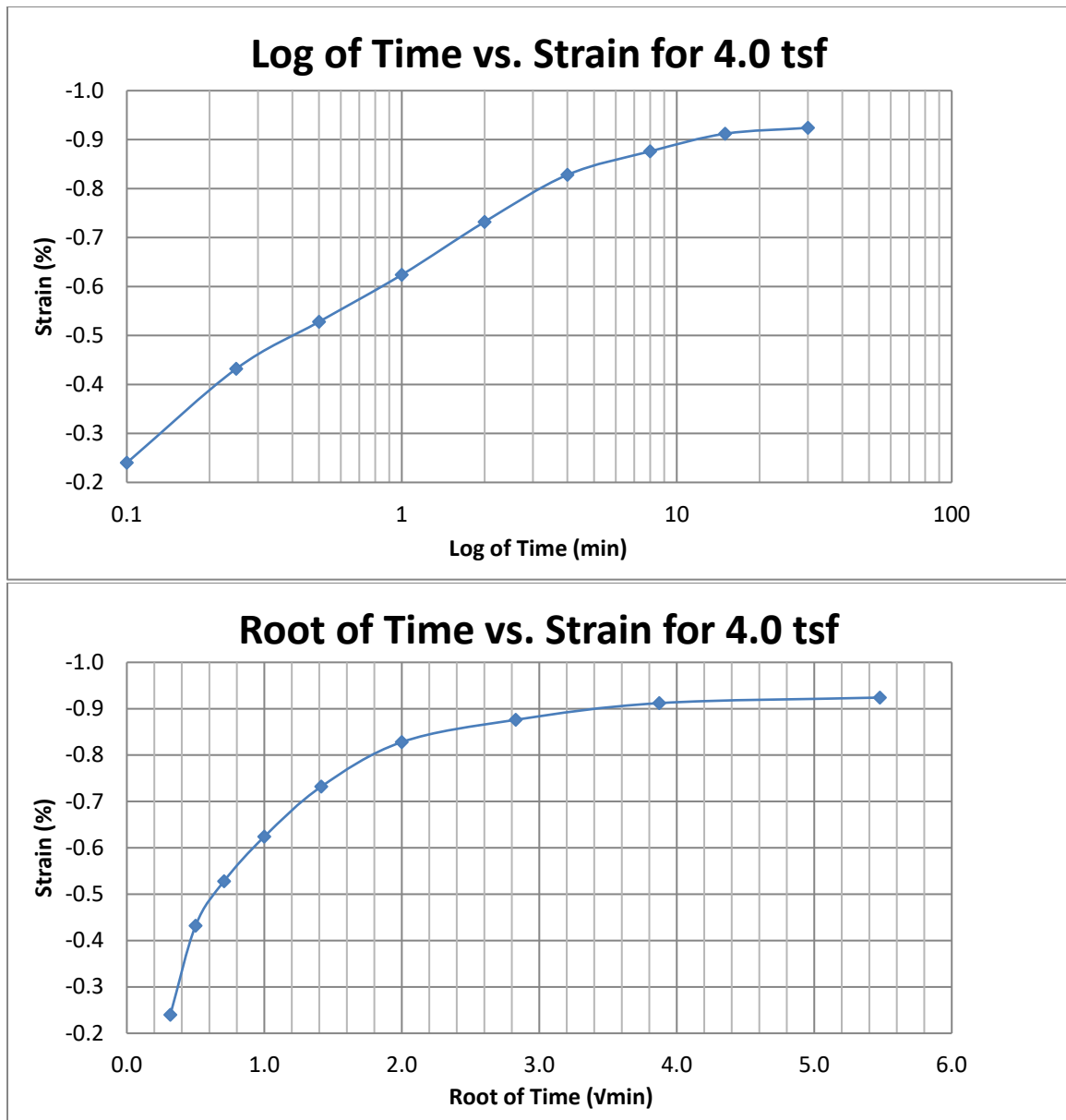


Figure A162 Springville at 75-77 feet



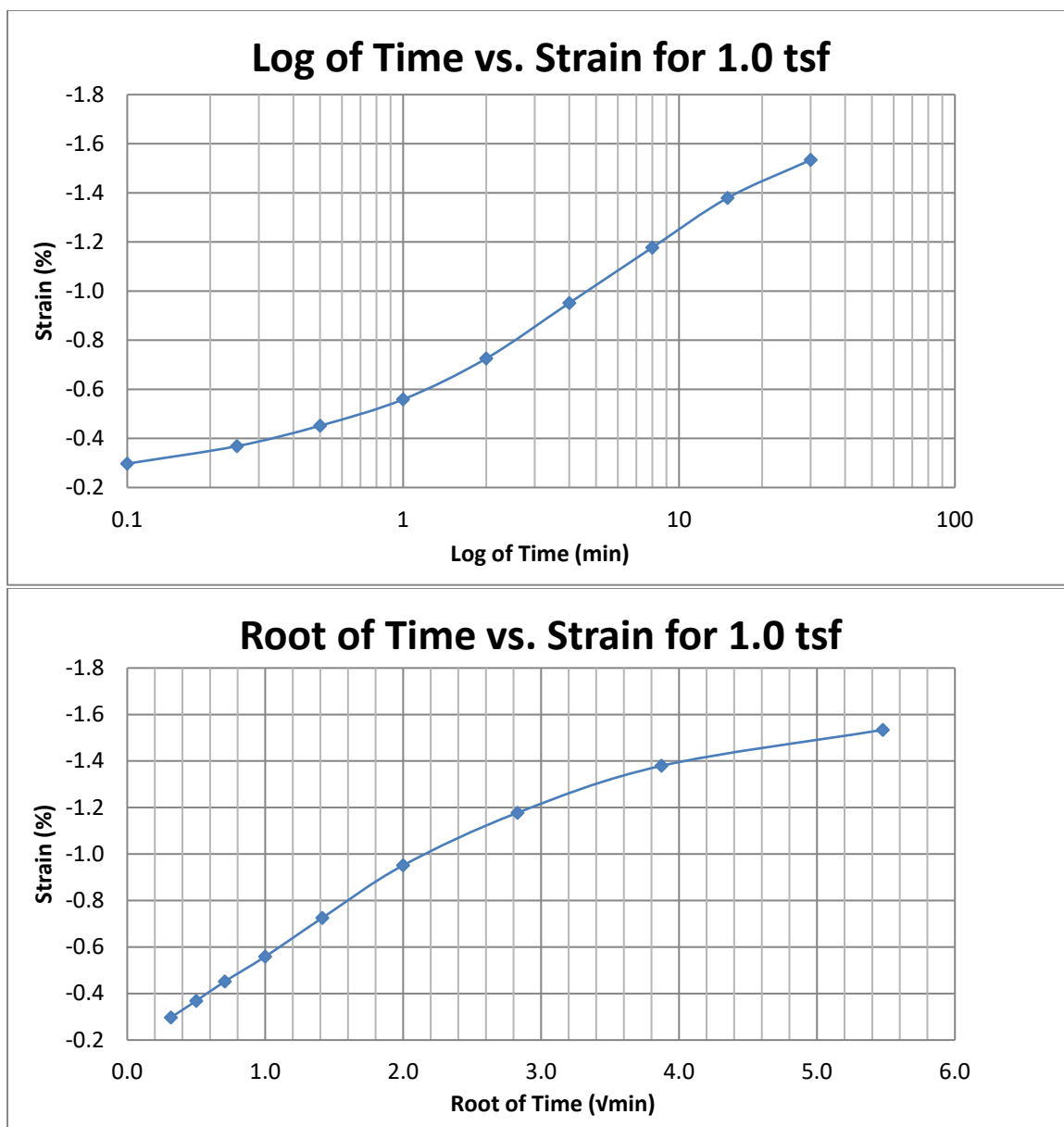


Figure A163 Springville at 75-77 feet

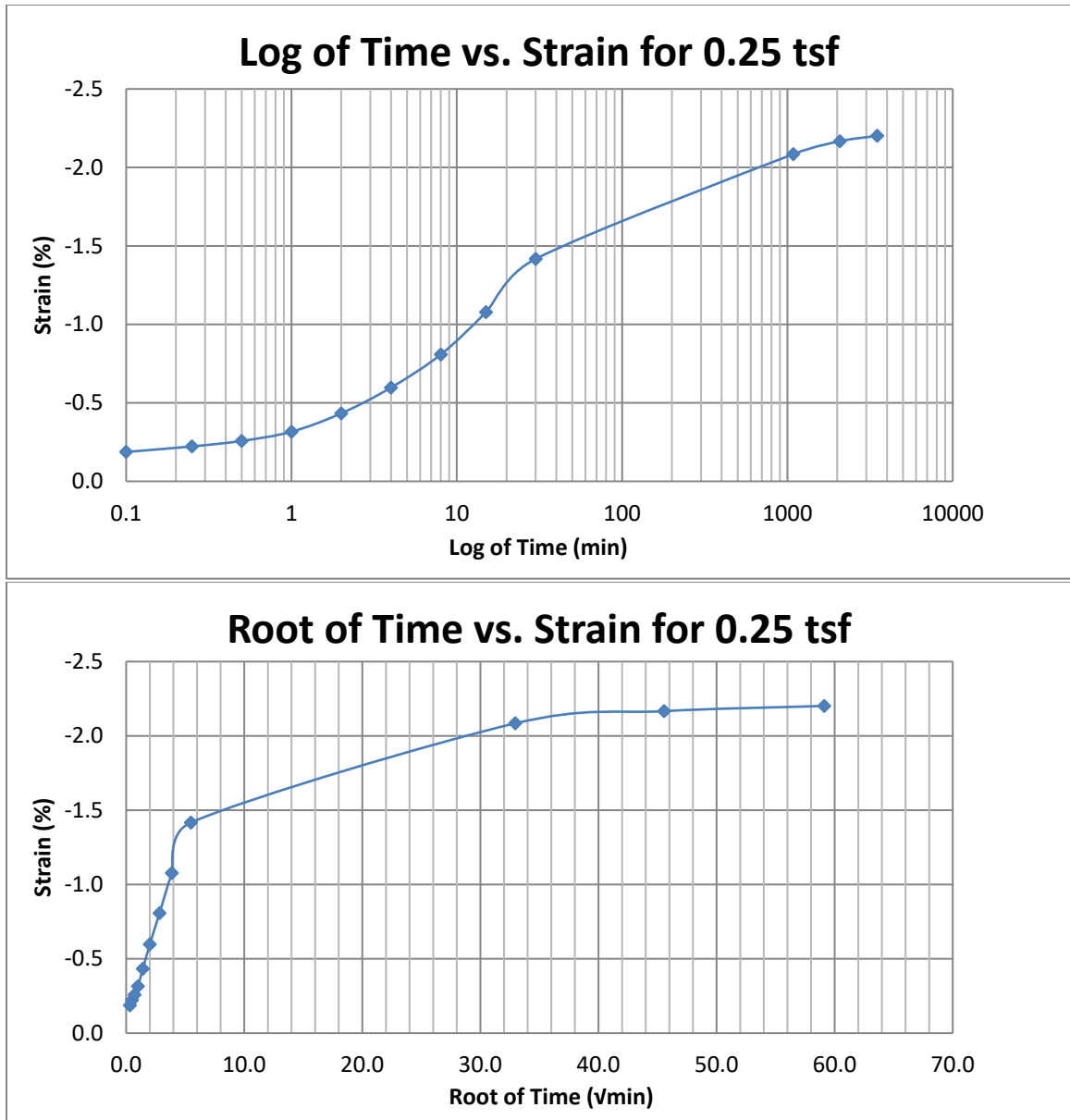


Figure A164 Springville at 75-77 feet

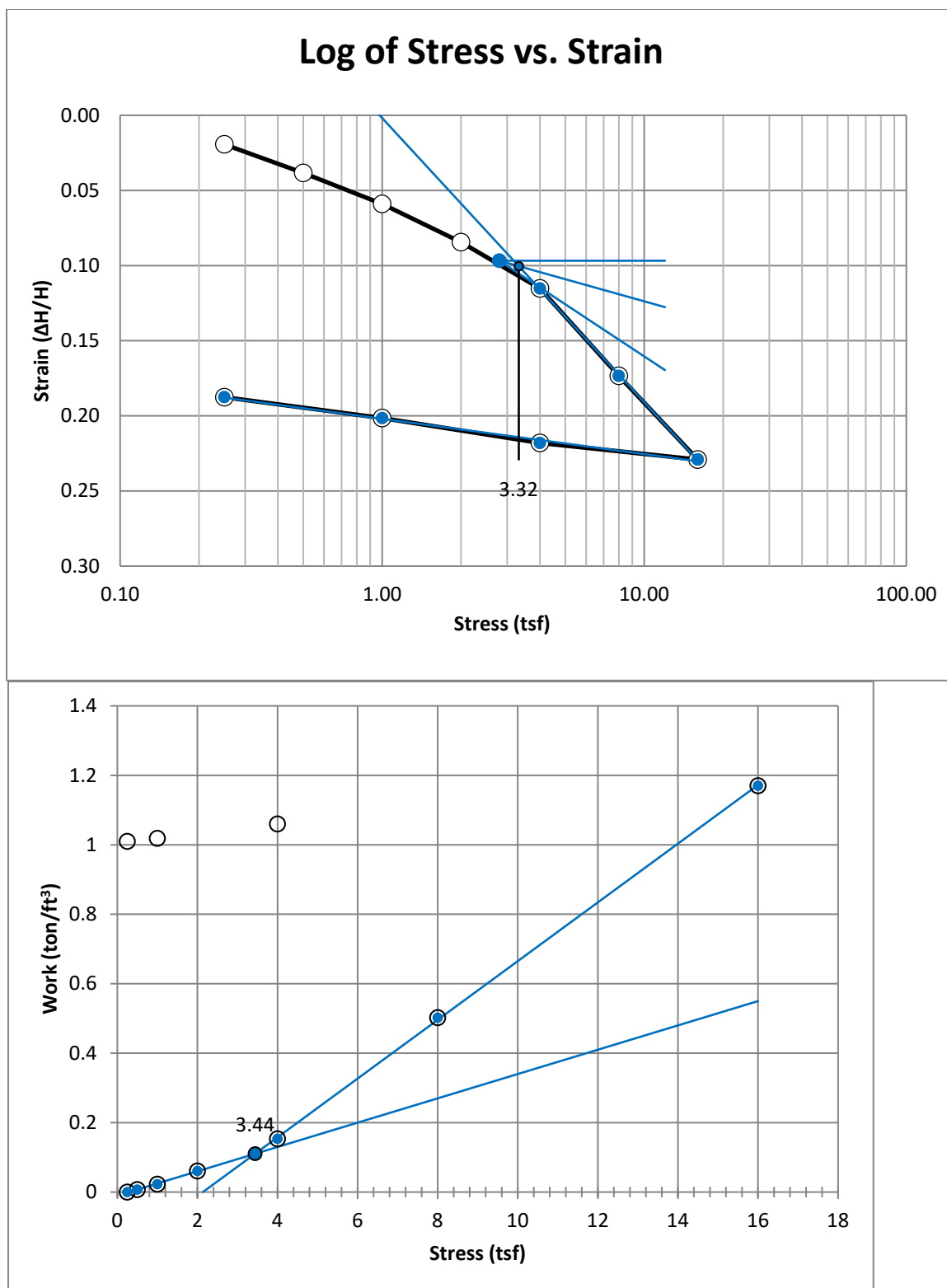


Figure A165 Springville at 80-82 feet

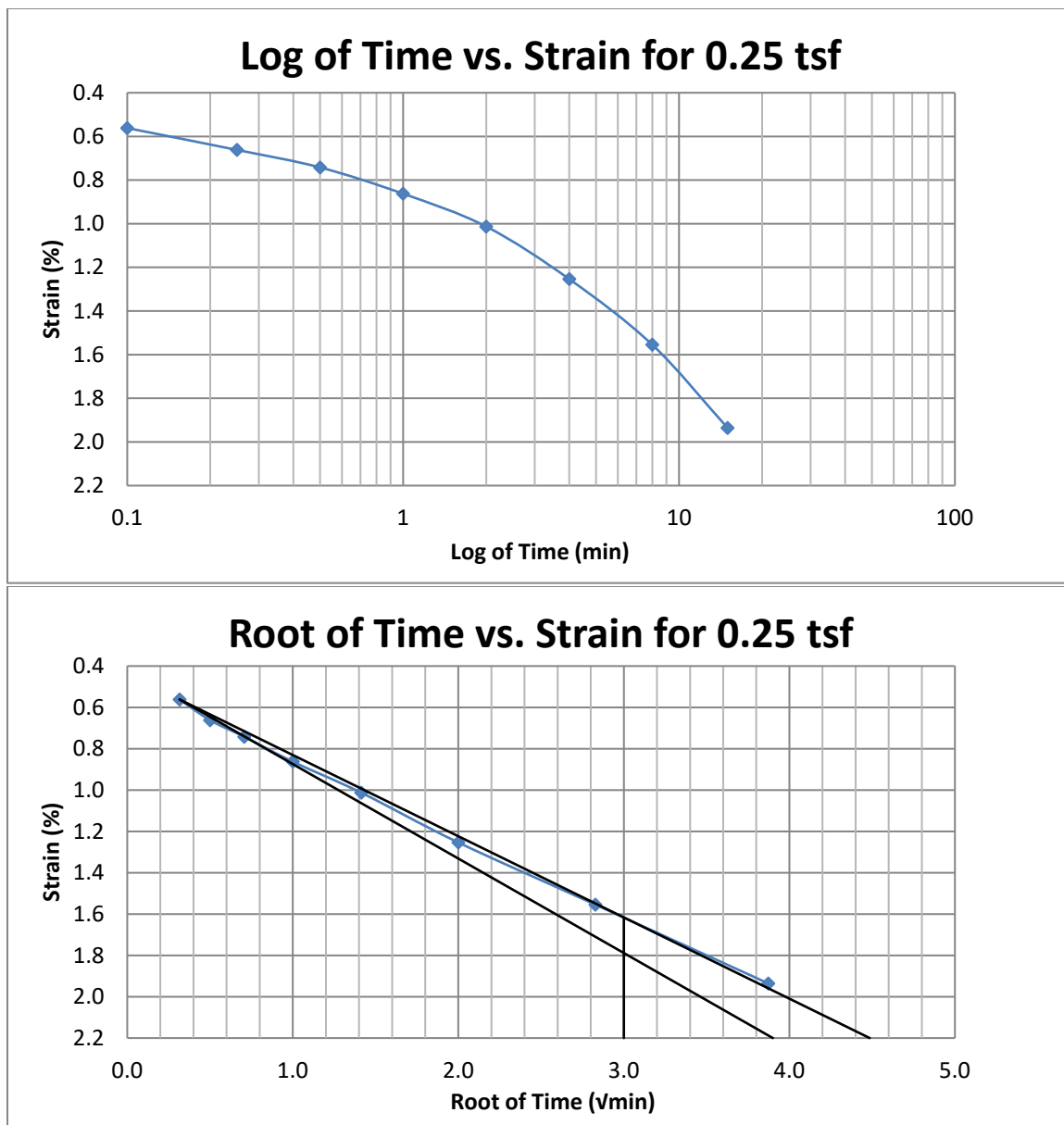


Figure A166 Springville at 80-82 feet

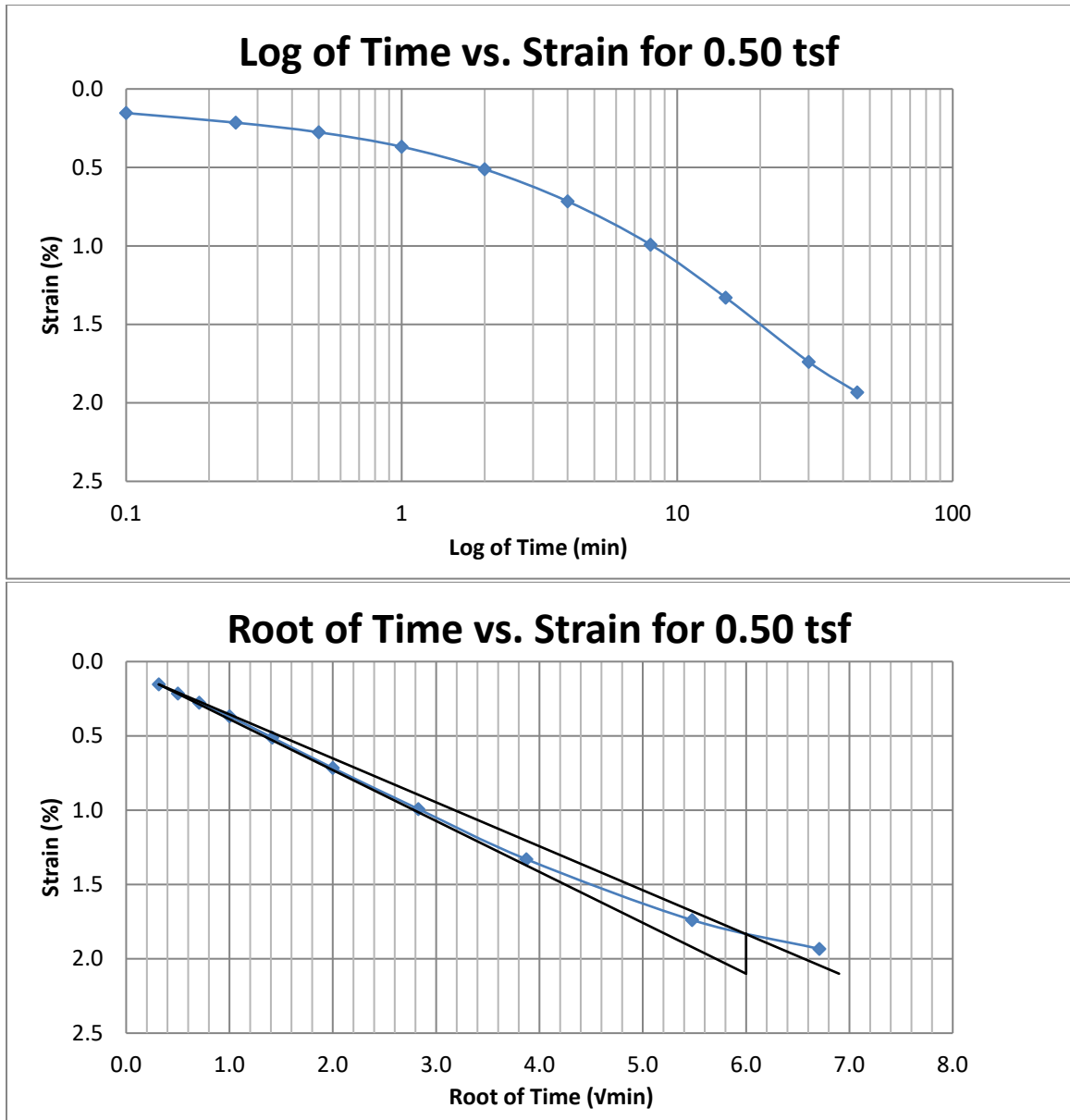


Figure A167 Springville at 80-82 feet

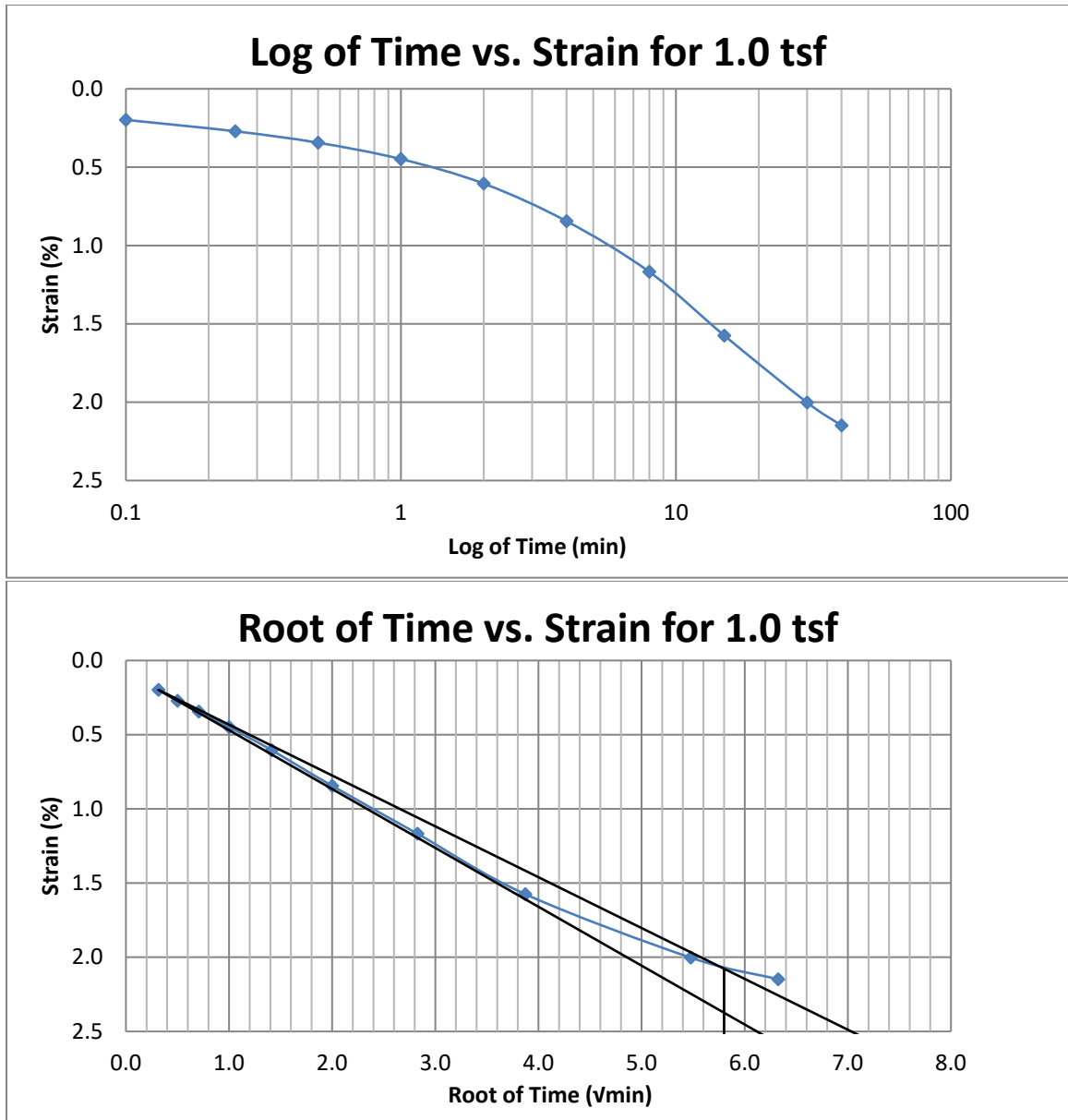


Figure A168 Springville at 80-82 feet

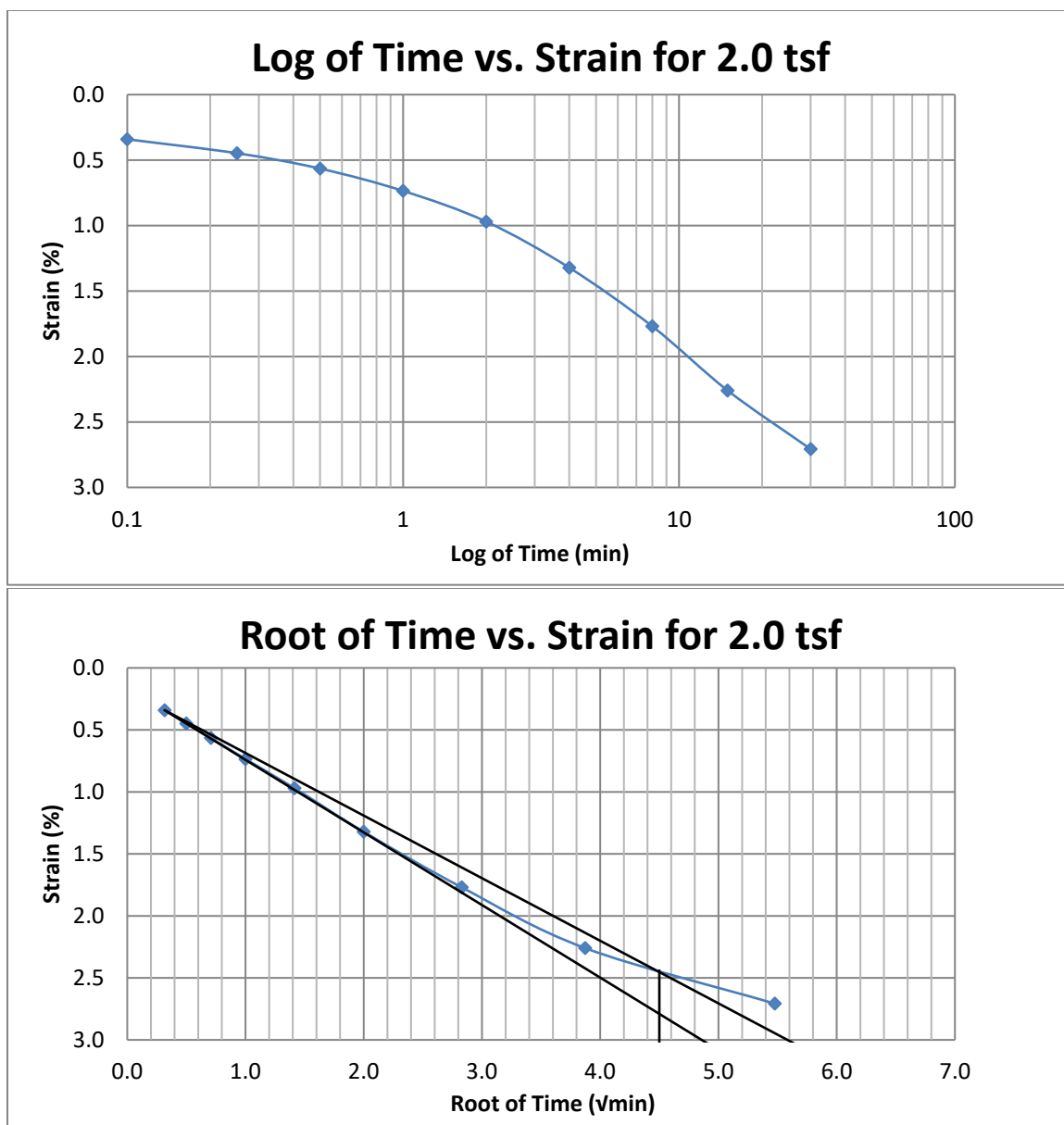


Figure A169 Springville at 80-82 feet

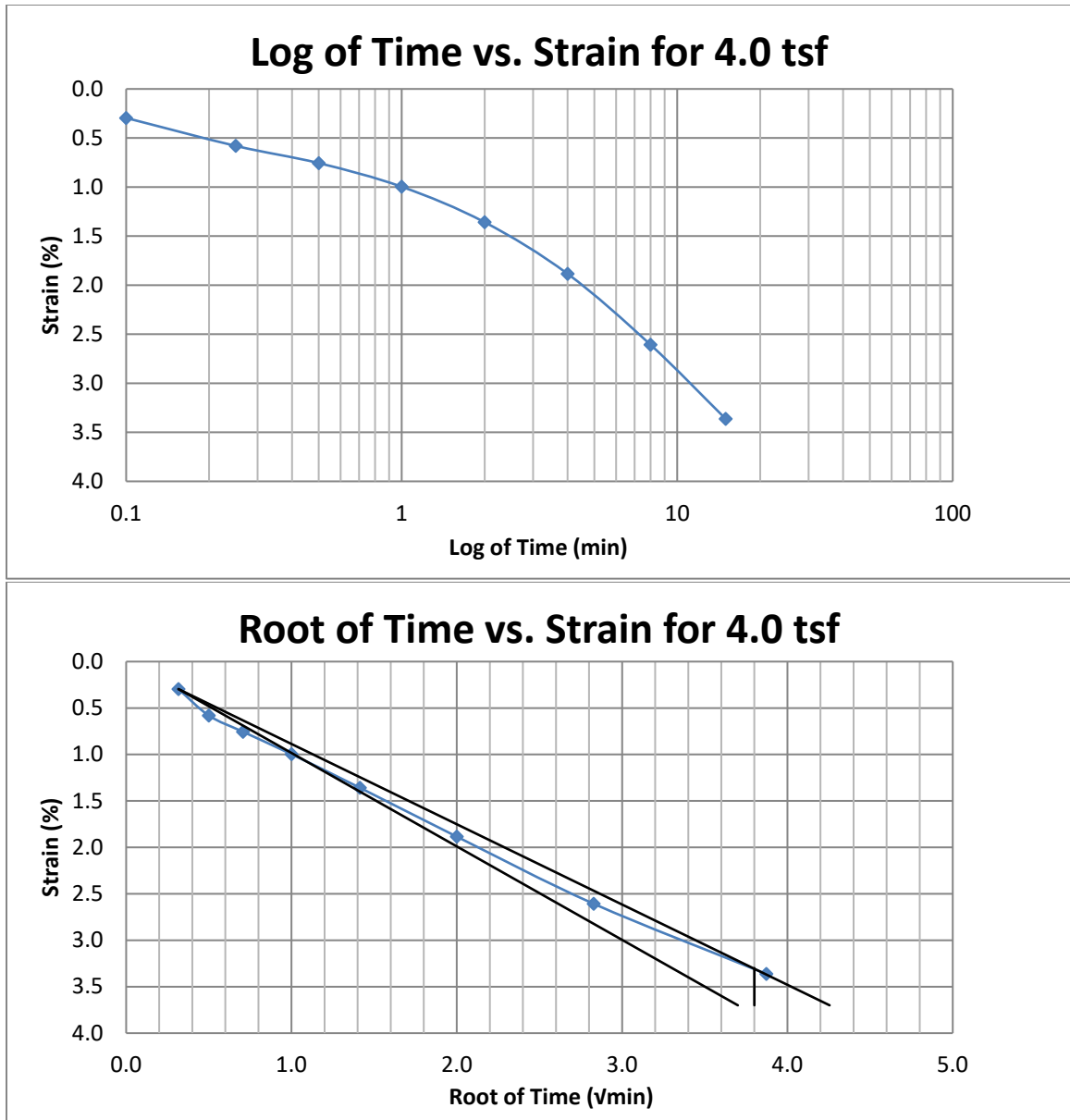


Figure A170 Springville at 80-82 feet



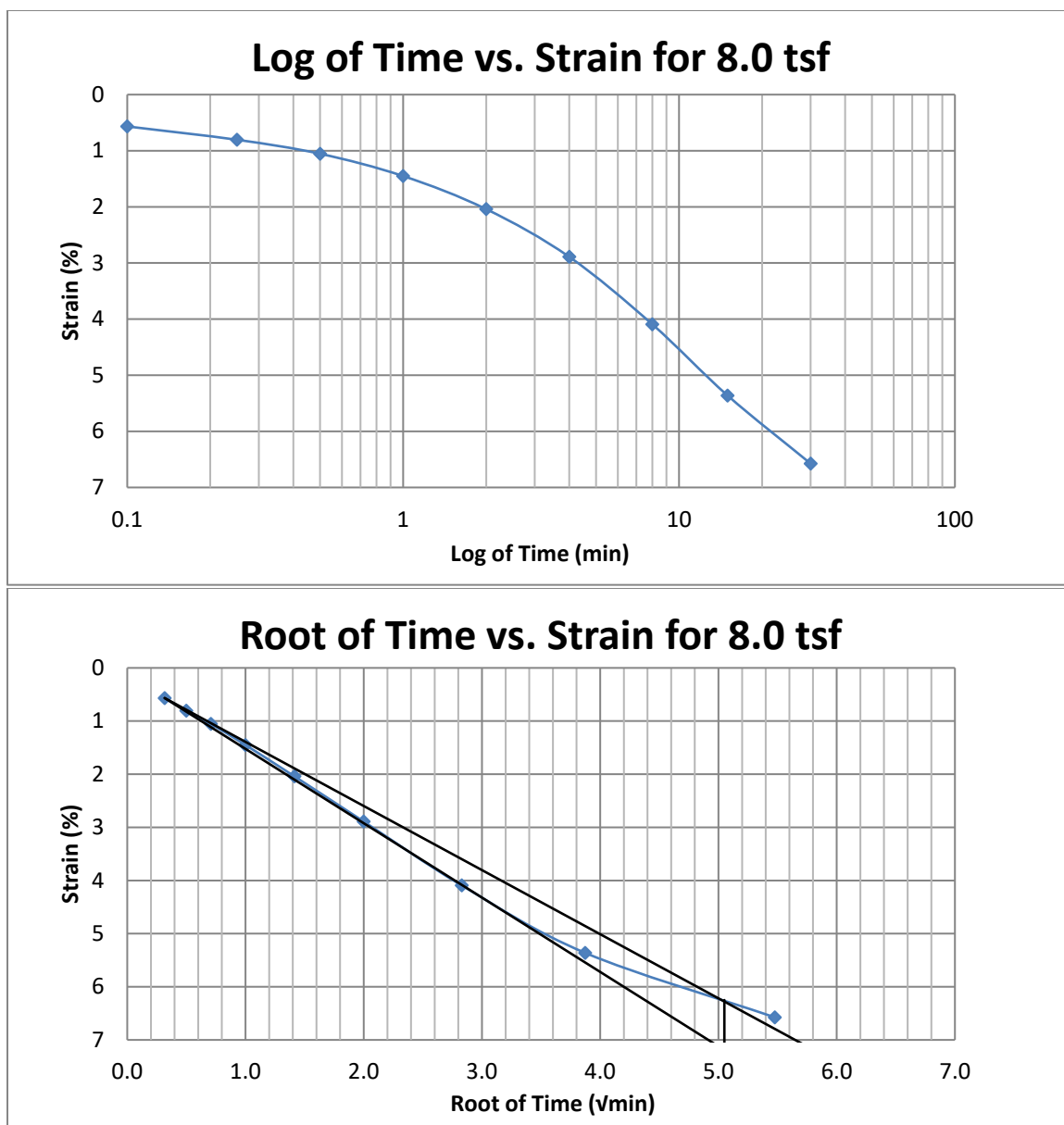


Figure A171 Springville at 80-82 feet

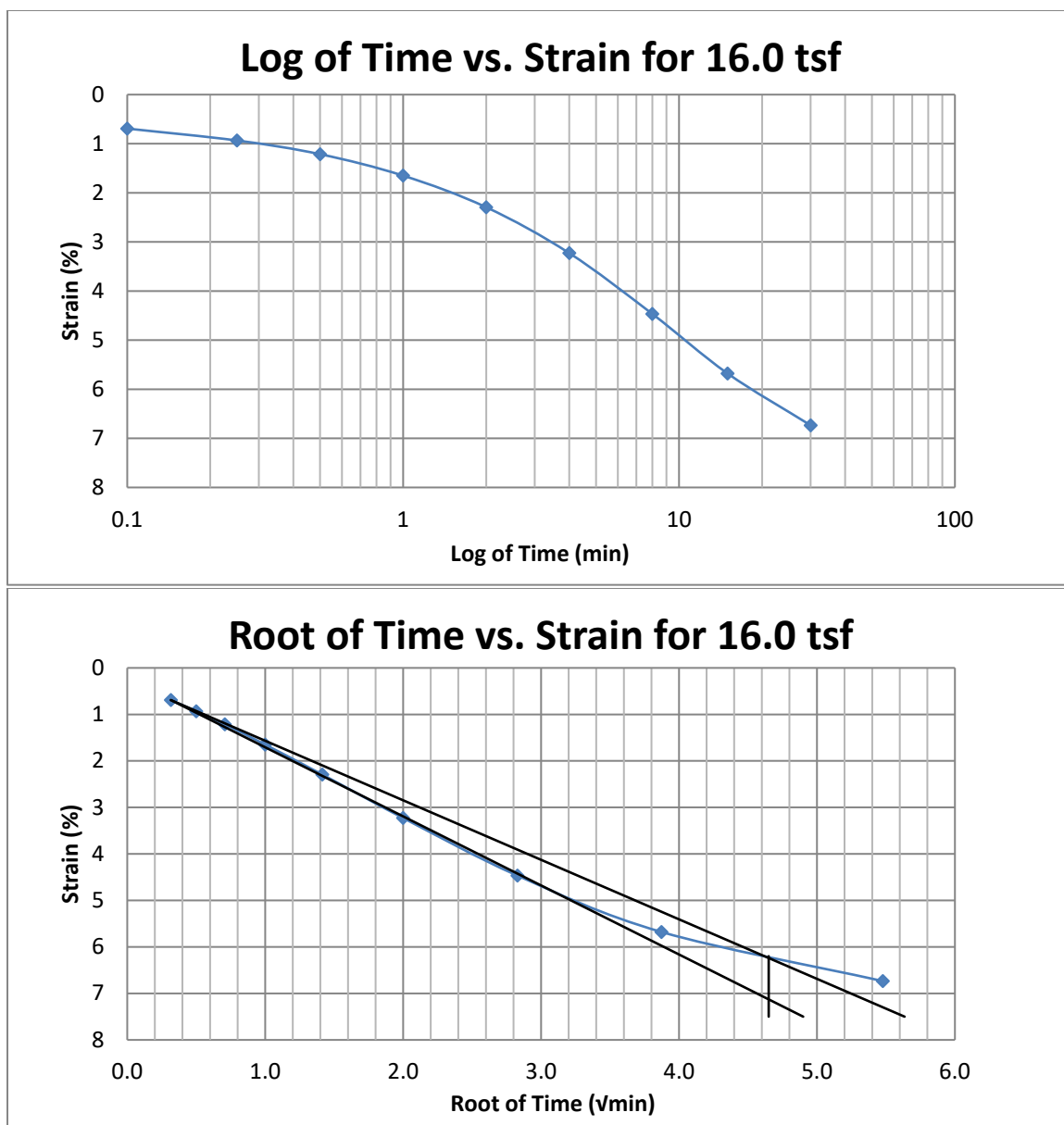


Figure A172 Springville at 80-82 feet

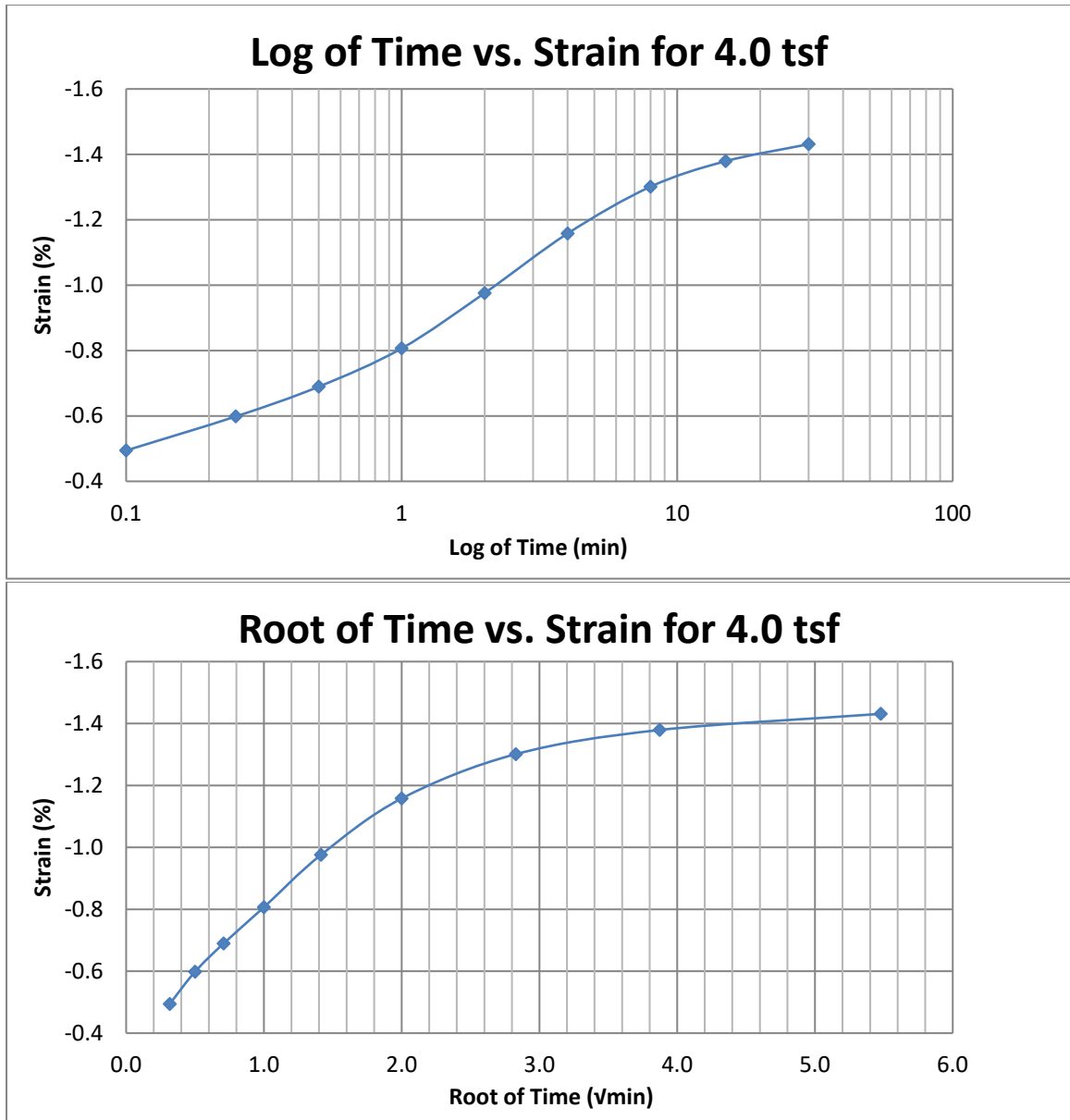


Figure A173 Springville at 80-82 feet

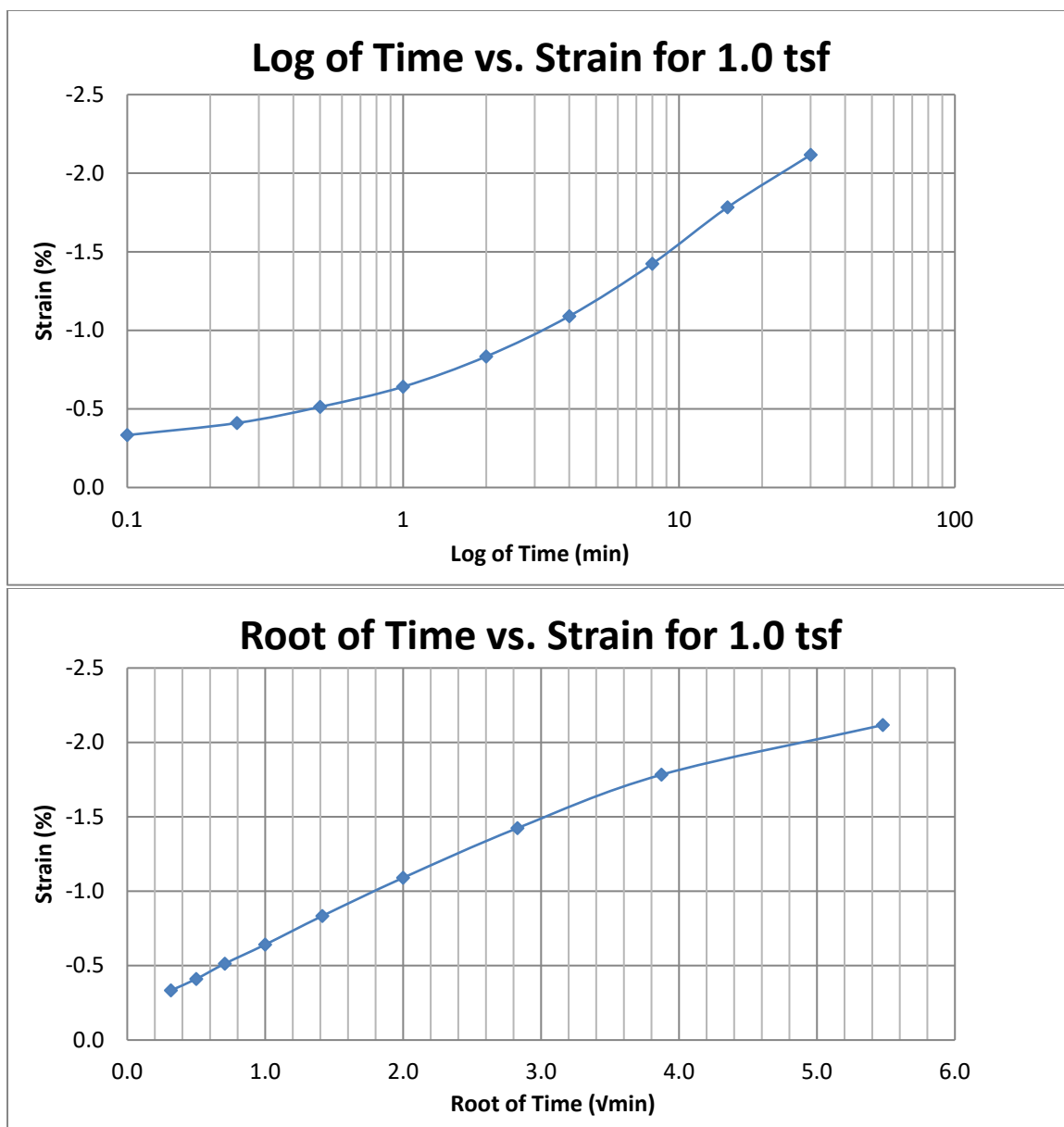


Figure A174 Springville at 80-82 feet

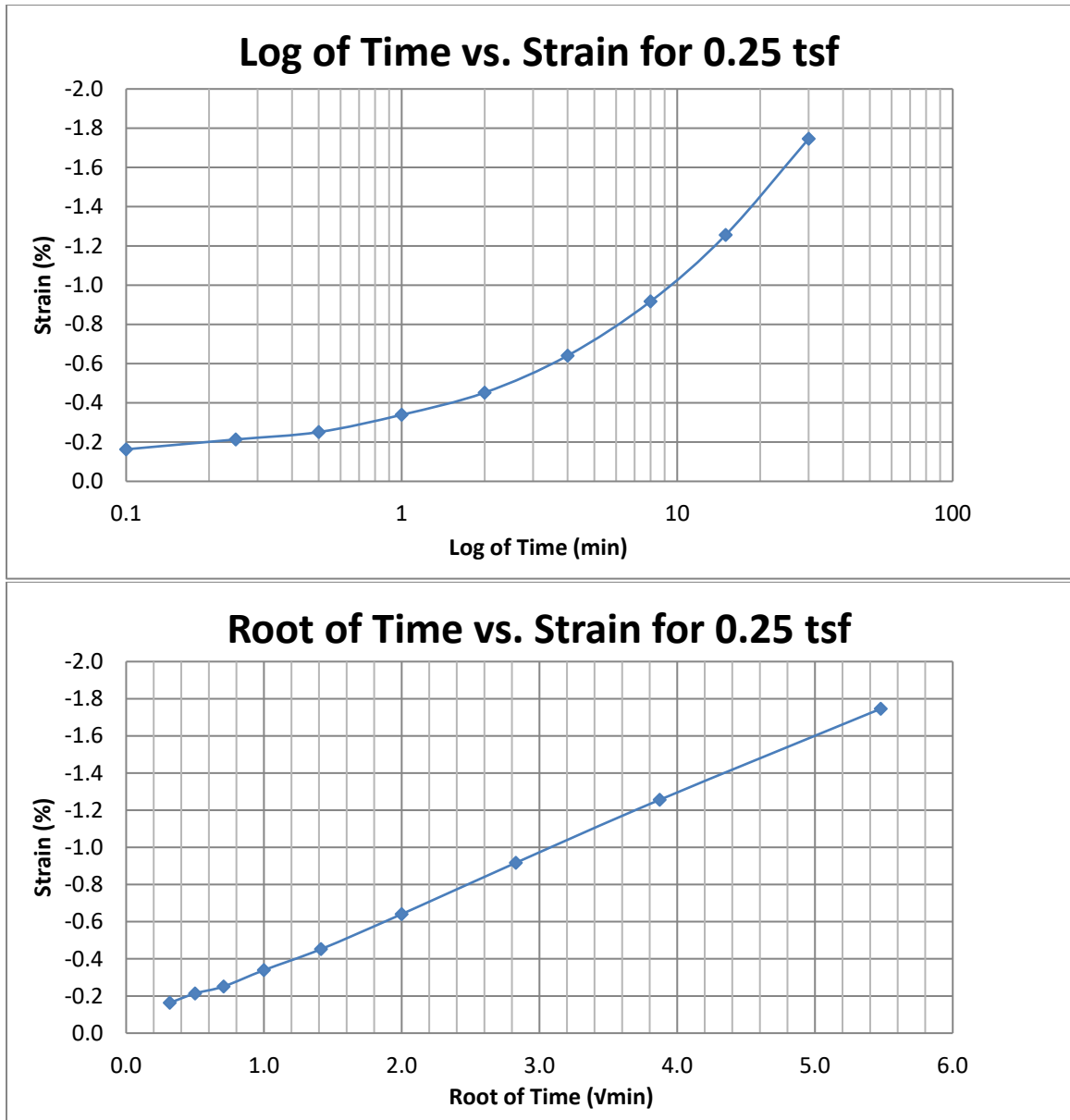


Figure A175 Springville at 80-82 feet

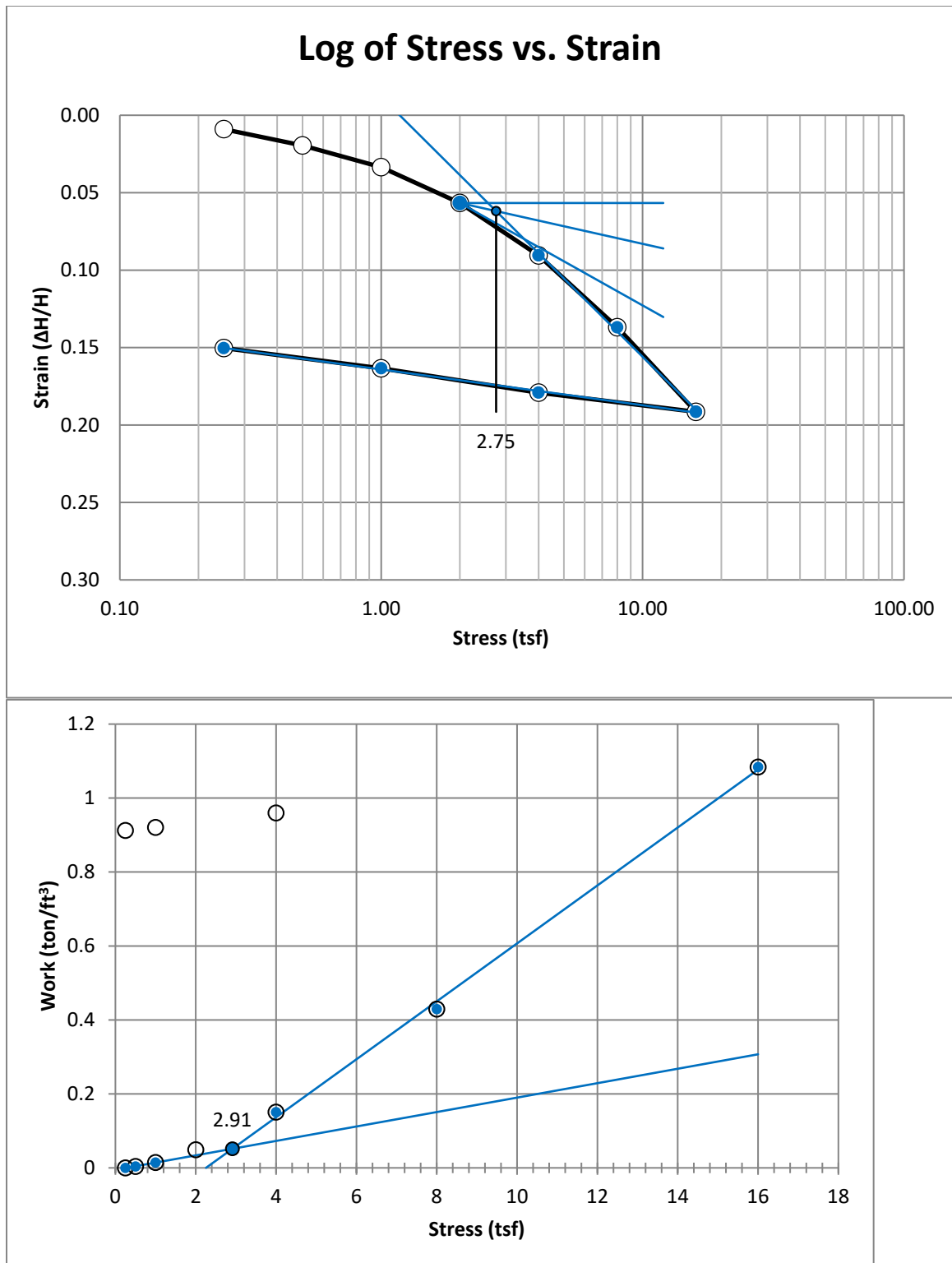


Figure A176 Springville at 84-86 feet

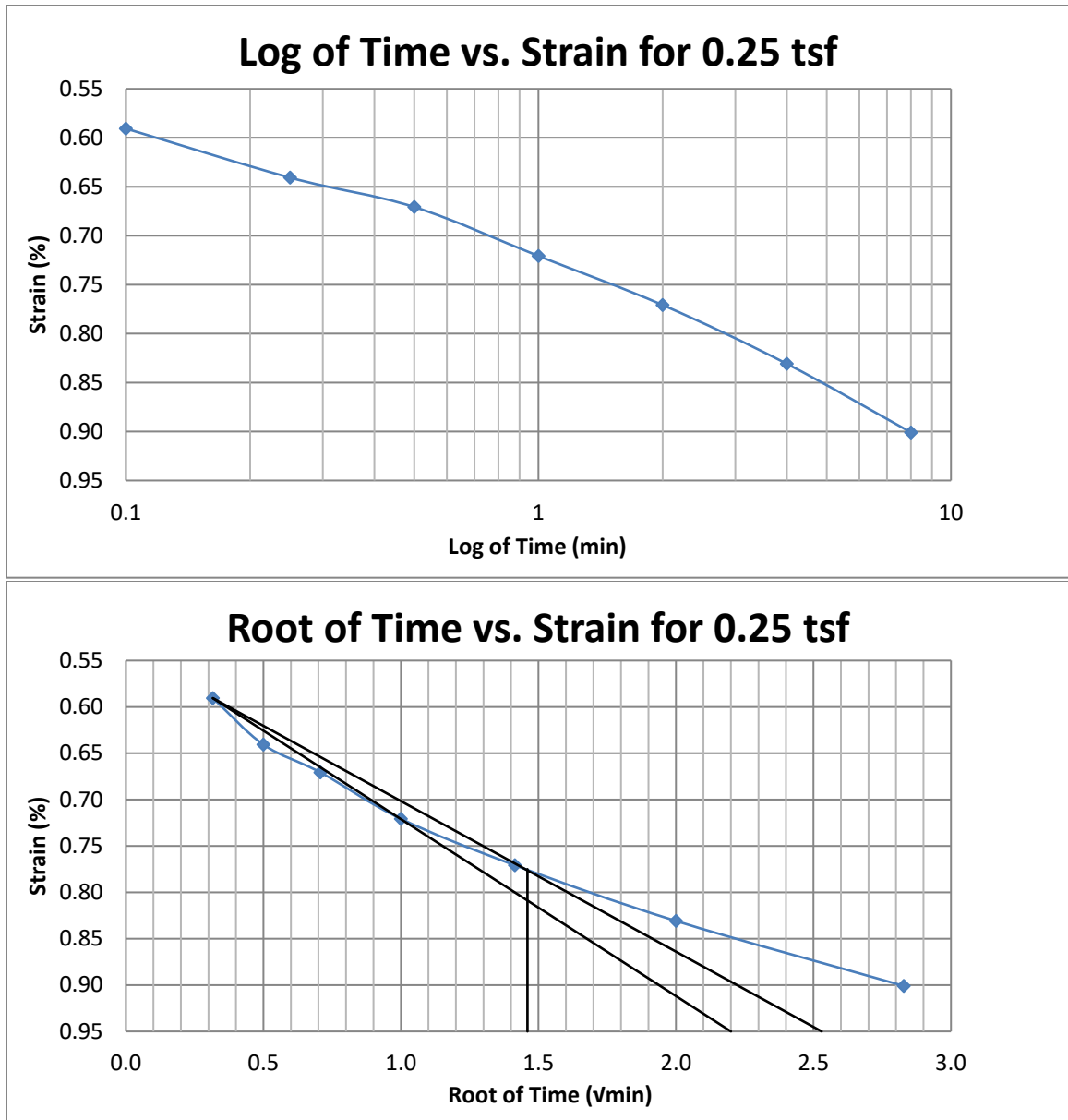


Figure A177 Springville at 84-86 feet

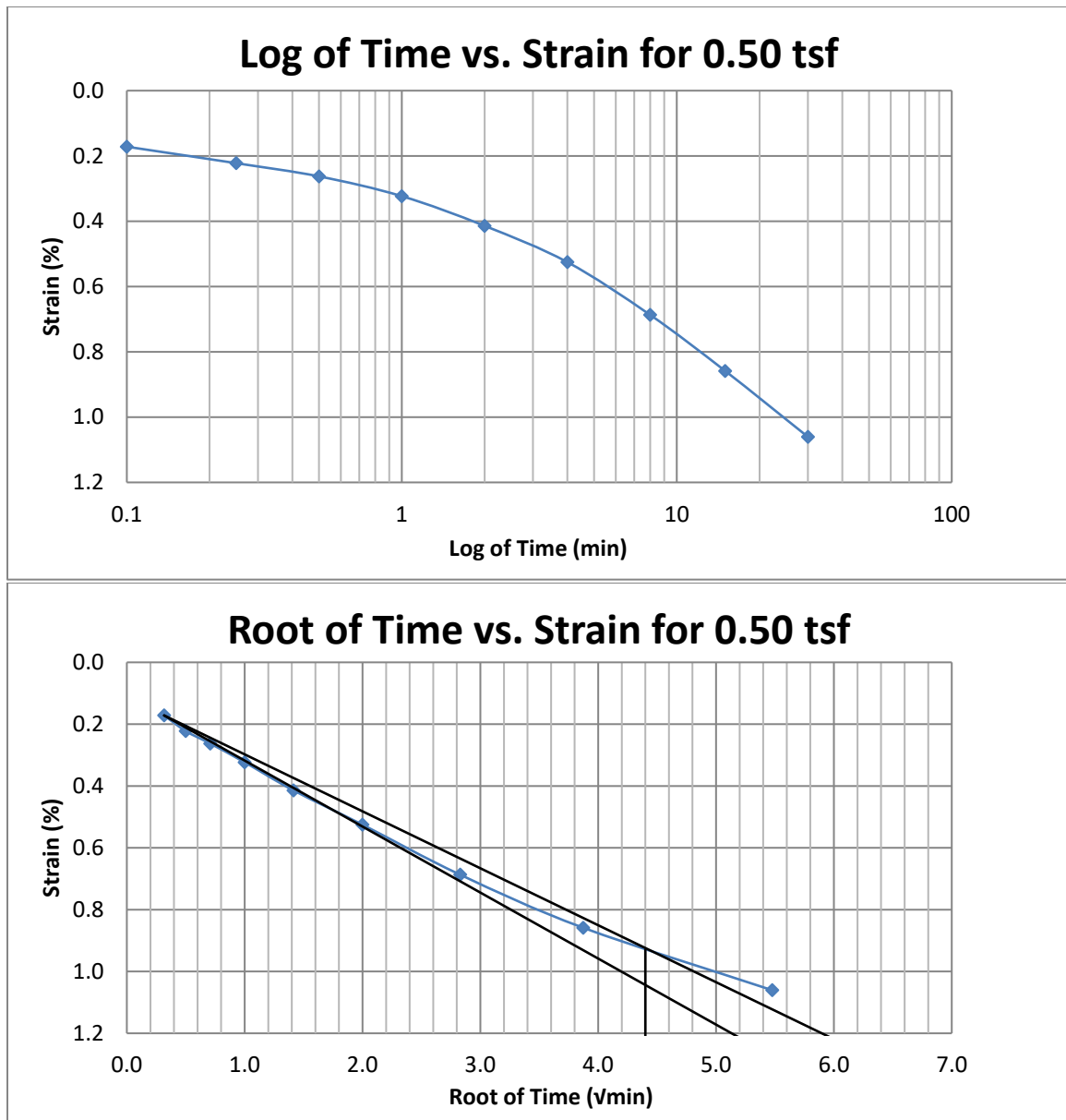


Figure A178 Springville at 84-86 feet



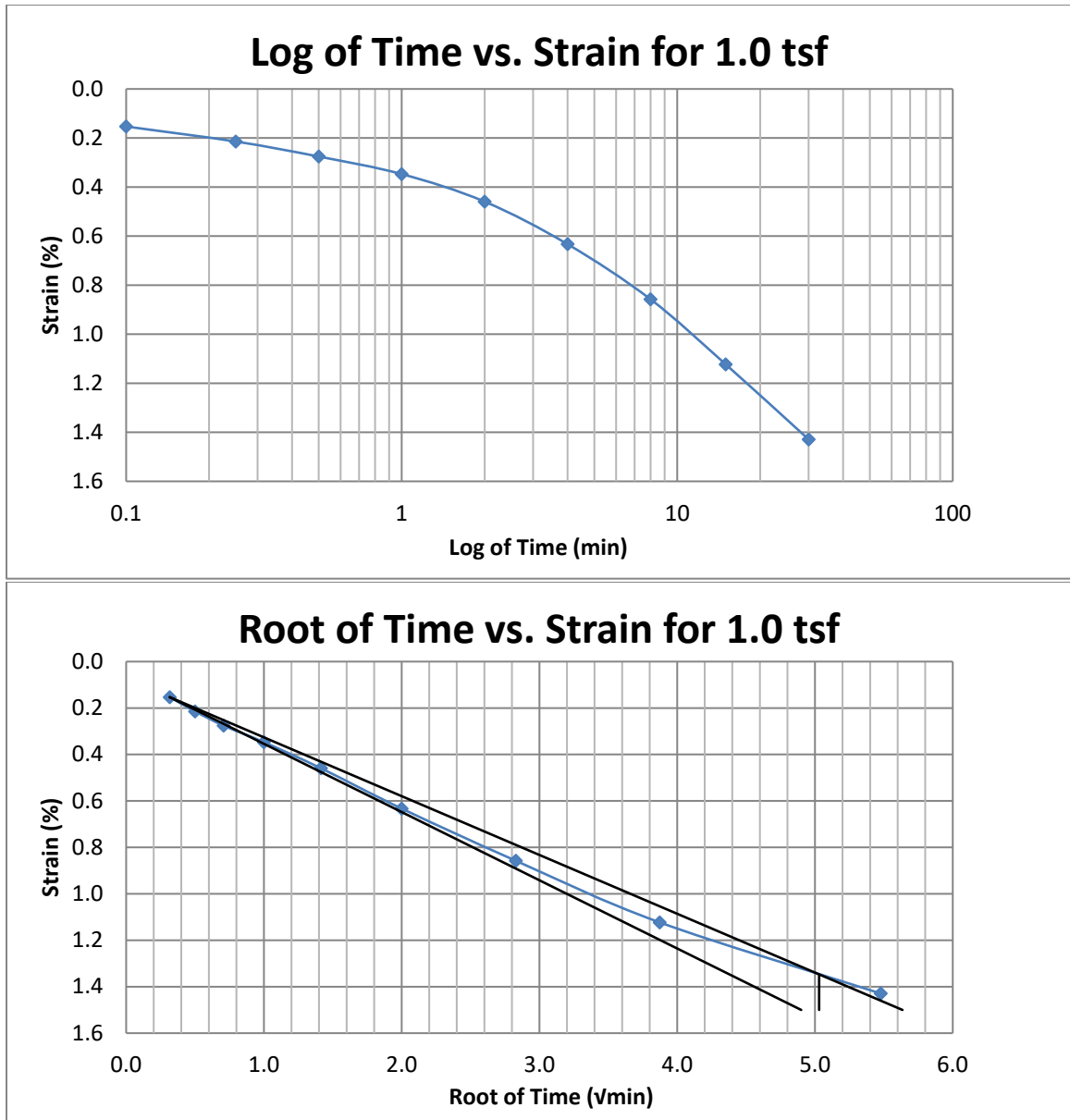


Figure A179 Springville at 84-86 feet

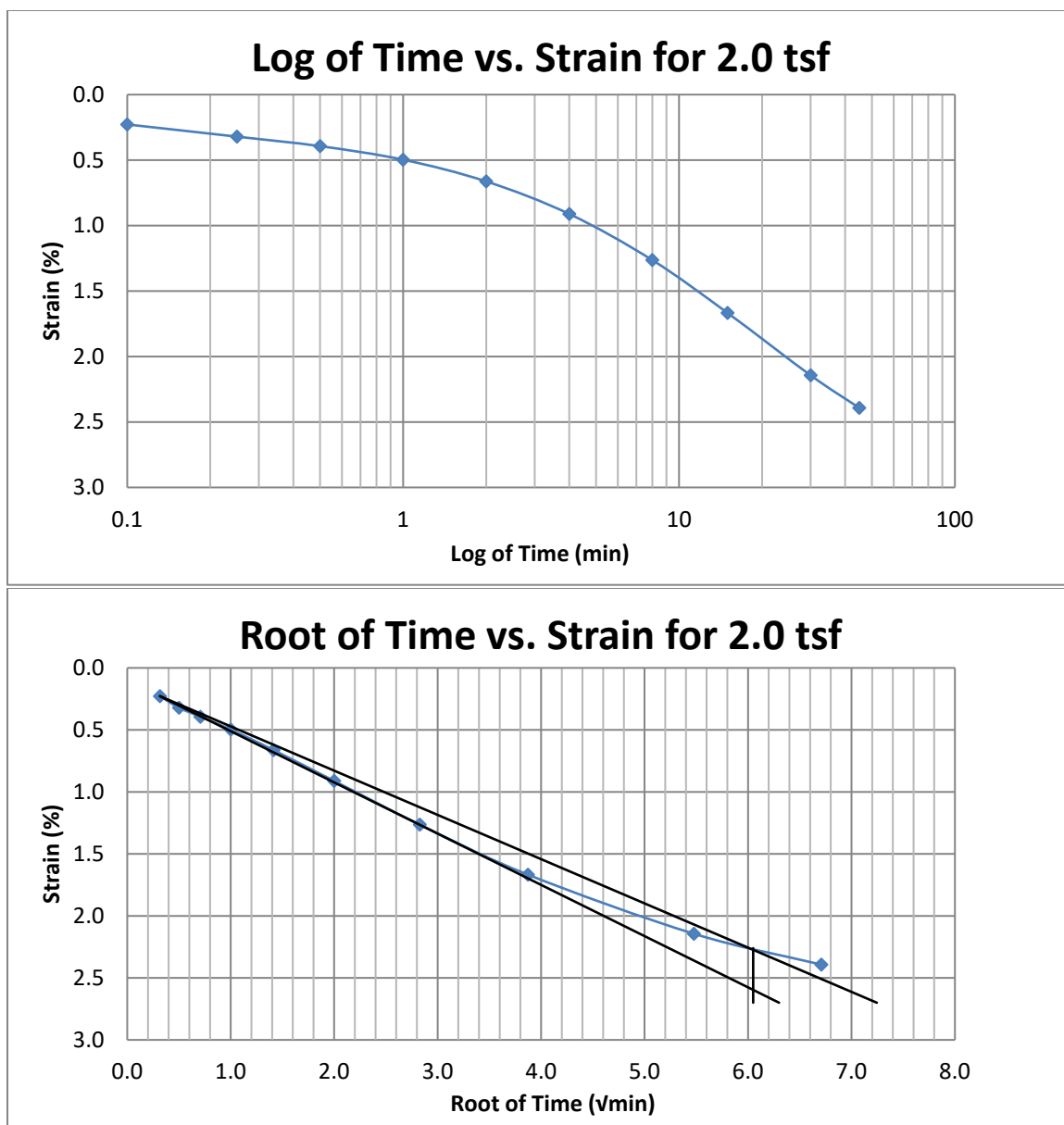


Figure A180 Springville at 84-86 feet

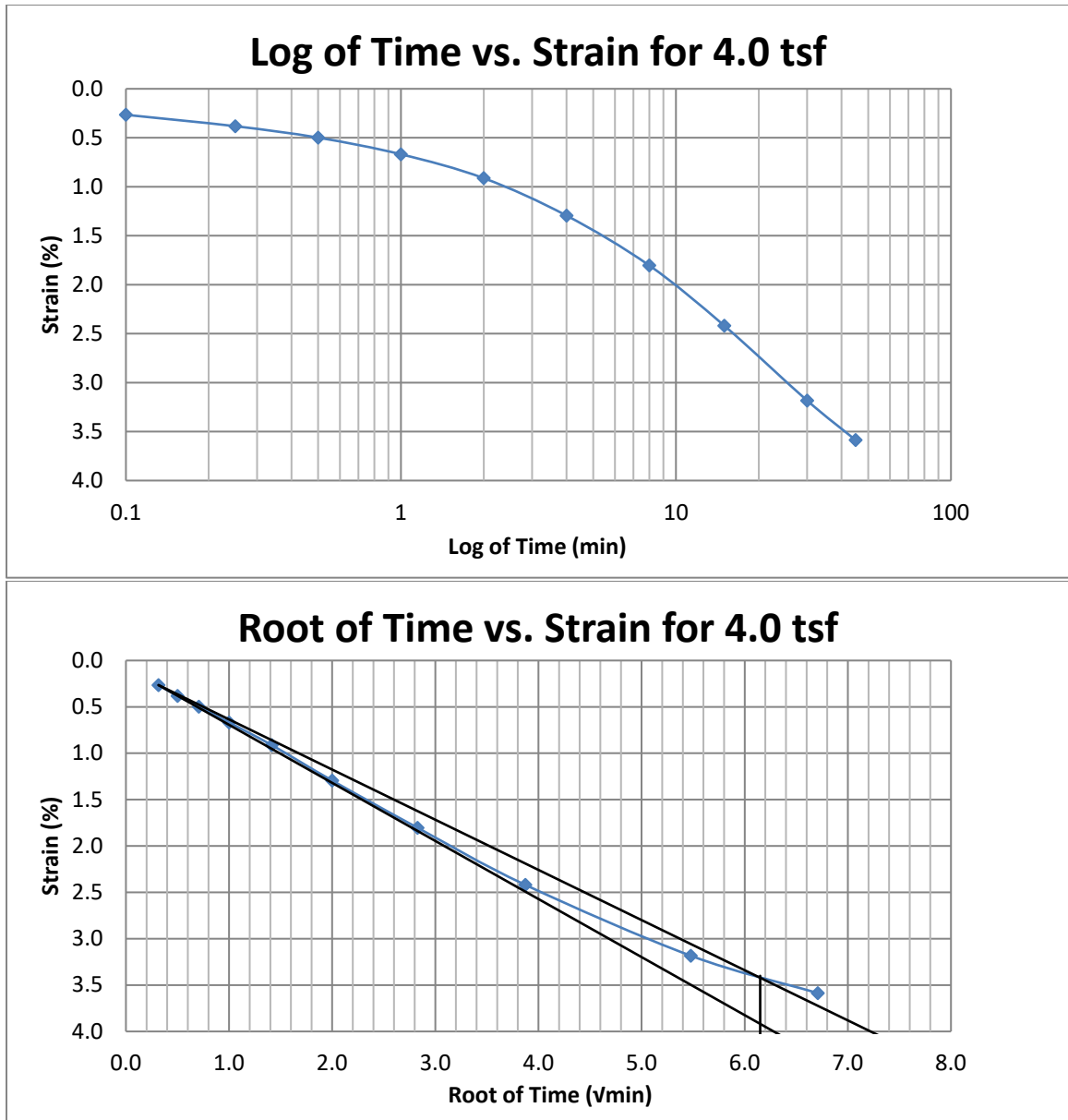


Figure A181 Springville at 84-86 feet

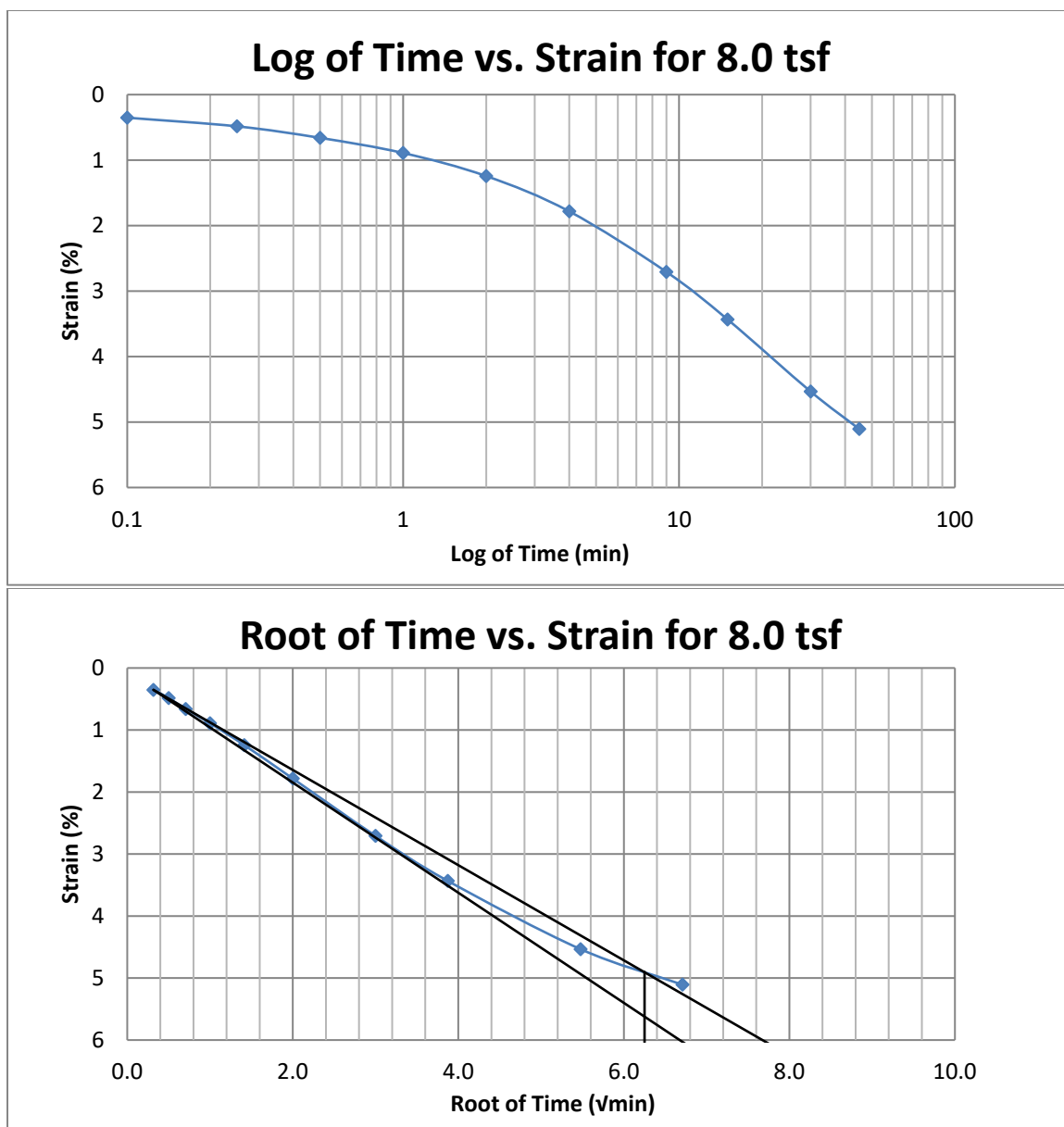


Figure A182 Springville at 84-86 feet

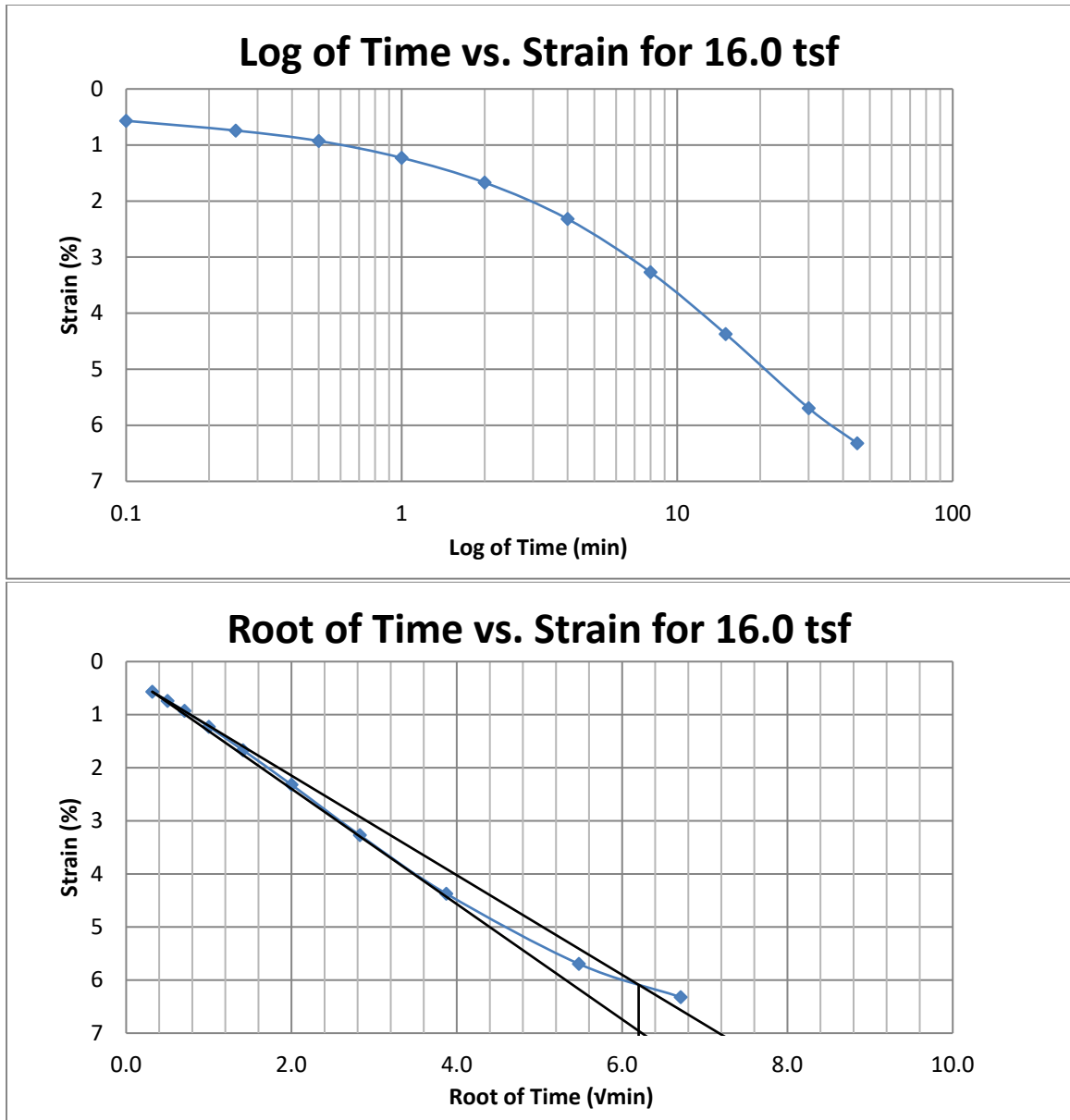


Figure A183 Springville at 84-86 feet

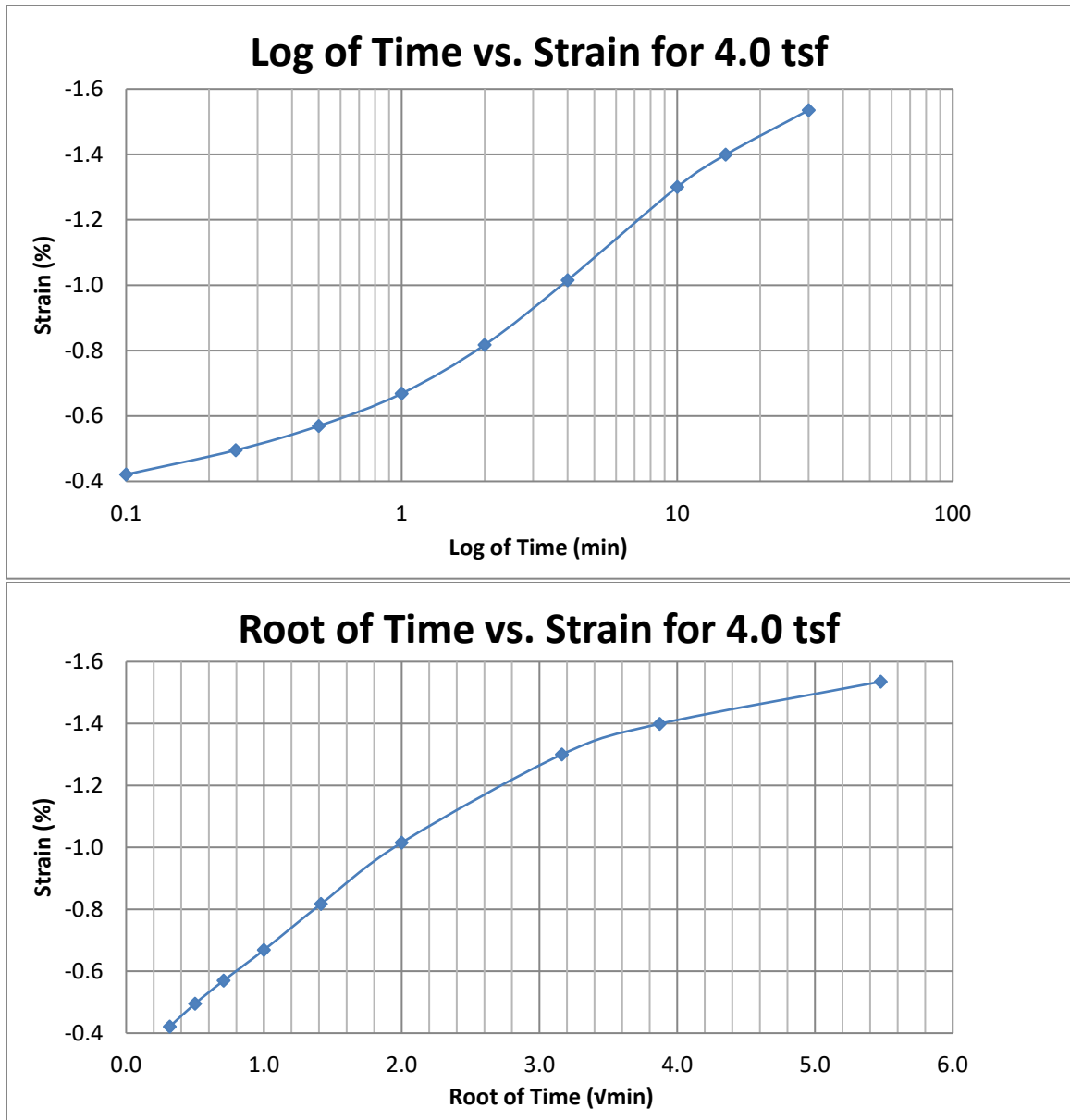


Figure A184 Springville at 84-86 feet

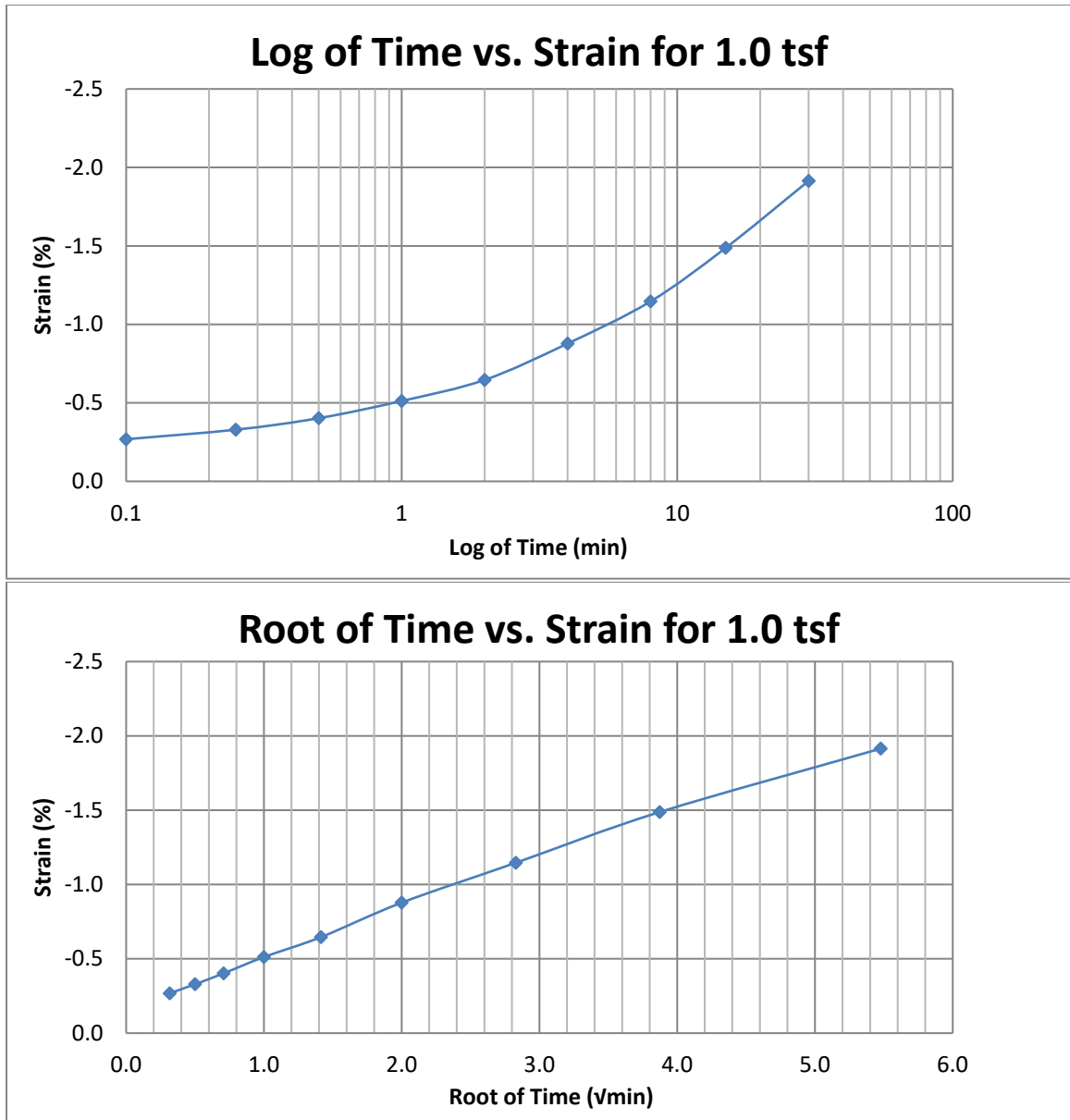


Figure A185 Springville at 84-86 feet

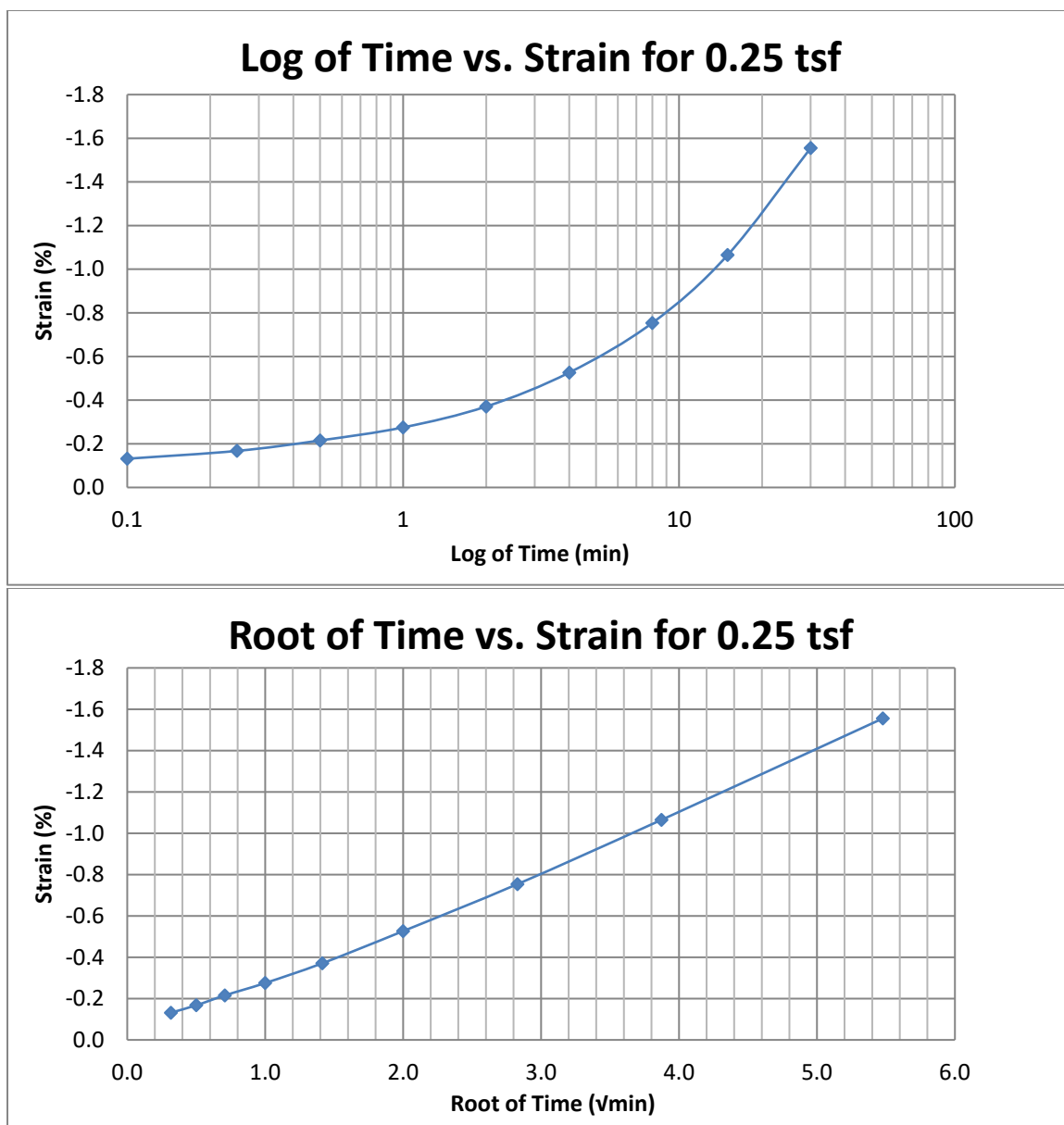
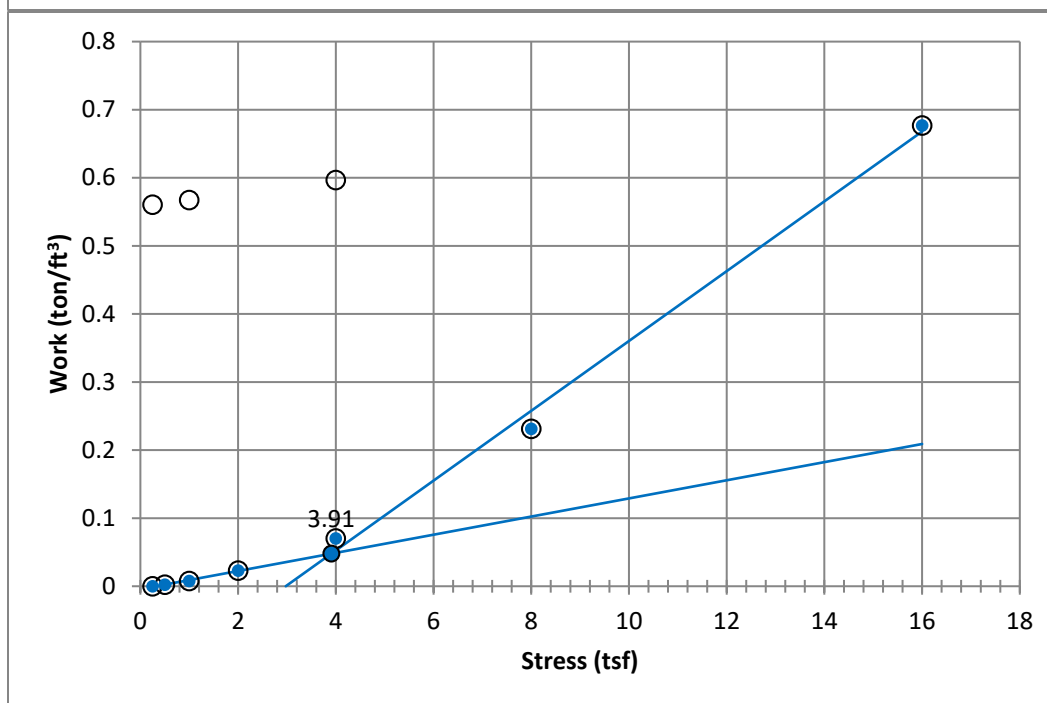
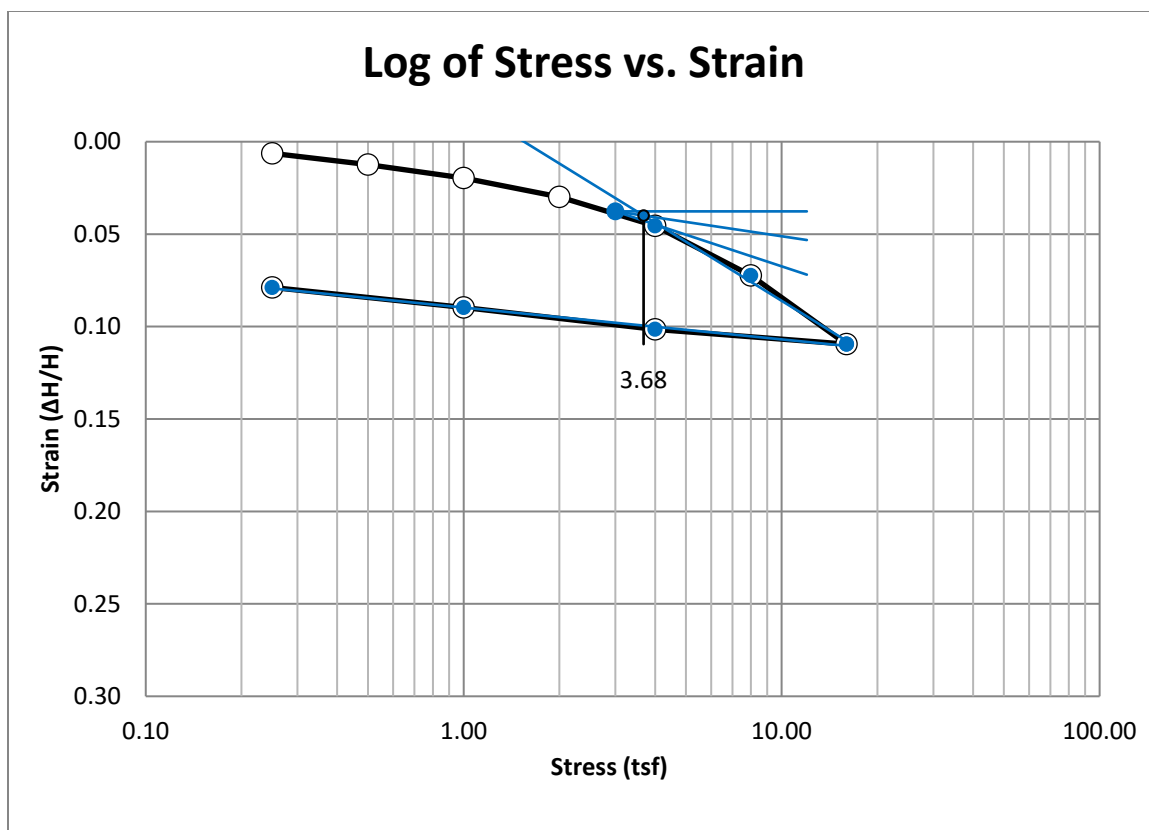


Figure A186 Springville at 84-86 feet





**Figure A187 Provo at 12-14 feet**

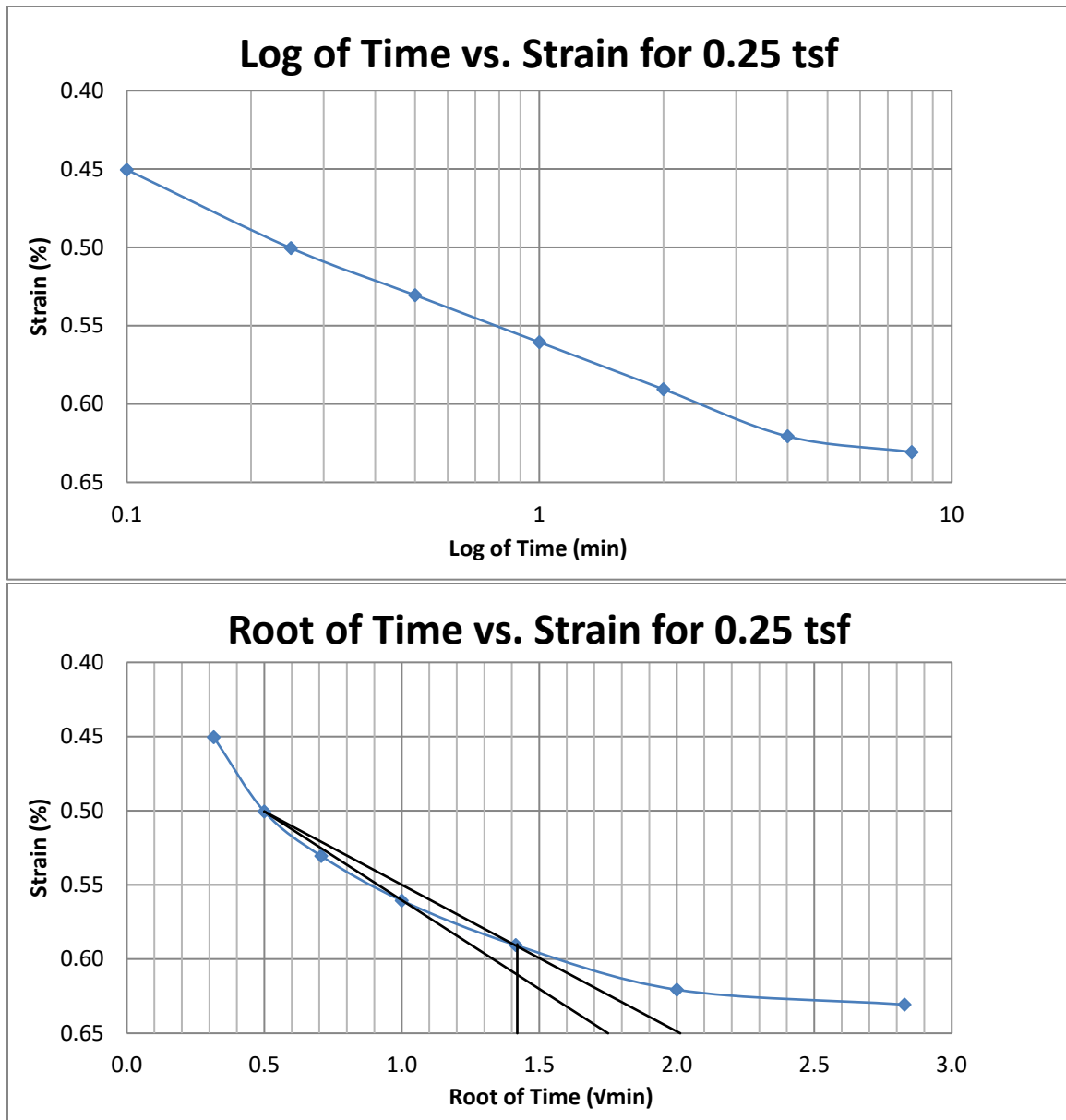
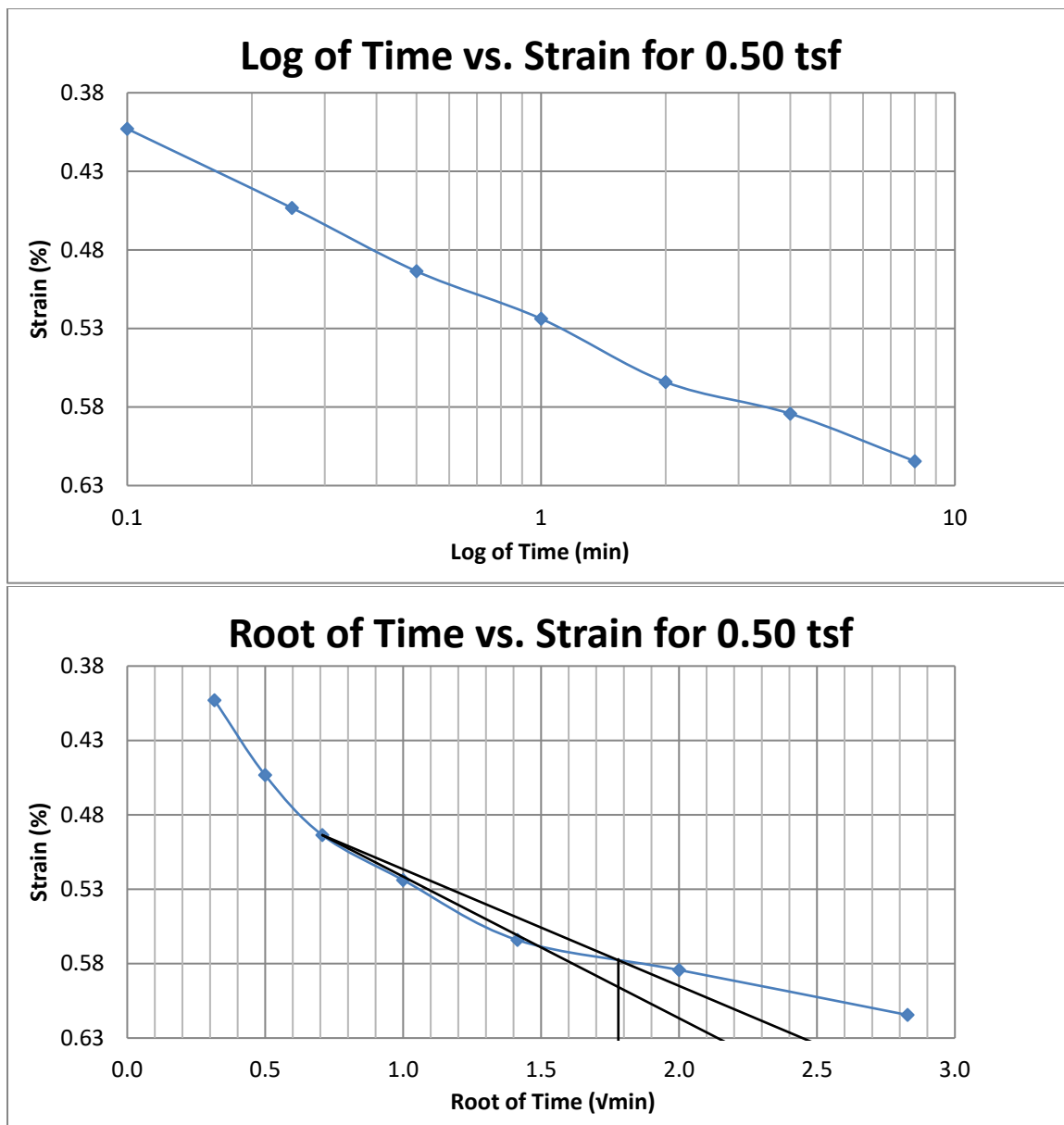


Figure A188 Provo at 12-14 feet



**Figure A189 Provo at 12-14 feet**

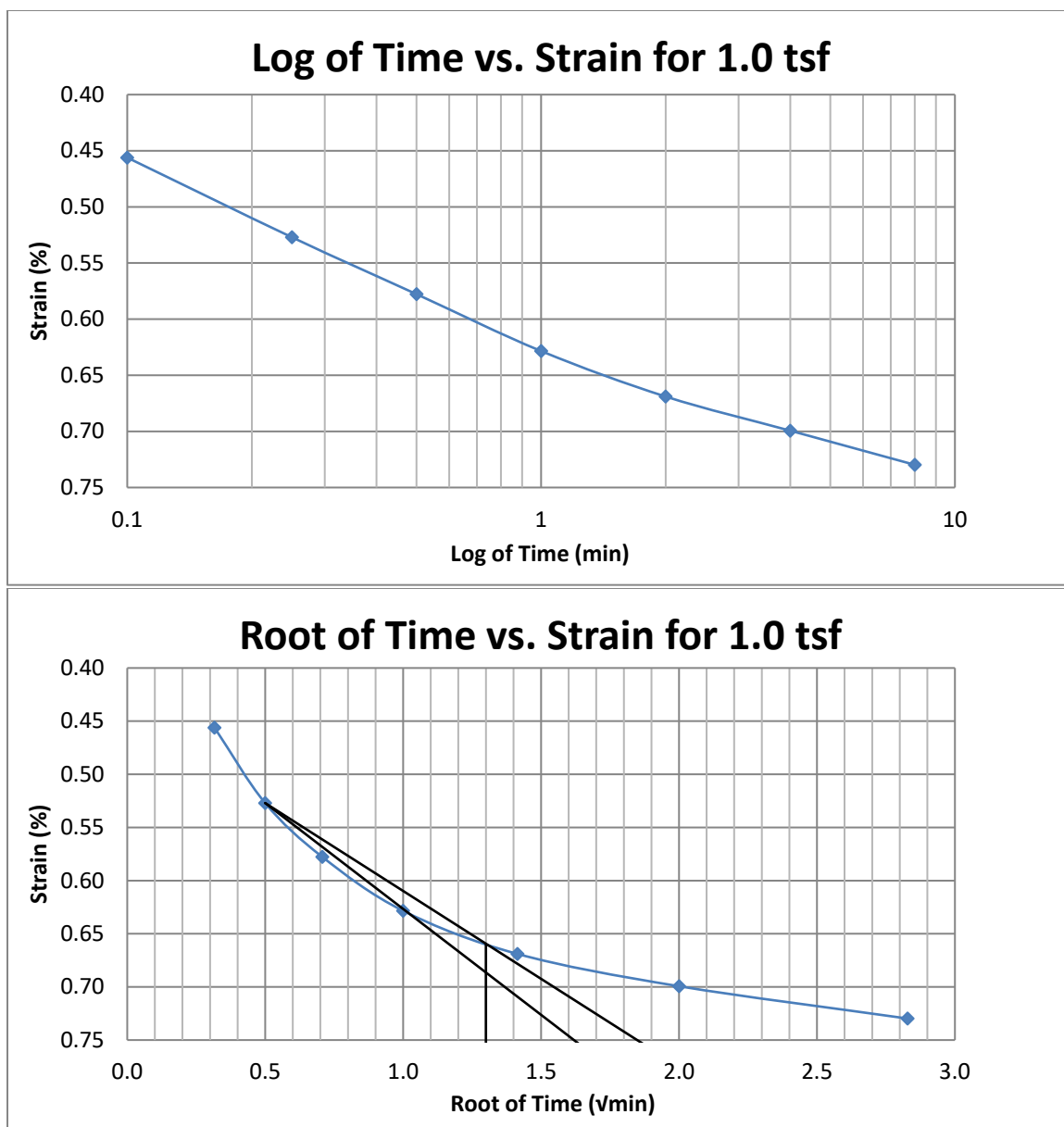


Figure A190 Provo at 12-14 feet

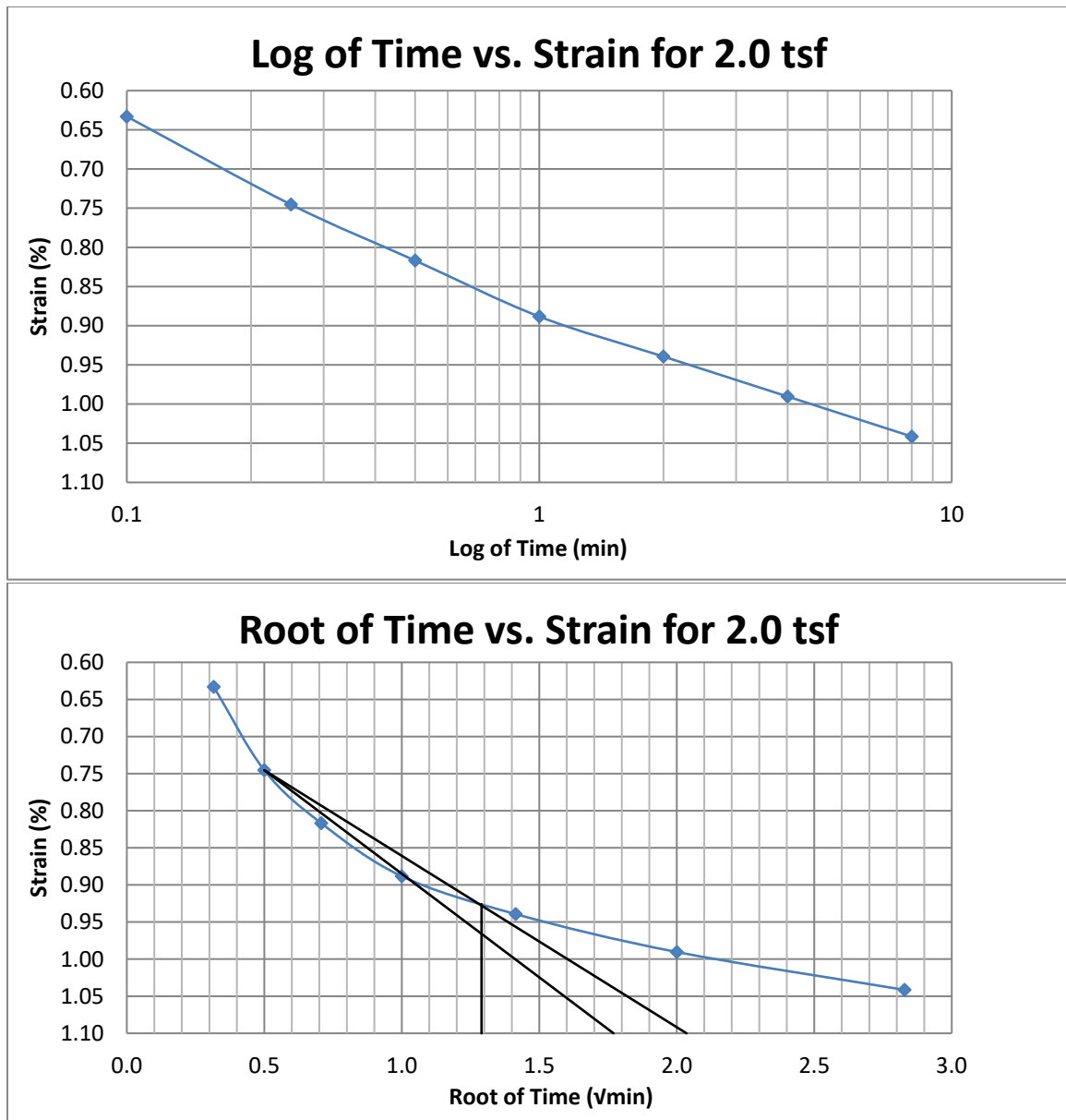


Figure A191 Provo at 12-14 feet

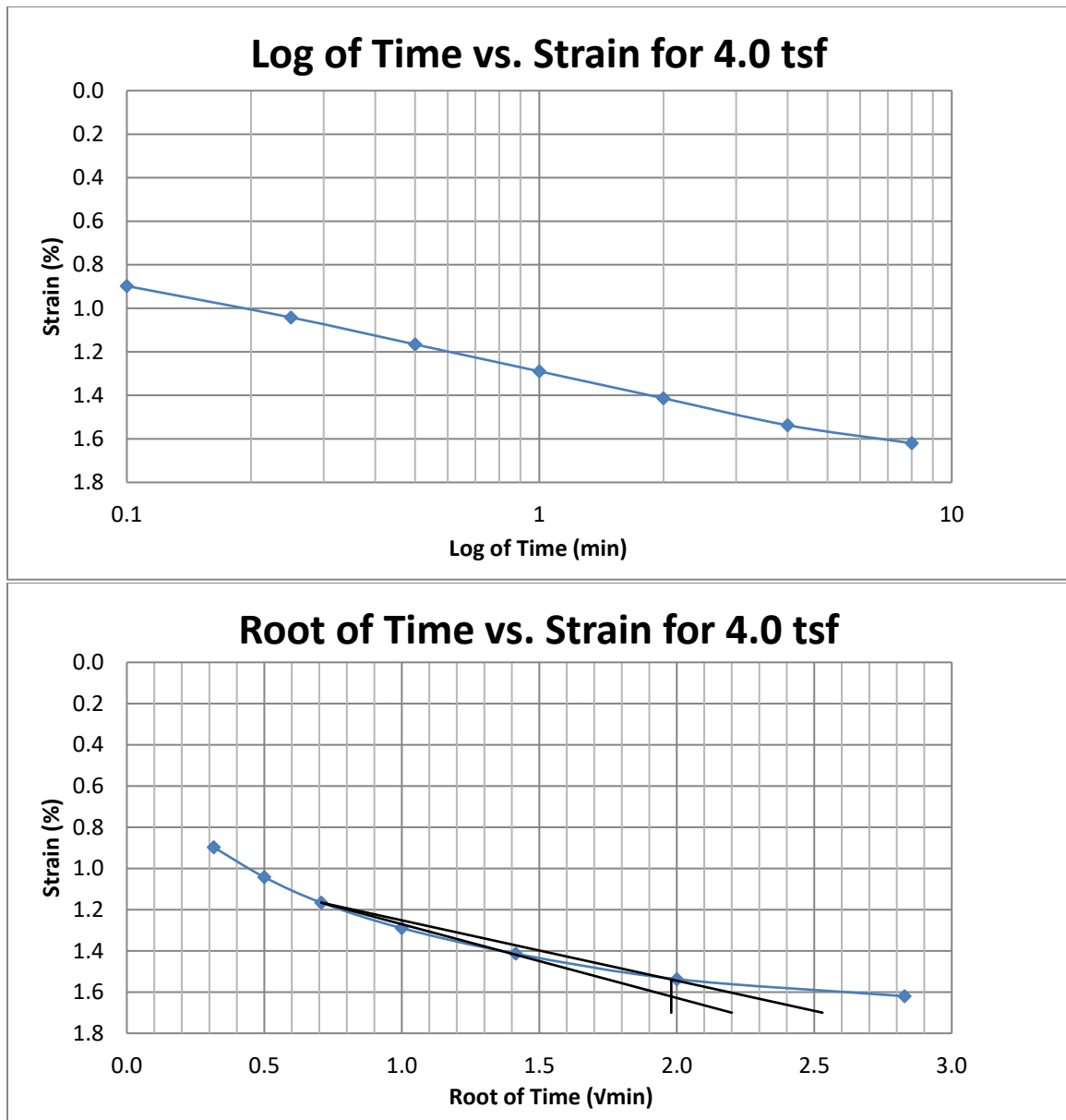


Figure A192 Provo at 12-14 feet

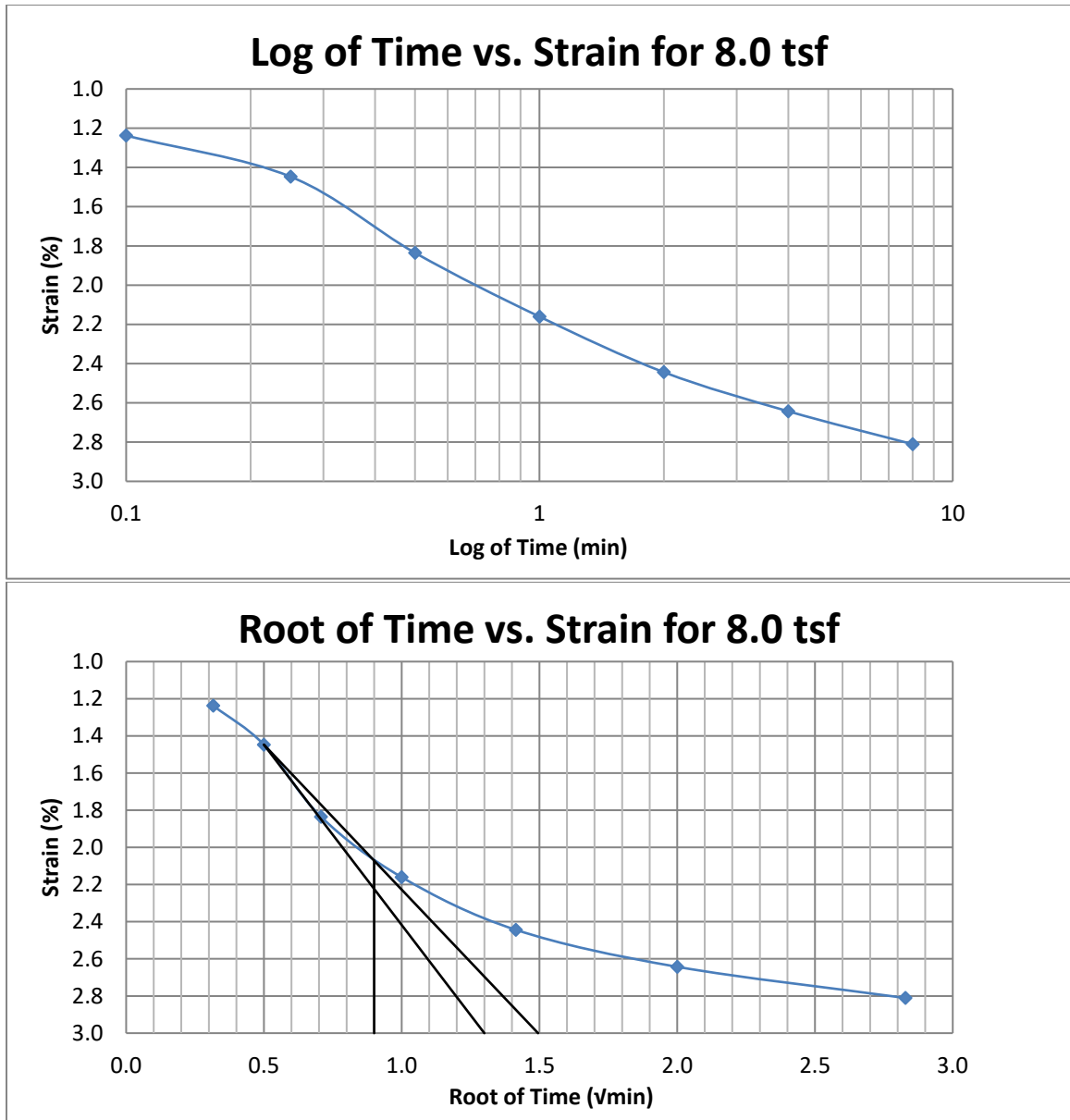


Figure A193 Provo at 12-14 feet

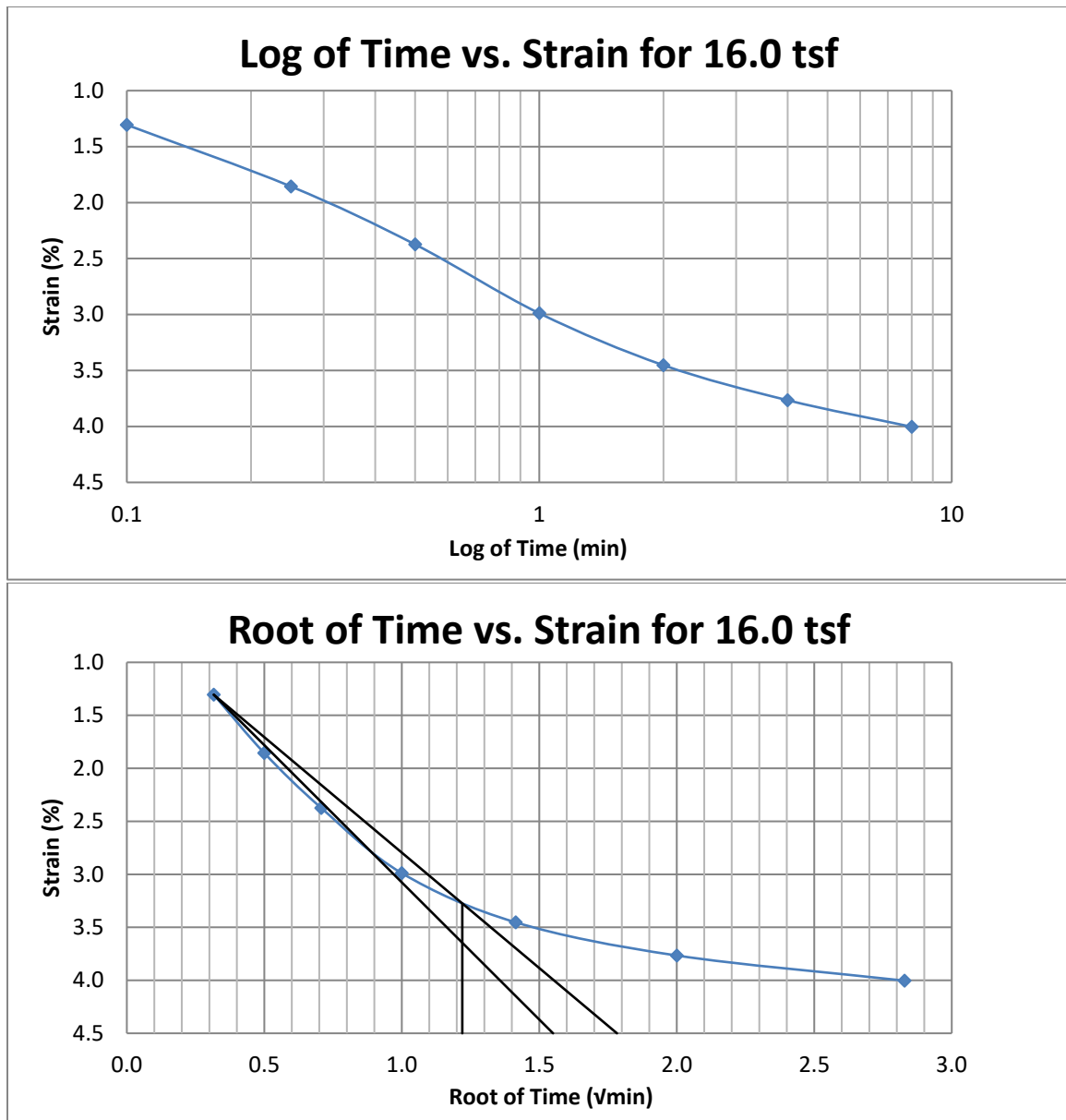


Figure A194 Provo at 12-14 feet



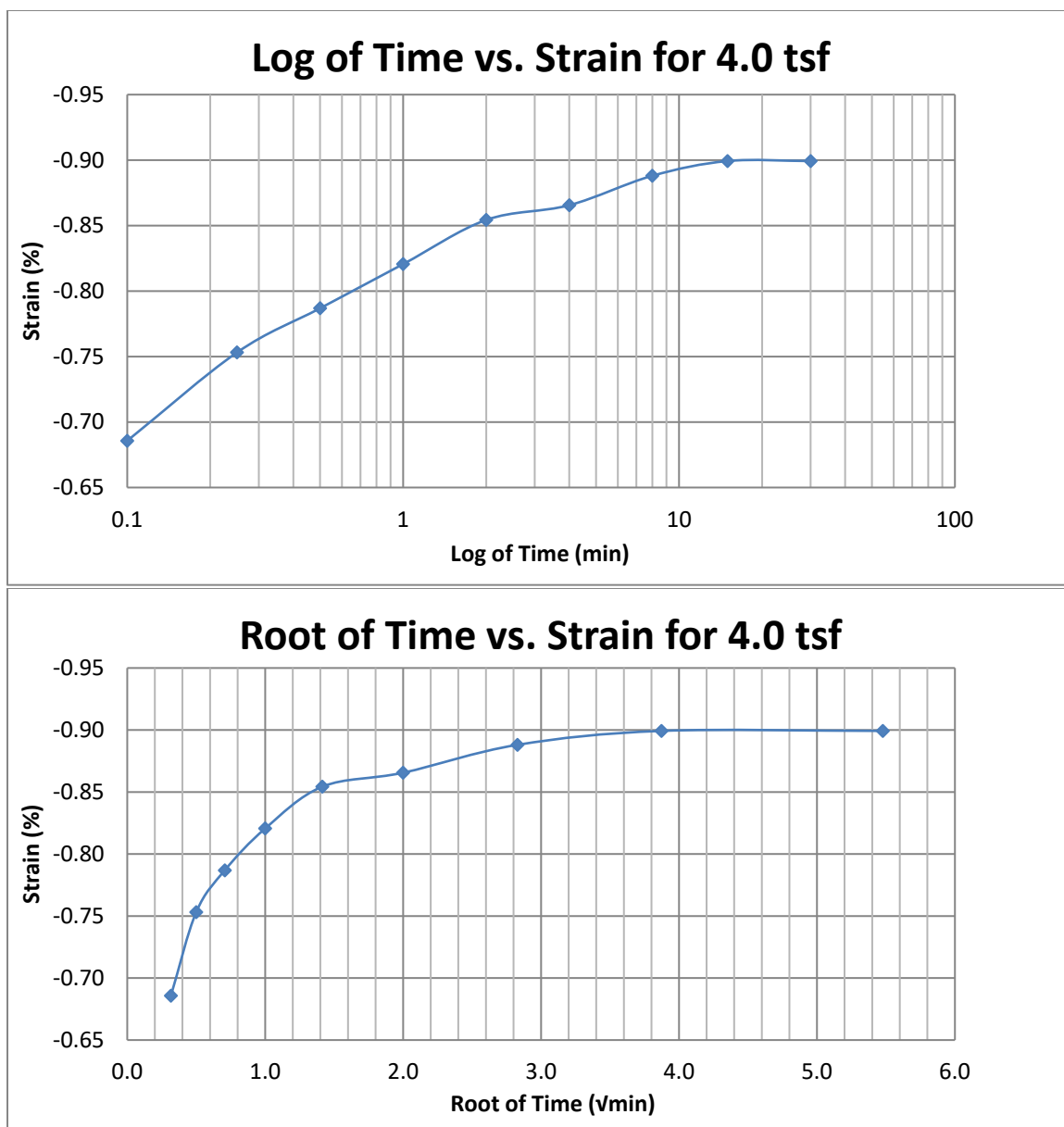
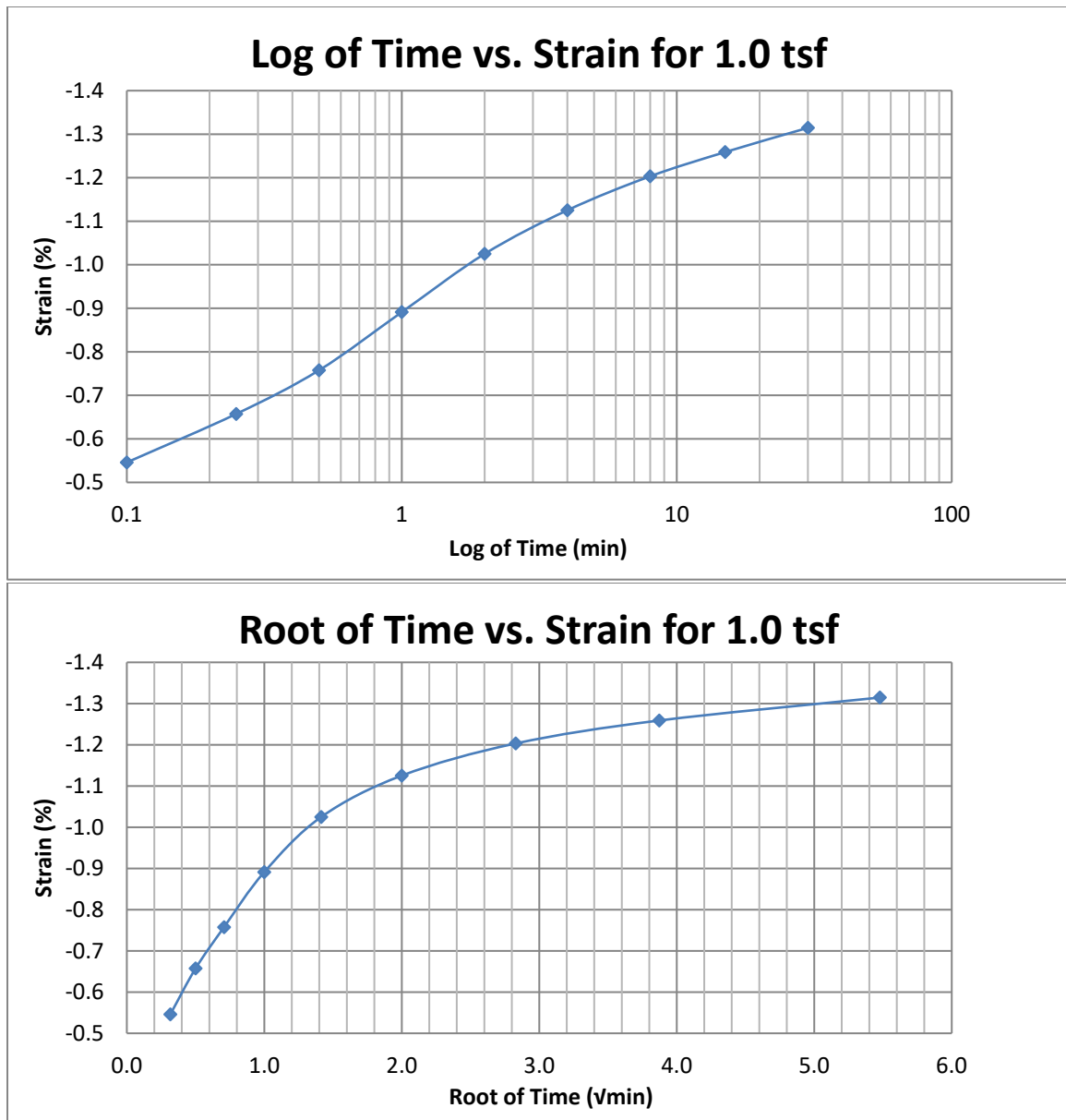


Figure A195 Provo at 12-14 feet



**Figure A196 Provo at 12-14 feet**

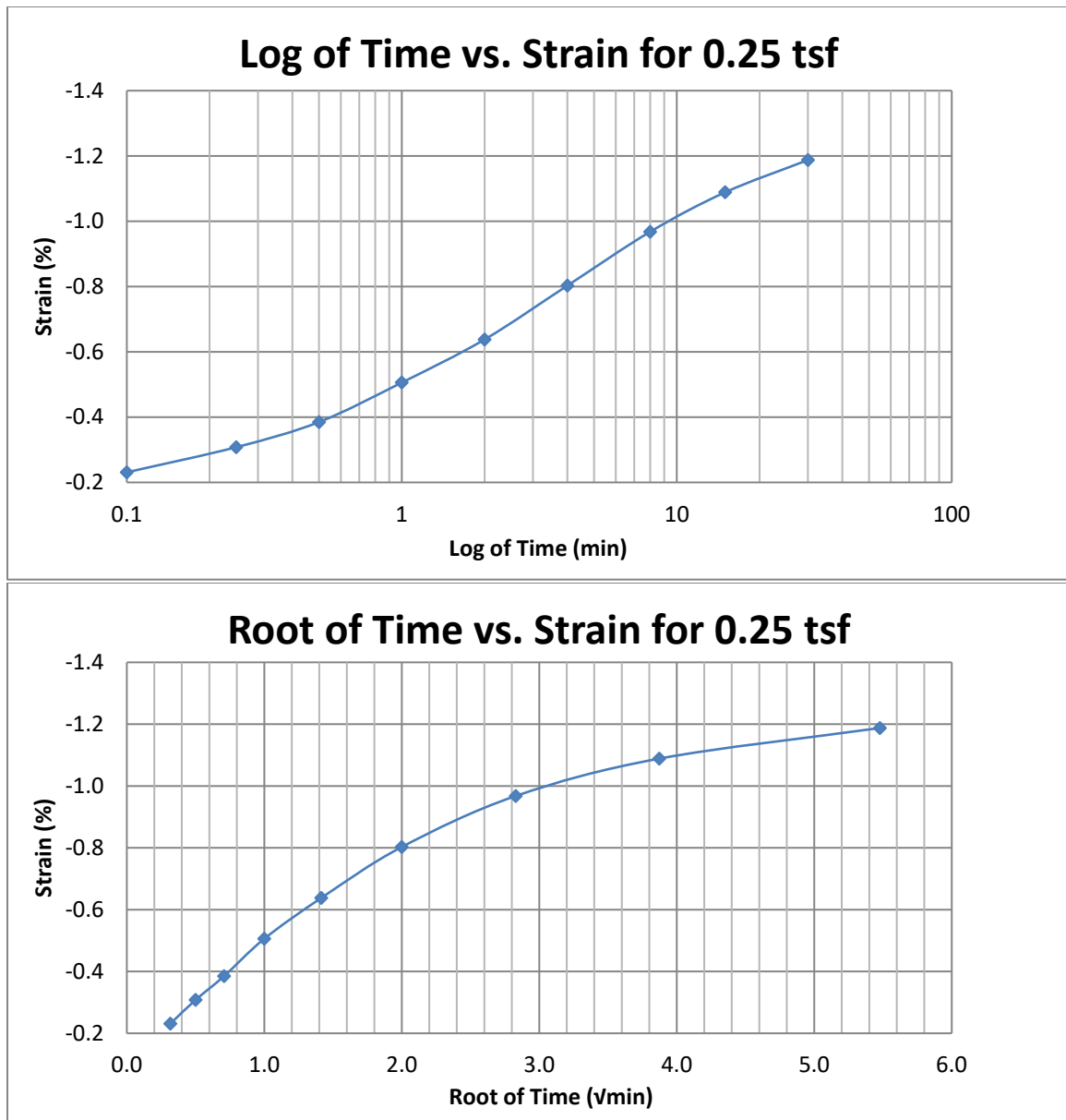


Figure A197 Provo at 12-14 feet

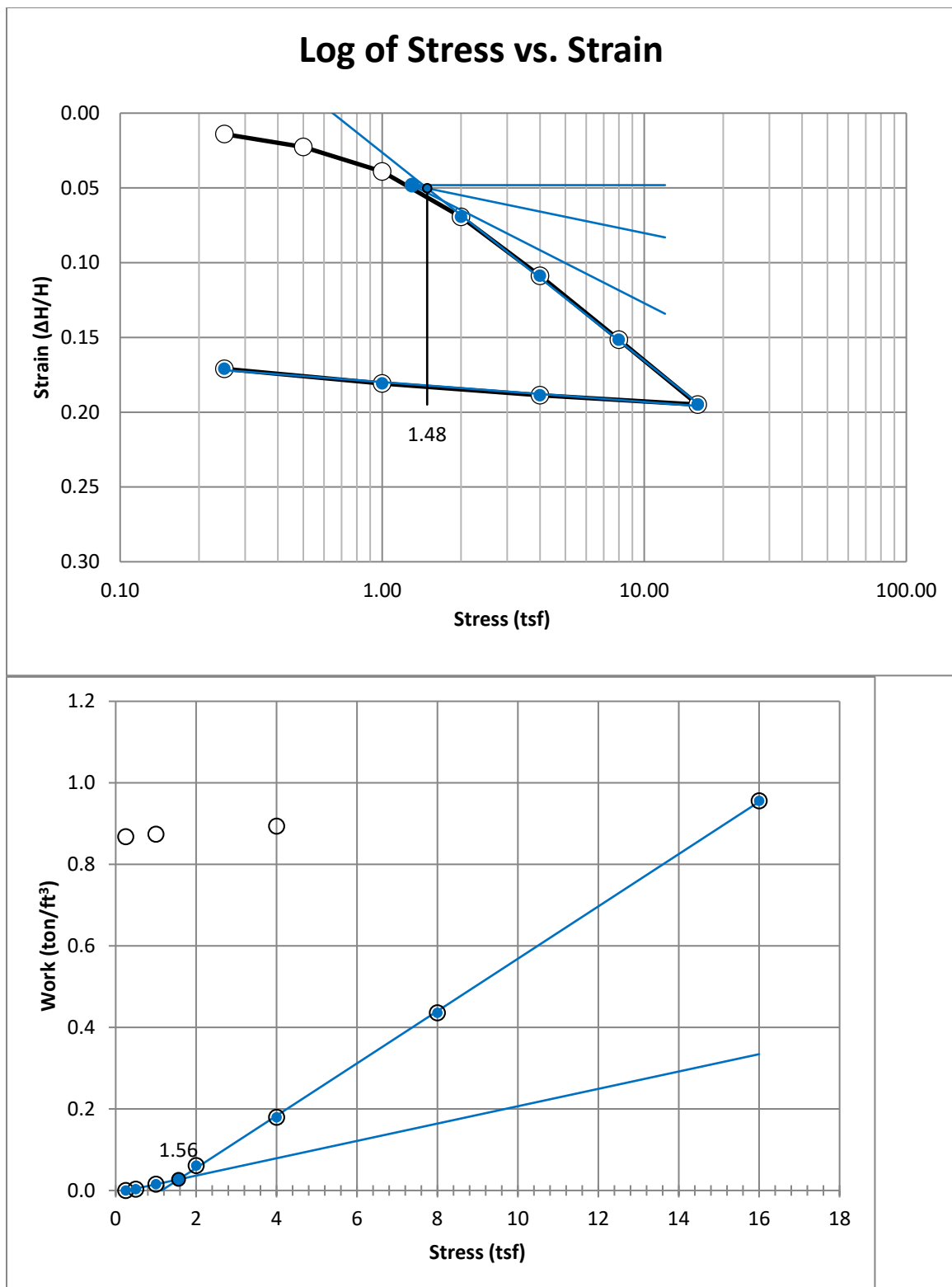


Figure A198 Provo at 17-19 feet

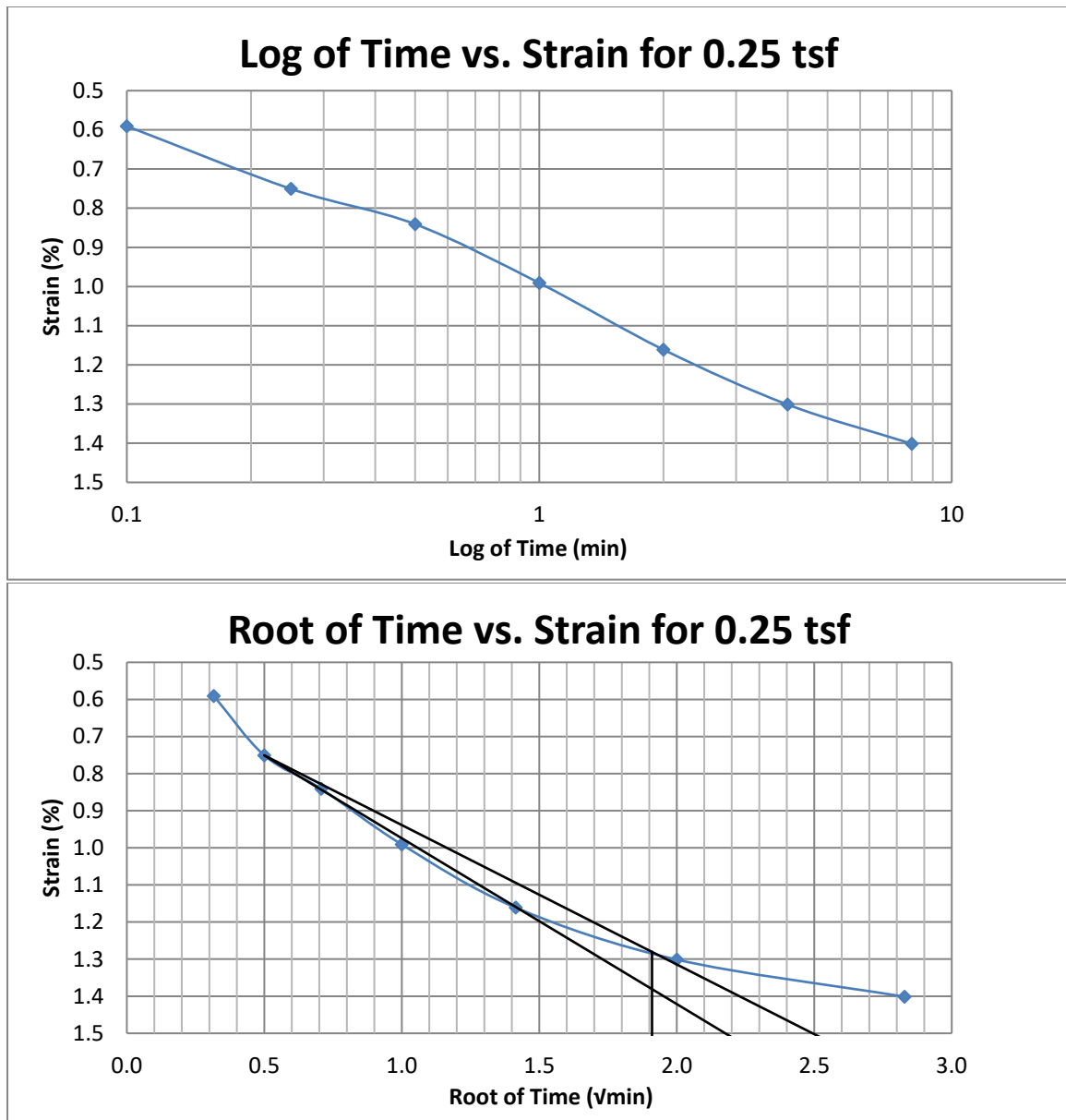


Figure A199 Provo at 17-19 feet

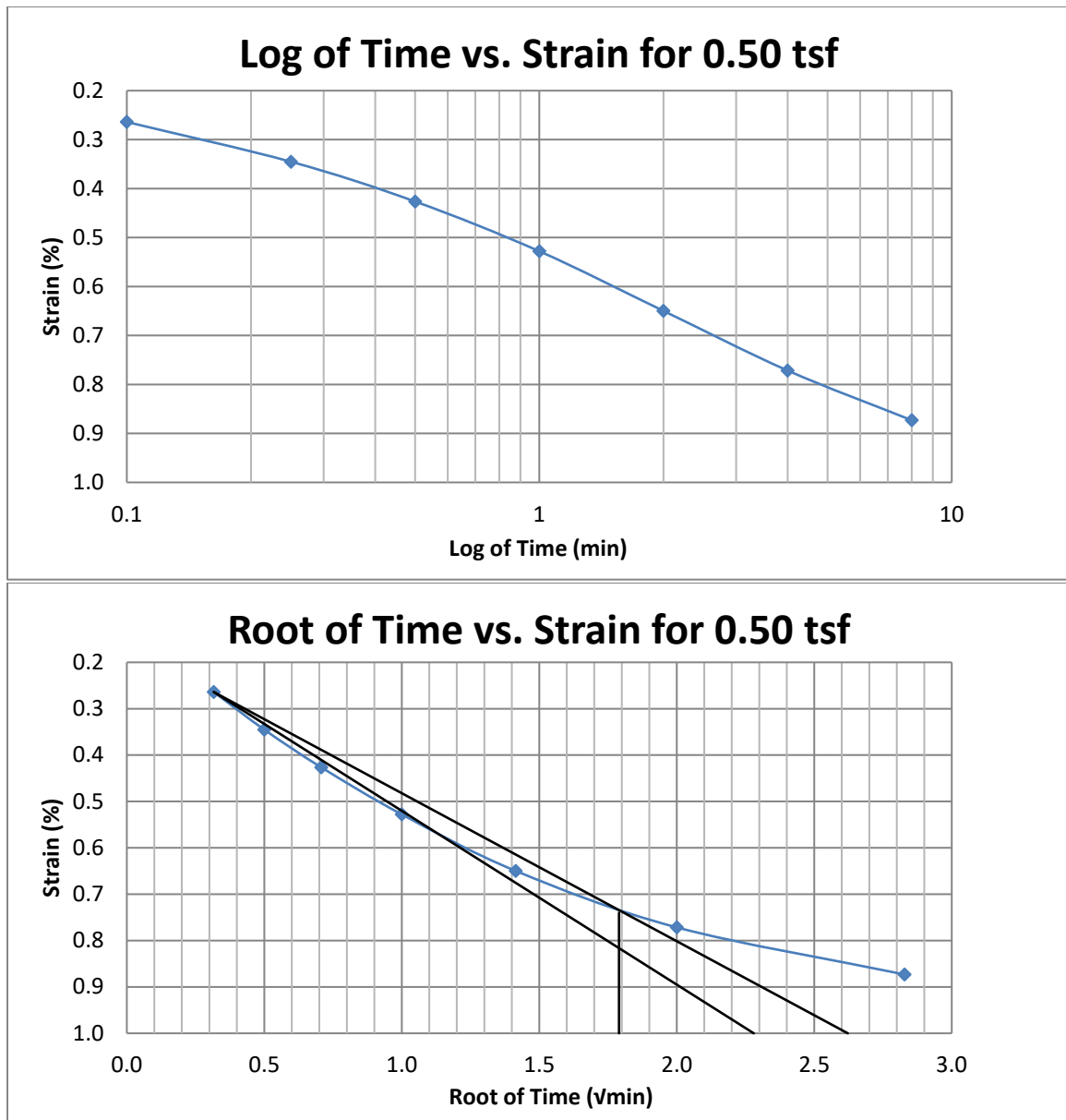


Figure A200 Provo at 17-19 feet

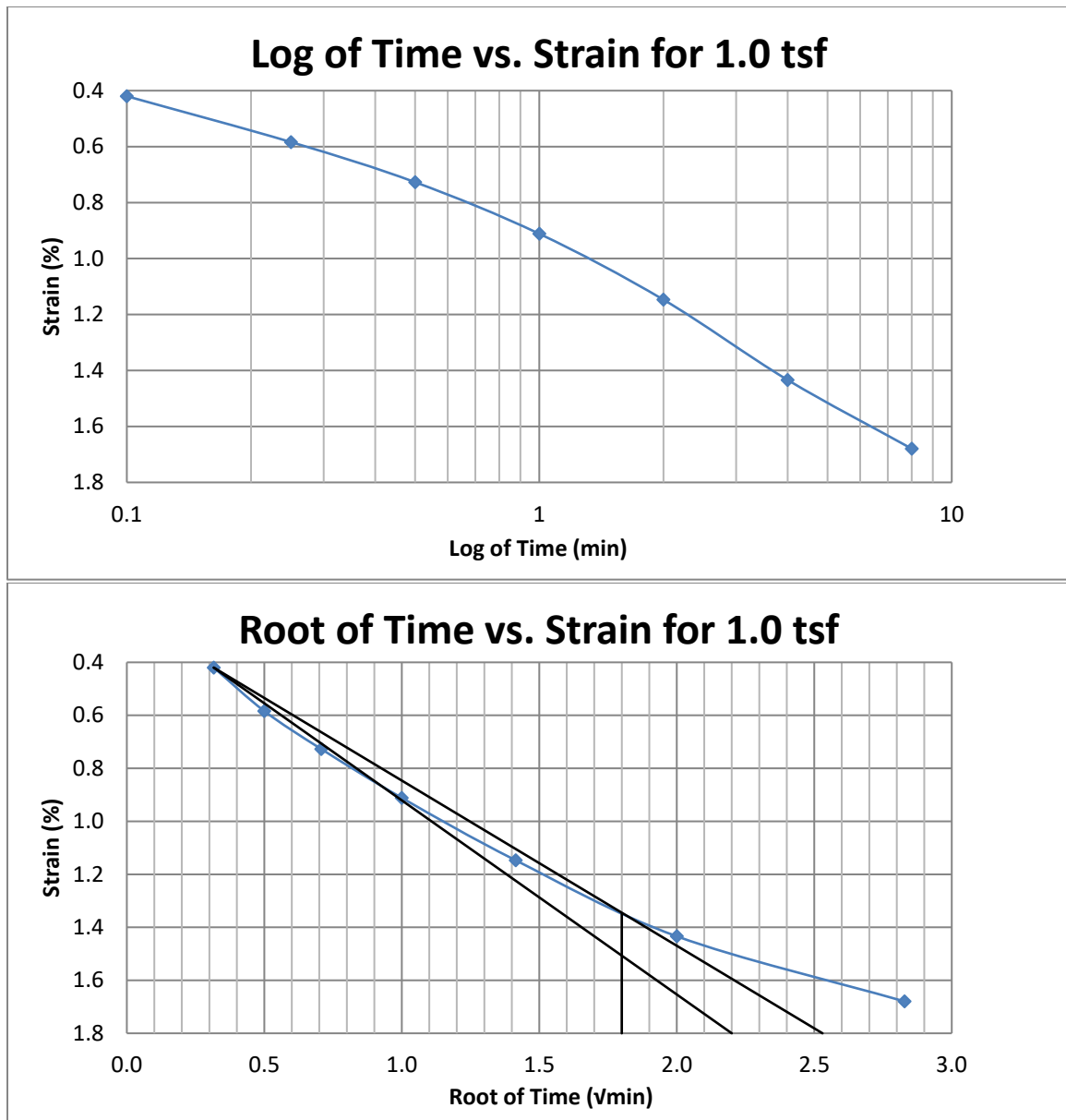


Figure A201 Provo at 17-19 feet

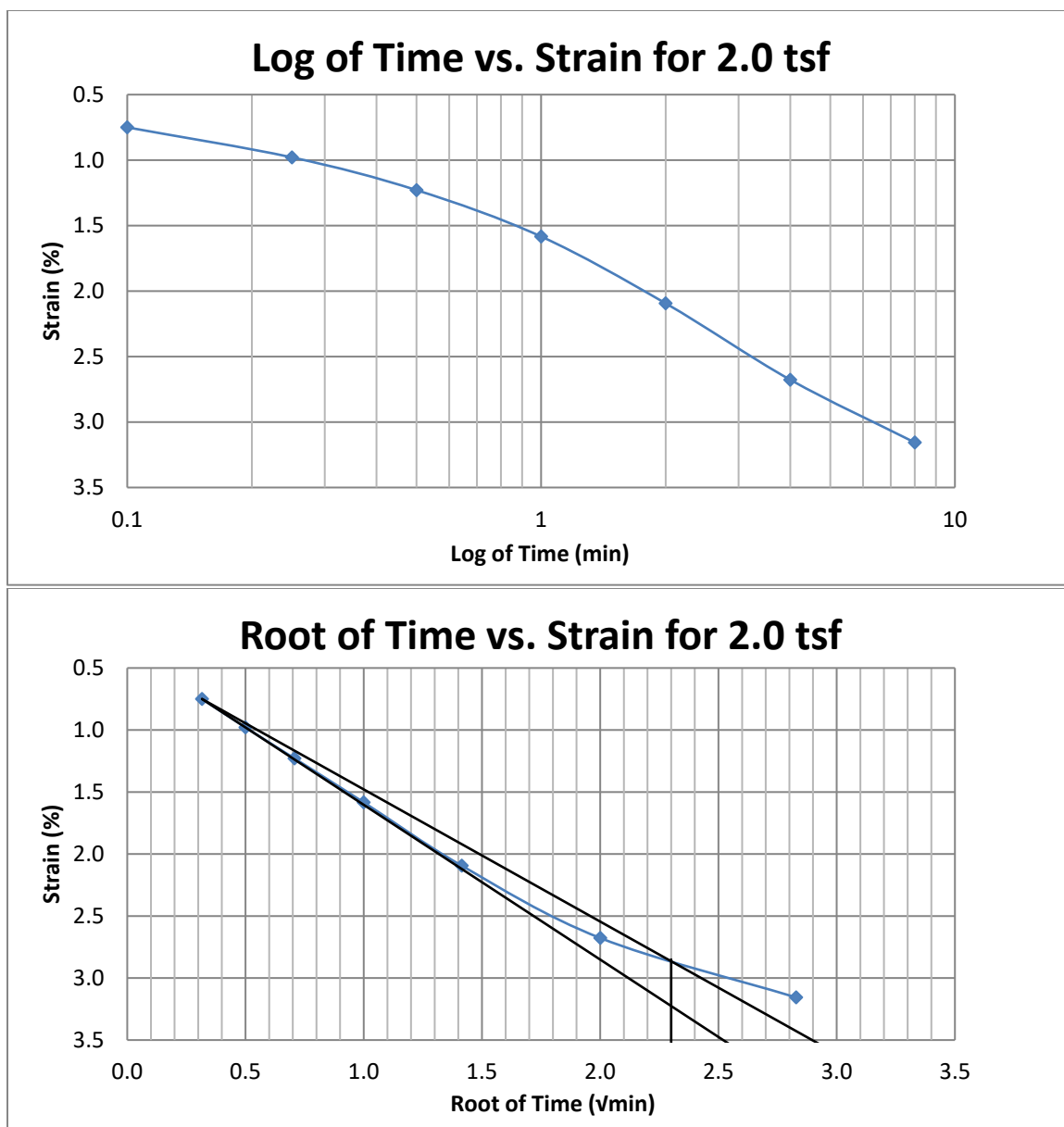


Figure A202 Provo at 17-19 feet



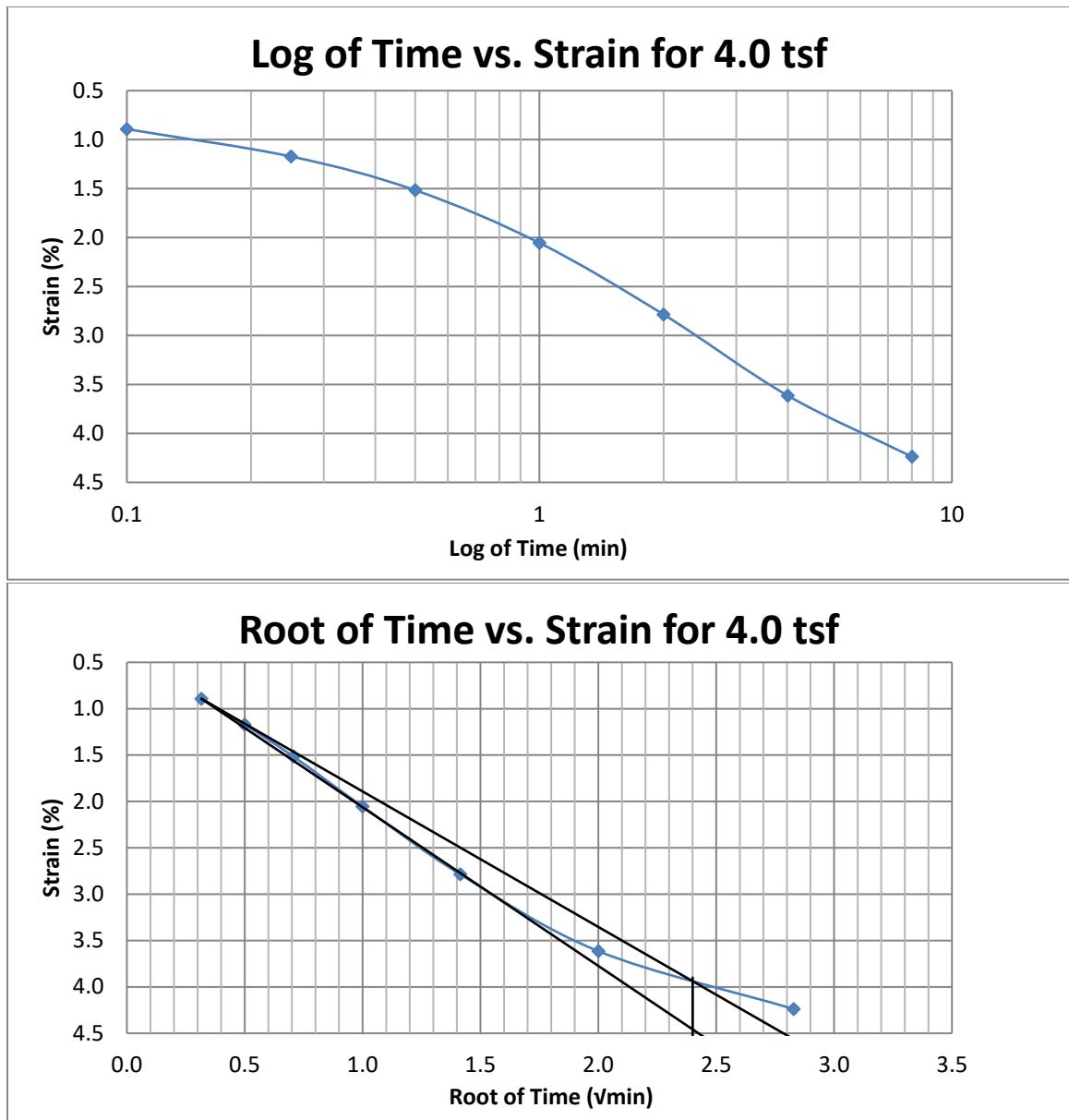


Figure A203 Provo at 17-19 feet

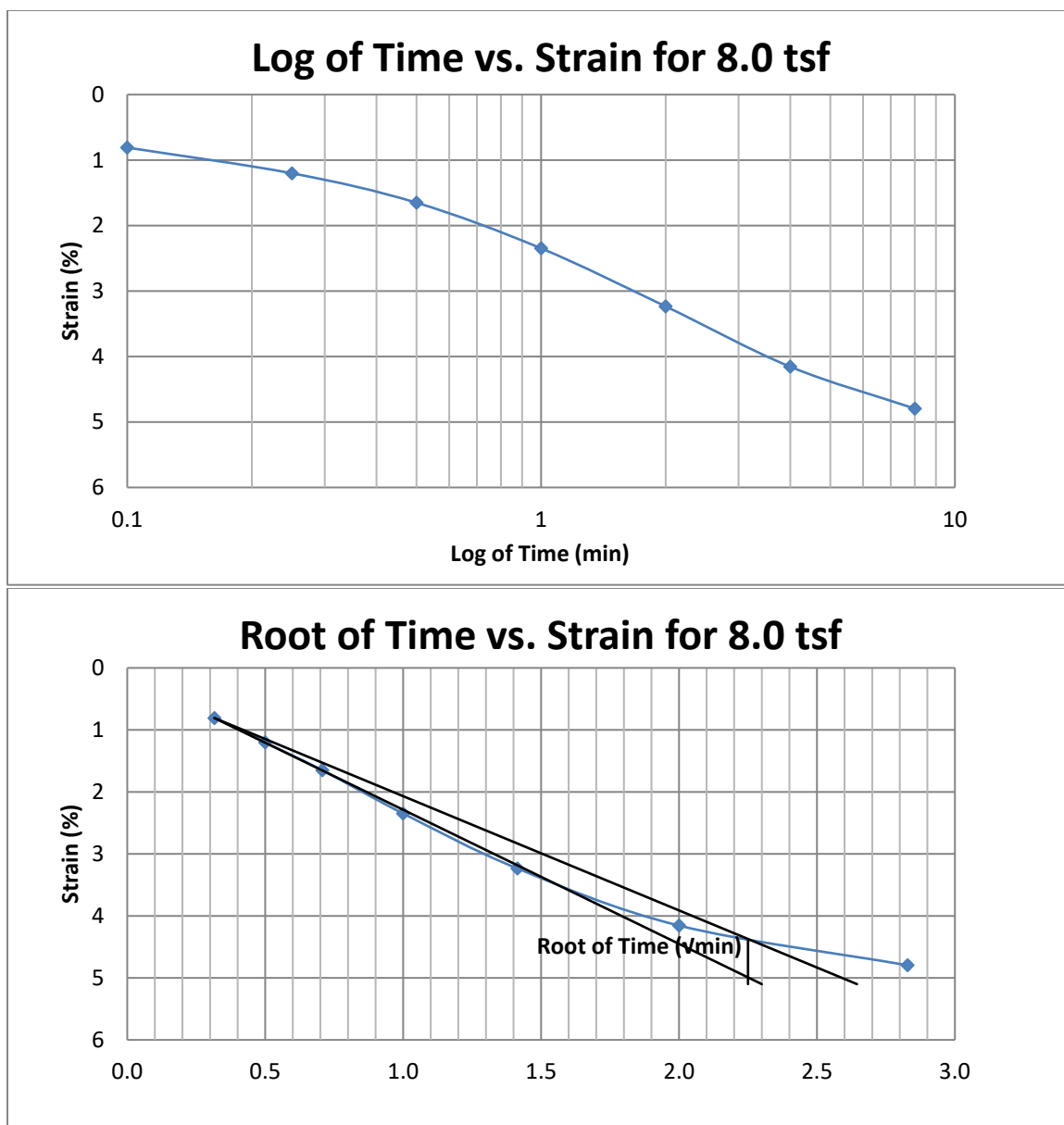


Figure A204 Provo at 17-19 feet

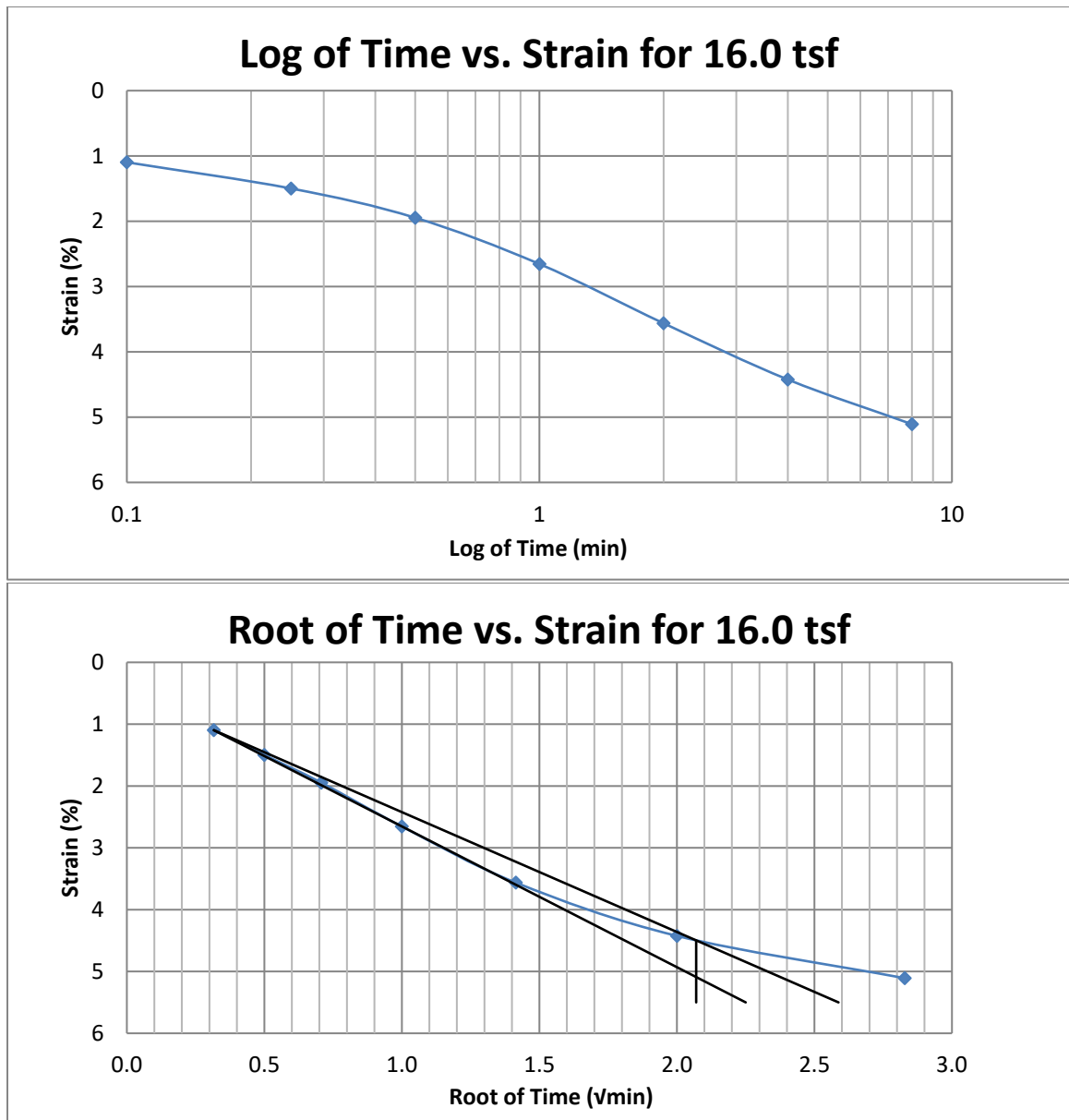


Figure A205 Provo at 17-19 feet

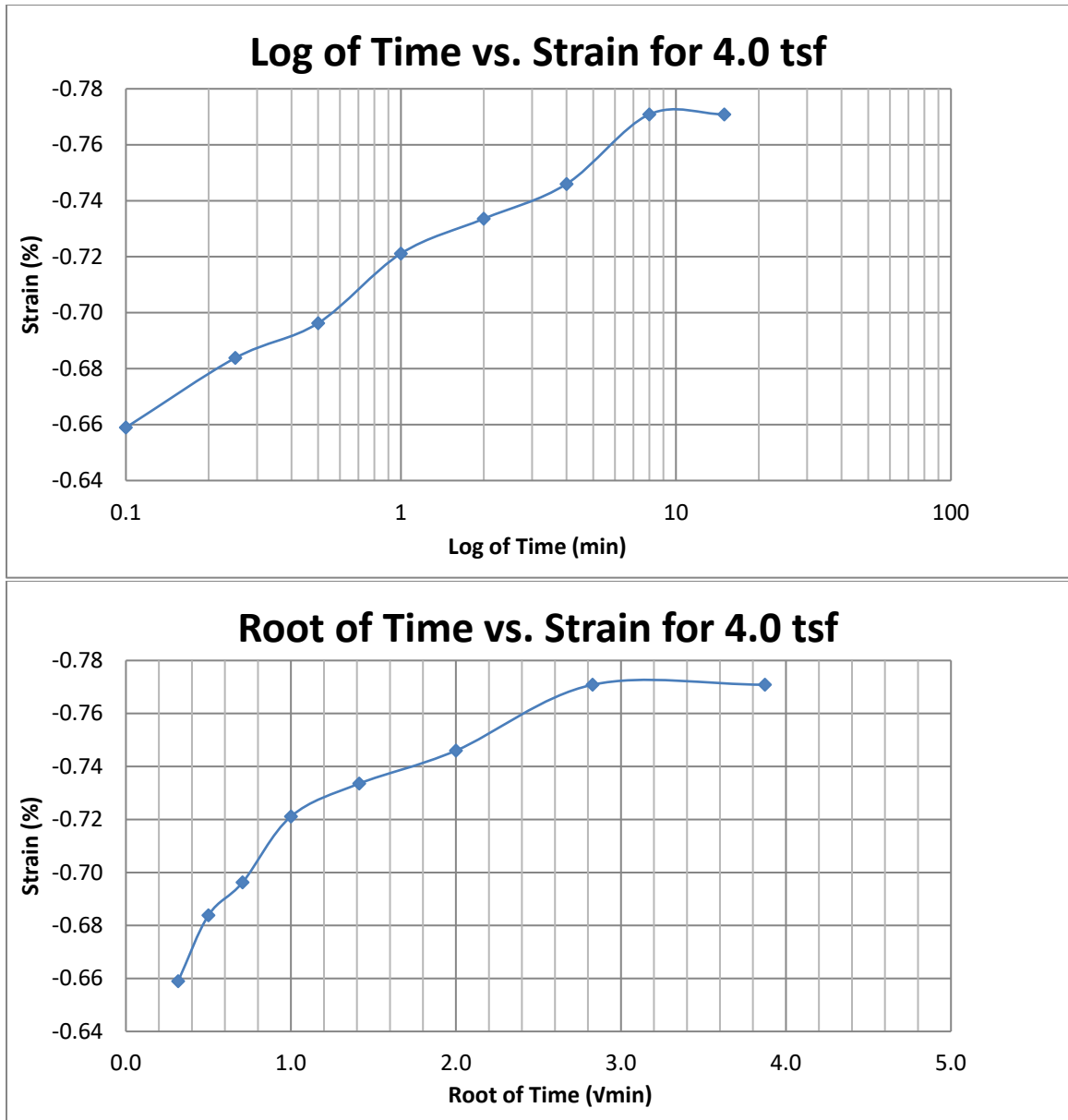


Figure A206 Provo at 17-19 feet

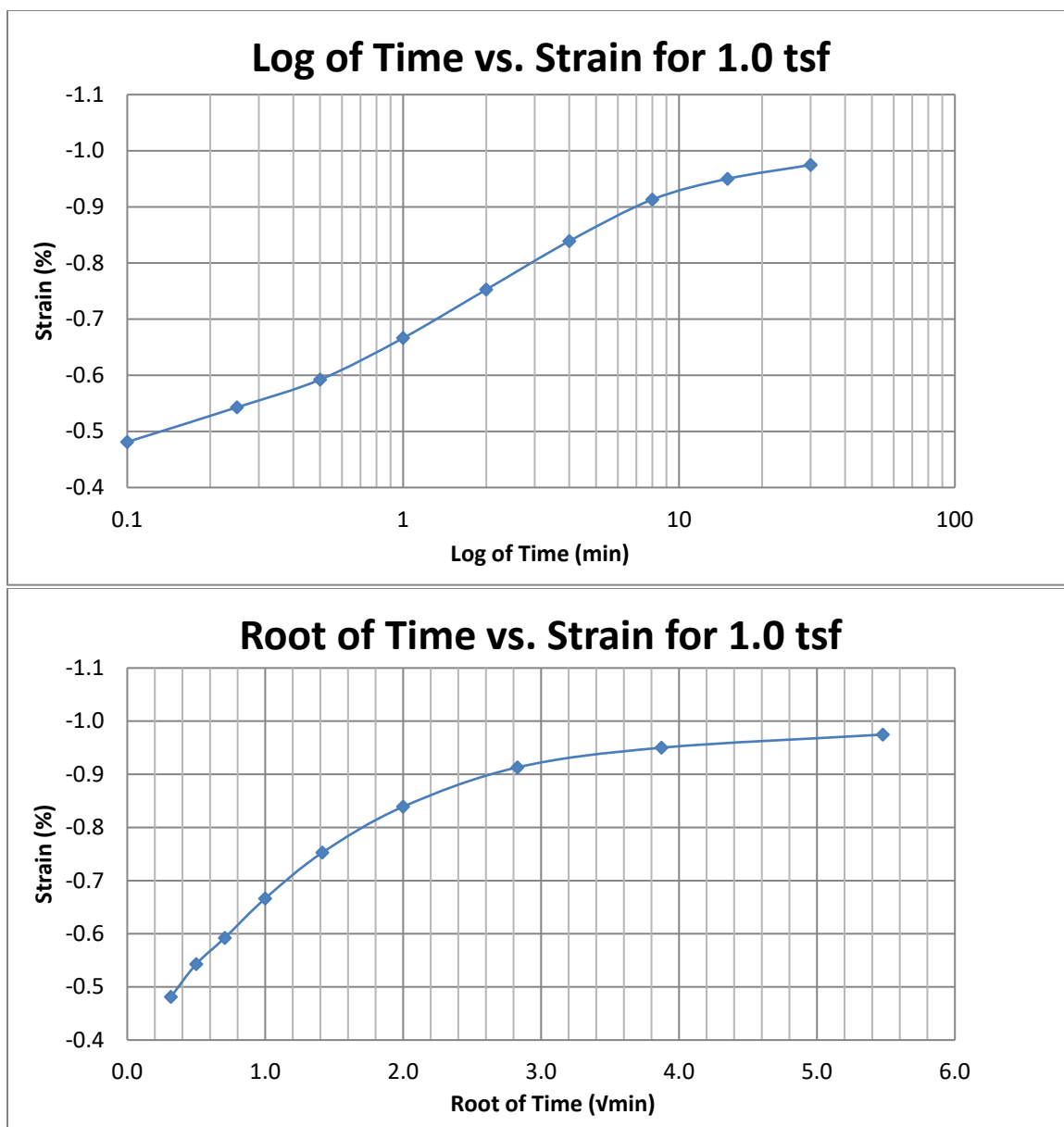


Figure A207 Provo at 17-19 feet

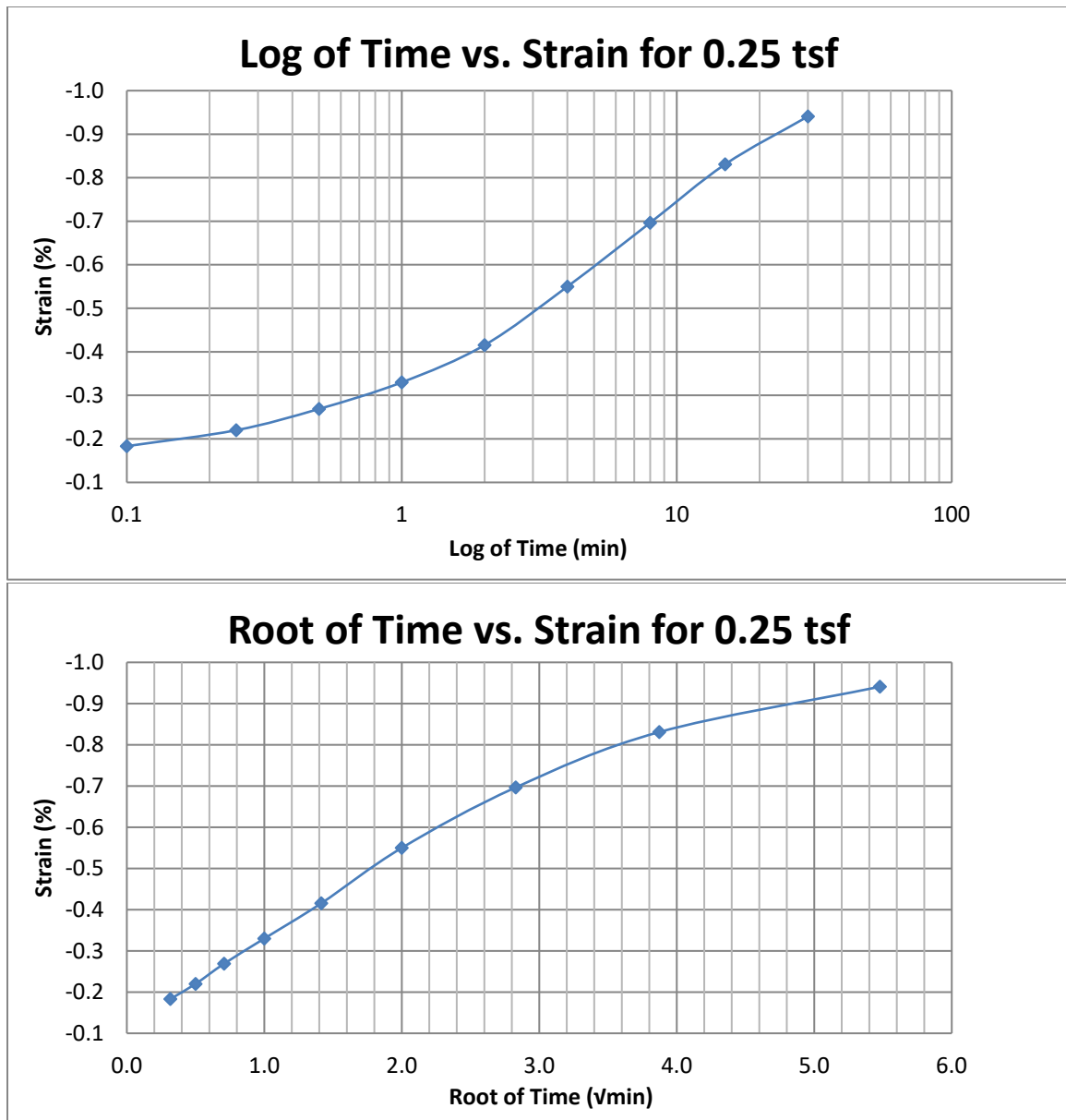
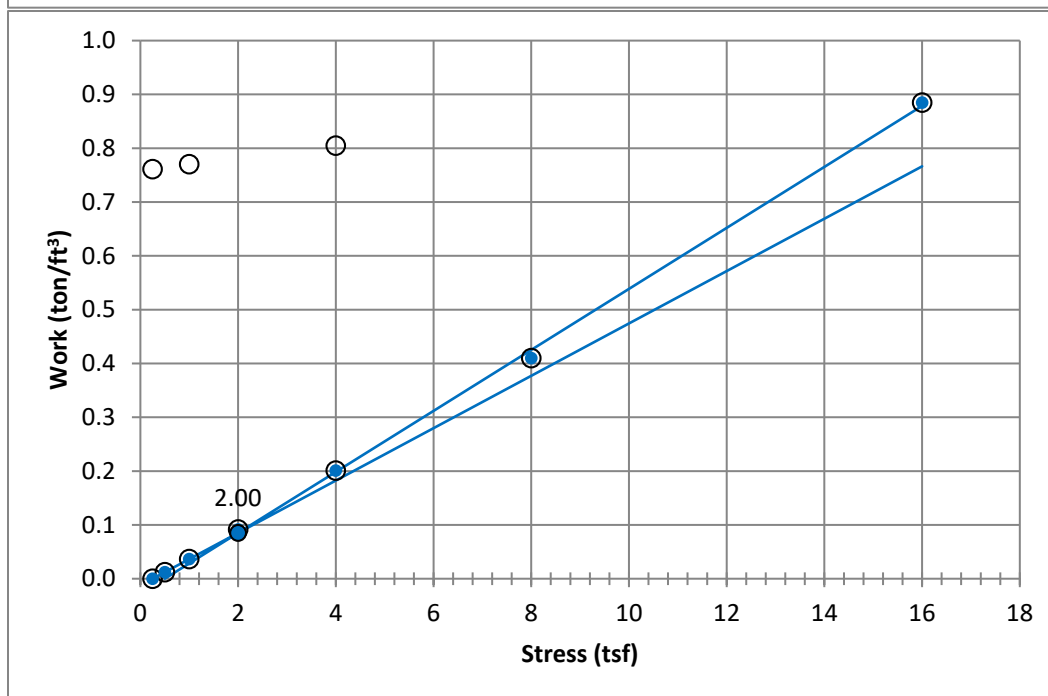
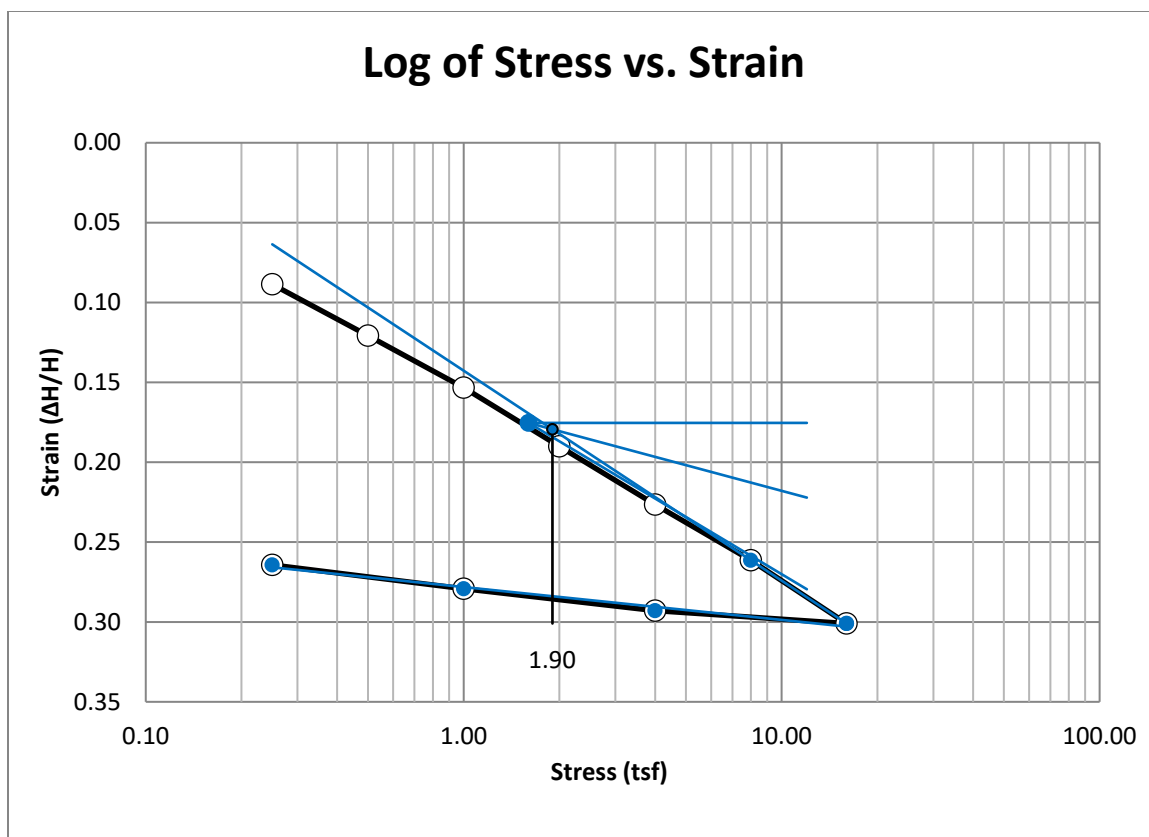


Figure A208 Provo at 17-19 feet



**Figure A209 Provo at 50-52 feet**

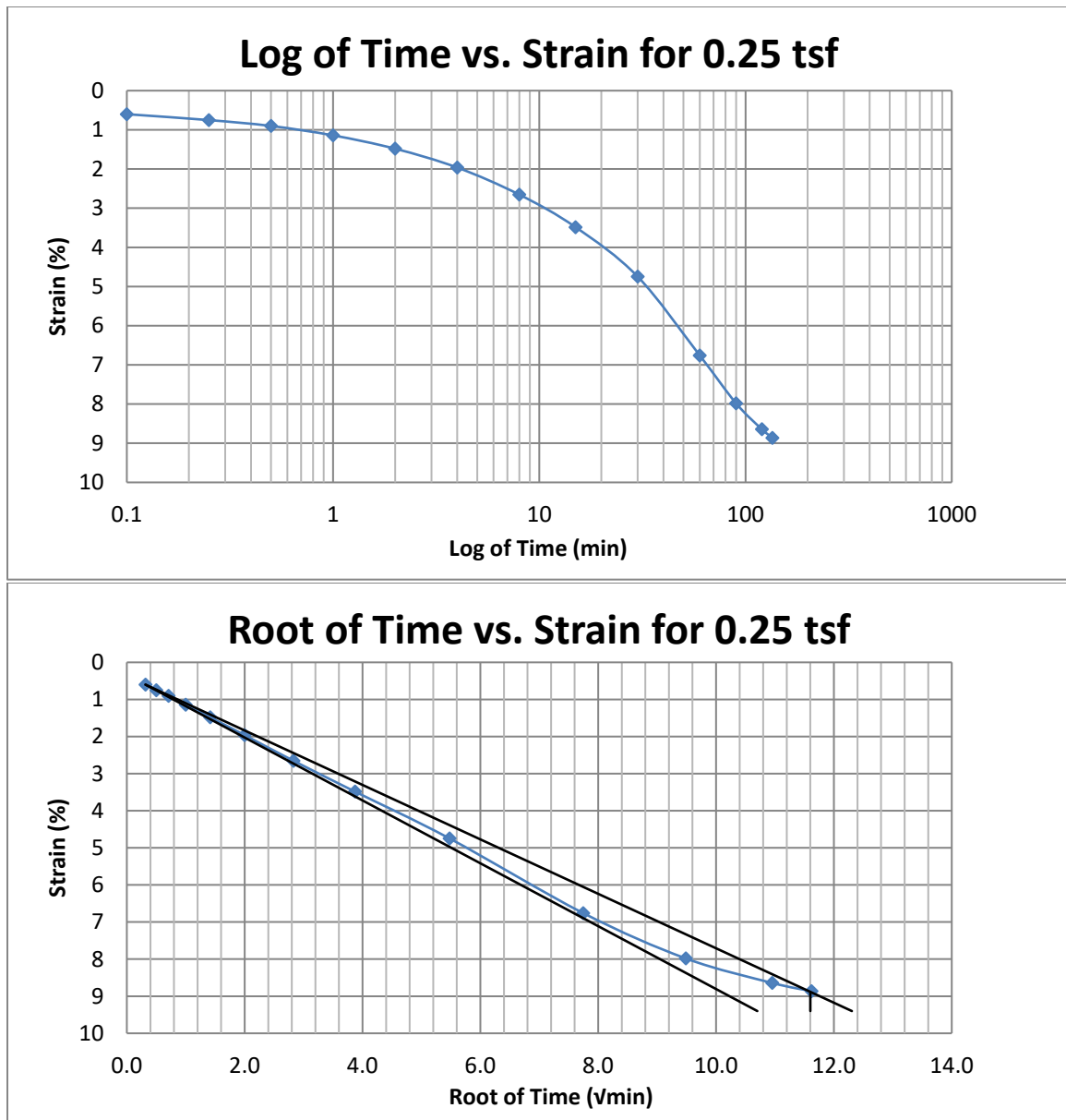


Figure A210 Provo at 50-52 feet



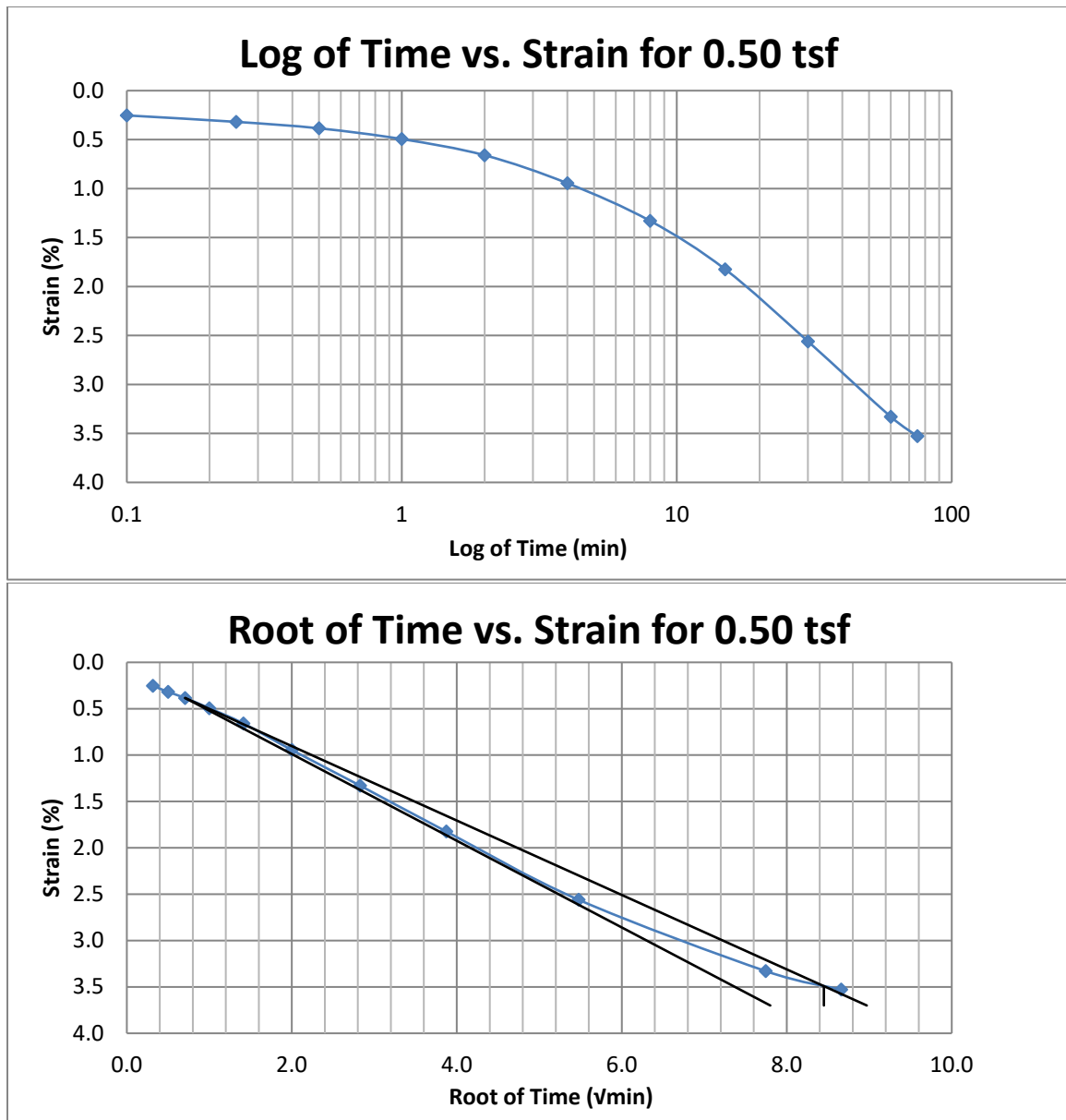


Figure A211 Provo at 50-52 feet

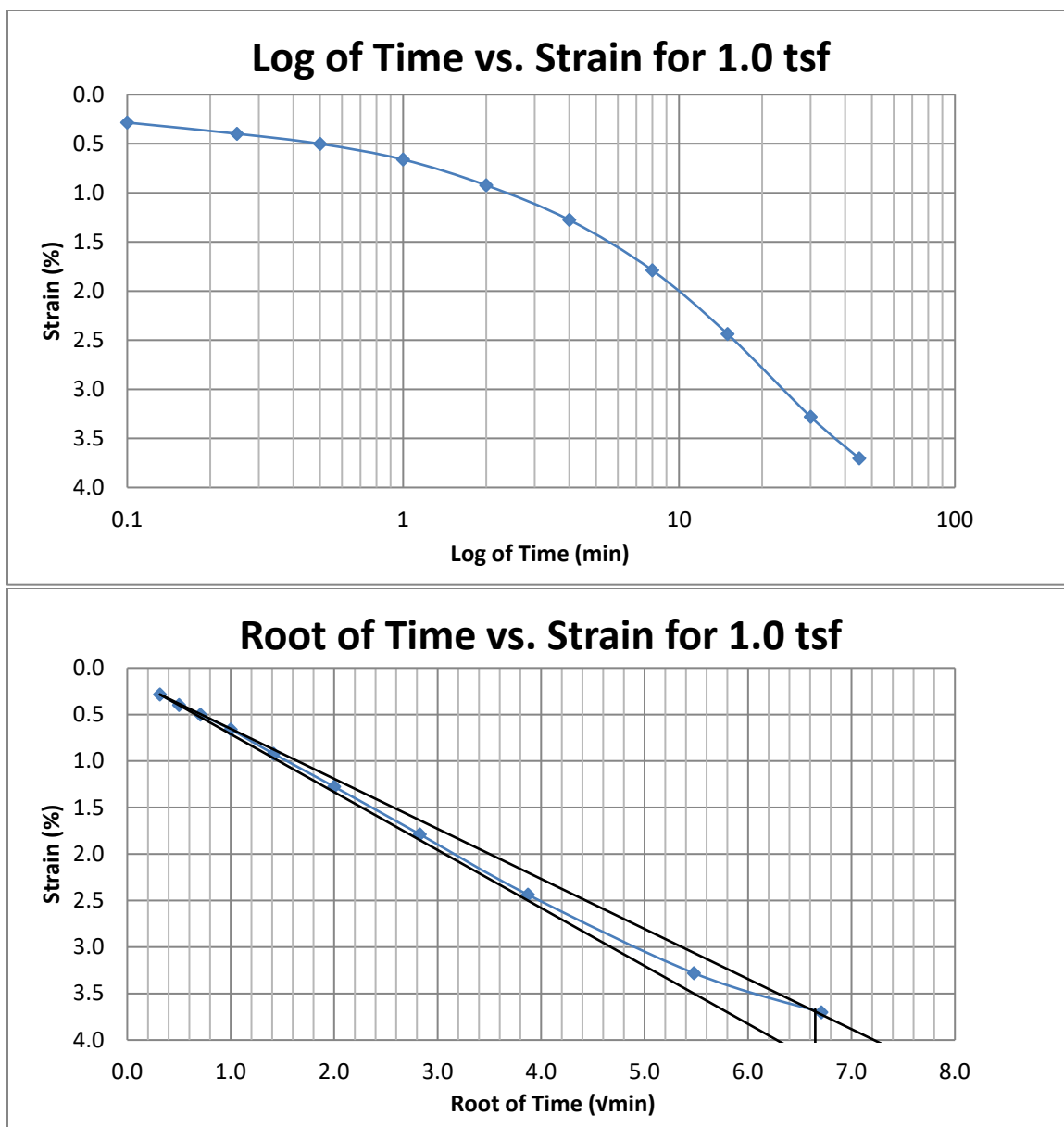


Figure A212 Provo at 50-52 feet

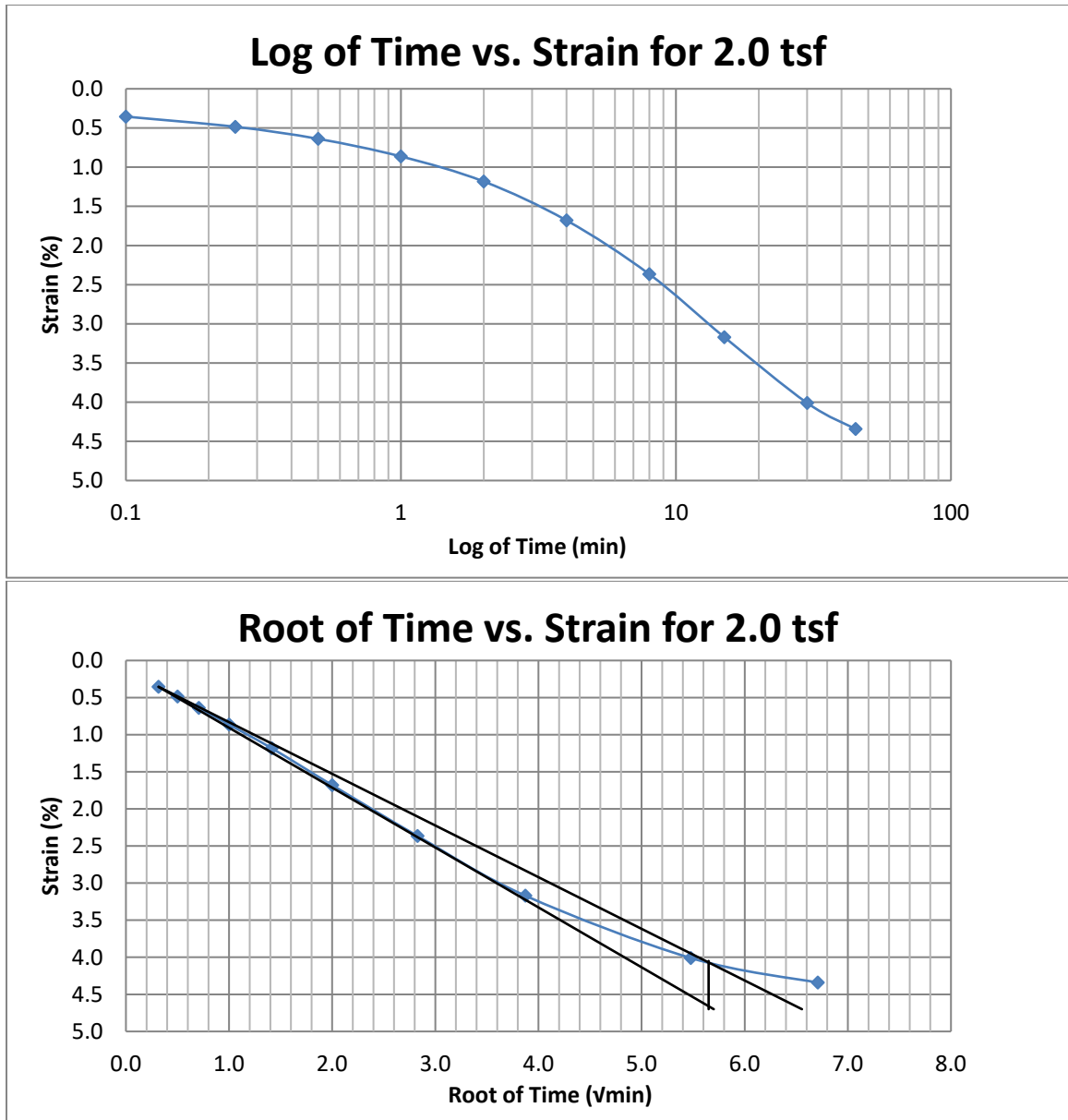


Figure A213 Provo at 50-52 feet

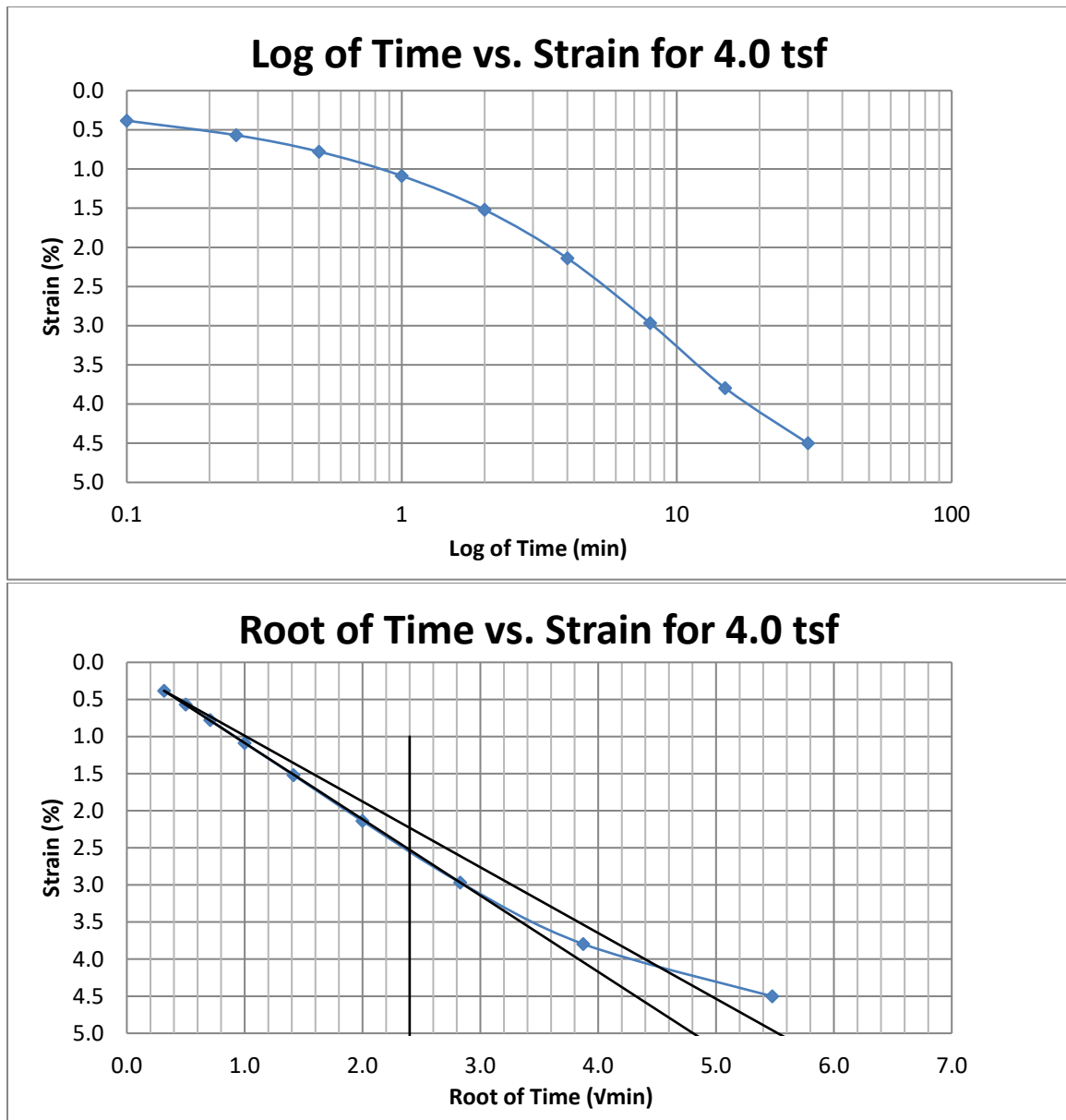
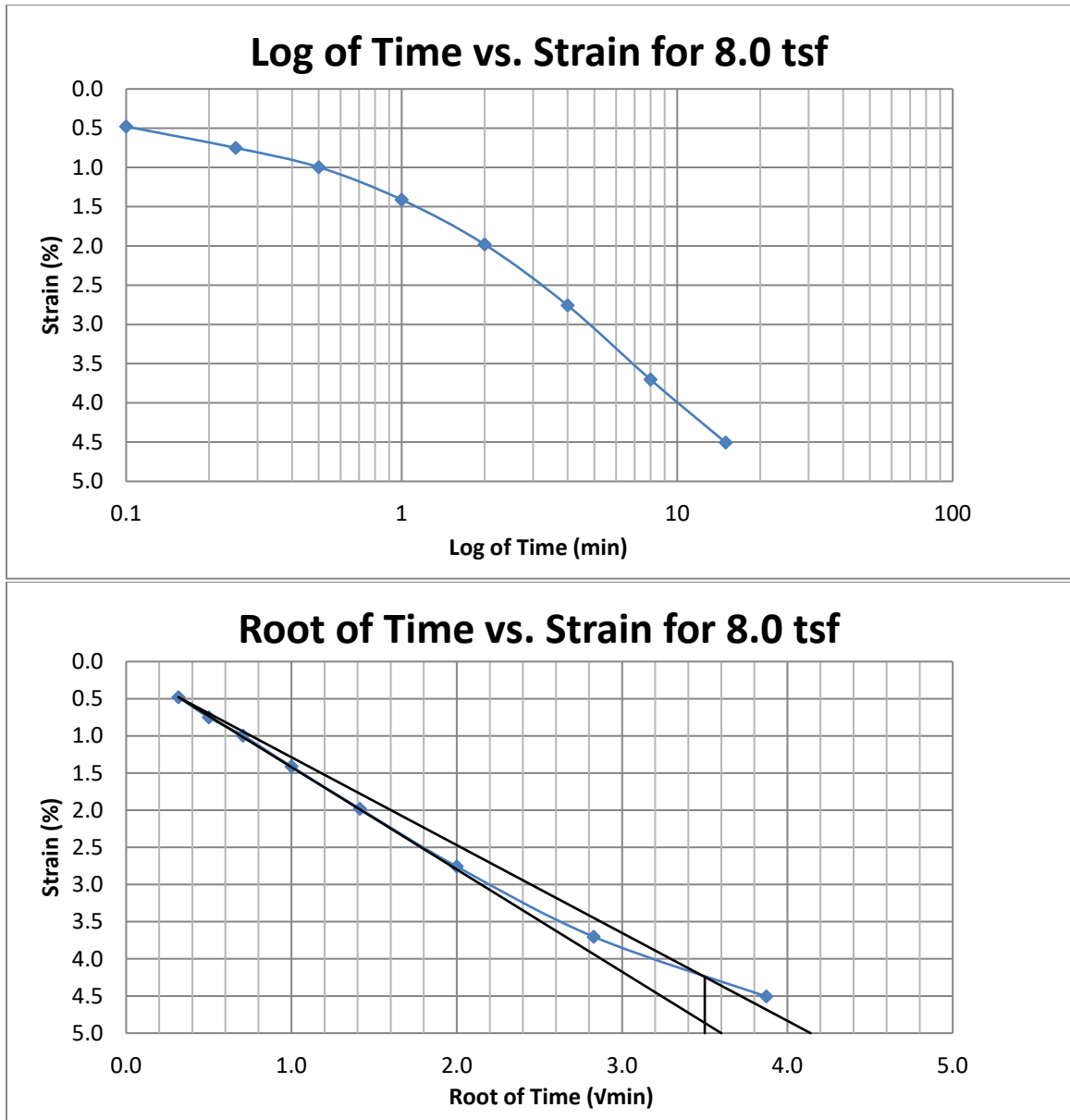


Figure A214 Provo at 50-52 feet



**Figure A215 Provo at 50-52 feet**

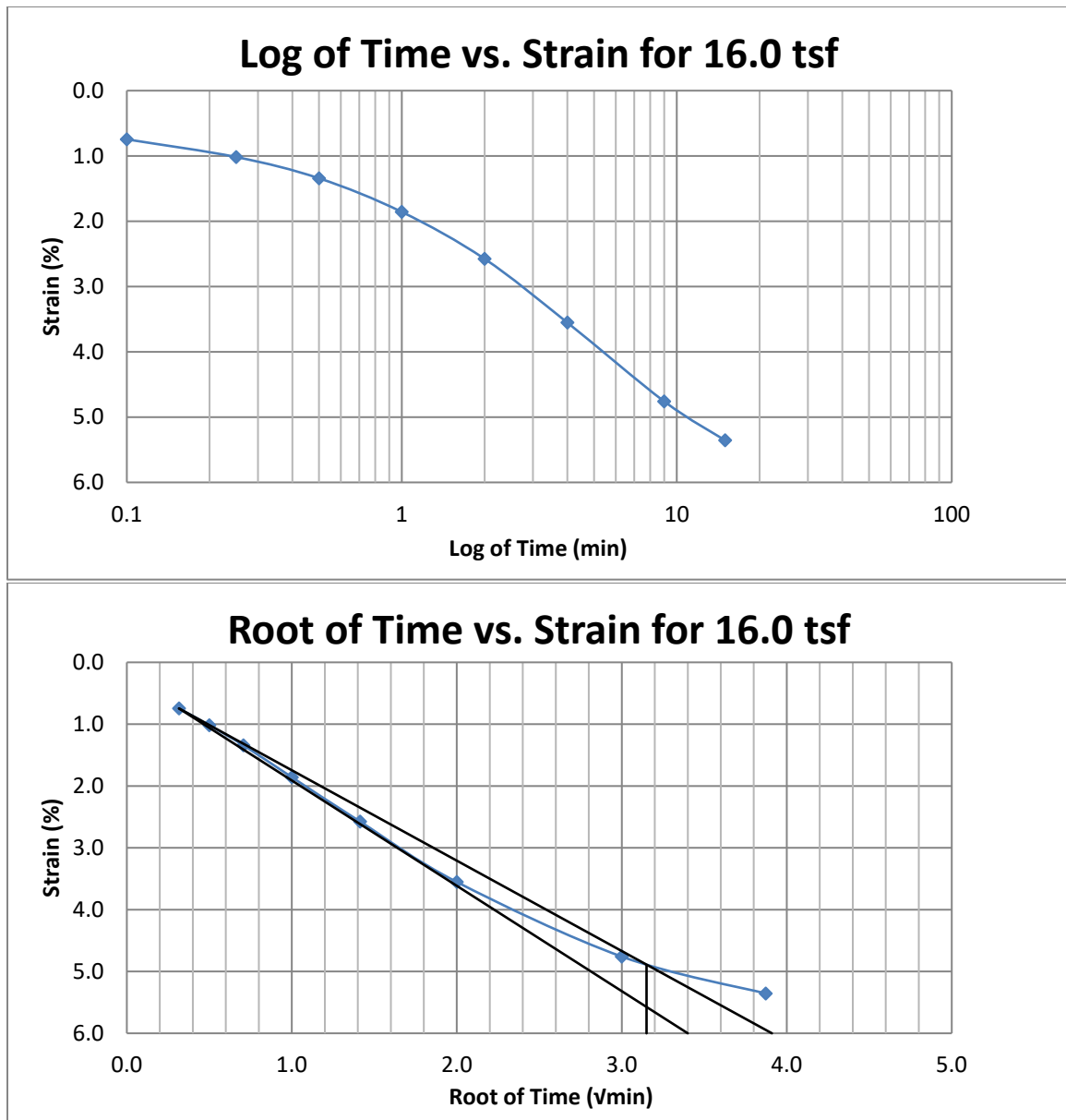
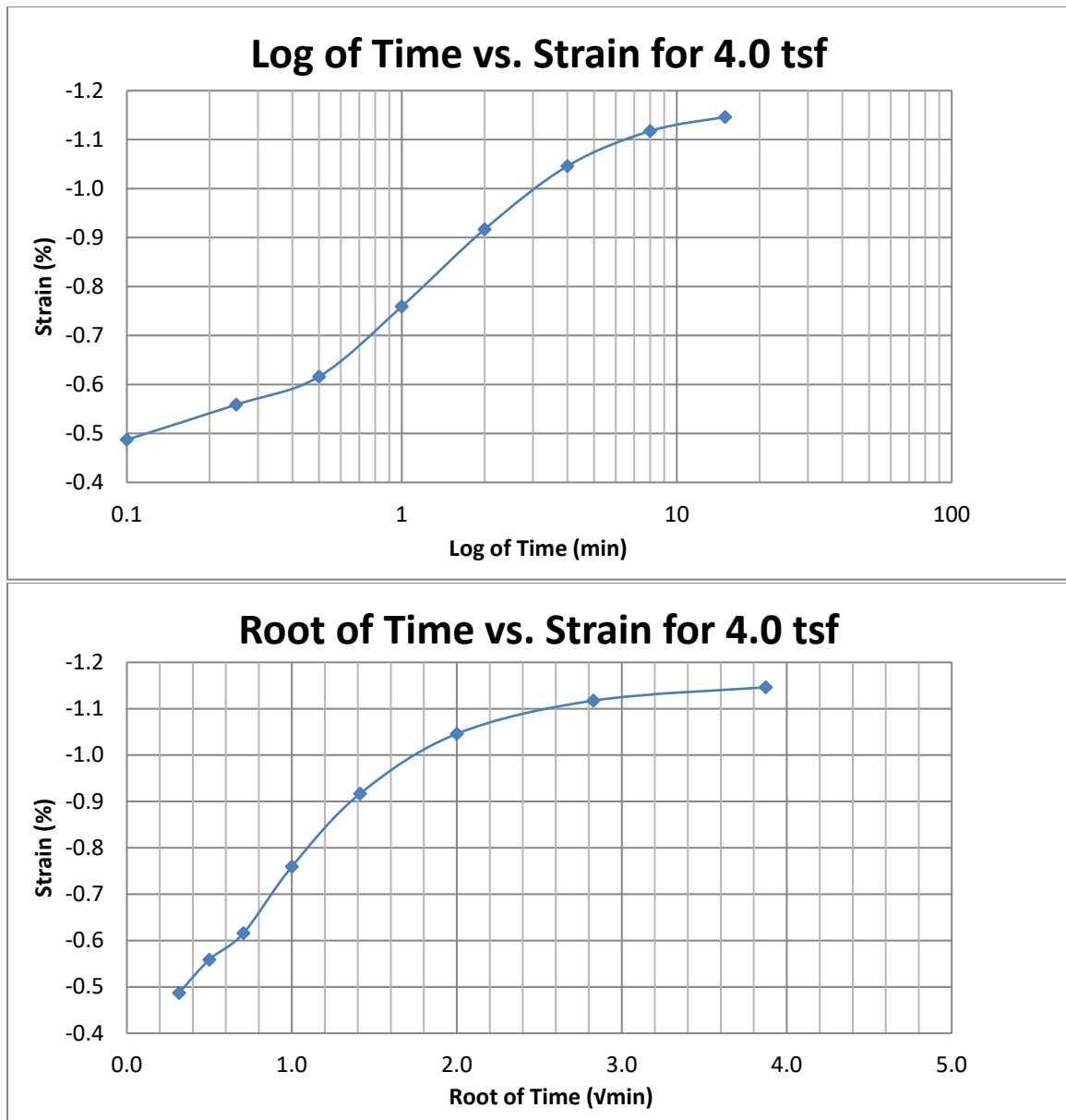


Figure A216 Provo at 50-52 feet



**Figure A217 Provo at 50-52 feet**

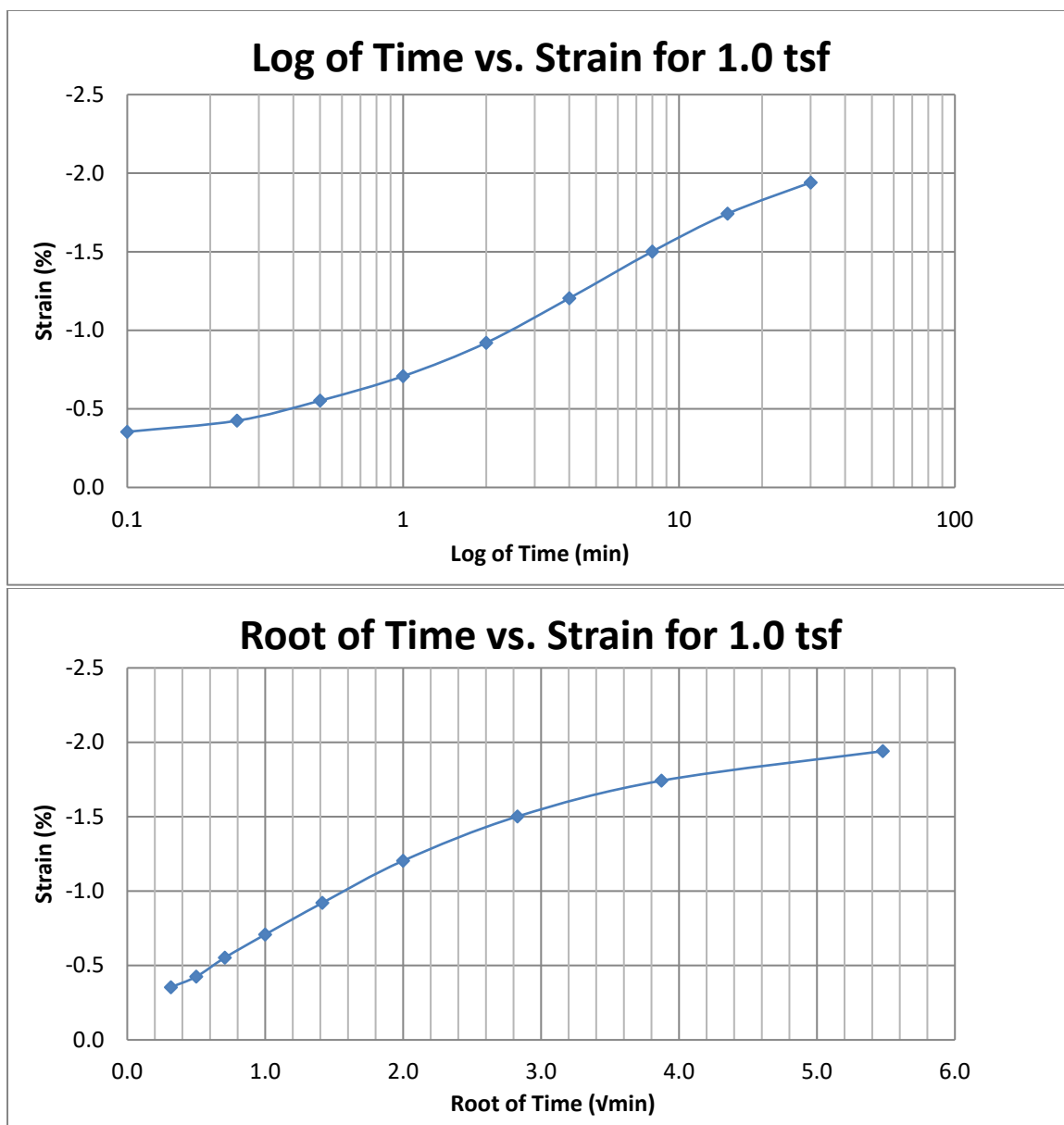
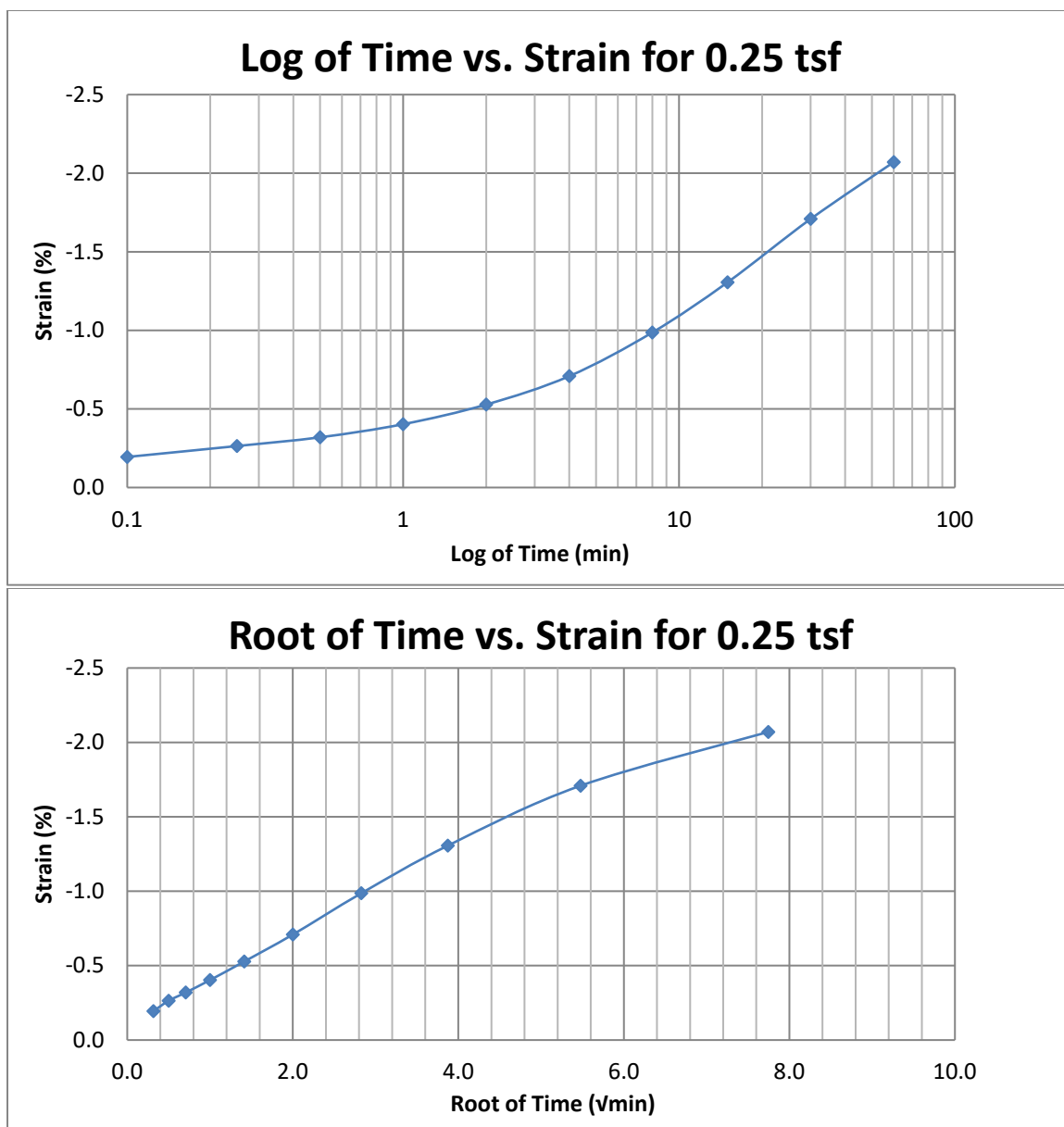


Figure A218 Provo at 50-52 feet





**Figure A219 Provo at 50-52 feet**

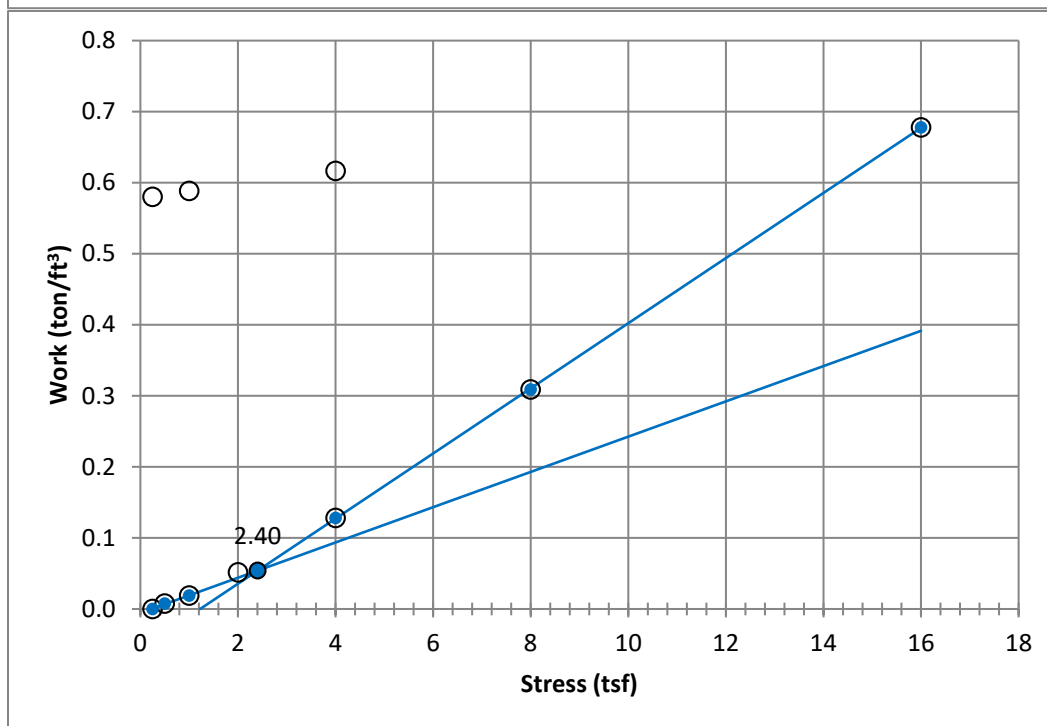
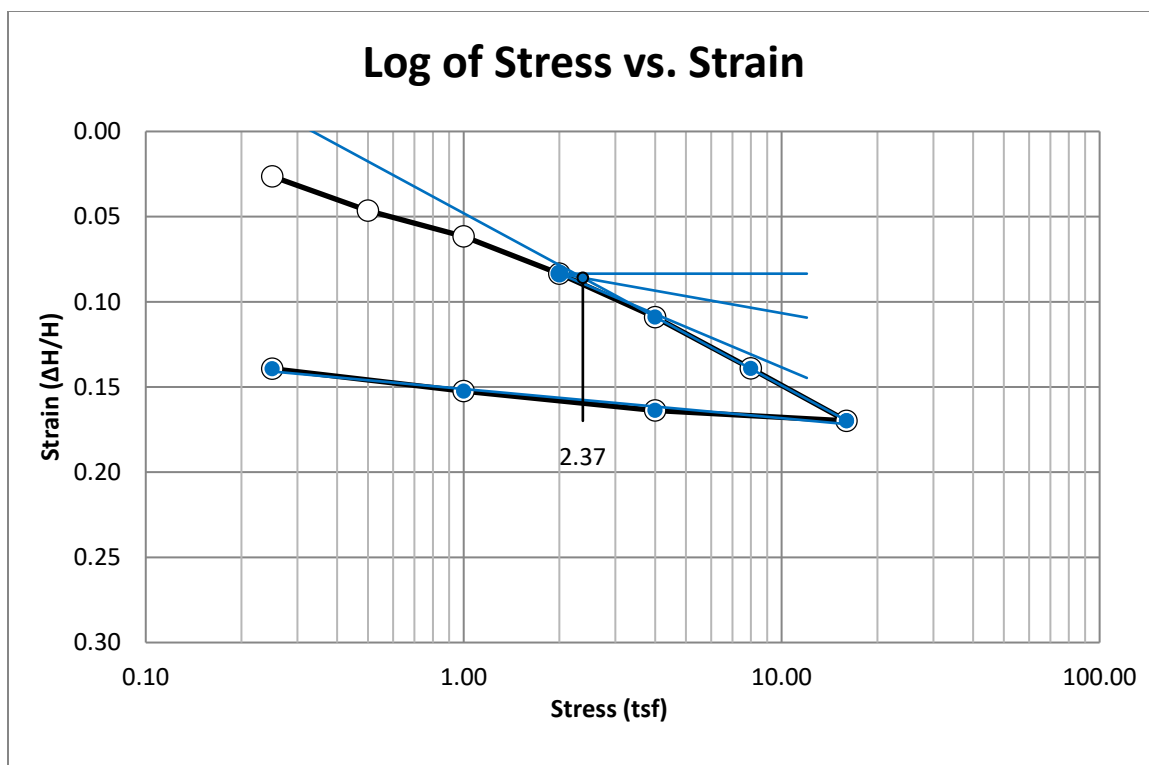


Figure A220 Provo at 60-62 feet

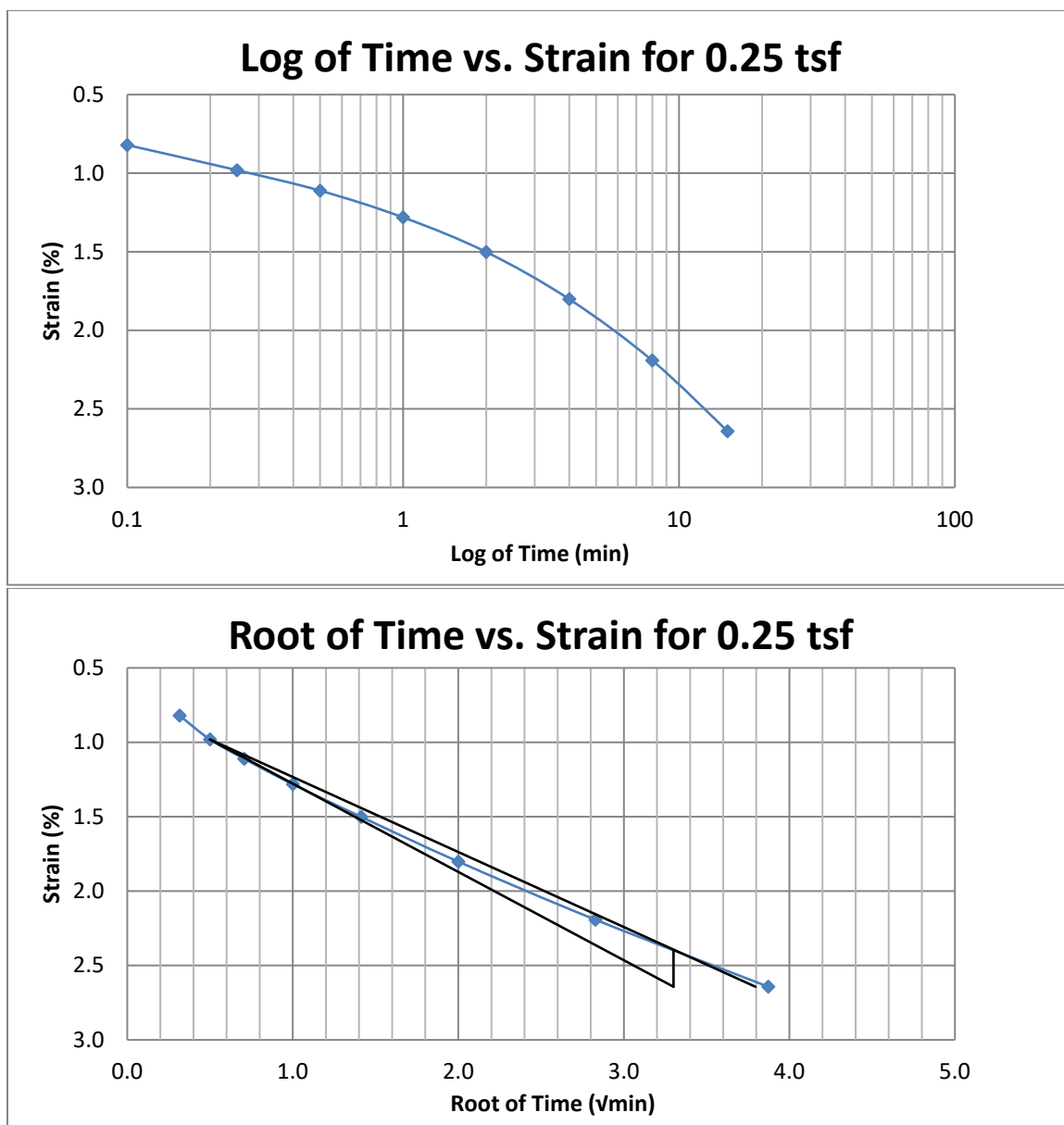


Figure A221 Provo at 60-62 feet

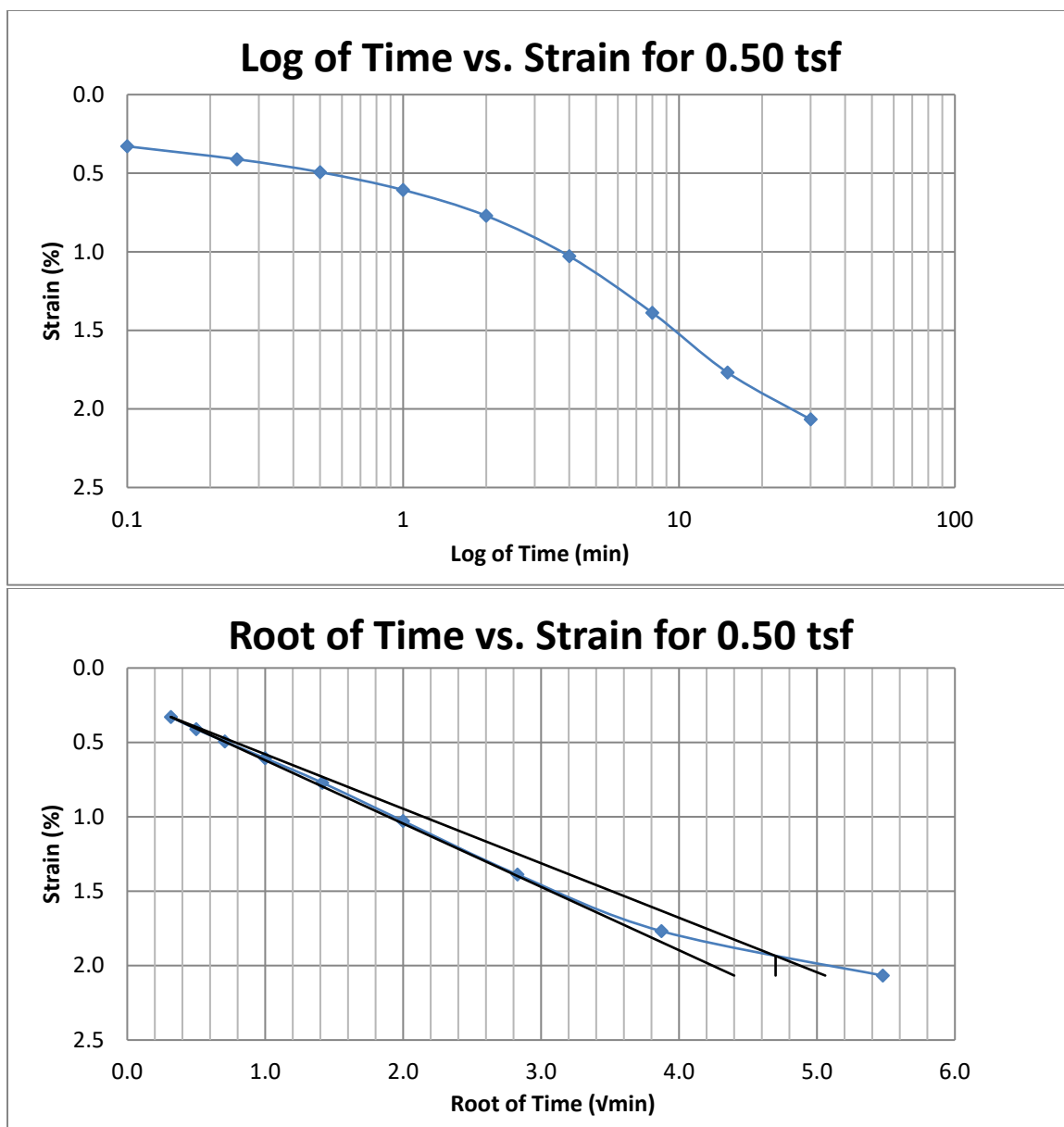


Figure A222 Provo at 60-62 feet

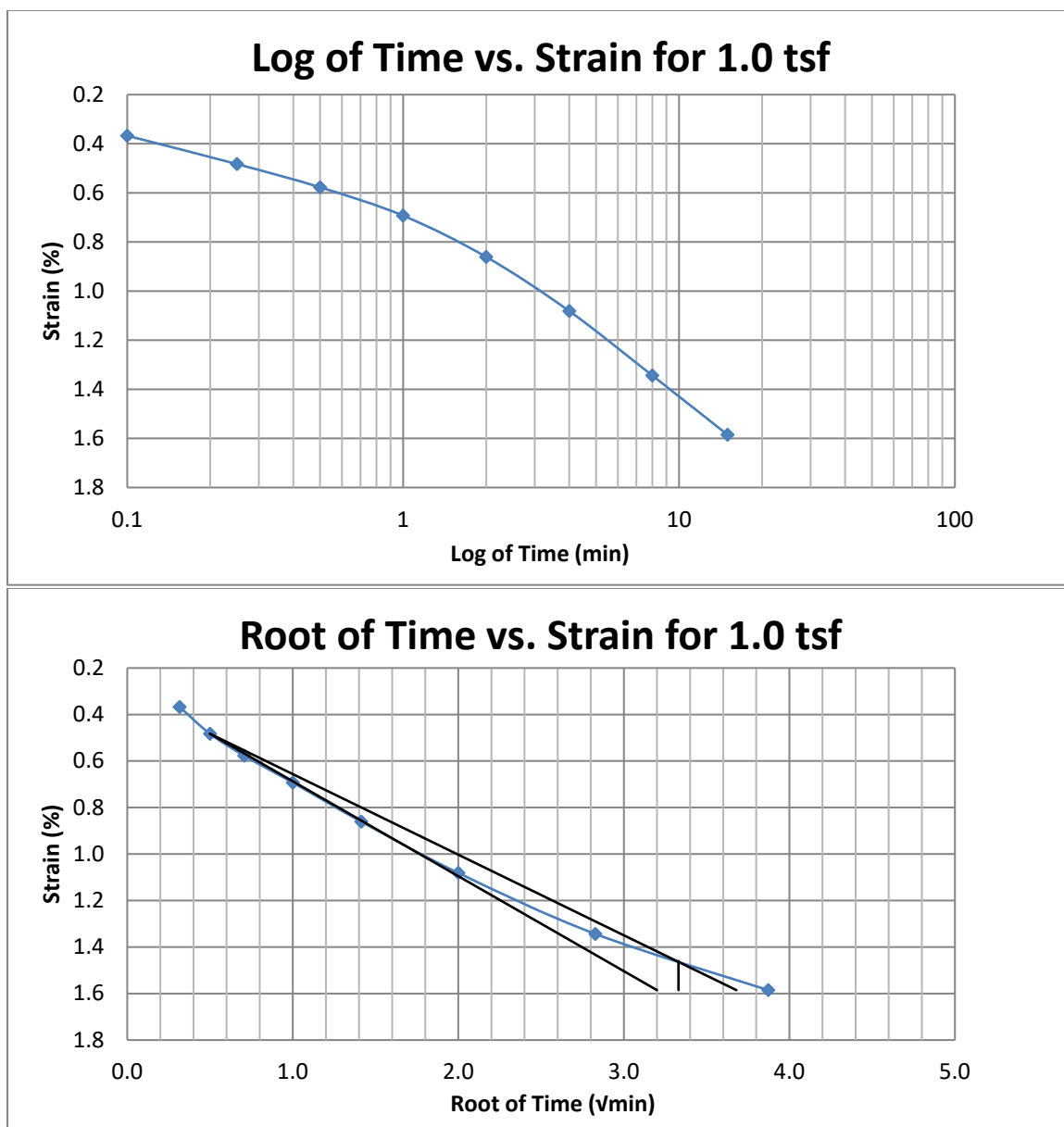


Figure A223 Provo at 60-62 feet

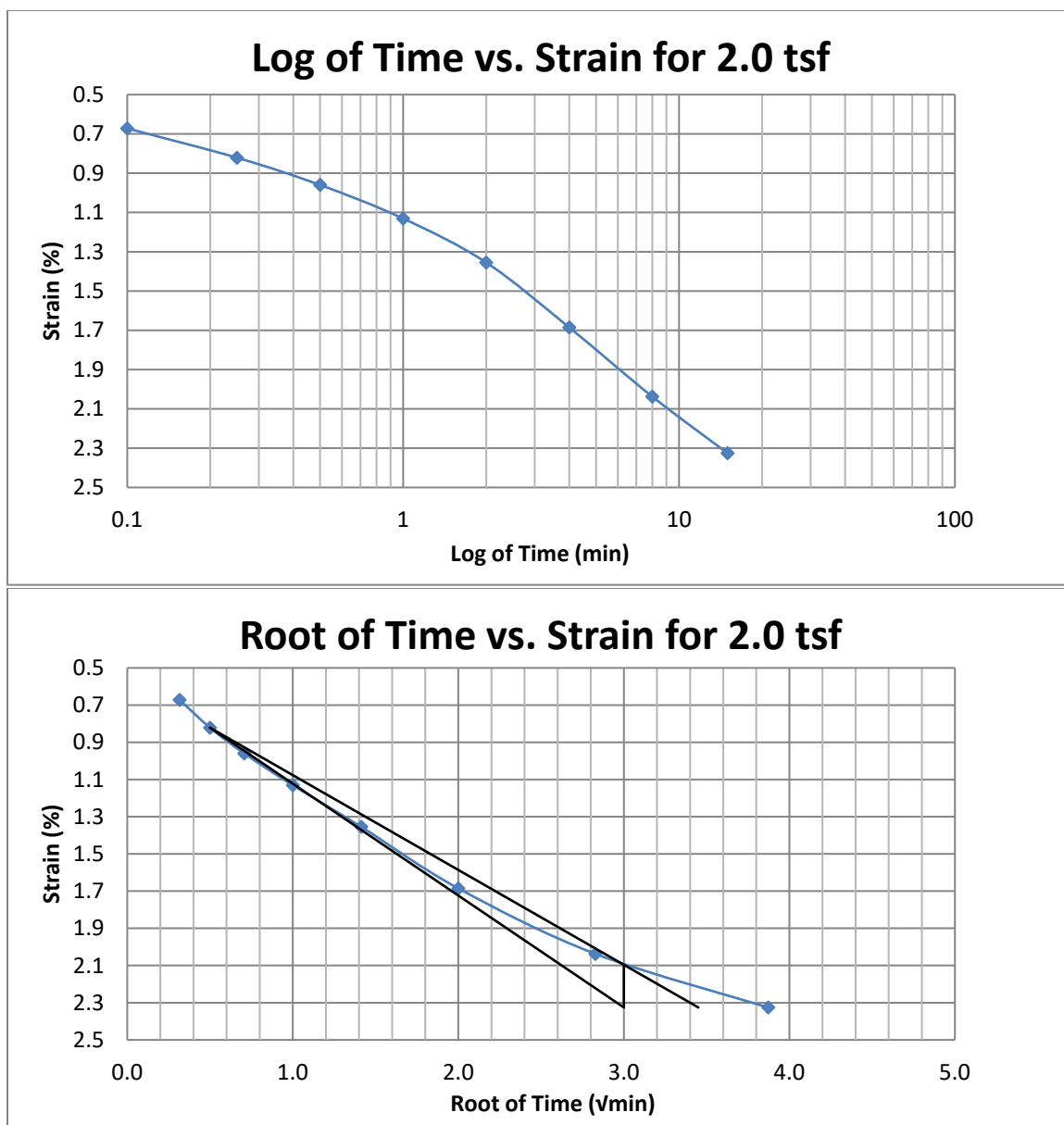


Figure A224 Provo at 60-62 feet

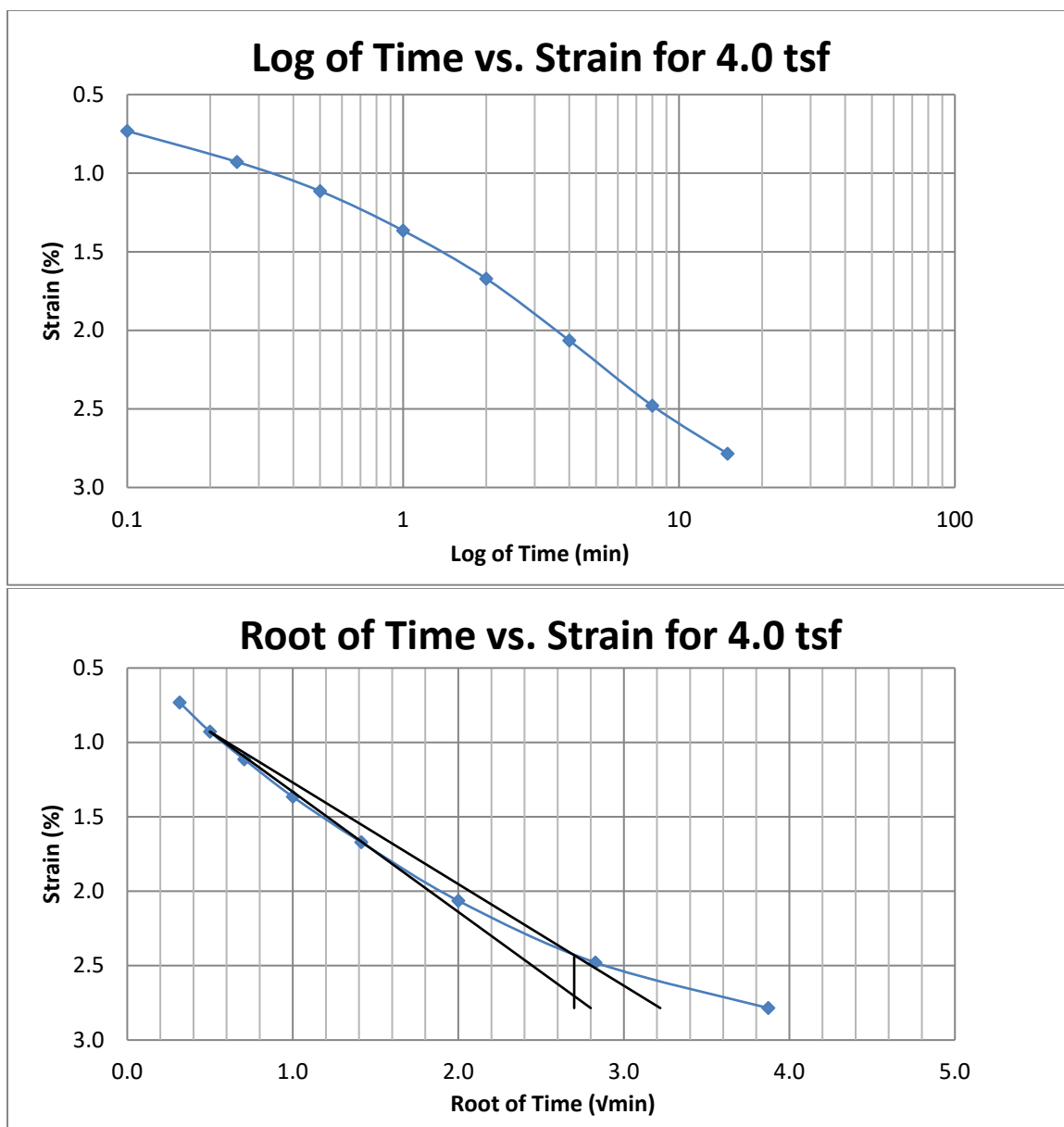


Figure A225 Provo at 60-62 feet

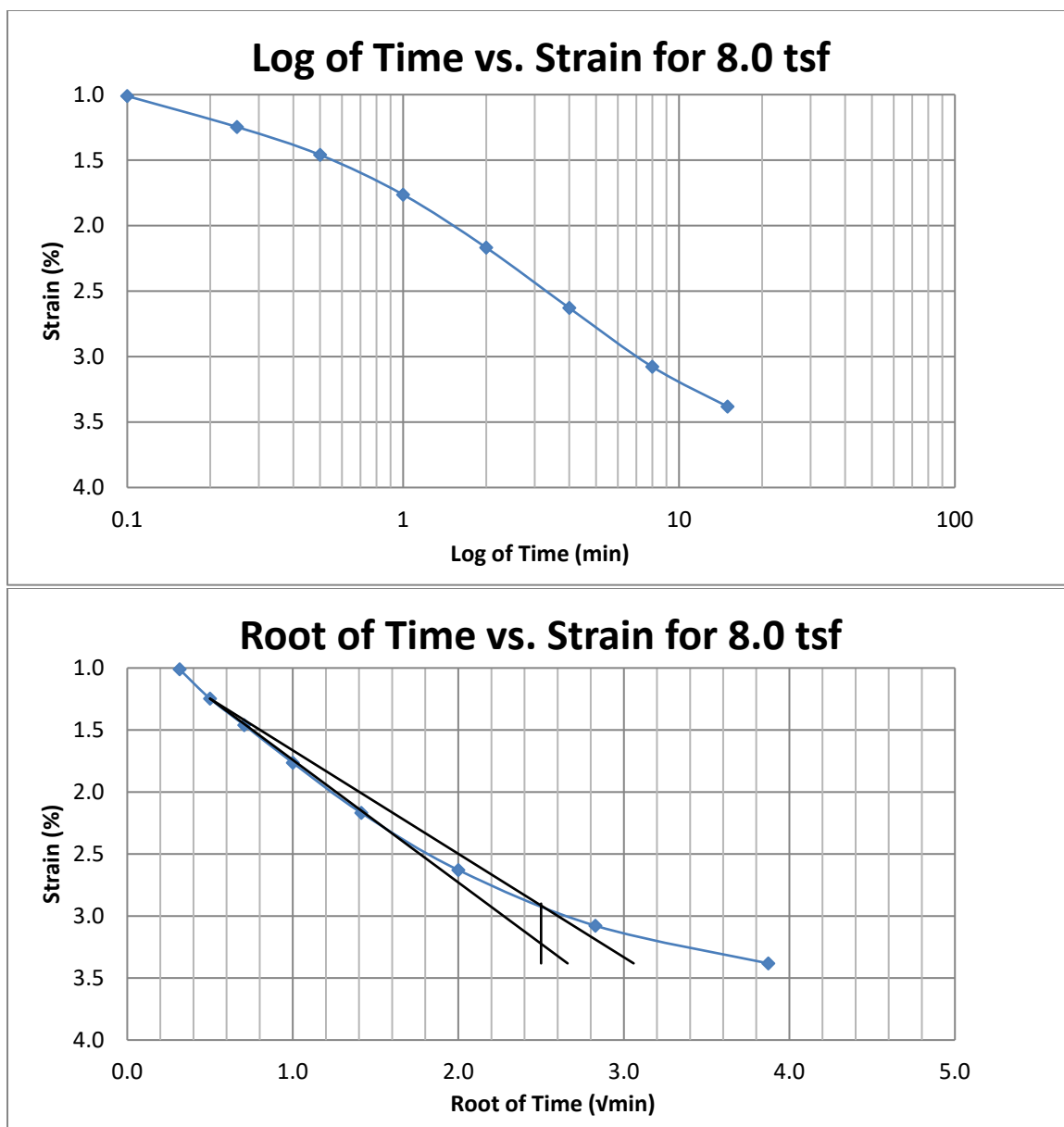
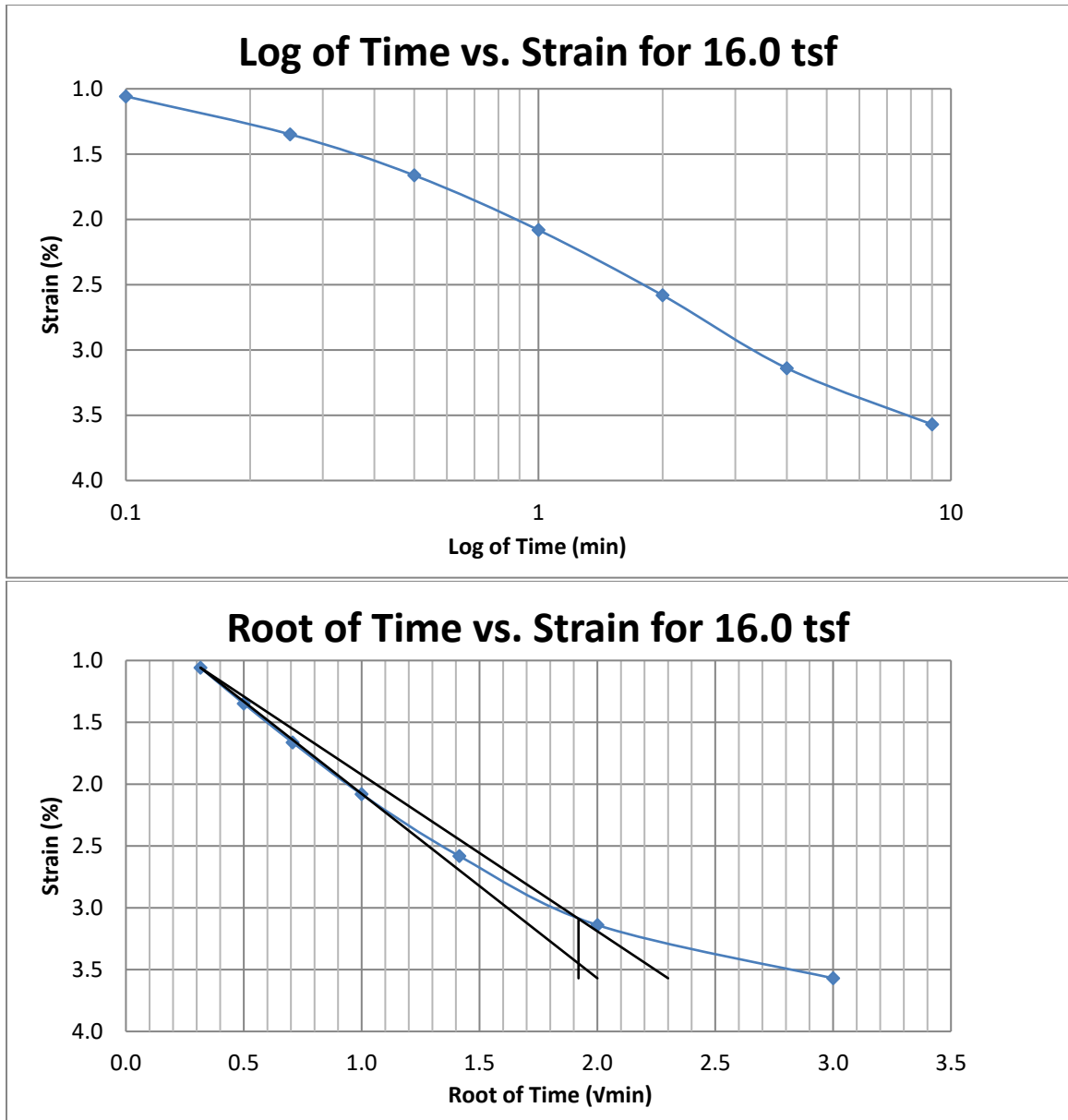


Figure A226 Provo at 60-62 feet





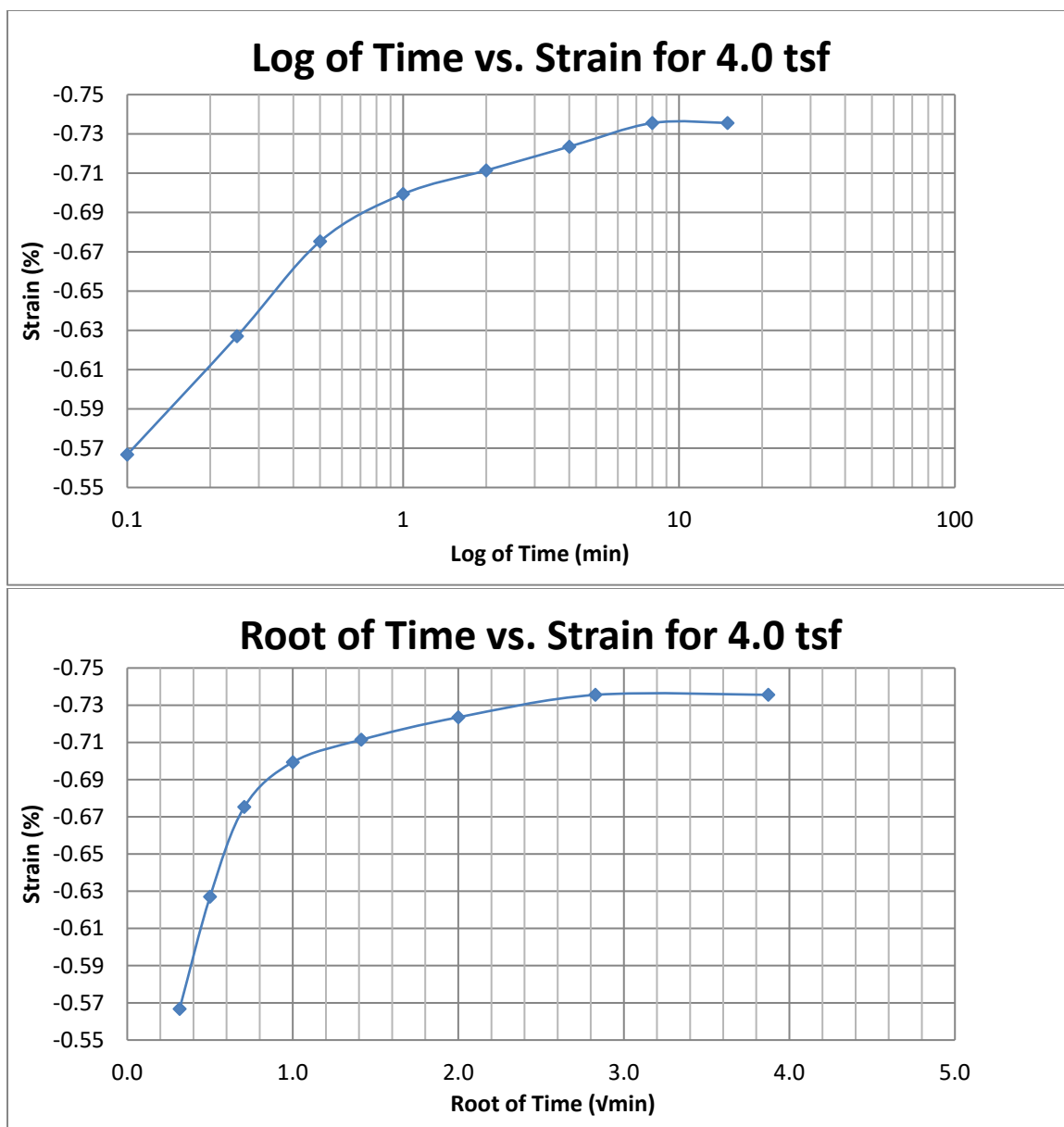


Figure A228 Provo at 60-62 feet

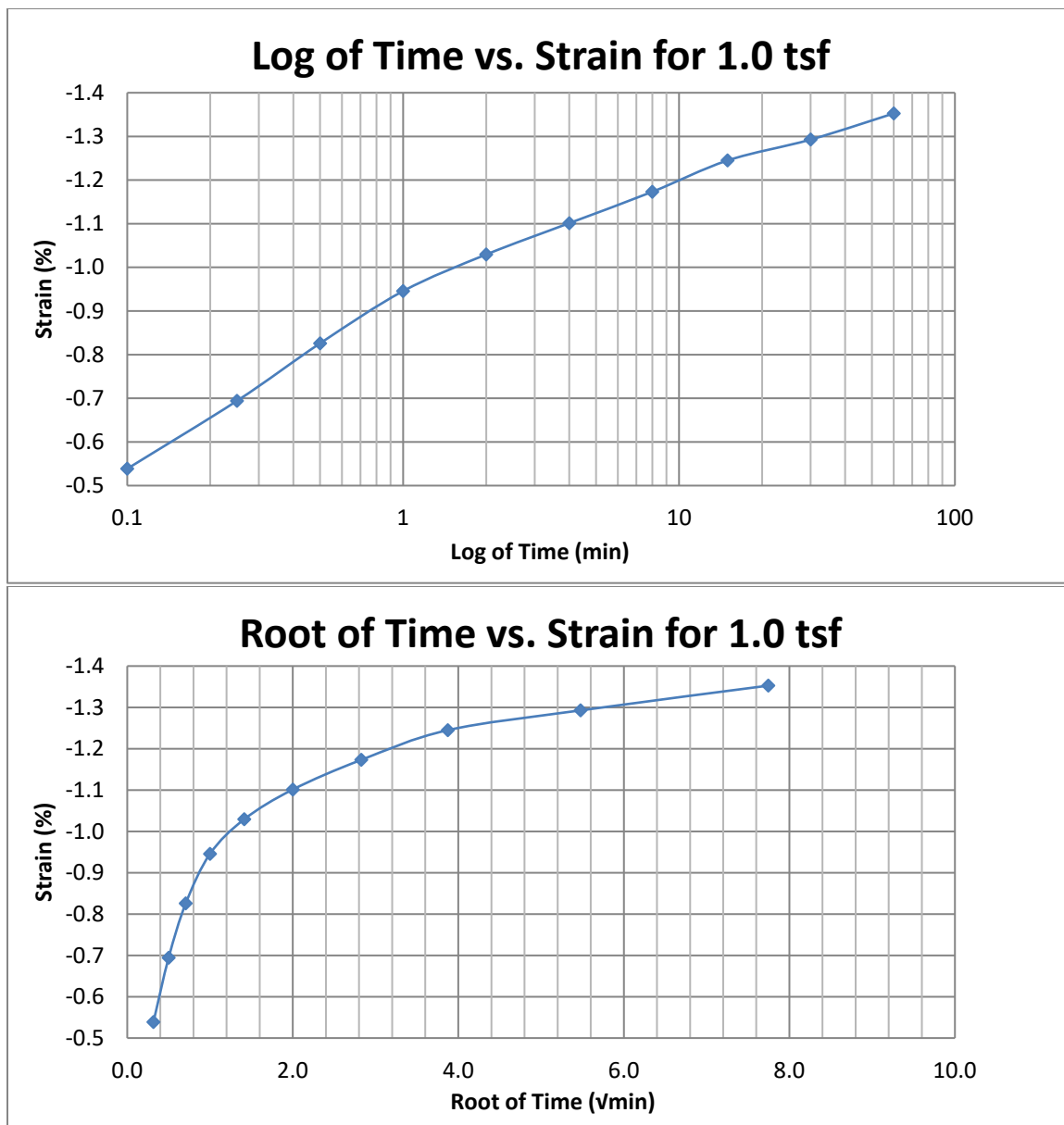


Figure A229 Provo at 60-62 feet

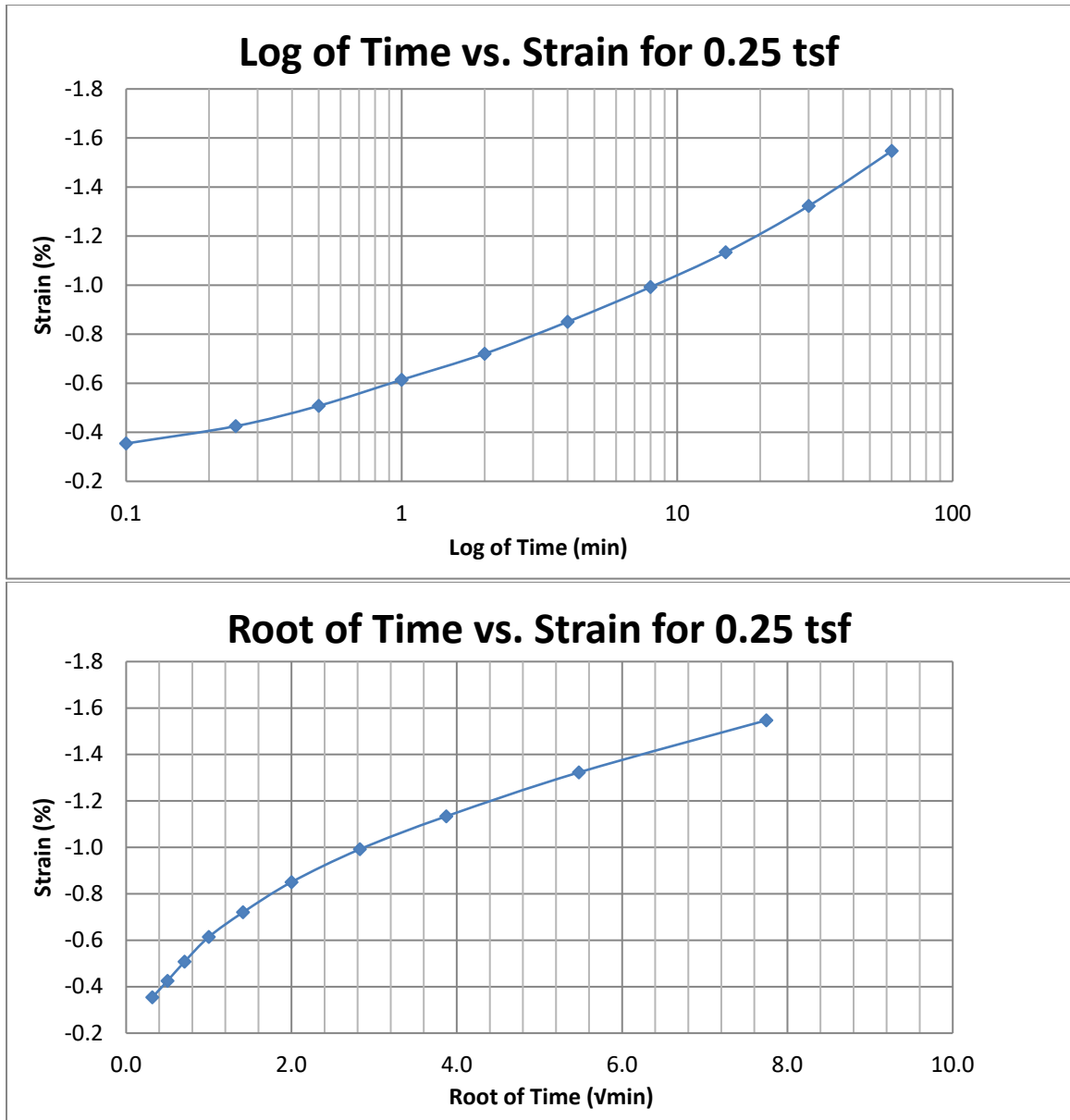


Figure A230 Provo at 60-62 feet

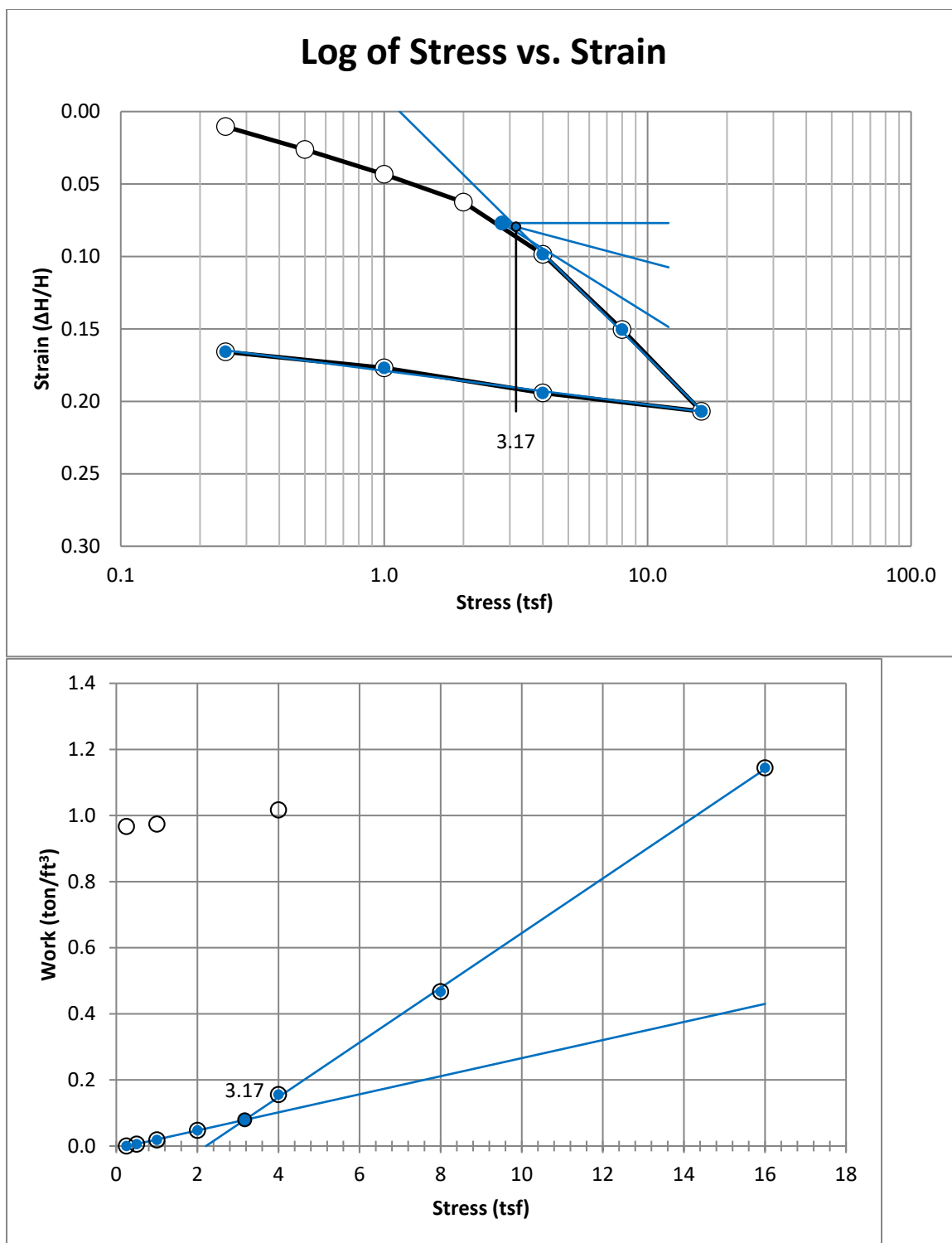
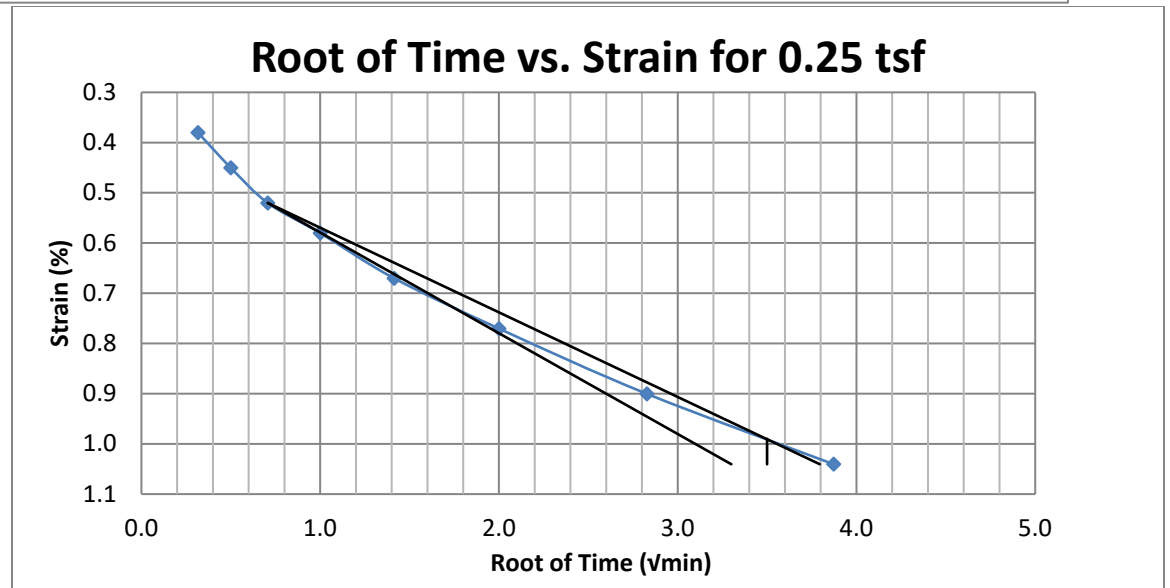
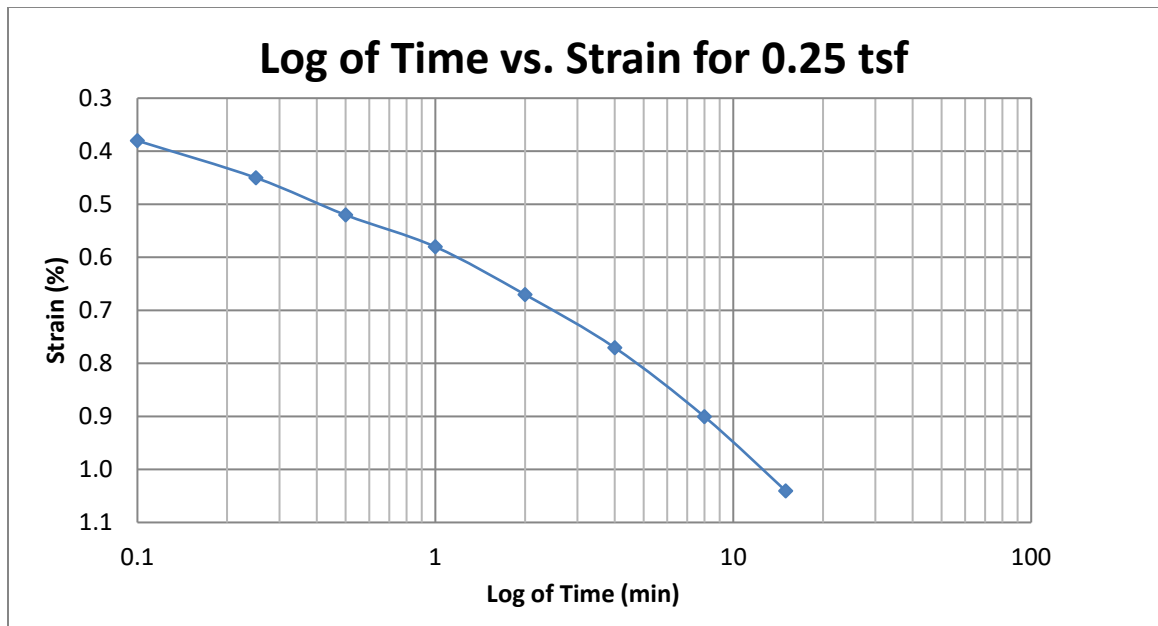


Figure A231 Provo at 80-82 feet



**Figure A232 Provo at 80-82 feet**

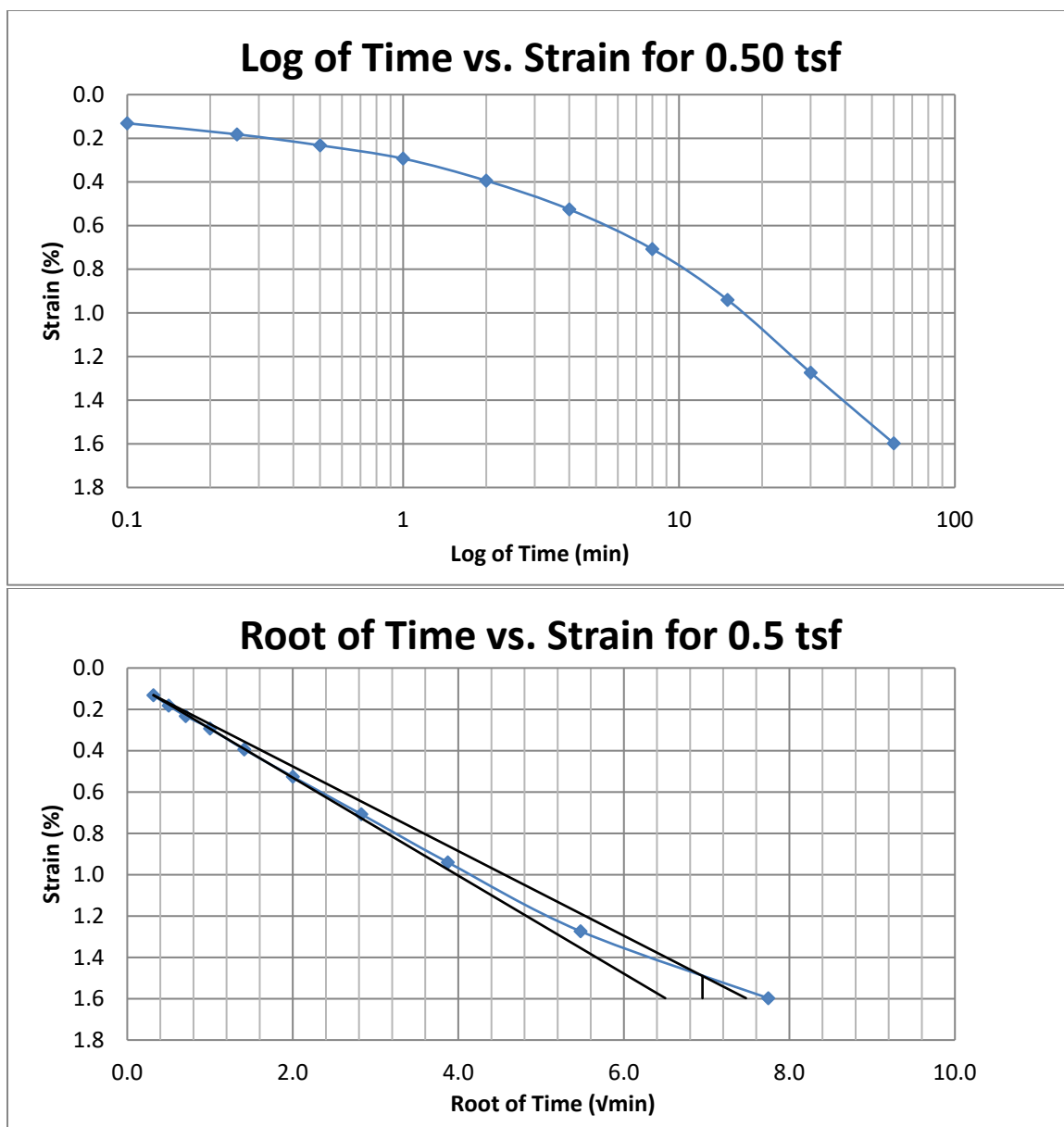


Figure A233 Provo at 80-82 feet

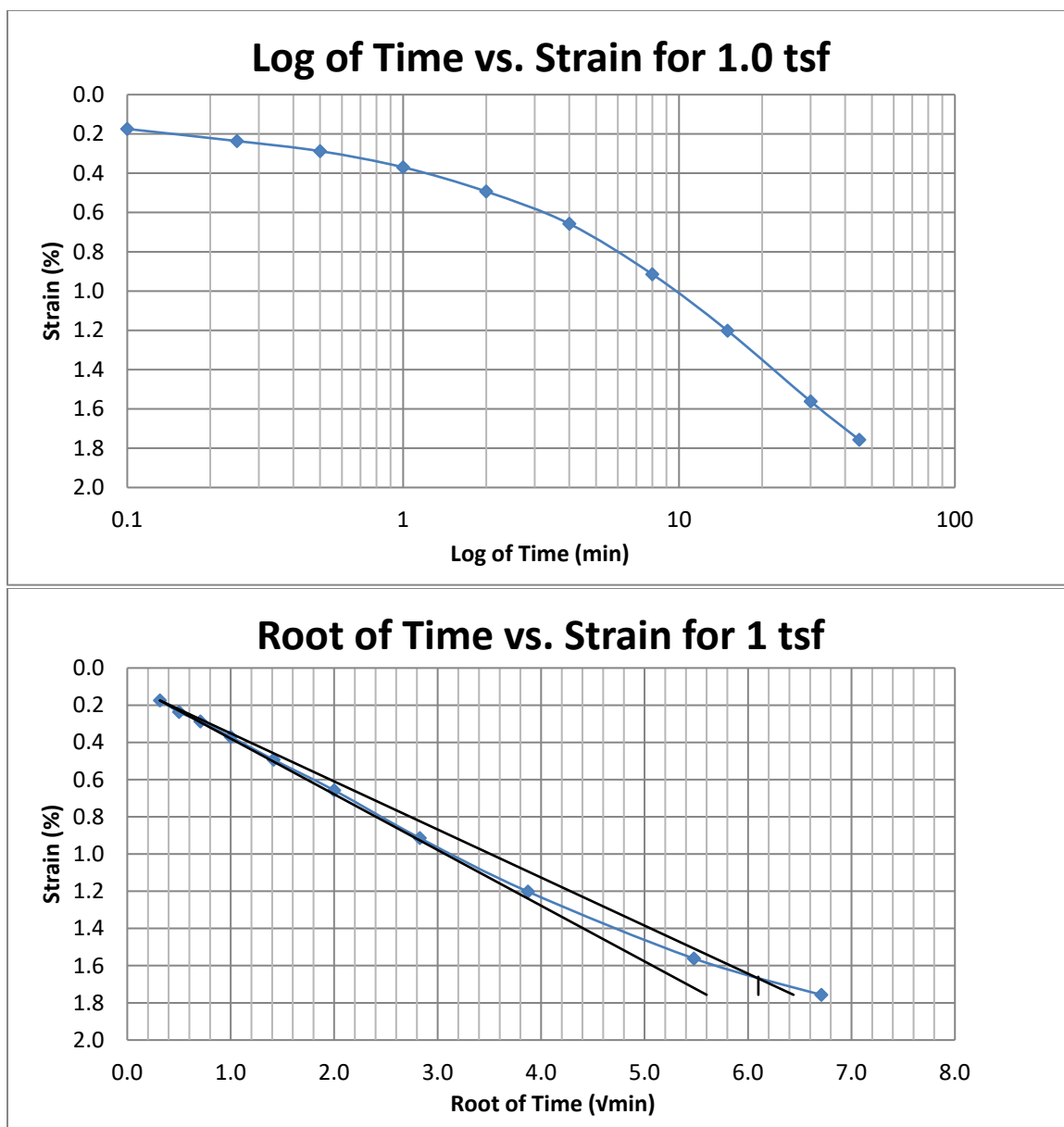


Figure A234 Provo at 80-82 feet



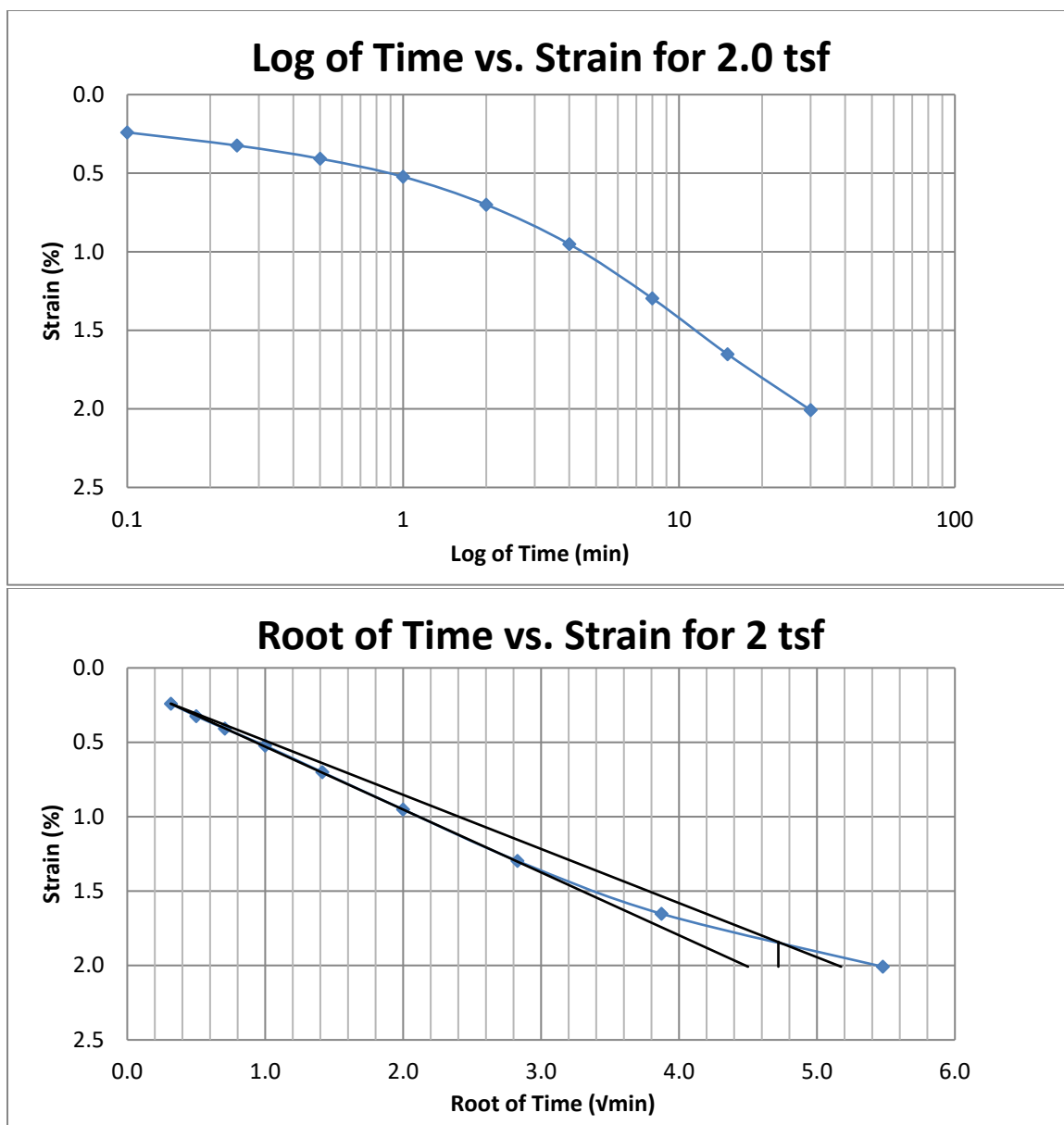


Figure A235 Provo at 80-82 feet

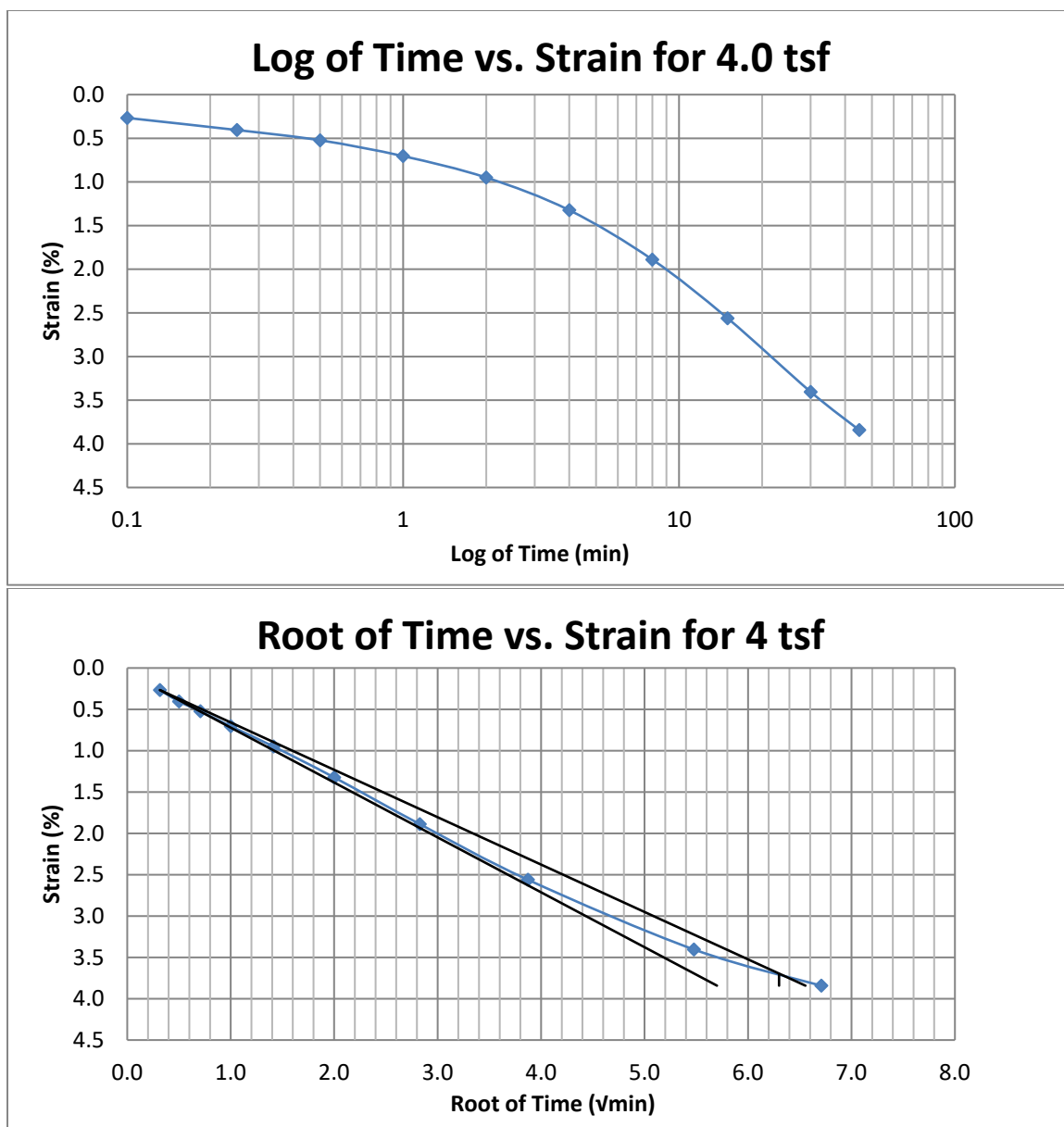


Figure A236 Provo at 80-82 feet

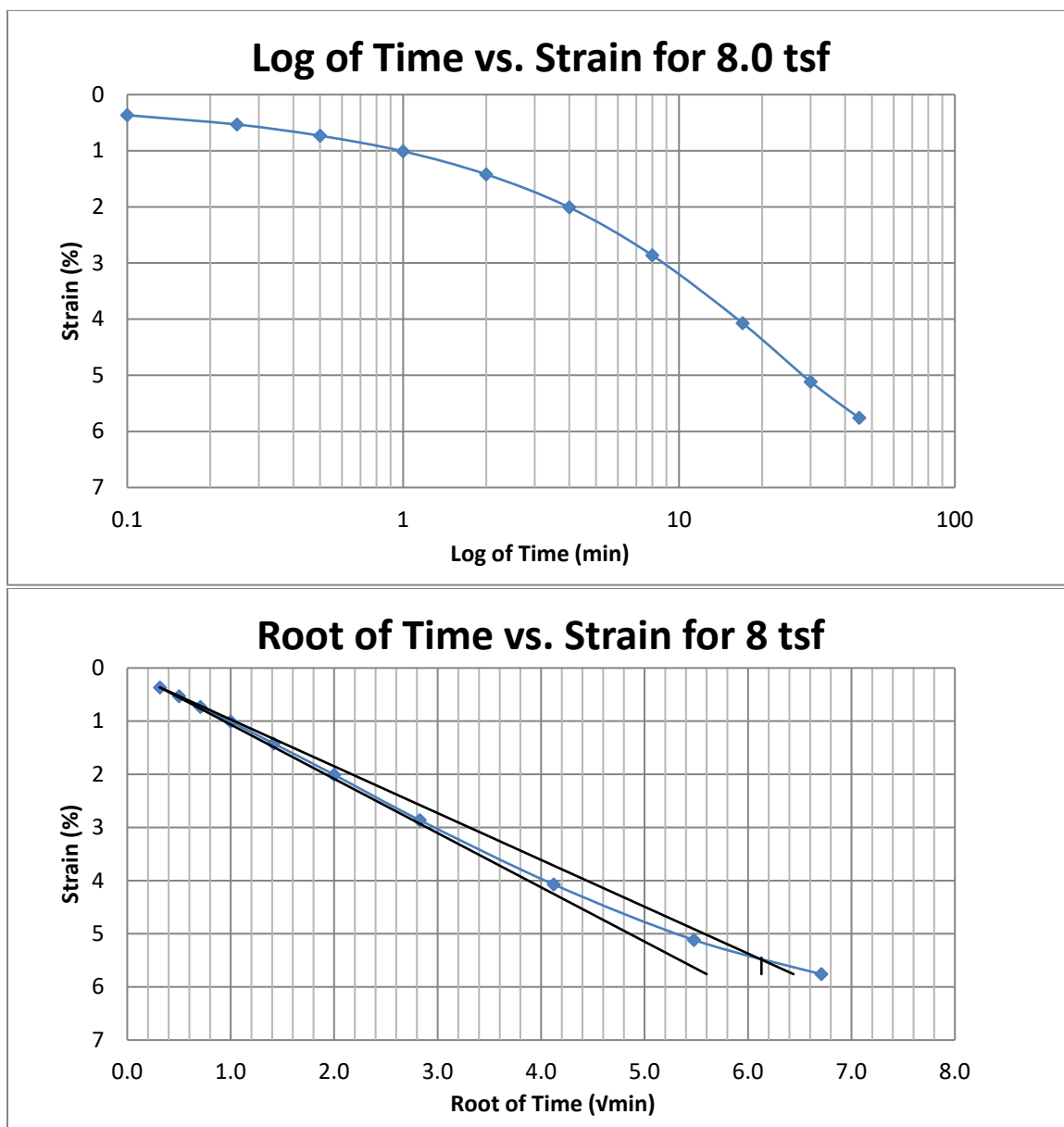


Figure A237 Provo at 80-82 feet

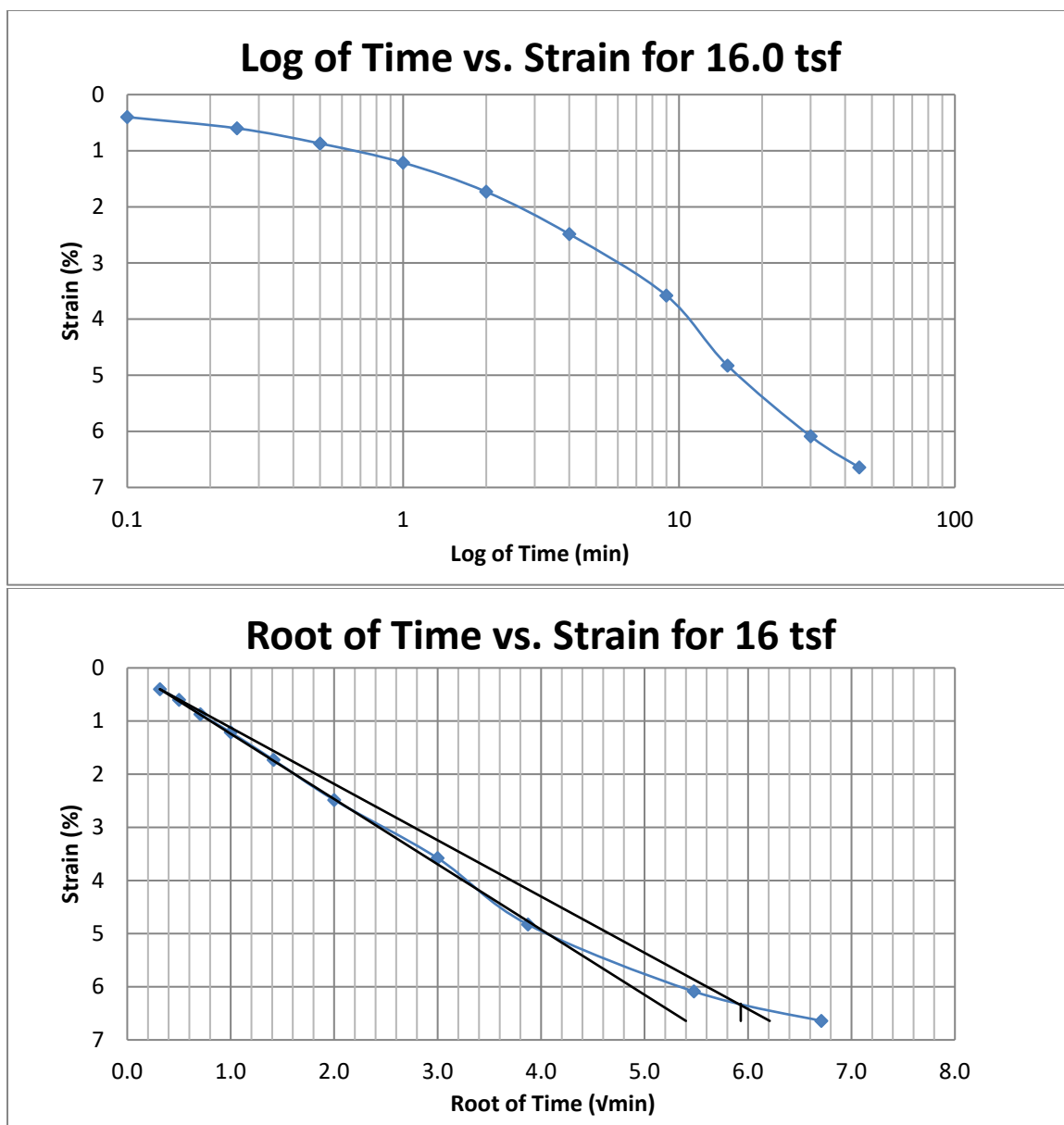


Figure A238 Provo at 80-82 feet

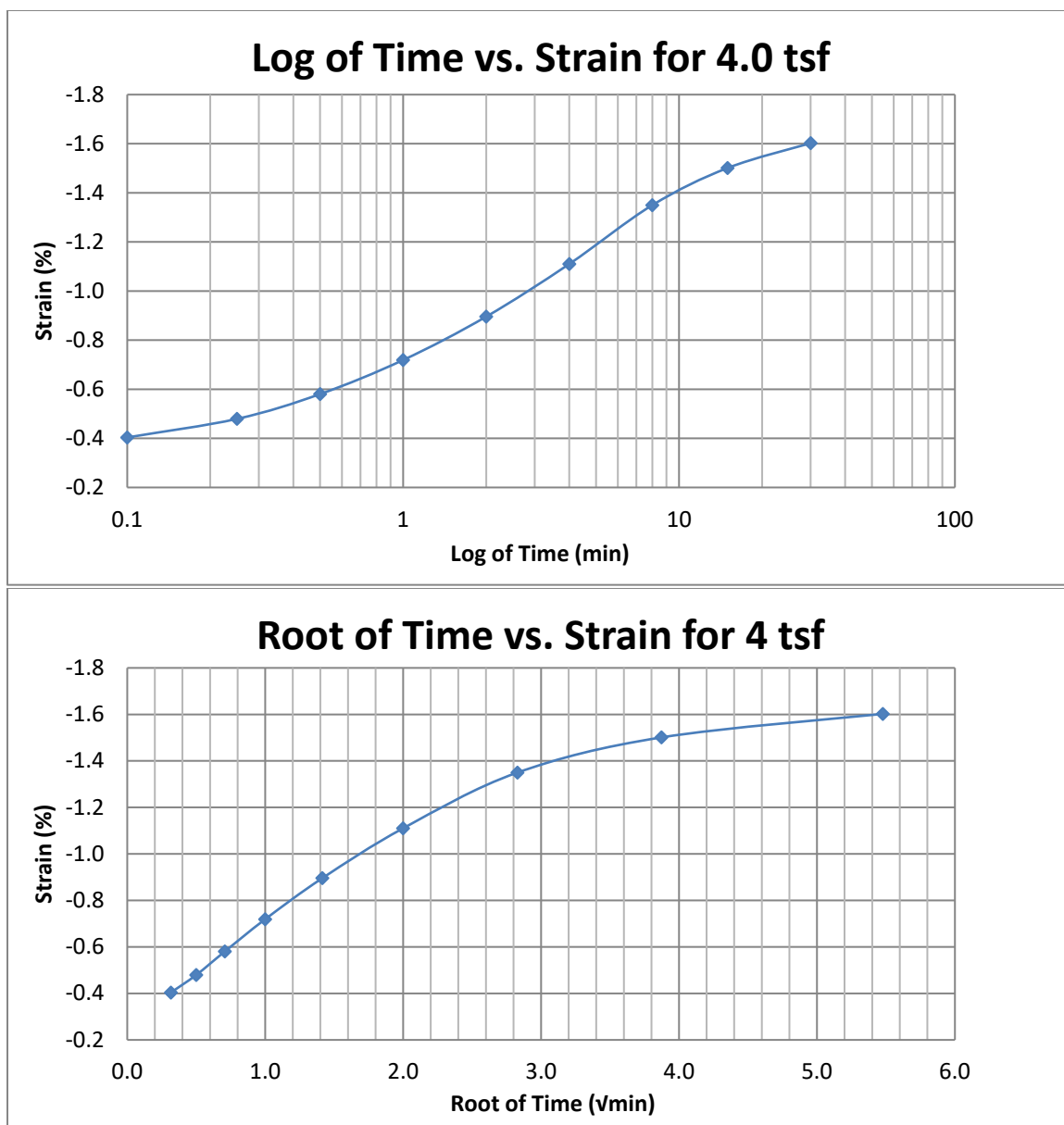


Figure A239 Provo at 80-82 feet

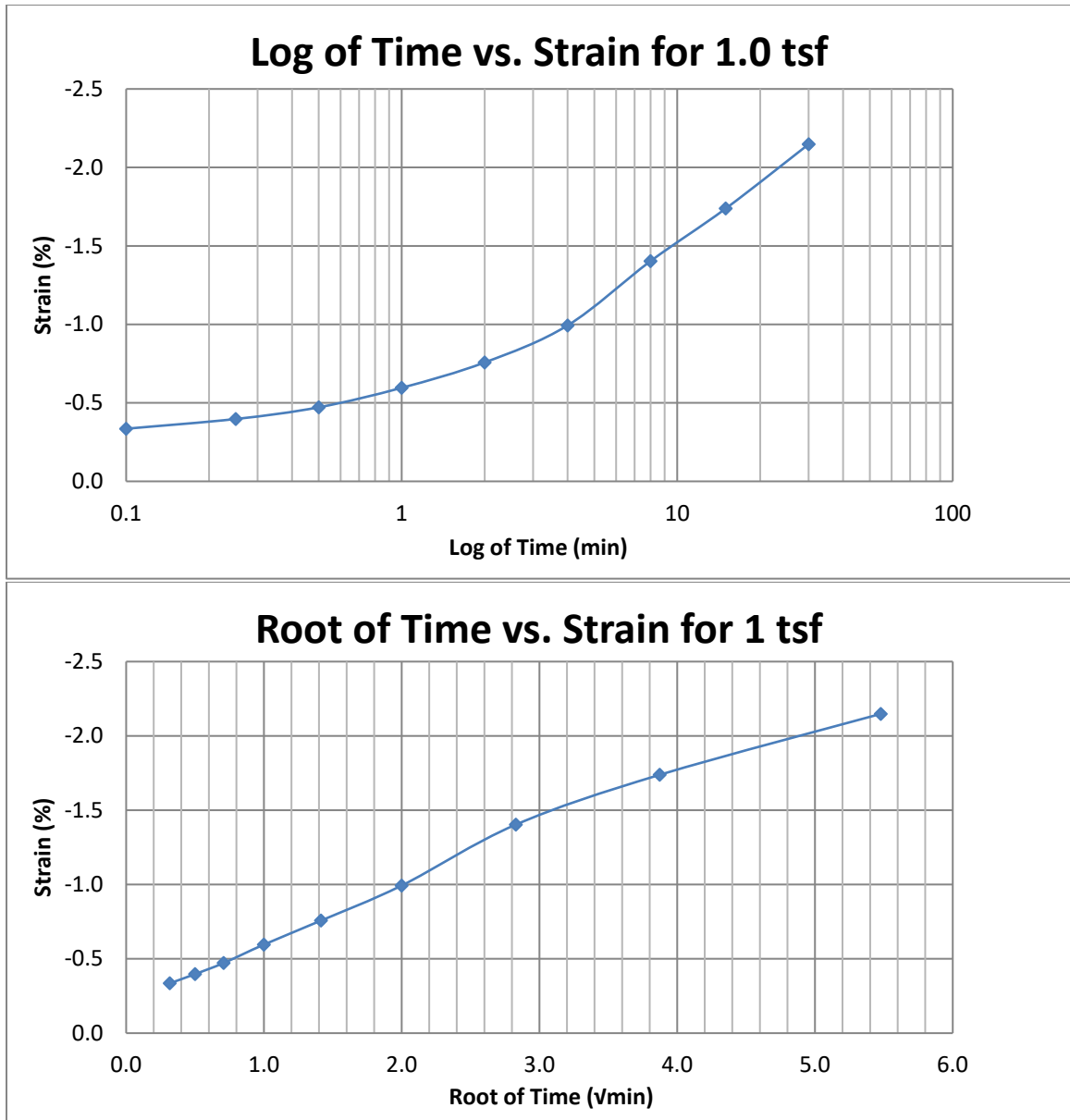


Figure A240 Provo at 80-82 feet

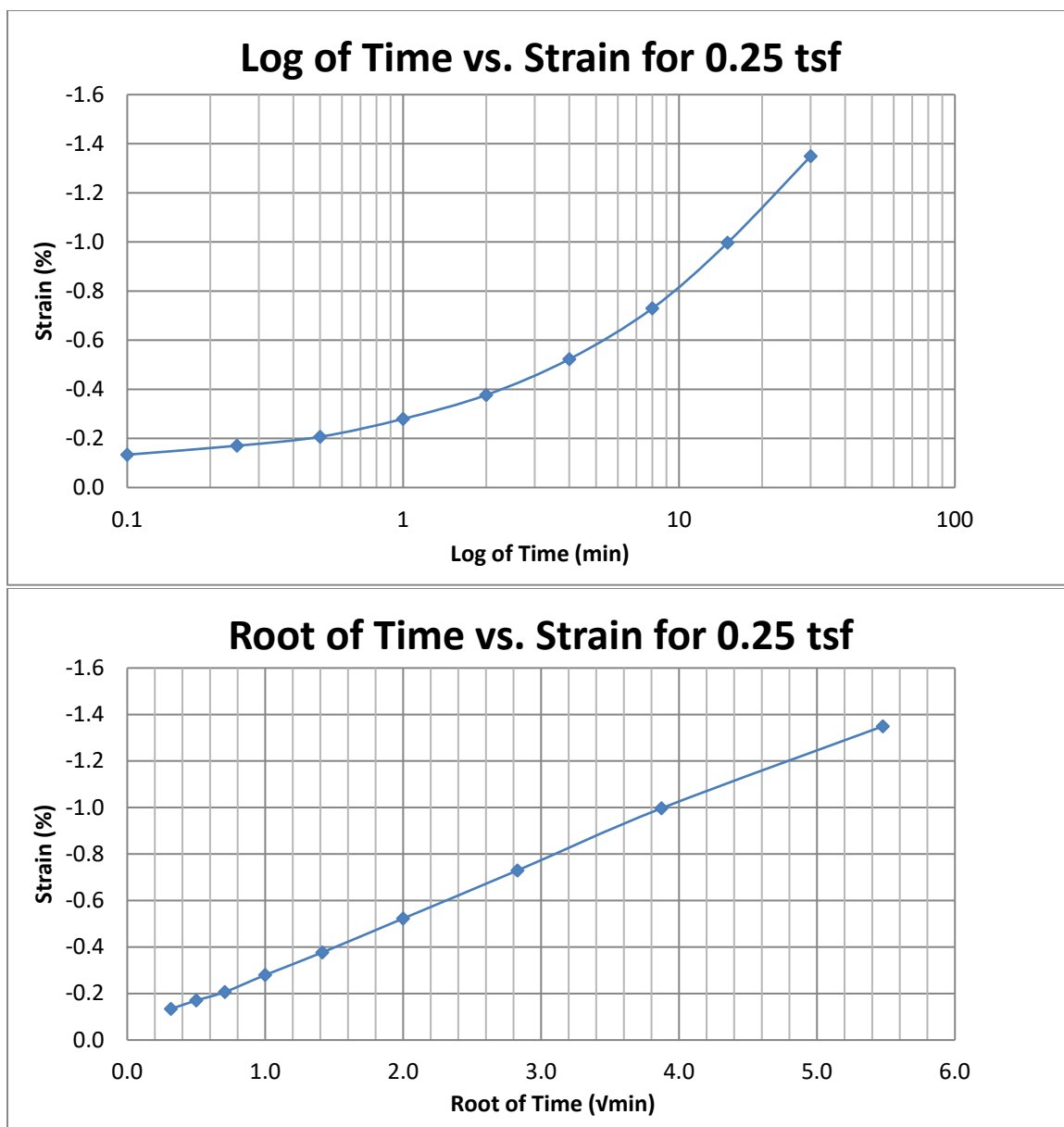


Figure A241 Provo at 80-82 feet

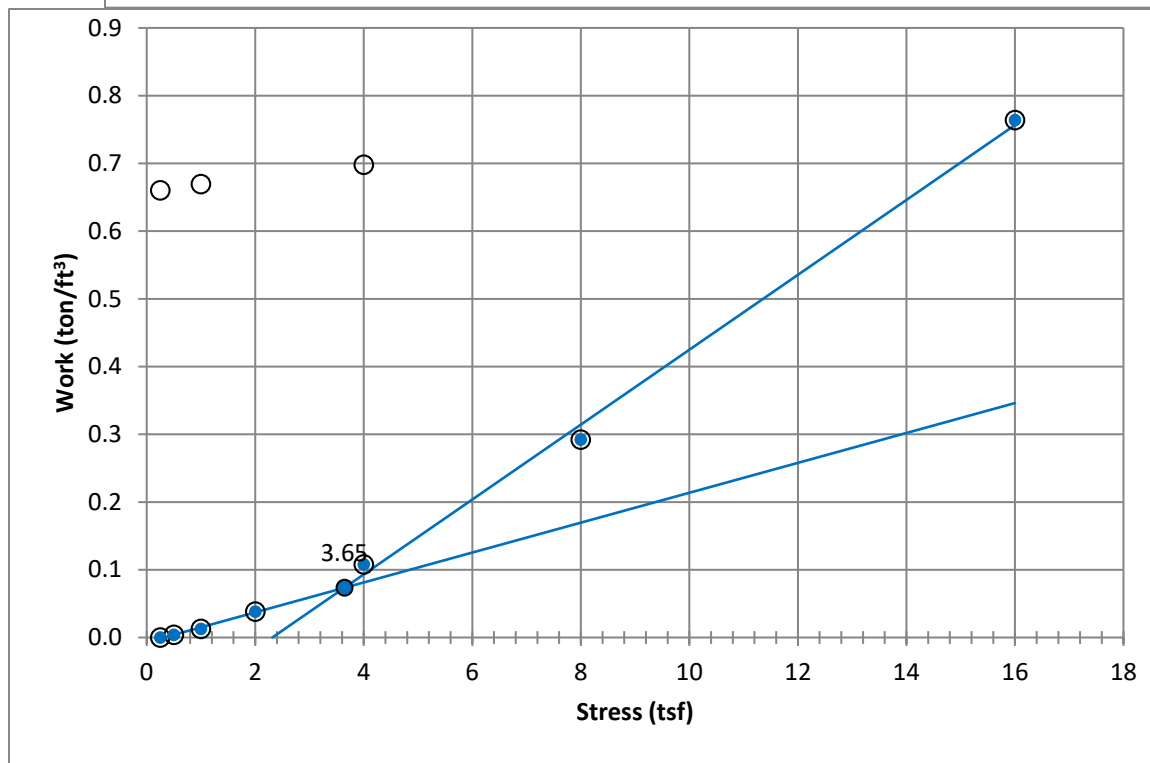
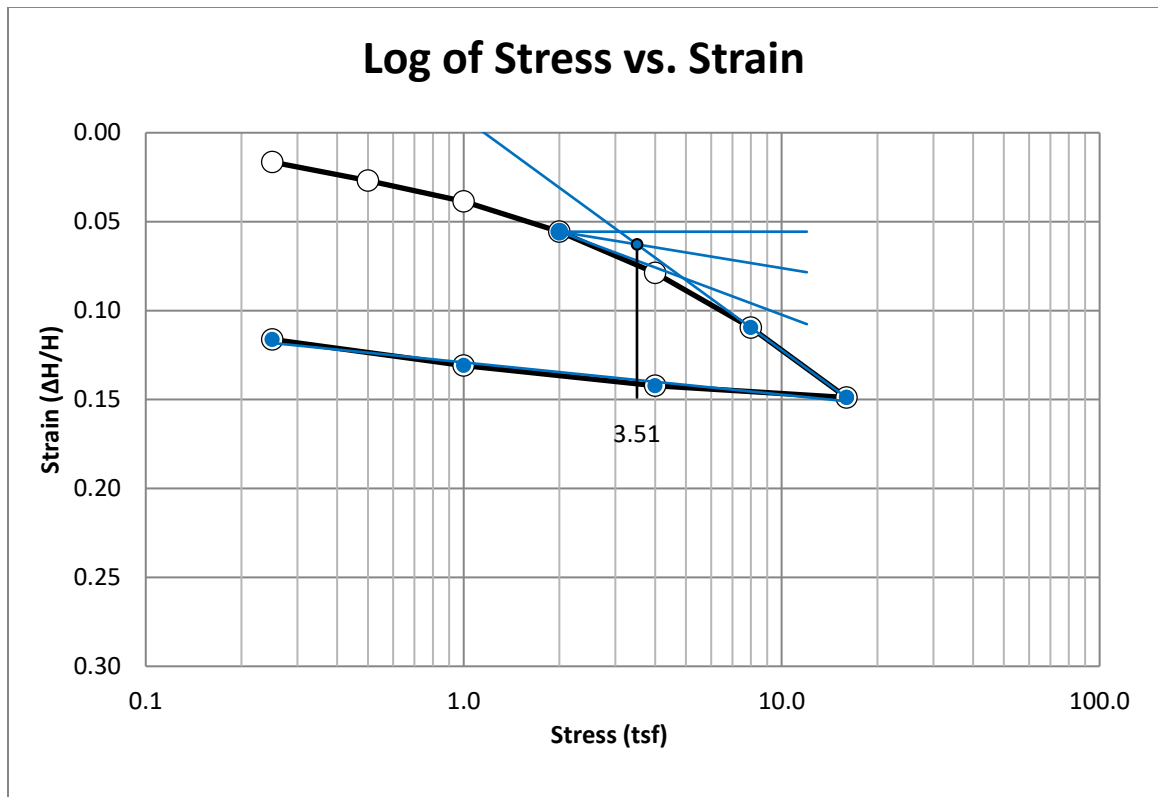


Figure A242 Provo at 90-92 feet



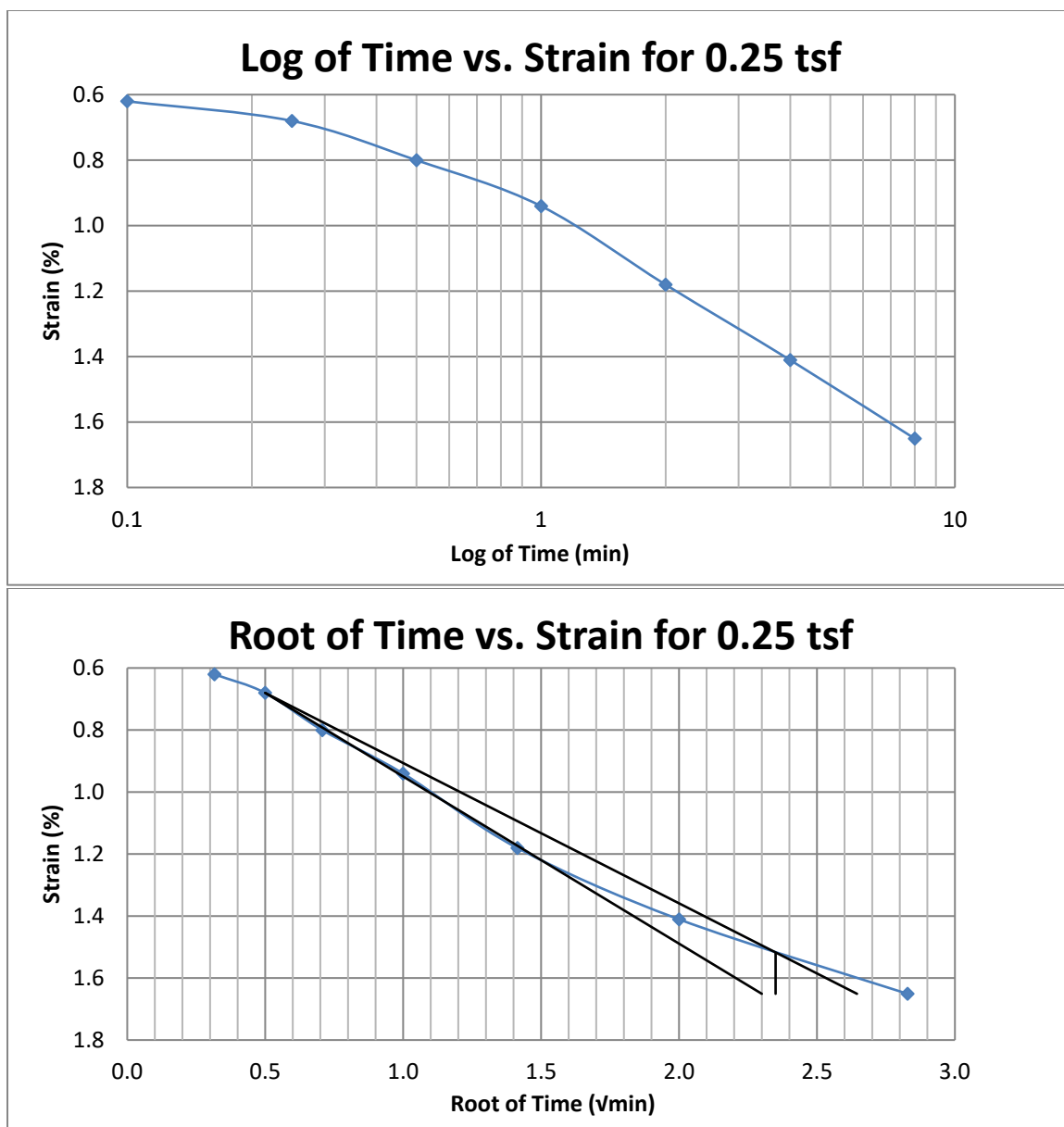


Figure A243 Provo at 90-92 feet

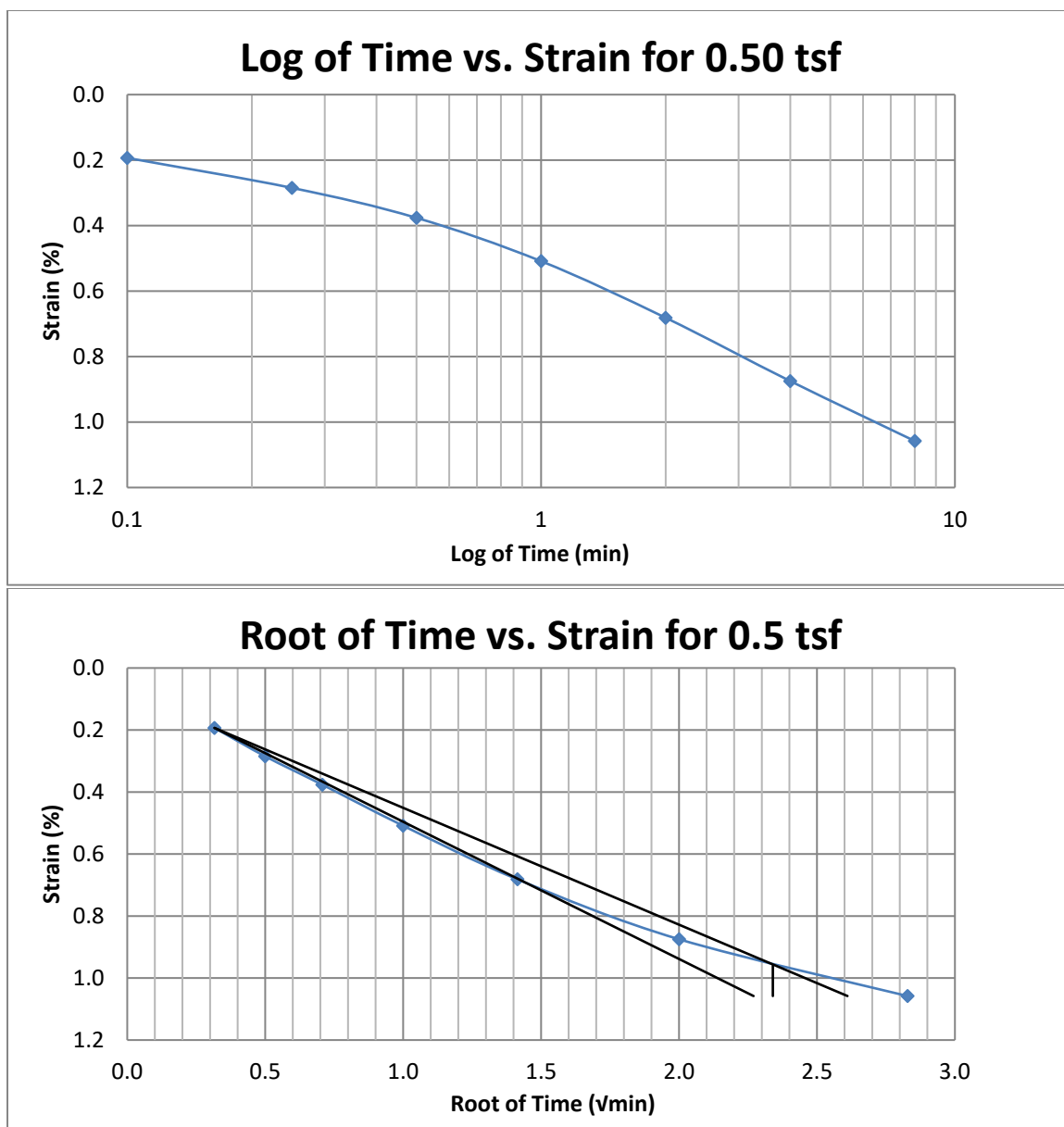


Figure A244 Provo at 90-92 feet

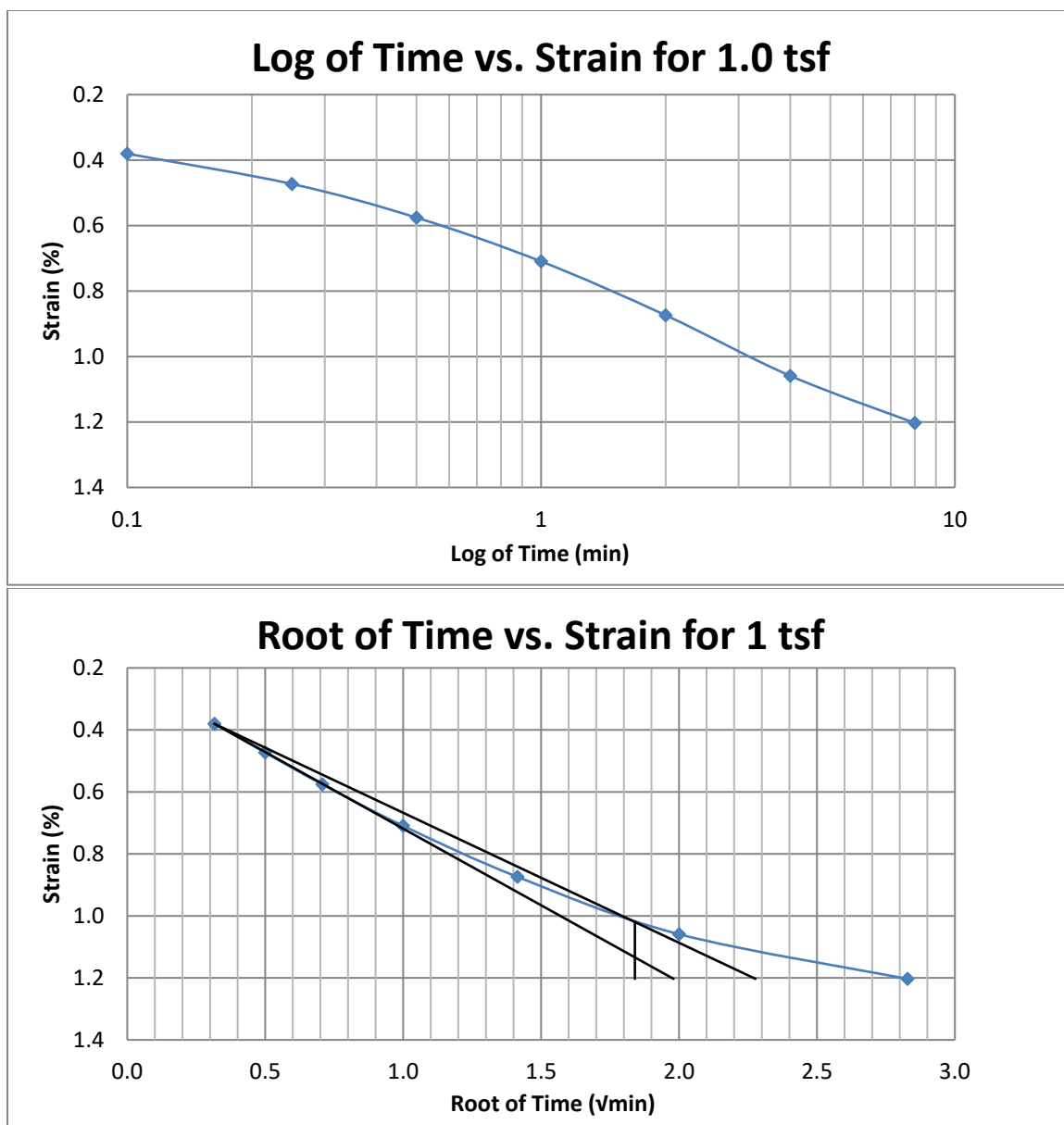


Figure A245 Provo at 90-92 feet

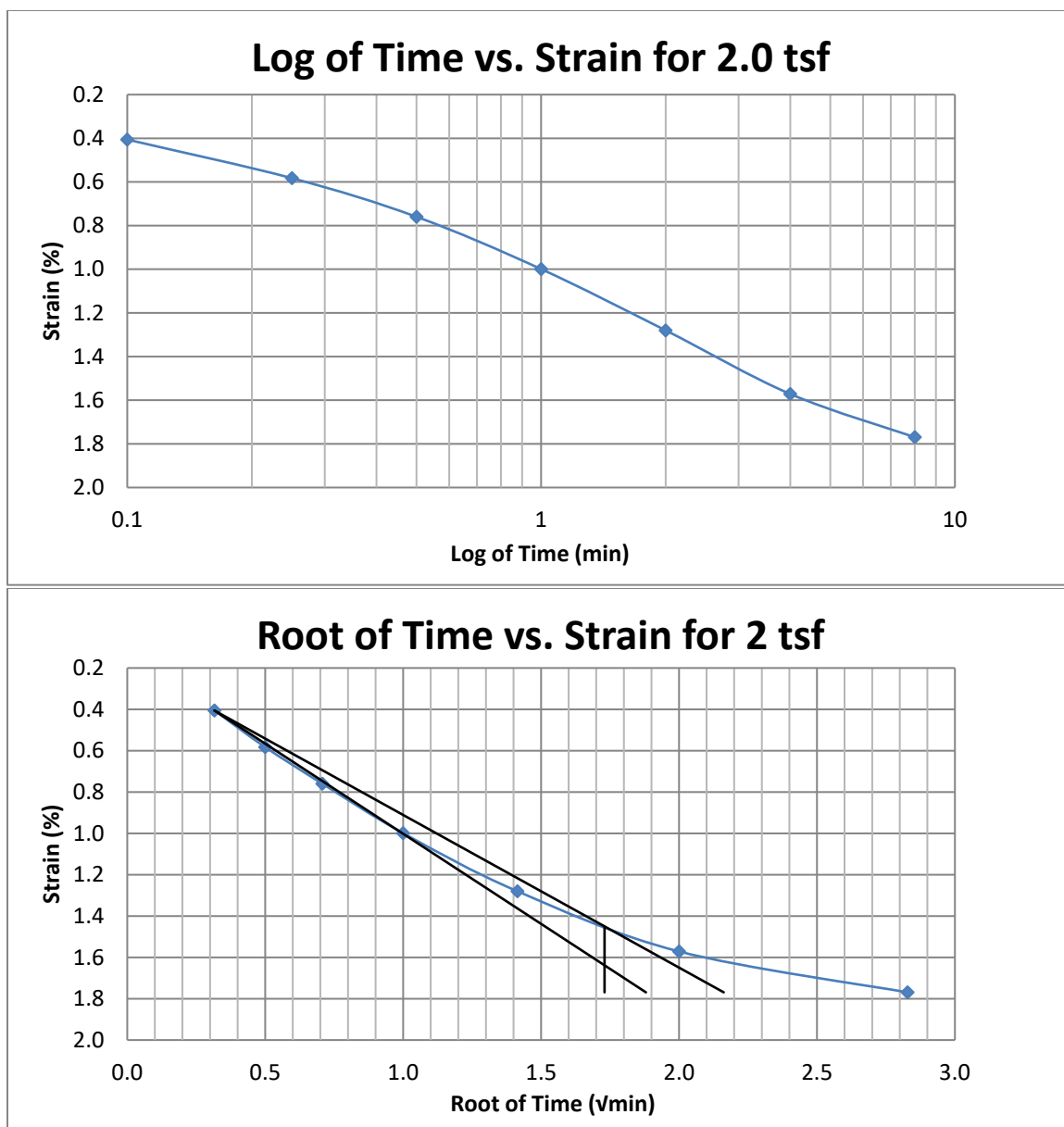


Figure A246 Provo at 90-92 feet

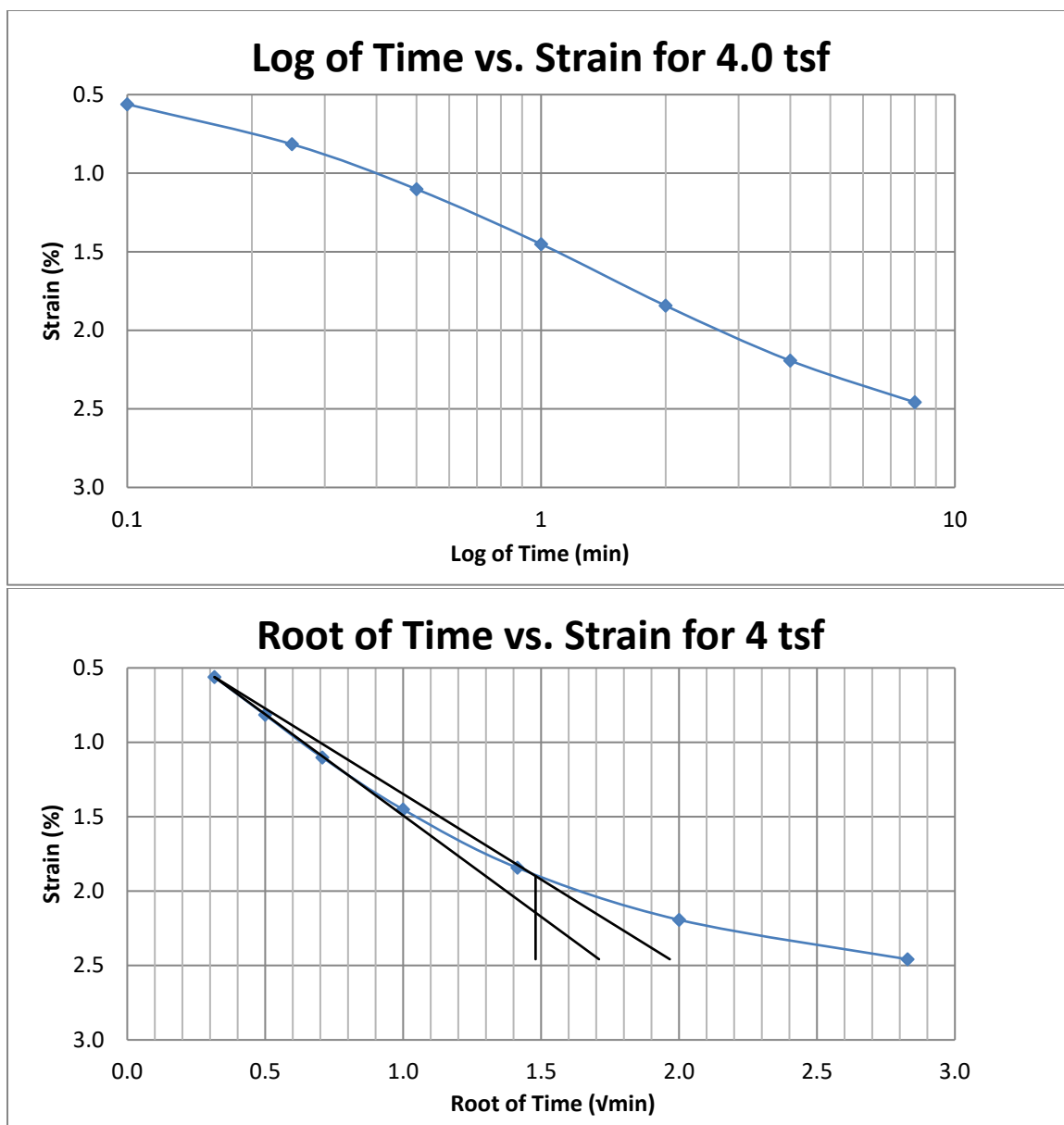


Figure A247 Provo at 90-92 feet

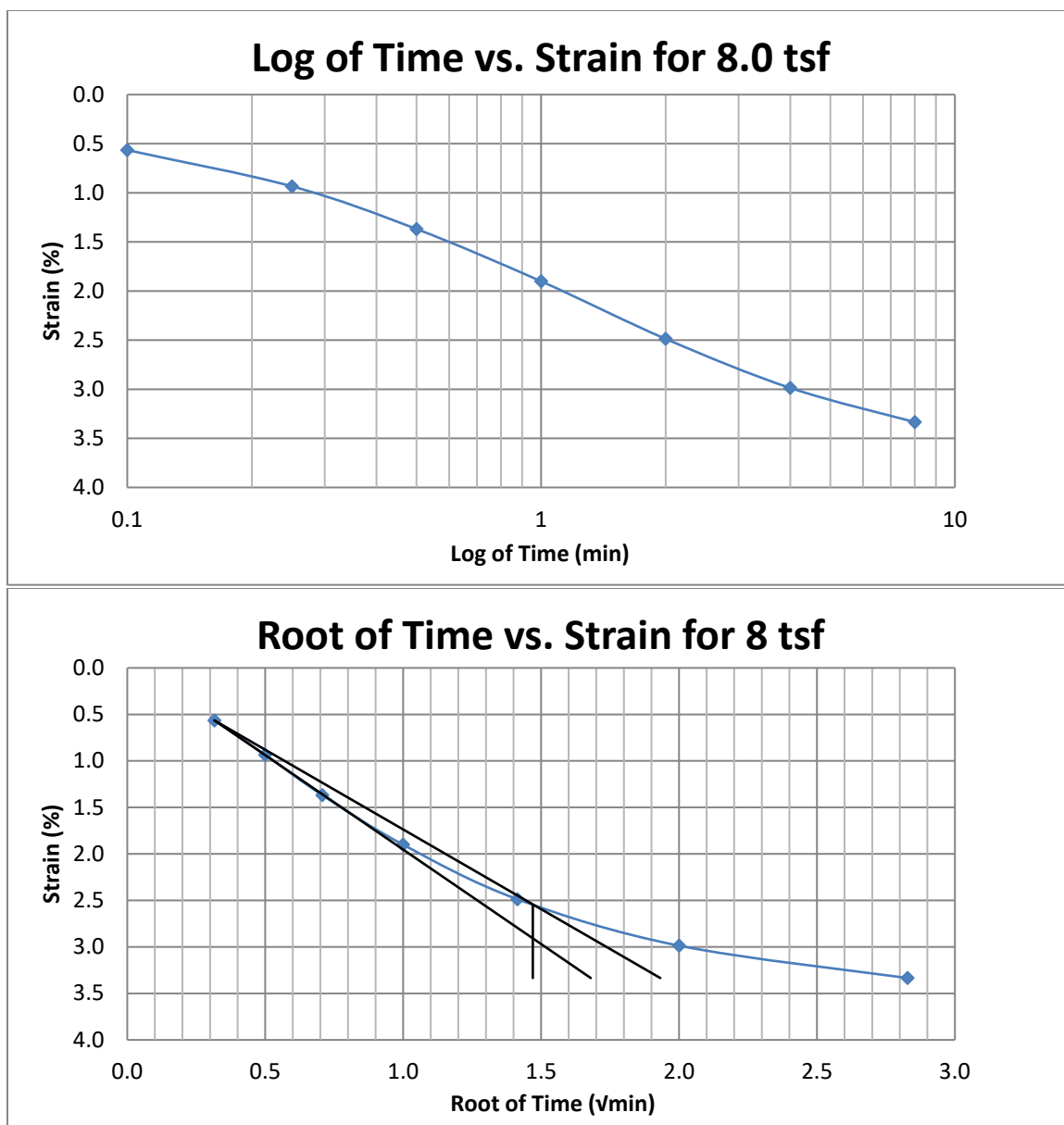


Figure A248 Provo at 90-92 feet

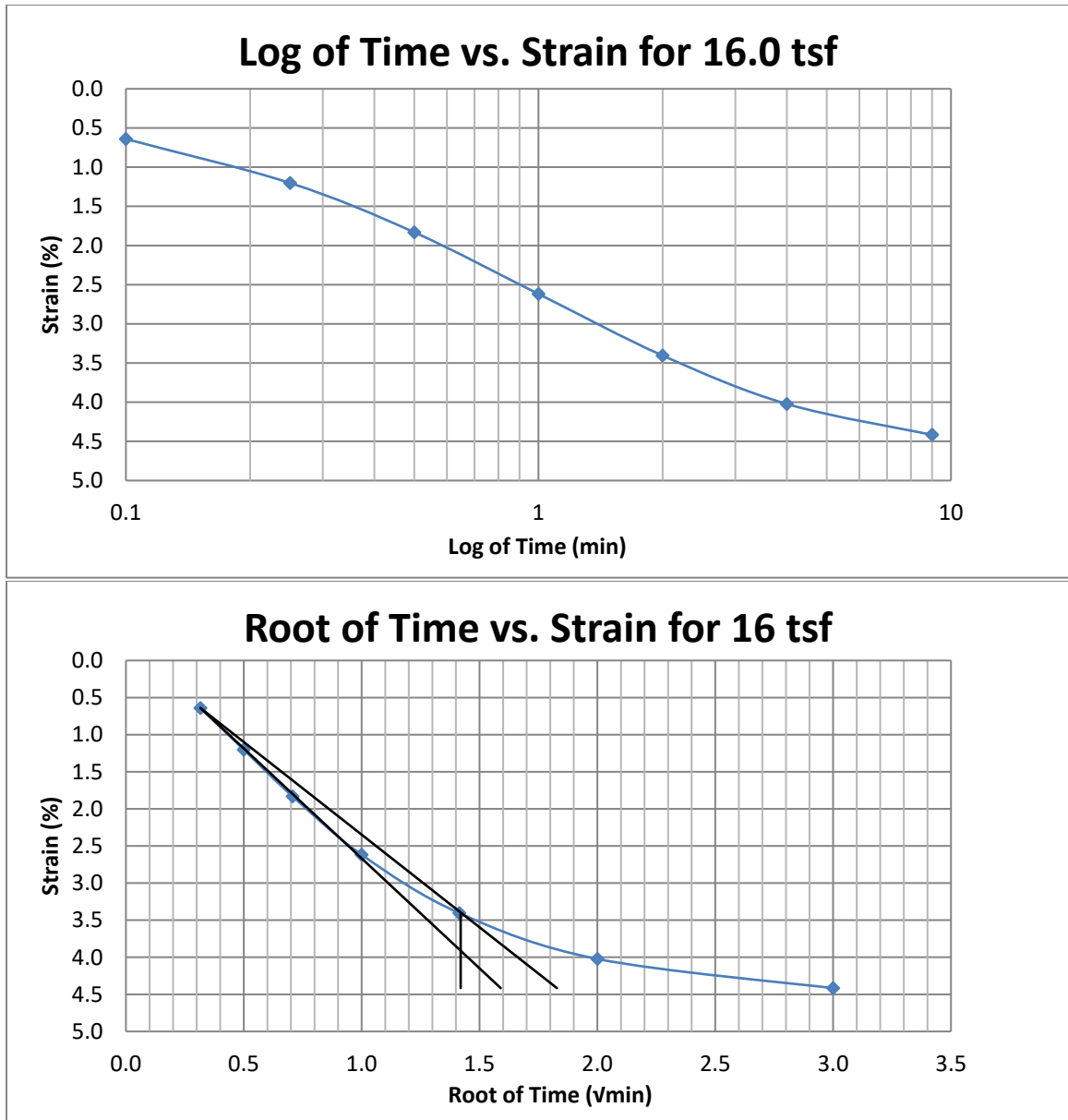


Figure A249 Provo at 90-92 feet

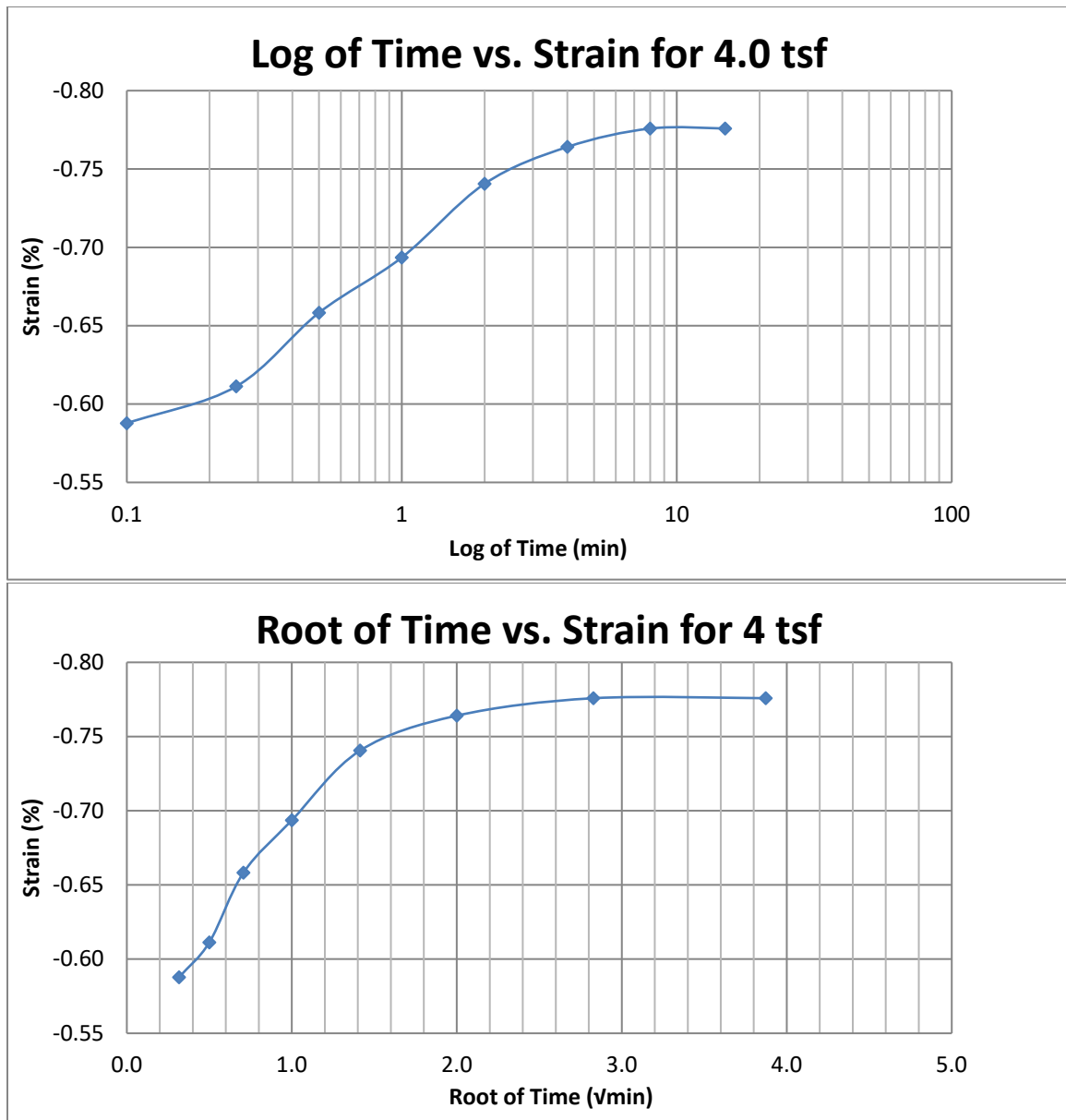


Figure A250 Provo at 90-92 feet



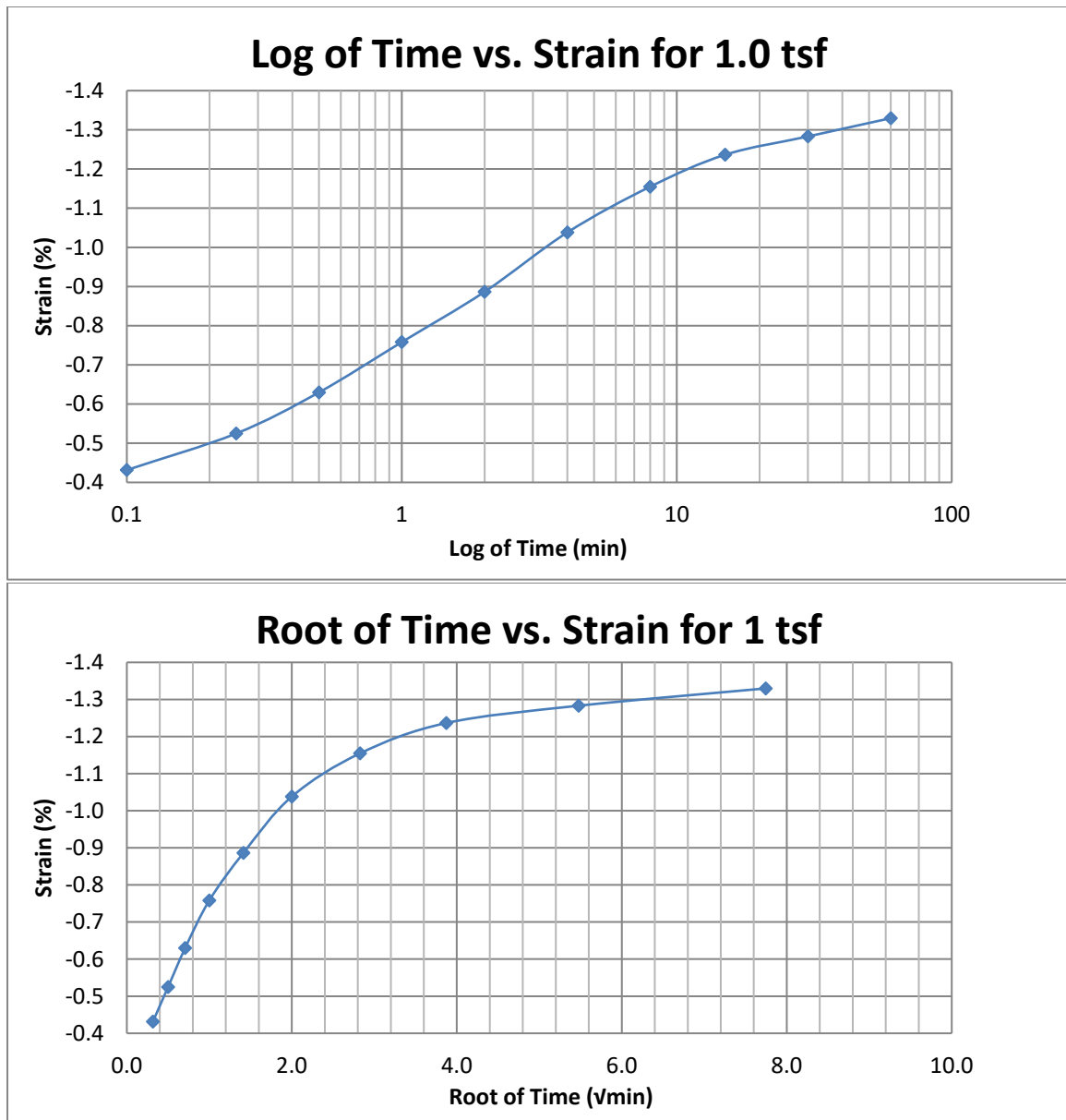


Figure A251 Provo at 90-92 feet

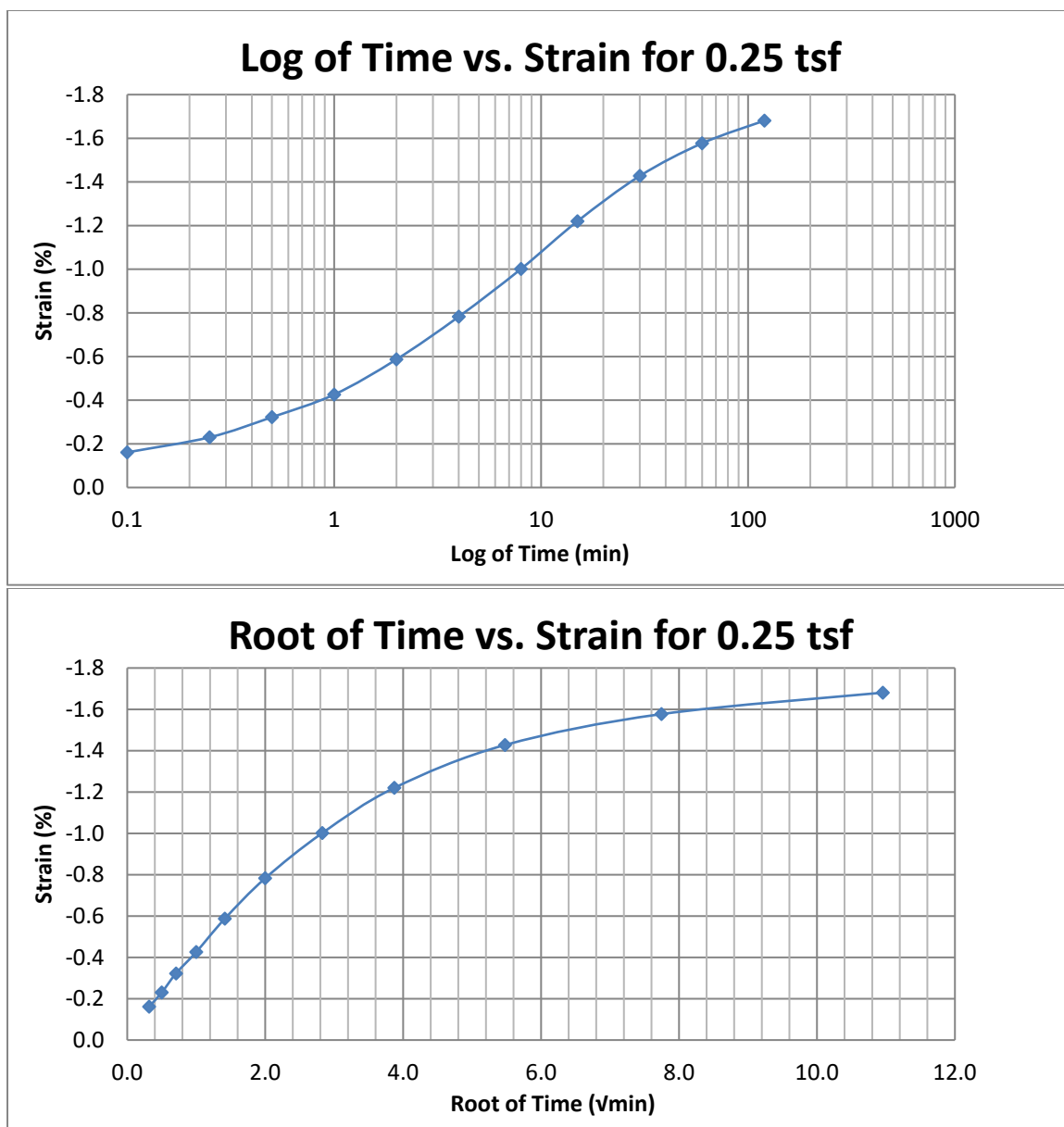


Figure A252 Provo at 90-92 feet

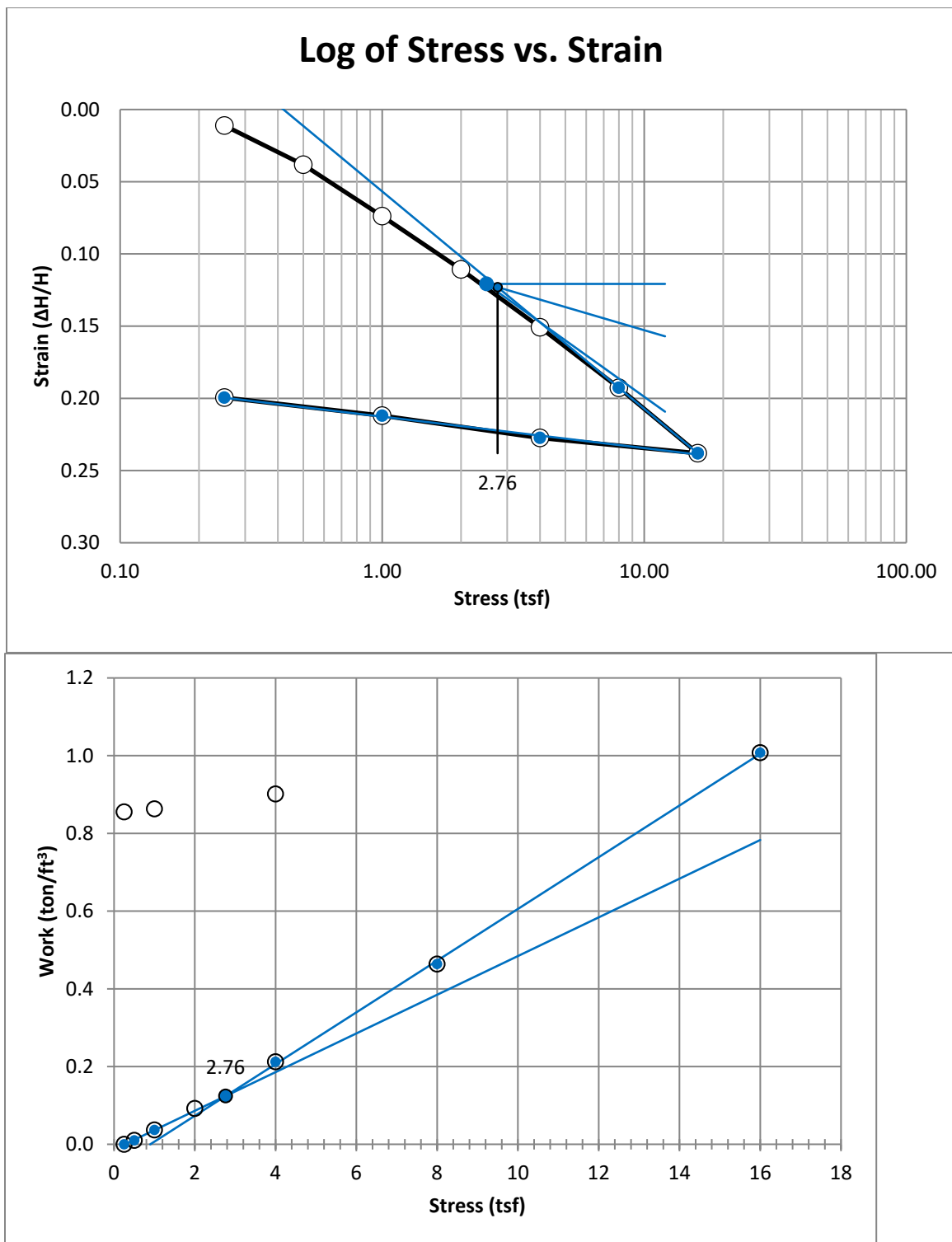


Figure A253 Provo at 110-112 feet

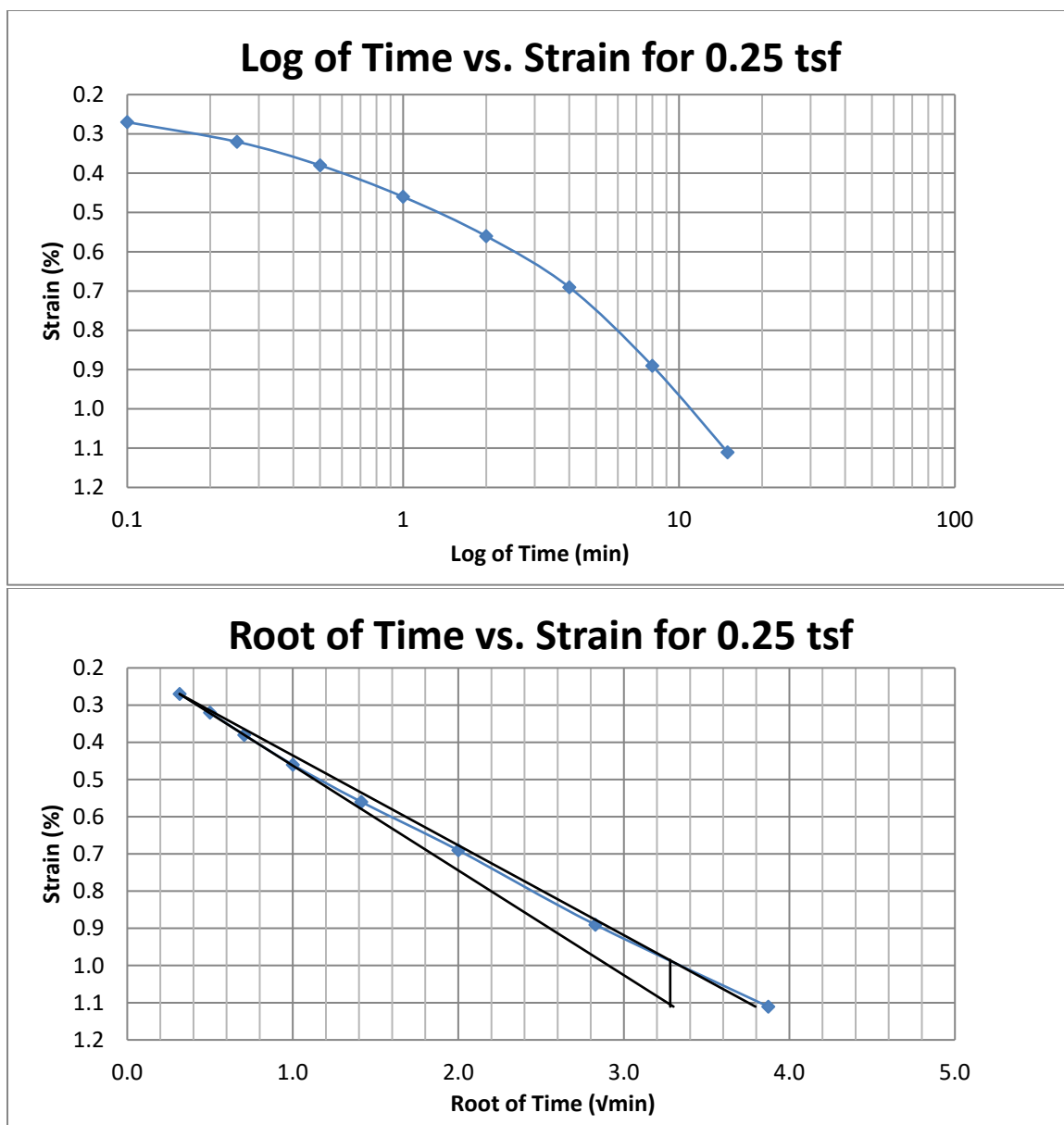


Figure A254 Provo at 110-112 feet

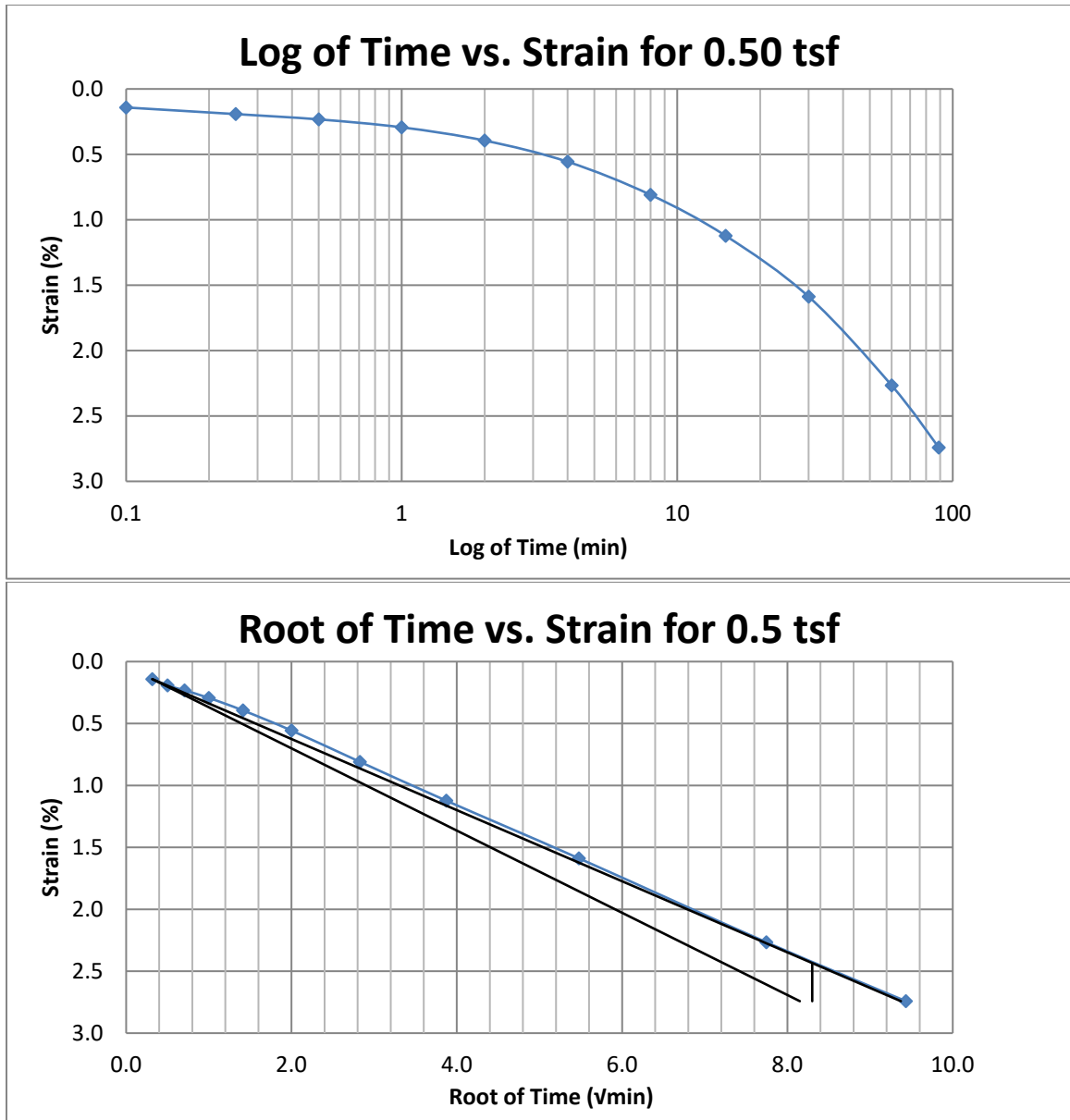


Figure A255 Provo at 110-112 feet

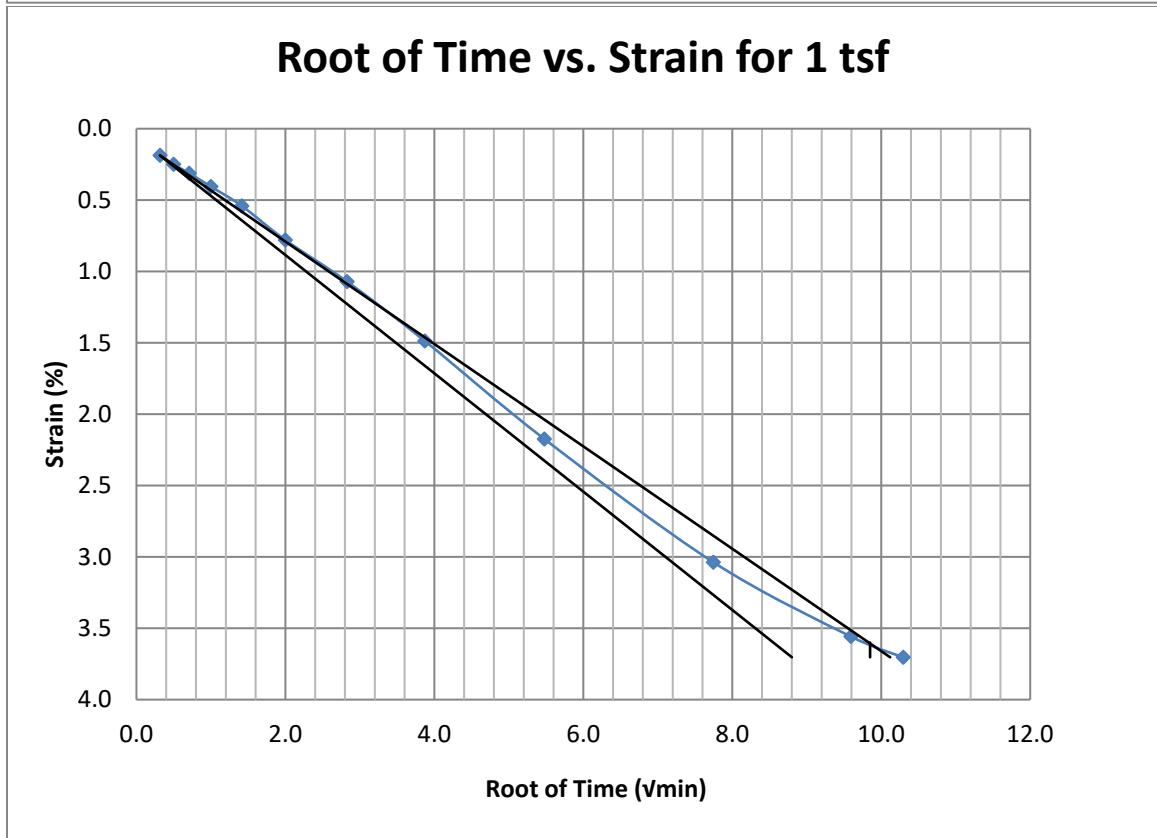
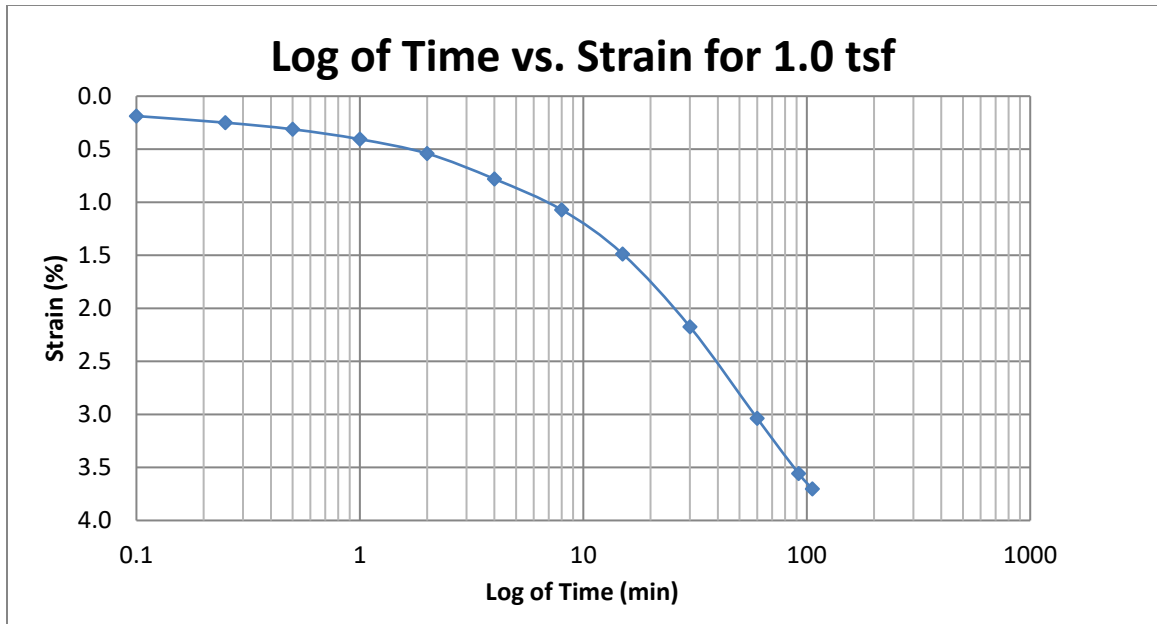


Figure A256 Provo at 110-112 feet

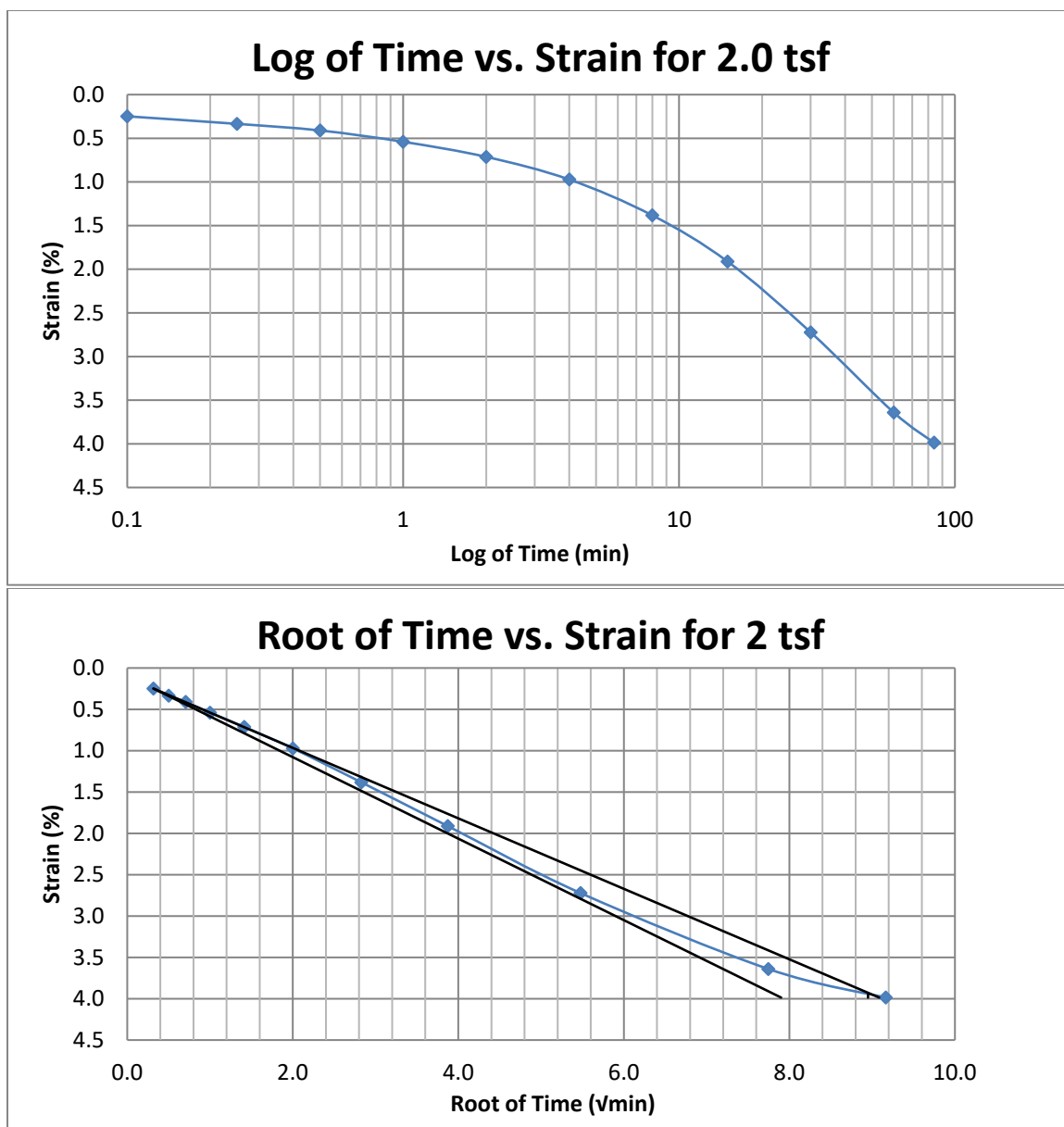


Figure A257 Provo at 110-112 feet

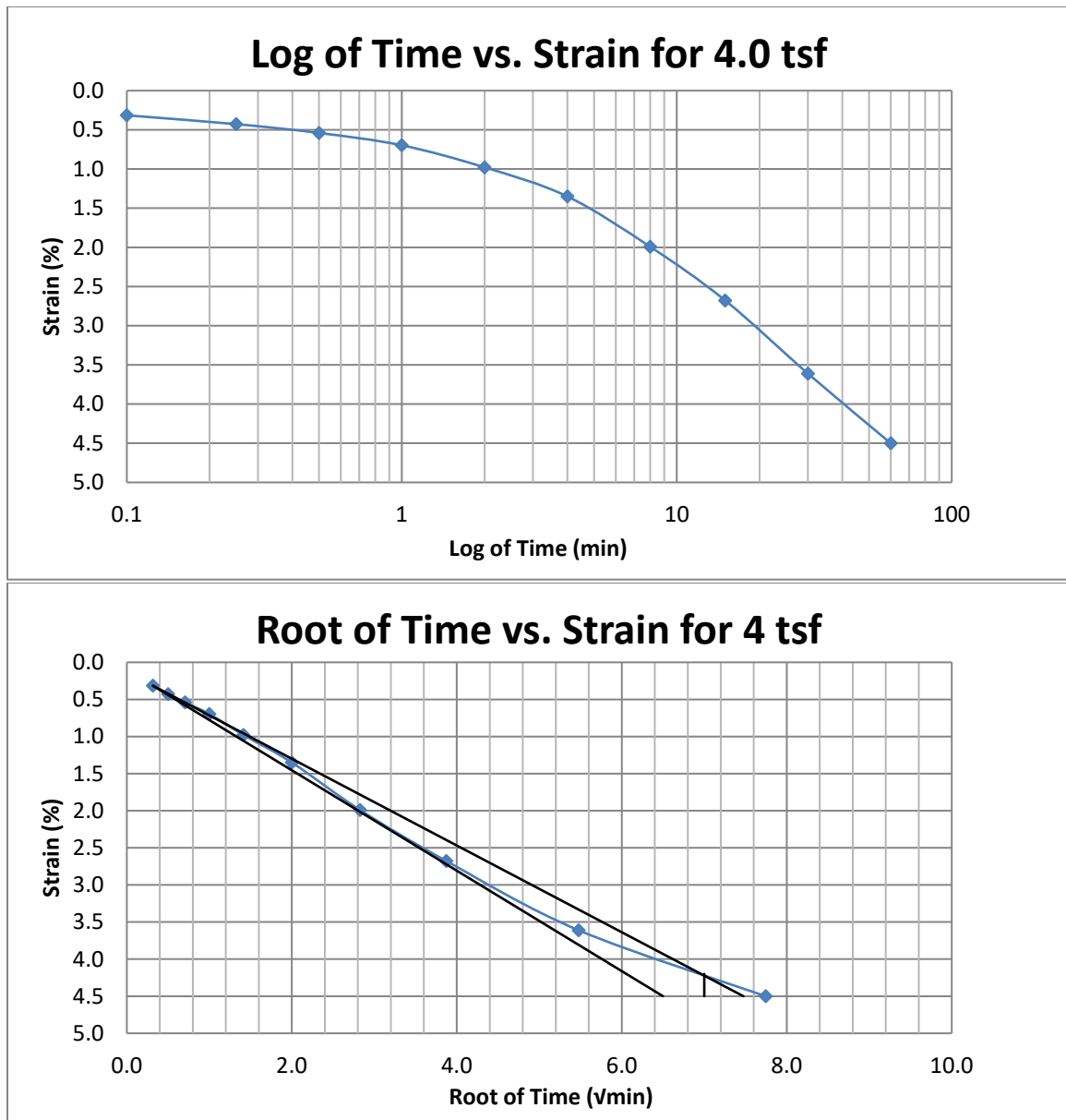


Figure A258 Provo at 110-112 feet



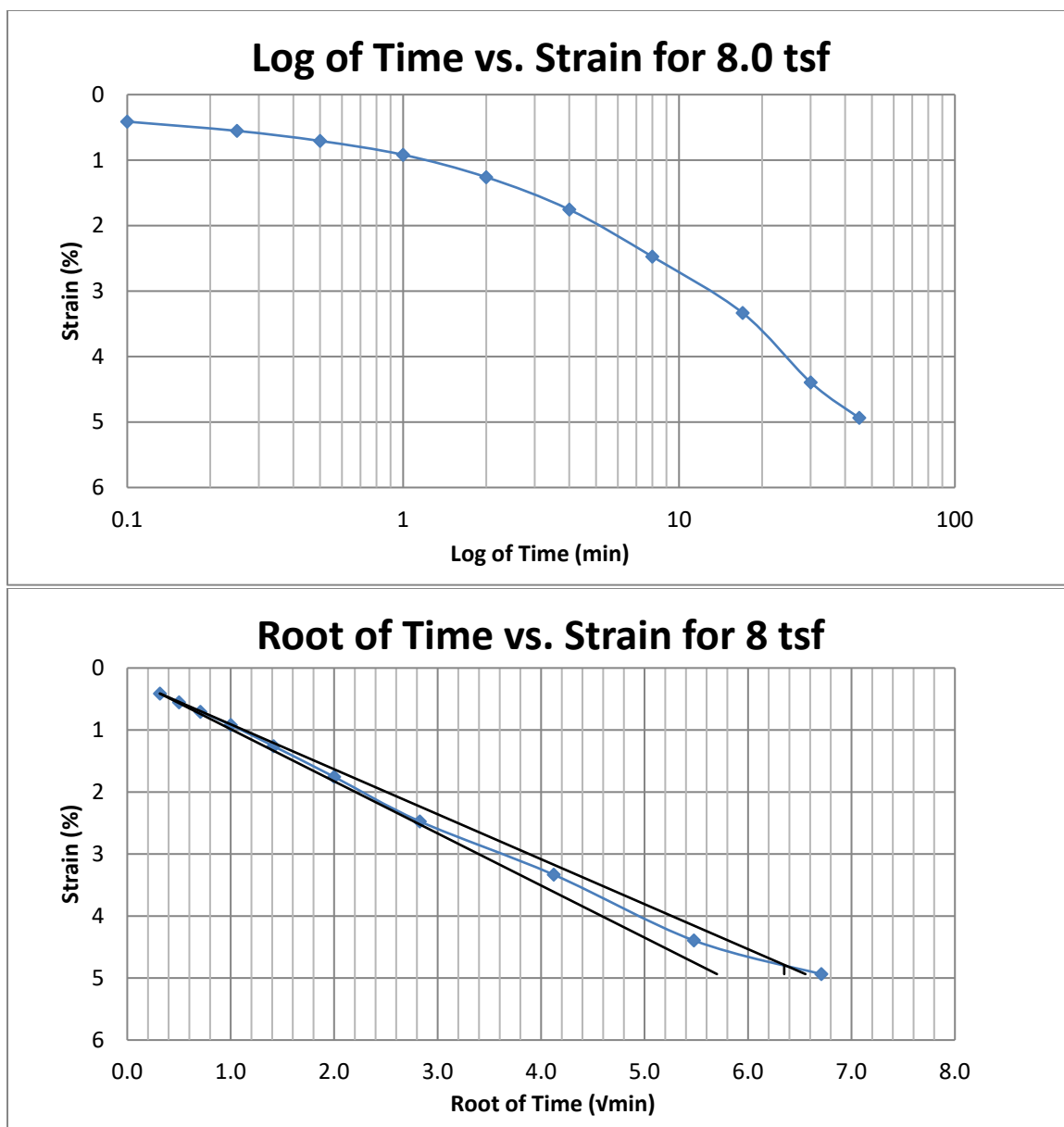


Figure A259 Provo at 110-112 feet

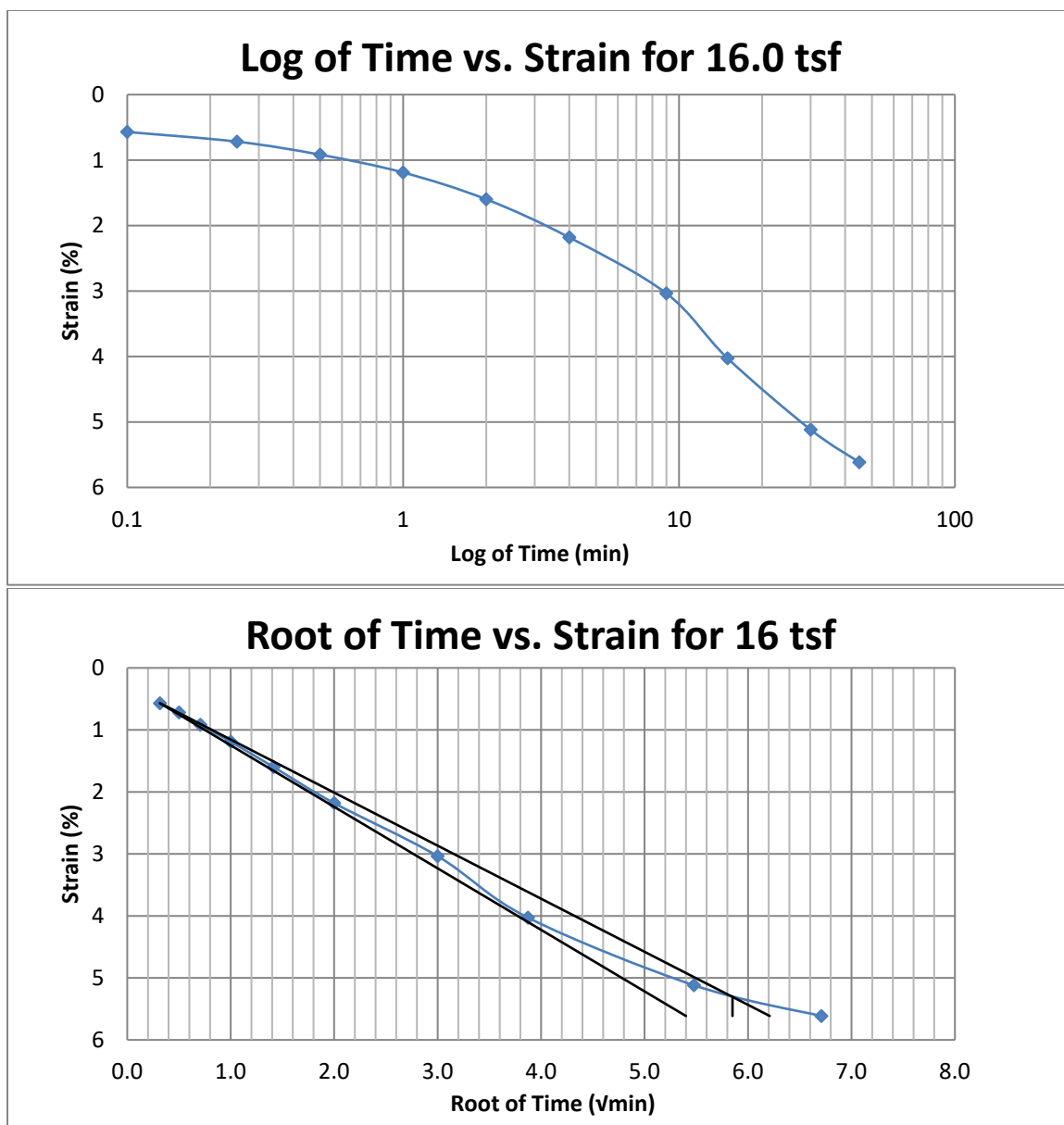
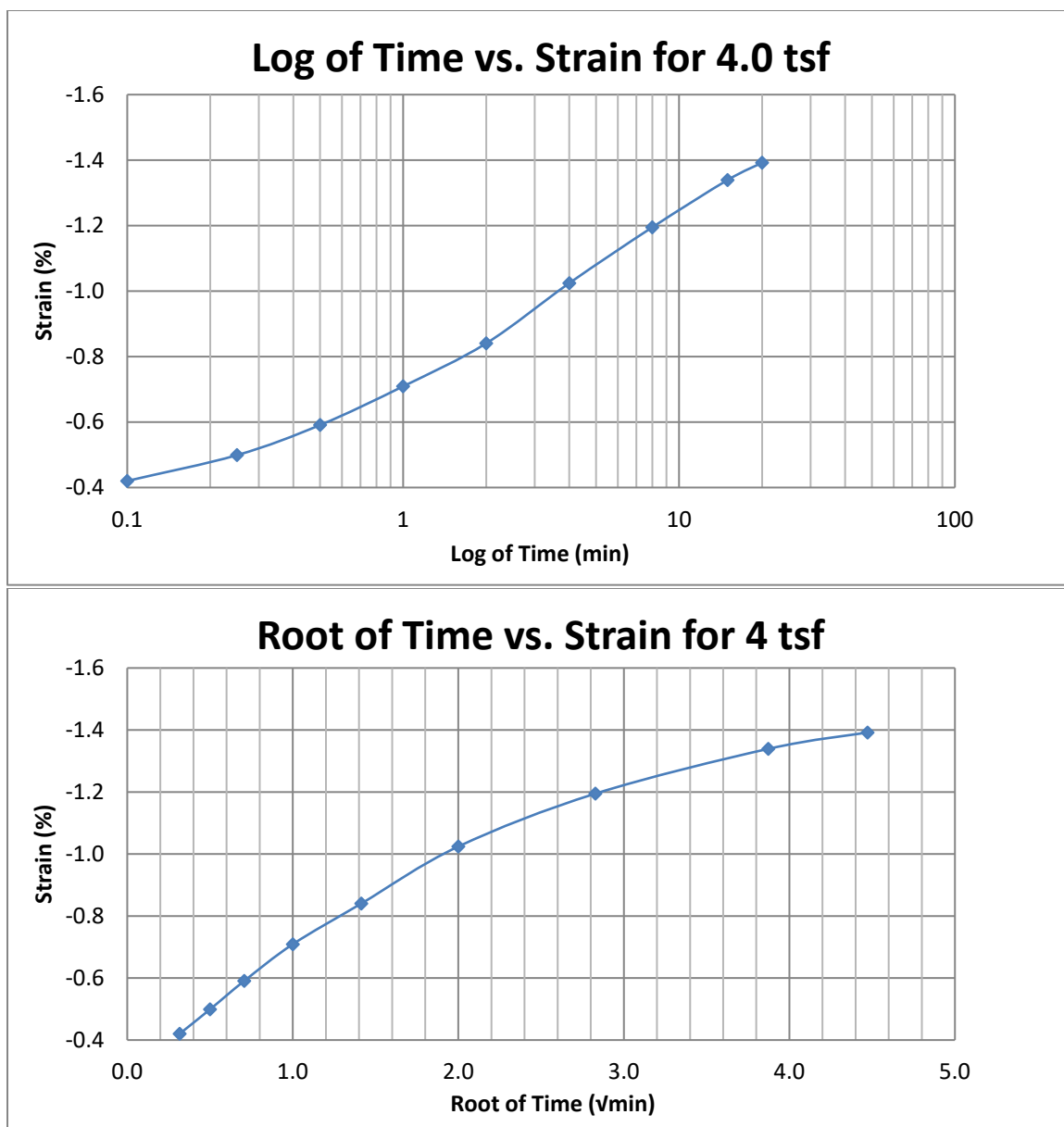
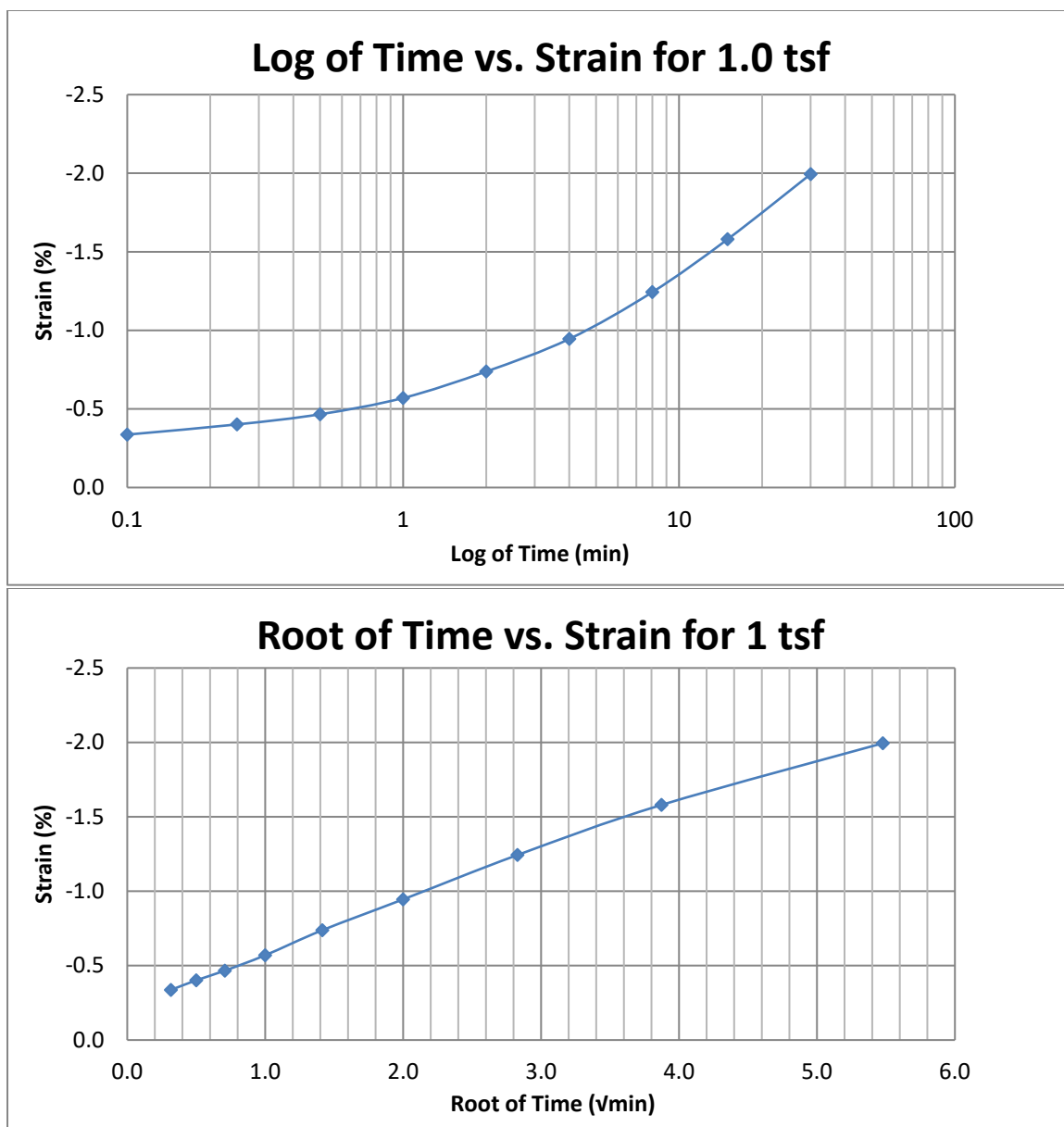


Figure A260 Provo at 110-112 feet



**Figure A261 Provo at 110-112 feet**



**Figure A262 Provo at 110-112 feet**

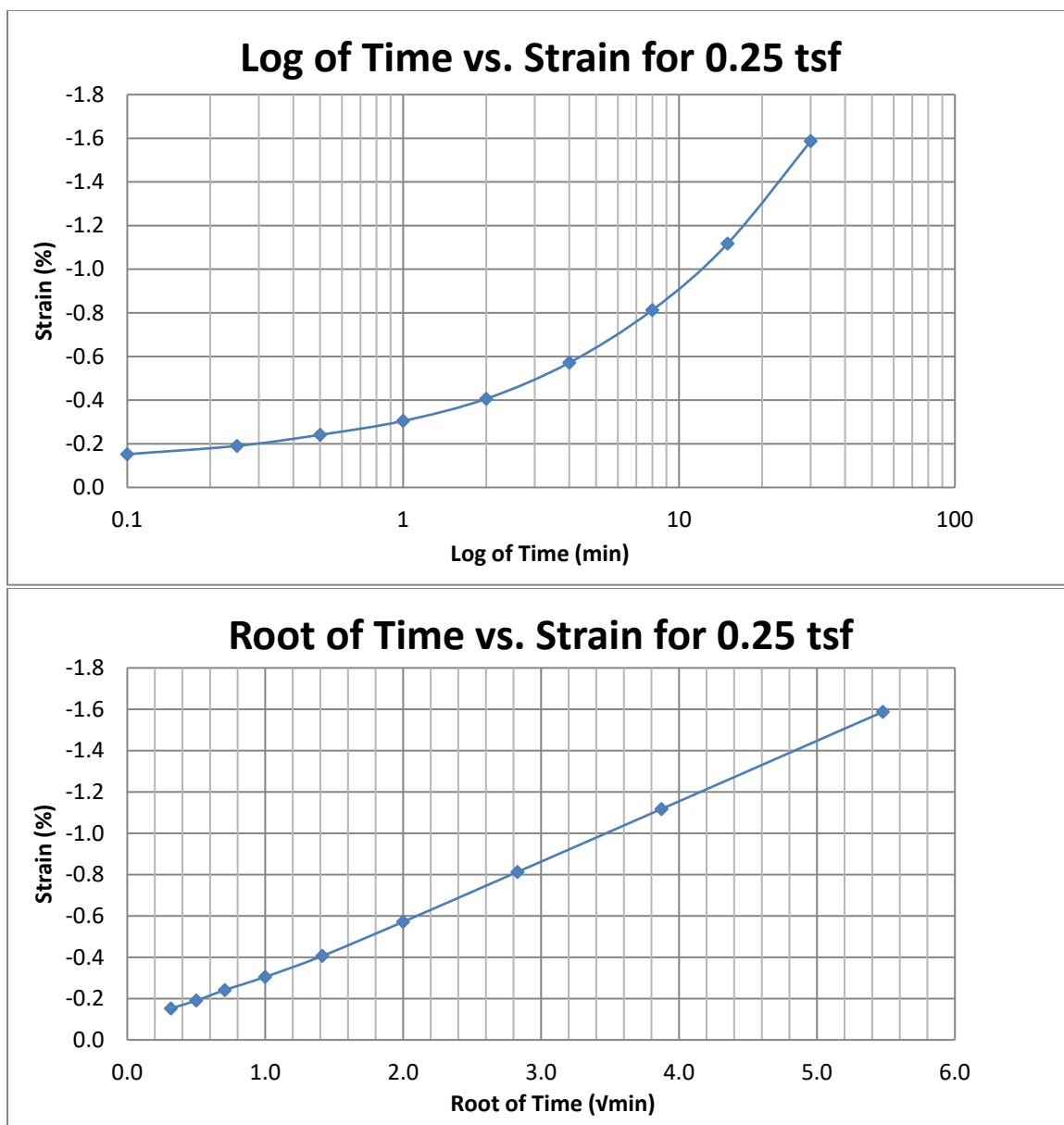


Figure A263 Provo at 110-112 feet

## **APPENDIX B PLOTS OF RATE OF SECONDARY SETTLEMENT**

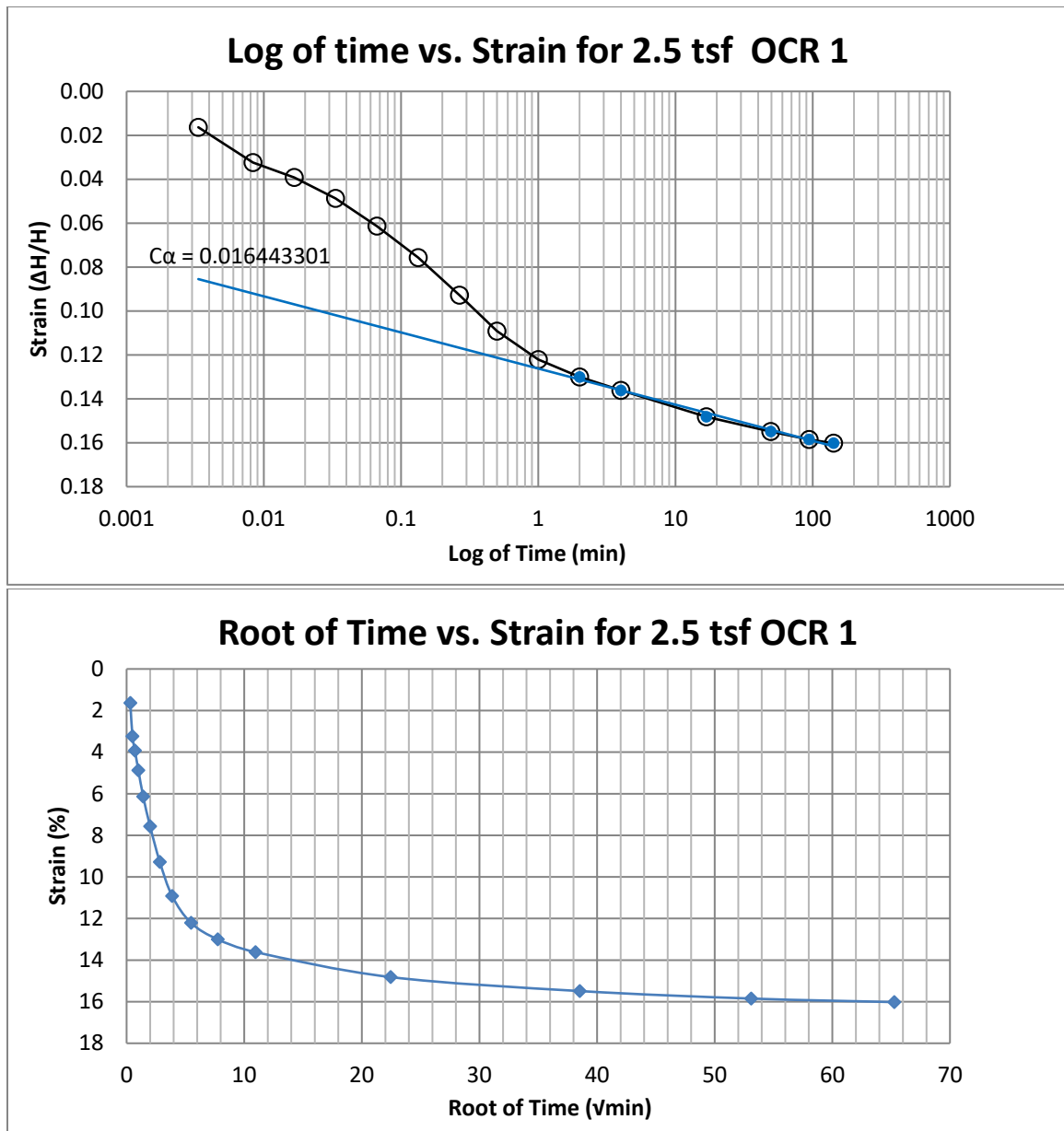
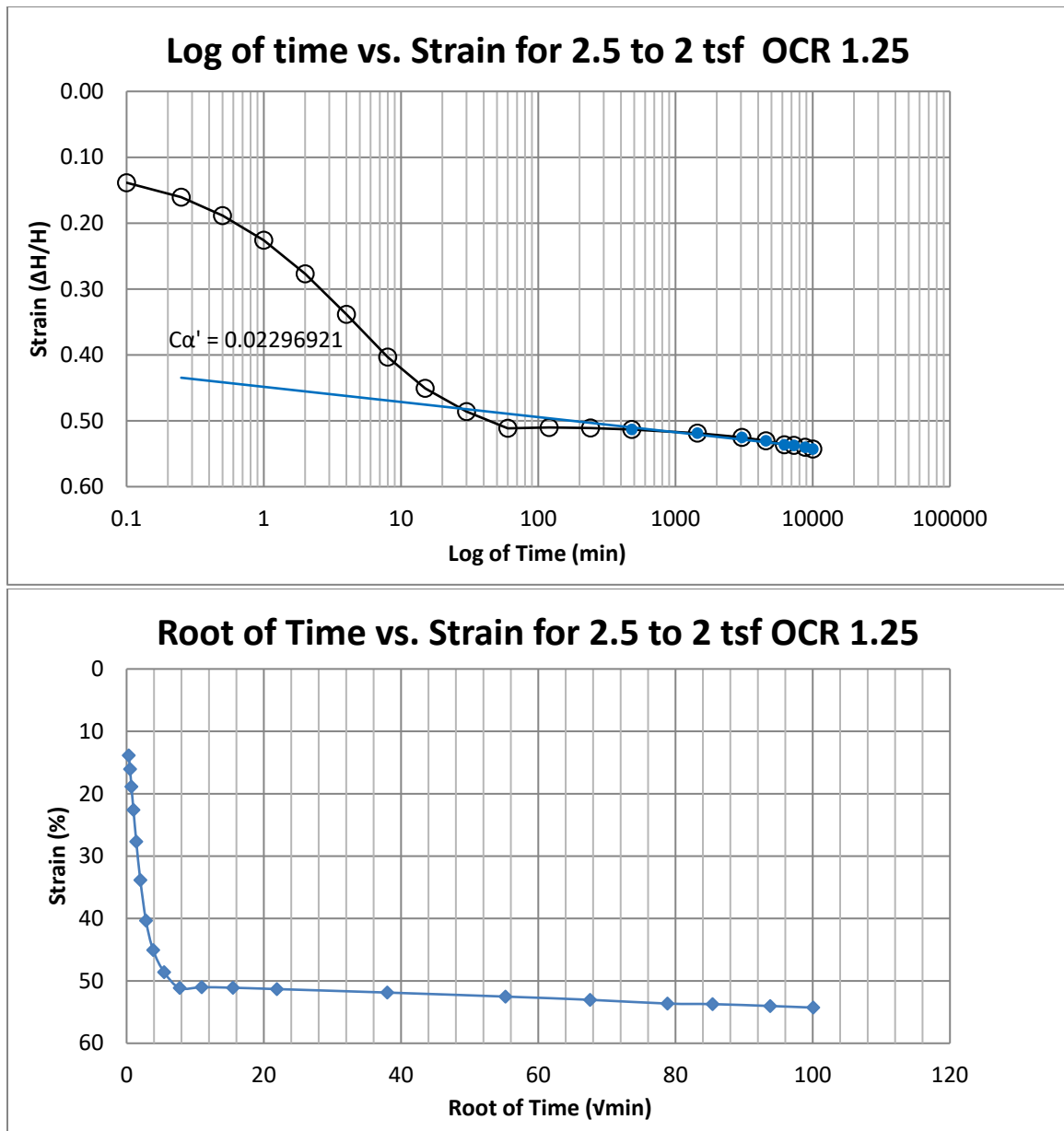


Figure B1 400 South at 15-17 feet



**Figure B2 400 South at 15-17 feet**



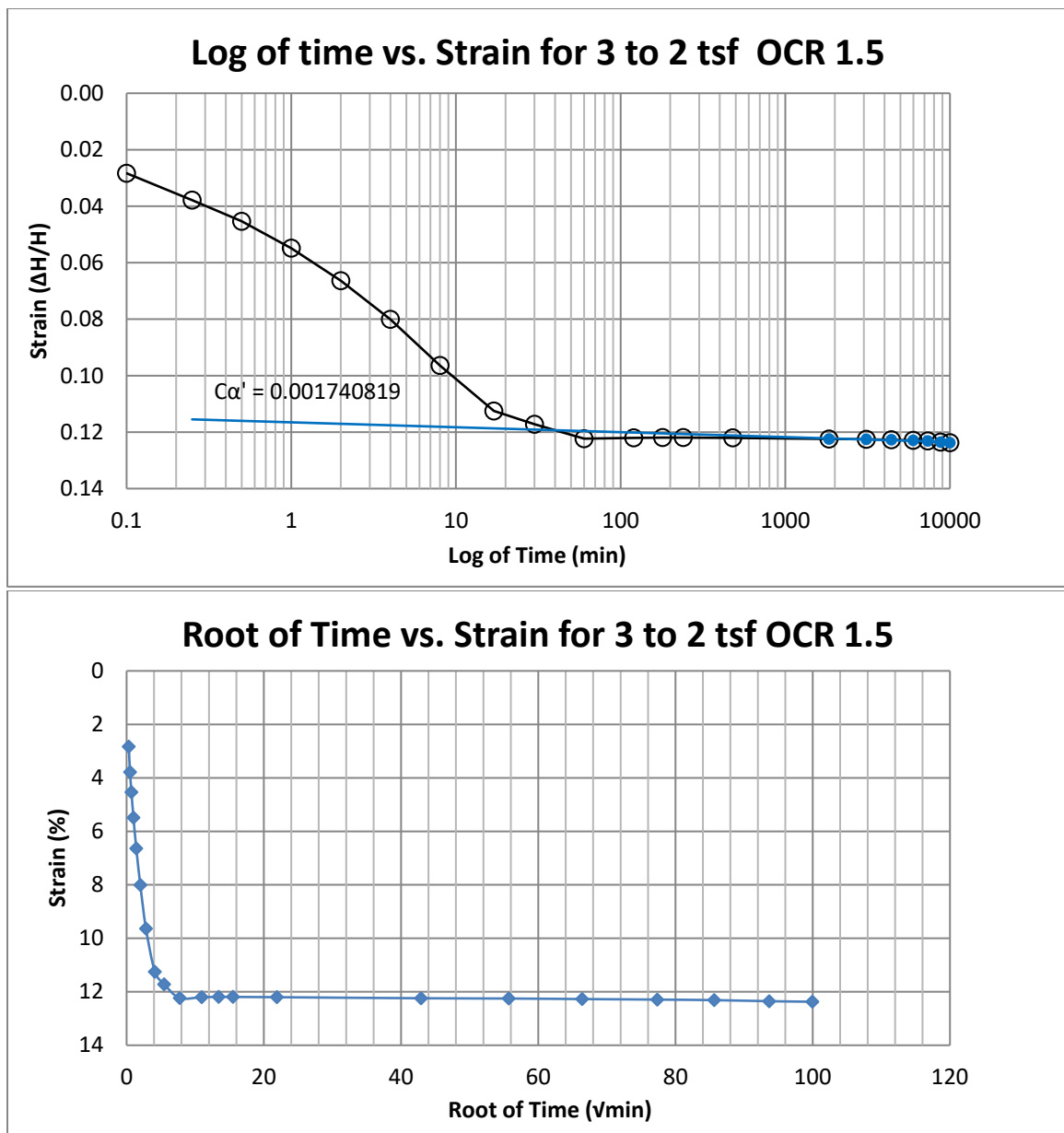


Figure B3 400 South at 15-17 feet

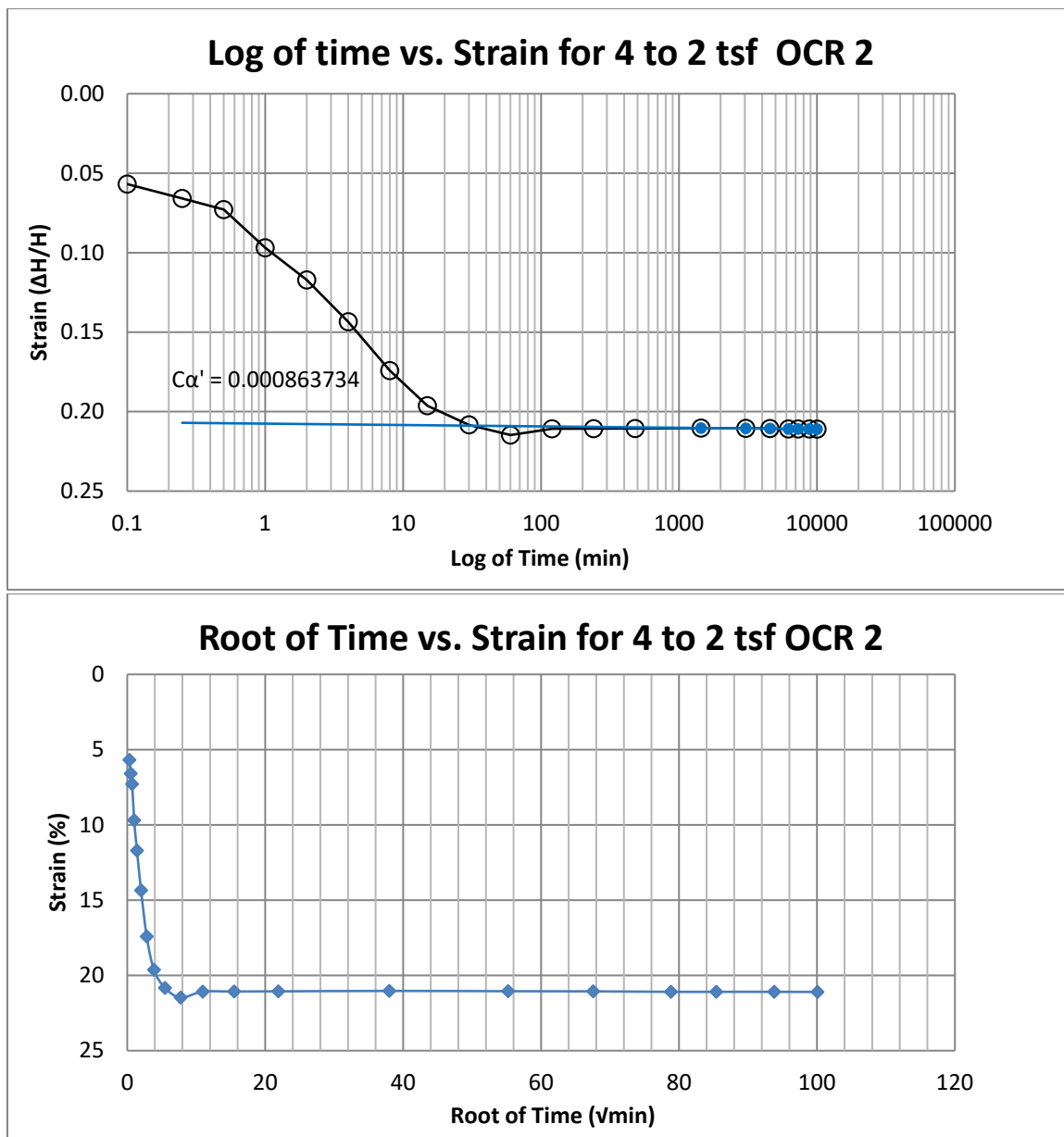


Figure B4 400 South at 15-17 feet

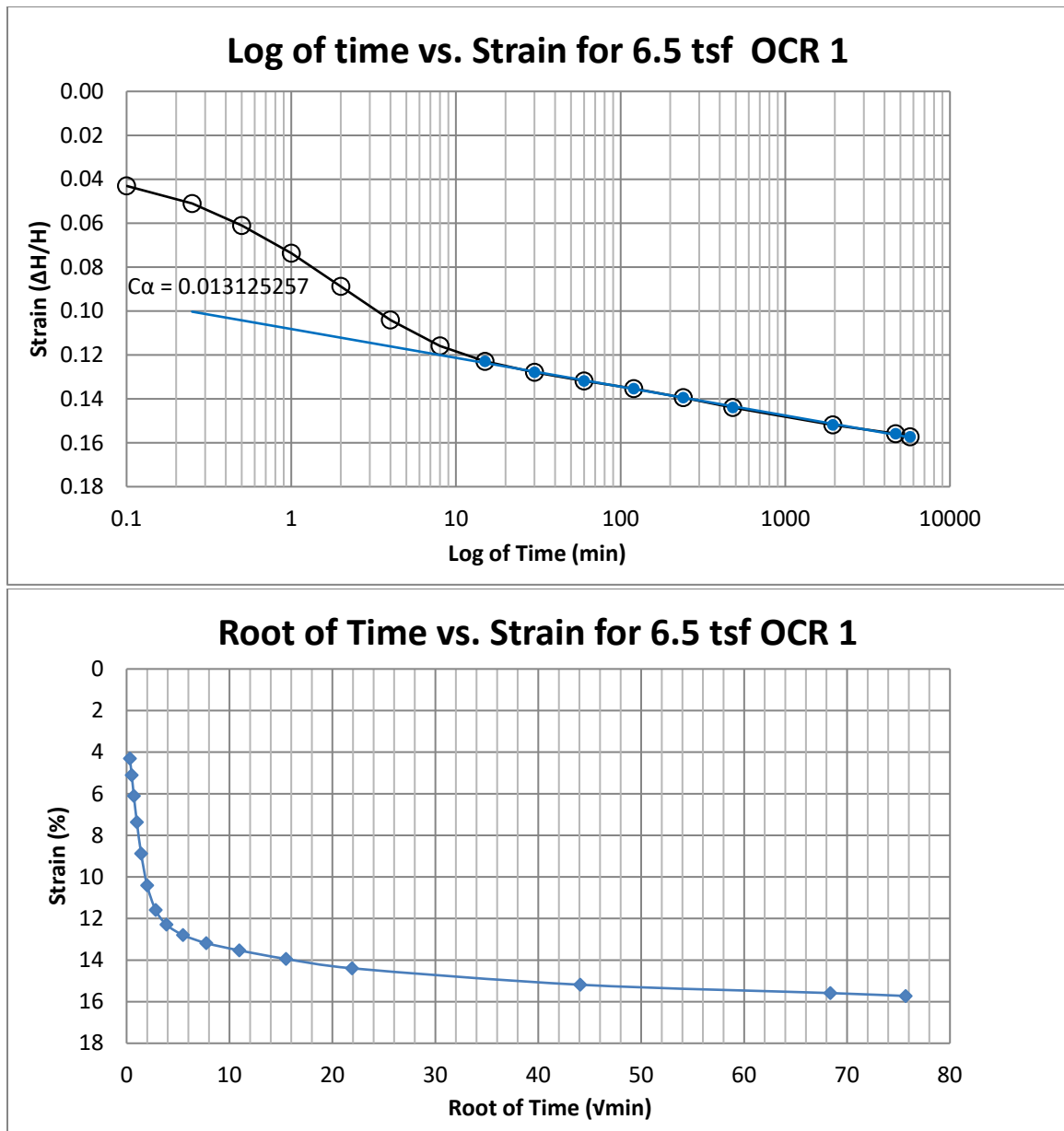


Figure B5 400 South at 20-22 feet

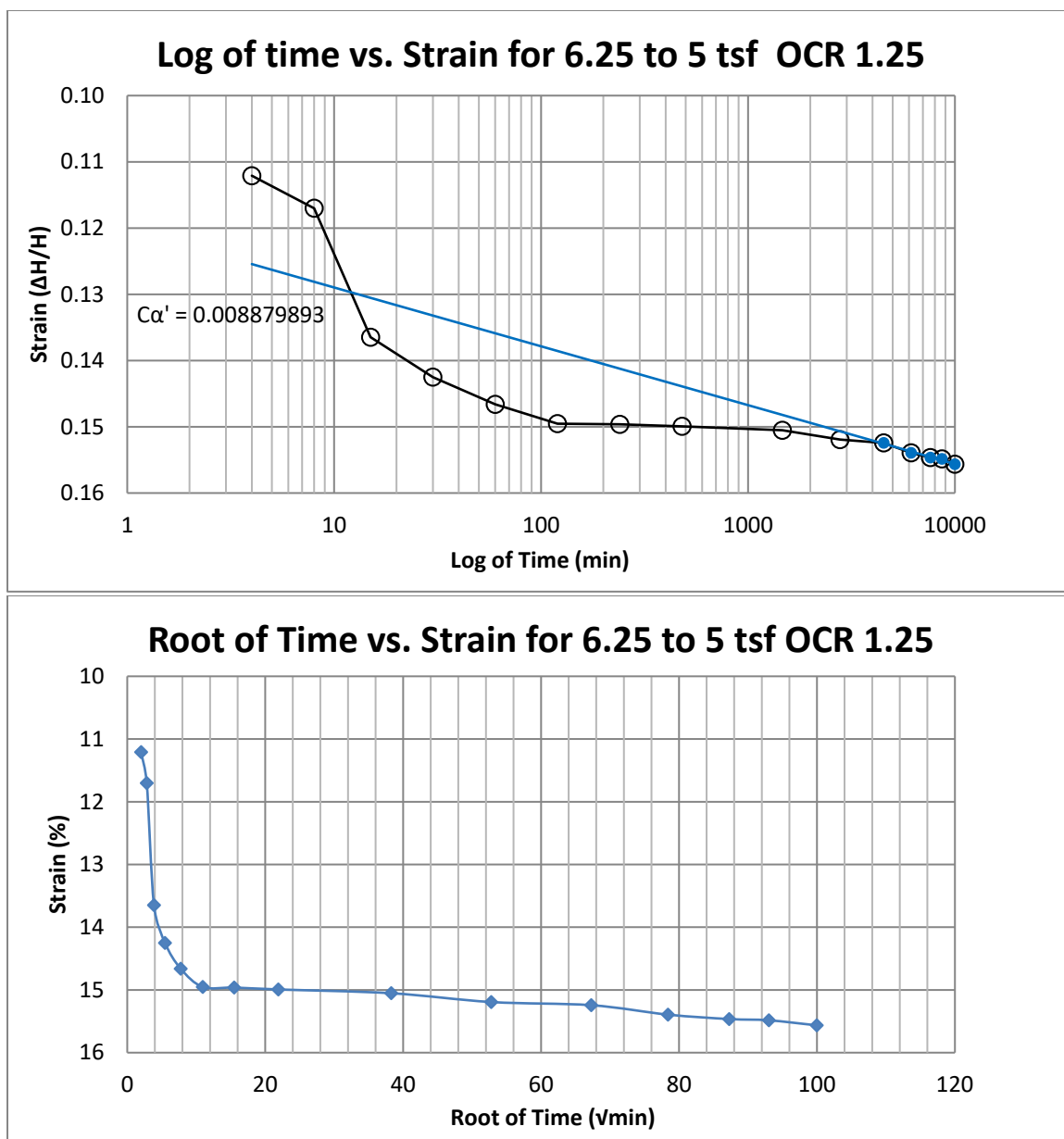


Figure B6 400 South at 20-22 feet

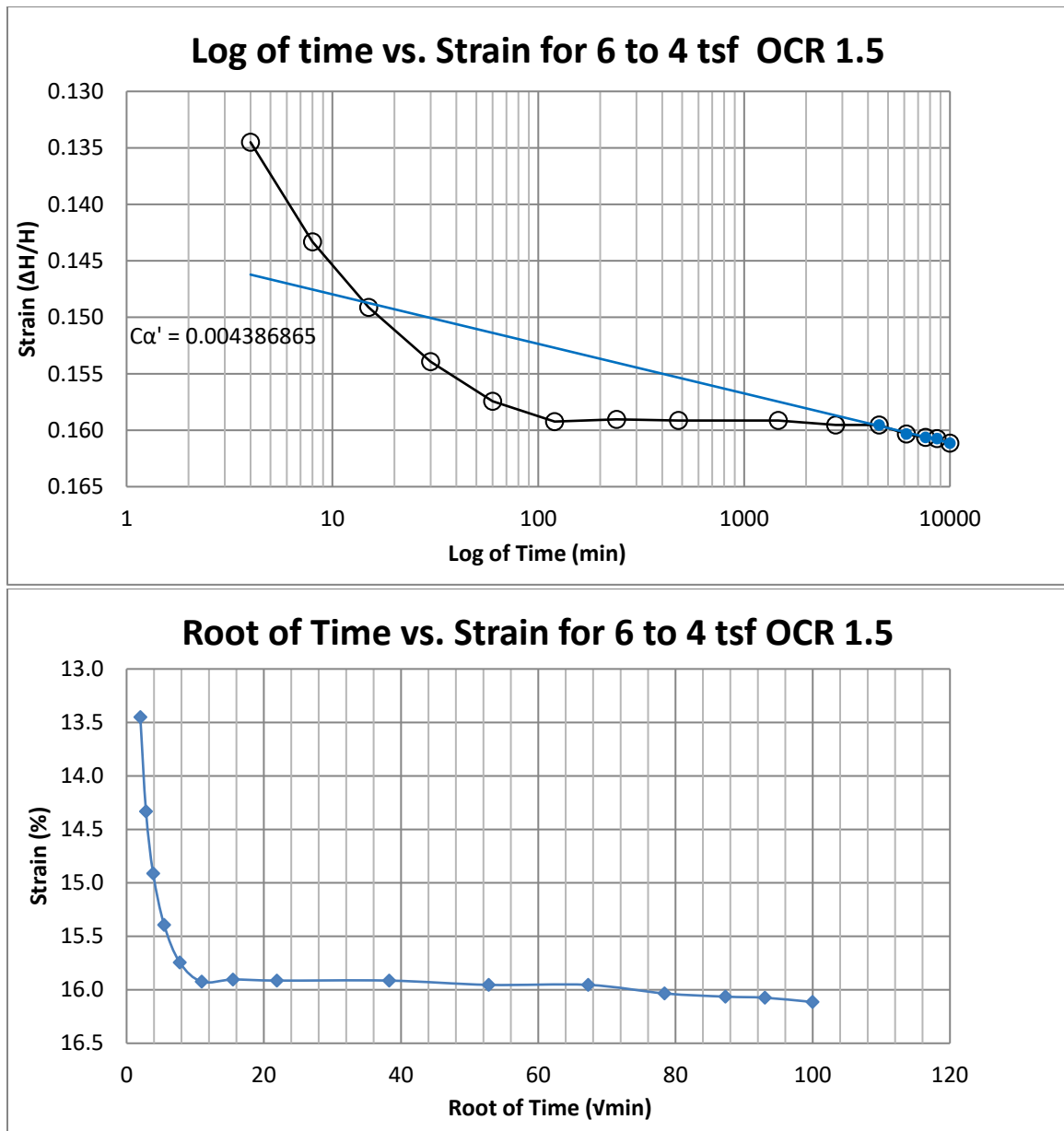


Figure B7 400 South at 20-22 feet

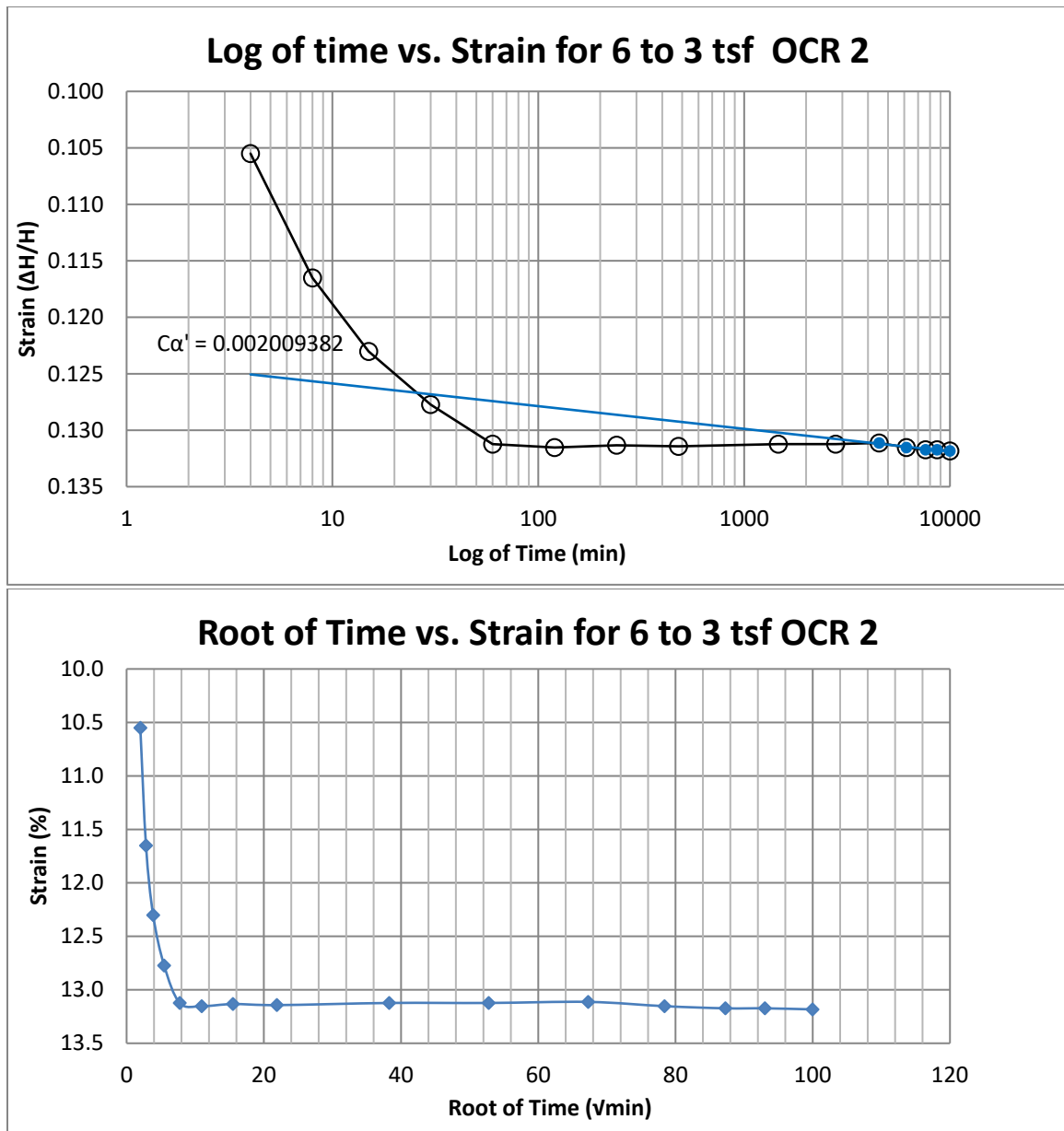


Figure B8 400 South at 20-22 feet

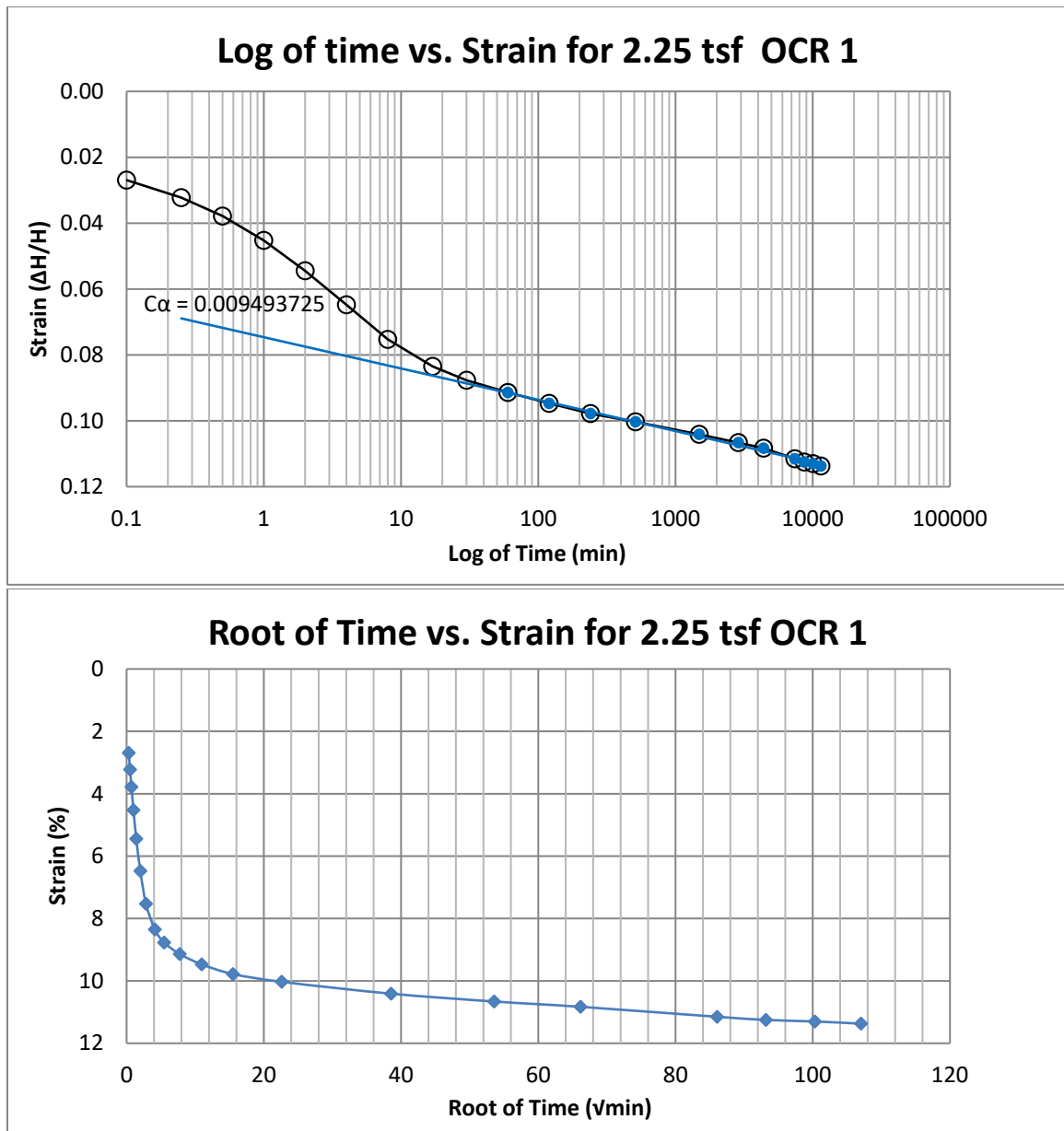


Figure B9 400 South at 25-27 feet

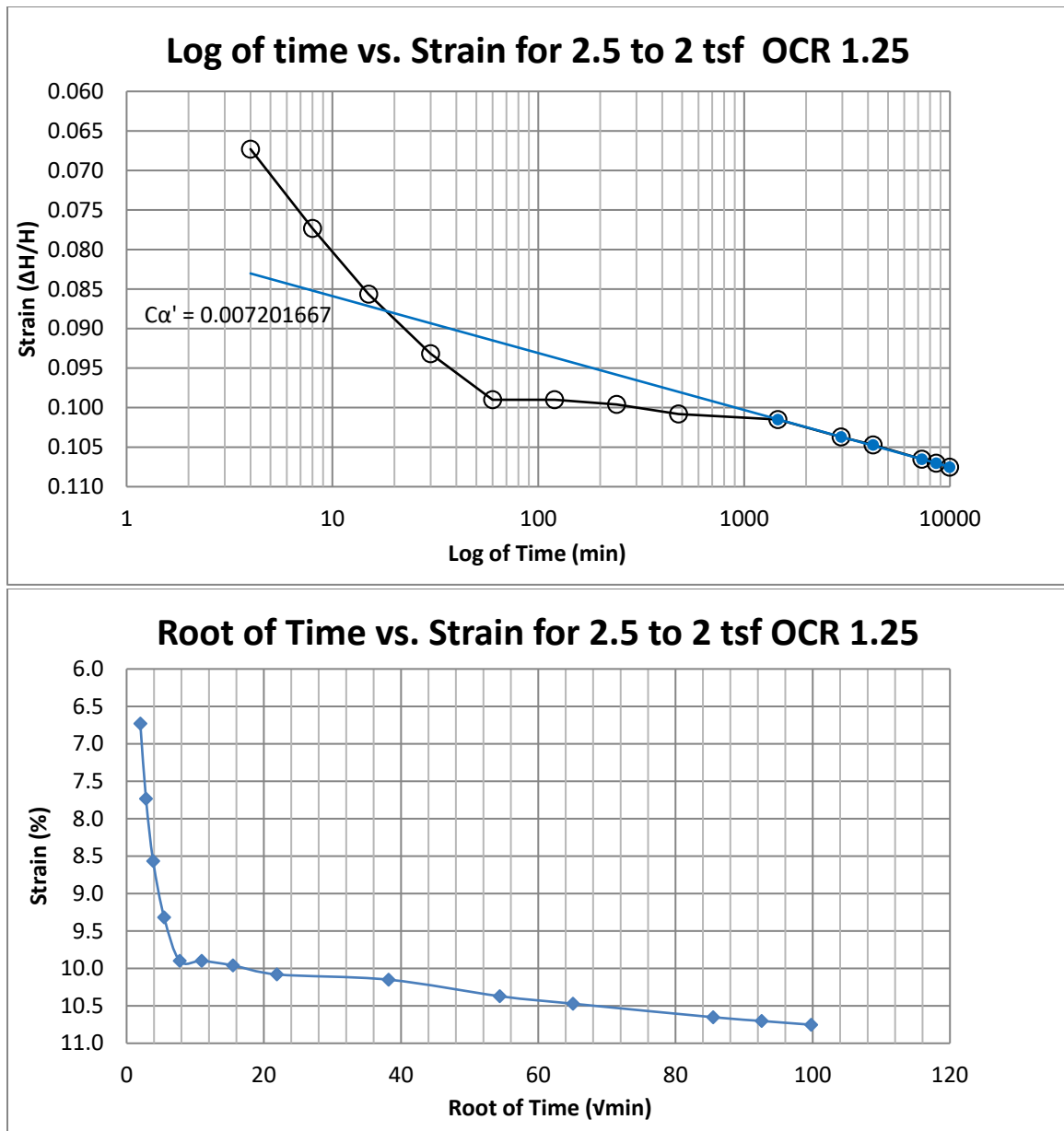


Figure B10 400 South at 25-27 feet



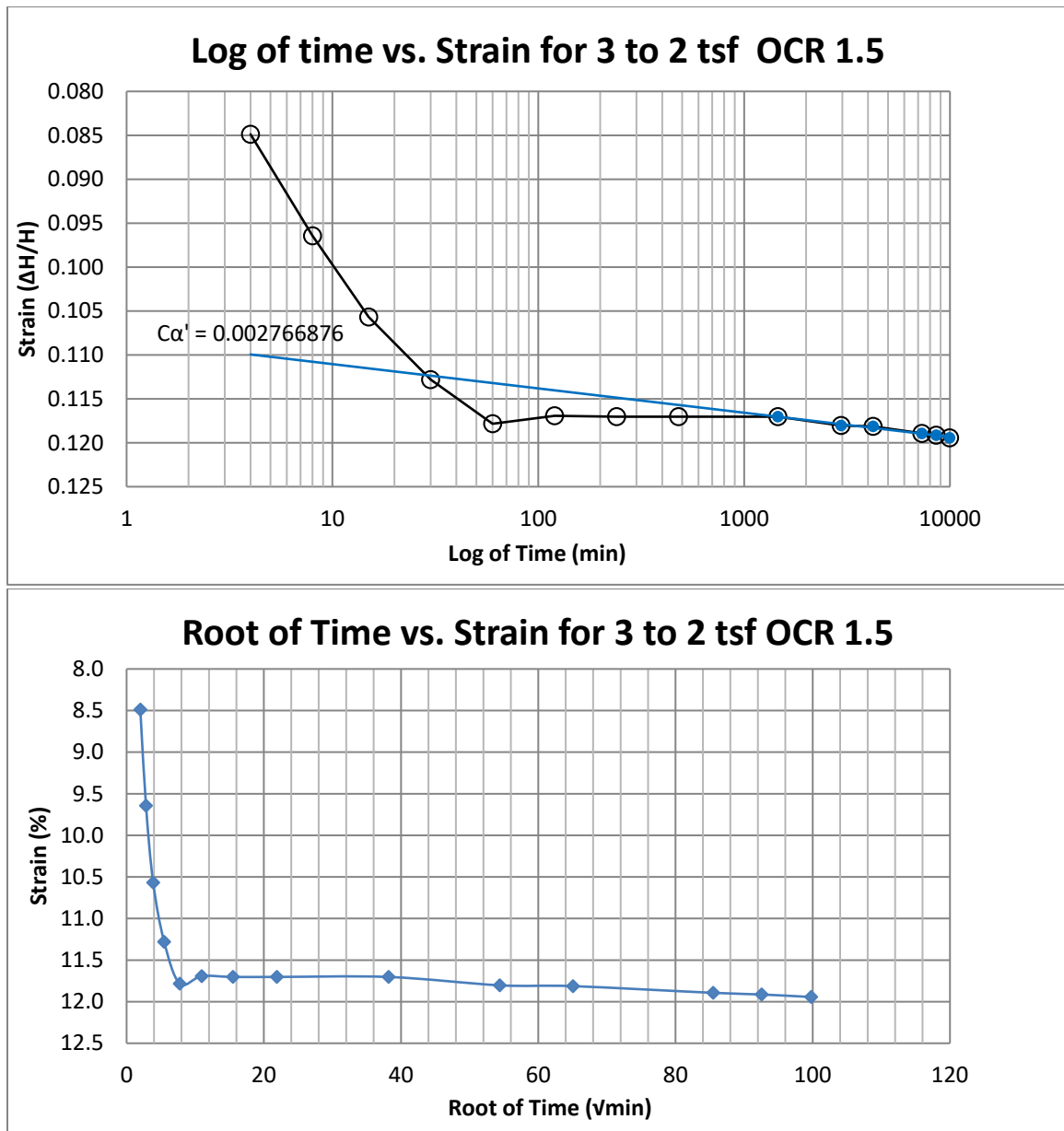


Figure B11 400 South at 25-27 feet

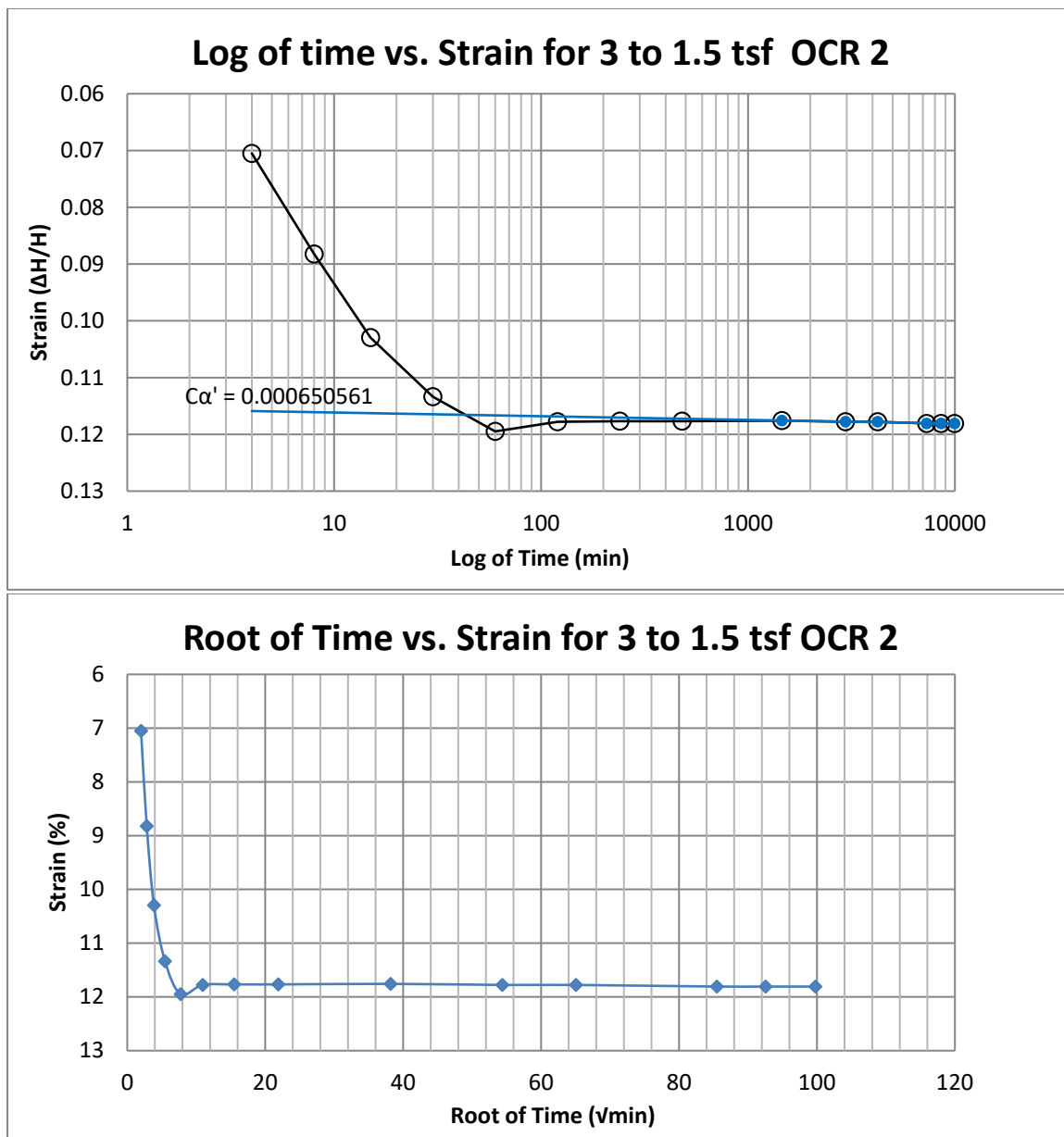


Figure B12 400 South at 25-27 feet

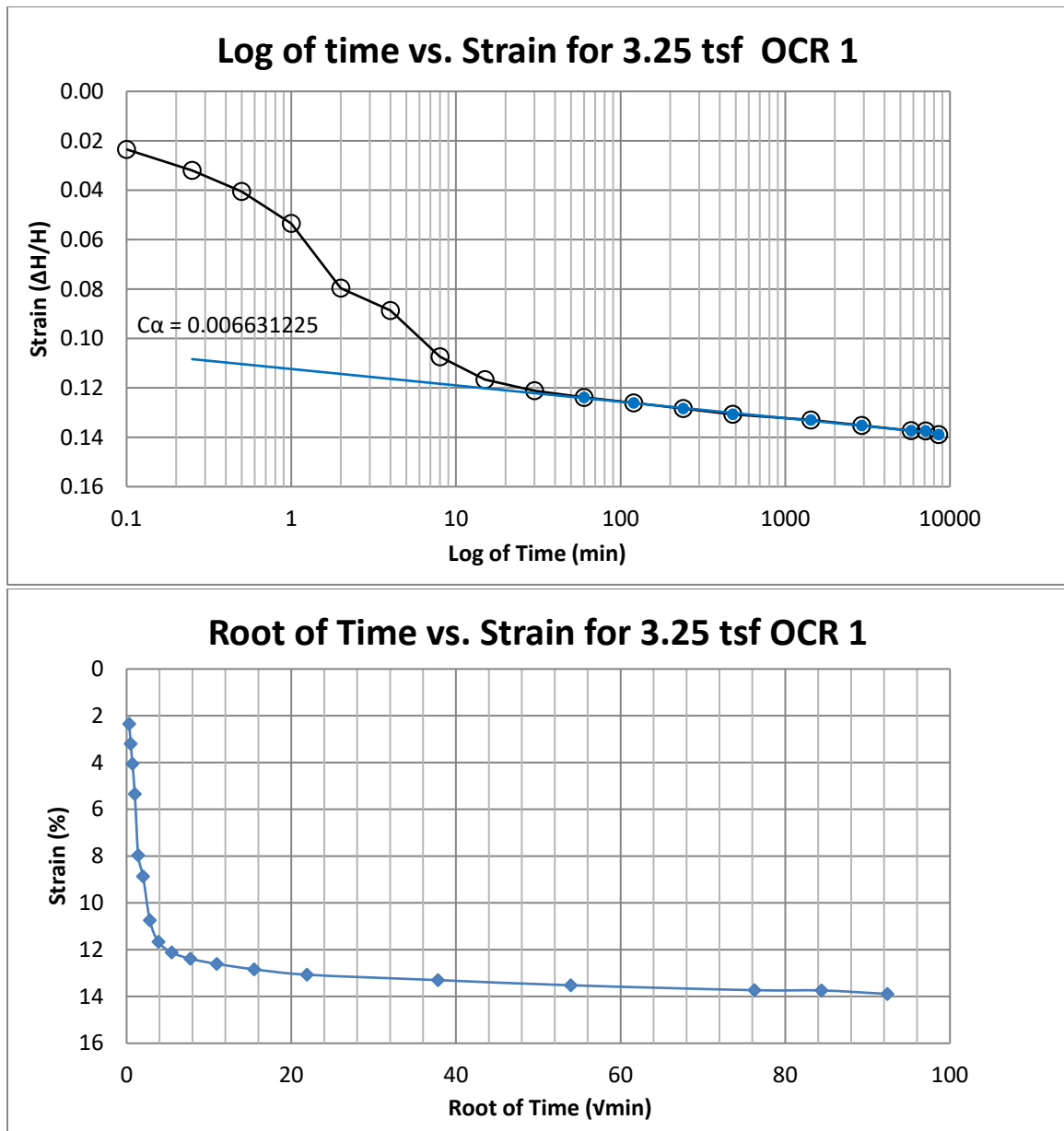


Figure B13 400 South at 30-32 feet

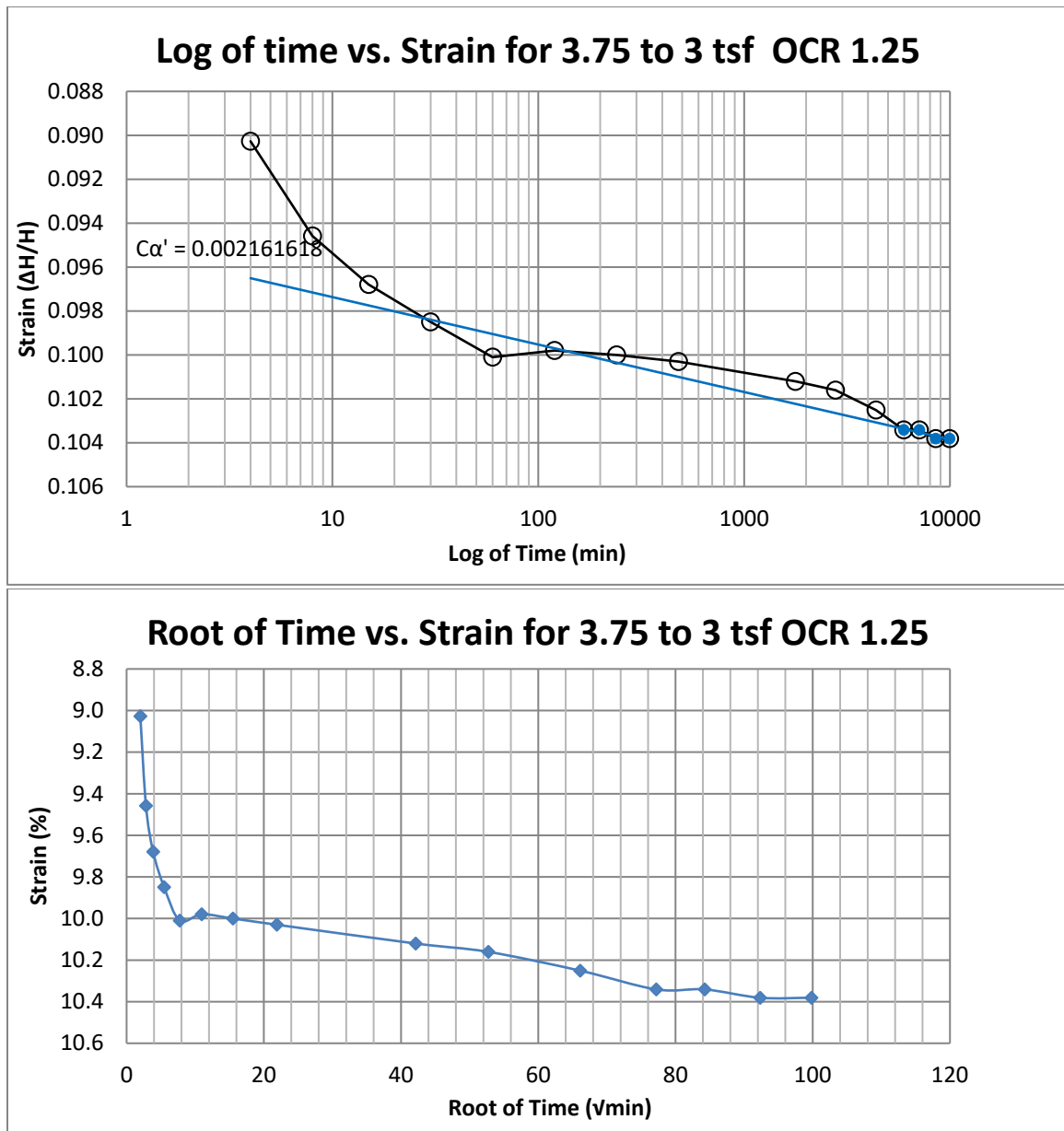


Figure B14 400 South at 30-32 feet

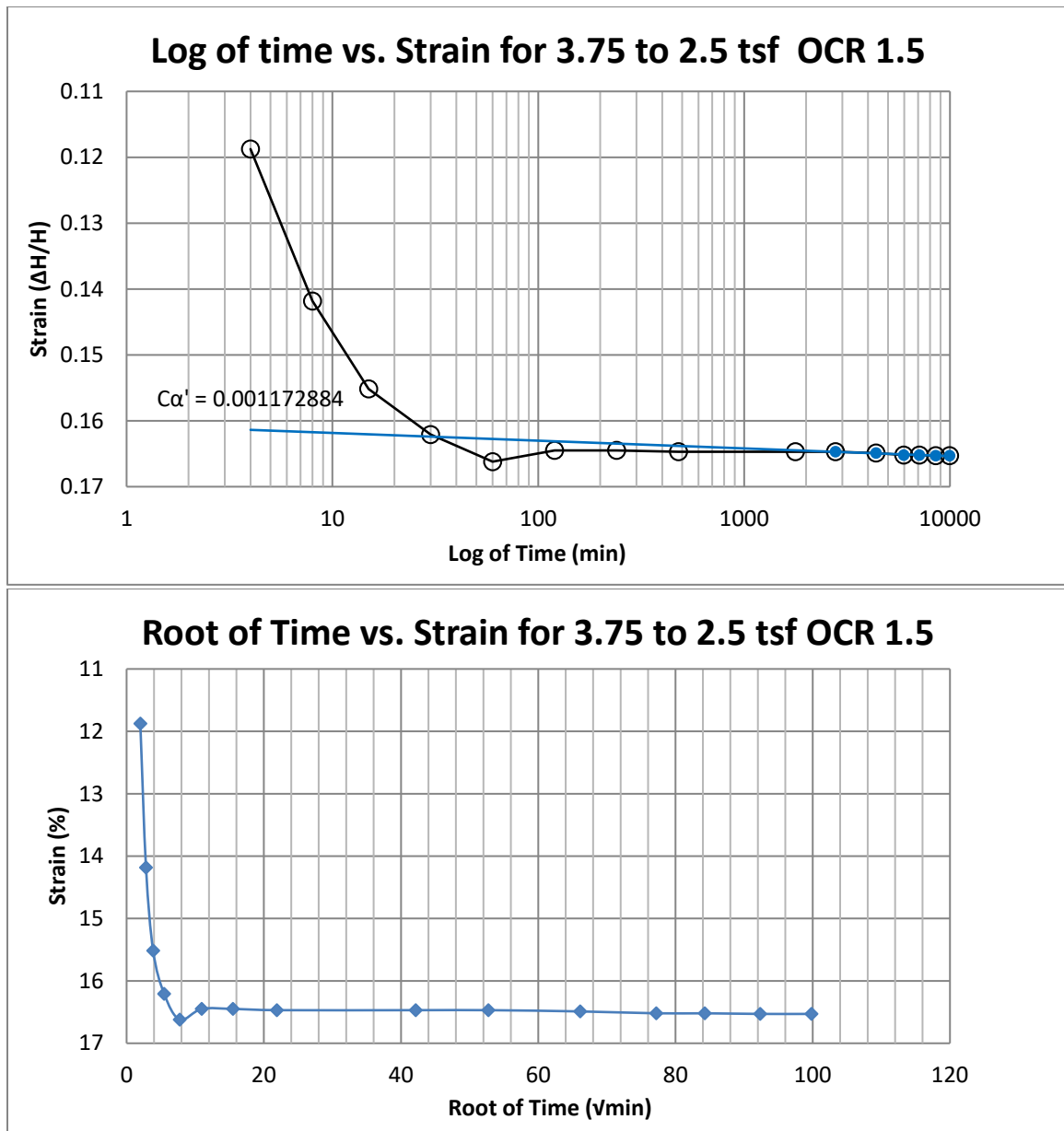


Figure B15 400 South at 30-32 feet

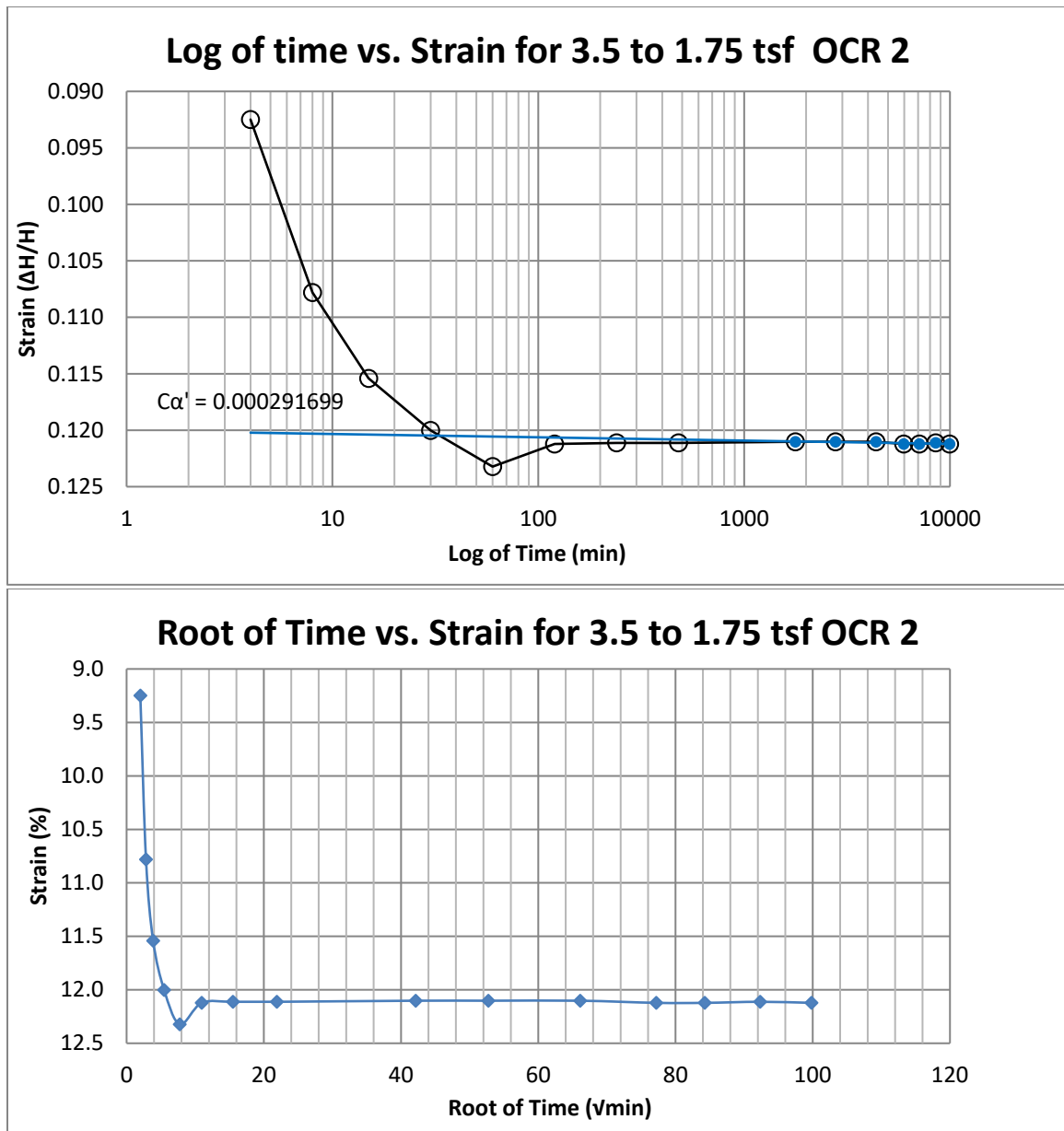


Figure B16 400 South at 30-32 feet

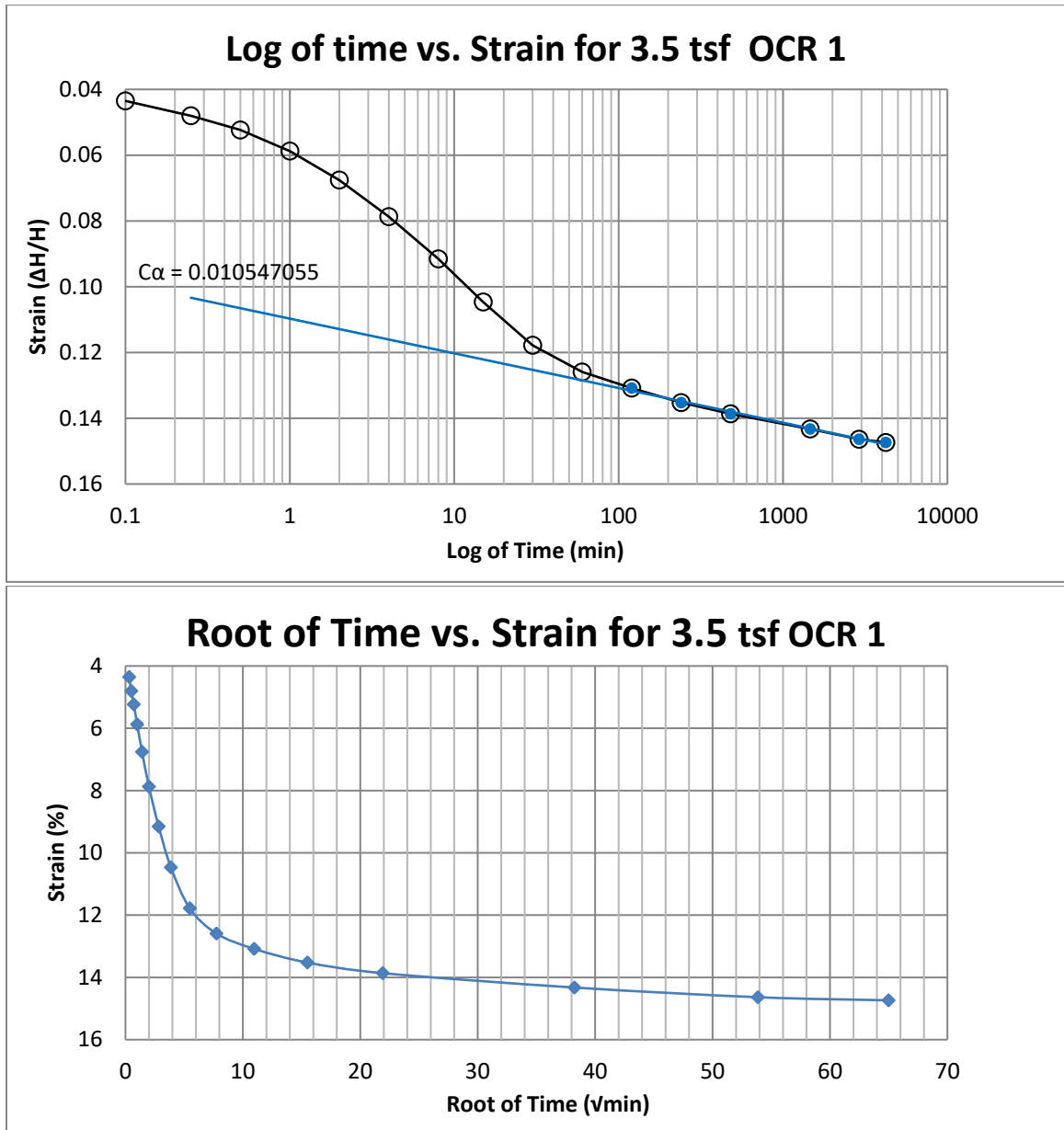


Figure B17 400 South at 37.5-39.5 feet

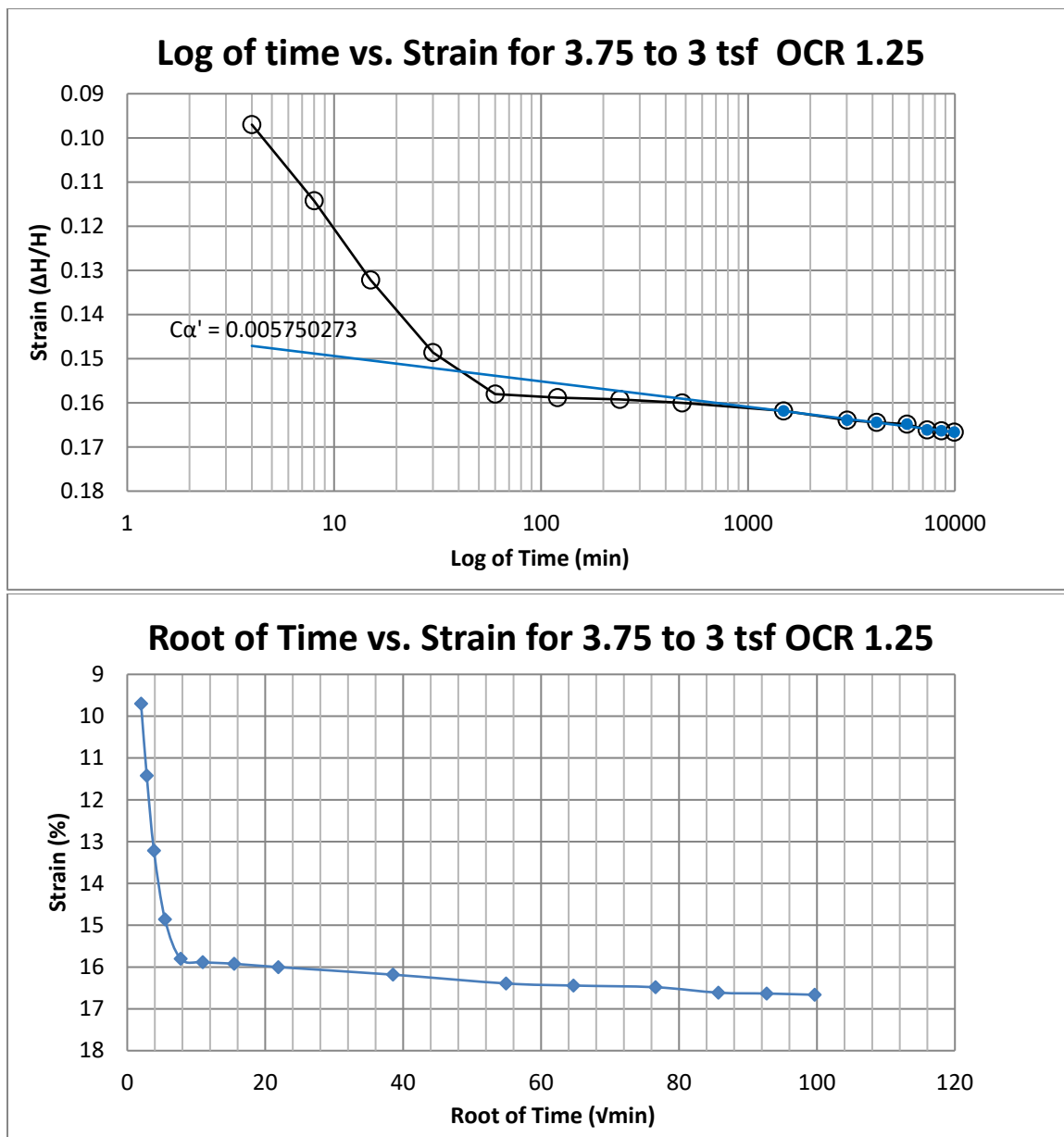


Figure B18 400 South at 37.5-39.5 feet



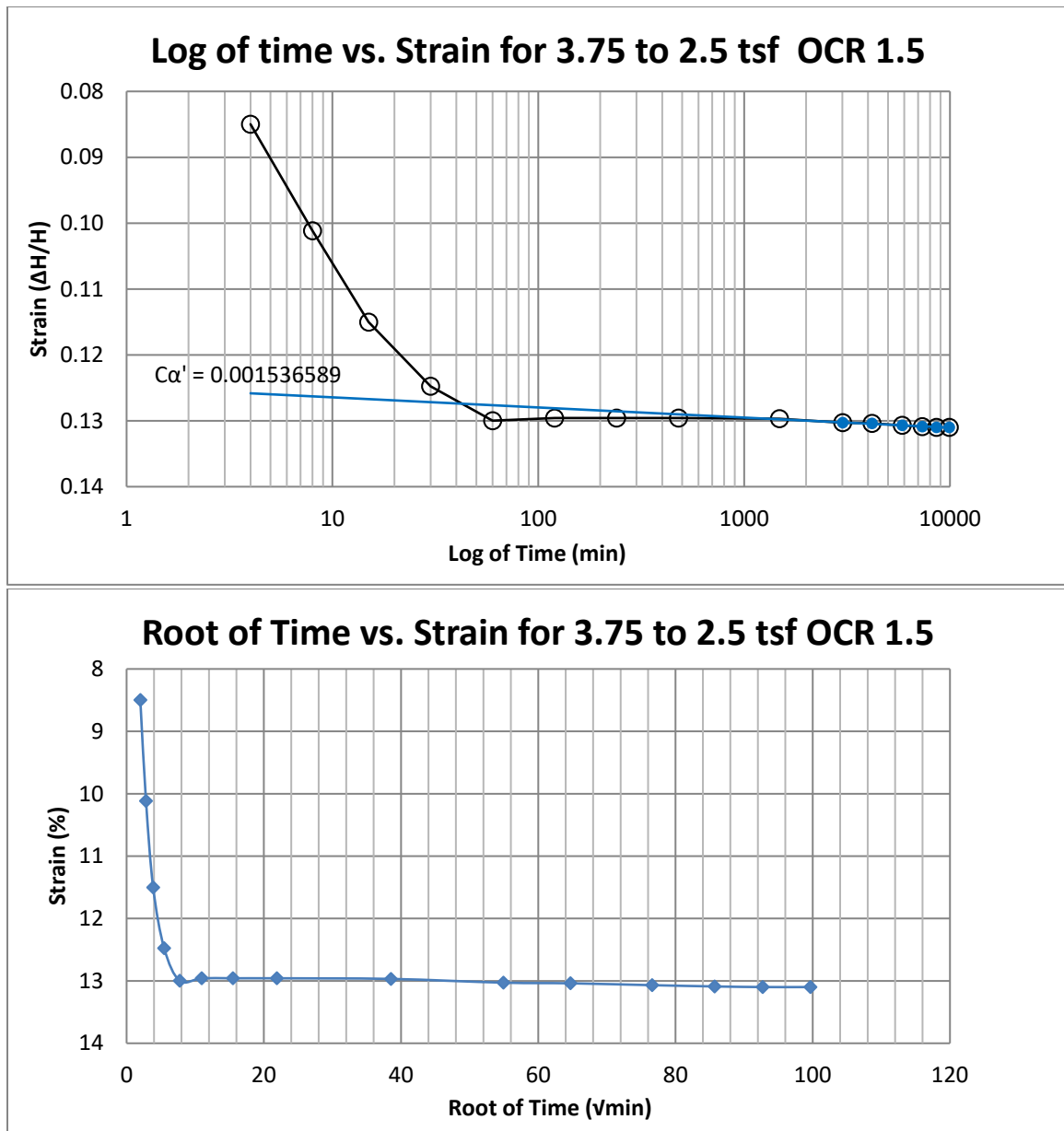


Figure B19 400 South at 37.5-39.5 feet

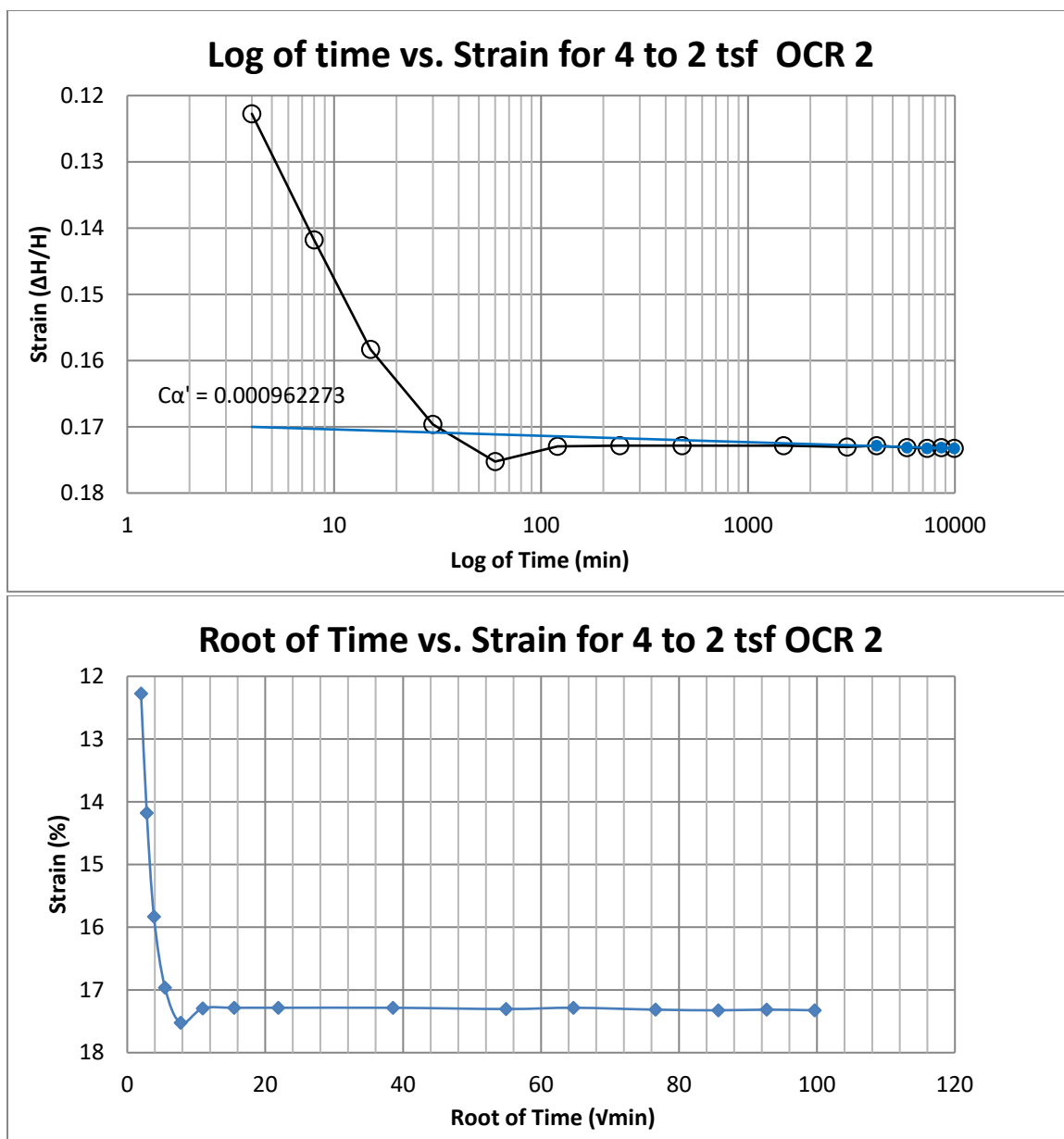


Figure B20 400 South at 37.5-39.5 feet

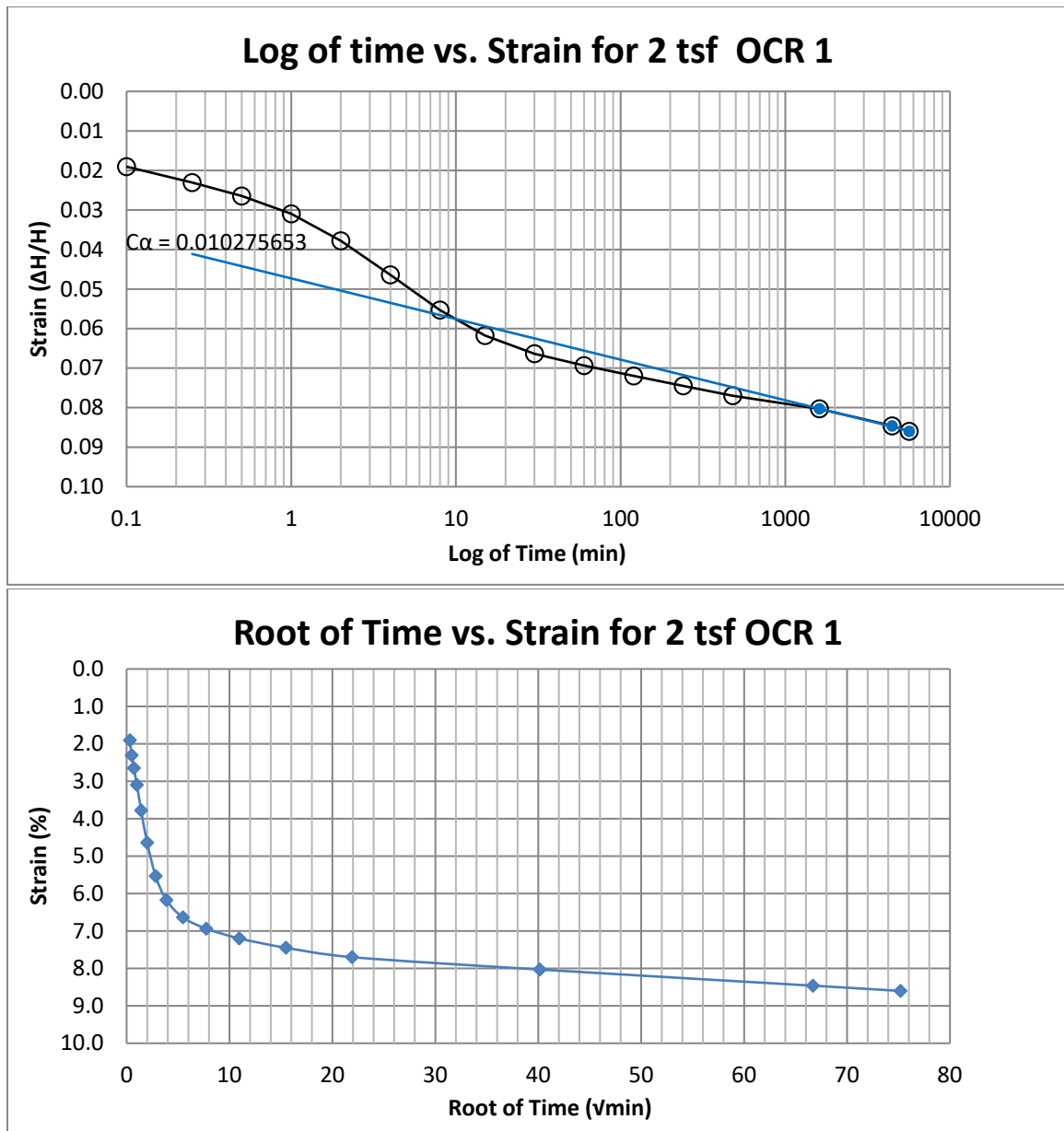


Figure B21 400 South at 40-42 feet

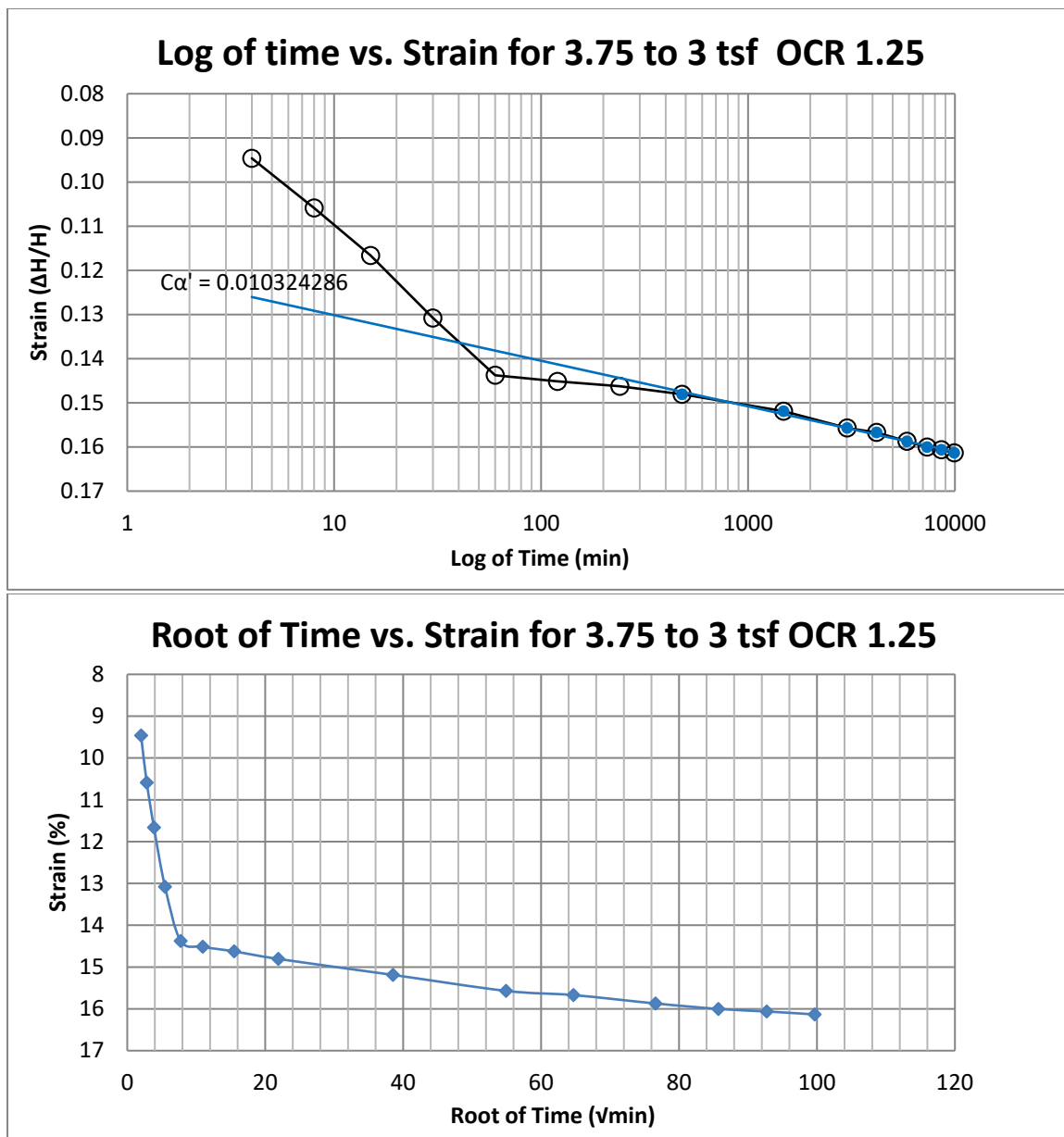


Figure B22 400 South at 40-42 feet

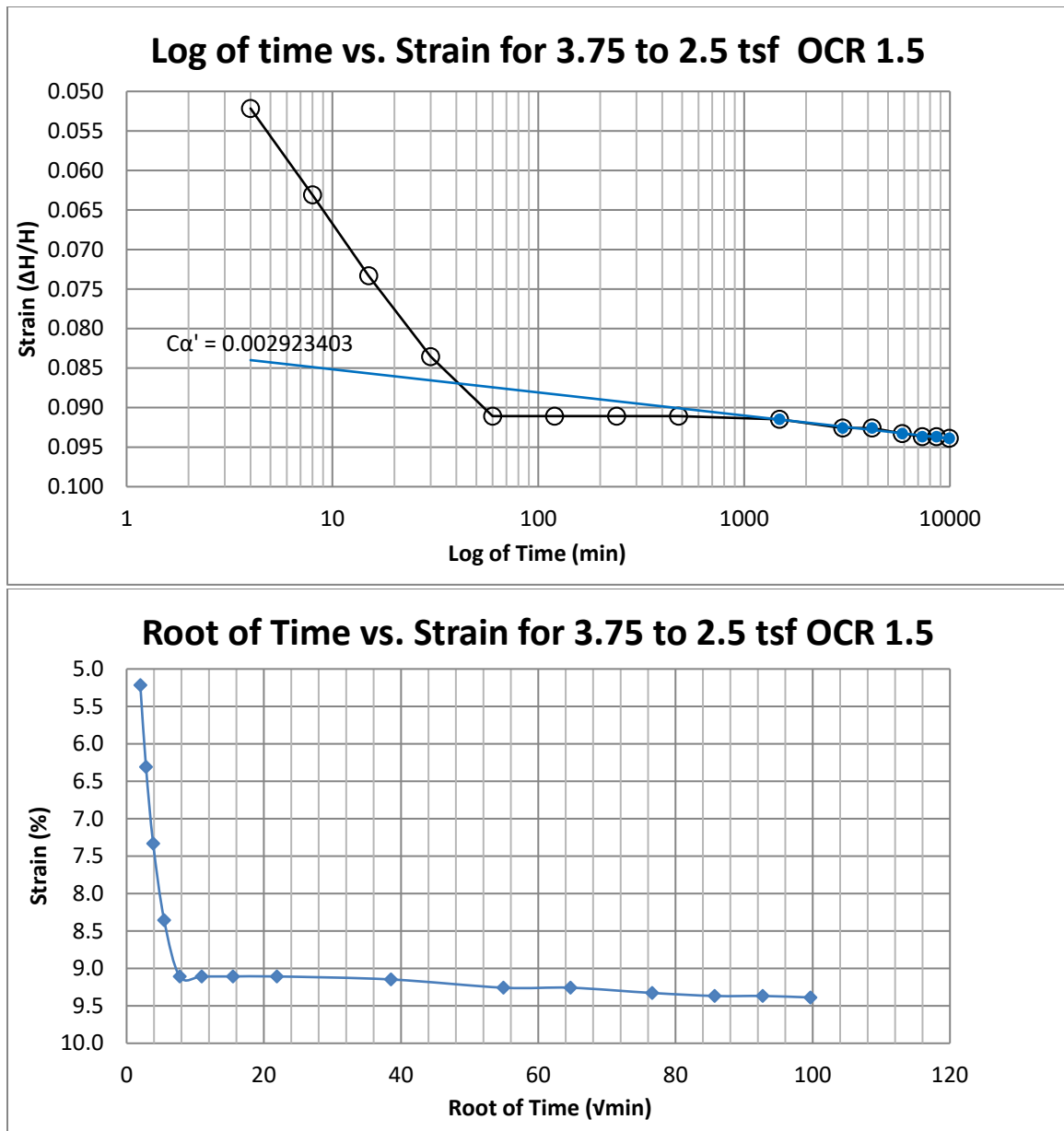


Figure B23 400 South at 40-42 feet

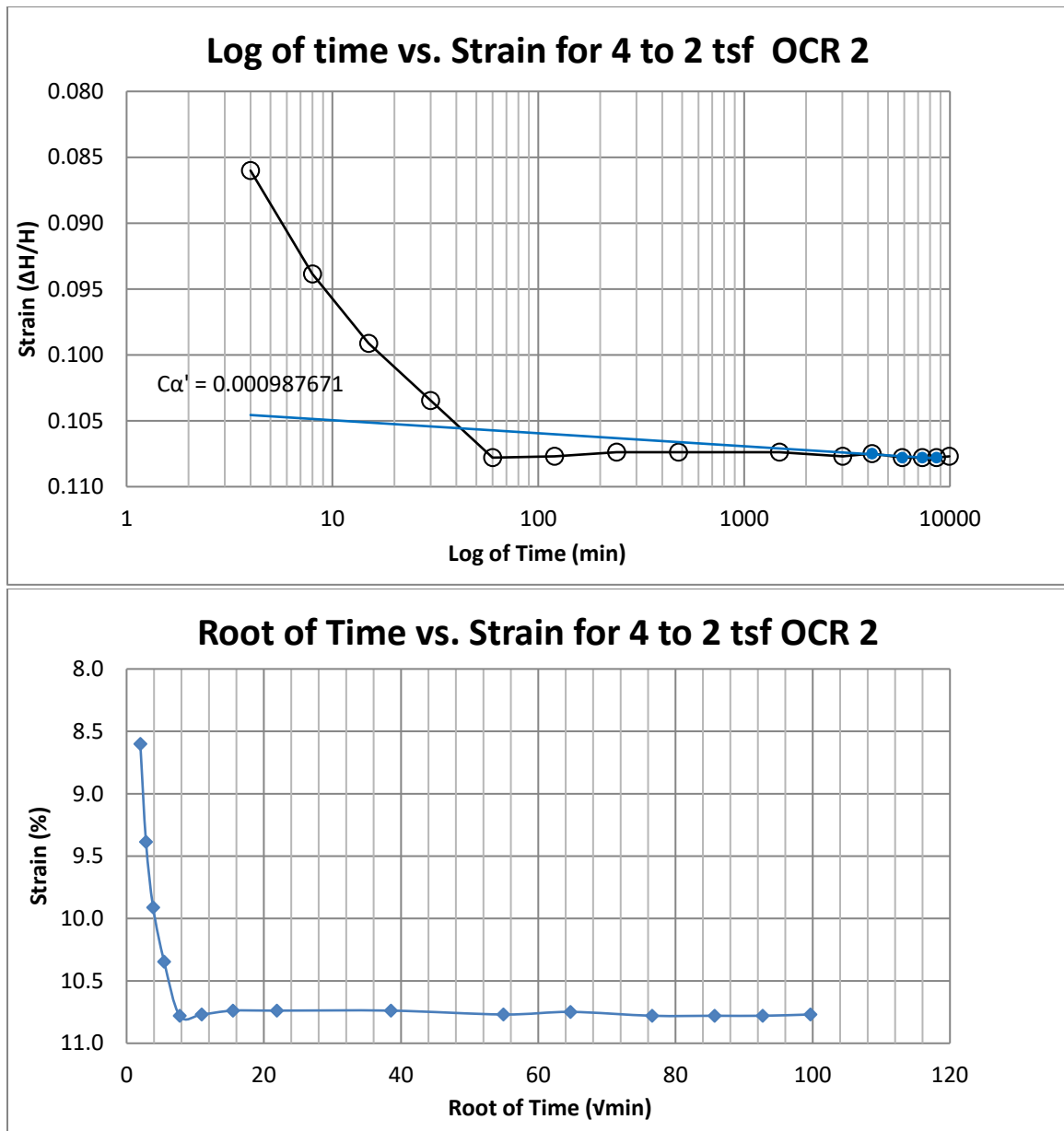


Figure B24 400 South at 40-42 feet

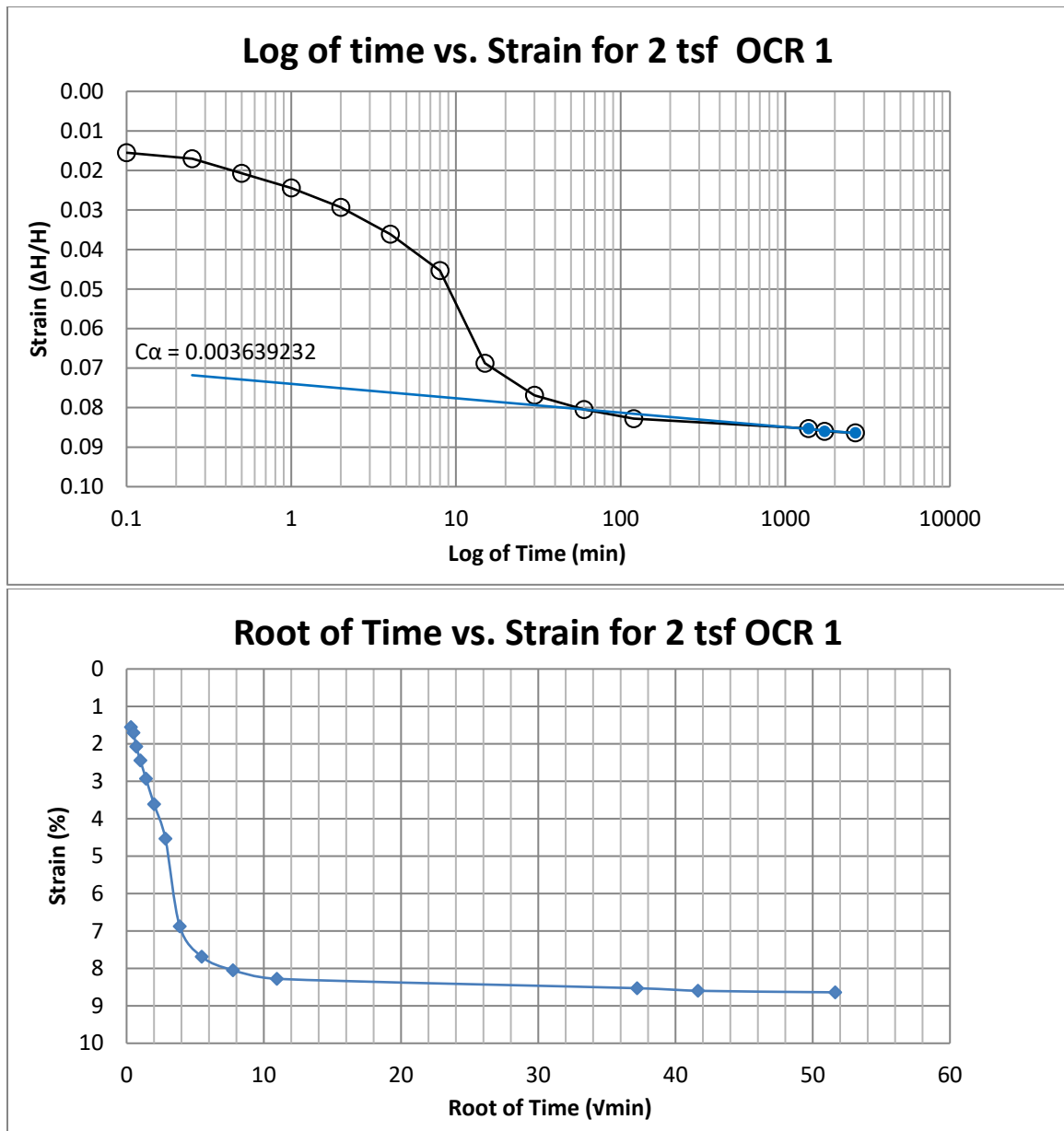


Figure B25 400 South at 45-47 feet

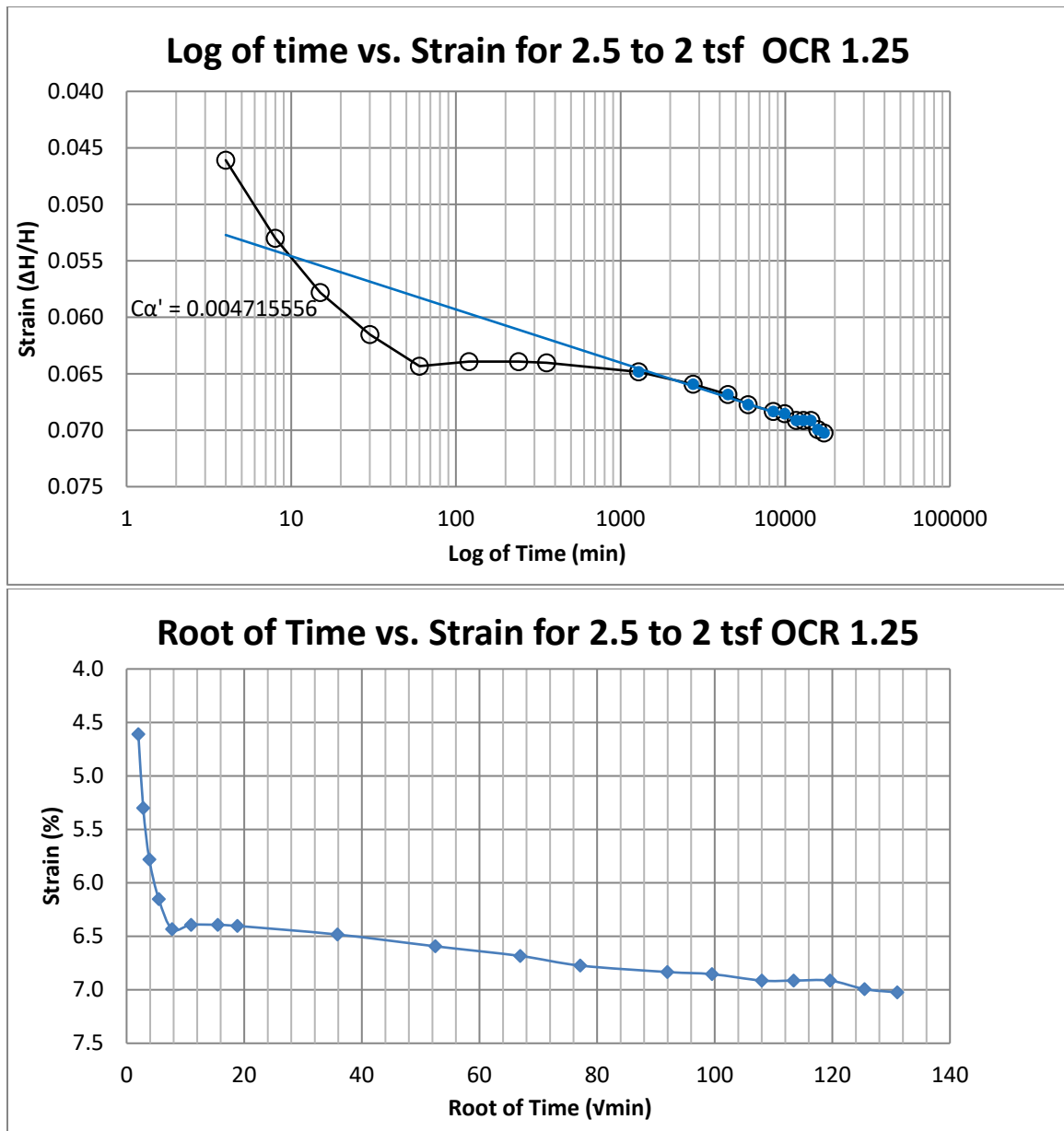


Figure B26 400 South at 45-47 feet



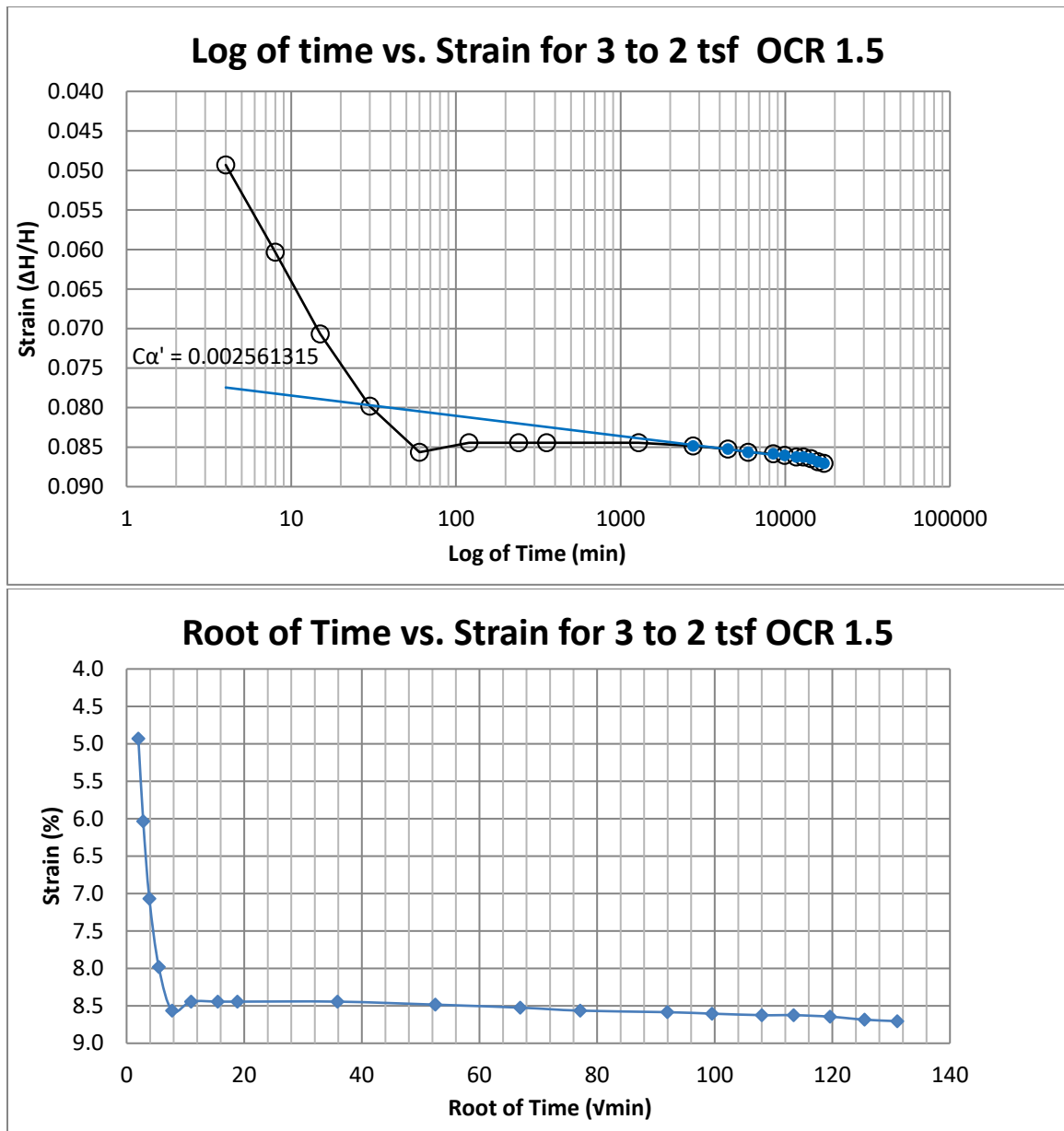


Figure B27 400 South at 45-47 feet

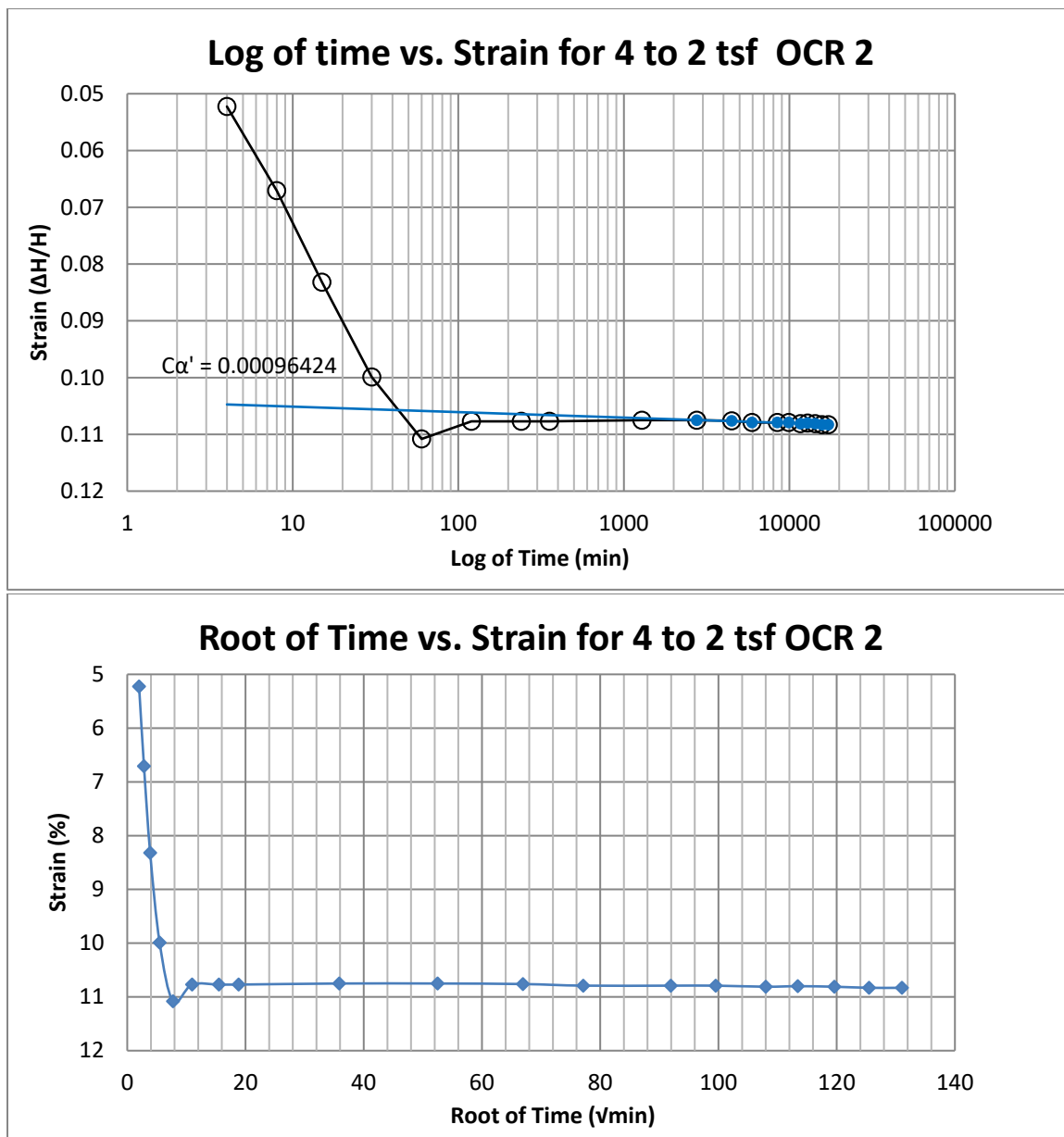


Figure B28 400 South at 45-47 feet

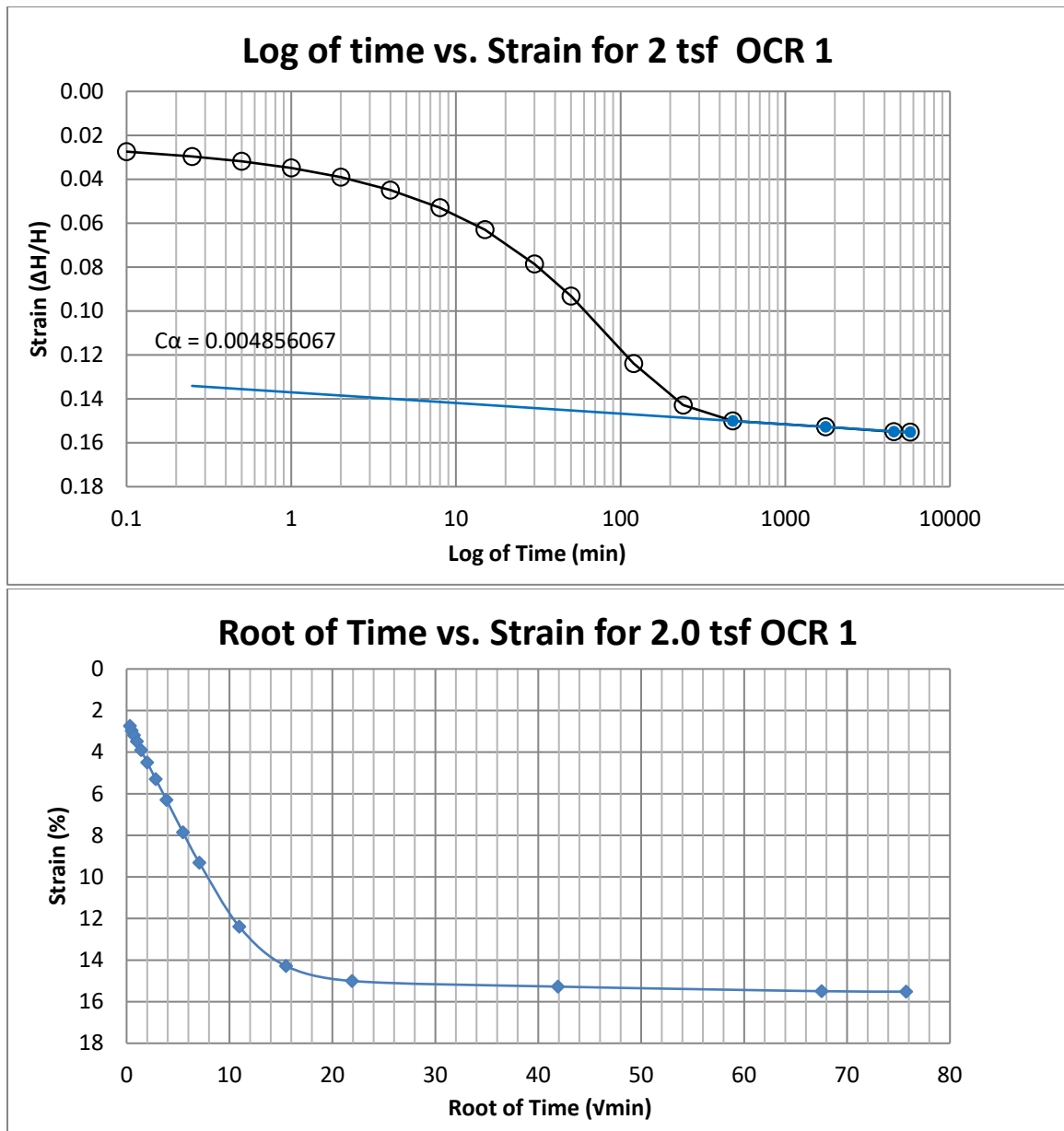


Figure B29 400 South at 50-52 feet

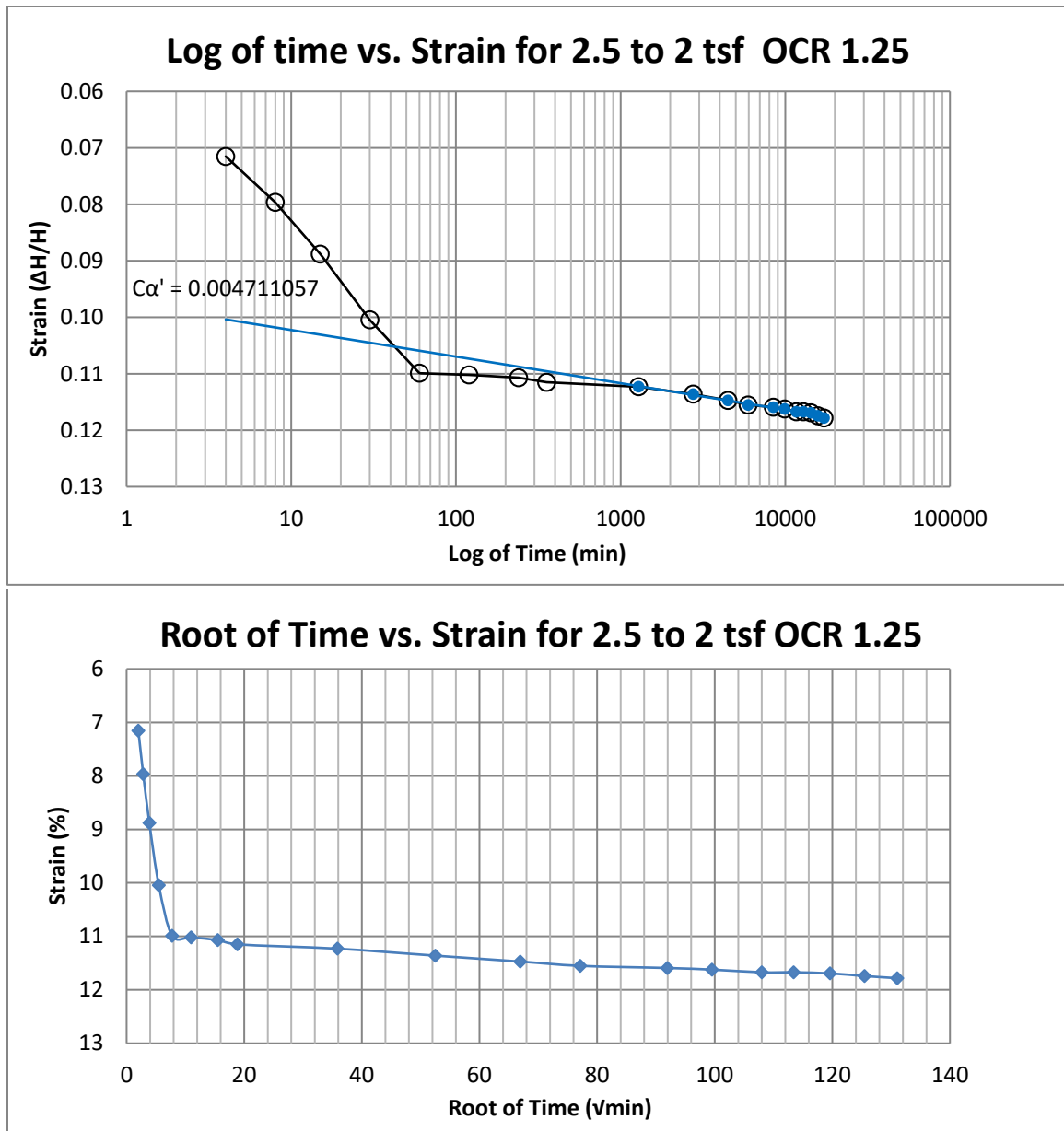


Figure B30 400 South at 50-52 feet

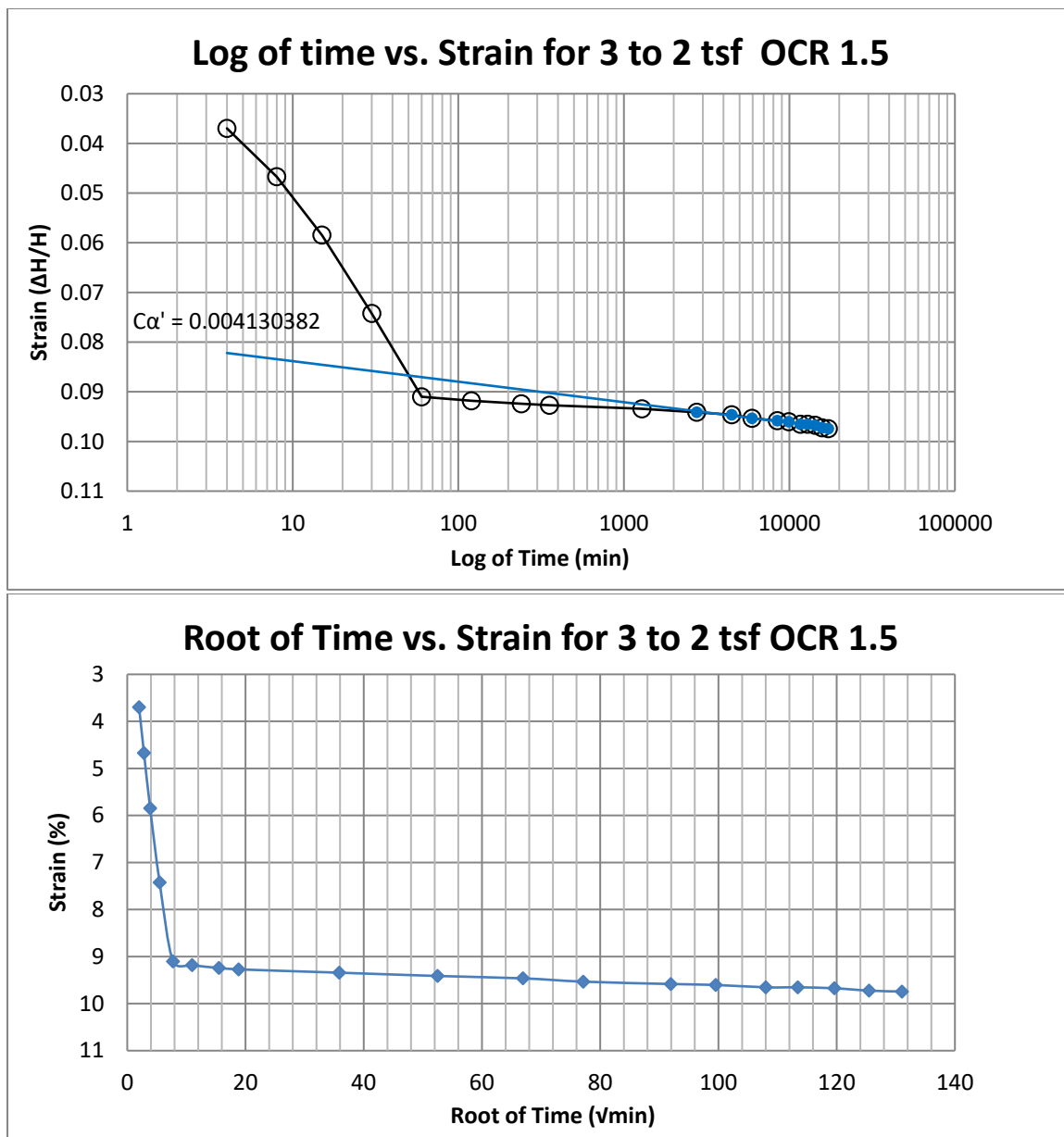


Figure B31 400 South at 50-52 feet

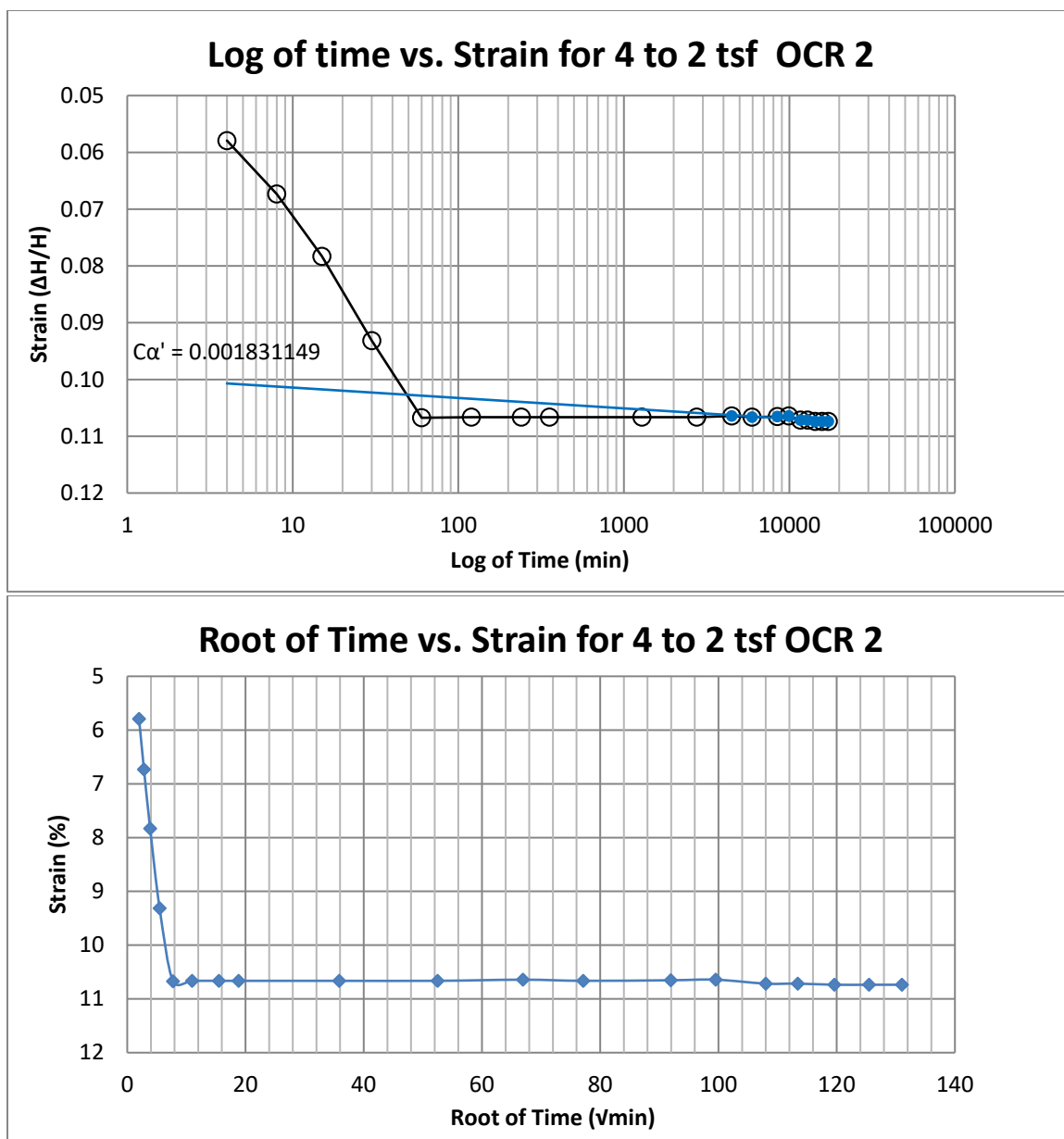


Figure B32 400 South at 50-52 feet

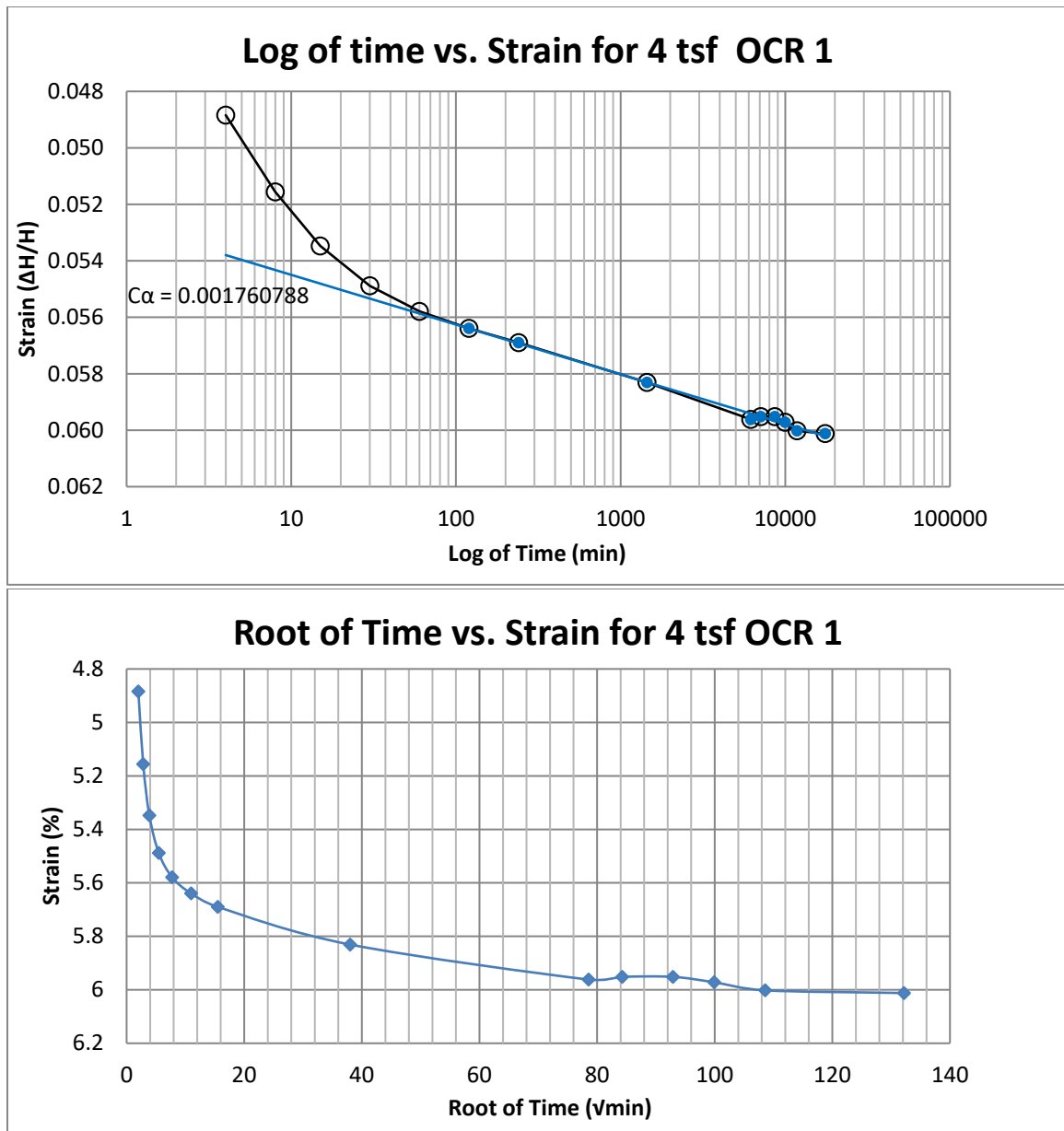


Figure B33 Springville at 30-32 feet

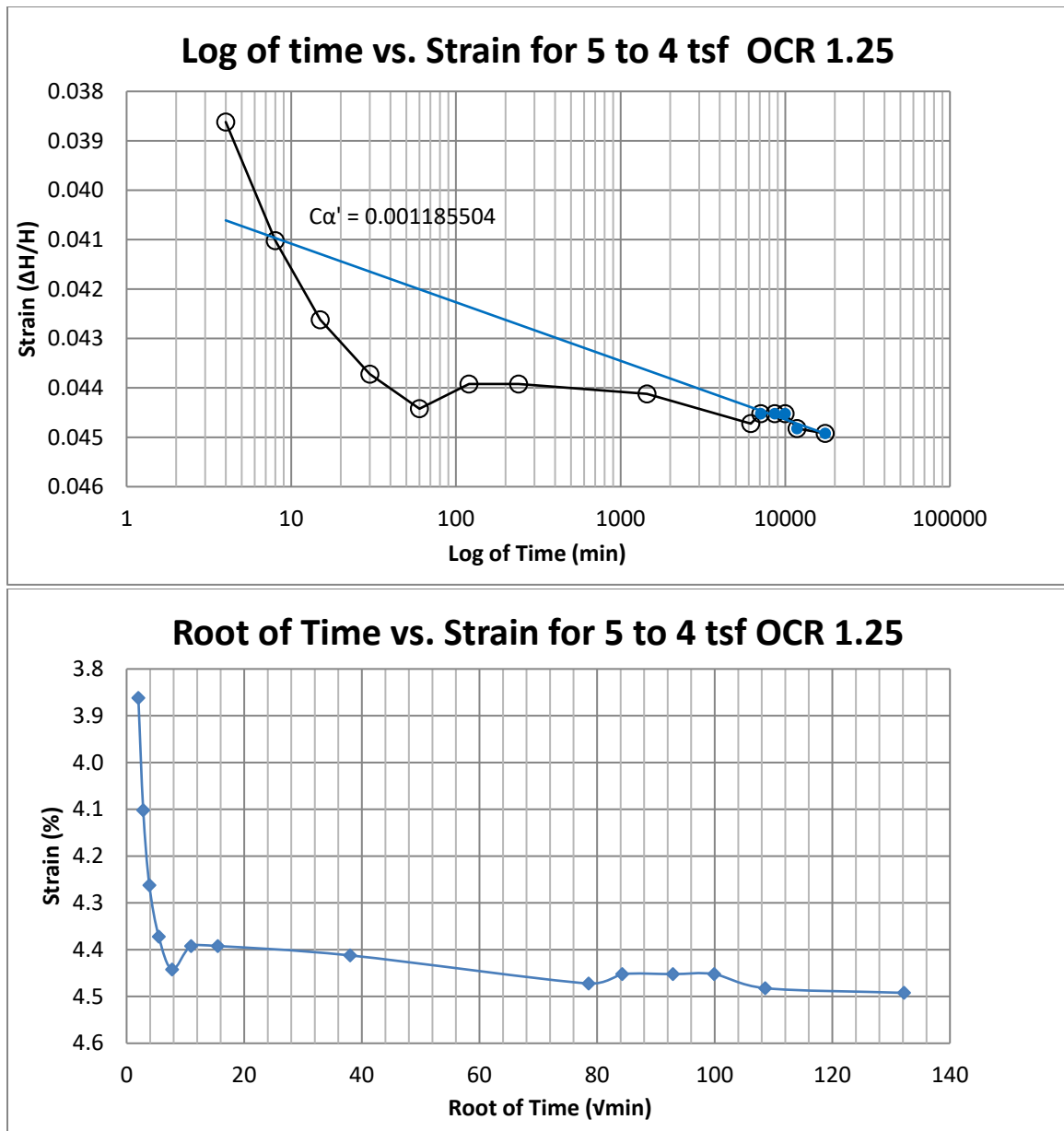


Figure B34 Springville at 30-32 feet



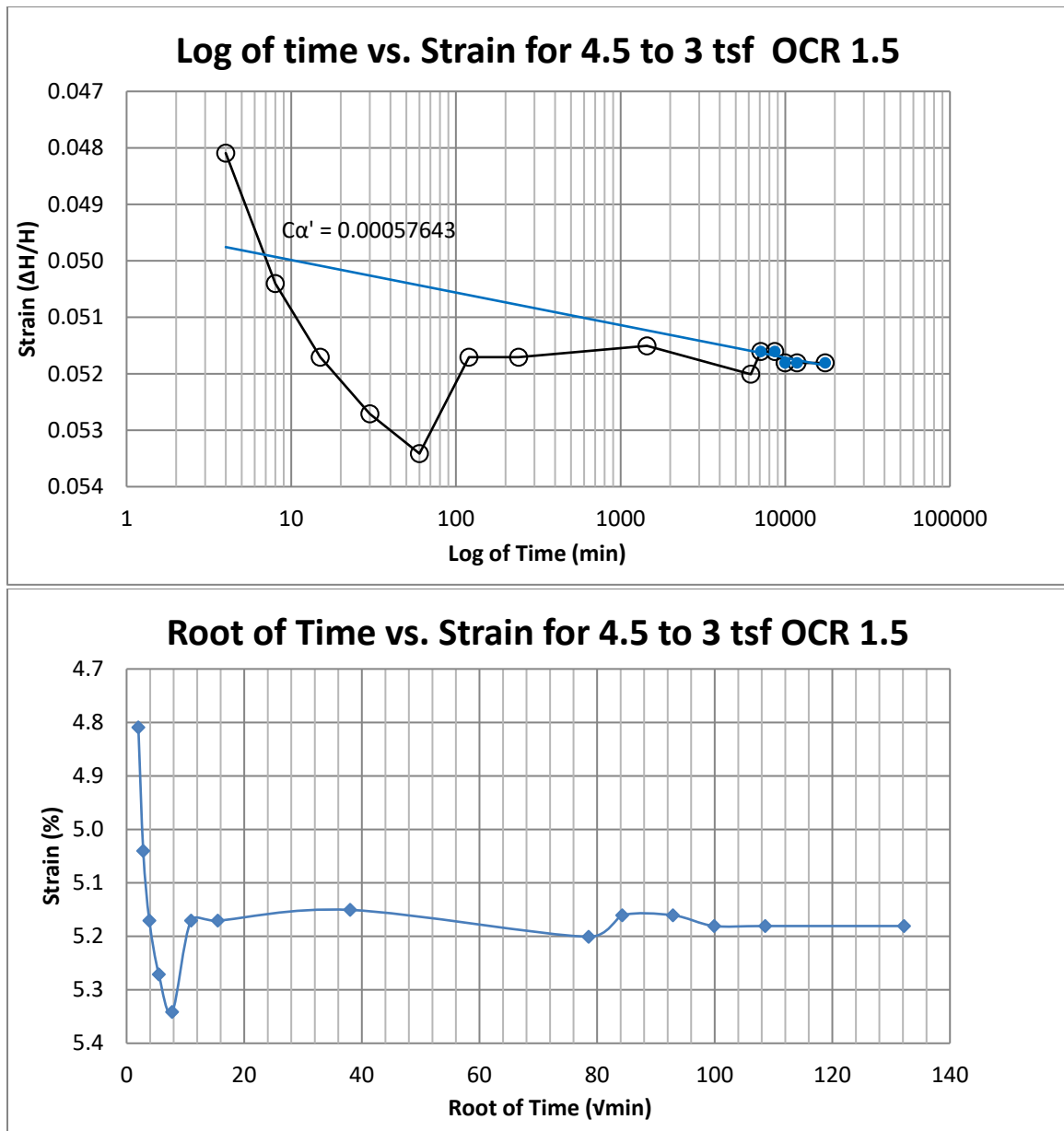


Figure B35 Springville at 30-32 feet

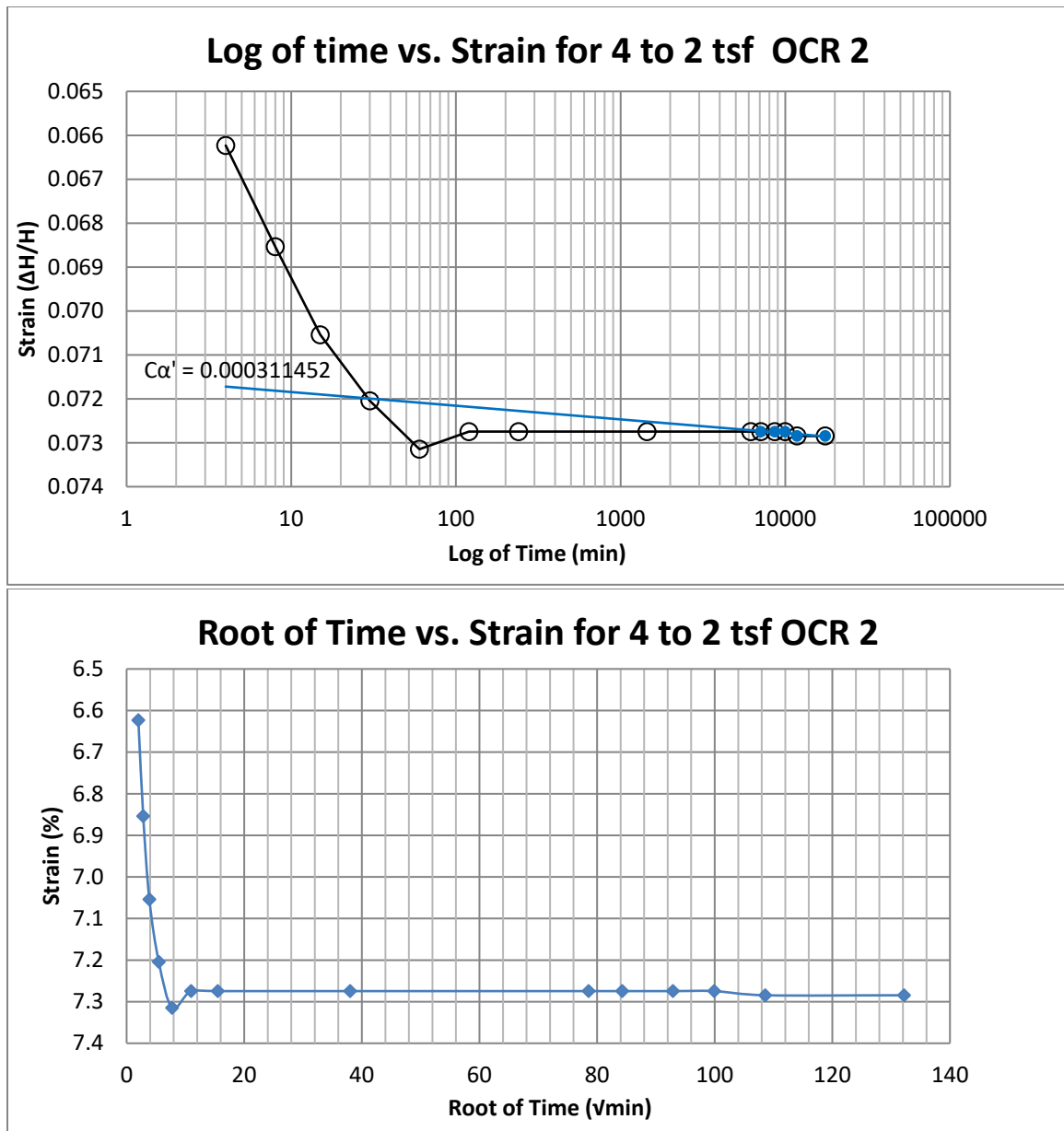


Figure B36 Springville at 30-32 feet

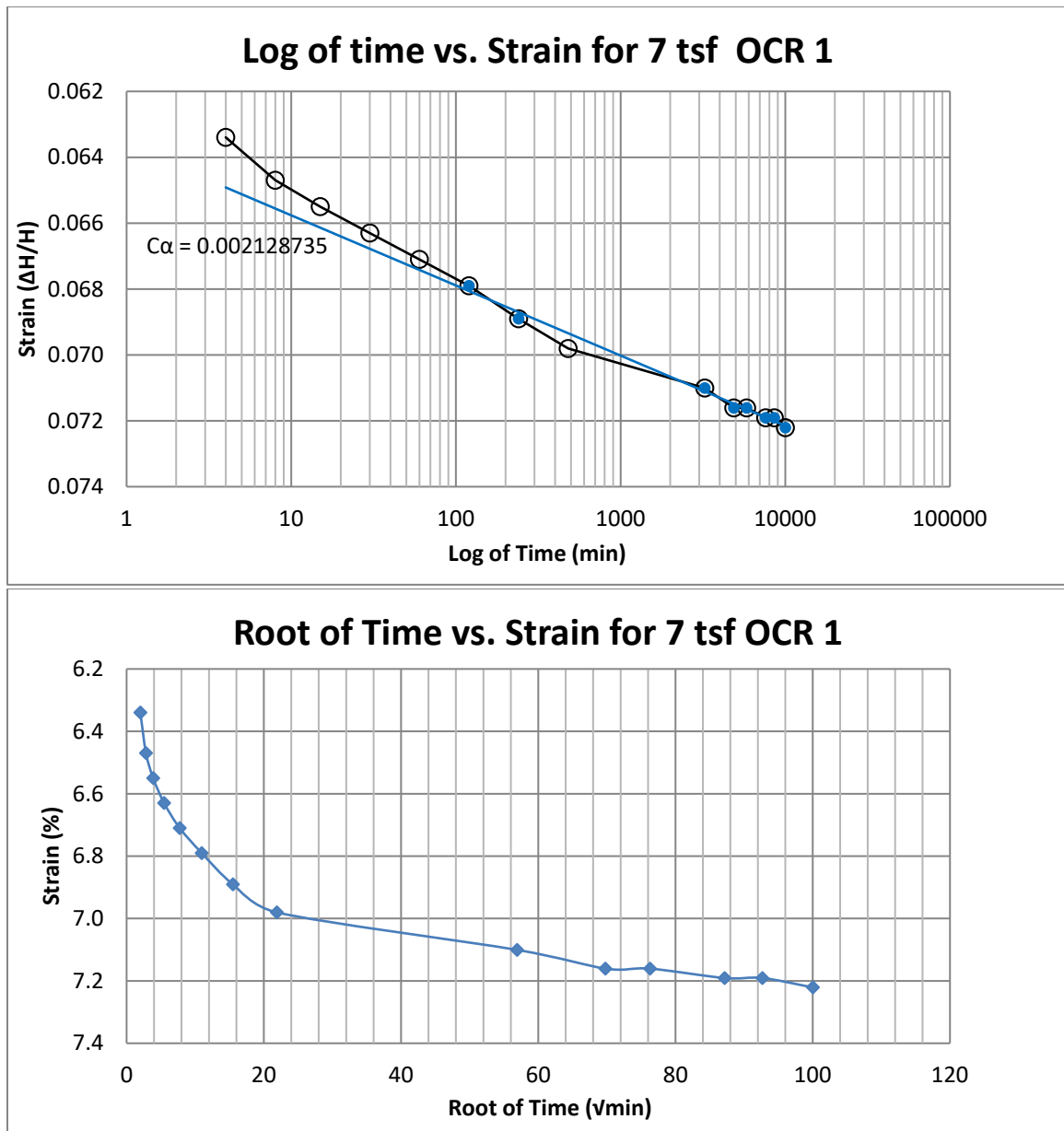
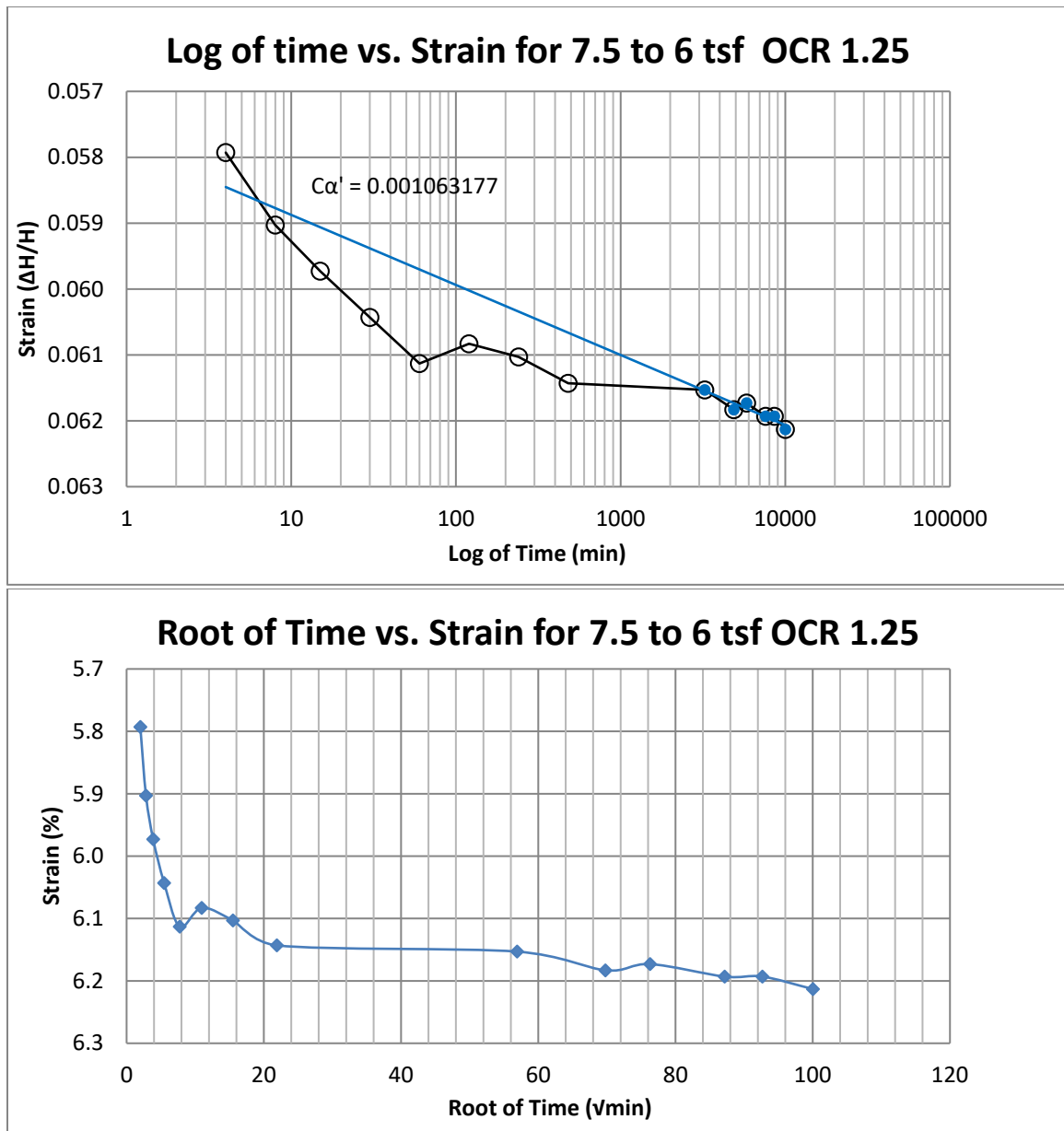


Figure B37 Springville at 40-42 feet



**Figure B38 Springville at 40-42 feet**

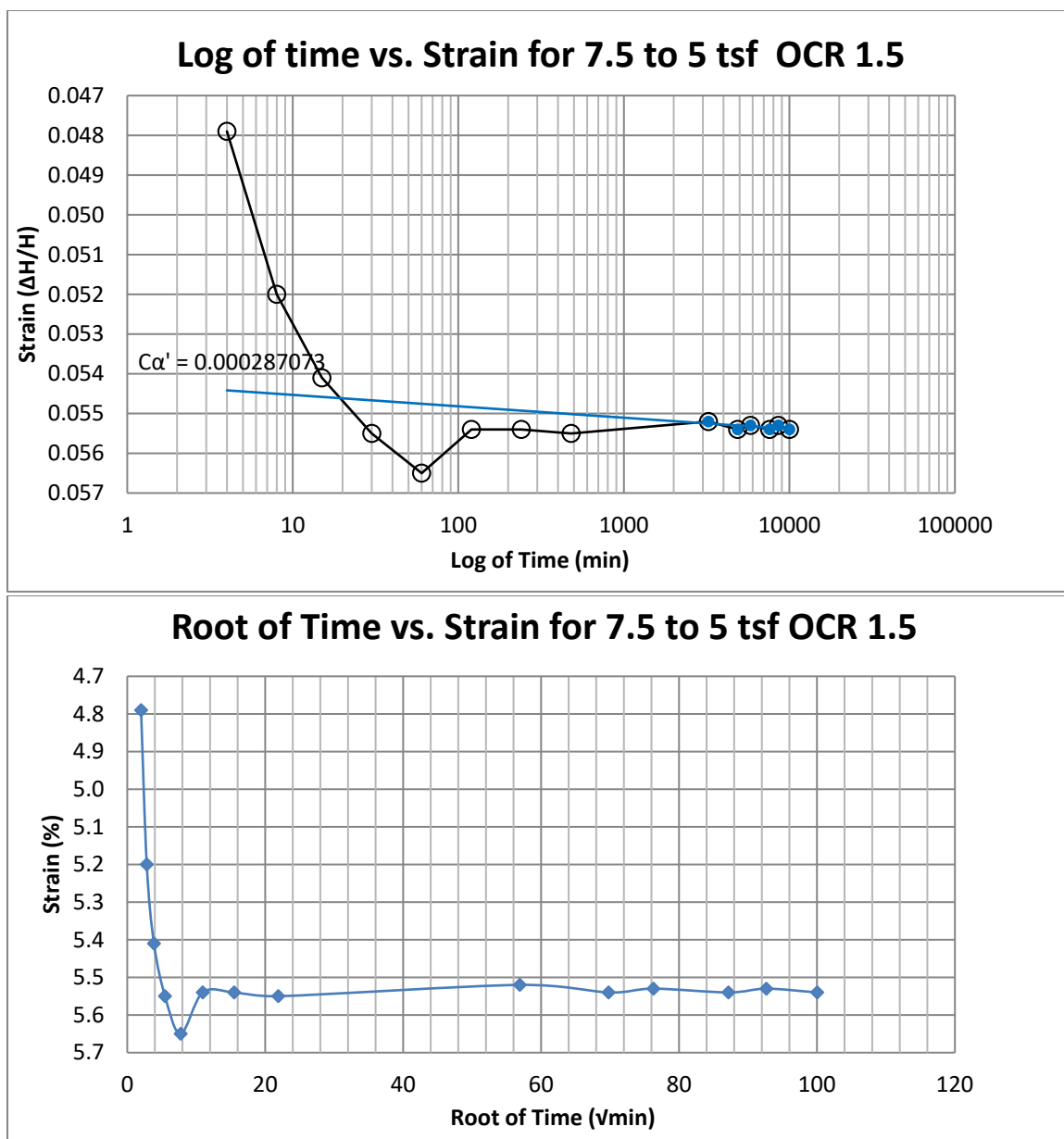


Figure B39 Springville at 40-42 feet

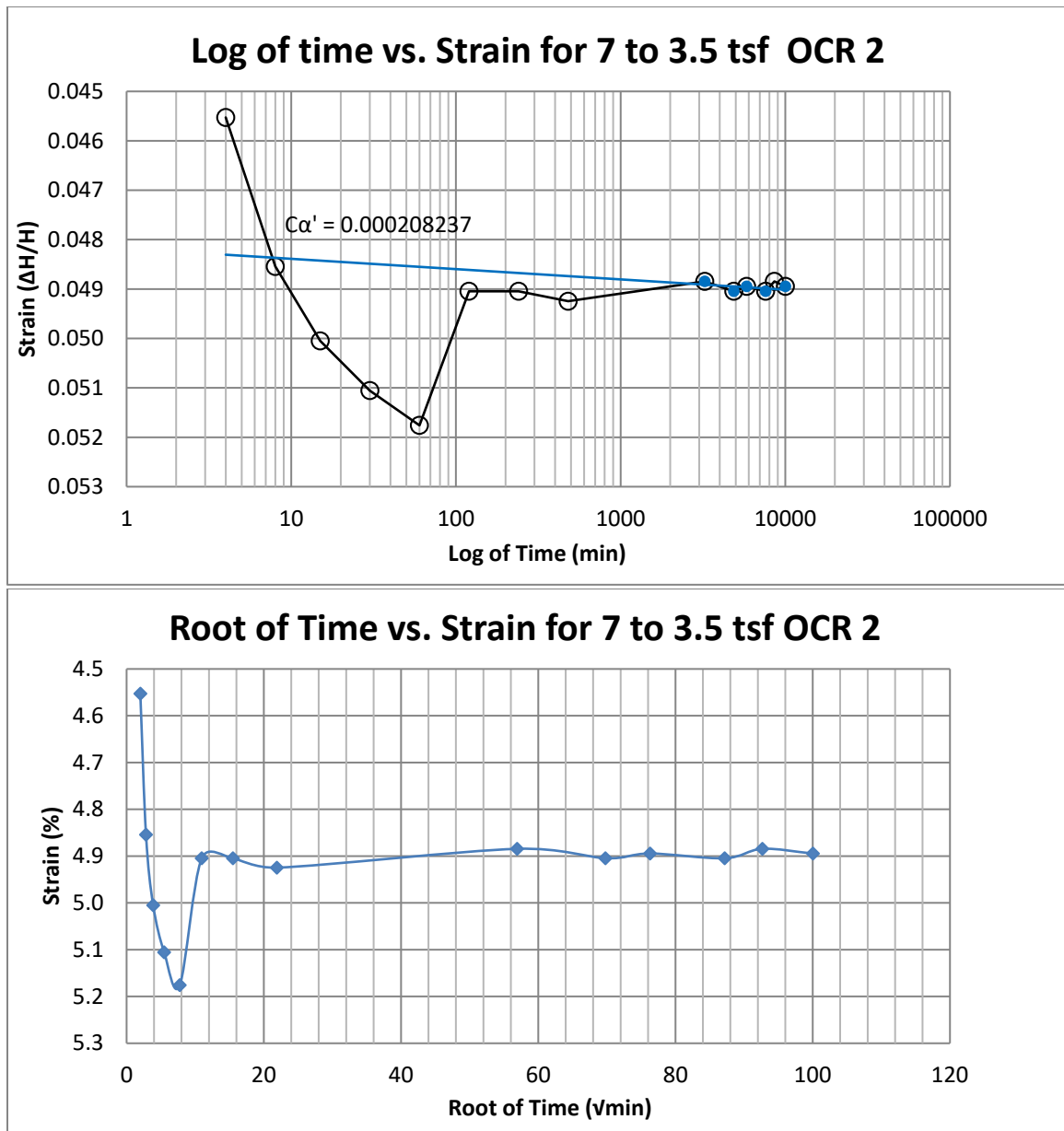


Figure B40 Springville at 40-42 feet

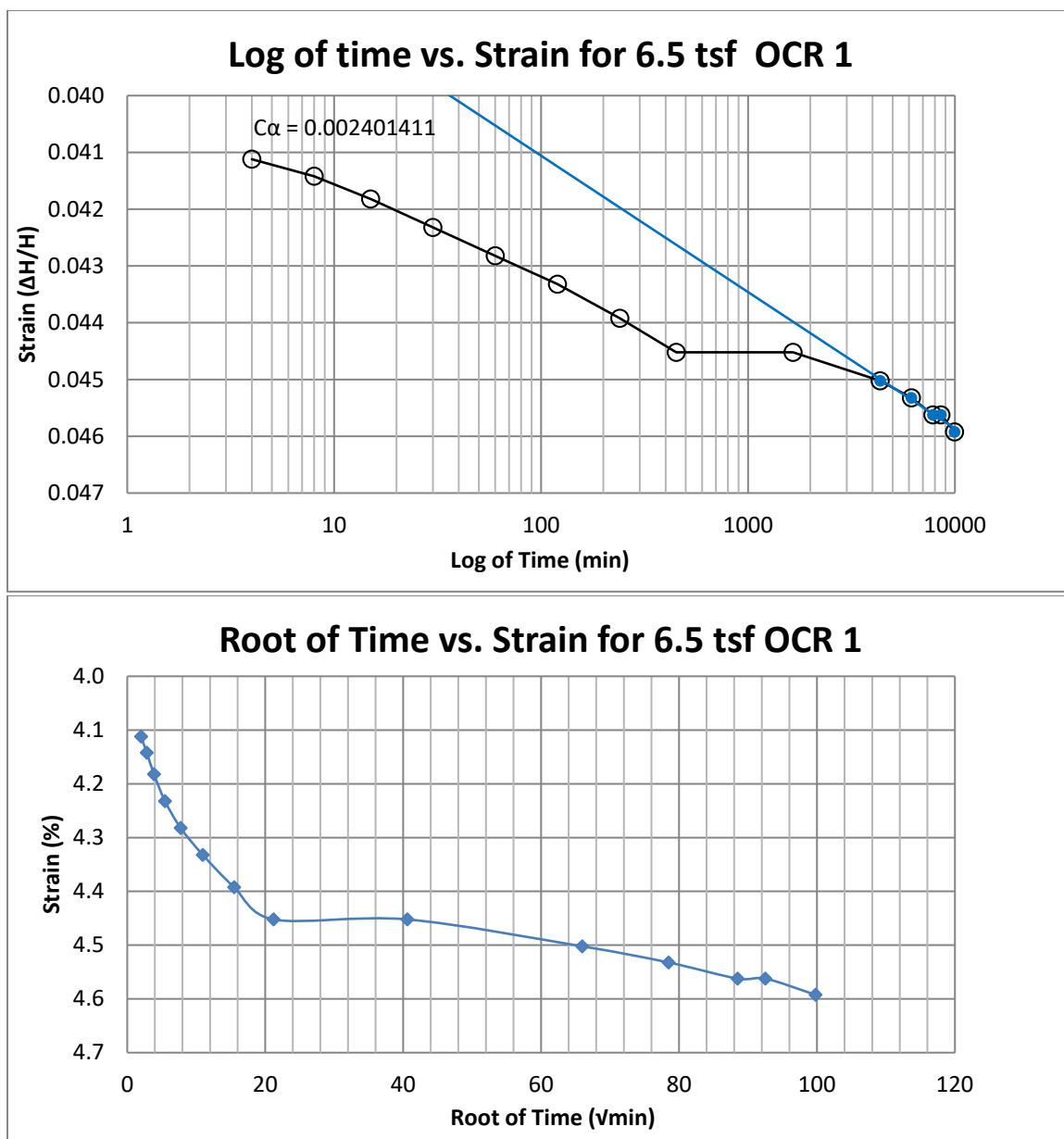


Figure B41 Springville at 65-67 feet

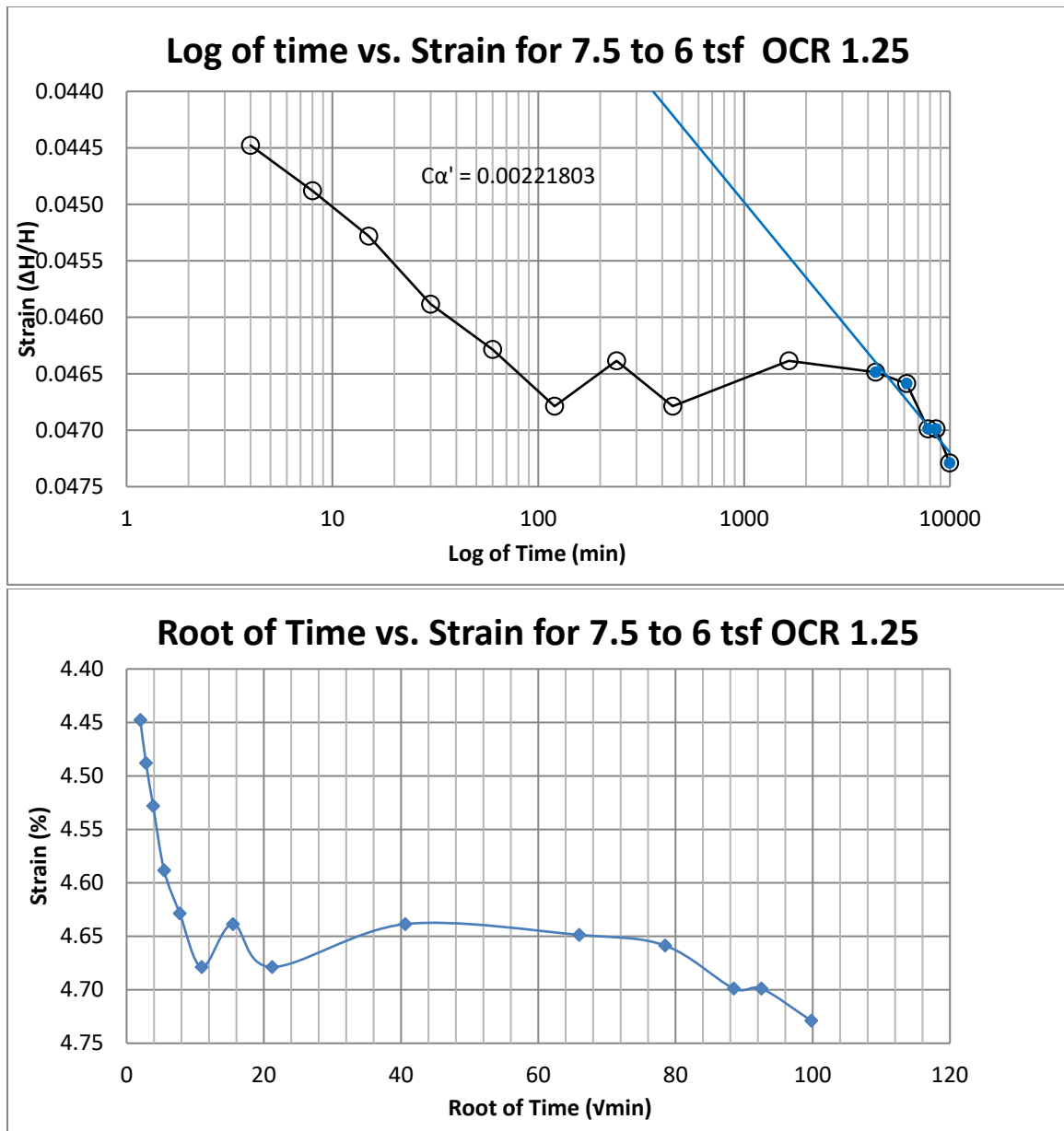


Figure B42 Springville at 65-67 feet



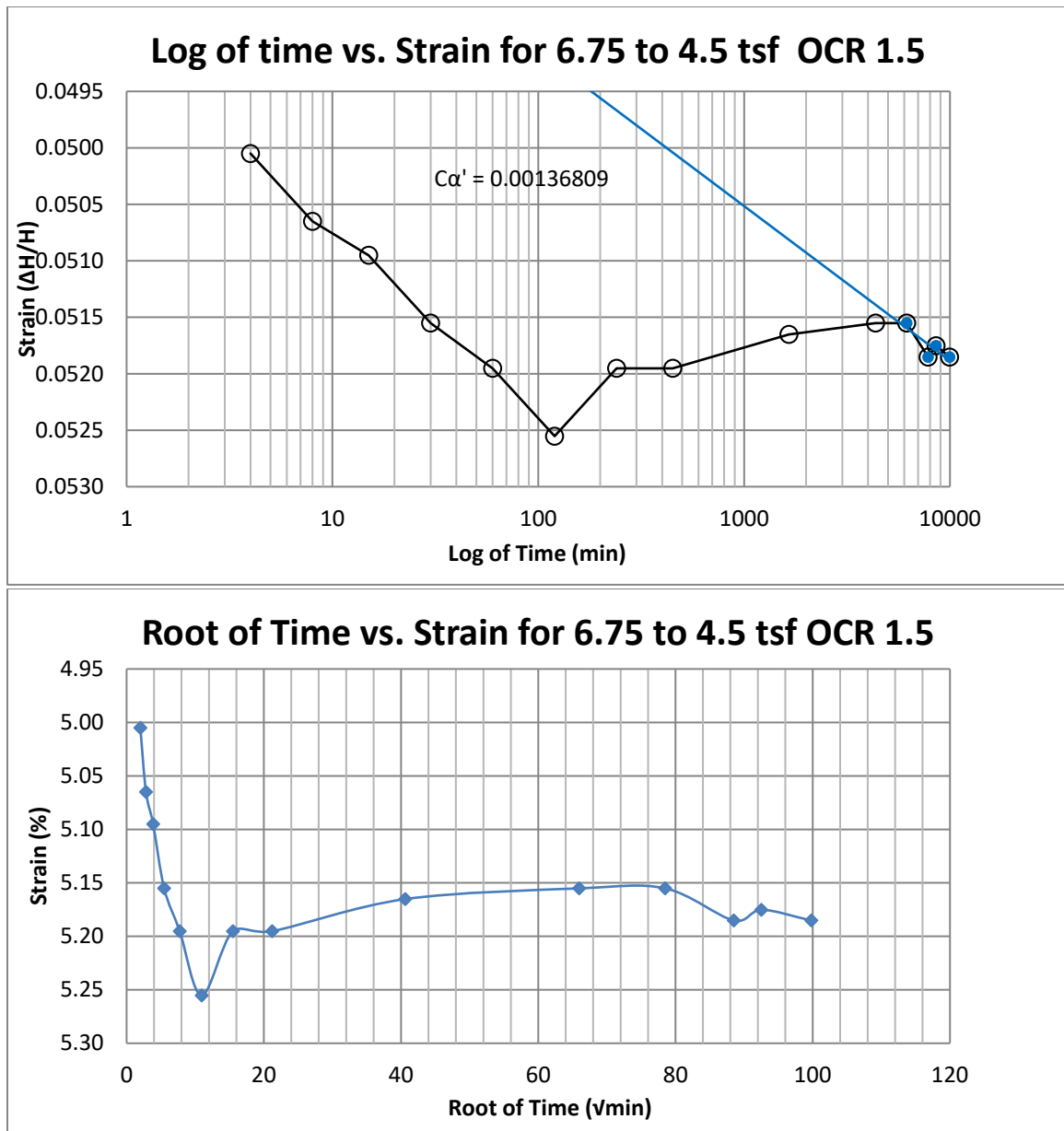


Figure B43 Springville at 65-67 feet

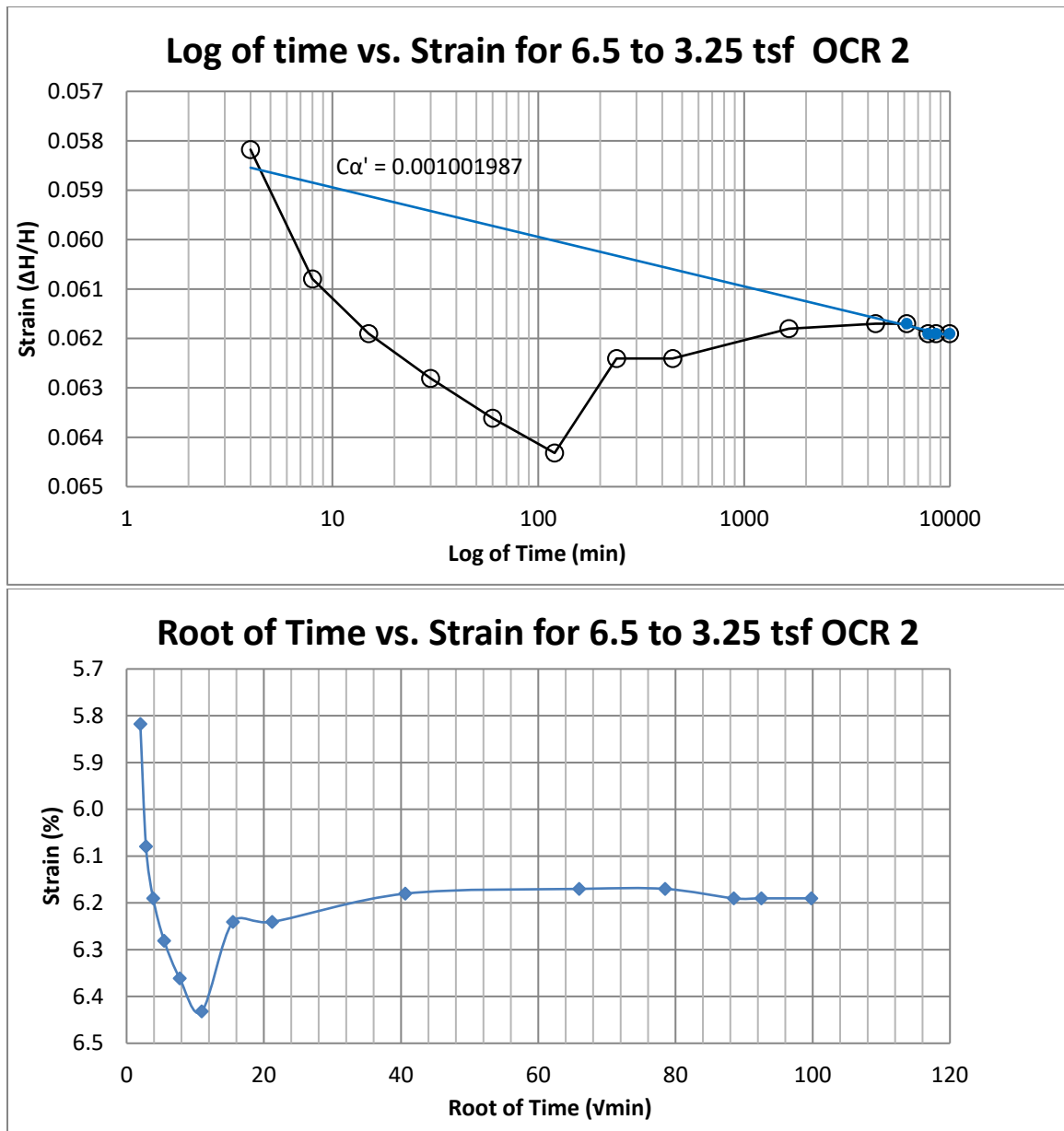


Figure B44 Springville at 65-67 feet

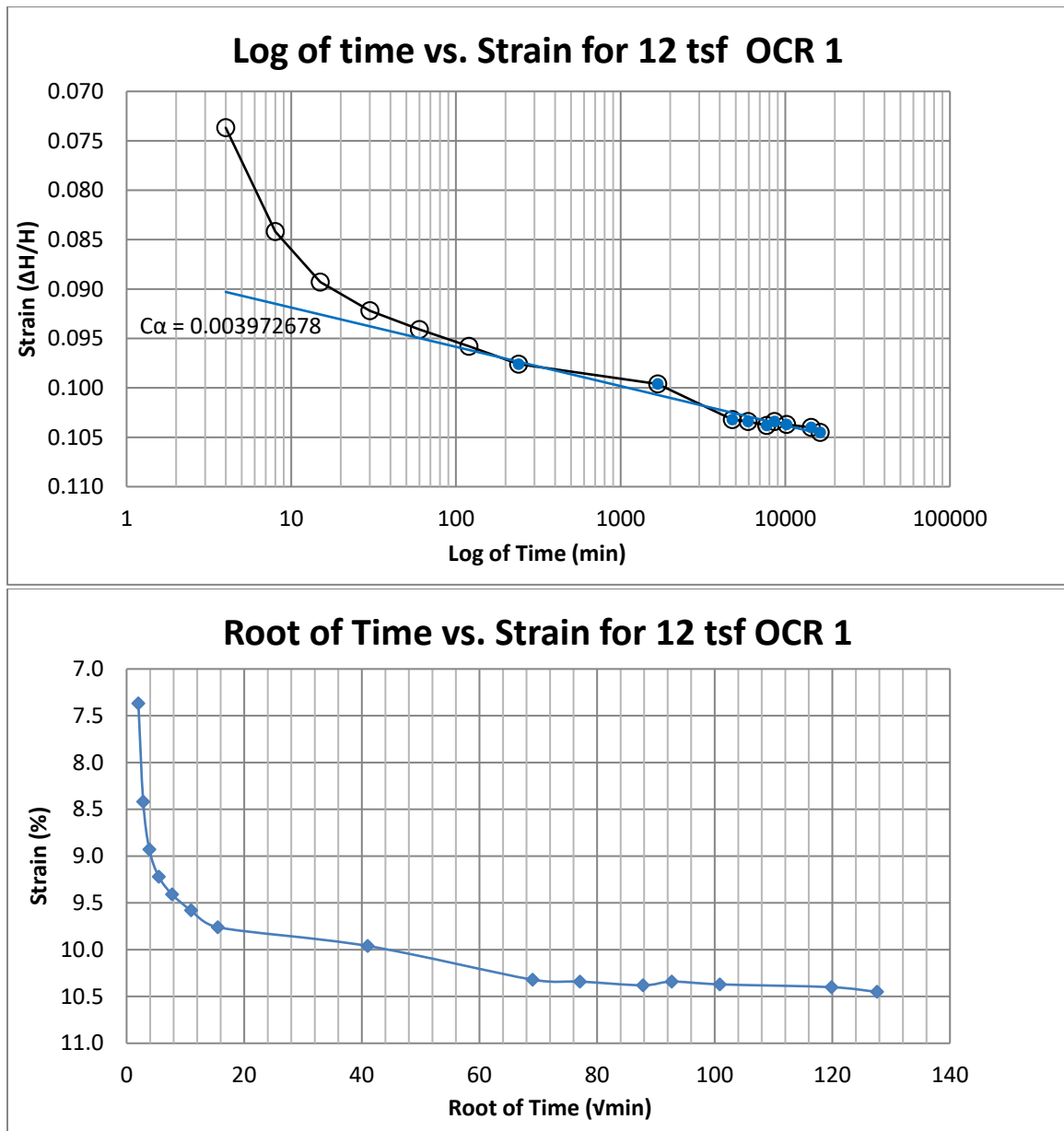


Figure B45 Springville at 70-72 feet

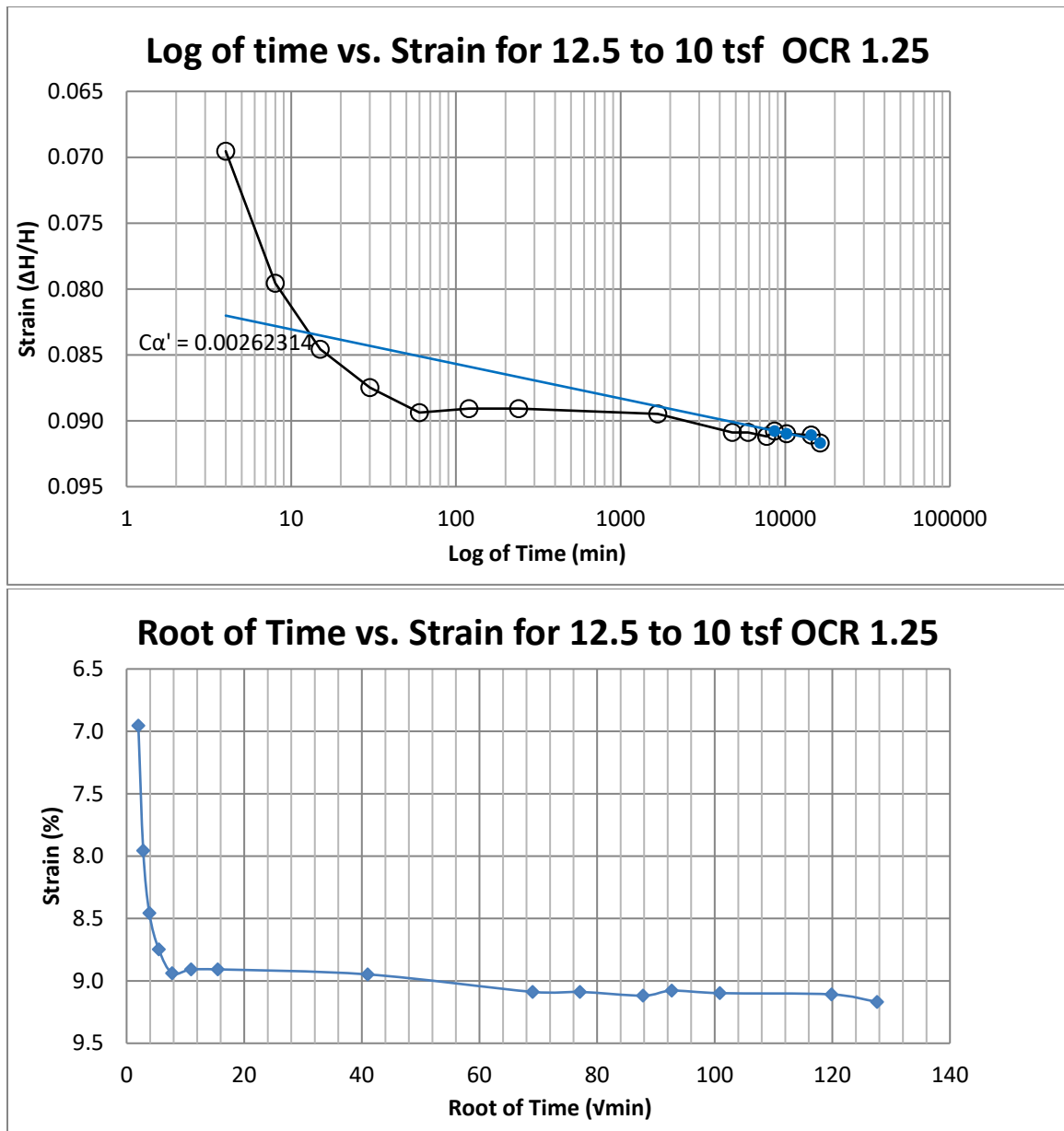


Figure B46 Springville at 70-72 feet

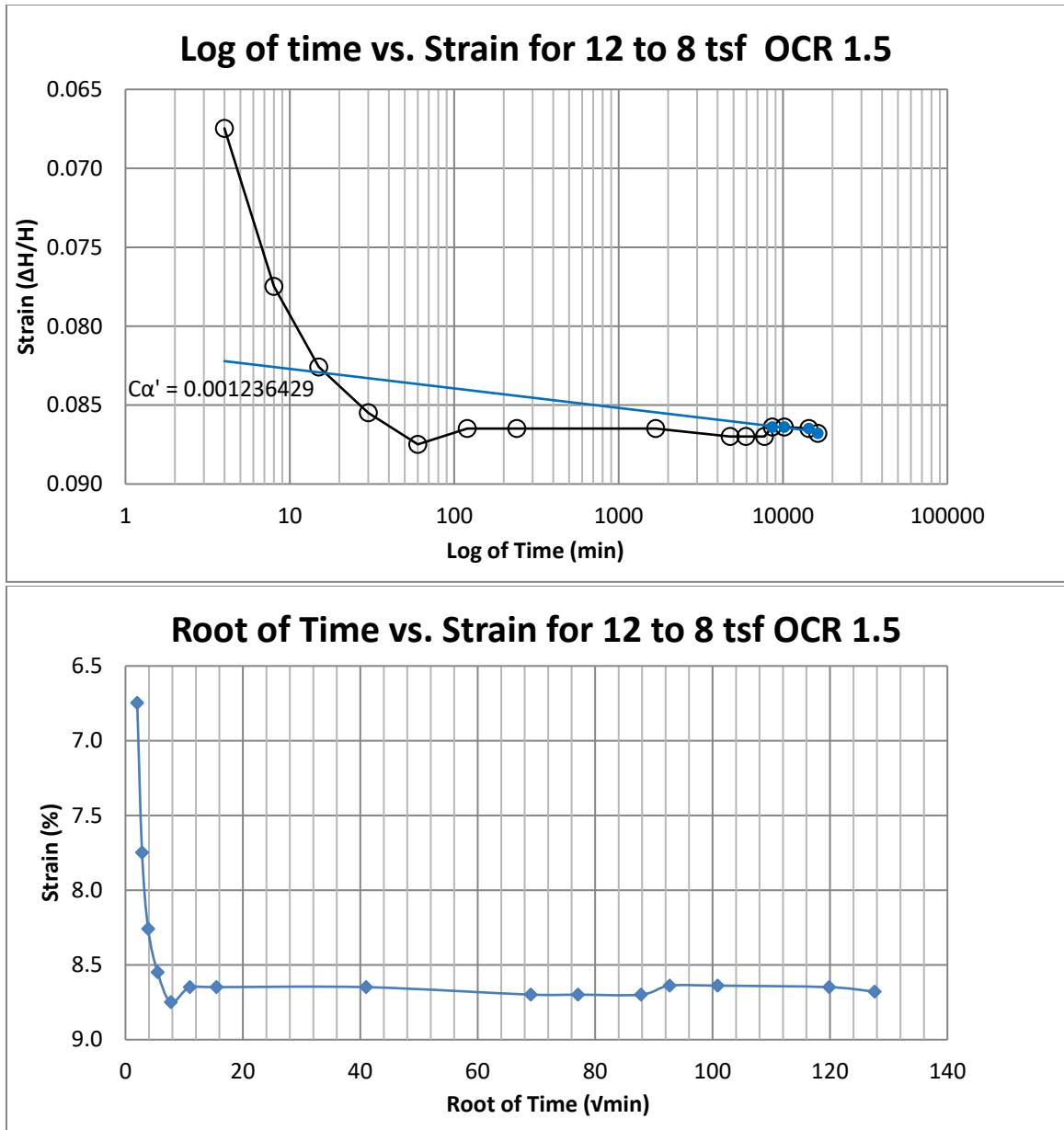


Figure B47 Springville at 70-72 feet

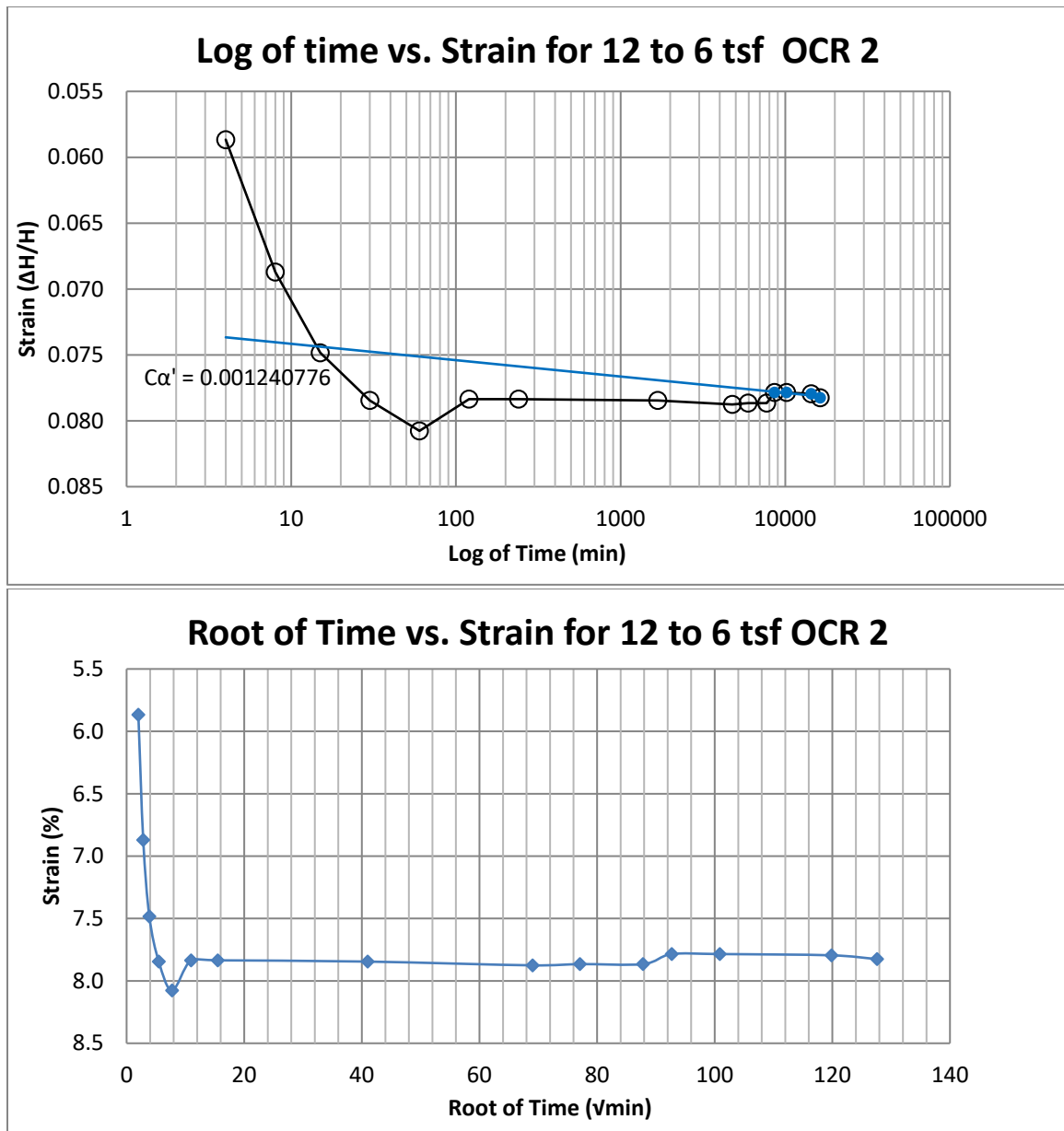


Figure B48 Springville at 70-72 feet

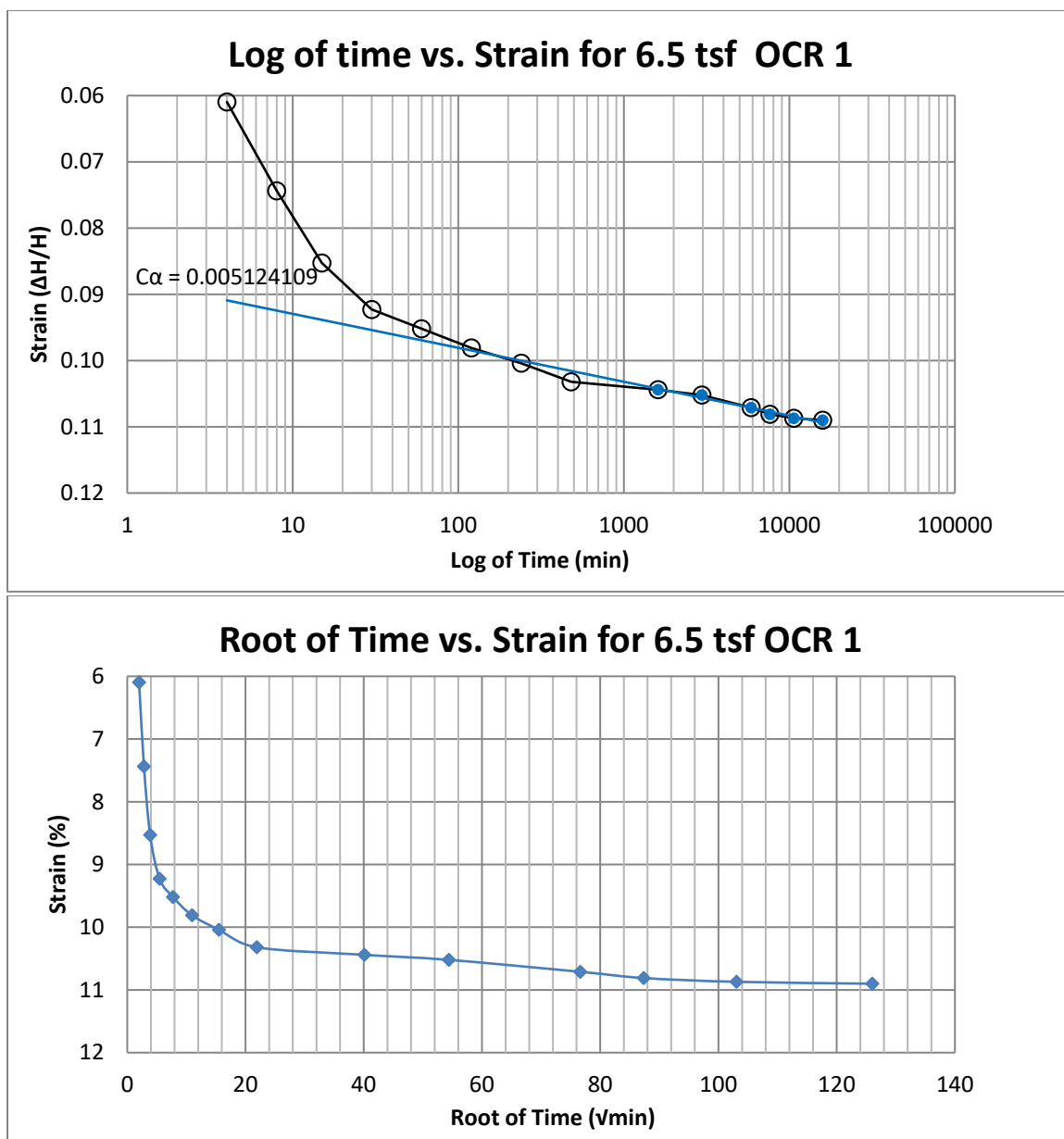


Figure B49 Springville at 75-77 feet

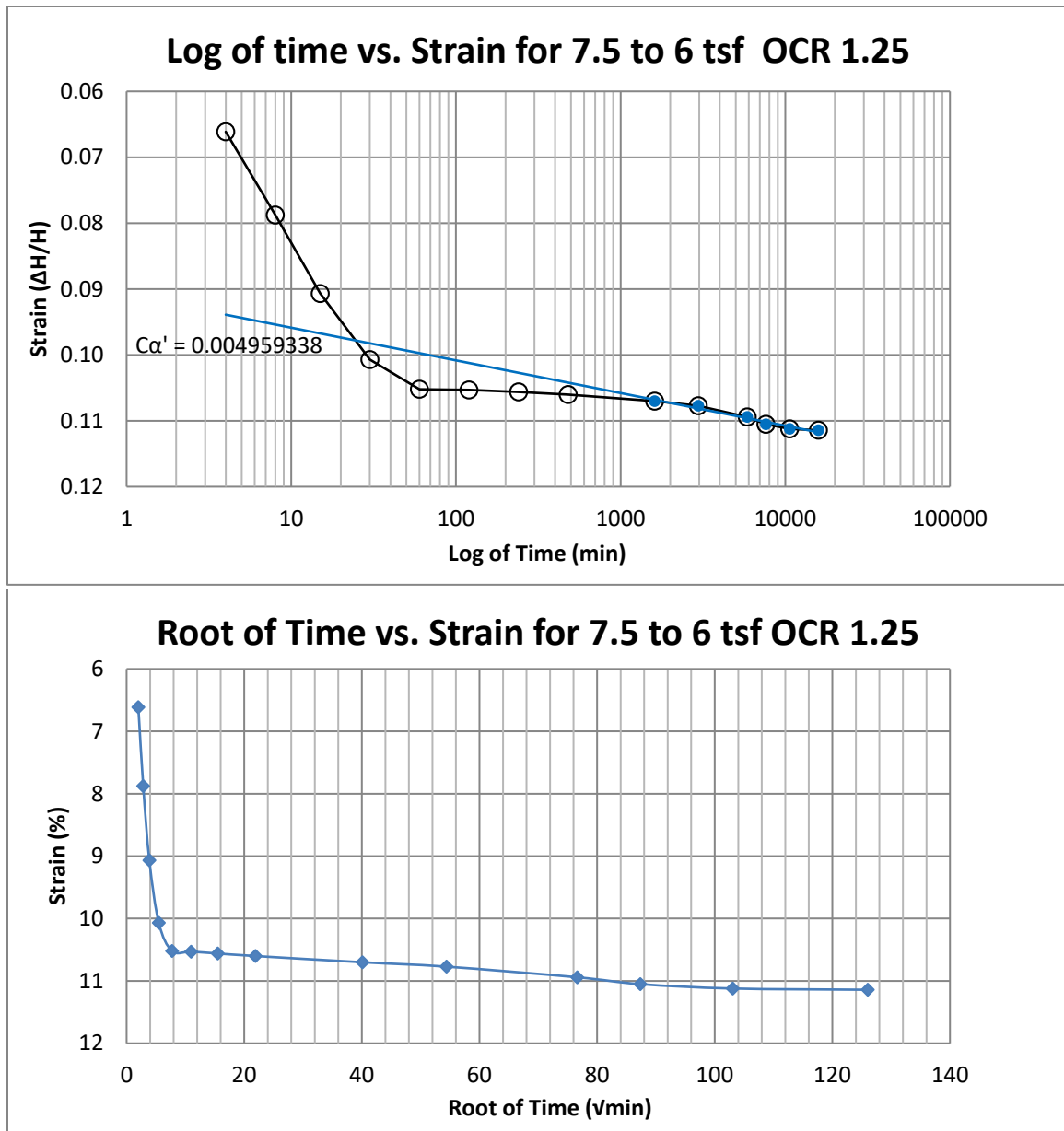


Figure B50 Springville at 75-77 feet



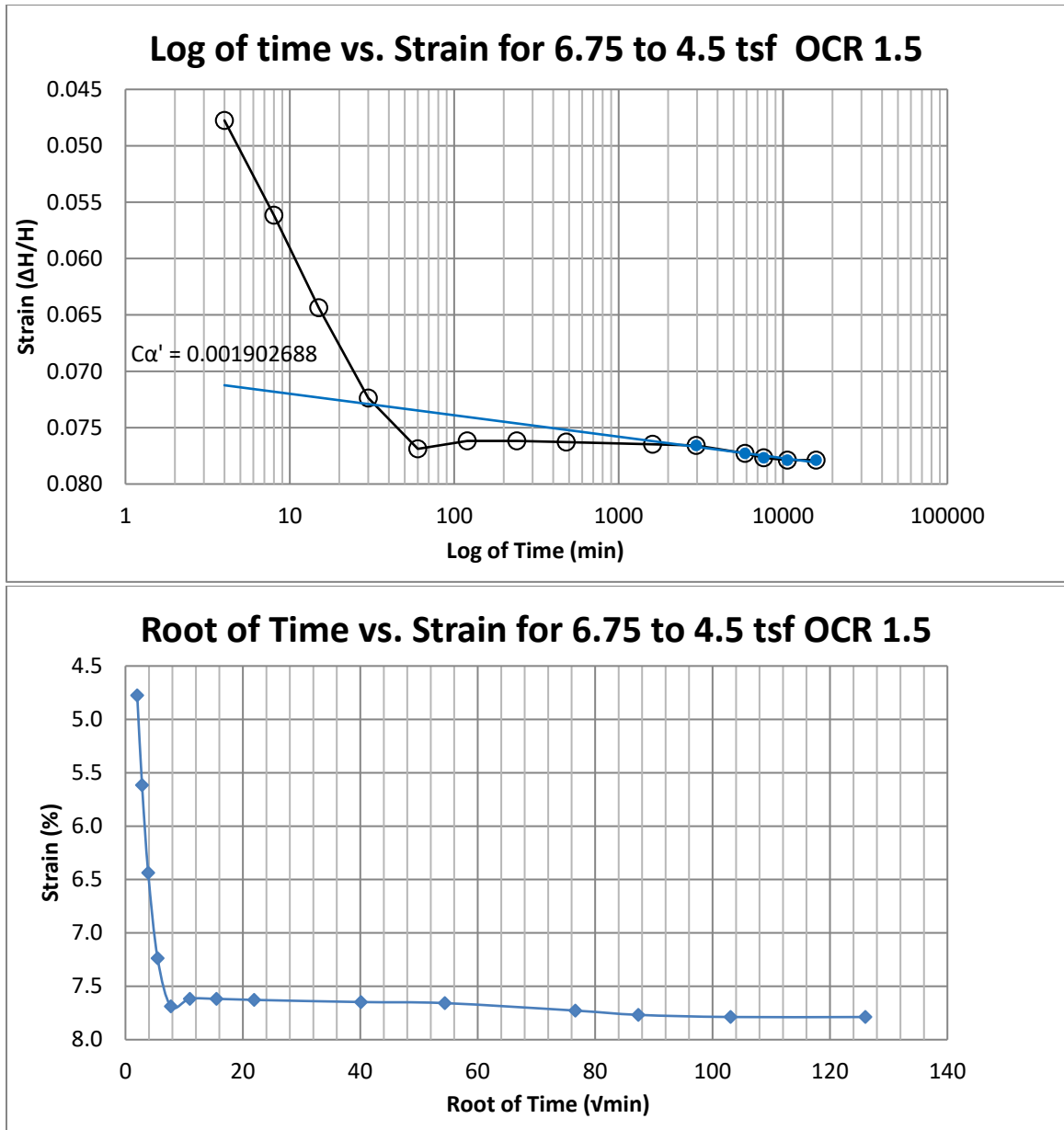


Figure B51 Springville at 75-77 feet

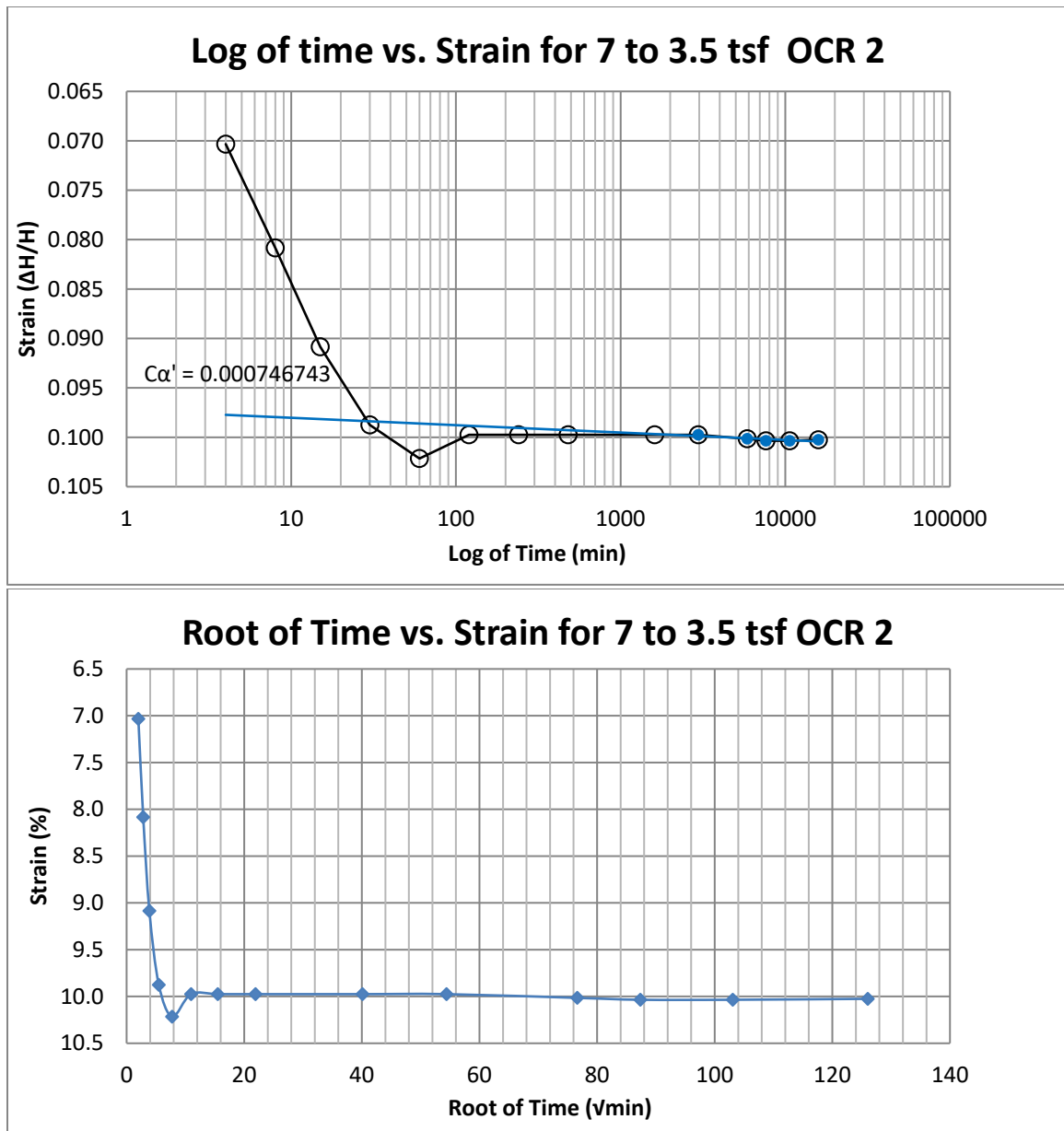


Figure B52 Springville at 75-77 feet

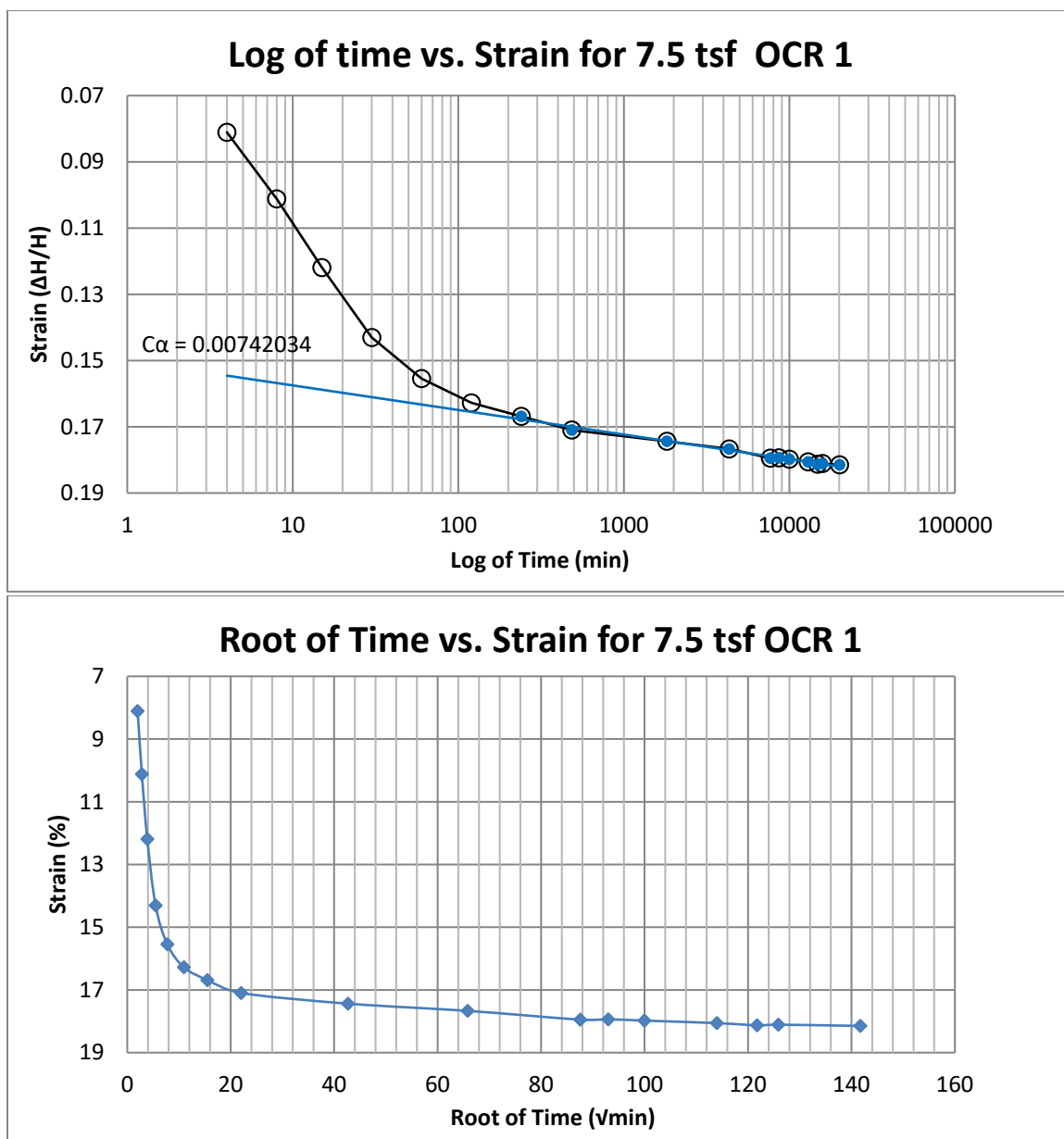


Figure B53 Springville at 80-82 feet

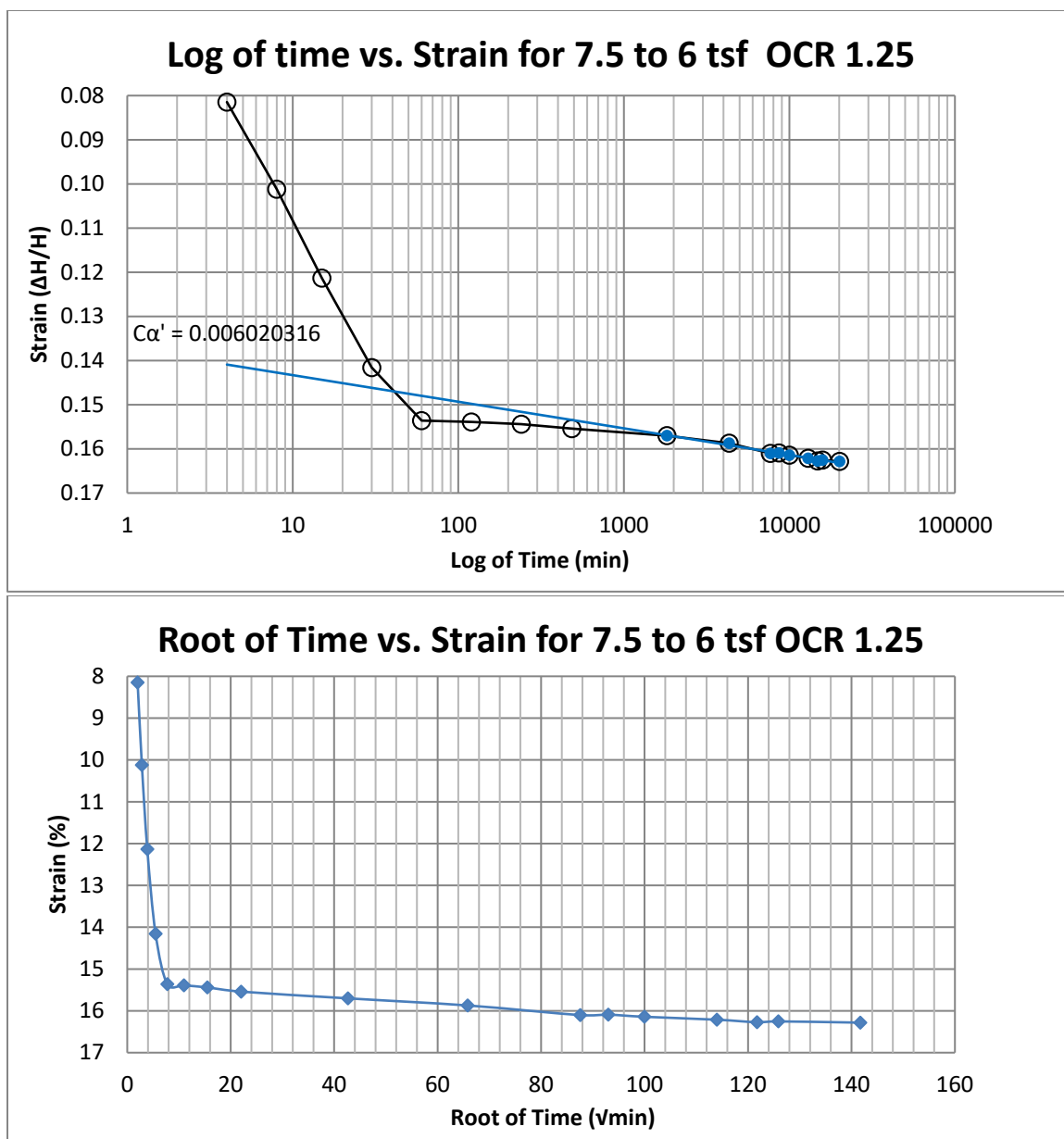


Figure B54 Springville at 80-82 feet

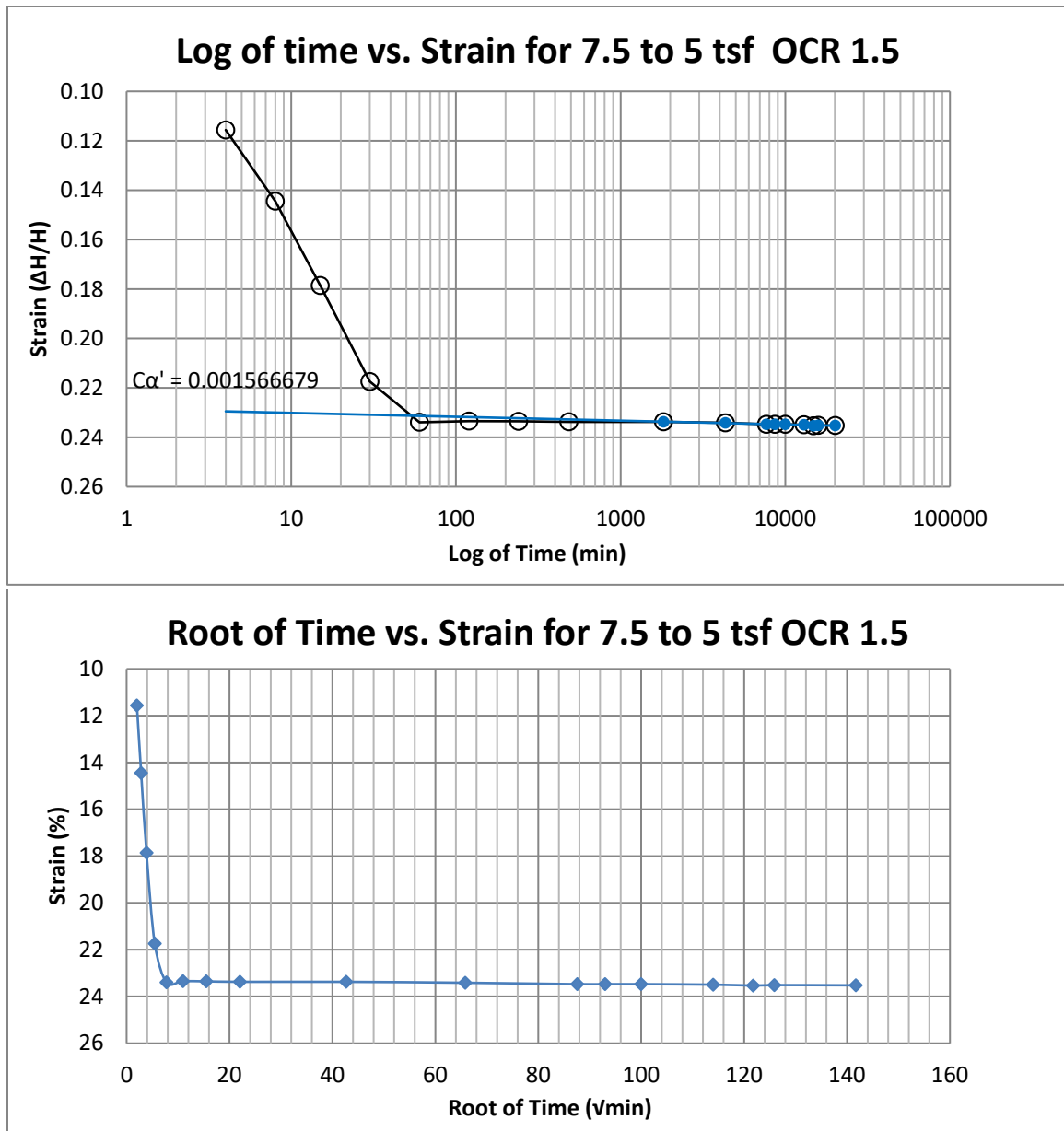


Figure B55 Springville at 80-82 feet

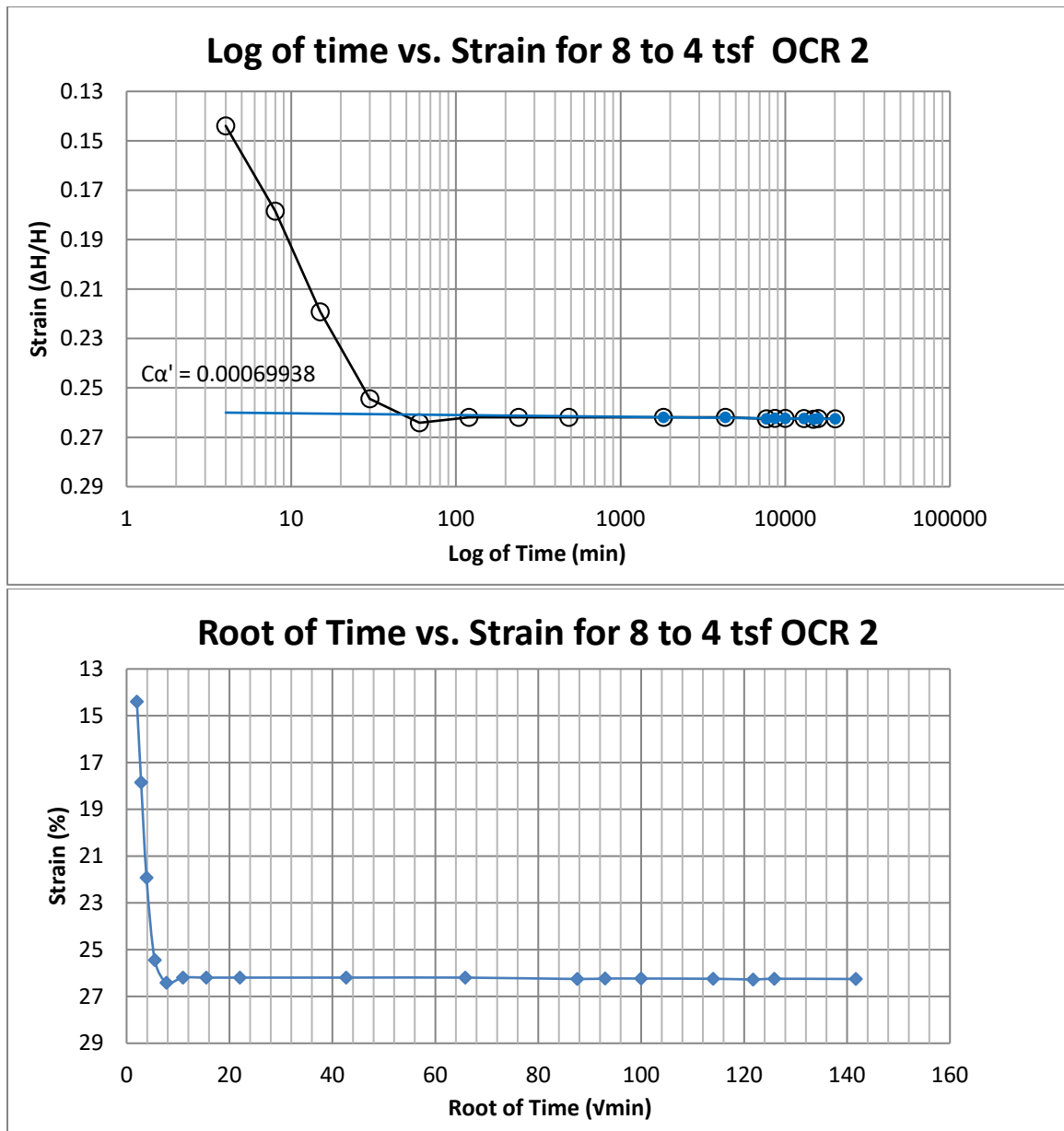


Figure B56 Springville at 80-82 feet

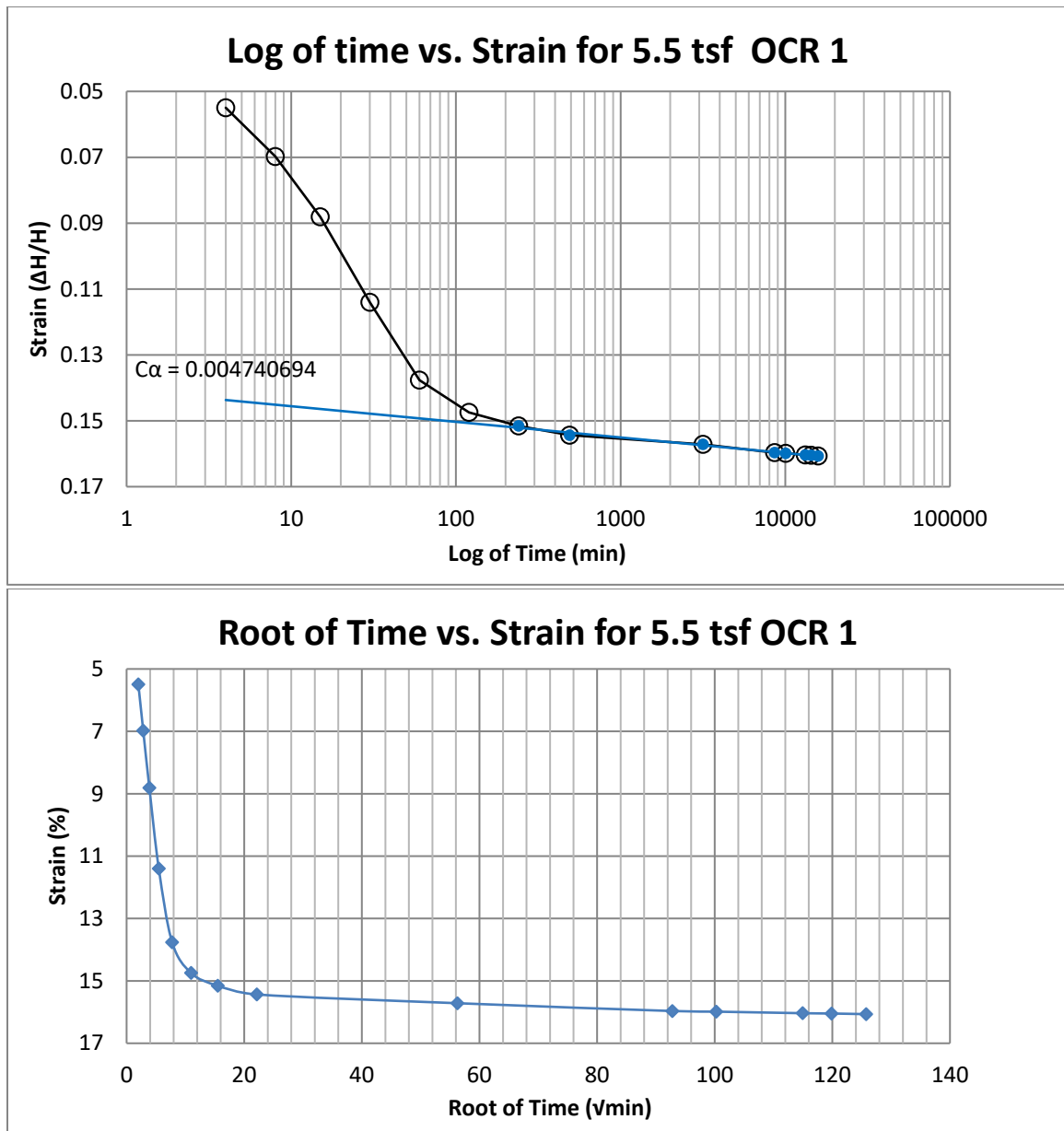


Figure B57 Springville at 84-86 feet

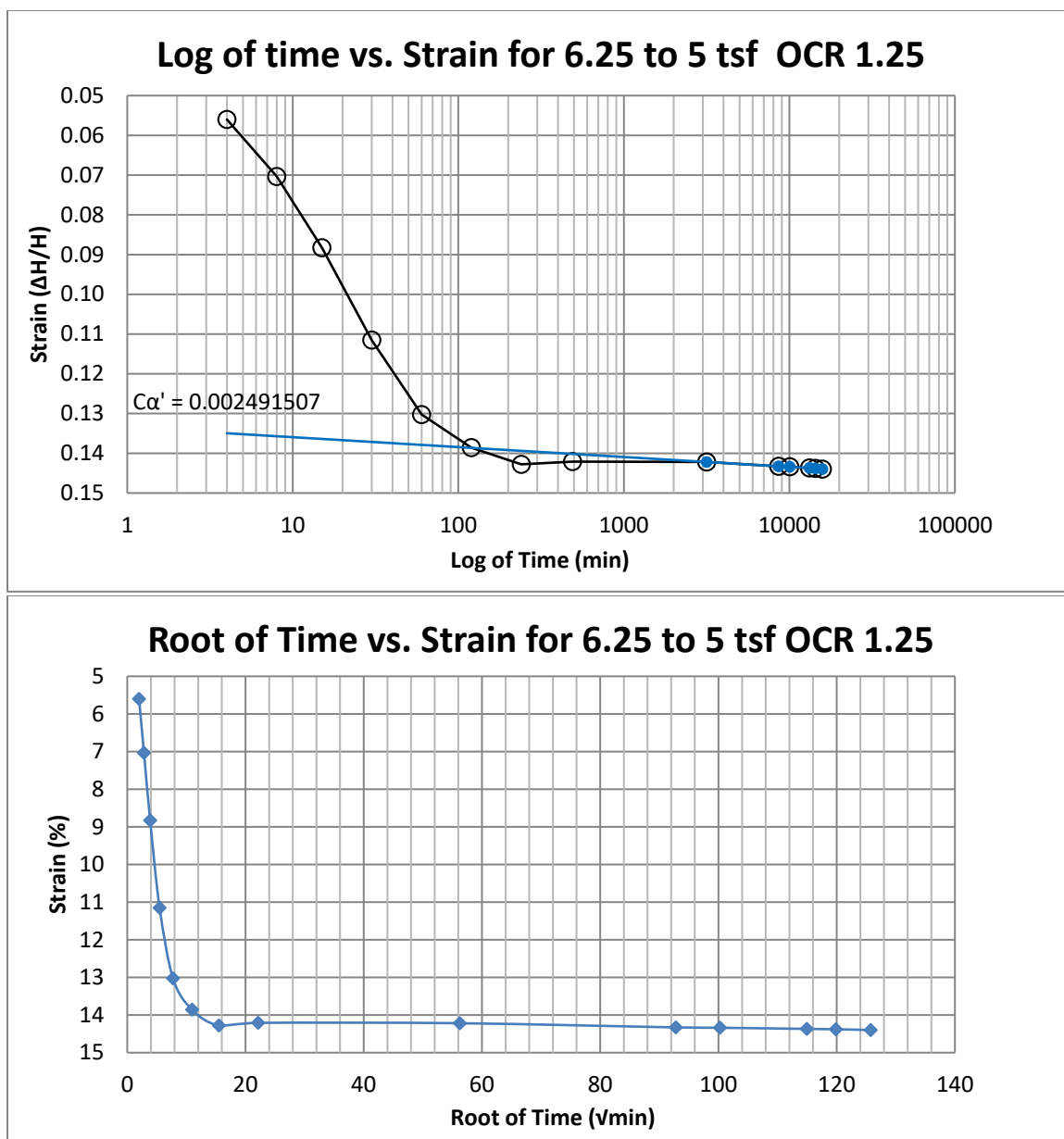


Figure B58 Springville at 84-86 feet



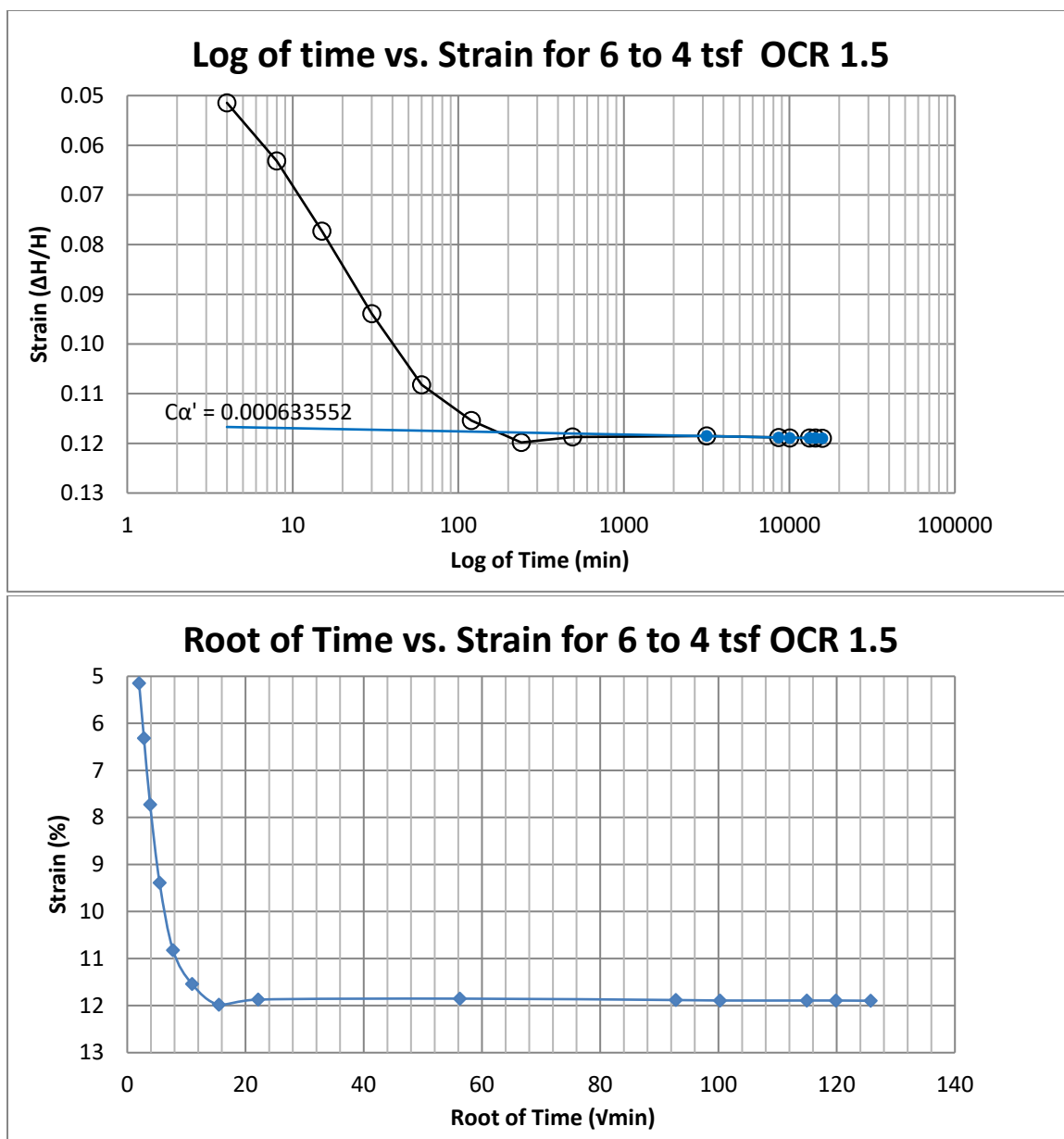


Figure B59 Springville at 84-86 feet

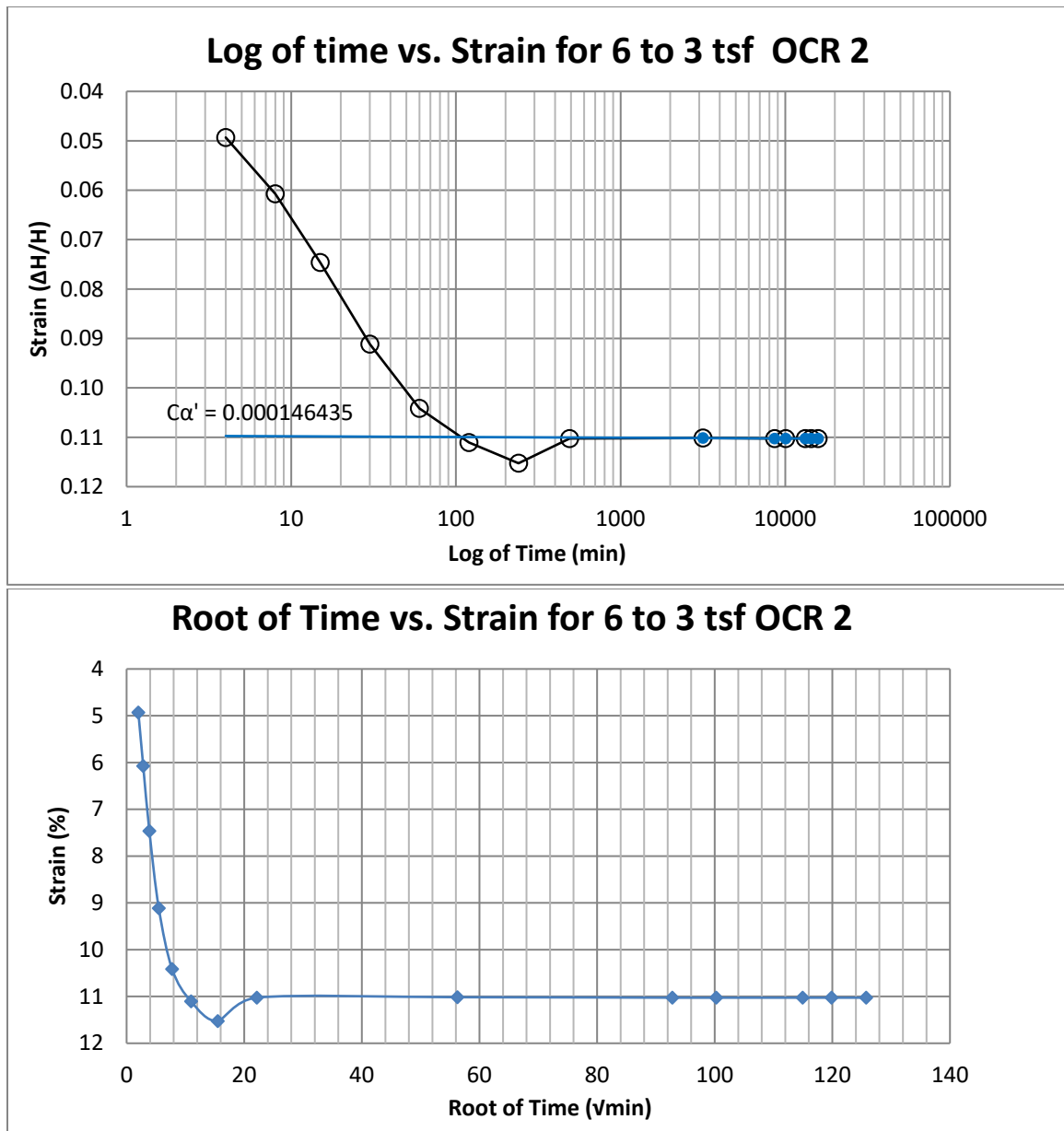


Figure B60 Springville at 84-86 feet

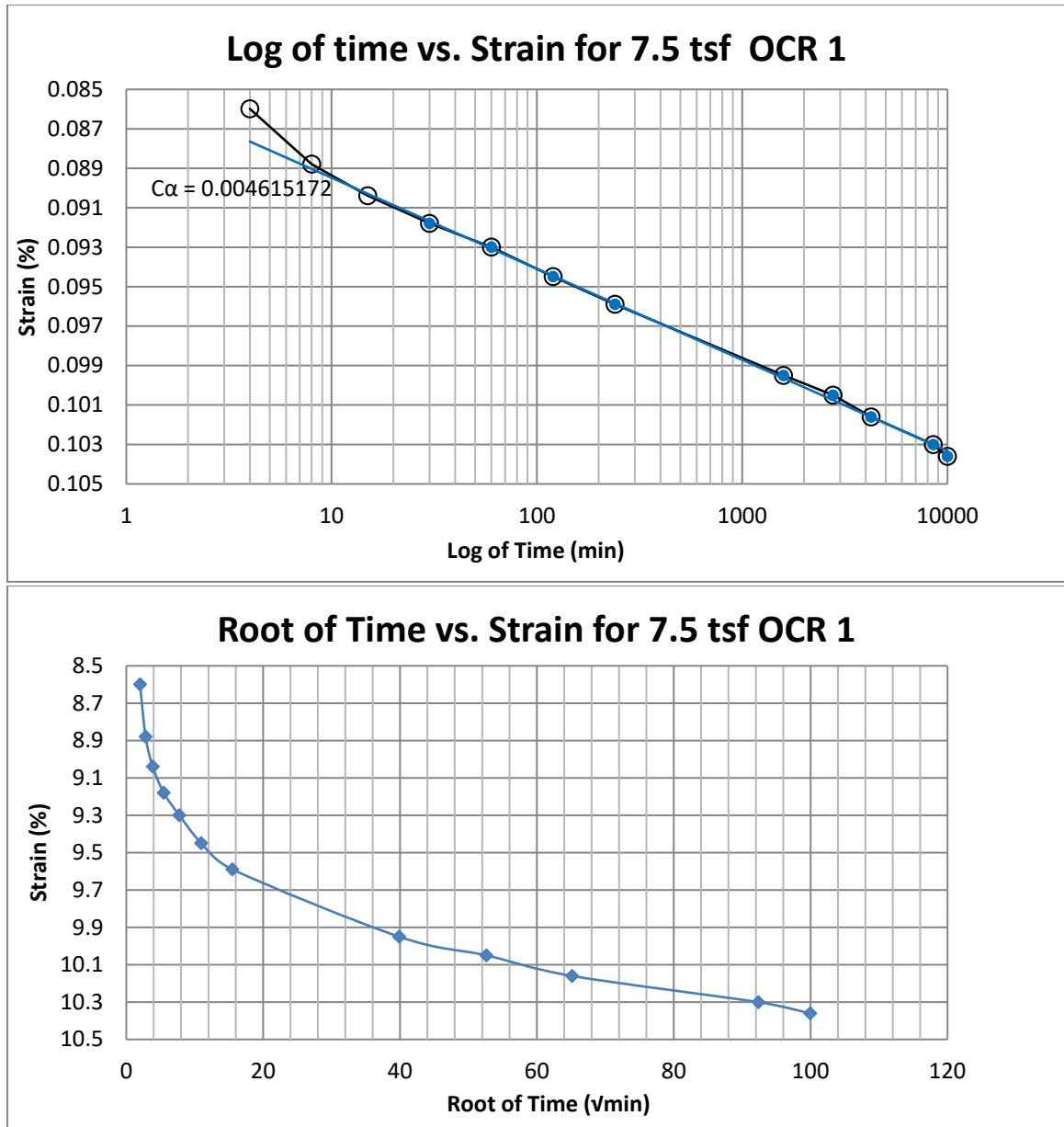


Figure B61 Provo at 12-14 feet

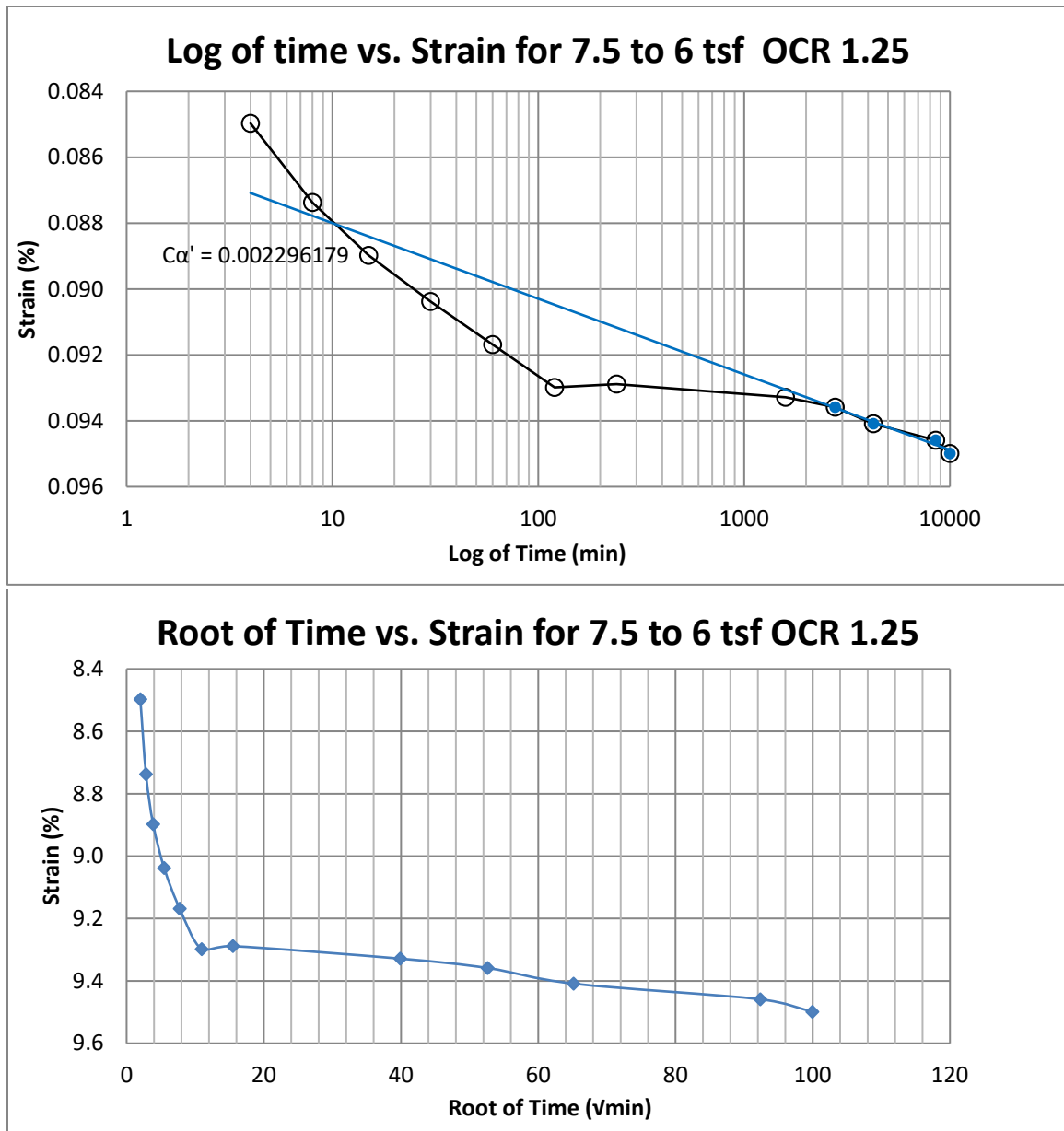


Figure B62 Provo at 12-14 feet

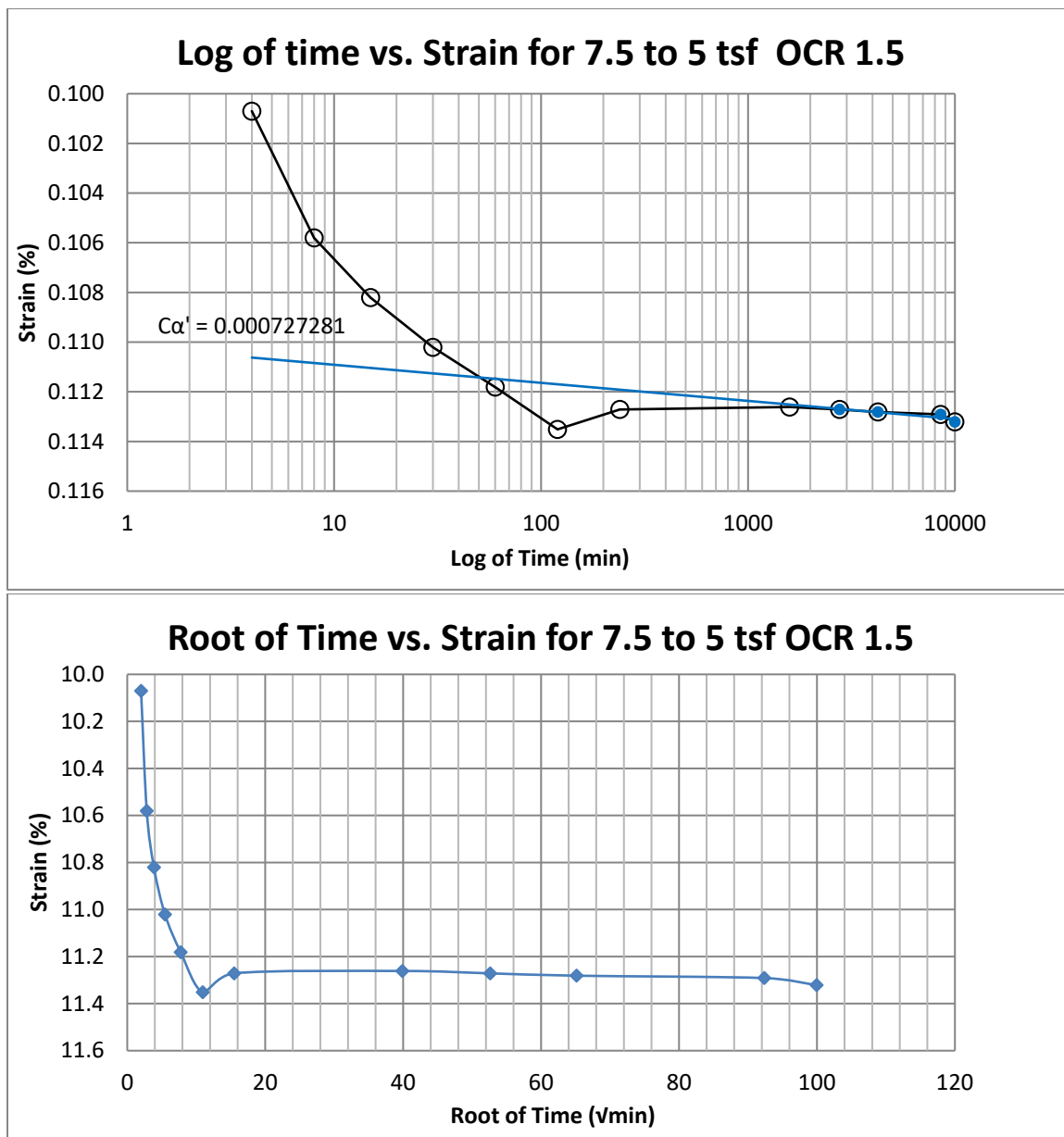


Figure B63 Provo at 12-14 feet

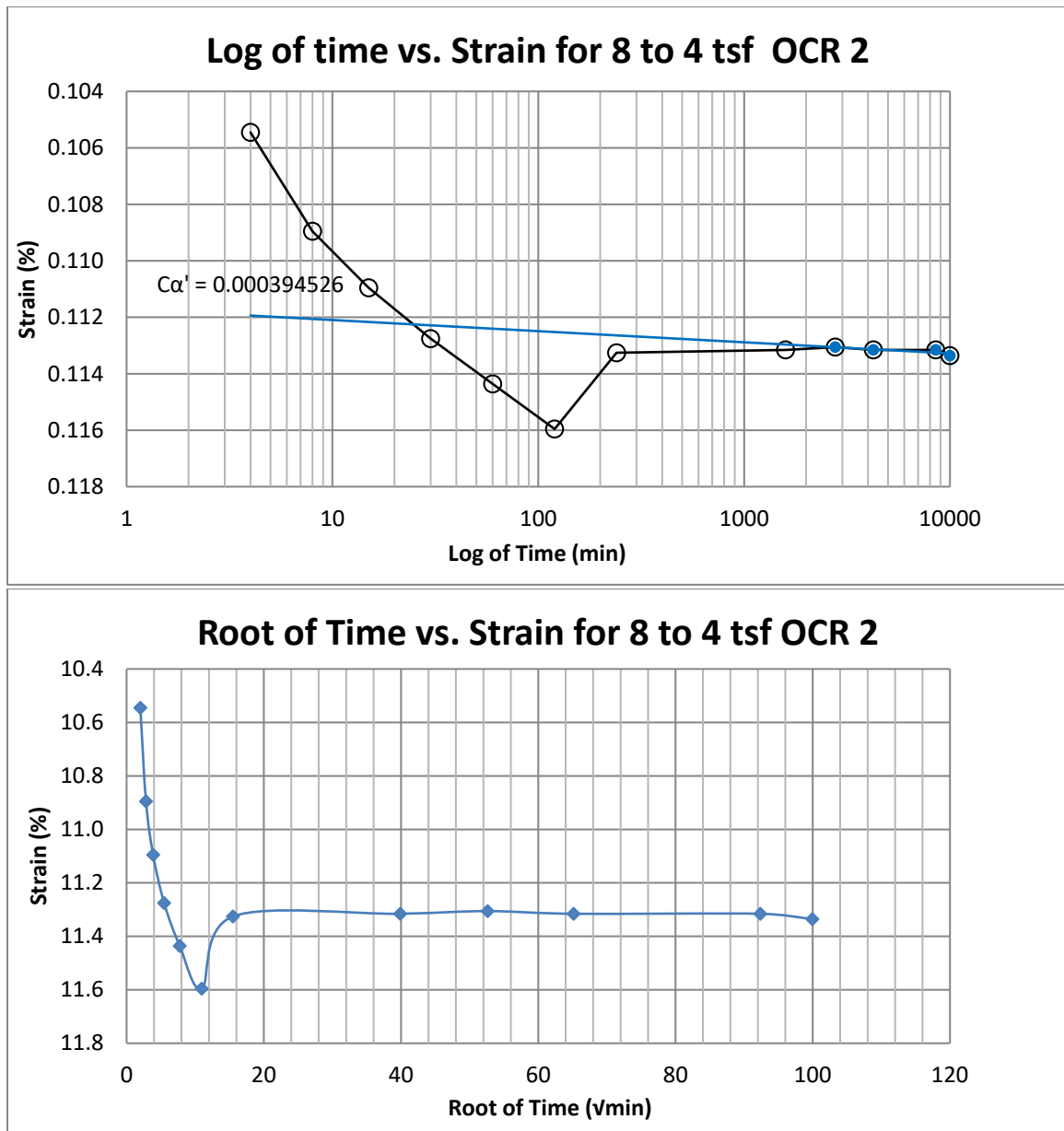


Figure B64 Provo at 12-14 feet

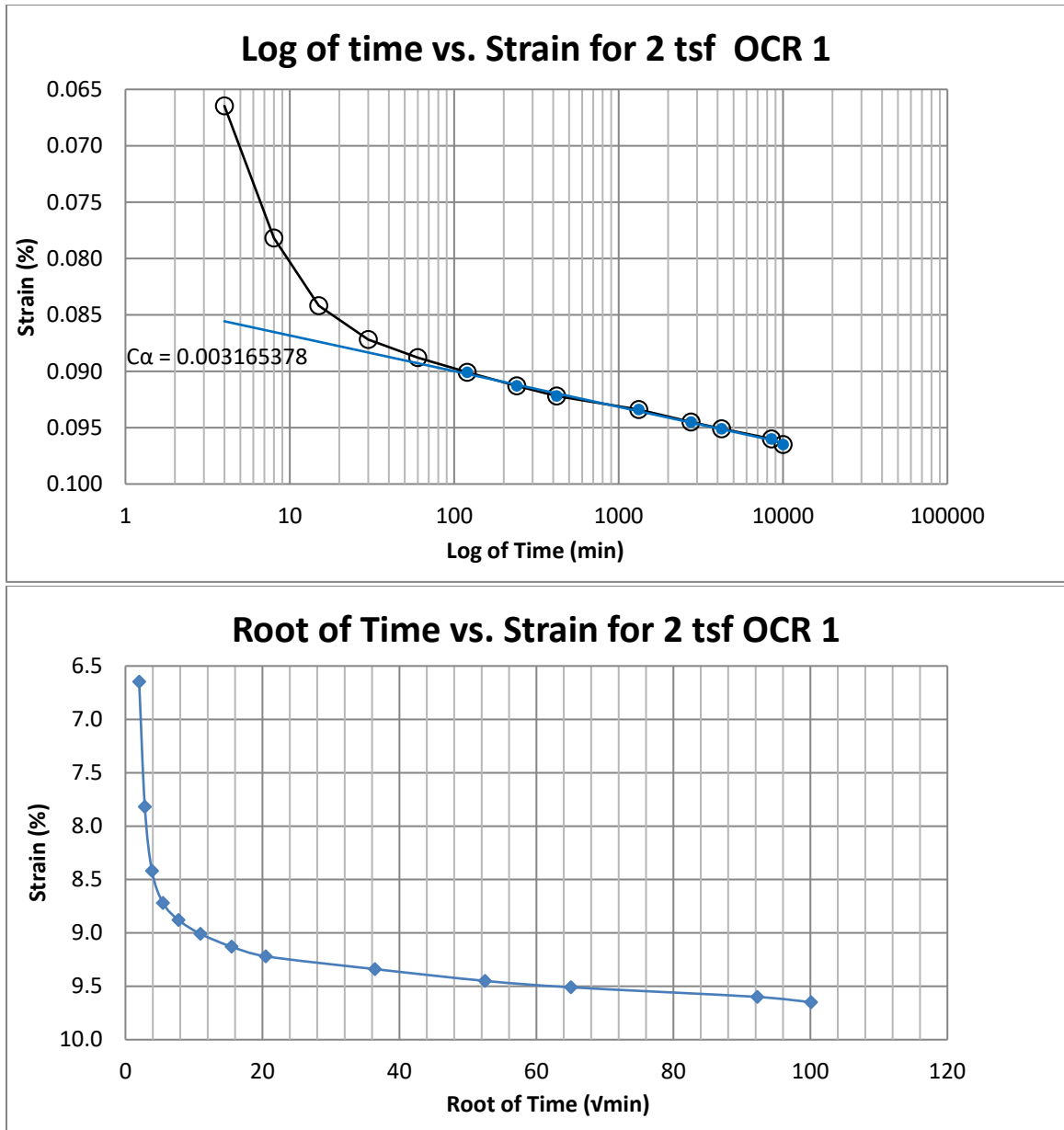


Figure B65 Provo at 17-19 feet

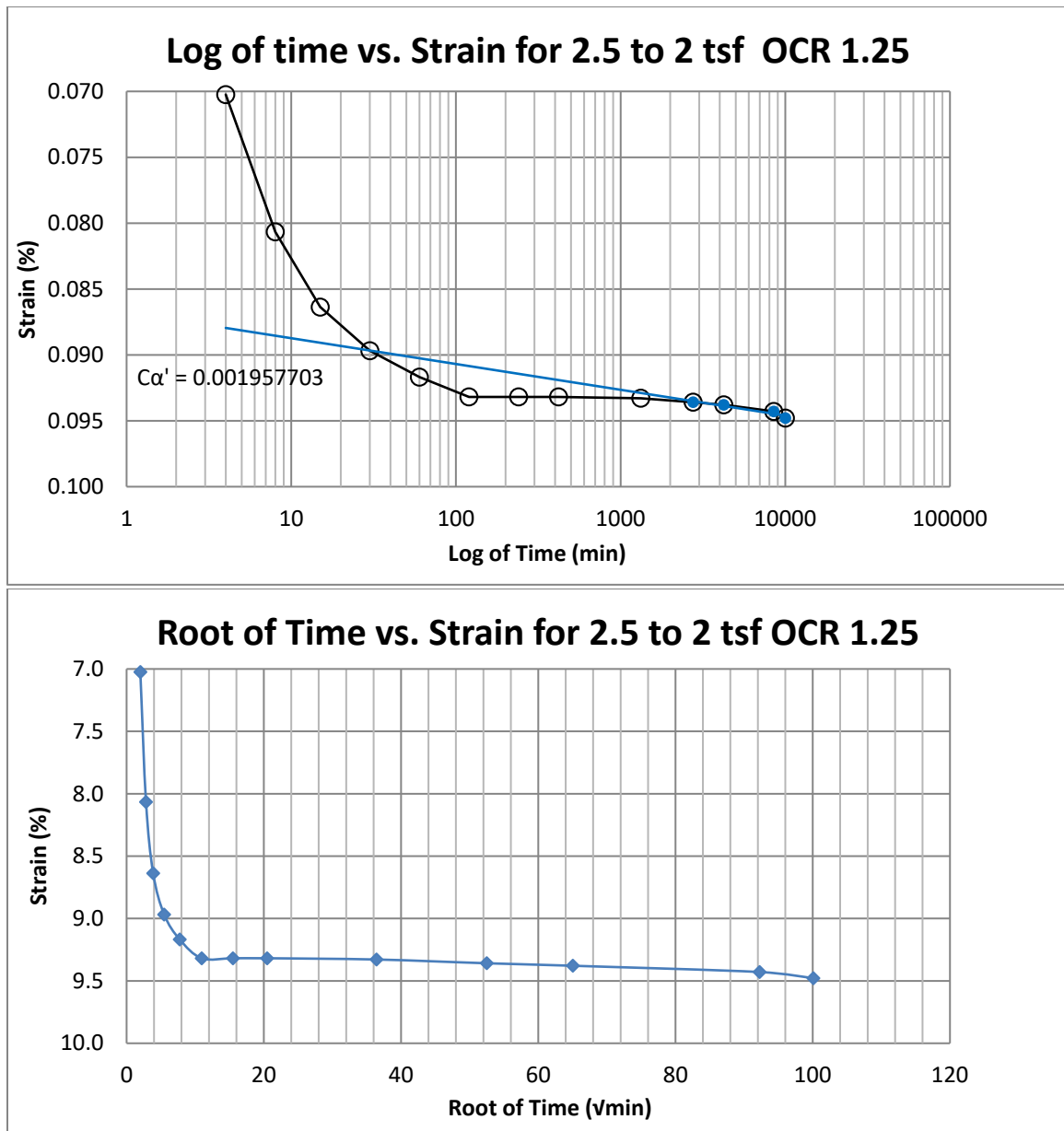


Figure B66 Provo at 17-19 feet



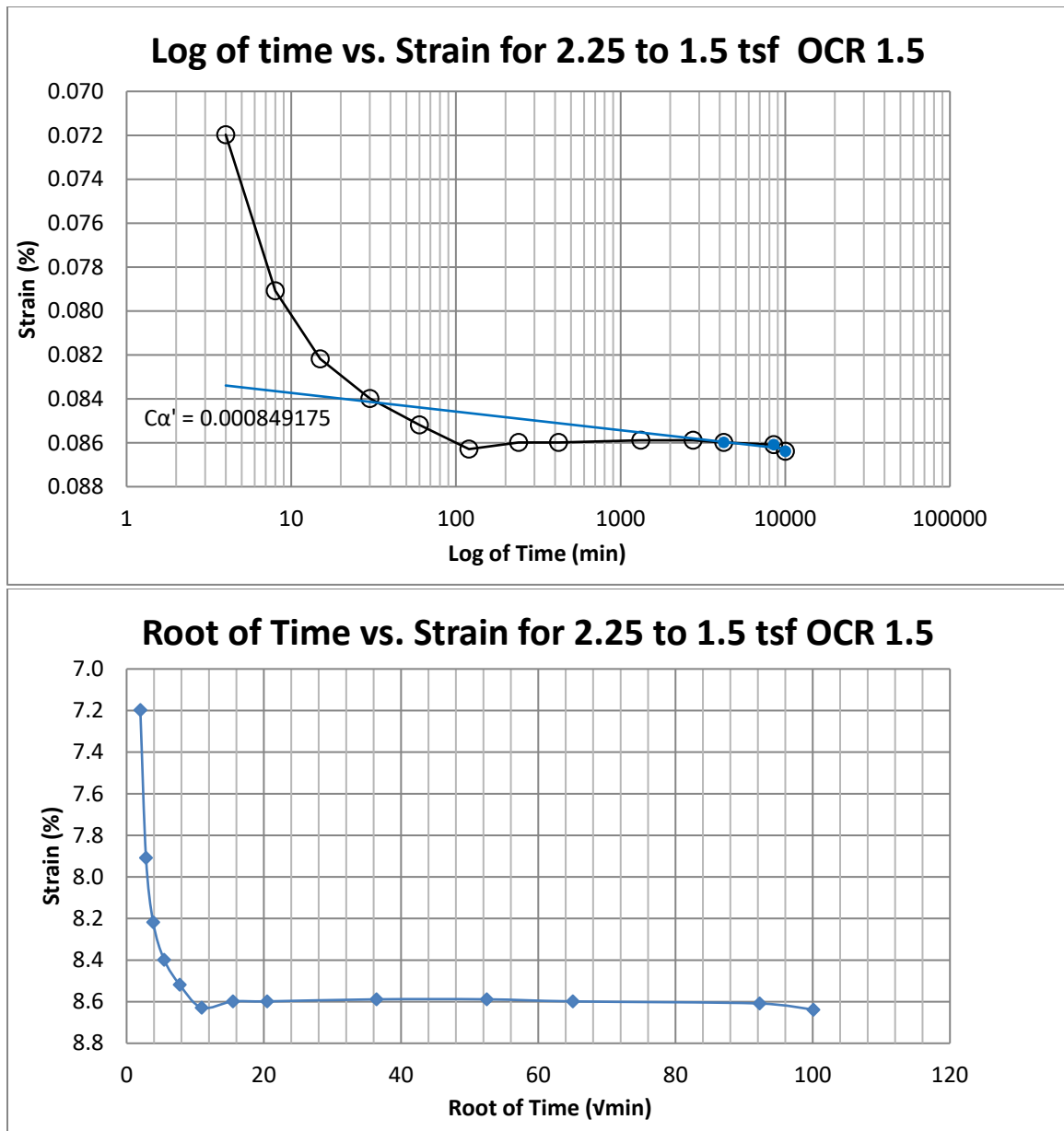


Figure B67 Provo at 17-19 feet

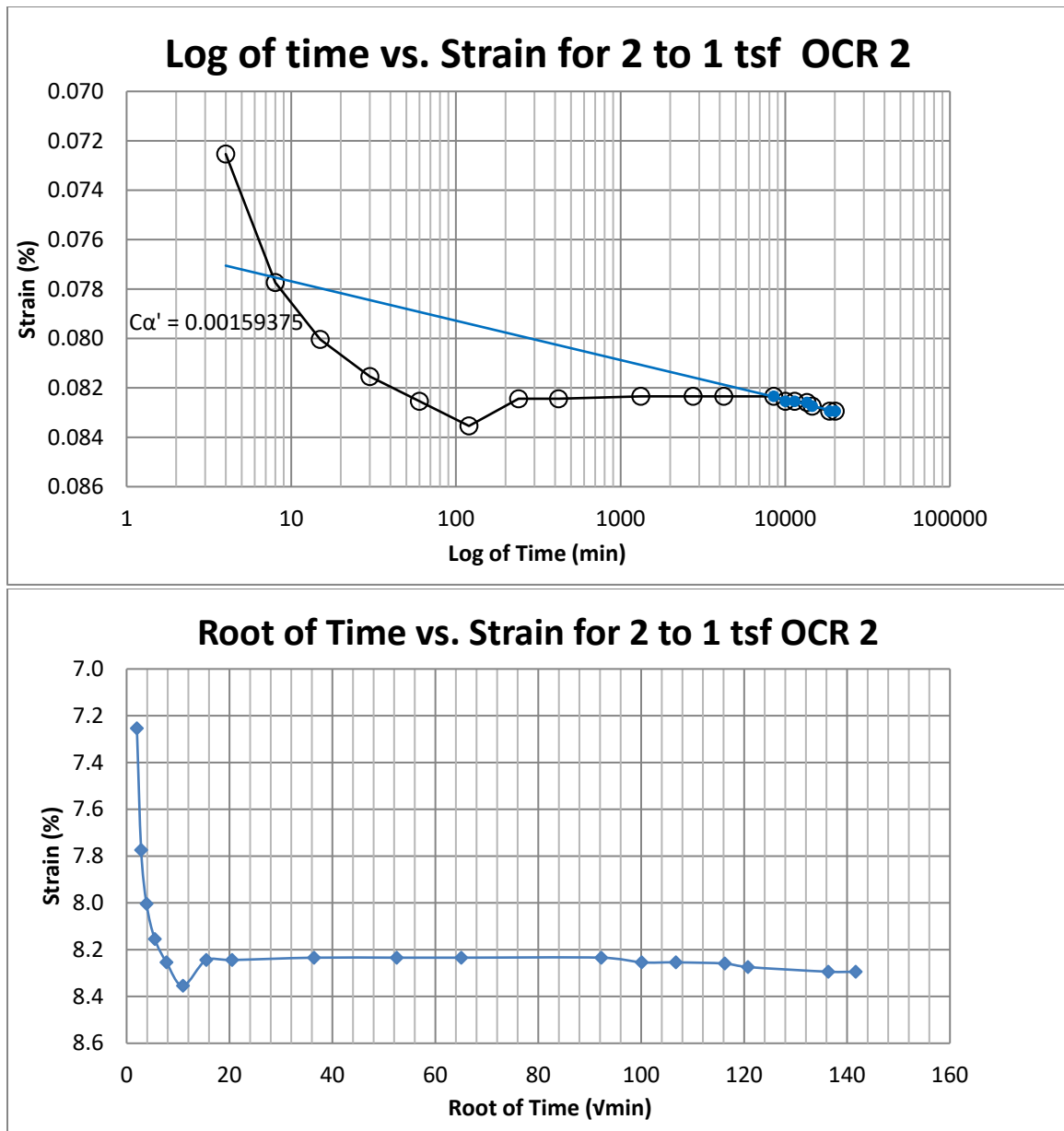


Figure B68 Provo at 17-19 feet

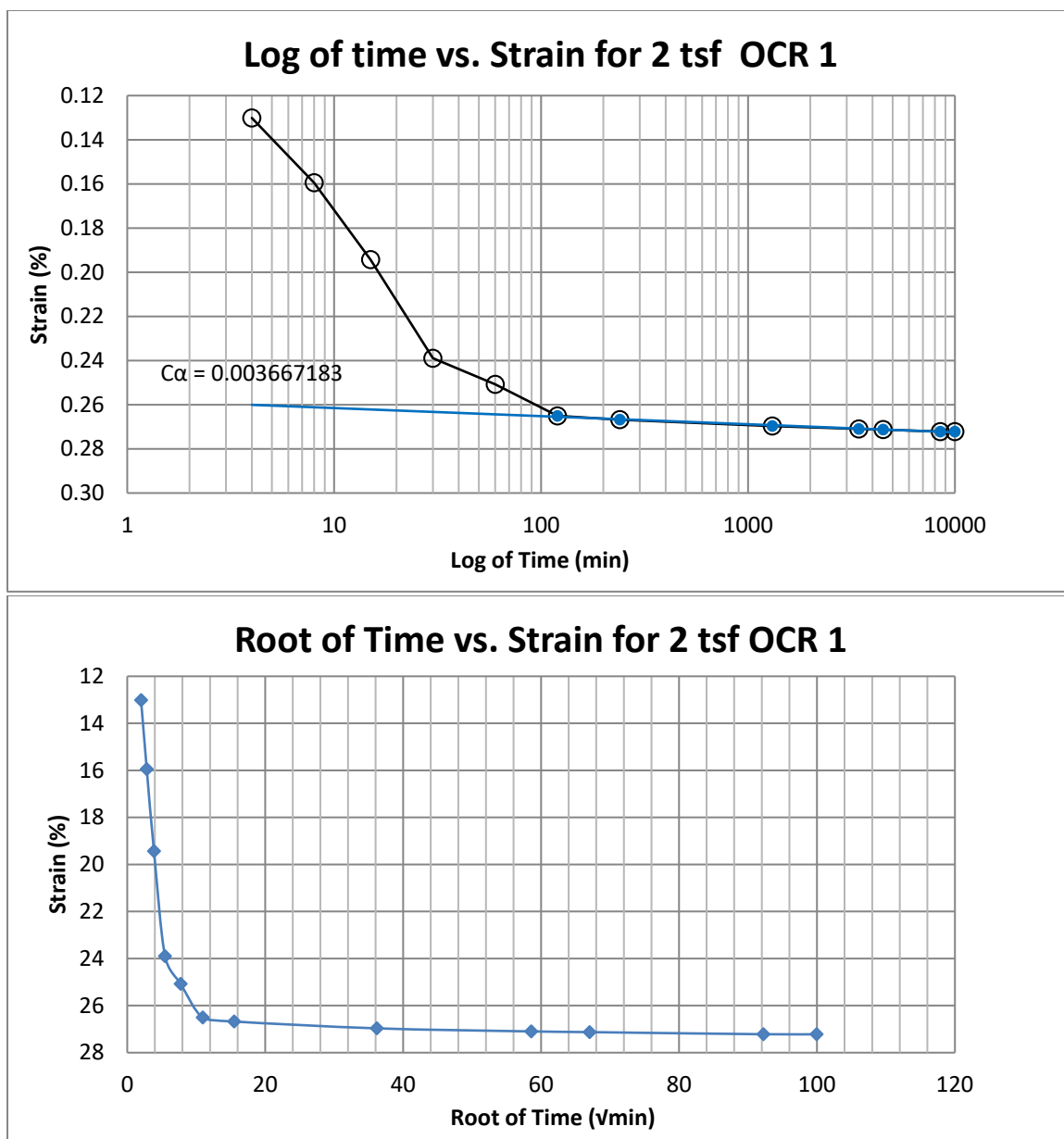


Figure B69 Provo at 50-52 feet

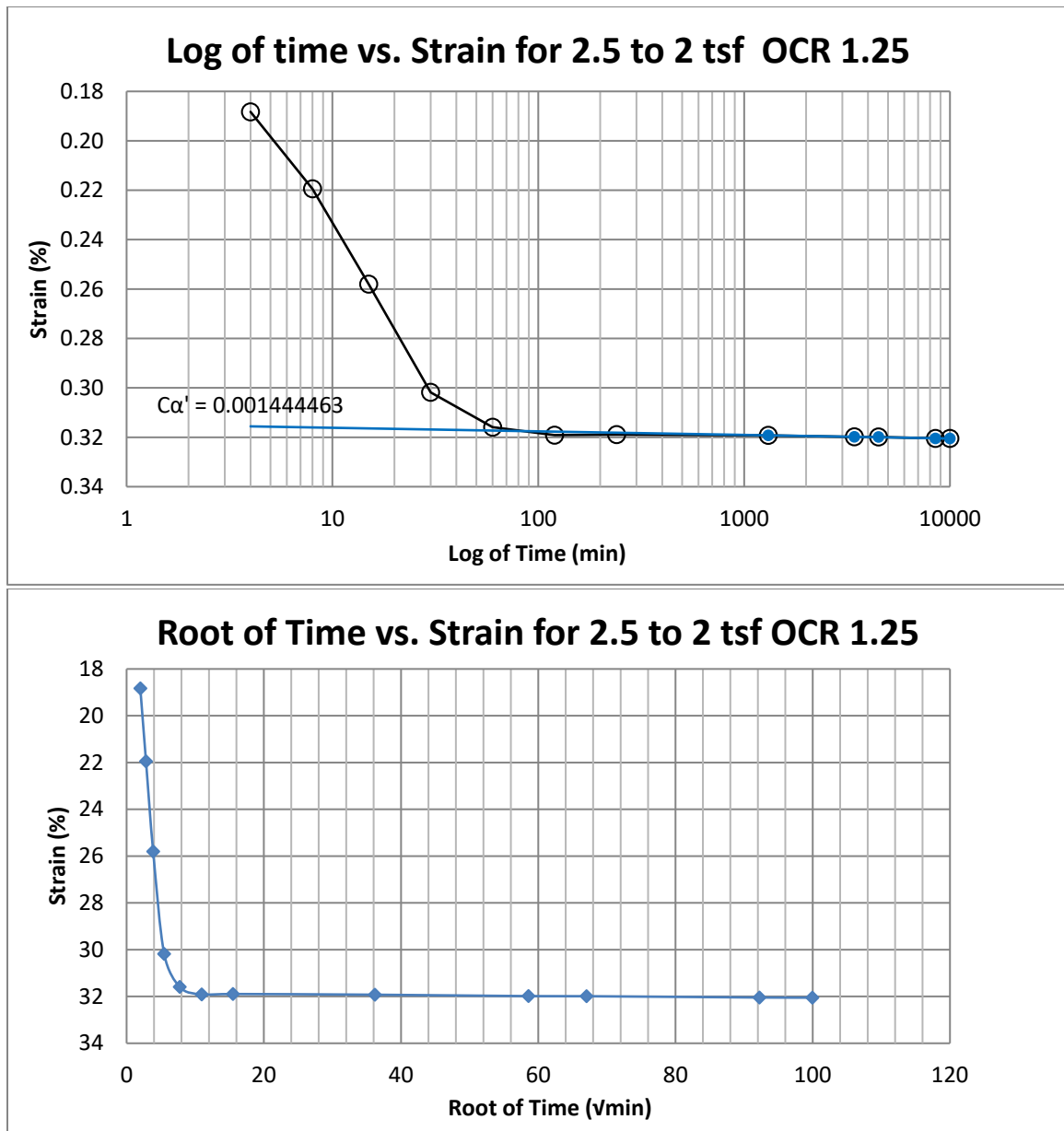


Figure B70 Provo at 50-52 feet

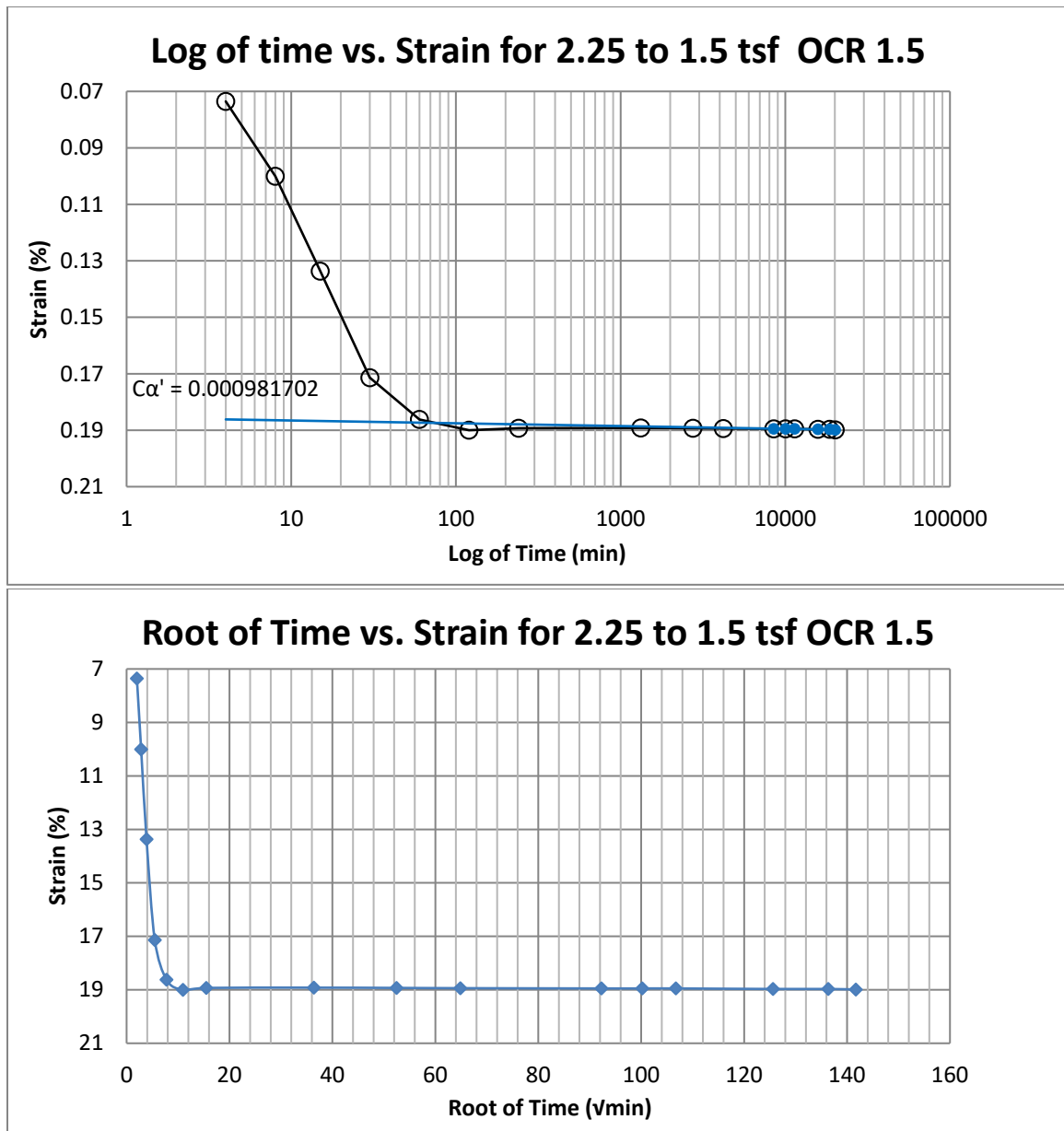


Figure B71 Provo at 50-52 feet

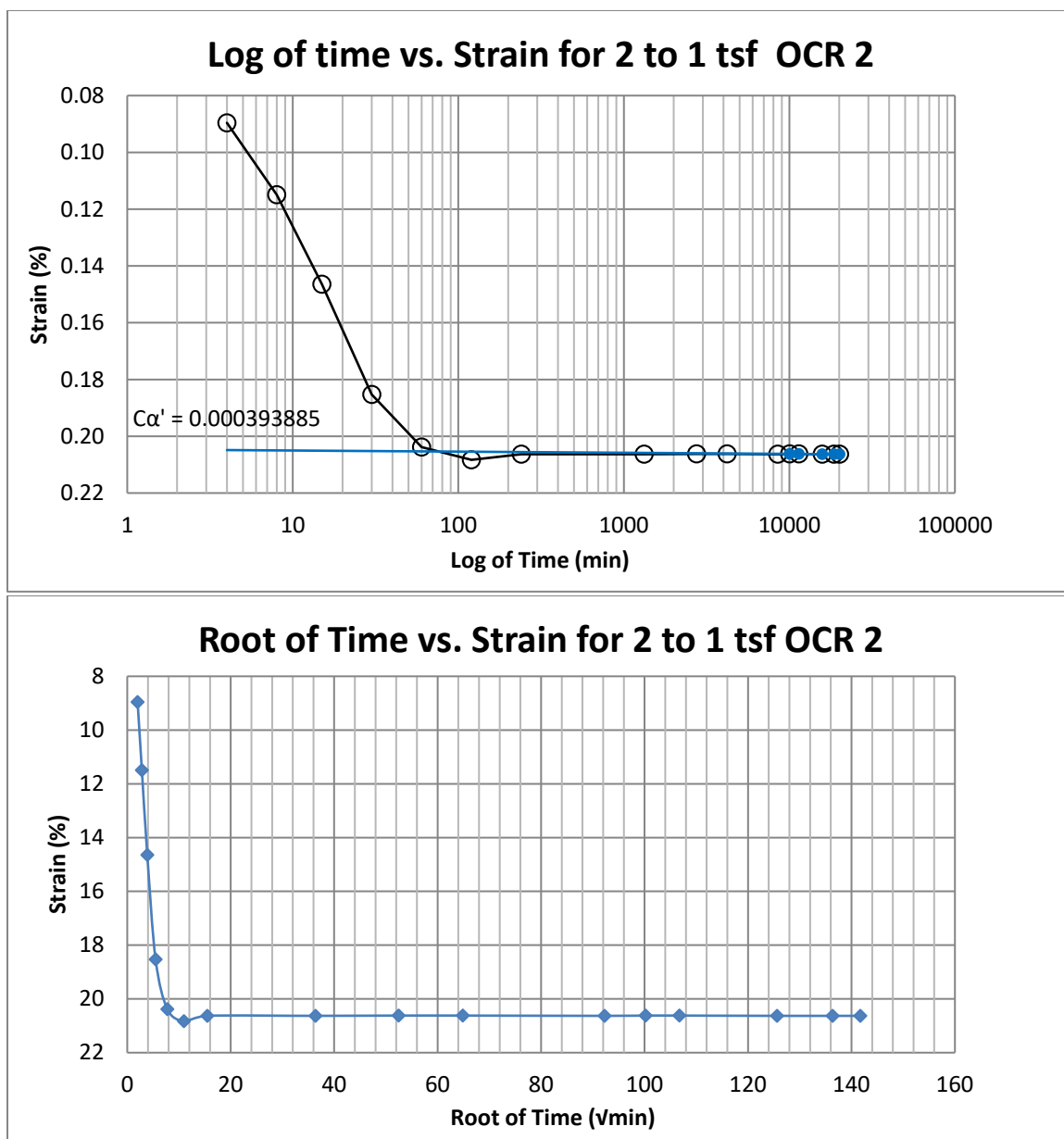


Figure B72 Provo at 50-52 feet

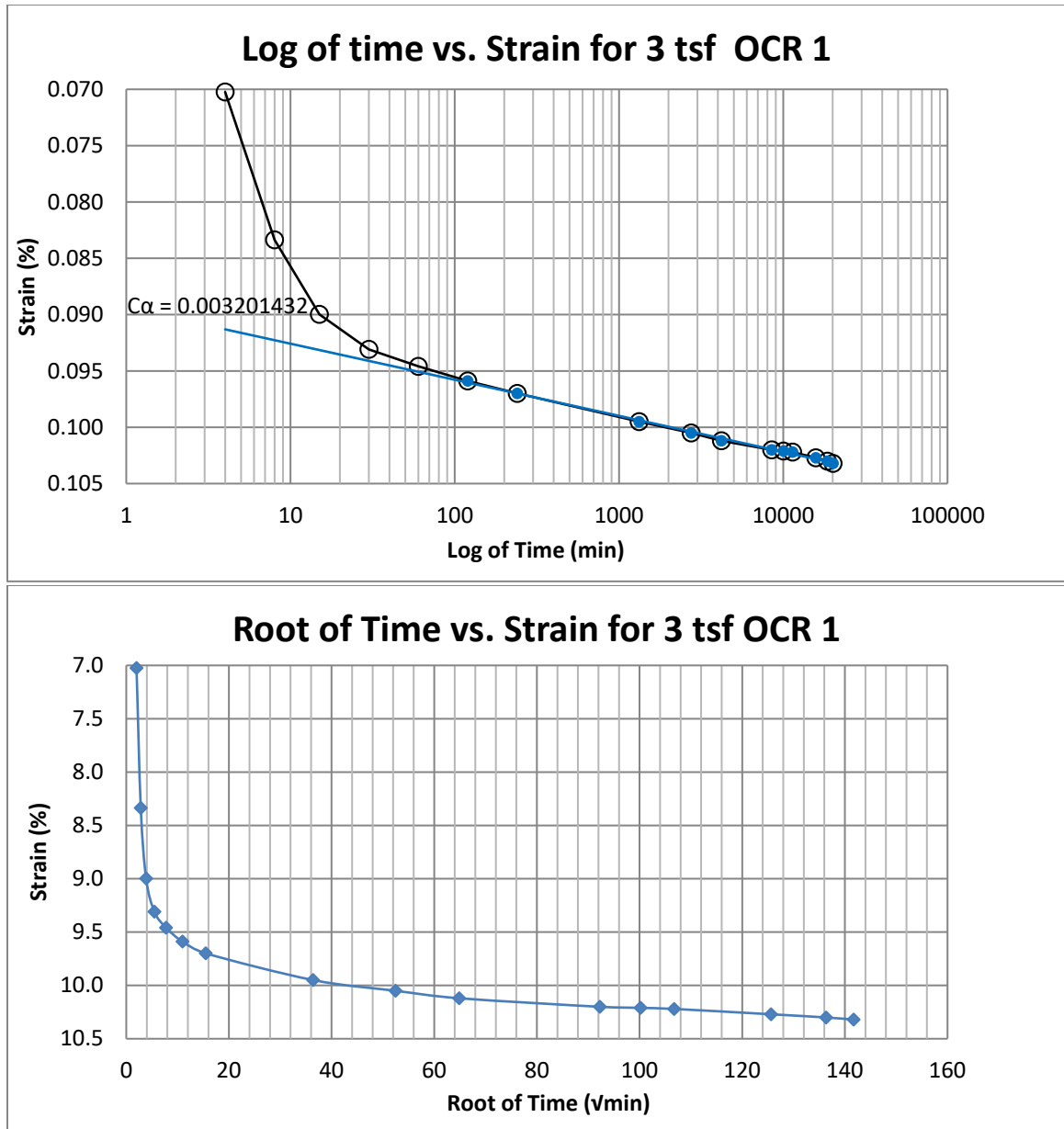


Figure B73 Provo at 60-62 feet

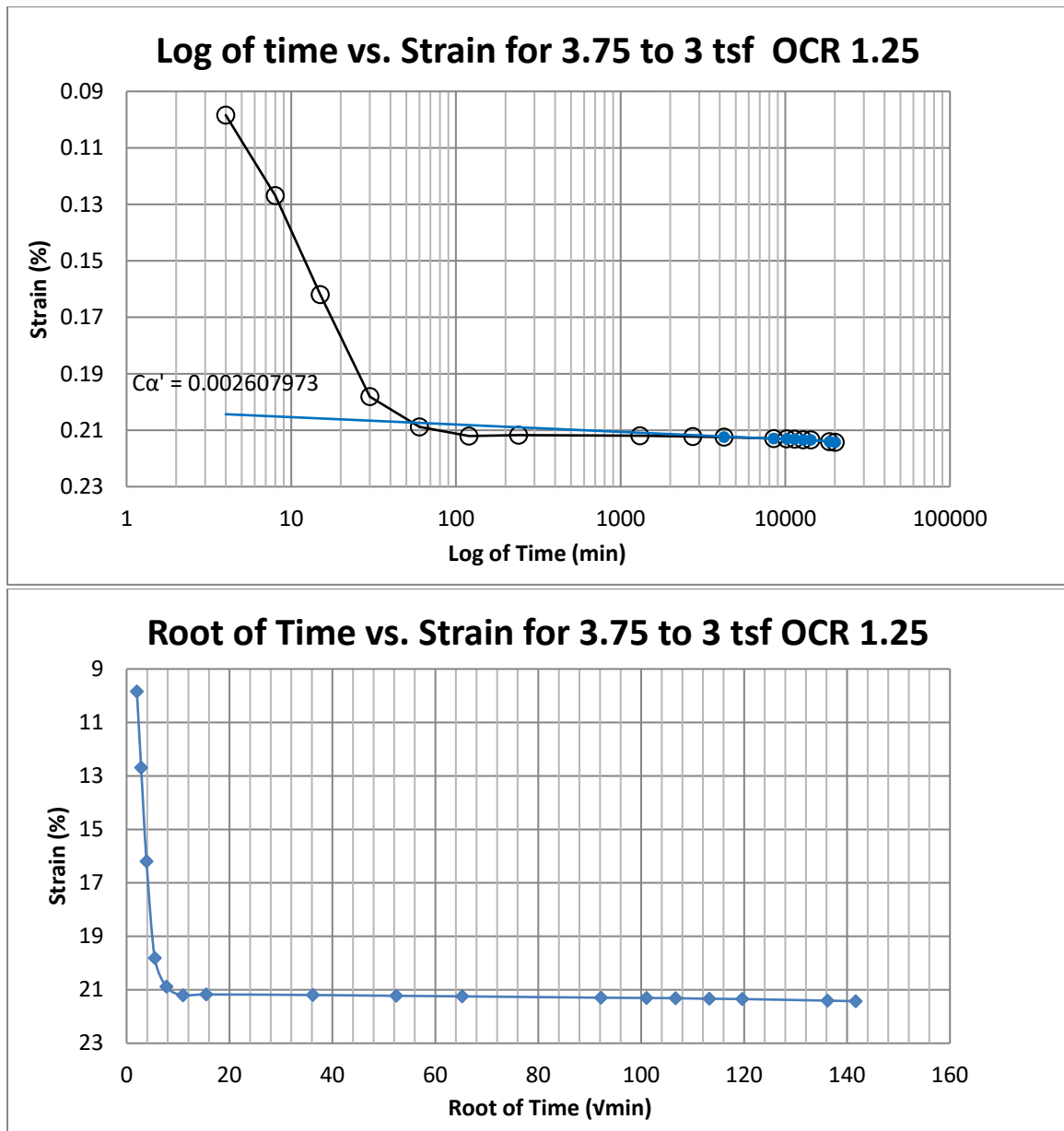


Figure B74 Provo at 60-62 feet



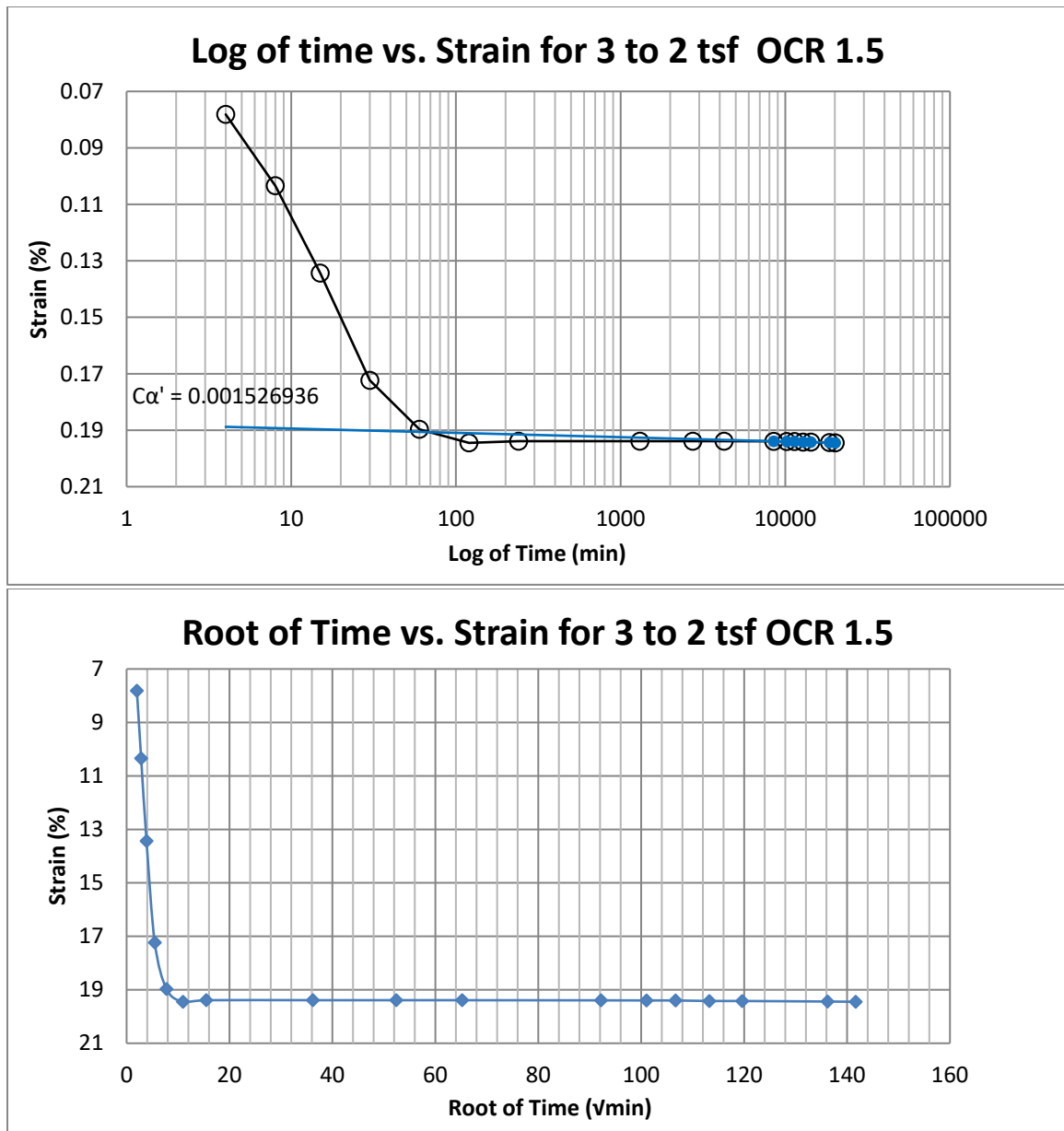


Figure B75 Provo at 60-62 feet

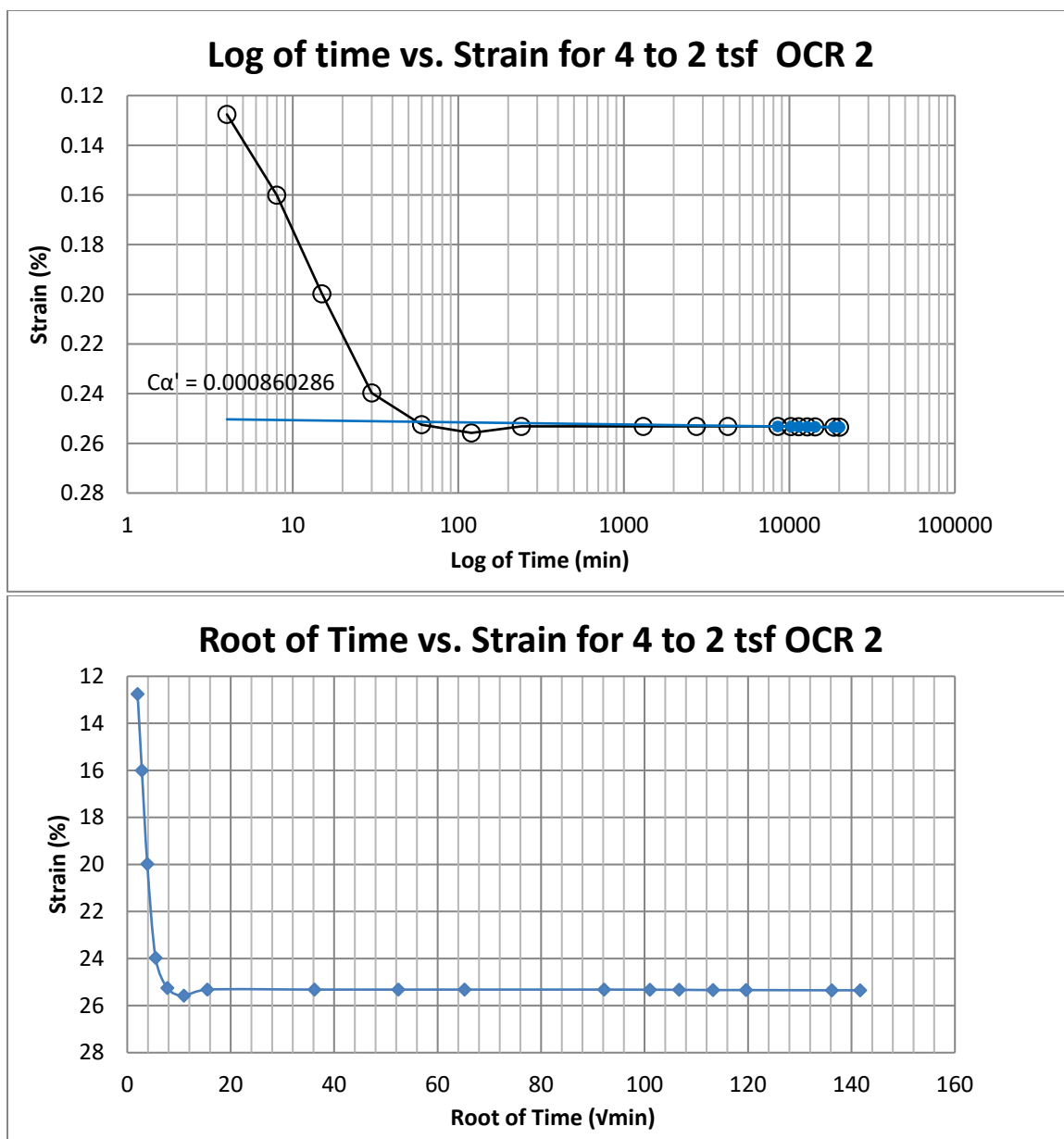


Figure B76 Provo at 60-62 feet

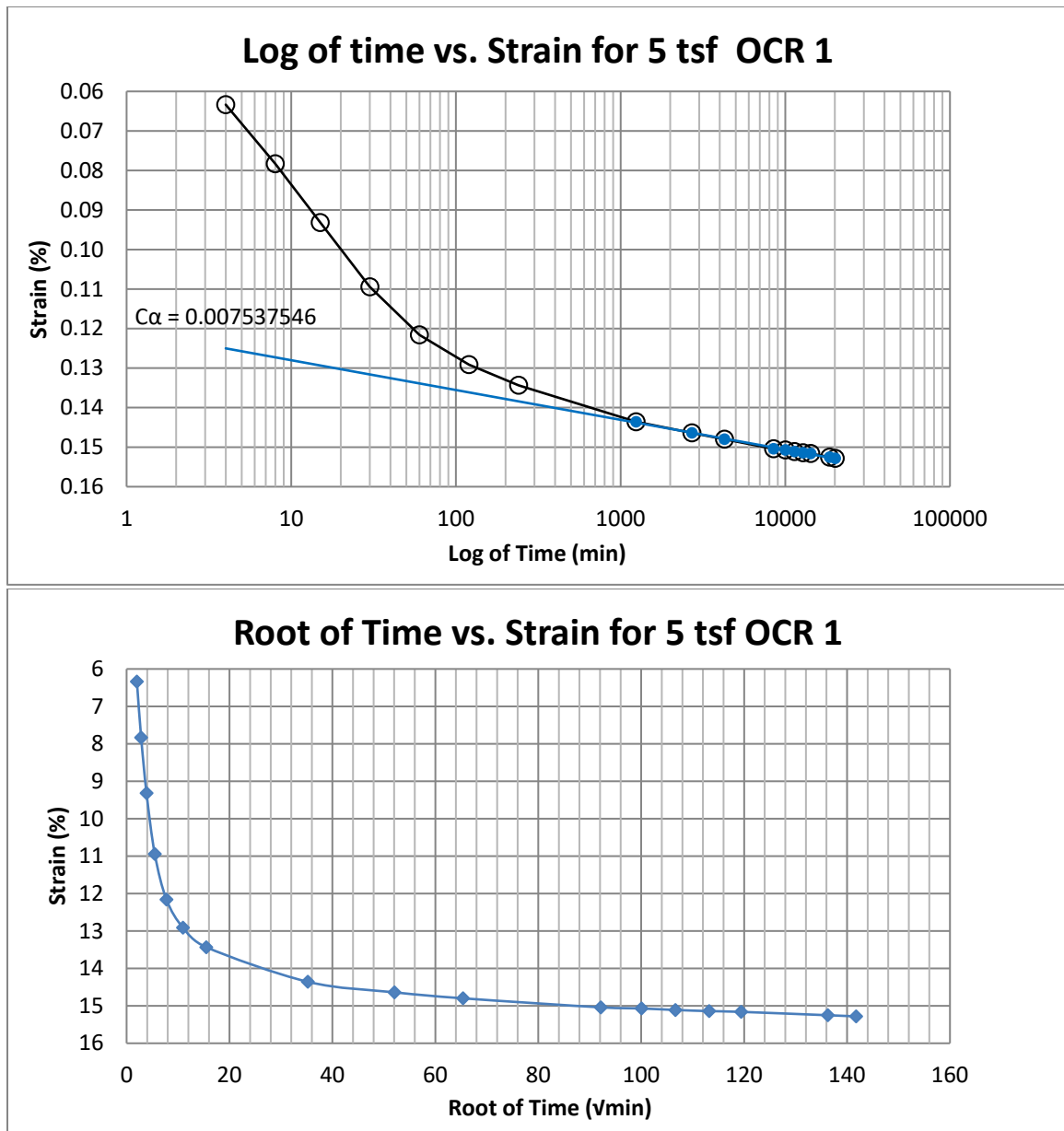


Figure B77 Provo at 80-82 feet

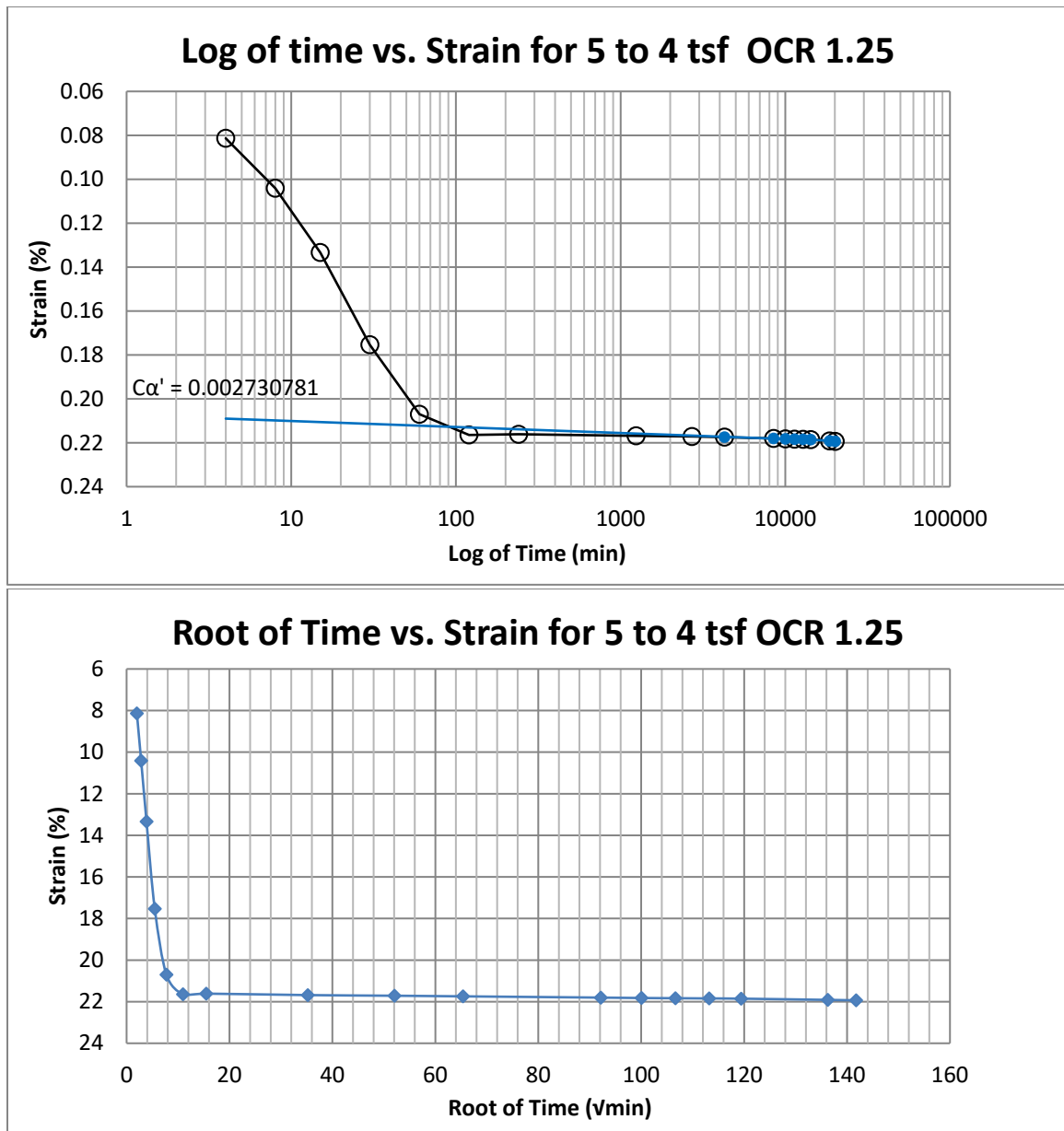


Figure B78 Provo at 80-82 feet

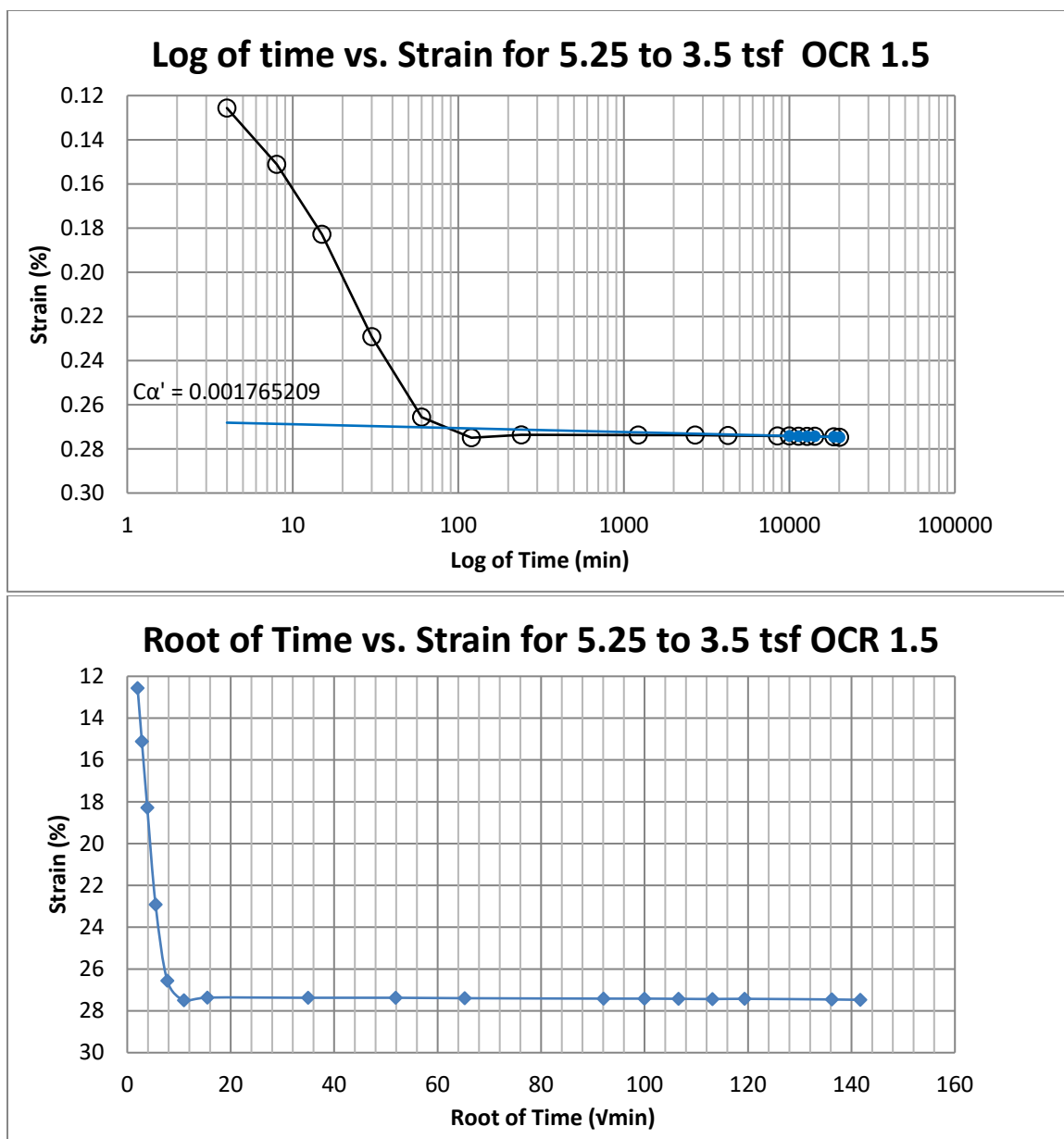


Figure B79 Provo at 80-82 feet

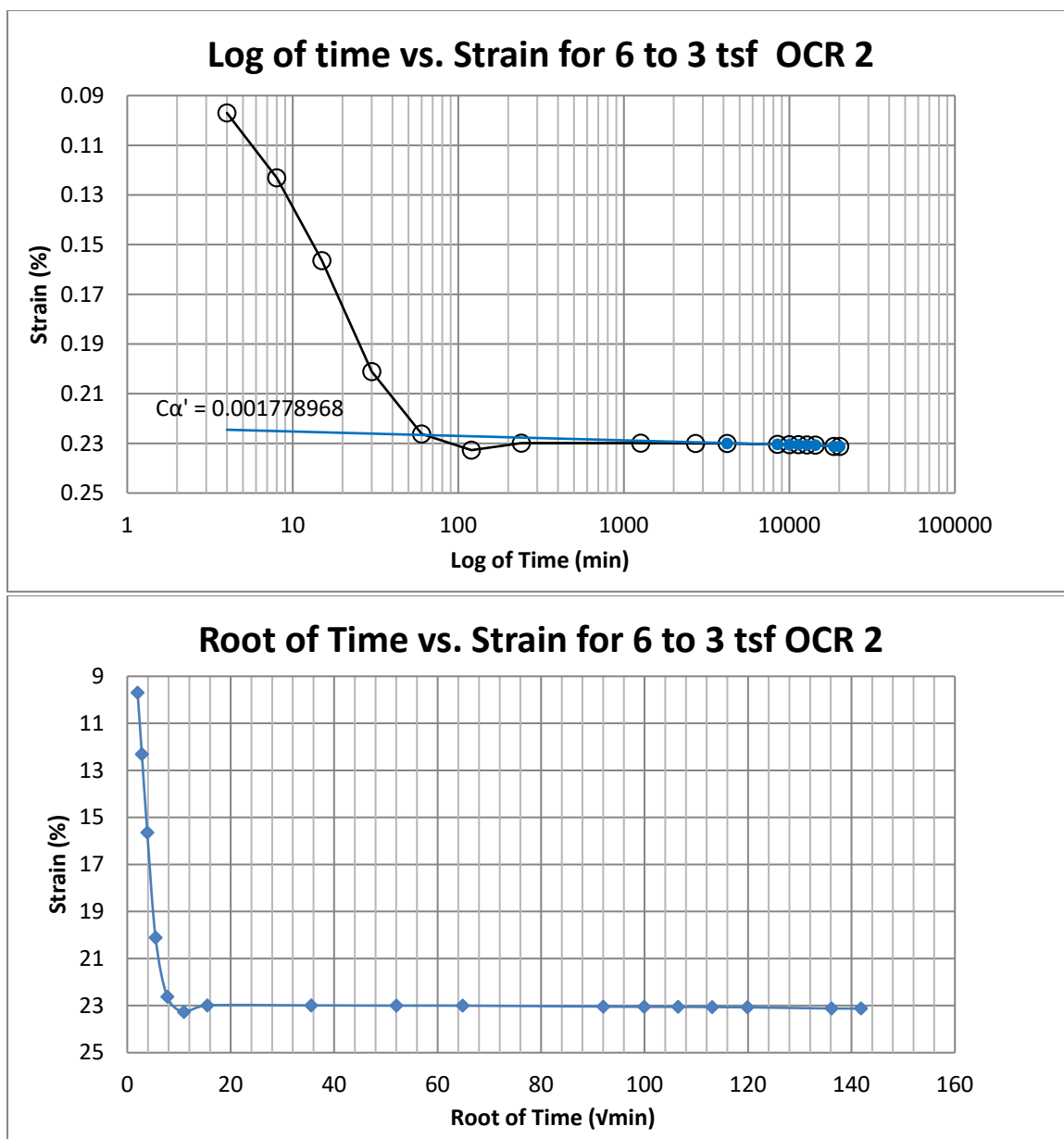


Figure B80 Provo at 80-82 feet

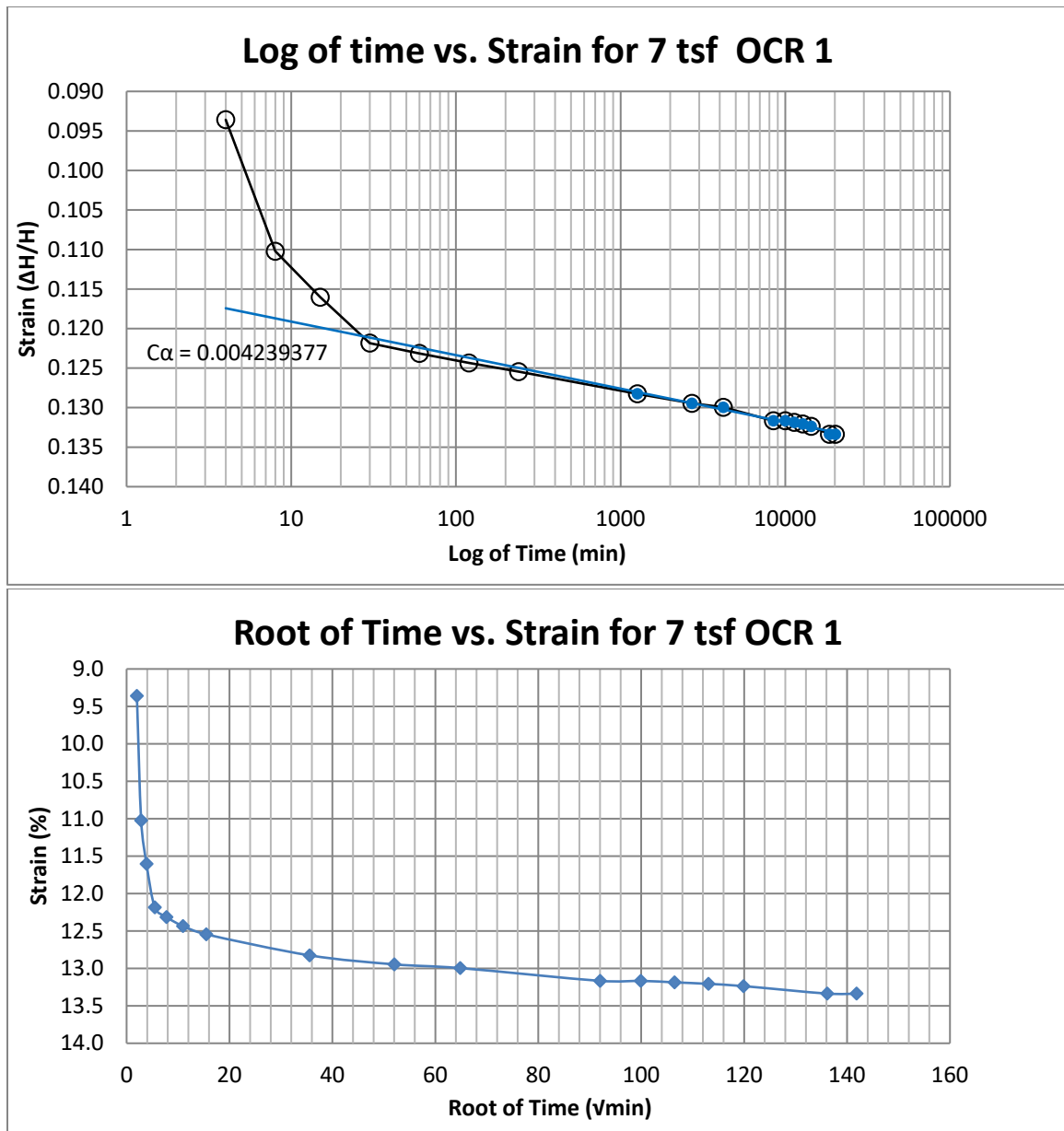
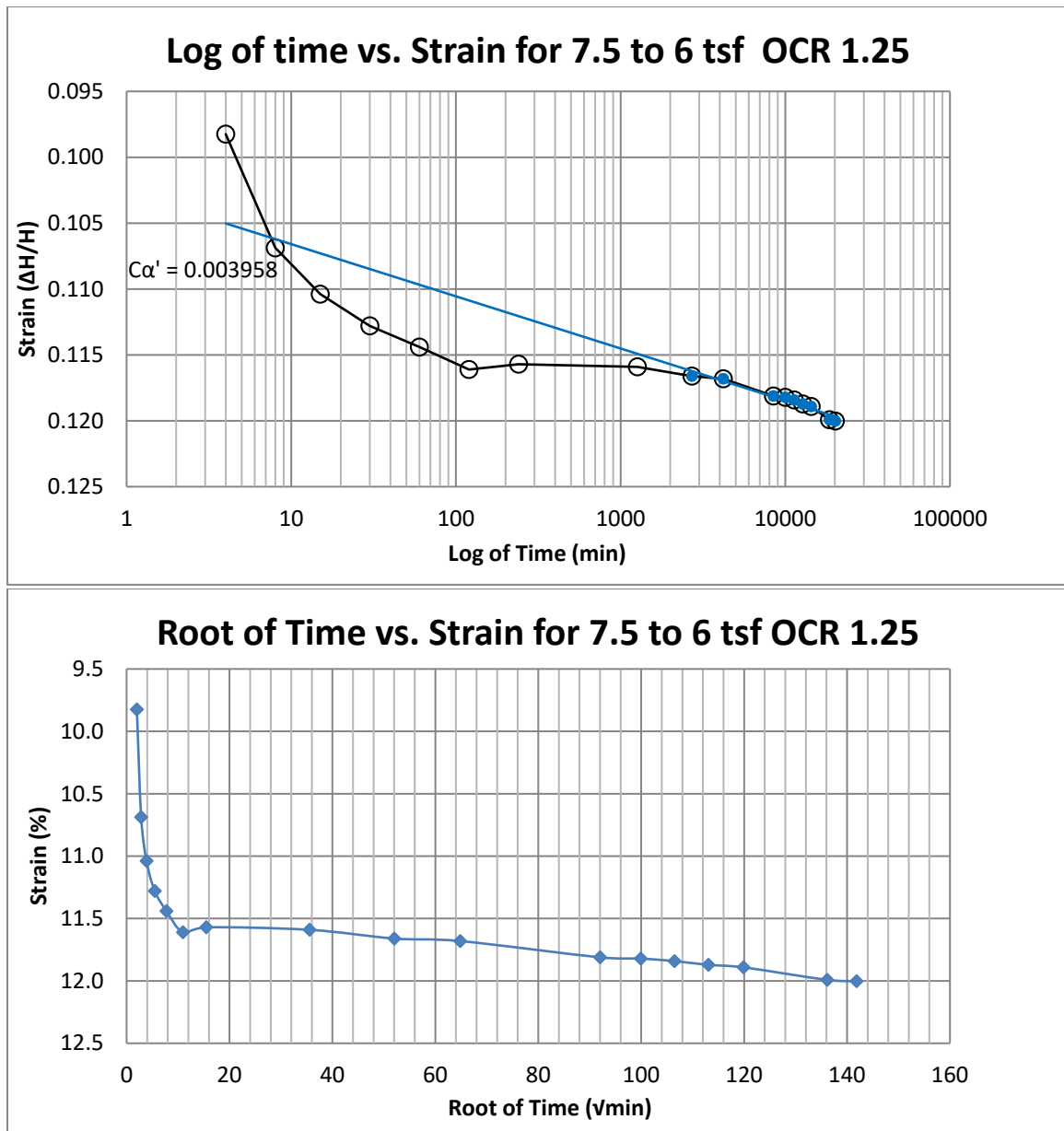


Figure B81 Provo at 90-92 feet



**Figure B82 Provo at 90-92 feet**



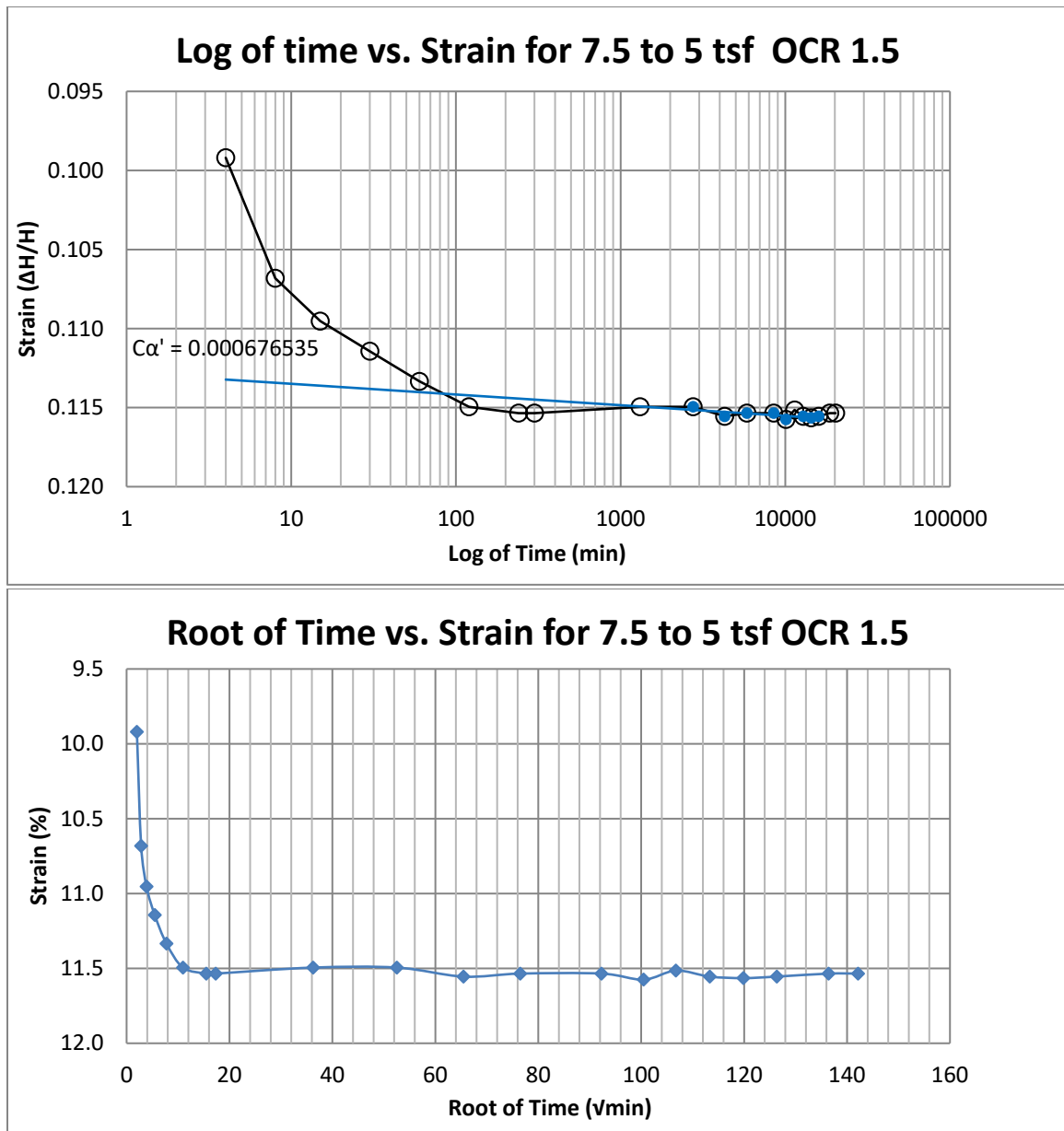


Figure B83 Provo at 90-92 feet

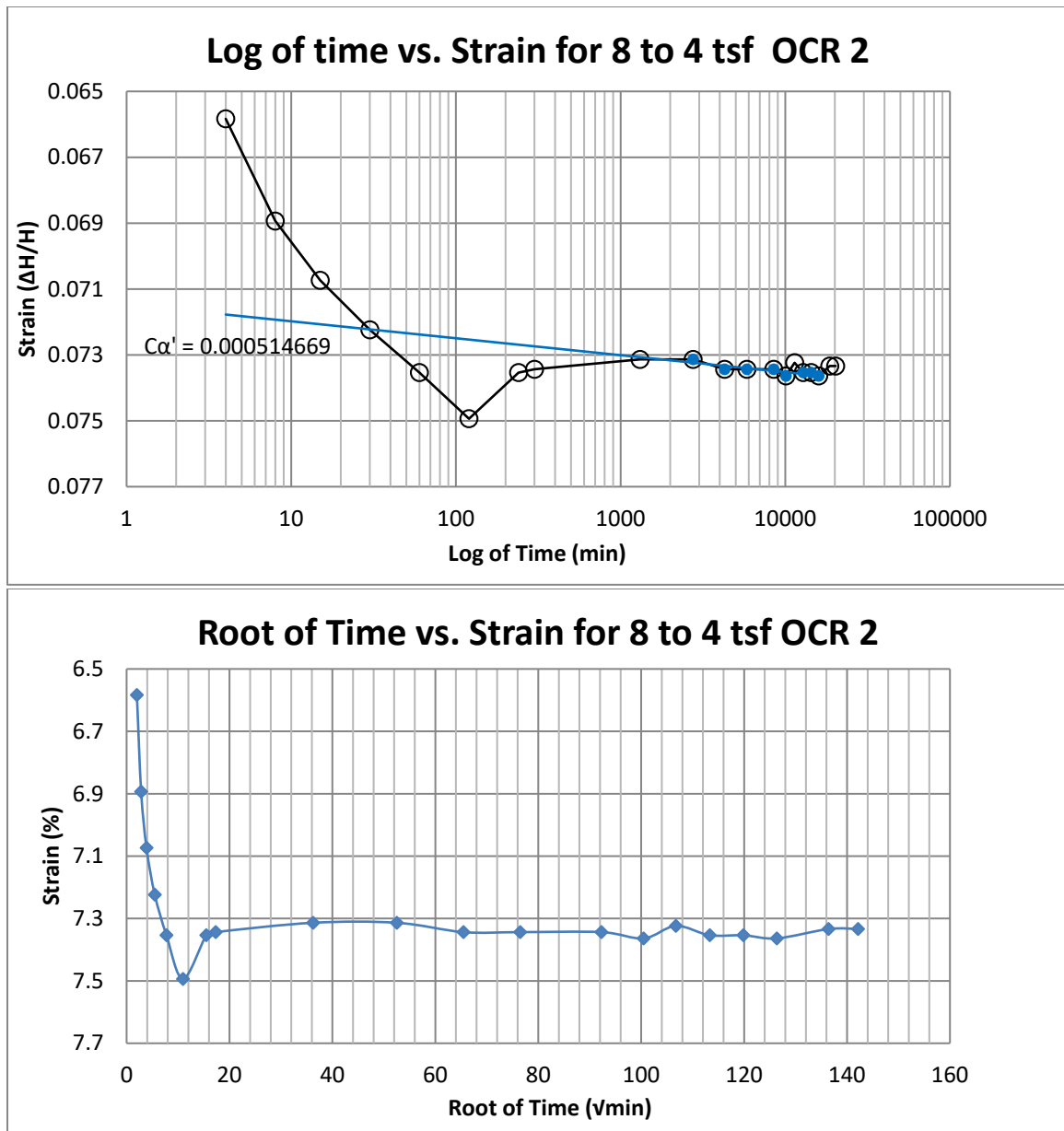


Figure B84 Provo at 90-92 feet

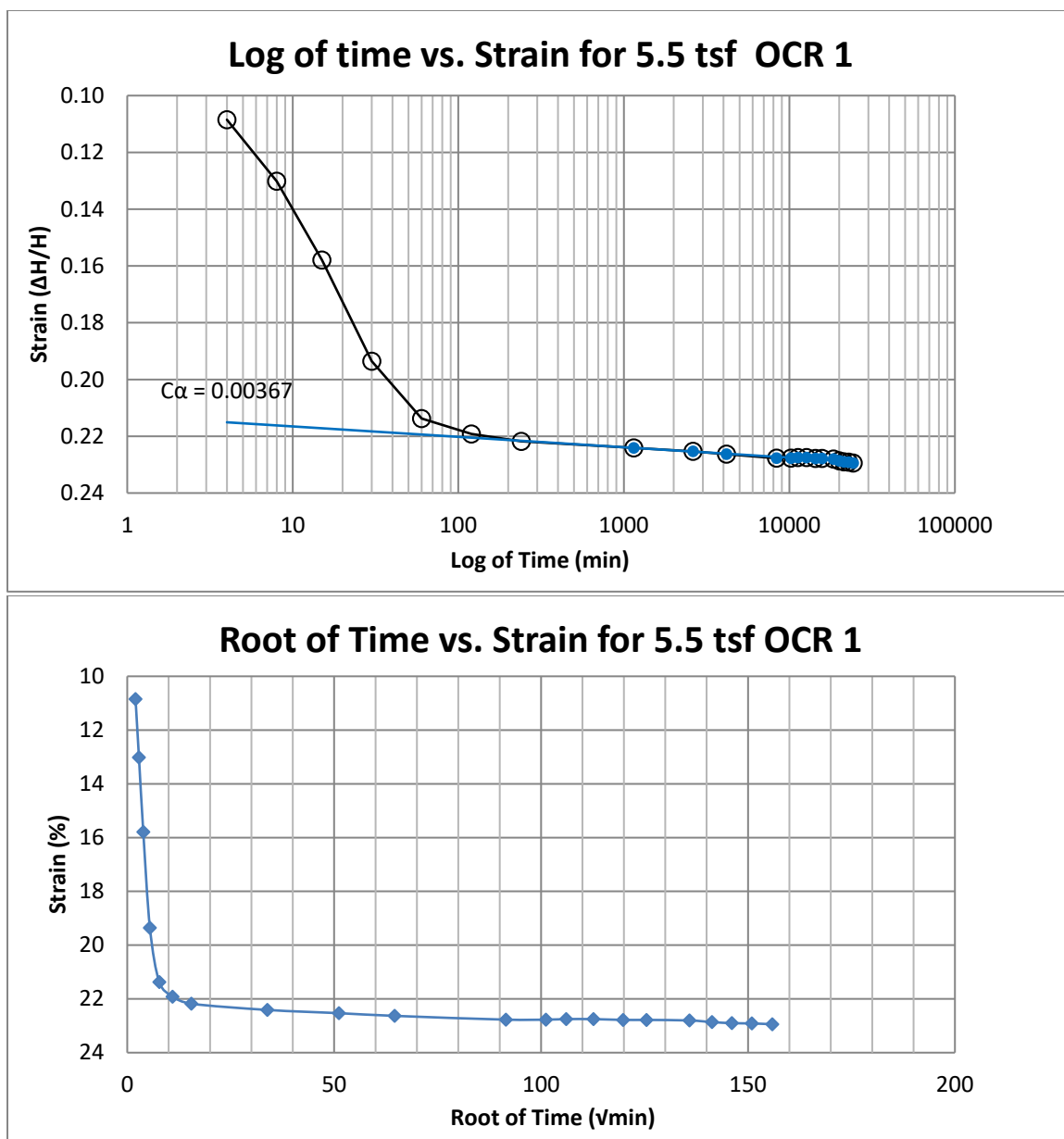


Figure B85 Provo at 110-112 feet

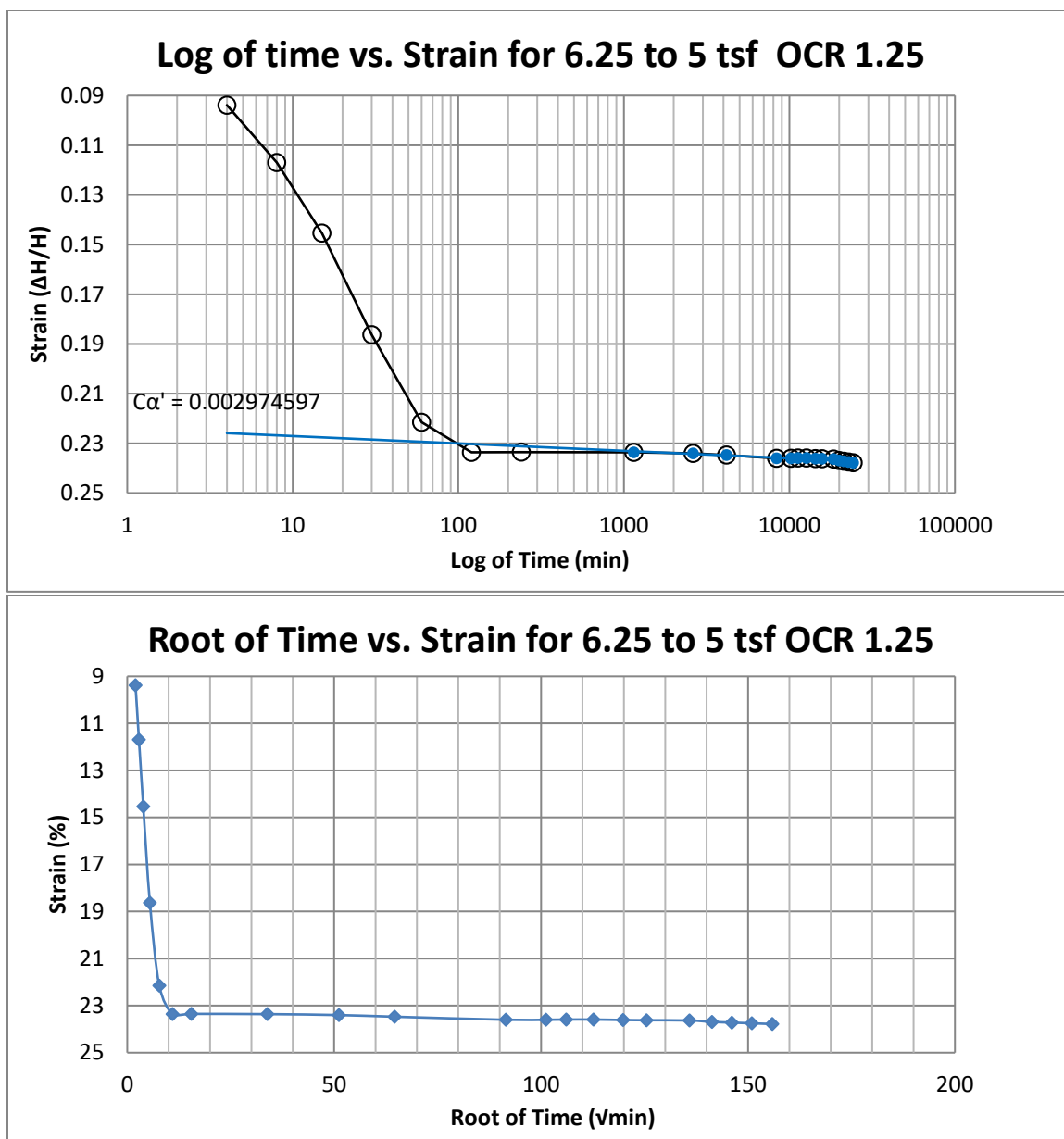
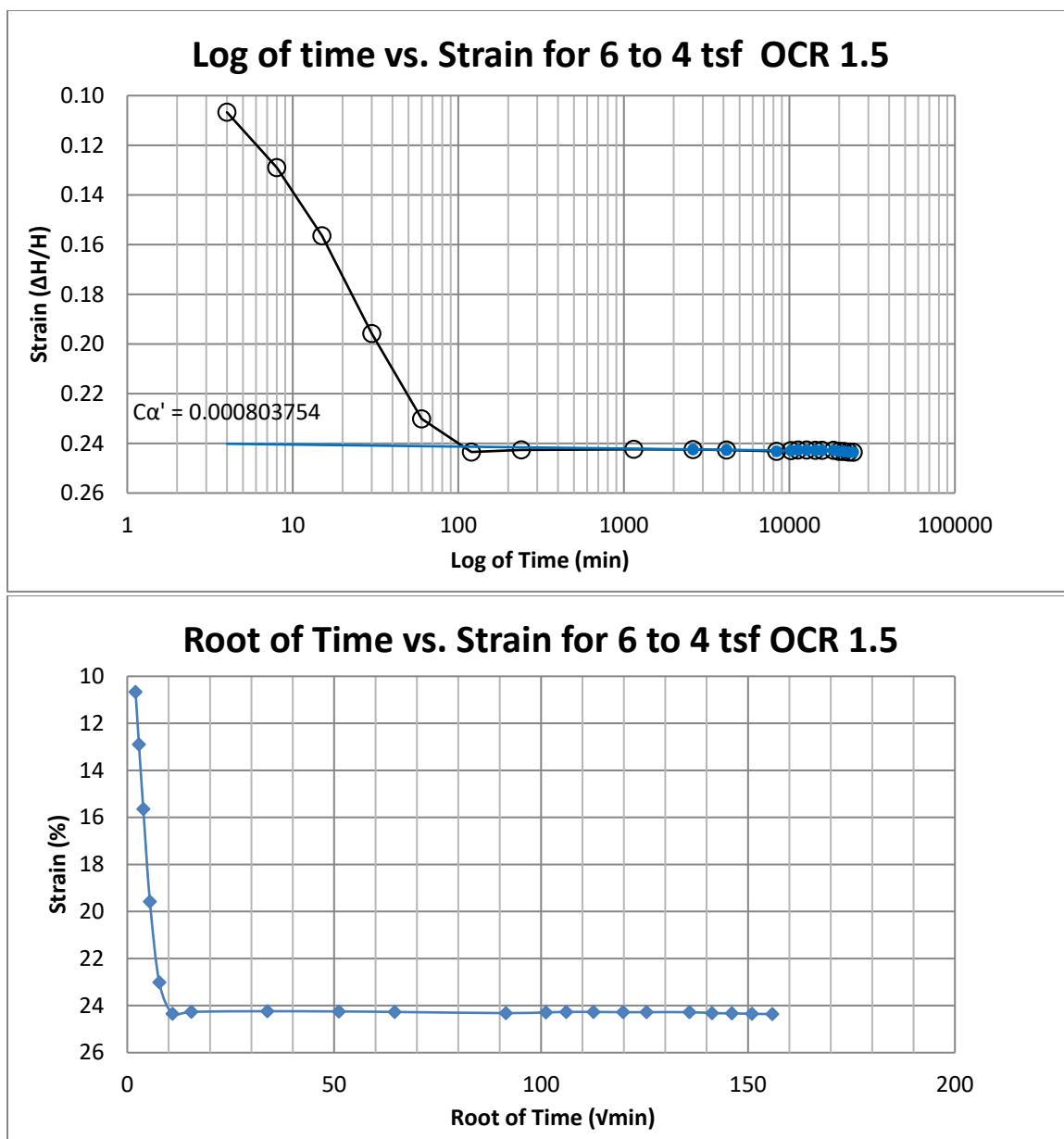


Figure B86 Provo at 110-112 feet



**Figure B87 Provo at 110-112 feet**

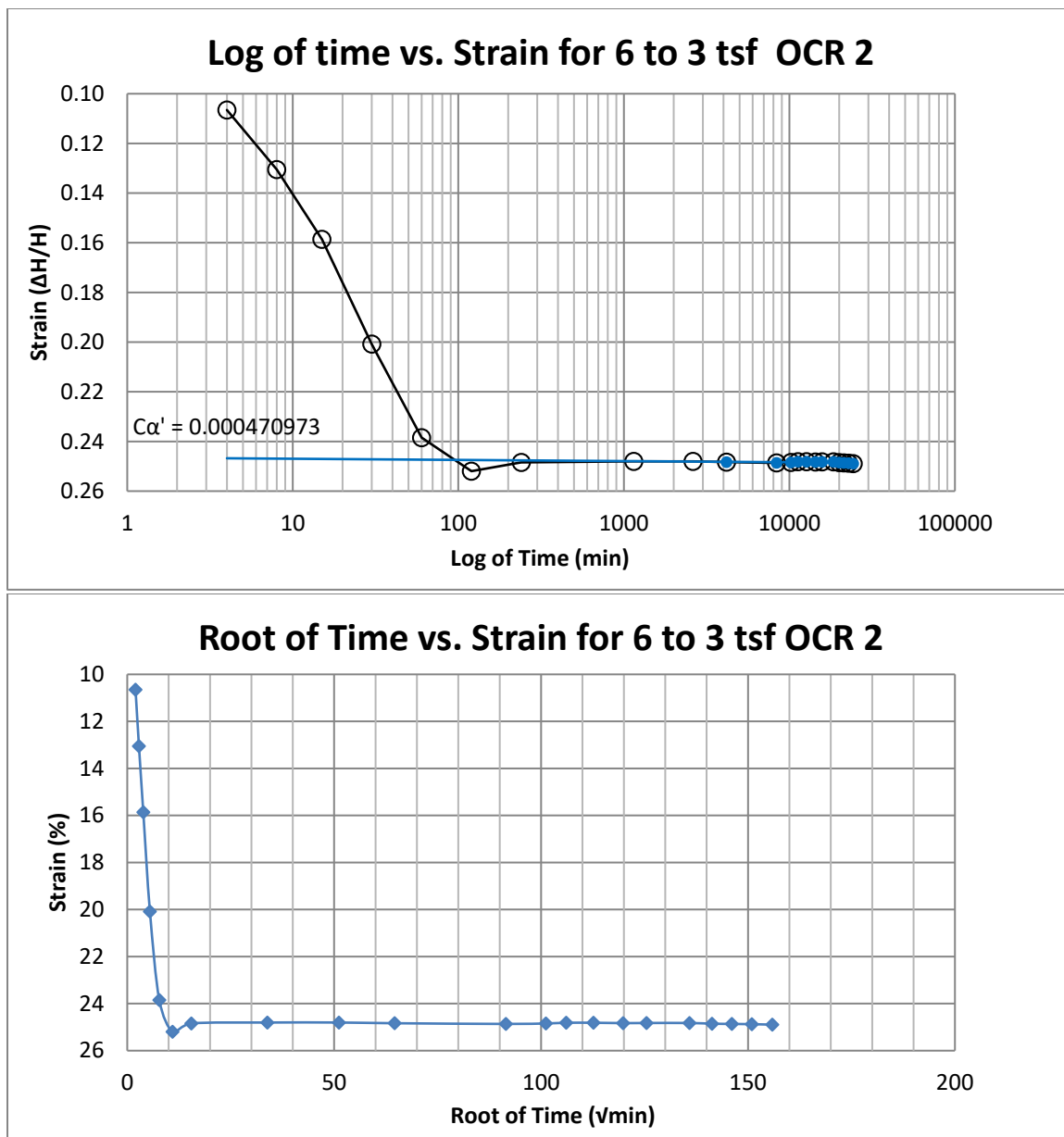


Figure B88 Provo at 110-112 feet

## **APPENDIX C LABORATORY TESTING PROCEDURE**

## C.1. Sample Preparation

C.1.1. Determine the mass, height and diameter of the consolidation ring.

C.1.2. Obtain an undisturbed sample from the selected test depth.

C.1.3. Trim the sample to size and insert it into the consolidation ring.

C.1.1.

C.1.2.

C.1.3.

C.1.3.1. When trimming the sample to size, for soft to medium soils it is recommended to use a wire saw for the trimming to minimize the disturbance to the sample.

C.1.3.2. Coating the inside of the consolidation ring with a silicon lubricant will reduce the amount of disturbance when inserting the soil into the ring.

C.1.4. Trim the sample flush with the top and bottom of the consolidation ring.

C.1.4.

C.1.4.1. For soft to medium soils use a wire saw to trim the sample flush with the top and bottom; after the excess soil is removed a straight edge with a sharp cutting edge may be used for the final trim. For stiff soils use the straightedge to trim the soil flush on the top and bottom.

C.1.4.2. If there are any small voids on the sample, carefully fill them with remolded trimming.

C.1.5. Determine the mass of the soil in the ring by getting the mass of the soil and ring and subtracting out the mass of the consolidation ring.

C.1.6. Use the trimmings to determine the moisture content.

C.1.7. Assemble the consolidometer and place in the loading device.



C.2. Determining the Preconsolidation Pressure

C.2.1. Apply the seating load and take the initial reading.

C.2.1.1. In ASTM D2435 it is recommended that the seating load to be used is 5 kPa (100 psf)

C.2.1.2. Inundate the specimen shortly after the application of the seating load with distilled water.

C.2.2. When determining the preconsolidation stress use a 1-D incremental loading test with time rate of consolidation measurements taken for each loading increment.

C.2.3. The loading schedule will have a load increment ratio (LIR) of one, which is obtained by doubling the pressure on the soil. LIR is defined as the added load divided by the previous total load on the specimen ( $\Delta P/P$ ).

C.2.3.1. Recommended loading schedule from ASTM D2435 is 12, 25, 50, 100, 200, etc. kPa (250, 500, 1000, 2000, 4000 psf etc.)

C.2.3.2. Recommended unloading schedule from ASTM D2435 is to either half the loading or to one-fourth the loading. When unloading it is recommended to use the one-fourth schedule to shorten the test time.

C.2.4. Apply the first loading and begin taking time rate readings.

C.2.4.1. Aging of the soil can affect the test results; to avoid aging, the next loading should be applied before significant secondary compression occurs. It is recommended to use Taylor's square root of time method to determine when 90% of primary settlement has occurred before applying the next loading. For an explanation of the square root of time method refer to Figure C1.

C.2.4.2. Procedure for the square root of time method:

C.2.4.2.1. Plot square root of time versus strain.

C.2.4.2.2. Draw a straight line through the points representing the initial readings that exhibit a straight line trend.

C.2.4.2.3. Draw a second straight line through the 0% ordinate so that the abscissa of this line is 1.15 times the abscissa of the first straight line through the data.

C.2.4.2.4. The point where the second line crosses the plotted data is the point that corresponds to 90% primary consolidation.

C.2.4.3. For each load increment the time rate readings are as follows; 0.1, 0.25, 0.5, 1, 2, 4, 8, 15, 30 minutes, and 1, 2, 4, 8, and 24 hours.

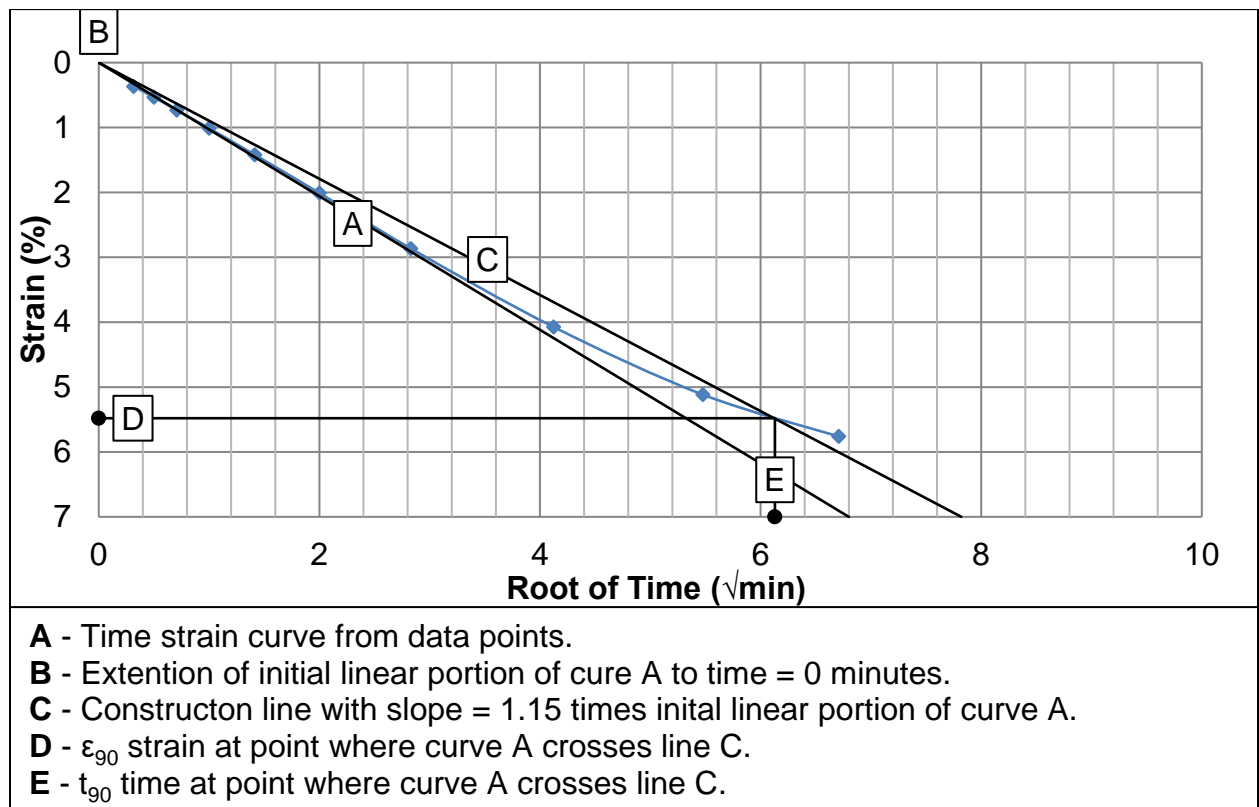


**Figure C1 Time-Deformation Curve from Square Root of Time Method**

C.2.5. Keep applying loads until the preconsolidation stress can be determined by having a minimum of two points after the break in the curve. After a minimum of two points have been determined past the break in the curve, start the unloading. Refer to Figure C2.

C.2.6. Use Casagrande's (1936) method and Becker et al (1987), also known as the work method, to determine the preconsolidation stress.

C.2.6.1. Procedure for Casagrande method (Figure C2):

C.2.6.1.1. Plot vertical effective stress versus strain.

- C.2.6.1.2. Estimate the point of maximum curvature on the consolidation curve.
- C.2.6.1.3. Draw a line tangent to the consolidation curve at the point of maximum curvature.
- C.2.6.1.4. Draw a horizontal line through the point of maximum curvature.
- C.2.6.1.5. Draw a line that bisects the angle between lines drawn in steps 3 and 4 through the point of maximum curvature.
- C.2.6.1.6. Draw a line tangent to the steep, linear portion of the consolidation curve (virgin compression branch) upwards to intersect line drawn in step 5.
- C.2.6.1.7. The point of intersection of the lines drawn in step 5 and 6 corresponds to the estimated preconsolidation pressure.

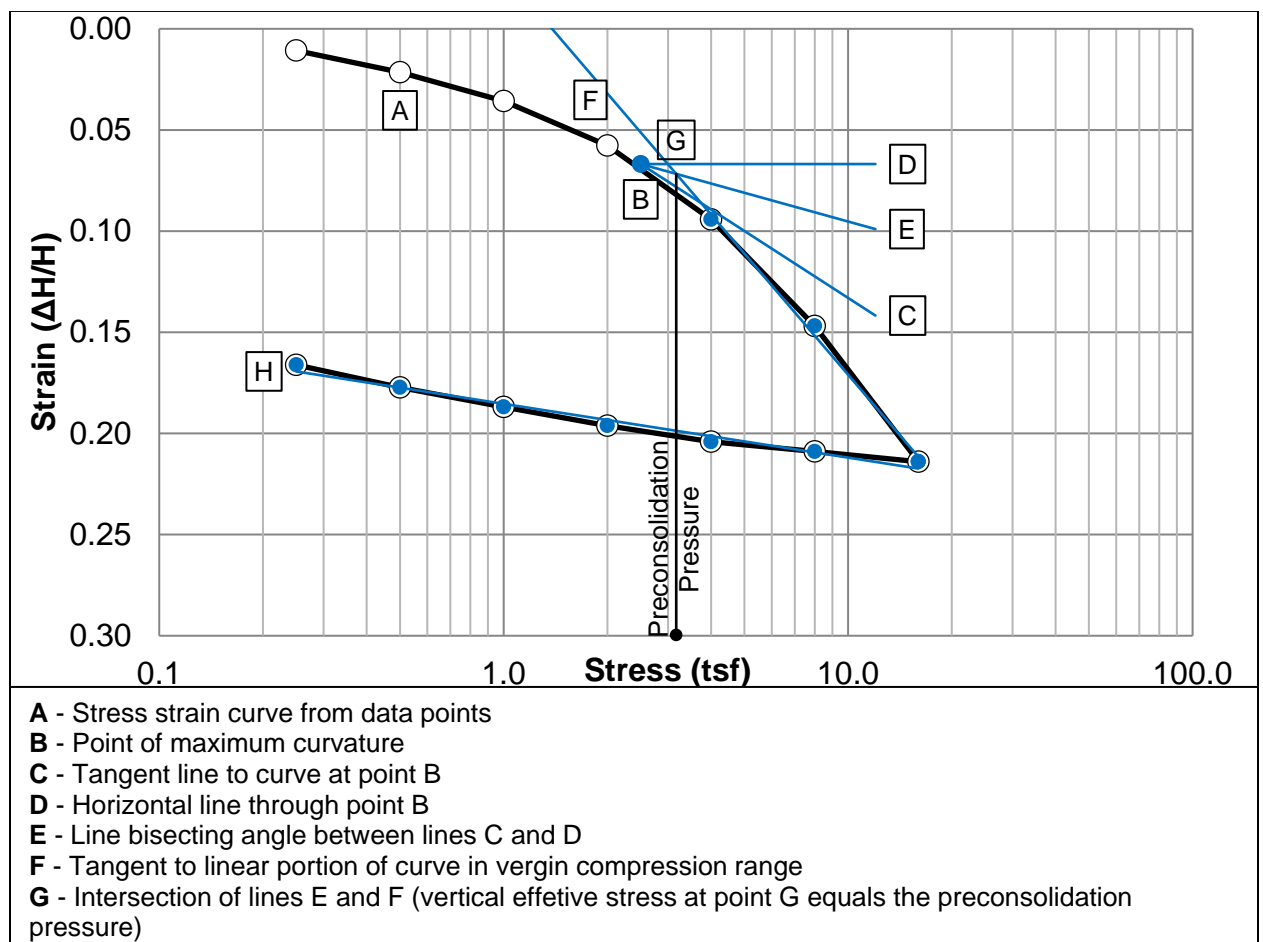


**Figure C2 Evaluation for Preconsolidation Pressure Using Casagrande Method**

C.2.7. Procedure for Becker et al (1987)/Work method (Figure C3):

C.2.7.1. Calculate the incremental work for each loading step using the equation C.1 below

$$\Delta W = \left[ \frac{(\sigma'_z)_{i+1} + (\sigma'_z)_i}{2} \right] \times [(\epsilon_z)_{i+1} - (\epsilon_z)_i]$$

C.1

where  $(\sigma'_z)_{i+1}$  and  $(\epsilon_z)_{i+1}$  are the vertical effective stresses and vertical strain at the end of the  $i+1$  increment and  $(\sigma'_z)_i$  and  $(\epsilon_z)_i$  are the vertical effective stresses and vertical strain at the end of the  $i$  increment.

C.2.7.2. Calculate the cumulative work by summing the incremental work determined in step 1.

C.2.7.3. Plot the cumulative work (ordinate, arithmetic scale) versus the vertical effective stress (abscissa, arithmetic scale). You would normally get two distinct averaged straight lines (see Figure C3).

C.2.7.4. Project the upper averaged straight line to intersect the projection of the lower averaged straight line.

C.2.7.5. The vertical effective stress at the intersection of the two lines in step 4 corresponds to the estimated preconsolidation pressure,  $\sigma'_p$ .

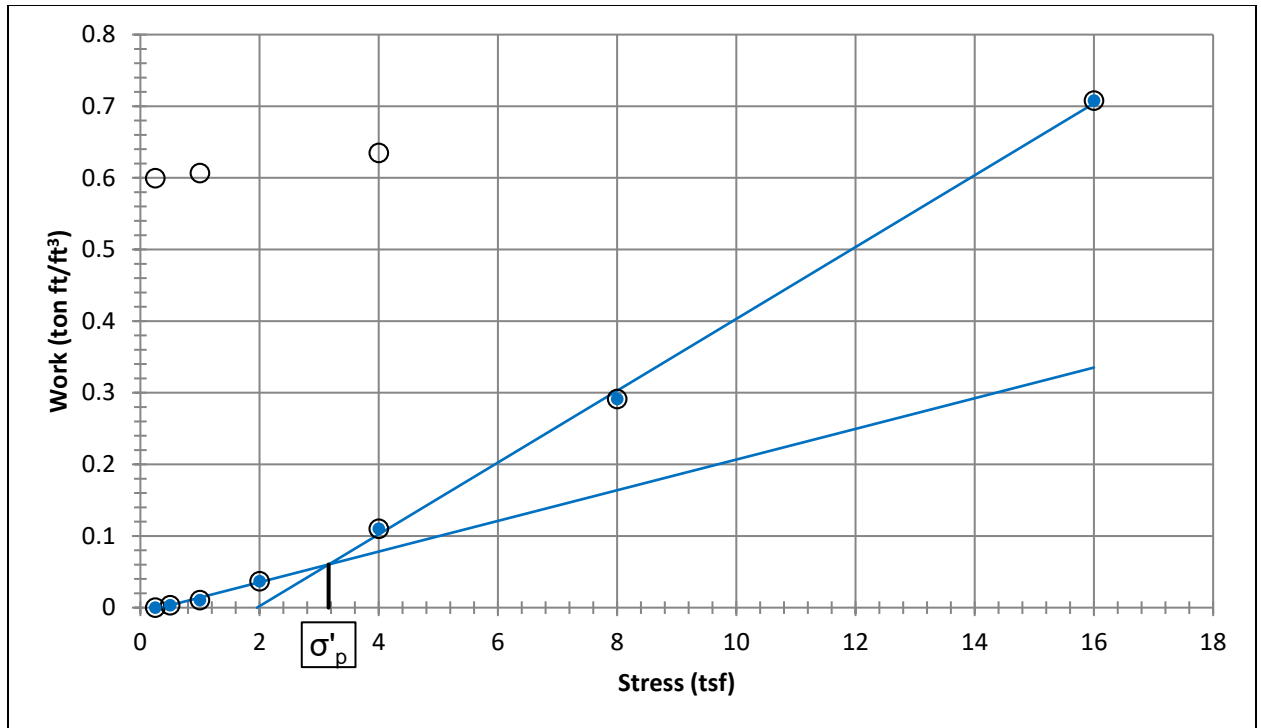


**Figure C3 Evaluation for Preconsolidation Pressure Using Becker et al. (1987) Work Method**

### C.3. Determining the Rate of Secondary Settlement Normally Consolidated $C_\alpha$

C.3.1. Using the preconsolidation stress determined from the incremental load test performed previously, load the sample to 1.5 to 2 times that of the preconsolidation stress.

C.3.1.1. This ensures that the samples have reached a new normally consolidated state and any effects of aging or past preconsolidation have been removed.

C.3.2. The standard reading schedule for the time rate testing are as follows:

6, 15, 30 seconds, 1, 2, 4, 8, 15, 30 minutes, 1, 2, 4, 8, 24 hours.

C.3.2.1. Take readings about every 24 hours after the initial 24 hours

C.3.2.2. Run the test long enough to be sure that a good value of  $C_\alpha$  is achieved; this test could run for 1 to 2 weeks.

C.3.3. Use Ladd's methodology to determine the value of  $C_\alpha$ .

C.3.3.1. Ladd's procedure for determining the rate of secondary settlement normally consolidated,  $C_\alpha$  (Figure C4):

C.3.3.1.1. Plot strain versus the log of time.

C.3.3.1.2. Determine the end of primary settlement,  $t_p$ .

C.3.3.1.2.1. This is done by extending forward the slope of the steep portion of the plotted data and extending backwards the shallow portion of the plotted data, after the steep portion, until they intersect.

C.3.3.1.2.2. Draw a line horizontal from this intersection point. Where this horizontal line crosses the plotted data is the time to end of primary settlement.

C.3.3.1.3. The rate of secondary settlement normally consolidated,  $C_\alpha$  is determined by the slope of the linear most portion of the data after primary consolidation has occurred, also known as end of primary  $t_p$ , on the strain vs. log of time plot. Refer to Figure C4.

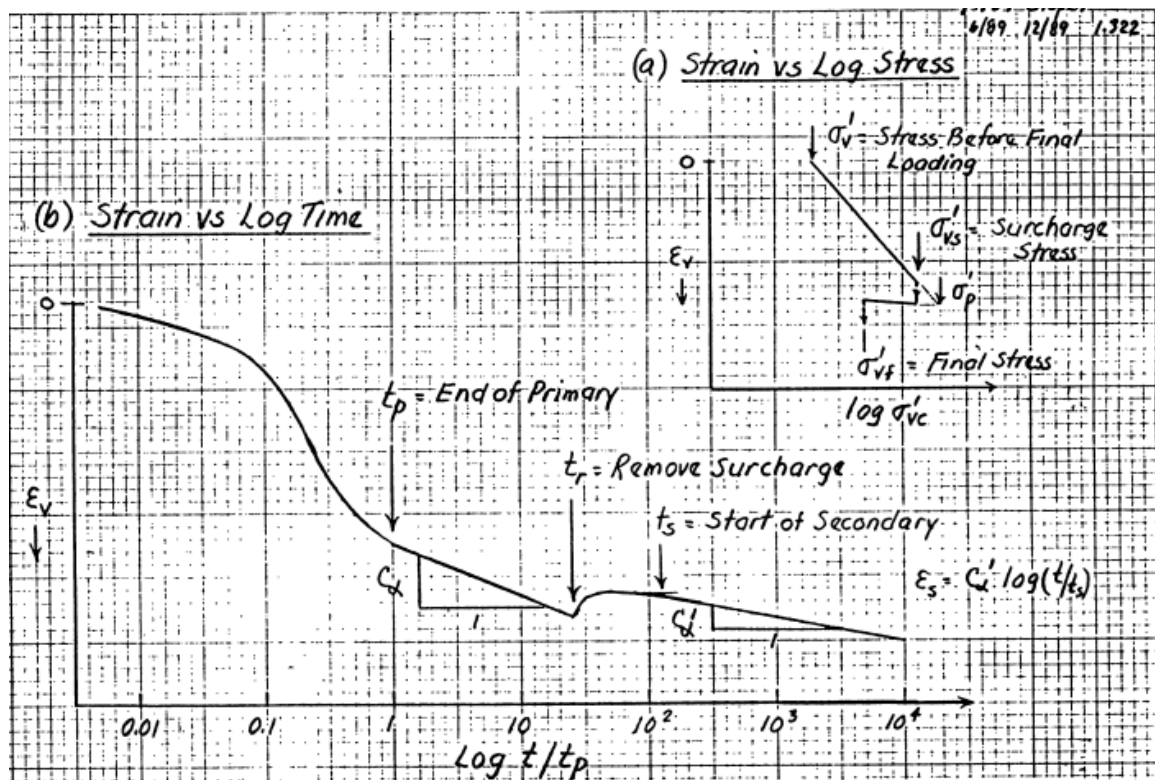


Figure C4 Ladd's method for determining the rate of secondary settlement (after Ladd, unpublished notes)

C.4. Determining the Rate of Secondary Settlement Over Consolidated  $C'_\alpha$

C.4.1. Using the preconsolidation stress determined from the incremental load test performed previously, load the sample to 1.5 to 2 times that of the preconsolidation stress.

C.4.1.1. This ensures that the samples have reached a new normally consolidated state and any effects of aging or past preconsolidation have been removed.

C.4.2. Using the same reading schedule as stated in section C.3.2 and the square root of time method stated in section C.2.4.2, determine when 90% of primary consolidation has occurred; this usually requires about 1 to 2 hours.

C.4.2.1. After 90% of primary consolidation has occurred, decrease the stress on the sample to a known OCR of either 1.25, 1.5, or 2.0.

C.4.2.1.1. It is important to keep the sample from undergoing a large amount of secondary settlement. If the sample undergoes secondary settlement this will cause an aging effect to occur in the sample and the effect of aging can have an impact on the rate of secondary settlement.

C.4.2.1.2. After the stress has been reduced, restart the reading schedule.

C.4.2.2. Run the test long enough to be sure that a good value of  $C'_\alpha$  is achieved; this test could run for 1 to 2 weeks.

C.4.3. Use Ladd's methodology to determine the value of  $C'_\alpha$ . (refer to Figure C4)

C.4.3.1. Plot strain versus the log of time.

C.4.3.2. Determine the end of primary settlement,  $t_p$  using the same procedure as stated in section C.3.3.1.2.

C.4.3.2.1. After the surcharge has been removed in step C.4.2.1 there is a brief heaving event before the beginning of the reduced rate of secondary settlement. This heaving event is the time between the removal of surcharge,  $t_r$  and start of secondary settlement,  $t_s$ .

C.4.3.2.2. The value of  $t_s$  is the point in time when the soil has reached its maximum heave value.

C.4.3.3. The rate of secondary settlement over consolidated,  $C'_\alpha$  is determined by the slope of the linear most portion of the data after  $t_s$ . Refer to Figure C4.



## **APPENDIX D CPT PLOTS OF SOIL BEHAVIOR TYPES**

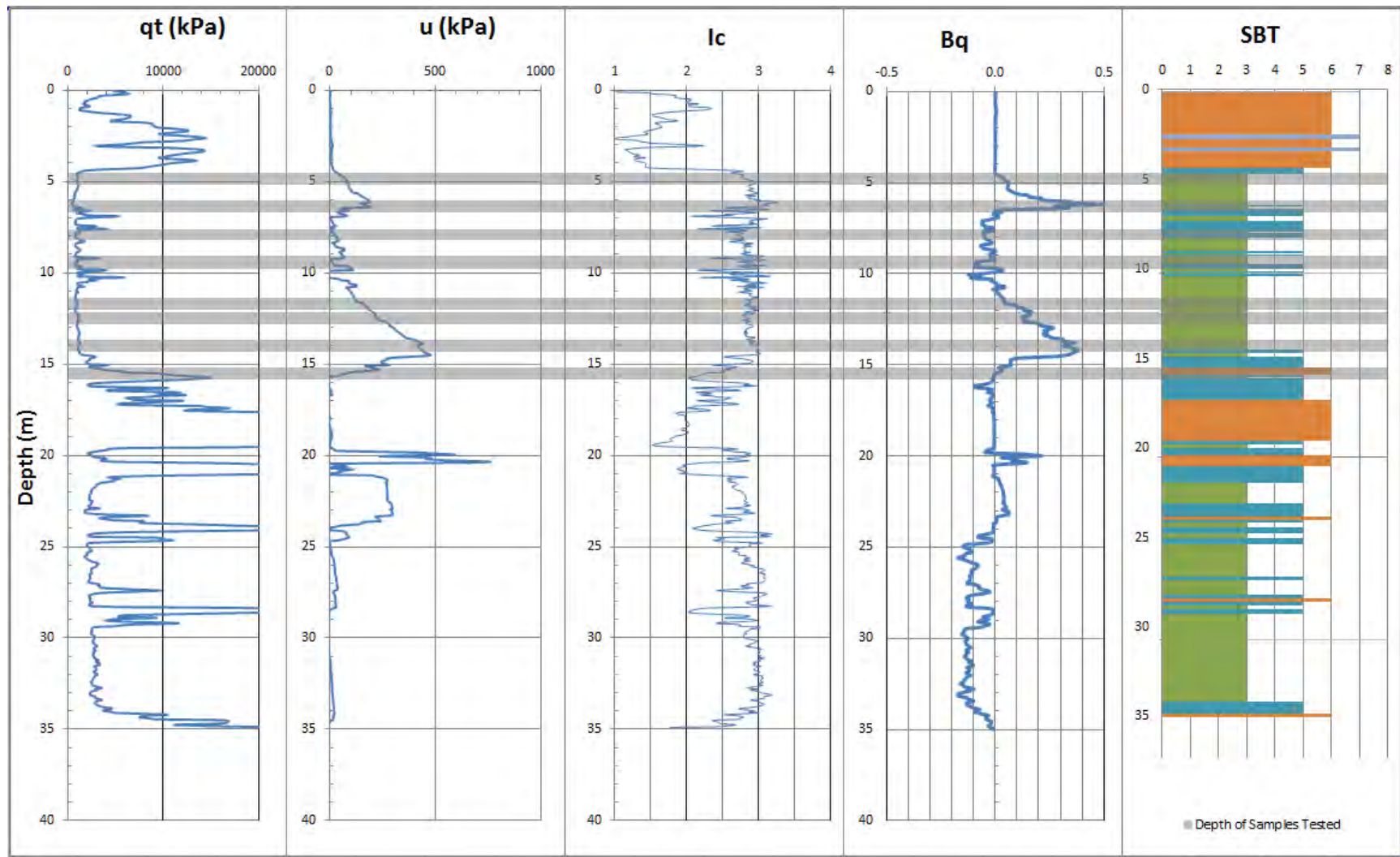


Figure D1 400 South CPT plots with Ic, Bq, and SBT and depths where samples were tested

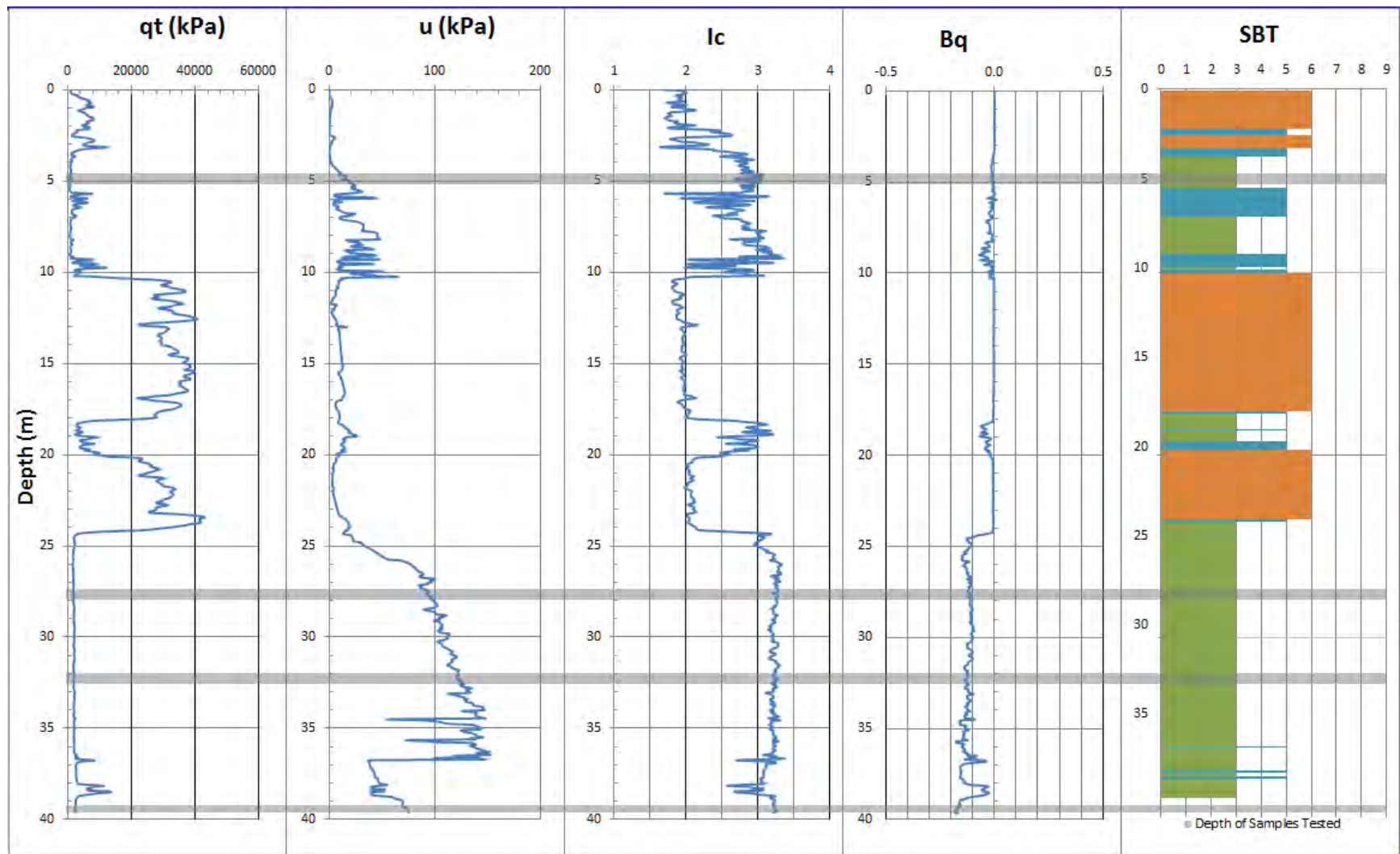


Figure D2 South Layton CPT plots with Ic, Bq, and SBT and depths where samples were tested

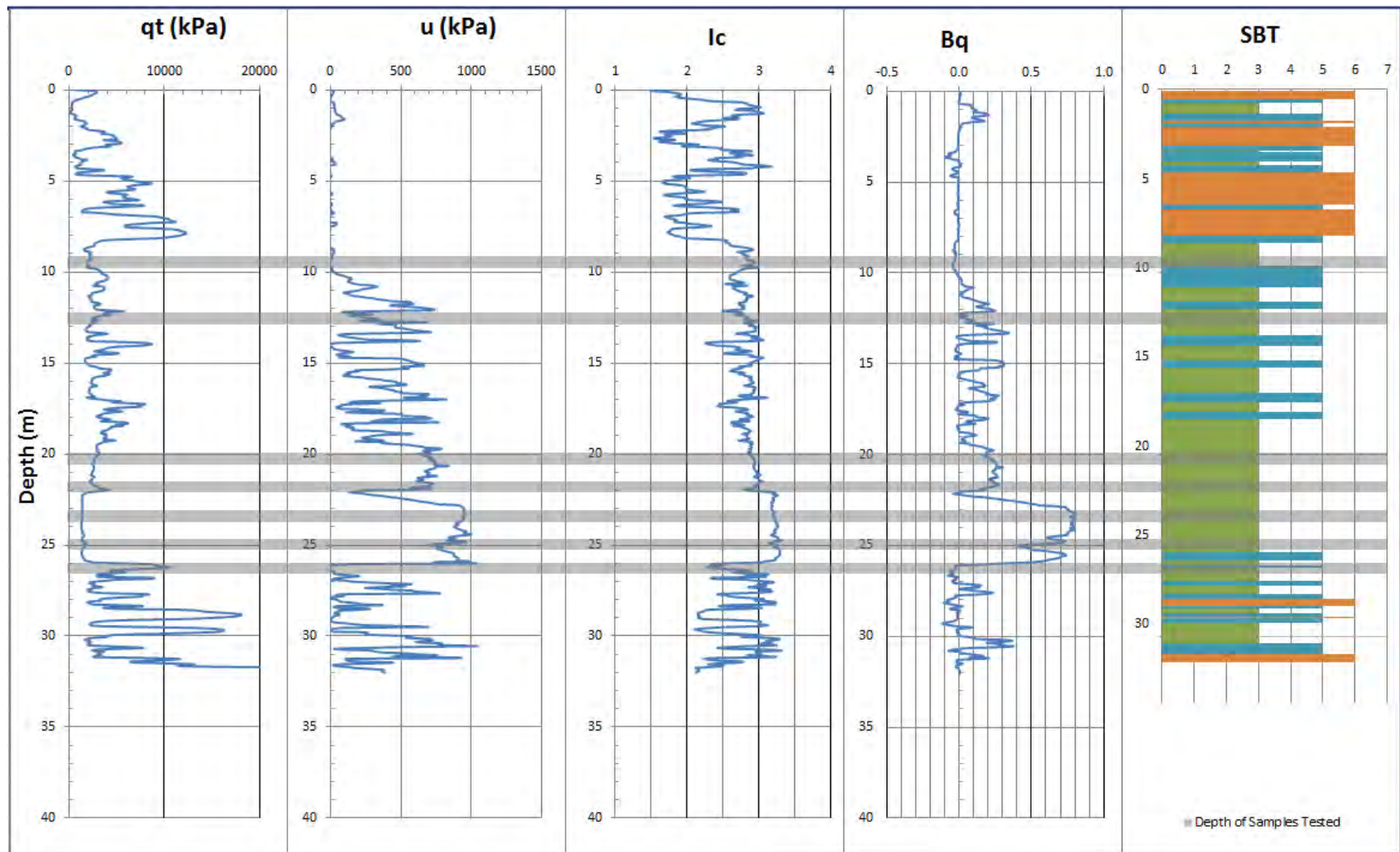


Figure D3 Springville CPT plots with Ic, Bq, and SBT and depths where samples were tested



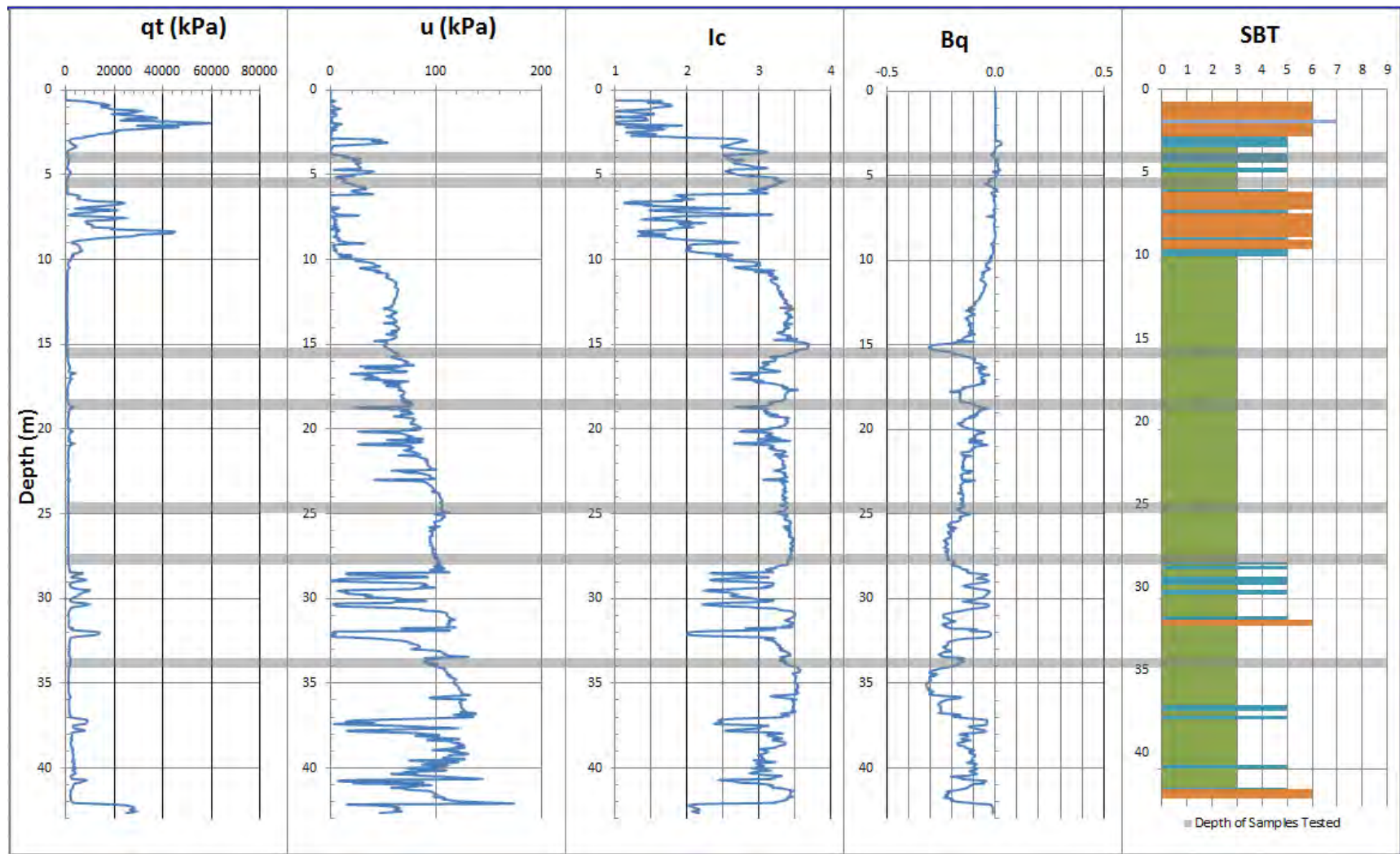


Figure D4 Provo CPT plots with Ic, Bq, and SBT and depths where samples were tested

## **APPENDIX E COMPARISON OF INCREMENTAL LOADING AND INSTANTANEOUS LOADING**

## E.1 Comparison of incremental loading and instant loading

When performing the laboratory testing to determine the value of  $C_\alpha$  and  $C'_\alpha$ , the samples were loaded to the desired stress in one step. This is the equivalent to loading the sample with a large load increment ratio, LIR, whereas incremental loading was used when determining the preconsolidation of the soil. Does a large LIR have an effect on the value of  $C_\alpha$  and  $C'_\alpha$ ? The literature seems to be mixed on the effect of what a large LIR will do to the test results.

Large LIRs will cause the soil to squeeze past the gap of the consolidation ring and the porous stone. This extrusion of soil is due to a large hydraulic gradient caused by the large step in stress. This will in turn cause an error in the measurement in the deformation due to the loss of soil (Germaine and Germaine, 2009). However, the value of  $C_\alpha$  is independent of the load increment ratio (LIR), as long as some primary consolidation occurs (Raymond and Wahls, 1976). This concept that the value of  $C_\alpha$  is not affected by LIR is what will be tested for this part of the report.

To determine if a large LIR has an effect on the value of  $C_\alpha$ , parallel tests will be run. One sample will have an instant loading where the soil will be brought to the desired stress in one step. The other sample will have an incremental loading where the soil will have an LIR of 1 and time rate readings will be taken, and the next loading will be added when more than 90% of primary consolidation has occurred. The samples were selected using data from nearby CPTs. These were soft soils with low tip resistance and high pore water pressures. A total of four samples were tested, one from each site. The results of each of these tests are in Table E1.

Table E1 Test Results for Incremental Loading and Instantaneous Loading

Site	Depth	$C_{\alpha}$ Incremental load (OCR=1)	$C_{\alpha}$ Instantaneous load (OCR=1)
400 South	20- 22	0.01163	0.01270
Provo	90- 92	0.00496	0.00454
South Layton	105- 107	0.00221	0.00227
Springville	75- 77	0.00512	0.00512

The data were then plotted with the instantaneous loading on the x-axis and the incremental loading on the y-axis. A 45-degree line was then added to the plot for reference to see how the values of  $C_{\alpha}$  instantaneous loading and  $C_{\alpha}$  incremental loading deviate from each other. The value of  $C_{\alpha}$ , determined using an incremental loading, didn't change much when compared to the value of  $C_{\alpha}$  that was determined using an instantaneous loading. This can be seen in Figure E1.

It should be noted that the samples that were subjected to the instantaneous loading tended to have a higher overall strain than the samples that underwent the incremental loading; this could be due to the squeezing effect stated earlier. However, this squeezing effect did not seem to affect the rate of secondary settlement. There may have been higher strains with the instantaneous loading, but once the pore water pressure dissipated and primary settlement had occurred, the value of  $C_{\alpha}$  did not change much regardless of the use of a large LIR. This higher strain could have an effect on the value of the compression ratio, CR, and the recompression ratio, RR, but the value of  $C_{\alpha}$  seems to be unaffected.



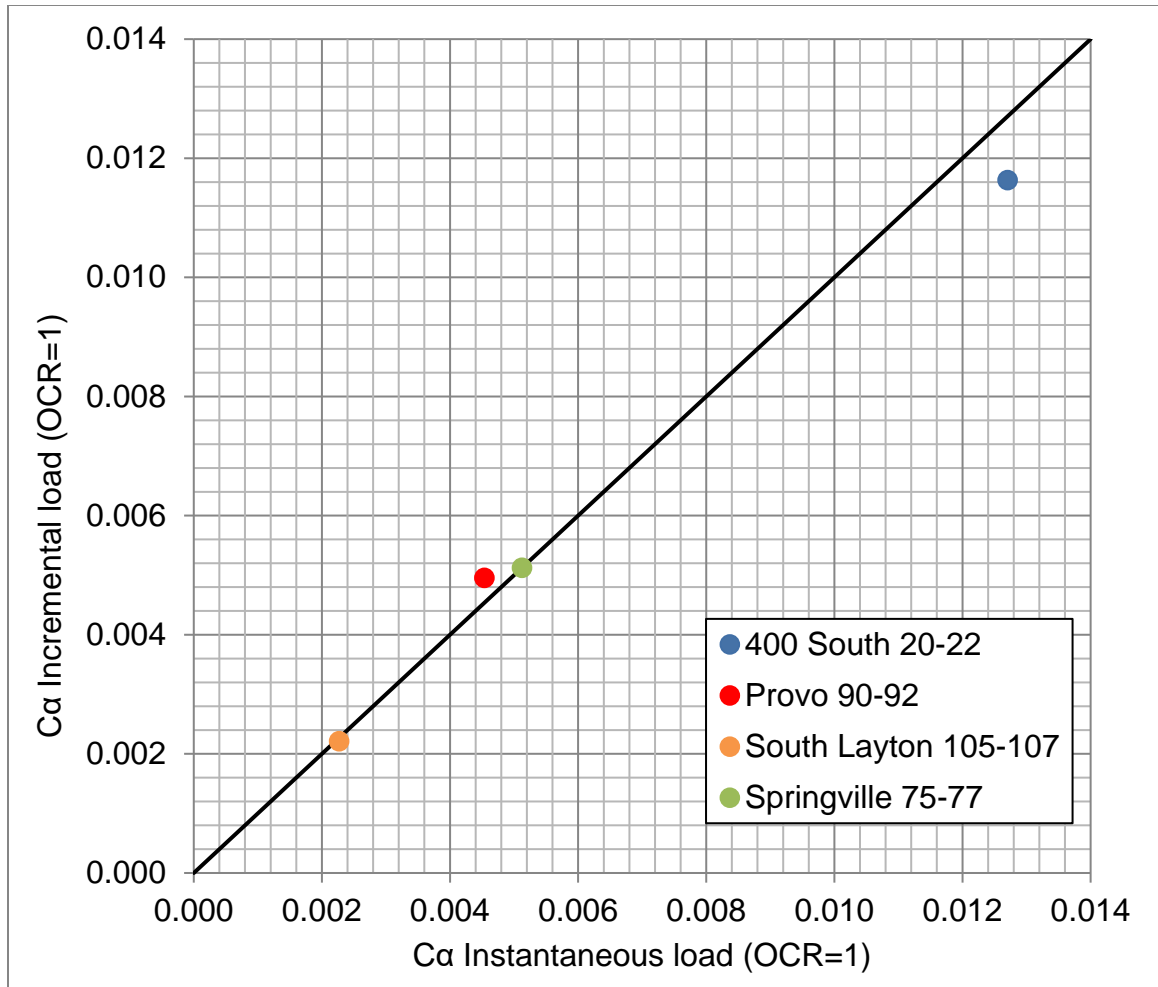


**Figure E1 Plot of  $C_\alpha$  instantaneous loading versus  $C_\alpha$  incremental loading**

In conclusion, two things were observed: 1) the value of  $C_\alpha$  is independent of the load increment ratio (LIR); when using large LIRs,  $C_\alpha$  seems to be constant for the same material; and 2) with large LIRs there seems to be larger overall strains on the sample, probably due to a loss of soil caused by high hydraulic gradient.

## **APPENDIX F METHOD FOR DESIGNING SURCHARGE FILLS CONSIDERING POST-CONSTRUCTION SECONDARY COMPRESSION SETTLEMENT**

## Introduction

This appendix describes the recommended method for designing surcharged embankments for highway construction. It provides the rationale for determining the height of required surcharge in order to reduce the amount of secondary compression to levels consistent with the performance goals of the projects. It is based on methods presented in Ladd (1989), Stewart et al. (1994), Saye and Ladd (1997), and information presented in the body of this report. Note that current UDOT Geotechnical Manual of Instruction (GMOI) requirements take precedence over the narrative here. Also, the recommended surcharge layouts and extents given here are general in nature, and some of the recommendations may not apply for all cases.

An allowable post-construction settlement of 76 mm (3 inches) in 10 years has been established by UDOT as a performance goal in certain past projects to meet lane smoothness requirements and reduce the amount of settlement at bridge approaches. An equivalent goal in terms of rate of settlement is to limit the post-construction settlement to 50 mm (2 inches) in 5 years. The following sections address the analysis of the foundation conditions, primary consolidation, secondary compression, and immediate settlements in terms of meeting this goal.

## Required Information and Design Inputs

The design of surcharged embankments and retaining structures requires several inputs including:

- profile and cross-section drawings of current ground or embankment configuration
- design profiles and cross-section drawings of proposed embankments or retaining walls
- design plan view sheets of proposed alignment including extent of current and planned embankment and its relationship to right-of-way (ROW)
- geotechnical borehole logs and other information (e.g., CPT soundings) to determine soil stratigraphy with depth
- geotechnical subsurface profile of pre-consolidation stress ( $\sigma_p'$ ) with depth
- geotechnical subsurface profile of compression ratio (CR) versus depth
- estimates of time rate of consolidation for untreated, natural ground and for various pre-fabricated vertical drain (PVD) spacing, if PVDs are planned
- site-specific laboratory testing expressing relations of  $C_\alpha$  and CR for compressible layers
- site-specific laboratory testing expressing relations of adjusted amount of surcharge (AAOS) versus the normalized rate of secondary settlement ( $C_\alpha'/C_\alpha$ ) for compressible layers (see body of report and Appendix C)

## Primary Consolidation Settlement

The Lake Bonneville deposits along the Wasatch Front consist of low and highly plastic silts and clays that exhibit a small amount of pre-consolidation, probably due to aging and fluctuations in groundwater level. In addition, in many locales, the overlying sediments have developed a “surface crust,” of less compressible soil due to repeated desiccation and the deposition of more granular recent alluvium.

The foundation soils beneath new embankments will exhibit large settlements due to primary consolidation when the newly applied stress at depth from embankment construction exceeds the pre-consolidation stress of compressible layers. The amount of differential settlement in the longitudinal and transverse directions of the roadway will be proportional to the height of the newly constructed embankment. In addition, experience has shown that lengthy settlement periods are required to allow for completion of primary consolidation settlement at many locales where a considerable thickness of

soft sediments exist. Pre-fabricated vertical (PV) drains are the main technology used to reduce the primary consolidation settlement period for fast-paced construction projects constructed atop compressible, clayey soils. In most cases, the installation of PV drains is necessary to implement a surcharge strategy. This is because without the installation of PV drains, the resulting primary consolidation time is generally too lengthy to meet project schedule constraints.

## **Estimation of Amount of Primary Consolidation Settlement for Design**

This topic is outside of the scope of this research in that this document is focused on methods to evaluate the amount of secondary compression associated with surcharging. Cline and Bartlett (2008) and Bartlett et al. (2011) used commercially available software to perform 2D embankment settlement analysis for embankments constructed in the Salt Lake Valley and compare traditional methods (i.e., Janbu) (Fang, 1991) (Cline and Bartlett, 2008) with 2D non-linear methods as represented by the hyperbolic non-linear elastic (HNLE) model as developed by Duncan et al. (1980). In general, traditional methods can provide reasonable estimates of the consolidation settlement occurring within the footprint of the newly added embankment; however, for estimates of settlement outside that footprint (e.g., determining settlement impacts to adjacent structures), the HNLE model is superior and is recommended for practice.

Considerable work has been done in determining and comparing methods for estimating the pre-consolidation stress ( $\sigma_p$ ) and compressibility parameters ( $C_c$ ,  $CR$ ,  $M$ ) of the Lake Bonneville deposits. Ozer (2005) used constant rate of strain (CRS) consolidation tests to obtain high quality estimates of  $\sigma_p$ ,  $C_c$  and used these measurements to develop regression equations for estimating these parameters based on CPT and DMT methods. These correlations can be used to make preliminary estimates of consolidation parameters pending the completion of more detailed undisturbed sampling and laboratory investigations. In addition, Bartlett and Lee (2004) have provided regression equations to predict the compressibility parameters for the Lake Bonneville sediments using laboratory determined values of natural moisture content and void ratio. These correlations were developed using the large geotechnical database obtained from the I-15 Reconstruction in Salt Lake Valley, Utah. These correlations may also be useful for preliminary evaluations.

## **Estimation of Time Rate of Primary Consolidation Settlement for Design**

Historic settlement records and monitoring suggest the presence of sandy layers within the Lake Bonneville deposits that control the drainage conditions and determine the maximum thickness of the major compressible layers. The highly layered structure of the Lake Bonneville sediments and considerable variations in the plasticity of the silty and clayey layers complicates the assessment of the coefficient of consolidation in both the vertical and horizontal directions (Farnsworth et al., 2015). The layering of the various sandy and silty sediments forms a macro fabric that increases the effective coefficient of consolidation of the deposits. This has been explored in terms of Terzaghi's theory of consolidation, which relates the elapsed time of primary consolidation to the thickness of the clay layer.

$$t = T_v H^2 / c_v \quad (1)$$

where:  $t$  is the elapsed settlement time,  $T_v$  is the dimensionless time factor for vertical drainage from Terzaghi's theory of 1-D consolidation,  $H$  is the maximum length of the drainage path for the layer undergoing primary consolidation and  $c_v$  is the coefficient of consolidation for vertical drainage.

However, foundation soils treated with PV drains undergo radial consolidation instead of vertical consolidation; hence, the process of vertical compression results from horizontal drainage. The processes of vertical and radial consolidation are similar, with the exception of the direction of excess pore pressure dissipation. However, radial consolidation is mathematically more complex because the distance between the flow paths decreases as the flow paths approach the PV drains, as opposed to remaining constant

throughout the vertical drainage system. In either case, the drainage of excess pore water pressure with respect to time is a function of the coefficient of consolidation, either  $c_v$  or  $c_h$ , for vertical or radial (i.e., horizontal) consolidation, respectively. Thin layers undergoing radial consolidation experience some effect from vertical drainage, but these effects are minor when the compressible layer is over 5 m in thickness (Bartlett et al. 2001). To be conservative for thinner layers, the effect of vertical drainage is often disregarded.

To calculate the average degree of consolidation for radial drainage,  $U_r$ , (e.g., where PV drains have been used), the equation given by Barron (1948) may be used:

$$U_r = 1 - e^{-8T_r / F(n)} \quad (2)$$

where:  $U_r$  is the degree of consolidation with radial drainage,  $T_r$  is the radial drainage time factor, and  $F(n)$  is equal to:

$$F(n) = \ln(n) * [n^2 / (n^2 - 1)] - [(3n^2 - 1) / (4n^2)] \quad (3)$$

and  $n$  is the drain spacing ratio defined by:

$$n = d_e / d_w \quad (4)$$

and  $d_e$  is the equivalent diameter of influence and  $d_w$  is the diameter of the drain. The parameter  $T_r$  is similar to the dimensionless vertical drainage time factor,  $T_v$ , but  $T_r$  is a function of the coefficient of horizontal consolidation,  $c_h$ , the length of the horizontal drainage path,  $d_e$ , (which is equal to two times the radius of an equivalent soil cylinder from which radial drainage occurs), and the time of consolidation,  $t$ . Values of  $T_r$  are related to these parameters by  $c_h / d_e^2$ . Thus,  $t$  can be calculated from:

$$t = T_r d_e^2 / c_h \quad (5)$$

and  $c_h$  is related to hydraulic conductivity and compressibility of the soil layer by:

$$c_h = k_h / m_v \rho_w g \quad (6)$$

where:  $k_h$  is the horizontal hydraulic conductivity,  $m_v$  is the 1D compressibility of the soil,  $\rho_w$  is the mass density of water and  $g$  is the acceleration of gravity. In order to calculate  $t$  for radial drainage, values of  $T_r$  as a function of  $n$  are required. These can be obtained from Figure F1 below (Barron, 1948).

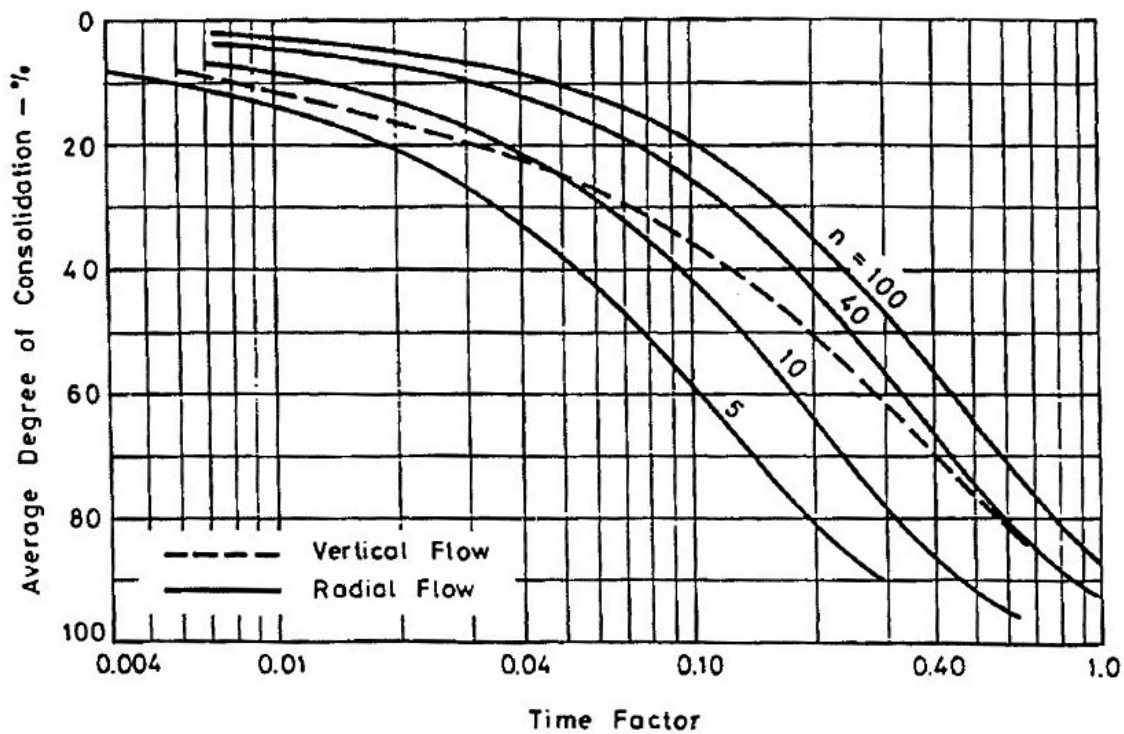


**Figure F1. Average degree of consolidation for radial flow as a function of  $n$  and  $T_r$  (after Barron, 1948).**

Obtaining reasonable estimates of the horizontal drainage characteristics of the soil layers is critical for making reliable evaluations of the time required to complete primary consolidation settlement for soils treated with PV drains. Farnsworth et al. (2015) compared the results from three different methods used to obtain  $c_h$ : (1) back calculation using the Asaoka method and data from borehole magnet extensometers, (2) cone penetrometer pore pressure dissipation testing (CPTU), and (3) laboratory Rowe cell testing (Figure F2). They demonstrated that Rowe cell testing can provide results very similar to those obtained from the back calculated field behavior. However, the CPTU pore pressure dissipation test provided results that were 5 to 10 times larger, which is unconservative in that calculations based on such tests may significantly underestimate the required settlement time.

Back calculation of field performance data was found to be a reliable approach for obtaining estimates of the effective values of the coefficient of horizontal consolidation,  $c_{he}$  (Farnsworth et al., 2013). The term effective is used because back calculated values represent the average horizontal coefficient of consolidation for the selected interval between two downhole magnets which is influenced by the disturbed zone that typically develops around the PV drain during installation. However, because this method is calibrated to the actual subsurface settlement behavior, this method can be used to calculate average parameters for the global subsurface settlement performance, or when used in conjunction with magnet extensometer data, estimating the settlement parameters of individual compressible layers. Unfortunately, this method requires full-scale embankment settlement data and subsurface monitoring of compression obtained from initial embankment loading through the duration of primary consolidation; therefore it is not always practical to implement, especially during routine projects (Farnsworth et al., 2015).

CPTU pore pressure dissipation is another commonly used technique because of its relative simplicity and wide availability. However, as shown in Farnsworth et al. (2015) the results from CPTU tests can vary greatly and tend to be heavily influenced by adjacent drainage layers. The  $c_h$  estimates

obtained from this method were significantly higher than those calculated from field settlement behavior. Thus, one should exercise prudent judgment in selecting design values using this methodology.

Rowe cell testing provided horizontal drainage results that best matched actual field behavior when considering the lower bound of the data range. Like most laboratory tests, there is a great deal of opportunity to introduce disturbance and error between obtaining undisturbed samples from the field and performing the test in the laboratory, and caution must be exercised to minimize unnecessary error. Although the results exhibited some minor scatter, thus demonstrating the variability of the soil, in this case the lower bound data provided the most accurate representation of the controlling behavior of the macro-fabric of the entire soil layer.

In addition to the above methods, the results from standard 1D laboratory consolidation tests might be utilized effectively to estimate  $c_h$ , if the relationship between the horizontal and vertical drainage characteristics are readily understood (Farnsworth et al., 2015). The method commonly employed is to approximate values of  $c_h$  from values of  $c_v$  obtained from the 1D consolidation test by determining the relationship between the horizontal and vertical conductivity of the layer. To this end, prior testing has shown that the hydraulic conductivity in the horizontal direction is greater than the vertical direction for the Lake Bonneville deposits. This ratio is thought to be somewhere between 2 and 5. For example, research performed by Ozer (2005) measured the  $c_v$  values for the Lake Bonneville clay layers using constant rate of strain (CRS) laboratory consolidation testing as shown in Figure F3. The values of  $c_v$  shown in this figure were obtained at the in situ stress state, between the in situ stress and pre-consolidation stress, and beyond the pre-consolidation stress through the end of the test. Because of this, there was considerable scatter in the results prior to reaching the pre-consolidation stress. Nonetheless, the values of  $c_v$  measured after exceeding the pre-consolidation stress best represent the stress levels achieved in the foundation soils beneath large embankments; therefore, these values are controlling the rate of primary consolidation settlement (Farnsworth et al., 2015). Therefore, only  $c_v$  values beyond the pre-consolidation stress were selected for comparison with this research. The values of  $c_v$  varied between about 1 and 32 mm<sup>2</sup>/min with an average value of 12 mm<sup>2</sup>/min, and 2 and 10 mm<sup>2</sup>/min with an average value of 5 mm<sup>2</sup>/min, for the Upper and Lower Bonneville clay layers, respectively. When compared with the results obtained by back calculation and the Rowe cell test, the values of  $c_h$  are approximately 1.0 and 1.8 times larger than the values of  $c_v$ , for the Upper and Lower Bonneville clay layers, respectively (Figure F2). This indicates that anisotropy associated with respect to hydraulic conductivity within the Lake Bonneville deposits may be as large as about 2 for this test location at 100 South and I-15 located near downtown Salt Lake City, Utah. If  $k_h/k_v$  ratios are used to estimate  $c_h$  using Equation (6), then a  $k_h/k_v$  of 1.0 is recommended, unless demonstrated otherwise using project specific testing.

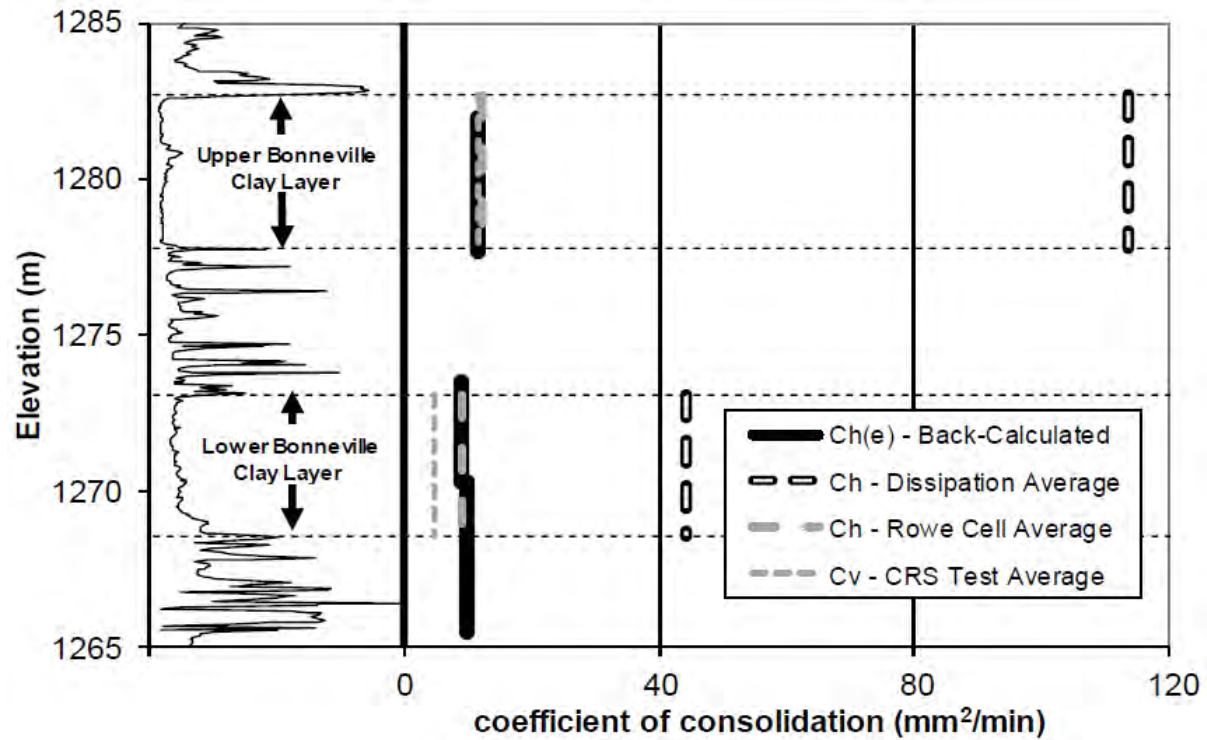


Figure F2. Comparison of average  $c_h$  values for the Lake Bonneville deposits, Salt Lake City, Utah (Farnsworth et al., 2015)

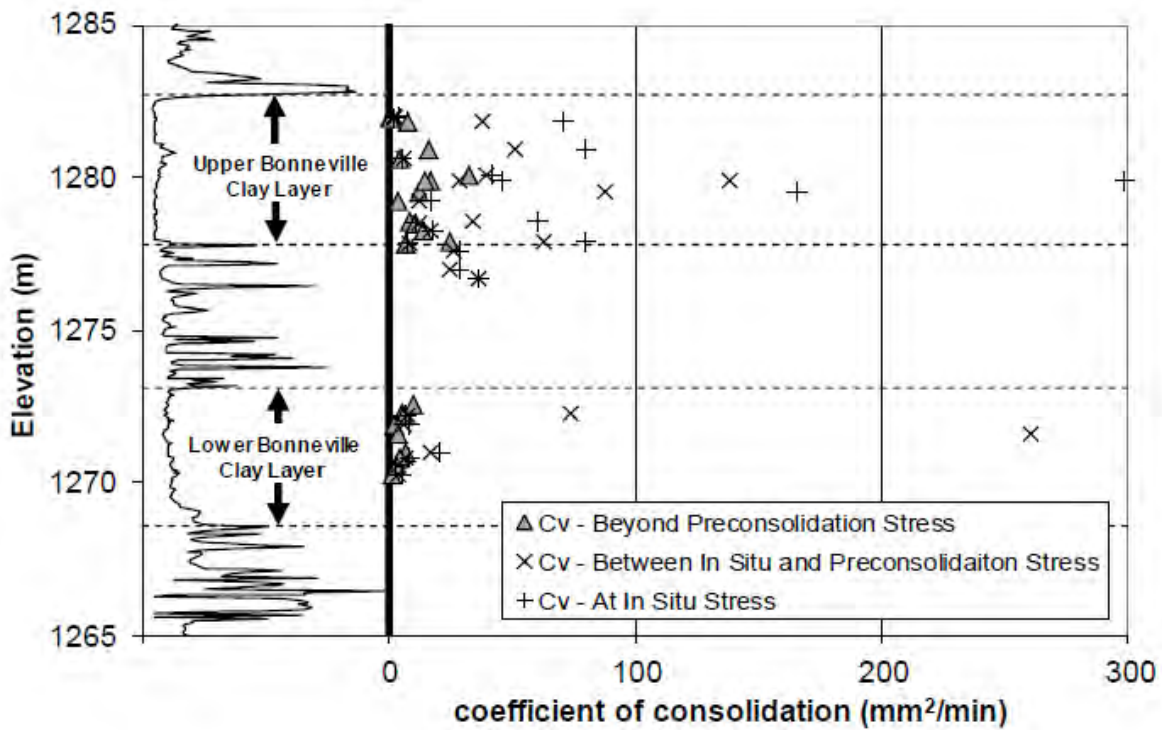


Figure F3. Values of  $c_v$  obtain from constant rate of strain (CRS) testing (after Ozer, 2005).



## Secondary Consolidation Settlement

Secondary compression, secondary settlement or creep settlement, is defined as settlement that occurs after the end of primary (EOP) consolidation settlement, which is taken to be the settlement that occurs after the dissipation of excess pore water pressure (i.e., pressure above hydrostatic caused by the placement of the new embankment).

### Estimation of Secondary Compression for Normally Consolidated Soils

The amount of secondary compression settlement expected for normally consolidated soil layer is:

$$S_s = C_{\alpha\epsilon} H \log (t/t_p) \quad (7)$$

where:  $S_s$  is the secondary compression settlement at time  $t$ ,  $C_{\alpha\epsilon}$  is the rate of secondary compression for normally consolidated soils,  $H$  is the thickness of the compressible layer,  $t$  is the elapsed time since the initial placement of embankment, and  $t_p$  is the elapsed time since the initial placement of embankment until the EOP consolidation settlement. Values of  $C_{\alpha}$  should be determined from a laboratory test program as described in Appendix C of this report. Equation (7) is only valid for cases where the compressible layer has undergone virgin compression from the new embankment loading and no surcharge load has been applied to cause over-consolidation.

### Estimation of Secondary Compression for Surcharged Soils

Post-surge secondary compression must account for unloading resulting from removal of surcharge and any over-consolidation of the foundation soil by that surcharging. Figure F4 illustrates the concepts associated with surcharging. All references to time,  $t$ , correspond to the time of initial placement of the final surcharge load. When the surcharge load is removed at time  $t_r$ , some rebound (swelling) is expected until time  $t_s$  if the surcharge has been left on until EOP. After this time, secondary compression resumes at an average rate, measured over one log cycle, which is equivalent to  $C'_{\alpha\epsilon}$ . Hence, in this design procedure,  $C'_{\alpha\epsilon}$  is approximated as a constant value over one log cycle following  $t_s$ . The nomenclature  $C'_{\alpha\epsilon}$  is used to designate  $C'_{\alpha}$  values that have been calculated based on the change in vertical strain and not void ratio.

The effectiveness of surcharging is judged by using laboratory tests on representative soil samples to determine the ratio of  $C'_{\alpha\epsilon} / C_{\alpha\epsilon}$  for various amounts of adjusted amount of surcharge (AAOS) (Figure F5). The value of AAOS for field applications is the vertical effective stress reduction caused by the removal of the surcharge,  $\Delta\sigma'_{vs}$  at the depth of interest, divided by the final vertical effective stress at the depth of interest, which is usually calculated at the center point of each sublayer being evaluated.

$$AAOS = \Delta\sigma'_{vs} / \sigma'_{vf} \quad (8)$$

For 1D calculations,  $\Delta\sigma'_{vs}$  is equivalent to the average height of the surcharge,  $H_s$ , multiplied by the average unit weight of the surcharge,  $\gamma_s$ . Alternatively, it can be calculated from Figure F4a as:

$$\Delta\sigma'_{vs} = \sigma'_{vs} - \sigma'_{vf} \quad (9)$$

The value of  $\sigma'_{vs}$  incorporates the vertical effective stress at depth resulting from the full height of the surcharged embankment during the last stage of embankment construction at the EOP. The value of  $\sigma'_{vf}$  incorporates the vertical effective stress at depth at EOP resulting from the final embankment

configuration including the additional vertical stresses resulting from the dead load due to weight of the pavement system and underlying roadbase.

If complex embankment construction or other irregular geometries or embankment configurations are planned, it may become necessary to estimate  $\Delta\sigma'_{vs}$  by numerical means to account for 2D and 3D loading effects using methods and geotechnical software similar to that of Cline et al. (2008) and Lingwall et al. (2013).

The procedures for determining the reduced rate of secondary compression due to surcharging,  $C'_{\alpha\epsilon}$ , are found in Appendix C. Based on the results shown in Figure F5, it can be seen that  $C'_{\alpha\epsilon} / C_{\alpha\epsilon}$  relations are somewhat variable and should be determined on a project-specific basis. Therefore, the relations shown in this figure are given for information purposes only and are only recommended for preliminary evaluations. For such evaluations, the mean line from Figure F5 is recommended, which is:

$$C'_{\alpha\epsilon} / C_{\alpha\epsilon} = -0.336 \ln(AAOS) + 1.679 \quad (10)$$

where:  $\Delta\sigma'_{vs}$  is the increase in vertical effective stress resulting from the surcharge load. The mean line used for the I-15 Reconstruction Project, also shown in this figure, is not recommended for preliminary evaluations. Post-construction settlement monitoring for the I-15 Reconstruction Project in Salt Lake Valley has shown that the actual settlement exceeded the design value (Figure 6-6, Section 6.2); hence, use of this line may not be conservative.

It is strongly recommended that the surcharge fill should remain in place until primary consolidation is essentially completed, or longer if possible, for the final embankment stage.

When the surcharge remains past EOP, then compressible layers at depth are “aged” (i.e., allowed to undergo secondary compression under the surcharged load). This will improve the effectiveness of the surcharging in reducing the amount of secondary compression. This aging effectively increases the pre-consolidation stress of each subsurface layer, hence reducing the subsequent amount of secondary compression. This additional pre-consolidation stress caused by aging can be estimated for each layer by:

$$\sigma'_{p \text{ aged}} = \sigma'_{vs} (t_r / t_p)^{(C_{\alpha\epsilon}/CR)} \quad (11)$$

where:  $t_r / t_p$  is the ratio of time when surcharged is removed to the time to EOP consolidation,  $C_{\alpha\epsilon}$  is the normally consolidated rate of secondary compression and CR is the compression ratio, which is equal to:

$$CR = C_c / (1+e_o) \quad (12)$$

where:  $C_c$  is the compression index and  $e_o$  is the initial void ratio of the specimen or layer.

As primary consolidation is completed and the surcharge is removed, there will be a small rebound or heaving of compressible layers. The duration of this heave event is the elapsed time between the removal of surcharge,  $t_r$ , and start of secondary settlement,  $t_s$  where the value of  $t_s$  is taken as the point in time when the soil has reached its maximum heave value. Based on the laboratory testing performed as part of this research, an average value for  $t_s$  is calculated from:

$$\log(t_s / t_r) = x_0 * AAOS \quad (13)$$

where the average value of  $x_0$  is 0.0174 as obtained from the laboratory tests program. Hence,

$$t_s = 10^{x_0 * AAOS} * t_r \quad (14)$$

Lastly, the amount of secondary compression (cm) for each compressible layer is calculated from:

$$\Delta S_s = H * C'_{\alpha\epsilon} * \log(t / t_s) * 100 \quad (15)$$

where:  $S_s$  is the secondary compression in the sublayer (cm),  $H$  is the thickness (m) of the sublayer,  $C'_{\alpha\epsilon}$  is the rate of secondary compression for the sublayer,  $t$  is the elapsed time (days) since the EOP consolidation for the sublayer and  $t_s$  is calculated from Equation 14 for each sublayer, and 100 is a conversion to convert m to cm. In order to calculate the total secondary compression settlement for the soil profile, the following is applied:

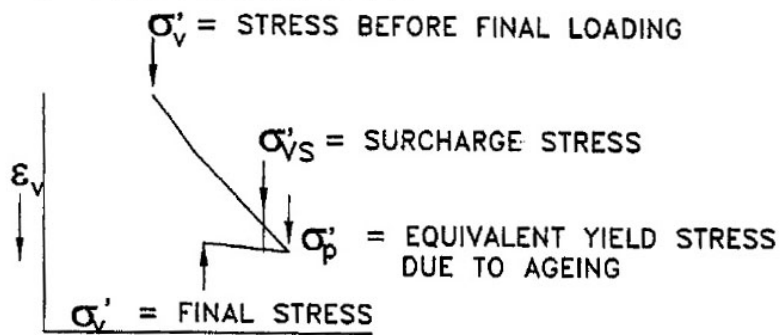
$$S_s = \sum \Delta S_s \quad (16)$$

where: Eq. 16 is summed for  $n = 1$  to  $n$  compressible sublayers.

A spreadsheet calculation for estimating the amount of secondary compression is given in Table F1. Note that in this spreadsheet the ratio of  $C_{\alpha\epsilon} / CR$  for interbedded and silty sediments was assumed to be 75% of the  $C_{\alpha\epsilon} / CR$  value for clays. This was done as an expediency, but this assumption has not been verified by laboratory testing or field monitoring.

This spreadsheet can be modified using project-specific data and used to determine the required height of surcharge to meet the post-construction settlement performance goal established by the project team.

A) STRAIN vs. LOG STRESS



B) STRAIN vs. LOG TIME

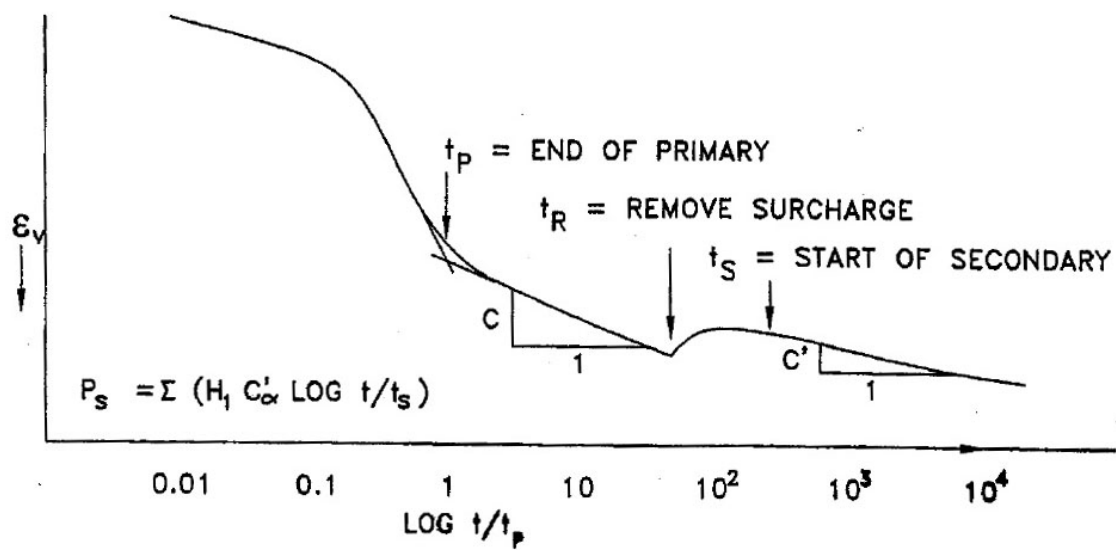


Figure F4. Effects of Surcharge on Secondary Compression (after Ladd, 1989).

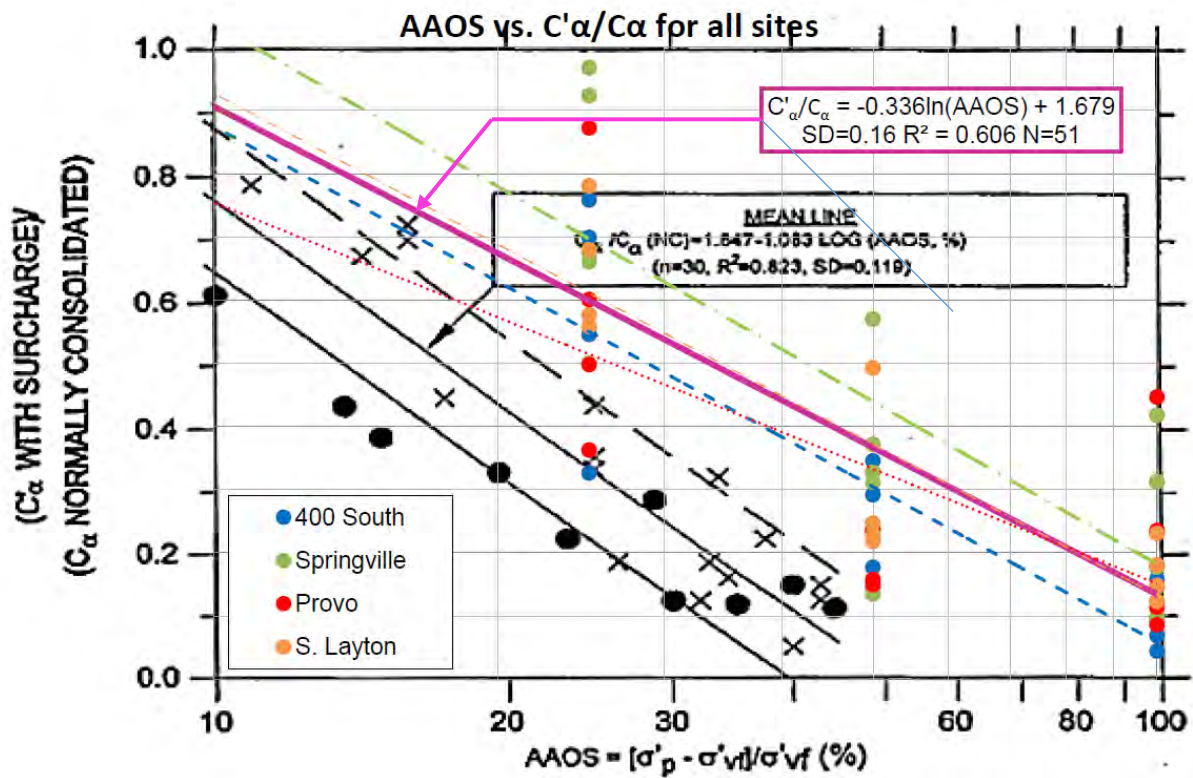


Figure F5. Comparison plot of AAOS vs.  $C'_\alpha / C_\alpha$  from this research with that used by the I-15 Reconstruction Project.

**Table F1 Spreadsheet Example of Calculation of the Amount of Secondary Compression Settlement**

**CALCULATION OF MAGNITUDE OF POSTCONSTRUCTION SECONDARY COMPRESSION**

Location: **Example**

Average Unit Weight of Embankment  $\gamma_e$  21.2 kN/m<sup>3</sup>

Average Unit Weight of Surcharge  $\gamma_s$  21.2 kN/m<sup>3</sup>

Height of Embankment,  $H_e$  12 m

Height of Surcharge,  $H_s$  6 m

Depth of Watertable 2 m

Ratio of  $C_{\alpha\alpha}$  / CR for clays

0.0442

(Recommended average value)

Ratio of  $C_{\alpha\alpha}$  / CR for interbeds or silts

0.03315

(Recommend 75% of ratio for clays, if unknown)

Time of surcharge removal,  $t_r$

200 days

(Set  $t_r = t_p$  if surcharge is removed at or near EOP, (i.e., not aged))

Elapsed time after EOP,  $t - t_p$

3650 days

Layer	Soil Type	Layer Thickness $\Delta H$ (m)	Layer Middepth $z$ (m)	Soil Unit Weight $\gamma_{sat}$ (kN/m <sup>3</sup> )	Bottom Vertical Total Stress $\sigma_{vo}$ (kPa)	Midlayer Vertical Total Stress $\sigma_{vm}$ (kPa)	Midlayer Hydrostatic Porewater Pressure $u_e$ (kPa)	Midlayer Vertical Effective Stress $\sigma'_{vm}$ (kPa)	Layer Compression Ratio CR (unitless)	Initial Pre-consolidation Stress $\sigma'_p$ (kPa)	Aged Pre-consolidation Stress $\sigma'_{p,aged}$ (kPa)	Final Vertical Effective Stress w/o surcharge $\sigma'_{vf}$ (kPa)	Final Vertical Effective Stress w surcharge $\sigma'_{vs}$ (kPa)	Time Req'd for EOP consolidation with surcharge $t_p$ (days)	Adjusted Amount of Surcharge AAOS (%)	$B_0$ (see note 1)	$B$ (see note 1)	$C_{\alpha\alpha} / C_{\alpha\alpha}$ (see note 1)	$C_{\alpha\alpha}$	$C_{\alpha\alpha}$	$x_s$ (see note 2)	$\log(t_r / t_e)$	$t_e$	$\log(t / t_e)$	$\Delta S_v$ (cm)
1	silt	1.5	0.75	18.6	28	14	0	14	0.09	250	405	268	396	100	47.40	1.679	0.336	0.382	0.0030	0.001	0.0174	0.825	1336	0.44	0.07
2	sand	3	3	18.6	84	56	10	46	0.02	99	428	300	428	100	42.34	1.679	0.336	0.429	0.0000	0.000	0.0174	0.737	1001	0.52	0.00
3	clay	2	5.5	18.6	121	102	34	68	0.175	122	464	322	450	100	39.46	1.679	0.336	0.444	0.0077	0.003	0.0174	0.687	972	0.57	0.39
4	interbeds	4	8.5	18.6	195	158	64	94	0.15	148	487	349	476	100	36.47	1.679	0.336	0.471	0.0050	0.002	0.0174	0.635	862	0.63	0.59
5	clay	4.5	12.75	18.6	279	237	105	132	0.24	183	529	386	513	100	32.95	1.679	0.336	0.505	0.0106	0.005	0.0174	0.573	740	0.69	1.66
6	sand	6	18	18.6	391	335	157	178	0.02	226	559	432	559	100	29.43	1.679	0.336	0.543	0.0000	0.000	0.0174	0.512	650	0.75	0.00
7	clay	3	22.5	18.6	446	419	201	217	0.19	312	618	472	599	100	26.96	1.679	0.336	0.572	0.0084	0.005	0.0174	0.469	589	0.79	1.14
8	interbeds	6	27	18.6	558	502	245	257	0.2	353	653	511	639	100	24.88	1.679	0.336	0.599	0.0066	0.004	0.0174	0.433	542	0.83	1.97
9	clay	3.5	31.75	18.6	623	591	292	299	0.2	397	701	553	680	100	23.00	1.679	0.336	0.626	0.0088	0.006	0.0174	0.400	503	0.86	1.67
10																									

**NOTES:**

1  $C_{\alpha\alpha} / C_{\alpha\alpha} = -B \ln(AAOS) = B_0$

2  $\log(t_r / t_e) = x_s / AAOS$ , Recommend using 0.0174 for preliminary evaluations

Total post construction secondary compression =

Secondary compression for design life of

$\Sigma \Delta p_v =$

7.5 cm

3650 days

## Recommended Surcharge Layout and Extents

The overconsolidation of compressible sediments subjected to surcharging will be less at the edge of the surcharge fill. Therefore, extension of the surcharge laterally beyond the pavement edge is generally used to increase the effectiveness of the surcharge.

The recommended limits of the surcharge fill that is to be constructed in combination with new embankment is shown in Figure F6. The height of the surcharge fill should be determined using the method outlined in the previous section. In addition, the side slope of the new embankment should also be surcharged as shown in Figure F6 to insure that large differential settlement does not occur at the planned edge of pavement.

The recommended limits of the surcharge fill that is to be constructed adjacent to existing embankments in widened areas is shown in Figures F7 and F8. The recommended extents of the surcharge take into consideration the effectiveness of the surcharge and have been developed to reduce the potential deleterious impact of increased post-construction settlement at the outside edge of the new roadway. Figure F7 is for the case where the height of the new embankment does not exceed the height of the existing embankment by 0.75 m. Hence, for this case, the surcharge does not extend across the entire new roadway alignment; instead, it terminates at 5 m right of the shoulder of the new roadway. For cases where the new embankment height exceeds the height of the existing embankment by 0.75 m, then the layout shown in Figure F8 should be applied.

In addition, for the case of vertical embankment when PV drains (i.e., wick drains) are planned to accelerate construction, it is recommended that the zone of installation extend 4 m beyond the face of the wall (i.e., extend 4 m outside of the wall face into the zone of original ground at the foot of the wall).

Figures F7 and F8 also show the recommended zone of PV drain installation extends into the footprint of the existing embankment. If this portion of the embankment is not removed to accommodate PV drain installation, then pre-drilling of pilot holes for PV drain installation may be required, depending on the height and stiffness of the existing embankment and the push capacity of the PV drain installation rig.

If a vertical embankment (e.g., MSE wall) is to be constructed, then it is recommended that the height of the MSE wall be increased by means of a temporary geosynthetic wall perched atop the permanent wall to accommodate the construction of the surcharge. Replacement of the temporary wall with a sloped surcharge embankment is not recommended. Such an approach will increase the amount of secondary compression settlement at the edge of the roadway and, depending on the slope used, might pose a safety hazard to construction personnel if the soil is not retained in some manner.

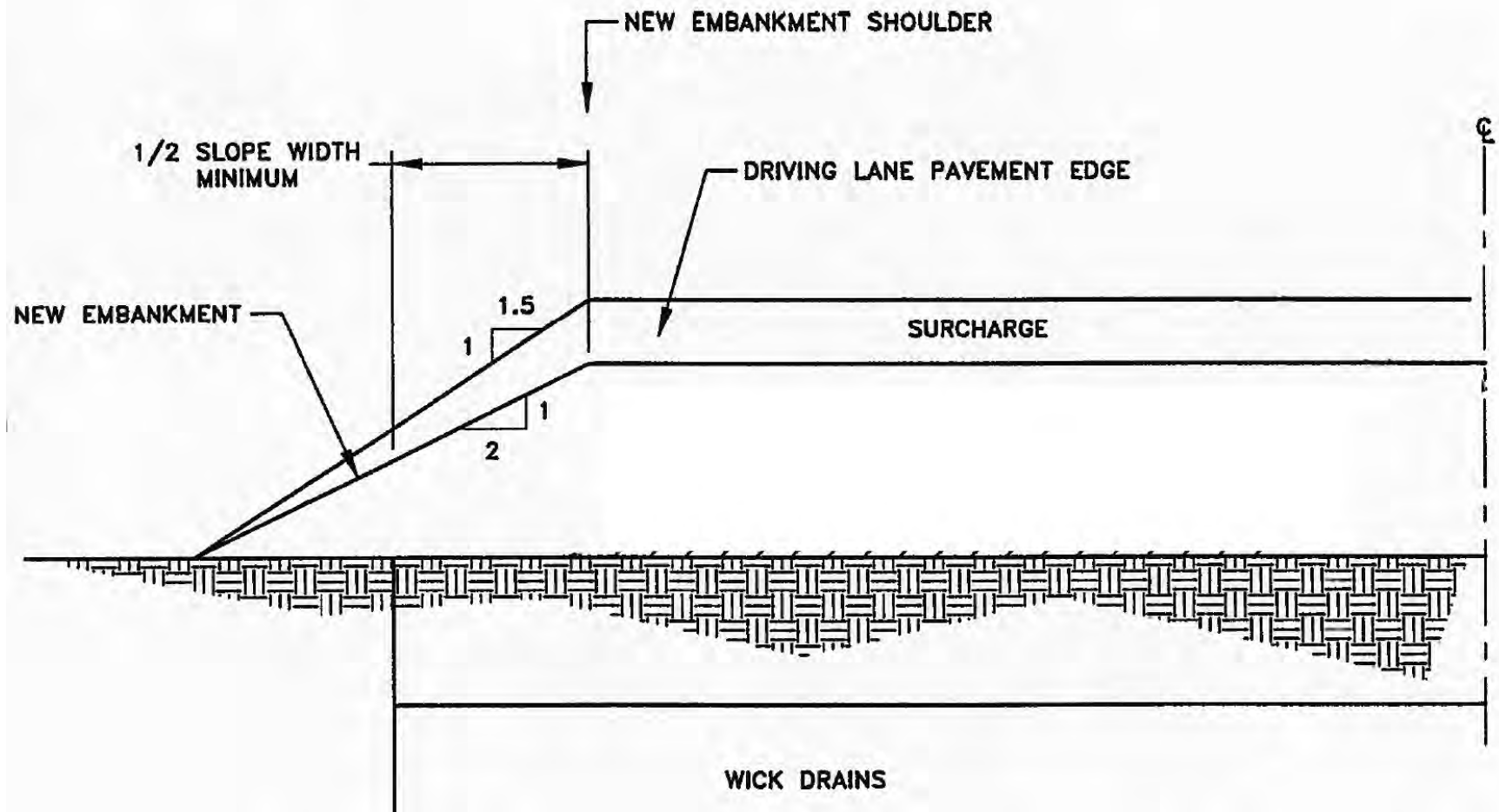


Figure F6. Recommended surcharge layout for new embankment. Wick drains may be optional depending on project schedule constraints.



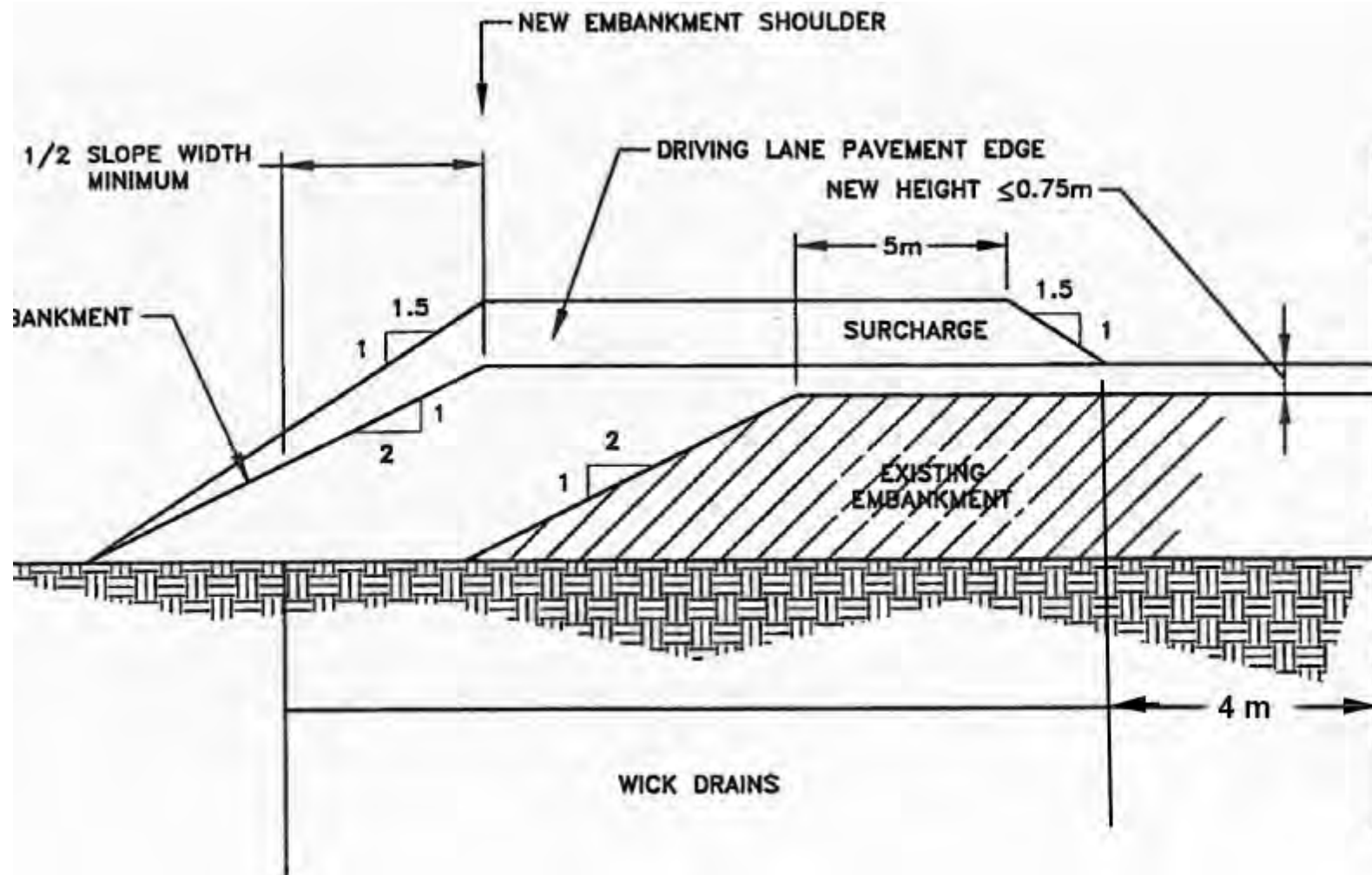


Figure F7. Recommended surcharge layout for cases where new embankment increases the existing embankment height by 0.75 m, or less, above the existing embankment.

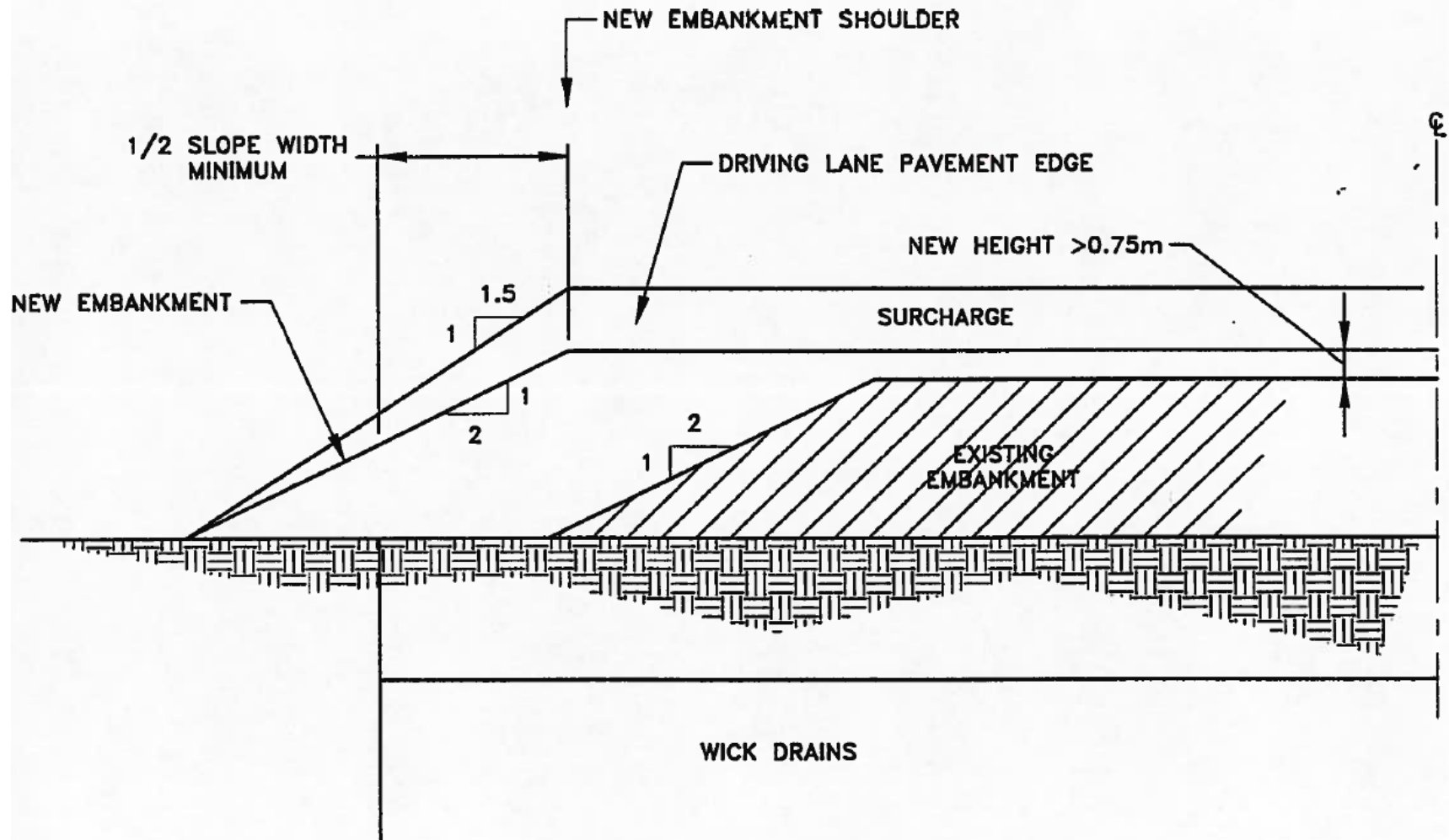


Figure F8. Recommended surcharge layout for cases where new embankment increases the existing embankment height by greater than 0.75 m above the existing embankment

## **Instrumentation for Monitoring Progression of Primary Consolidation**

The instrumentation plan should focus on developing and implementing a monitoring program to safely and efficiently monitor embankment construction and surcharge release. The goals of the monitoring program may vary depending on ground conditions and type of construction; hence, other types of instrumentation might be considered beyond those discussed in this section. This section focuses solely on the recommended instrumentation required to monitor the rate of primary consolidation settlement.

The primary objectives of the construction settlement monitoring program are to: (1) provide a systematic program for determining the completion date of primary settlement to facilitate the removal of surcharge fill, (2) monitor the time rate of primary consolidation, and (3) verify important design inputs and assumptions. For fast-paced projects, instrumentation is vital in verifying design and ultimately limiting the amount of post-construction settlement. To meet the construction and post-construction monitoring objectives outlined above, the project team may be required to deploy several types of instruments, including surface settlement plates, surface survey points, fluid-filled settlement manometers, vibrating wire (VW) piezometers, magnetic extensometers, and monitoring wells (Figure F9). A good summary of lessons learned from instrumentation on the I-15 Reconstruction Project in Salt Lake Valley is given by Bartlett et al., (2001) and Bartlett and Farnsworth (2004).

### **Settlement Plates**

Settlement plates and survey points can be an economical means of monitoring the magnitude and time-rate of primary consolidation settlement during construction. Settlement plates are typically constructed of 600-mm-square metal plates located on compacted level fill at an elevation approximately 1 m above the original ground surface. Iron riser pipe can be attached to the plates and pipe sections added as the fill is constructed to extend the pipe through the fill. Precision elevation surveying is subsequently performed to obtain a baseline reading and subsequent readings referenced to a stable bench mark that is sufficiently distant from the fill to be outside the zone of settlement influence.

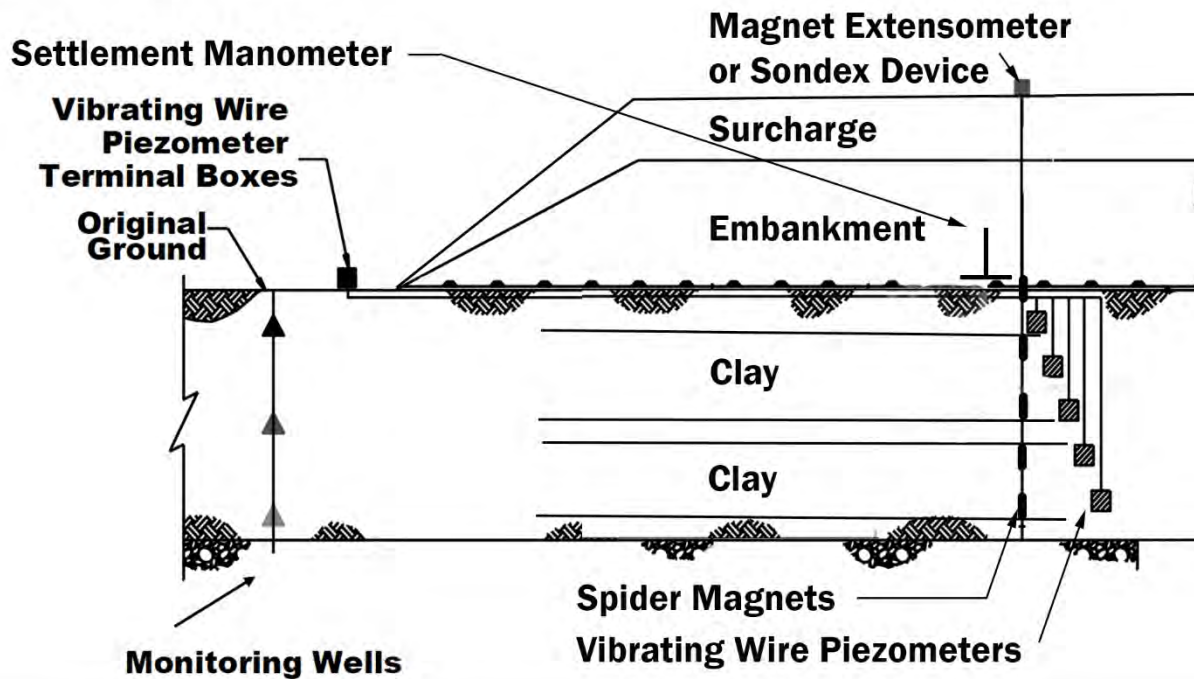


**Figure F9.** Schematic drawing of a typical instrumentation array for monitoring consolidation settlement.

### Settlement Manometer

For cases where settlement plates and their corresponding riser pipes may be subject to damage due to construction, it is recommended that settlement manometers be considered (Figure F10). A settlement manometer is used to monitor foundation soil settlement below the embankment. The settlement manometer readout station is located away from the construction area, outside the zone of settlement. Changes in elevation, or settlement, can be measured and are used to determine the rate and magnitude of primary consolidation settlement.

The settlement manometer consists of plastic tubing filled with de-aired ethylene glycol attached to a metal standpost on one end and a measuring staff on the other. A PVC casing with cap is used to protect the metal standpost from the backfill and to ensure that the tubing is not obstructed. As settlement occurs, the elevation of the standpoint and plastic tubing decrease correspondingly. Because one of the tubes is fluid-filled and open-ended, this causes the fluid elevation to decrease correspondingly. This also causes a corresponding and equal change in fluid elevation in the other end of the tubing, which is attached to a measuring staff in the readout housing. Note that the other open-ended tube is not fluid filled, but remains empty so that the pressure inside the manometer casing and the readout housing are equal to atmospheric pressure. Settlement is measured by comparing the current liquid level in the fluid-filled tube with the initial level made during the baseline readings. In addition, optical survey is done to account for any settlement of the readout housing.



**Figure F10. Settlement manometer standpoint (left). Plastic tubing (center). Housing box with measuring staff inside (right). Note inclinometer casing and pressure cell have also been installed at this site.**

Settlement manometers are installed beneath embankments, before the fill is placed. A narrow trench is excavated in the native ground inside the footprint of the fill and approximately perpendicular to the alignment. This trench should extend to a safe point outside of the embankment footprint. After the instrumentation has been placed, medium-grained, clean sand is used as bedding for the plastic tubing. The plastic tubing is then laid in the bottom of the trench in a snaking pattern to allow extra slack in the line to accommodate settlement. The line that is to be fluid-filled is attached to the full-height of the standpipe and the other used for pressure equilibrium can be attached at any convenient height.

The standpipe is typically constructed of wood or metal, and the tubing is attached to the post by hose clamps. This attachment should be secure enough so that the tubing will move in unison with the post, but not so tightly that fluid flow is constricted. The post is covered with a capped piece of four- to six-inch PVC pipe to protect the tubing and standpipe during the subsequent backfilling operation and to allow unimpeded movement. Sand bedding is also placed around the standpipe to protect it from oversized material within the fill.

The standpipe outside the fill is protected in a “birdhouse” where the plastic tubing is mounted against a ruler or measuring tape attached to the back wall of the house. The trench can be backfilled with relatively clean sand to protect the plastic tubing. The plastic tubing is filled with the de-aired ethylene glycol and a baseline reading is taken. Care should be taken to ensure the line is completely filled with fluid. This is done by over-filling the tube and allowing the fluid level to drop to the equilibrium position. (Note that the top of the tube in the birdhouse should be slightly higher than that found on the standpipe. This will allow the tube in the birdhouse to be overfilled and the fluid to escape out the top of the tube connected to the standpipe until an equilibrium level is reached.)

The reading frequency of the settlement manometer is dependent upon the rate of foundation settlement. During construction, the rate and magnitude of settlement may be very large, and daily readings are usually required. When the rate of construction settlements decreases, the frequency of readings can decrease (e.g., weekly). When read, the date and time of each reading should be recorded to the nearest minute.

To account for evaporation of the liquid within the plastic tubing, the tube must be filled above the equilibrium level and allowed to reach equilibrium before each reading. Topping off the liquid level replaces any liquid that may have been lost due to evaporation. A plastic squeeze bottle filled with extra liquid can be used for this purpose.

Also, if the birdhouse is located in the zone of settlement influence, then an optical survey should be performed for each reading. The benchmark for this survey should be located outside the zone of settlement.

There are two common problems associated with reading manometers. The first problem is not ensuring that the liquid level is completely filled within the plastic tubing when making the reading. The second is operator error. Care must be taken in correctly and consistently reading the height of the fluid in the manometer from the same eye elevation on the measurement tape or staff.

## **Magnet Extensometer**

The magnet extensometer (also known as a borehole or magnet reed extensometer) is used to measure settlement in foundations and embankments (Figure F11). Data gathered from the extensometer indicate the depths at which settlement has occurred as well as the total amount of settlement. This type of extensometer is especially useful for identifying the total compression (immediate settlement, primary consolidation, and creep settlement) that occurs within targeted layers. For example, borehole magnet “spider magnets” that bracket the critical layer(s) can greatly improve the accuracy of EOP projections. Data obtained from such instrumentation make it possible to evaluate the percent of consolidation completed for each subsurface layer and allow a more rational decision regarding the release of the surcharge fill for final construction. Bracketing layers means placing borehole spider magnets at the top and bottom of each compressible layer, so that the differential settlement within each layer can be calculated.

The magnet extensometer system consists of an access pipe, magnets strategically placed along the pipe, a survey tape, a tape reel with built-in light and buzzer and a magnet extensometer probe. The access pipe used for the I-15 Reconstruction in Salt Lake Valley consisted of 1-inch (25.4 mm) diameter flush-coupled PVC pipe. Telescoping sections were used to allow the pipe strand to compress in a manner compatible with the settlement of the adjacent soil column. Magnets placed in boreholes consisted of a datum magnet and spider magnets. The datum magnet is fixed to the bottom of the access pipe and serves as a reference or datum for the bottom of the extensometer. (If the datum magnet is placed below the zone of significant settlement, then it is generally assumed that this magnet is stationary and settlement is calculated in reference to this point.) (However, an alternative approach is to not assume that the datum magnet is stationary and use the top of the access pipe as a reference. If this point is used, the top of casing must be surveyed each time the magnet extensometer is read to determine the absolute settlement of each of the magnets.)

The spider magnets have a cylindrical body with a hollow center that is free to slide over the access pipe and six spring-steel legs. During installation, the legs of the spider magnet are compressed and then released when the magnet is positioned at the specified depth. Upon release, the legs spring into place into the adjacent soil column, locking the magnet in place. By this action, the magnets are coupled to the surrounding soil. They will then displace downward as settlement occurs.





**Figure F11. Magnet extensometer equipment. Tape reel (left). Spider magnet (right). Base plate magnet (left center middle).**

For installations where the embankment or wall is to be constructed during the installation, then plate magnets can be used (Figure F11). The plates are positioned at the desired lift within the fill or wall and backfill is placed over them and around the access pipe.

The magnet extensometer probe is connected to a survey tape, which is in turn housed on a tape reel. The tape reel has a light and buzzer that identify when the probe is in position with a magnet (i.e., at the same depth in the standpipe). Readings are made by lowering the probe down the access pipe and recording the corresponding magnet depths.

The position of the magnets must be pre-planned to capture settlement within specific layers of interest. Generally, a magnet is placed at the top and bottom of a compressible layer to measure the compression of that interval with time. Geotechnical subsurface explorations (e.g., CPT soundings) are a valuable tool for identifying important soil layers and positioning of the magnets. The first step in the installation of a borehole magnet extensometer is to drill a borehole to the desired final depth. The complete magnet extensometer system (magnets and PVC casing) is then assembled adjacent to the borehole. The datum magnet is fixed to the bottom piece of the access pipe. It is generally placed several inches from the bottom of the tube to account for any silt collection that may occur in the bottom of the access tube. The bottom of the tube is also capped to keep the access pipe free from soil during installation. Spider magnets are positioned in a retracted position along the access pipe at the appropriate depths. A locking cable is wrapped around the spider legs and an anchor pull pin holds the locking cable in place. An anchor pull cable is attached to the anchor pull pin. The locking cable not only holds the spider legs in the retracted position but also secures the spider magnet at the appropriate depth during installation. When the setup is complete, the access pipe sections are connected and placed down the borehole. The anchor pull cables are pulled, releasing the locking cables, and allowing the spider legs to spring into place. The borehole is grouted through a tremie pipe using a soft bentonite grout that will not impede the settlement of the ground.

Magnet extensometers that are installed in an embankment or MSE wall are installed as construction progresses. The access pipe must be brought up through the embankment with magnet plates being placed at various levels as the fill is placed. In this type of installation, the access pipe must be protected from construction equipment and extended to the surface as the system is constructed. For magnet extensometers with telescoping sections used in borehole installations, the depth from the top of the casing to the bottom may decrease with time as the telescoping sections compress.

For all installations, a protective casing is often placed around the top of the magnet extensometer. This keeps the access pipe free from debris and serves as a protective cushion. In addition, because the magnet extensometer must be read from the top, reading access and safety must be taken into consideration in determining the instrument location.

Care should be taken in selecting the reference point for collecting and reducing the magnet extensometer data. Three possible reference points can be used: (1) bottom of the access tube casing, (2) depth to the bottom magnet, (3) top of casing access tube. If the extensometer is installed to a depth that is greater than the compressible layers, then reference point (1) is often used. Selection of this reference point essentially assumes that the bottom of the casing will not settle significantly. If settlement does occur below this depth, it will not be possible to measure or estimate its magnitude. However, the results may still be used to calculate the relative movement and compression of specific layers between the magnets. Reference point (1) can also give erroneous readings if soil, obstructions, or other items are present or can enter and settle to the bottom of the casing. For this reason, it is often preferable to use reference point (2), where the bottom magnet is usually placed below the depth of the compressible zone. However, selecting reference point (2) also suffers from the same limitation of (1) in not being able to measure settlement occurring below the reference point.

Reference point (3) can be used for installations where it is desirable, or necessary, to measure settlement occurring below the bottom of the casing or the bottom magnet. Using the reference point requires a corresponding optical survey to be done of the top of the casing for each set of extensometer readings. With this information, it is possible to establish elevations for the top of casing and each magnet position versus time. The settlement that has occurred below the bottom of the casing is simply the elevation of the bottom of the casing at the time of interest, minus the elevation for the same point established during the baseline reading. However, a slight caution is warranted for cases where rigid casing has been installed and where very small settlement measurements are being attempted. In this case, it is possible to have minor thermal expansion and contraction of the casing, which introduce a few millimeters of error into the calculations.

## **Sondex System**

An alternative system to the magnet extensometer for reading settlement versus depth is the Sondex<sup>TM</sup> System (Slope Indicator, 2004). This device includes a relatively rigid plastic inner pipe that is allowed to slip freely inside corrugated plastic tubing. Metal rings are fitted inside the corrugations at a vertical spacing of about 1 meter, and bentonite/cement grout is placed between the corrugated tubing and the borehole sidewall. The corrugated tubing compresses in response to foundation settlement, and an electric induction probe lowered inside the rigid pipe measure changes in the position of the metal rings resulting from settlement of the foundation.

An advantage of the Sondex<sup>TM</sup> system is that compression can occur along the entire length of the outer corrugated tubing in response to vertical deformation; whereas, compression along the access tubing of the magnet extensometer is mostly transferred to the telescoping couplings and the PVC pipe, which may bend or shear. Thus, where very large settlement is expected, the Sondex<sup>TM</sup> system may be more reliable in terms of not kinking or deforming, and thus allowing unblocked passage of the reading probe.

## **Piezometers**

Piezometers are used to monitor the development and decay of pore water pressure in compressible layers. They are vital to understanding the progression of primary consolidation and are used in conjunction with the borehole settlement devices to determine the release date of surcharged fills. Piezometers are of two general types: (1) standpipe piezometers and (2) diaphragm piezometers consisting of either vibrating wire, pneumatic, or strain gauge internal construction (Slope Indicator, 2004).

Type 1 piezometers are useful as monitoring wells to determine the initial water levels in various layers (Figure F9). Monitoring wells should be positioned outside the zone of influence of the planned embankment and read before and during embankment construction. Their construction essentially consists of a screened or slotted pipe installed in the layer of interest. Unslotted PVC casing is used to extend the



pipe to the surface, which allows water to rise or fall within the pipe. Readings are obtained using a water level indicator, which is lowered in the pipe via a reel tape.

Type 2 piezometers are electronic devices that measure the pore water pressure via a readout wire and box. These devices can be installed below the embankment and read periodically via a terminal box (Figure F9). Vibrating wire (VW) piezometers can be installed without a sand intake zone and bentonite seal. Instead, the entire borehole is backfilled with bentonite cement grout.

## **Interpretation of Field Data for Surcharge Release**

Generally, the surcharge is released for construction (i.e., released for removal) when the primary consolidation settlement reaches about 96% to 98% EOP after placement of the final embankment stage.

A common technique for determining the degree of consolidation is the Asaoka (1978) method (see also Jamiolkowski et al., 1985). Using this method, the field time-settlement curve is used to select a series of settlement values,  $S_{n1} \dots S_{ni}$  such that  $S_{ni}$  is the settlement at time  $t_i$ . To use this method, the time interval between readings,  $\Delta t$ , is constant and the embankment loading is not changing with time. From this series of measurements, a plot similar to that shown in Figure F12 is made on an arithmetic scale. The total primary consolidation settlement,  $S_n$ , is given where a straight line fitted through the points plotted as  $(S_{n-1}, S_n)$  intersects the 45° line (i.e.,  $S_{n-1} = S_n$  line), as shown in Figure F12. For example, this figure shows that the projected primary consolidation is about 710 mm. Thus, if the current measured settlement is about 680 mm, then the percentage of primary consolidation completed at this last reading is  $680/710 \times 100$ , or 95.8%. Obviously, the reliability of the Asaoka method improves as more settlement measurements are gathered.

In addition to estimating the time to reach EOP, the slope of the line  $\beta_1$  is related to the coefficient of consolidation in the vertical direction,  $c_v$ , which can also be estimated using consolidation theory and compared with values obtained from a laboratory test program, as was done in Farnsworth et al. (2013).

Research performed by Farnsworth et al. (2013) has shown that monitoring of the time rate of consolidation using the Asaoka (1978) method applied to surface monuments solely is unreliable. This is especially true when the deposits consist of relatively thick clay layers consolidating at different rates. The Asaoka (1978) method suffers from a significant decrease in accuracy for such cases. In short, the relatively fast settlement rate in the early consolidation stages contributed by the faster draining layers, and the much slower settlement rates in the late stages contributed by the slower draining layers, tend to cause the settlement line in the Asaoka (1978) method to bow upwards toward the 45-degree convergence line (Figure F13).

Hence, to overcome this, separate Asaoka projection evaluations are required on each compressible layer using the calculated settlement within each layer, as obtained by differencing the settlement readings that bracket the compressible layer as obtained from periodic readings of the magnet extensometer or Sondex<sup>TM</sup> systems (Farnsworth et al., 2013).

In addition, in order to limit the potential for underestimating the time to EOP using the Asaoka (1978) method, it is recommended that such Asaoka projections not be attempted until 80% of the consolidation settlement has been completed in the slowest consolidating layer, and that approximately 10 or more settlement measurements have been obtained from the monitoring program at a relatively uniform time interval (i.e., constant value of  $\Delta t$ ).

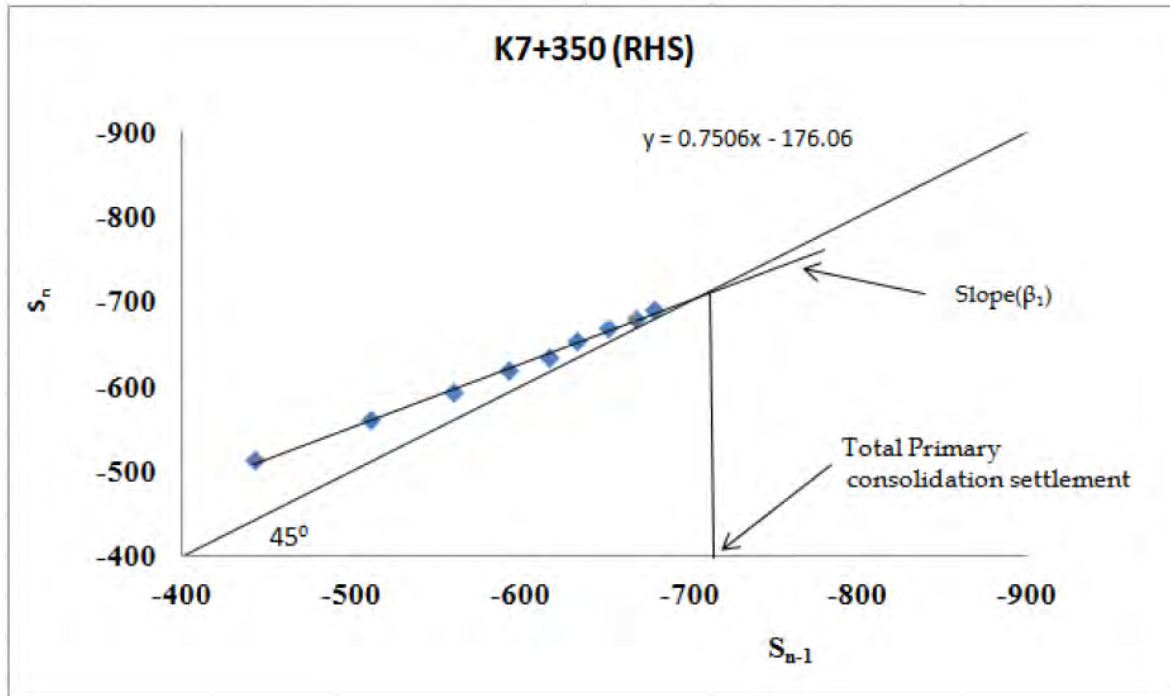


Figure F12 Typical plot of determining the amount of primary consolidation using the Asaoka (1978) method (after Premalal et al., 2012).

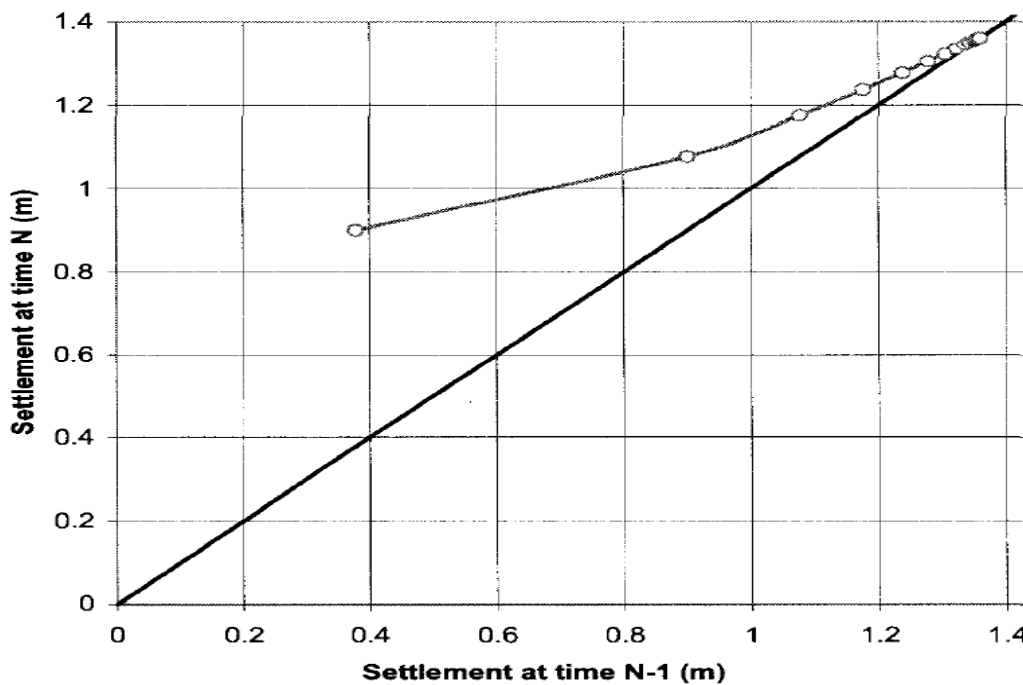


Figure F13. Surface settlement measurements plotted using Asaoka (1978) method. Strong non-linearity in the data indicates multi-layers consolidating at different rates.

Also, the degree of consolidation in soils treated with PV drains can be estimated using the piezometer measurements. The procedure for doing this was developed by Orleach (1983) and summarized in Jamiolkowski et al. (1985).

## Consequences of Premature Surcharge Removal

The premature removal of surcharge may have deleterious effects on the post-construction settlement behavior of the foundation/embankment system and this may, in turn, affect pavement performance and drainage. Premature removal may cause pavement unevenness and noticeable, unsafe differential settlement, especially at bridge approaches.

In some projects, where embankment construction and settlement duration become critical path activities on the construction schedule, there may be pressure on the project team to decide to remove the surcharge fill prior to completion of EOP consolidation. This should be avoided whenever possible.

Depending on the settlement performance goal of the project and as a practical matter, it is recommended that the surcharge remain in place until at least 96% to 98% of EOP consolidation has been reached during the last stage of embankment construction. Premature removal of the surcharge prior to this time will result in increased secondary compression settlement.

In order to estimate the increase in post-construction settlement resulting from premature surcharge removal, a geotechnical monitoring array, as discussed in the previous section, is essential in measuring  $\Delta u$  in each of the critical layers. These measurements can then be used to evaluate the consequences of premature surcharge removal. For such cases, the AAOS value must be reduced to account for remaining  $\Delta u$  measured in the compressible soils. In addition,  $t_r$  will occur earlier due to early surcharge removal, and this will add to increasing the amount of secondary compression settlement. The vertical effective stress reduction caused by the removal of the surcharge,  $\Delta \sigma'_{vs}$ , at the depth of interest should be revised using Equation 17:

$$\Delta \sigma'_{vs} = \sigma'_{vs} - \Delta u - \sigma'_{vf} \quad (17)$$

where:  $\sigma'_{vs}$  and  $\sigma'_{vf}$  have been previously defined and  $\Delta u$  is the remaining excess pore water pressure in each of the consolidating layers above the hydrostatic pressure:

$$\Delta u = u - u_o \quad (18)$$

where:  $u$  is the measured pore pressure in each layer prior to surcharge removal and  $u_o$  is the hydrostatic pore water pressure prior to embankment construction. The revised AAOS is then calculated from:

$$AAOS = \Delta \sigma'_{vs} / \sigma'_{vf} \quad (19)$$

If the surcharge fill is removed too early, it is possible that additional primary consolidation may occur in some of the thicker, cohesive layers because of the existence of a significant amount of excess pore water pressure in critical layers. The possibility for additional primary consolidation resulting from premature surcharge release should be checked for each cohesive layer by ensuring that the following inequality is true:

$$\sigma'_{vs} - \Delta u > \sigma'_{v \text{ final}} \quad (20)$$

where:  $\sigma'_{vs}$  incorporates the vertical effective stress at depth resulting from the full height of the surcharged embankment during the last stage of embankment construction at the EOP, and  $\sigma'_{vf}$  incorporates the vertical effective stress at depth at EOP resulting from the final embankment

configuration, including the additional vertical stresses resulting from the dead load due to the weight of the pavement system and underlying roadbase.

If this inequality is not true, then some amount of primary consolidation remains in the layer(s) of interest and more time is required before the surcharge can be released.

If this inequality is true, EOP consolidation has not been reached and premature surcharge removal is being considered by the project personnel; then it becomes vital that measurements of the remaining excess pore water pressure,  $\Delta u$ , be obtained from project-specific geotechnical monitoring using piezometers placed in the critical consolidating layers. These measurements are used to calculate the consequences of premature surcharge release in terms of additional secondary compression settlement using the above equations to estimate the revised AAOS.

If such piezometers were not placed during initial construction, or they have become dysfunctional during construction, then it becomes imperative that they be placed or replaced and monitored prior to release of the surcharged fill.

Lastly, the ramifications of increased secondary compression settlement resulting from premature surcharge removal should be discussed among the project team. In some cases, it may be necessary to use lightweight fill to achieve project post-construction settlement goals. In concept, the surcharge and a portion of the embankment could be removed and replaced with lightweight fill to effectively increase the AAOS; hence, aiding in the reduction of the estimated amount of post-construction settlement.

## References (Appendix F only)

- Asaoka, A. (1978). Observational Procedure of Settlement Prediction. *Soils and Foundations*, Vol. 18, No. 4, 1978, pp. 87–101.
- Barron, R.A. (1948). Consolidation of Fine-Grained Soils by Drain Wells. *ASCE Transactions*, Vol. 113, pp. 718-742.
- Bartlett, S. F., Lawton E. C., Lingwall, B. N., and Cline M. F., (2011). "Hyperbolic Model Parameters and Settlement Modeling for the I-15 Reconstruction Project," Prepared for the Utah Department of Transportation Research Division, Report, Oct. 2011, 93p.
- Bartlett, S.F., G. Monley, A. Soderborg, and A. Palmer (2001). Instrumentation and Construction Performance Monitoring for the I-15 Reconstruction Project, Salt Lake City, Utah. *Transportation Research Record: Journal of the Transportation Research Board*, No. 1772, pp. 40-47.
- Bartlett, S.F., and Farnsworth, C.B., 2004. "Monitoring and Modeling of Innovative Foundation Treatment and Embankment Construction Used on the I-15 Reconstruction Project, Project Management Plan and Instrument Installation Report," UDOT Research Report No. UT-04.19, 202 p.
- Bartlett, S. F., and Lee, H., (2004). "Estimation of Compression Properties of Clayey Soils, Salt Lake Valley, Utah," Utah Department of Transportation Research Report No. UT-04.28, 44 p.
- Cline, M. D., and Bartlett S. F., (2008). "Numerical Modeling of Settlement Behavior of Treated and Untreated Foundation Soils Underlying MSE Wall for the I-15 Reconstruction Project, Salt Lake City, Utah," Utah Department of Transportation Research Report No. UT-04.18, 62 p.
- Duncan, J. M., Byrne, P., Wong, K. S., and Mabry, P. (1980). "Strength, stress-strain and bulk modulus parameters for finite element analyses of stresses and movements in soil masses." Rep. No. UCB/GT/80-01, College of Engrg., Univ. of Calif., Berkeley, Calif.
- Fang, H-Y. (1991). *Foundation engineering handbook*, 2nd Ed., Van Nostrand Reinhold, New York.
- Farnsworth, C. B., Ozer, T. A, Bartlett, S. F., and Lawton, E. C., (2015). "A Case Study Comparison of Methodologies for Establishing Horizontal Drainage Design Properties in Soft Cohesive Soils," *Transportation Research Record*, 2511:1-8, July 2015.
- Farnsworth, C. F., Bartlett, S. F., and Lawton, E. C., (2013). "Estimation of the Time-Rate of Settlement for Multi-Layered Clays Undergoing Radial Drainage," *Transportation Research Record: Journal of the Transportation Research Board*, No. 2363, Transportation Research Board of the National Academies, Washington, D.C., 2013, pp. 3–11.
- Jamiolkowski, et al. (1985). "New Developments in Field and Laboratory Testing of Soils." Proc. of the 11th Intl. Conf. on Soil Mech. and Found. Engrg., San Francisco, Vol. 1, pp. 57-153.
- Ladd, C. C. (1989). Unpublished class notes for course 1.322, Soil Behavior, Department of Civil and Environmental Engineering, MIT, Cambridge, MA.
- Lingwall, B. N., and Bartlett, S. F. (2013). "Settlement of Structures Adjacent to Large Embankment Construction – A Case History in Settlement Estimates," ASCE GeoCongress, 2013.
- Orleach P. (1983). "Techniques to evaluate the field performance of vertical drains," Thesis (M.S.) Massachusetts Institute of Technology, Dept. of Civil Engineering, 1983, 159 p.
- Ozer, A.T. (2005). *Estimation of Consolidation and Drainage Properties for Lake Bonneville Clays*. Ph.D. Dissertation, Department of Civil and Environmental Engineering, University of Utah, Salt Lake City, Utah.
- Premalal, R.P.D.S., Jayasinghe, T.W.A.S.L, Indrachap, K.R.T.H, and Thilakasiri, H.S. (2012). "Use of the Observational Approach for Embankment Construction on Organic Soil Deposits in Sri Lanka," ICSBE-2012: International Conference on Sustainable Built Environment, 14-16 December 2012, Kandy, Sri Lanka.
- Slope Indicator (2004). "Guide to Geotechnical Instrumentation," 52 p.

- Stewart, J.P., Lacy, H. S., and Ladd, C. C. (1994). "Settlement of large mat on deep compressible soil. *Proceedings, Settlement '94*, ASCE Specialty Conference, Geotechnical Special Publication No. 40, 2, p. 842-859.
- Saye, S., and Ladd, C. C. (1997). "Methodology for Estimating Surcharge Heights and Secondary Compression Settlements," Woodward-Clyde Consultants Memorandum, I-15 Reconstruction Project, Salt Lake City, Utah, November 21, 1997.